

P54/WGI-14 - Changes to the underlying scientific-technical assessment to ensure consistency with the approved SPM
These trickle backs will be implemented in the Chapter during copy-editing

SPM Page:Line	Chapter/Su pp. Material	Chapter Page:Line	Summary of edit to be made
SPM14:4	9	7:4	Please change "There is low confidence in model simulations of past and future Antarctic sea ice evolution due to deficiencies..." to " There is <i>low confidence</i> in model simulations of future Antarctic sea ice decrease, and lack of decrease, due to deficiencies... "
SPM-9:4	9	8:40	Please add the sentence in bold after the existing sentence: "While ocean thermal expansion (38%) and mass loss from glaciers (41%) dominate the total change from 1901 to 2018, ice sheet mass loss has increased and accounts for about 35% of the sea level increase during the period 2006–2018 (<i>high confidence</i>). Because of the increased ice-sheet mass loss, the total loss of land ice (glaciers and ice sheets) was the largest contributor to global mean sea-level rise over the period 2006-2018 (<i>high confidence</i>). "
SPM14:4	9	51:1-2	Please change "there remains low confidence in existing future projections of Antarctic sea-ice evolution." to " there remains <i>low confidence</i> in existing future projections of Antarctic sea-ice decrease and lack of decrease. "
SPM-9:4	9	96:4	Please add the sentence in bold after the existing sentence: "However, all contributions to GMSL rise show their largest rate during 2006 to 2018, with the ice sheets accounting for about 35% of the total change during this period. Because of the increased ice-sheet mass loss, the total loss of land ice (glaciers and ice sheets) was the largest contributor to GMSL rise over the period 2006-2018 (<i>high confidence</i>). "

AR6 WGI Report – List of corrigenda to be implemented

The corrigenda listed below will be implemented in the Chapter during copy-editing.

CHAPTER 9

Document (Chapter, Annex, Supp. Mat...)	Section	Page :Line (based on the final pdf FGD version)	Detailed info on correction to make
9	Author list	1: 25	Replace “Hong Kong” with “Hong Kong, China”
9	ES	5:30	Replace “1971 to 2018 by [0.28–0.55] yottajoules” by “1971 to 2018 by 0.396 [0.329–0.463, <i>likely range</i>] yottajoules”
9	ES	5:31	The long time scale also implies that the amount of deep-ocean warming will only become scenario-dependent after about 2040 (<i>medium confidence</i>), and that the warming is irreversible over centuries to millennia (<i>very high confidence</i>).
9	ES	7:9	Replace: Over the 21st century, the majority of coastal locations have a median projected regional sea-level rise within +/- 20% of the median projected GMSL change (<i>medium confidence</i>). with: Approximately 60% (SSP1-1.9) to 70% (SSP5-8.5) of the global coastline has a projected median 21st century regional relative sea-level rise within ±20% of the global mean increase (<i>medium confidence</i>).
9	ES	8:37	Change ‘While ocean’ to ‘Ocean’
9	ES	8:38-40	Change ‘to 2018, ice sheet mass loss has increased and accounts for about 35% of the sea level increase during the period 2006-2018 (high confidence). {2.3.3, 9.6.1, 9.6.2, Cross-Chapter Box 9.1, Box 7.2}’ To ‘to 2018. The contribution of Greenland and Antarctica to GMSL rise was four times larger during 2010-2019 than during 1992-1999 (high confidence). {2.3.3, 9.6.1, 9.6.2, Cross-Chapter Box 9.1, Table 9.A.1, Box 7.2}’
9	ES	9:10	Page 9-9: Over the 21st century, the majority of coastal locations will experience a median projected regional sea level rise within +/- 20% of the median projected GMSL change (<i>medium confidence</i>). {9.6.3, 9.6.4}
9	ES	9:16	Considering only processes for which projections can be made with at least <i>medium confidence</i>, relative to the period 1995–2014 GMSL will rise by 2050 between 0.18 [0.15–0.23, <i>likely range</i>] m (SSP1-1.9) and 0.23 [0.20–0.29, <i>likely range</i>] m (SSP5-8.5), and by 2100 between 0.38 [0.28–0.55, <i>likely range</i>] m (SSP1-1.9) and 0.77 [0.63–1.01, <i>likely range</i>] m (SSP5-8.5).
9	Figure 9.1 caption	11: 4 202: 6	Replace “Visual guide to chapter 9 with relevant chapter numbers indicated in red.” with “Visual guide to chapter 9. Sections dealing with the cryosphere are highlighted with a snowflake. ”
	8.3.1.7.1	12	Change ‘22.1%’ to ‘22.2%’
9	9.2.1.1	14 : 41	Replace “Chen et al., 2019b” by “J.-L. Chen et al., 2019”
9	9.2.1.1	14 : 46	Replace “Marshall et al., 2015b” by “J. Marshall et al., 2015”
9	9.2.1.1	15 : 32	Replace “Wang et al., 2014a” by “C. Wang et al., 2014”
9	9.2.1.1	15 : 32	Replace “Li et al., 2019b” by “Q. Li et al., 2019”
9	9.2.1.1	15 : 38	Replace “Li et al., 2016a” by “Q. Li et al., 2016”
9	9.2.1.2	16 : 50	Replace “Zanna et al., 2019a” by “Zanna et al., 2019”
9	9.2.1.2	17 : 48	Replace “Yang et al., 2016a” by “Yang et al., 2016”
9	9.2.1.2	18 : 8	Replace “Li et al., 2020” by “J.-L.F. et al., 2020b”
9	9.2.1.2	18 : 11	Replace “Jackson et al., 2020a” by “L.C. Jackson et al, 2020”

9	9.2.1.3	18 : 33 18 : 35-36 18 : 40	Replace “Li et al., 2020a” by “G. Li et al., 2020”
9	9.2.1.3	18 : 44	Replace “Cummins and Ross, 2020a” by “Cummins and Ross, 2020”
9	9.2.1.3	19 : 32 19 : 35	Replace “Lique et al., 2018a” or “Lique et al., 2018b” by “Lique et al., 2018”
9	9.2.1.3	19 : 38-39 19 : 43	Replace “Li et al., 2016a” or “Li et al., 2016b” by “Q. Li et al., 2016”
9	9.2.1.3	19 : 45-46	Replace “Li et al., 2016a” by “Q. Li et al., 2016” Replace “Li et al., 2019b” by “Q. Li et al., 2019”
9	Box 9.2	20 : 10	Replace “Hayashida et al., 2020a” by “Hayashida et al., 2020”
9	Box 9.2	20 : 17	Replace “Li et al., 2019c” by “Y. Li et al., 2019”
9	Box 9.2	21 : 17 21 : 24	Replace “Hayashida et al., 2020b” by “Hayashida et al., 2020”
9	9.2.2.1	22 : 13	Replace “Wang et al., 201b” by “L. Wang et al., 2021”
9	9.2.2.1	22 : 31	Replace “Zanna et al., 2019a” by “Zanna et al., 2019”
9	9.2.2.1	22 : 55	Replace “Purkey et al., 2019a” by “Purkey et al., 2019”
9	9.2.2.1	23 : 29 23 : 30-31	Replace “Couldrey et al., 2020” by “Couldrey et al., 2021”
9	9.2.2.1	23 : 43	Replace “Williams et al., 2015b” by “R.G. Williams et al., 2015” Replace “Zanna et al., 2019a” by “Zanna et al., 2019”
9	9.2.2.1 (Figure 9.8 caption)	23:52	Replace “and simulated by CMIP5 models over the historical period (1951-2011) and under the RCP8.5 future (2011-2060) versus” by “and simulated by CMIP5 models over the historical period (1972-2011) and under the RCP8.5 future (2021-2060) versus”
9	9.2.2.1	24 : 12 24 : 17	Replace “Wang et al., 2019b” by “Q. Wang et al., 2019”
9	9.2.2.1	24 : 22	Replace “Oldenburg et al., 2018a” by “Oldenburg et al., 2018”
9	9.2.2.1	24 : 36	Replace “Miller et al., 2012a” by “G.H. Miller et al., 2012”
9	9.2.2.1	24 : 52	Replace “Jackson et al., 2020a” by “L.C. Jackson et al., 2020”
9	9.2.2.1	25:22	Replace “will increase 2 to 5 times” by “will increase 2 to 4 times”
9	9.2.2.1	25 : 33 25 : 43 25 : 49	Replace “Couldrey et al., 2020” by “Couldrey et al., 2021”
9	9.2.2.1	25 : 40	Replace “Roberts et al., 2020a” by “Roberts et al., 2020”
9	9.2.2.1	26 : 7	Replace “Ehlert and Zickfeld, 2018a” by “Ehlert and Zickfeld, 2018”
9	9.2.2.1	26:26	In summary, there is <i>very high confidence</i> that there is a long-term commitment to increased OHC in response to anthropogenic CO2 emissions, which is essentially irreversible on human timescales.
9	9.2.2.2	27 : 13	Replace “Cummins and Ross, 2020b” by “Cummins and Ross, 2020”
9	9.2.2.2	27 : 29 27 : 35	Replace “Dukhovskoy et al., 2019a” by “Dukhovskoy et al., 2019”
9	9.2.2.2	27 : 39	Replace “Li et al., 2019a” by “G. Li et al., 2019”
9	9.2.2.2	27 : 48-49 28 : 8-9	Replace “Silvy et al., 2020a” by “Silvy et al., 2020”
9	9.2.2.3	28 : 22 28 : 33-34 28 : 36 28 : 55	Replace “Silvy et al., 2020a” or “Silvy et al., 2020b” by “Silvy et al., 2020”
9	9.2.2.3	29 : 26	Replace “Wang et al., 2015b” by “H. Wang et al., 2015”
9	9.2.2.3	29 : 36-37	Replace “Purkey et al., 2019b” by “Purkey et al., 2019”
9	9.2.2.3	29 : 39	Replace “Zhang et al., 2019b” by “L. Zhang et al., 2019”
9	9.2.2.3	30 : 13	Replace “Golledge et al., 2019a” by “Golledge et al., 2019”
9	9.2.3.1	30 : 43	Replace “Wang, Legg and Hallberg, 2015” by “H. Wang et al., 2015”
9	9.2.3.1	30 : 49 30 : 50	Replace “Roberts et al., 2020a” or “Roberts et al., 2020b” by “Roberts et al., 2020”

		32 : 46	
9	9.2.3.1	30 : 52	Replace “Jackson et al., 2020a” by “L.C. Jackson et al., 2020”
9	9.2.3.1	31 : 49	Replace “Zhang et al., 2019d” by “R. Zhang et al., 2019”
9	Figure 9.10 caption	32, Row 47	Replace “A compilation (Jackson and Wood, 2018) of percentage changes” with “A compilation of percentage changes”
9	9.2.3.1	32 : 2 32 : 44-45	Replace “Menary et al., 2020c” by “Menary et al., 2020b”
9	9.2.3.1	32 : 35	Replace “Menary et al., 2020b” by “Menary et al., 2020a”
9	9.2.3.2	35 : 25 35 : 35	Replace “Golledge et al., 2019a” by “Golledge et al., 2019”
9	9.2.3.4	37 : 8-9	Replace “Yang et al., 2016b” by “Yang et al., 2016”
9	9.2.3.4	37 : 10	Replace “Wang et al., 2016c” by “Y.-L. Wang et al., 2016”
9	9.2.3.4	37 : 20	Replace “Oldenburg et al., 2018b” by “Oldenburg et al., 2018”
9	9.2.3.4	37: 43-44	Replace “Zhang et al., 2016c” by “Z. Zhang et al., 2016”
9	9.2.3.4	38 : 55	Replace “Yang et al., 2016a” by “Yang et al., 2016”
9	9.2.3.5	39 : 34	Replace “Wang et al., 2015a” by “D. Wang et al., 2015”
9	9.2.3.5	39 : 52 40 : 3	Replace “Oerder et al., 2015a” or “Oerder et al., 2015b” by “Oerder et al., 2015”
9	9.2.3.6	40 : 38	Replace “Oerder et al., 2015a” or “Oerder et al., 2015b” by “Oerder et al., 2015” Replace “Zhang et al., 2016a” by “Y. Zhang et al., 2016”
9	9.2.3.6	40 : 43-44	Replace “Wang et al., 2014b” by “Q. Wang et al., 2014” Replace “Zhang et al., 2016b” by “Y.J. Zhang et al., 2016”
9	9.2.4.1	41 : 10	Replace “Church et al., 2013a” by “Church et al., 2013b”
9	9.2.4.1	41 : 13	Replace “Hobbs et al., 2016b” by “Hobbs et al., 2016a”
9	Table 9.1	42	Replace “Church et al., 2013a” by “Church et al., 2013b”
9	9.2.4.2	43 : 1	Replace “Couldrey et al., 2020” by “Couldrey et al., 2021”
9	9.2.4.2	43 : 51-52	Replace “Church et al., 2013a” by “Church et al., 2013b” Replace “Slangen et al., 2014a” by “Slangen et al., 2014b” Replace “Chen et al., 2019a” by “C. Chen et al. 2019” Replace “Couldrey et al., 2020” by “Couldrey et al. 2021”
9	9.2.4.2	44 : 1 44 : 7 44 : 9-10 44 : 11 44 : 18 44 : 23	Replace “Couldrey et al., 2020” by “Couldrey et al. 2021”
9	9.2.4.2	44 : 11	Replace “Chen et al., 2019a” by “C. Chen et al. 2019”
9	9.2.4.2	44 : 21	Replace “Zanna et al., 2019a” by “Zanna et al., 2019”
9	9.2.4.2	44 : 26	Replace “Slangen et al., 2014a” by “Slangen et al., 2014b”
9	9.2.4.2	44 : 51	Replace “Comiso et al., 2017b” by “Comiso et al., 2017a”
9	9.3.2.1	49 : 28	Replace “Comiso et al., 2017a” by “Comiso et al., 2017b”
9	9.3.2.1	49 : 49	Replace “Zhang et al., 2019b” by “L. Zhang et al., 2019”
9	9.3.2.1	50 : 16	Replace “Wang et al., 2019a” by “G. Wang et al., 2019”
9	9.3.2.1	51 : 29-30	Replace “Hobbs et al., 2016a; Jones et al., 2016b” by “Hobbs et al., 2016b; J.M. Jones et al., 2016”
9	9.3.2.1	51 : 36	Replace “Hobbs et al., 2016a” by “Hobbs et al., 2016b”
9	9.3.2.1	51 : 37 51 : 39-40	Replace “Zhang et al., 2019c” by “L. Zhang et al., 2019”
9	9.3.2.2	52 : 8 52 : 16	Replace “Williams et al., 2015a” by “G. Williams et al., 2015”
9	9.4.1.1	53 : 11	Replace “The IMBIE Team (2020)” with “Shepherd et al. (2021)” https://doi.org/10.5285/77B64C55-7166-4A06-9DEF-2E400398E452
9	Figure 9.17 Caption	54 232:10	Replace “likely range of the ISMIP6 emulation” by “17th to 83rd, 5th to 95th percentile ranges of the ISMIP6 emulation”
9	9.4.1.1	54 : 17	Replace “Miller et al., 2012b” by “K.G. Miller et al., 2012”

9	9.4.1.1	54 : 41	Replace “Zhang et al., 2019a” by “B. Zhang et al., 2019”
9	9.4.1.1	54 : 57	Replace “Wang et al., 2019” by “W. Wang et al., 2019c”
9	9.4.1.1	55 : 37	Replace “Jackson et al., 2020b” by “R.H. Jackson et al., 2020”
9	9.4.1.1	55 : 40	Replace “Slater et al., 2017b” by “D.A. Slater et al., 2017”
9	9.4.1.1	56 : 4	Replace “Slater et al., 2020b” by “T. Slater et al., 2020”
9	9.4.1.2	56 : 47	Replace “Alexander et al., 2019a” by “Alexander et al., 2019”
9	9.4.1.2	56 : 50	Replace “Alexander et al., 2019b” by “Alexander et al., 2019”
9	9.4.1.2	57 : 7	Replace “Morlighem et al., 2016a” by “Morlighem et al., 2016b”
9	9.4.1.2	57 : 29	Replace “Morlighem et al., 2016b” by “Morlighem et al., 2016a”
9	9.4.1.3	57 : 52	Replace “Church et al., 2013a” by “Church et al., 2013b”
9	9.4.1.3	58 : 31	Replace “Edwards et al., 9998” by “Edwards et al., 2021”
9	9.4.1.3	59 : 10	Replace “Golledge et al., 2019a” by “Golledge et al., 2019”
9	9.4.1.4	61 : 7	Replace “Church et al., 2013a” by “Church et al., 2013b”
9	9.4.1.4	61 : 19	Replace “Slater et al., 2020b” by “T. Slater et al., 2020”
9	Box 9.3	62 : 20	Replace “Church et al., 2013a” by “Church et al., 2013b”
9	Box 9.3	62 : 34 63 : 5-6	Replace “Barthel et al., 2020a” or “Barthel et al., 2020b” by “Barthel et al., 2020”
9	Box 9.3	62 : 54	Replace “Levermann et al., 2020a” by “Levermann et al., 2020”
9	Box 9.3	63 : 13	Replace “Slater et al., 2019, 2020a” by “D.A.Slater et al., 2019, 2020”
9	Box 9.3	63 : 34-35	Replace “Levermann et al., 2014, 2020a” by “Levermann et al., 2014, 2020”
9	Box 9.3	63 : 50	Replace “Church et al., 2013a” by “Church et al., 2013b”
9	9.4.2.1	64 : 33 64 : 51	Replace “The IMBIE Team (2020)” with “Shepherd et al. (2021)” https://doi.org/10.5285/77B64C55-7166-4A06-9DEF-2E400398E452
9	9.4.2.1	64 : 55 65 : 2	Replace “Li et al., 2016b” by “X. Li et al., 2016”
9	9.4.2.1	65 : 33-34	Replace “Miller et al., 2012b” by “K.G. Miller et al., 2012”
9	9.4.2.1	65 : 39	Replace “WCRP Global Sea Level Budget Group, 2018a” by “WCRP Global Sea Level Budget Group, 2018”
9	9.4.2.2	67 : 35	Replace “Church et al., 2013a” by “Church et al., 2013b”
9	9.4.2.2	68 : 7 69 : 8 70 : 35-36	Replace “Levermann et al., 2020a” by “Levermann et al., 2020”
9	9.4.2.2	68 : 16	Replace “Golledge et al., 2019a” by “Golledge et al., 2019”
9	9.4.2.2	69 : 21	Replace “Edwards et al., 2019a” by “Edwards et al., 2019”
9	9.4.2.3	71 : 15	Replace “DeConto et al., (9998)” by “DeConto et al., (2021)”
9	9.4.2.3	71 : 20	Replace “Golledge et al., 2019a” by “Golledge et al., 2019”
9	9.4.2.4	72 : 30	Replace “DeConto et al., (9998)” by “DeConto et al., (2021)”
9	9.4.2.5	73 : 13 73 : 16-17	Replace “Golledge et al., 2019b” by “Golledge et al., 2019”
9	9.4.2.5	73 : 30 74 : 34	Replace “Levermann et al., 2020b” by “Levermann et al., 2020”
9	9.4.2.5	73 : 37 73 : 46	Replace “Barthel et al., 2020b” by “Barthel et al., 2020”
9	Table 9.3	75 : 1	Replace “Church et al., 2013a” by “Church et al., 2013b”
9	Table 9.3	75 : 1	Replace “Levermann et al., 2020b” by “Levermann et al., 2020”
9	9.4.2.6	77 : 11	Replace “DeConto et al., (9998)” by “DeConto et al., (2021)”
9	9.4.2.6	77 : 15 77 : 43	Replace “Edwards et al., 2019b” by “Edwards et al., 2019”
9	9.4.2.6	77 : 21	Replace “Levermann et al., 2020a” by “Levermann et al., 2020”
9	9.5.1.2	82 : 54-55 83 : 13	Replace “Maussion et al., 2019a” by “Maussion et al., 2019”
9	9.5.1.3	83 : 55	Replace “Maussion et al., 2019a” by “Maussion et al., 2019”
9	9.5.1.3	84 : 10	Replace “Church et al., 2013a” by “Church et al., 2013b”
9	Table 9.4	84	Replace “Church et al., 2013a” by “Church et al., 2013b”
9	Table 9.4	85 : 1	Replace “Maussion et al., 2019a” by “Maussion et al., 2019”

9	9.5.2.1	87 : 6-7	Replace “Jones et al., 2016a” by “B.M. Jones et al., 2016” Replace “Gibson et al., 2018a” by “Gibson et al., 2018”
9	9.5.2.2	87 : 39	Replace “Gibson et al., 2018b” by “Gibson et al., 2018”
9	9.5.2.2	87 : 52	Replace “Chadburn et al., 2015a” by “S. Chadburn et al., 2015”
9	9.5.2.2	88 : 3	Replace “Wang et al., 2016b” by “W. Wang et al., 2016”
9	9.5.2.2	88 : 4-5	Replace “Chadburn et al., 2015b” by “S. Chadburn et al., 2015”
9	9.5.3.2	93 : 16	Replace “Slater et al., 2017a” by “A.G. Slater et al., 2017”
9	9.5.3.2	93 : 28	Replace “Wang et al., 2016a” by “L. Wang et al., 2016”
9	9.6.1.1	95 : 48	Replace “Zanna et al., 2019b” by “Zanna et al., 2019”
9	9.6.1.2	96 : 23	Replace “WCRP Global Sea Level Budget Group, 2018b” by “WCRP Global Sea Level Budget Group, 2018”
9	9.6.1.2	96:34	Change ‘about 35%’ to ‘27%’
9	Table 9.5	Row2, col4	Change ‘50.3%’ to 50.4%’
9	Table 9.5	Row2, col5	Change ‘45.7%’ to 45.9%’
9	Table 9.5	Row2, col6	Change ‘34.4%’ to ‘38.6%’
9	Table 9.5	Row4, col4	Change ‘22.1%’ to ‘22.2%’
9	Table 9.5	Row4, col5	Change ‘19.3%’ to ‘19.4%’
9	Table 9.5	Row4, col6	Change ‘15.4%’ to ‘17.3%’
9	Table 9.5	Row6, col5	Change ‘10.9 [9.0 to 12.8]’ To ‘10.8 [8.9 to 12.7]’
9	Table 9.5	Row6, col6	Change ‘10.9 [9.5 to 12.2] (22.3%)’ To ‘7.5 [6.2 to 8.9] (17.3%)’
9	Table 9.5	Row7, col5	Change ‘0.44’ to ‘0.43’
9	Table 9.5	Row7, col6	Change ‘0.91 [0.79 to 1.02]’ To ‘0.63 [0.51 to 0.74]’
9	Table 9.5	Row8, col4	Change ‘6.8 [-3.9 to 17.5 (7.2%)]’ To ‘6.7 [-4.0 to 17.3] (7.1%)’
9	Table 9.5	Row8, col5	Change ‘6.4 [4.3 to 8.5] (9.0%)’ To ‘6.1 [4.0 to 8.3] (8.6%)’
9	Table 9.5	Row8, col6	Change ‘6.4 [4.8 to 8.0] (13.1%)’ To ‘4.4 [2.9 to 6.0] (10.2%)’
9	Table 9.5	Row8, col7	Change ‘6.9 [-3.8 to 17.5] (4.2%)’ To ‘6.7 [-4.0 to 17.4] (4.1%)’
9	Table 9.5	Row9, col4	Change ‘-0.08’ to ‘-0.09’
9	Table 9.5	Row9, col5	Change ‘0.26 [0.17 to 0.34]’ To ‘0.25 [0.16 to 0.33]’
9	Table 9.5	Row9, col6	Change ‘0.53 [0.40 to 0.66]’ To ‘0.37 [0.24 to 0.50]’
9	Table 9.5	Row10, col5	Change 10.8% to 10.9%
9	Table 9.5	Row10, col6	Change 14.8% to 16.6%
9	Table 9.5	Row13, col4	Change ‘94.4 [71.7 to 117.1]’ to ‘94.2 [71.5 to 117.0]’
9	Table 9.5	Row13, col5	Change ‘71.6 [60.5 to 82.6]’ to ‘71.2 [60.2 to 82.3]’
9	Table 9.5	Row13, col6	Change ‘48.7 [39.9 to 57.5]’ to ‘43.4 [34.5 to 52.2]’
9	Table 9.5	Row13, col7	Change ‘164.8 [117 to 212.5]’ to ‘164.6 [116.9 to 212.4]’
9	Table 9.5	Row14, col4	Change ‘2.01’ to ‘2.00’
9	Table 9.5	Row14, col5	Change ‘2.86 [2.42 to 3.30]’ to ‘2.85 [2.41 to 3.29]’
9	Table 9.5	Row14, col6	Change ‘4.06 [3.32 to 4.79]’ to ‘3.61 [2.88 to 4.35]’
9	9.6.1.4	99 : 24-25	Replace “Slangen et al., 2014a” by “Slangen et al., 2014b”
9	Box 9.1	101 : 17	Replace “Church et al., 2013a” by “Church et al., 2013b”
9	9.6.2	103 : 19	Replace “Church et al., 2013a” by “Church et al., 2013b”
9	9.6.3	106 : 12	Replace “Church et al., 2013a” by “Church et al., 2013b”
9	9.6.3.1	106 : 38	Replace “Church et al., 2013a” by “Church et al., 2013b”
9	9.6.3.1	106 : 49	Replace “Wang et al., 2021a” by “J. Wang et al., 2021”
9	9.6.3.1	106 : 51-52 107 : 1	Replace “Slangen et al., 2014a” by “Slangen et al., 2014b”
9	9.6.3.2	108 : 10	Replace “Church et al., 2013a” by “Church et al., 2013b”
9	Table 9.7	108	Replace “Levermann et al., 2020a” by “Levermann et al., 2020”

9	Table 9.7	3rd data row (Antarctica)	(2) LARMIP-2 simulations augmented by AR5 surface mass balance model applied to CMIP6 models
9	Table 9.7	109	Replace “Slangen et al., 2014a” by “Slangen et al., 2014b”
9	Table 9.8	112 :28	See highlighted changes to be made below
9	9.6.3.2	114 : 5 114 : 14	Replace “Slangen et al., 2014a” by “Slangen et al., 2014b”
9	9.6.3.2	114 : 13	Replace “Church et al., 2013a” by “Church et al., 2013b”
9	9.6.3.2	114 : 27	Replace “Li et al., 2020c” by “T. Li et al., 2020”
9	9.6.3.3	115:20	Beyond 2050, the scenarios increasingly diverge. Between the baseline period (1995 to 2014) and 2100, processes in whose projection there is <i>medium confidence</i> drive <i>likely</i> GMSL rise of 0.44 m (0.32-0.62) m and 0.77 (0.63-1.01) m under SSP1-2.6 and SSP5-8.5, respectively (Tables 9.8, 9.9).
9	Table 9.9	115 :46	See highlighted changes to be made below
9	9.6.3.3	116 : 15	Replace “Church et al., 2013a” by “Church et al., 2013b”
9	9.6.3.3	117:17	Replace: Over the 21st century, the majority of coastal locations have a median projected regional sea-level rise within +/- 20% of the median projected GMSL change (<i>medium confidence</i>). with: Approximately 60% (SSP1-1.9) to 70% (SSP5-8.5) of the global coastline has a projected median 21st century regional relative sea-level rise within ±20% of the global mean increase (<i>medium confidence</i>).
9	9.6.3.4	118:39	GMSL in a 4°C scenario is <i>likely</i> to rise by 0.58-0.92 m, similar to the projection for SSP3-7.0.
9	Table 9.10	118 :48	See highlighted changes to be made below
9	Table 9.11	120 :22	See highlighted changes to be made below
9	9.6.3.3	122 : 13	Replace “Ehlert and Zickfeld, 2018b” by “Ehlert and Zickfeld, 2018”
9	Box 9.4	122:46	the upper limit of 1.01 m of <i>likely</i> sea-level range by 2100 for the SSP 5-8.5 scenario will be exceeded in any future warming scenario on time scales of centuries to millennia (<i>high confidence</i>), but it is uncertain how quickly the long-term committed sea level will be reached (Section 9.6.3.5).
9	9.6.3.5	122:11	The slow response of the deep ocean to forcing leads to global-mean thermosteric sea-level fall occurring long afterward even if CO ₂ levels are restored after a transient increase: global mean thermosteric sea level rise takes over a millennium to reverse course (Ehlert and Zickfeld, 2018b)
9	Box 9.4	123 : 20 123 : 54	Replace “Golledge et al., 2019b” by “Golledge et al., 2019”
9	Box 9.4	123 : 26	Replace “Slater et al., 2020b” by “T. Slater et al., 2020”
9	9.6.4.1	124 : 14	Replace “Church et al., 2013a” by “Church et al., 2013b”
9	9.6.4.1	126 : 10	Replace “Marshall et al., 2015a” by “A.G. Marshall et al., 2015”
9	9.6.4.1	128 : 42	Replace “Collins et al., 2019b” by “Collins et al., 2019”
9	9.6.4.2	128 : 47	Replace “Couasnon et al., 2019” by “Couasnon et al., 2020”
9	FAQ9.1, Figure 1	131 :9 and 255 :6	Change ‘Table 9.SM.5’ to ‘Table 9.SM.9’.
9	FAQ 9.1	132 : 9	Remove “Table 9.SM.5”
9		128: 49	Replace ‘Taiwan’ with ‘Taiwan, China’
9	References	168:33-34	Wrong reference. Replace current ‘Le Cozannet et al., 2019 (Scientific Reports)’ by ‘Le Cozannet et al., 2019 (Water) Low end probabilistic sea level projections. https://www.mdpi.com/2073-4441/11/7/1507 ’
9	Figure 9.1	202	replace with updated visual roadmap, as all visual roadmaps have been harmonised (to have a set with a consistent visual identity. This does not alter the content of the chapter.)
9	CCB 9.1, Figure 1	244:1	Update of time series
9			Updates to figure data needed for Figures SPM.8, Box TS.4 Figure 1, 4.2, 9.25, 9.26, 9.27, 9.28, 9.29. None of these changes are visible in the figures.

Table 9.1: Observed contributions to global mean sea level (GMSL) change for five different periods. Values are expressed as the total change over each period (mm) along with the equivalent rate (mm yr⁻¹). The *very likely* ranges appear in parentheses based on the various section assessments as indicated. Uncertainties for the sum of contributions are added in quadrature, assuming independence.

Observed contribution to GMSL change		1901-1990 {9.6.1.1}	1971-2018 {CCBox 9.1}	1993-2018 {9.6.1.2}	2006-2018 {9.6.1.2}	1901-2018 {9.6.1.2}
Thermal expansion (Section 2.3.3.1, Table 2.7)	Δ (mm)	31.6 [14.7 to 48.5] (31.9%)	47.5 [34.3 to 60.7] (50.4%)	32.7 [23.8 to 41.6] (45.9%)	16.7 [8.9 to 24.6] (38.6%)	63.2 [47.0 to 79.4] (38.4%)
	mm yr ⁻¹	0.36 [0.17 to 0.54]	1.01 [0.73 to 1.29]	1.31 [0.95 to 1.66]	1.39 [0.74 to 2.05]	0.54 [0.40 to 0.68]
Glaciers (Excl. peripheral glaciers) (Section 9.5.1.1, Table 9.3)	Δ (mm)	51.8 [30.4 to 73.2] (52.3%)	20.9 [10.0 to 31.7] (22.2%)	13.8 [10.0 to 17.6] (19.4%)	7.5 [6.8 to 8.2] (17.3%)	67.2 [41.8 to 92.6] (40.8%)
	mm yr ⁻¹	0.58 [0.34 to 0.82]	0.44 [0.21 to 0.67]	0.55 [0.40 to 0.70]	0.62 [0.57 to 0.68]	0.57 [0.36 to 0.79]
Greenland ice sheet (Incl. peripheral glaciers) (Section 9.4.1.1)	Δ (mm)	29.0 [16.3 to 41.7] (29.3%)	11.9 [7.7 to 16.1] (12.6%)	10.8 [8.9 to 12.7] (15.2%)	7.5 [6.2 to 8.9] (17.3%)	40.4 [27.2 to 53.5] (24.5%)
	mm yr ⁻¹	0.33 [0.18 to 0.47]	0.25 [0.16 to 0.34]	0.43 [0.36 to 0.51]	0.63 [0.51 to 0.74]	0.35 [0.23 to 0.46]
Antarctic ice sheet (Incl. peripheral glaciers) (Section 9.4.2.1)	Δ (mm)	0.4 [-8.8 to 9.6] (0.4%)	6.7 [-4.0 to 17.3] (7.1%)	6.1 [4.0 to 8.3] (8.6%)	4.4 [2.9 to 6.0] (10.2%)	6.7 [-4.0 to 17.4] (4.1%)

	mm yr ⁻¹	0.00 [-0.10 to 0.11]	0.14 [-0.09 to 0.37]	0.25 [0.16 to 0.33]	0.37 [0.24 to 0.50]	0.06 [-0.03 to 0.15]
Land water storage* (Section 9.6.1.1)	Δ (mm)	-13.8 [-31.4 to 3.8] (-13.9%)	7.3 [-2.4 to 16.9] (7.7%)	7.8 [3.3 to 12.2] (10.9%)	7.2 [3.8 to 10.6] (16.6%)	-12.9 [-45.8 to 20.0] (-7.8%)
	mm yr ⁻¹	-0.15 [-0.35 to 0.04]	0.15 [-0.05 to 0.36]	0.31 [0.13 to 0.49]	0.60 [0.32 to 0.88]	-0.11 [-0.39 to 0.17]
Sum of observed contributions	Δ (mm)	99.0 [63.0 to 135.1]	94.2 [71.5 to 117.0]	71.2 [60.2 to 82.3]	43.4 [34.5 to 52.2]	164.6 [116.9 to 212.4]
	mm yr ⁻¹	1.11 [0.71 to 1.52]	2.00 [1.52 to 2.49]	2.85 [2.41 to 3.29]	3.61 [2.88 to 4.35]	1.41 [1.00 to 1.82]
Observed GMSL change (Section 2.3.3.3)	Δ (mm)	120.1^T [69.3 to 170.8]	109.6^{T/A} [72.8 to 146.4]	81.2^A [72.1 to 90.2]	44.3^A [38.6 to 50.0]	201.9^{T/A} [150.3 to 253.5]
	mm yr ⁻¹	1.35^T [0.78 to 1.92]	2.33^{T/A} [1.55 to 3.12]	3.25^A [2.88 to 3.61]	3.69^A [3.21 to 4.17]	1.73^{T/A} [1.28 to 2.17]

T, A and T/A indicate assessments based on tide gauge reconstructions, satellite altimetry, or a combination of both. The assessment uses tide gauge reconstructions before 1993 and satellite altimetry after 1993.

*For the periods 1971-2018, 1993-2018, 2006-2018 and 1901-2018 the Caceres et al (2020) linear trends are based on the period up to 2016.

[END TABLE 9.5 HERE]

Table 9.8

	RCP 2.6	SSP1-2.6
--	---------	----------

<i>m rel. to 1995-2014</i>	AR5	SROCC	Medium confidence processes	MICI	SEJ
Thermal expansion (9.2.4.1)	0.14 (0.10-0.19)		0.14 (0.11--0.18)		
Greenland (9.4.1.3)	0.07 (0.03-0.11)		0.06 (0.01--0.10)		0.13 (0.07--0.30)
Antarctica (9.4.2.4)	0.06 (-0.04-0.16)	0.04 (0.01-0.11)	0.11 (0.03--0.27)	0.08 (0.06--0.12)	0.09 (-0.01--0.25)
Glaciers (9.5.1.3)	0.10 (0.04-0.16)		0.09 (0.07--0.11)		
Land water storage (9.6.3.2)	0.05 (-0.01-0.11)		0.03 (0.01--0.04)		
Total (2100)	0.41 (0.25-0.58)	0.40 (0.26-0.56)	0.44 (0.32--0.62)	0.41 (0.35--0.48)	0.53 (0.38--0.79)
Total (2150)	0.29-0.63	0.56 (0.40-0.73)	0.68 (0.46--0.99)	0.74 (0.62--0.91)	0.84 (0.56--1.34)
GMSL rate, 2080-2100 (mm/yr)	4.4 (2.0-6.8)	4 (2-6)	5.2 (3.2-8.0)	5.1 (4.3-6.2)	5.9 (2.8-11.0)

	RCP 8.5		SSP5-8.5		
<i>m rel. to 1995-2014</i>	AR5	SROCC	Medium confidence processes	MICI	SEJ
Thermal expansion (9.2.4.1)	0.31 (0.24-0.38)		0.30 (0.24--0.36)		
Greenland (9.4.1.3)	0.14 (0.08-0.27)		0.13 (0.09--0.18)		0.23 (0.10--0.59)
Antarctica (9.4.2.4)	0.04 (-0.08-0.14)	0.12 (0.03-0.28)	0.12 (0.03--0.34)	0.34 (0.19--0.53)	0.21 (0.02--0.56)
Glaciers (9.5.1.3)	0.17 (0.09-0.25)		0.18 (0.15--0.20)		
Land water storage (9.6.3.2)	0.05 (-0.01-0.11)		0.03 (0.01--0.04)		
Total (2100)	0.71 (0.49-0.95)	0.81 (0.58-1.07)	0.77 (0.63--1.01)	0.99 (0.82--1.19)	1.00 (0.70--1.60)
Total (2150)	0.34-1.35	1.27 (0.80-1.79)	1.32 (0.98--1.88)	3.48 (2.57--4.82)	1.79 (1.22--2.94)
GMSL rate, 2080-2100 (mm/yr)	11.2 (7.5-15.7)	15 (10-20)	12.1 (8.6-17.6)	23.1 (17.5-30.1)	16.0 (9.8-28.9)

Table 9.9

	SSP1-1.9	SSP1-2.6	SSP2-4.5	SSP3-7.0	SSP5-8.5	SSP5-8.5 <i>Low Confidence</i>
Thermal expansion	0.12 (0.09--0.15)	0.14 (0.11--0.18)	0.20 (0.16--0.24)	0.25 (0.21--0.30)	0.30 (0.24--0.36)	0.30 (0.24--0.36)
Greenland	0.05 (0.00--0.09)	0.06 (0.01--0.10)	0.08 (0.04--0.13)	0.11 (0.07--0.16)	0.13 (0.09--0.18)	0.18 (0.09--0.59)
Antarctica	0.10 (0.03--0.25)	0.11 (0.03--0.27)	0.11 (0.03--0.29)	0.11 (0.03--0.31)	0.12 (0.03--0.34)	0.19 (0.02--0.56)
Glaciers	0.08 (0.06--0.10)	0.09 (0.07--0.11)	0.12 (0.10--0.15)	0.16 (0.13--0.18)	0.18 (0.15--0.20)	0.17 (0.11--0.21)
Land Water Storage	0.03 (0.01--0.04)	0.03 (0.01--0.04)	0.03 (0.01--0.04)	0.03 (0.02--0.04)	0.03 (0.01--0.04)	0.03 (0.01--0.04)
Total (2030)	0.09 (0.08--0.12)	0.09 (0.08--0.12)	0.09 (0.08--0.12)	0.09 (0.08--0.12)	0.10 (0.09--0.12)	0.10 (0.09--0.15)
Total (2050)	0.18 (0.15--0.23)	0.19 (0.16--0.25)	0.20 (0.17--0.26)	0.22 (0.18--0.27)	0.23 (0.20--0.29)	0.24 (0.20--0.40)
Total (2090)	0.35 (0.26--0.49)	0.39 (0.30--0.54)	0.48 (0.38--0.65)	0.56 (0.46--0.74)	0.63 (0.52--0.83)	0.71 (0.52--1.30)
Total (2100)	0.38 (0.28--0.55)	0.44 (0.32--0.62)	0.56 (0.44--0.76)	0.68 (0.55--0.90)	0.77 (0.63--1.01)	0.88 (0.63--1.60)
Total (2150)	0.57 (0.37--0.86)	0.68 (0.46--0.99)	0.92 (0.66--1.33)	1.19 (0.89--1.65)	1.32 (0.98--1.88)	1.98 (0.98--4.82)
Rate (2040-2060)	4.1 (2.8-6.0)	4.8 (3.5-6.8)	5.8 (4.4-8.0)	6.4 (5.0-8.7)	7.2 (5.6-9.7)	7.9 (5.6-16.1)
Rate (2080-2100)	4.2 (2.4-6.6)	5.2 (3.2-8.0)	7.7 (5.2-11.6)	10.4 (7.4-14.8)	12.1 (8.6-17.6)	15.8 (8.6-30.1)

Table 9.10

	1.5°C	2.0°C	3.0°C	4.0°C	5.0°C	SSP5-8.5 <i>Low Confidence</i>
Closest SSPs	SSP1-2.6	SSP1-2.6/SSP2-4.5	SSP2-4.5/SSP3-7.0	SSP3-7.0	SSP5-8.5	
Total (2050)	0.18 (0.16--0.24)	0.20 (0.17--0.26)	0.21 (0.18--0.27)	0.22 (0.19--0.28)	0.25 (0.22--0.31)	0.24 (0.20--0.40)
Total (2100)	0.44 (0.34--0.59)	0.51 (0.40--0.69)	0.61 (0.50--0.81)	0.70 (0.58--0.92)	0.81 (0.69--1.05)	0.88 (0.63--1.60)
Rate (2040-2060)	4.1 (2.9-5.7)	5.0 (3.7-7.0)	6.0 (4.6-8.1)	6.4 (5.0-8.6)	7.2 (5.7-9.8)	7.9 (5.6-16.1)
Rate (2080-2100)	4.3 (2.6-6.4)	5.5 (3.4-8.4)	7.8 (5.3-11.6)	9.9 (7.1-14.3)	11.7 (8.5-17.0)	15.8 (8.6-30.1)

2000-yr commitment	2-3	2-6	4-10	12-16	19-22	
10000-yr commitment	6-7	8-13	10-24	19-33	28-37	

Table 9.11 :

	Low	RCP 2.6		SSP1-2.6			
<i>m rel. to 1995-2014</i>	AR5	SROCC	Post-AR5 Published range	No ice-sheet acceleration after 2100	Assessed ice-sheet contribution	MICI	SEJ
Thermal expansion	0.07-0.46			0.19-0.35			
Greenland	0.14			0.22-0.39	0.11-0.25		0.28-- 1.28
Antarctica	0.21-0.25			-0.05-1.14	-0.14--0.78	0.71-- 1.35	-0.11-- 1.56
Glaciers	-			0.12-0.29			
Land water storage	-0.03	0.07- 0.37		0.05-0.10			
Total (2300)	0.38- 0.82	0.57- 1.04	0.3--2.9	0.8-2.0	0.6--1.5	1.4--2.1	1.0--3.1

	High	RCP 8.5					
<i>m rel. to 1995-2014</i>	AR5	SROCC	Post-AR5 Published range without (with) MICI	No ice-sheet acceleration after 2100	Assessed ice-sheet contribution	MICI	SEJ
Thermal expansion	0.28-1.80			0.92--1.51			
Greenland	0.30-1.18			0.53--0.88	0.32--1.75		0.40-- 2.23
Antarctica	0.02- 0.19	0.60- 2.89		-0.39--1.55	-0.28--3.13	6.87-- 13.54	0.03-- 3.05
Glaciers	0.29-0.39			0.32			
Land water storage	-			0.05-0.10			
Total (2300)	0.89- 3.56	2.25- 5.34	1.7--6.8 (up to 14.1)	1.7-4.0	2.2--5.9	9.5--16.2	2.4--6.3

Chapter 9: Ocean, cryosphere and sea level change**Coordinating Lead Authors:**

Baylor Fox-Kemper (United States of America), Helene T. Hewitt (United Kingdom), Cunde Xiao (China)

Lead Authors:

Guðfinna Aðalgeirsdóttir (Iceland), Sybren S. Drijfhout (The Netherlands), Tamsin L. Edwards (United Kingdom), Nicholas R. Golledge (New Zealand/United Kingdom), Mark Hemer (Australia), Robert E. Kopp (United States of America), Gerhard Krinner (France/Germany, France), Alan Mix (United States of America), Dirk Notz (Germany), Sophie Nowicki (United States of America/France, United States of America), Intan Suci Nurhati (Indonesia), Lucas Ruiz (Argentina), Jean-Baptiste Sallée (France), Aimee B. A. Slangen (The Netherlands), Yongqiang Yu (China)

Contributing Authors:

Cecile Agosta (France), Kyle Armour (United States of America), Mathias Aschwanden (Switzerland), Jonathan L. Bamber (United Kingdom), Sophie Berger (France/Belgium), Fábio Boeira Dias (Finland/Brazil), Jason E. Box (Denmark/USA), Eleanor J. Burke (United Kingdom), Kevin D. Burke (United States of America), Xavier Capet (France), John A. Church (Australia), Lee de Mora (United Kingdom), Chris Derksen (Canada), Catia M. Domingues (Australia, United Kingdom/Brazil), Jakob Dörr (Norway/Germany), Paul J. Durack (United States of America/Australia), Thomas L. Frölicher (Switzerland), Thian Y. Gan (Canada/Malaysia), Gregory G. Garner (United States of America), Sebastian Gerland (Norway/Germany), Heiko Goelzer (Norway/Germany), Natalya Gomez (Canada), Irina V. Gorodetskaya (Portugal/Belgium, Russian Federation), Jonathan M. Gregory (United Kingdom), Robert Hallberg (United States of America), F. Alexander Haumann (United States of America/Germany), Tim H. J. Hermans (The Netherlands), Emma M. Hill (Singapore/United States of America, United Kingdom), Regine Hock (United States of America, Norway/Germany), Stefan Hofer (Norway/Austria), Romain Hugonnet (France, Switzerland/France), Philippe Huybrechts (Belgium), Akm Saiful Islam (Bangladesh), Laura C. Jackson (United Kingdom), Nicolas C. Jourdain (France), Andreas Käab (Norway/Germany), Nicole S. Khan (Hong Kong, China/USA), Shfaqat Abbas Khan (Denmark), Matthew Kirwan (United States of America), James Kossin (United States of America), Anders Levermann (Germany), Sophie Lewis (Australia), Shiyin Liu (China), Daniel Lowry (New Zealand/United States of America), Marta Marcos (Spain), Ben Marzeion (Germany), Matthew Menary (France/United Kingdom), Sebastian H. Mernild (Norway, Denmark/Norway), Philip Orton (United States of America), Matthew D. Palmer (United Kingdom), Frank Pattyn (Belgium), Brodie Pearson (United States of America/United Kingdom), Cécile Pellet (Switzerland), Chris Perry (United Kingdom), Mark D. Pickering (United Kingdom), Johannes Quaas (Germany), Roshanka Ranasinghe (The Netherlands/Sri Lanka, Australia), Roelof Rietbroek (The Netherlands), Malcom J. Roberts (United Kingdom), Alessio Rovere (Germany/Italy), Mathew Koll Roxy (India), Maria Santolaria Otin (Spain, France/Spain), Abhishek Savita (Australia/India), Alex Sen Gupta (Australia/ United Kingdom, Australia), Helene Seroussi (United States of America/France), Sharon L. Smith (Canada), Olga N. Solomina (Russian Federation), Esther Stouthamer (The Netherlands), Fiametta Straneo (United States of America/Italy, United States of America), William V. Sweet (United States of America), Thomas Wahl (United States of America/Germany), Lisan Yu (United States of America), Jiacan Yuan (United States of America/China), Jan David Zika (Australia)

Review Editors:

Unnikrishnan Alakkat (India), Benjamin P. Horton (Singapore/United Kingdom), Simon Marsland (Australia)

Do Not Cite, Quote or Distribute

1
2
3
4
5
6
7
8
9
10
11
12
13
14
15
16
17
18
19

Chapter Scientists:

Gregory G. Garner (United States of America), Tim H. J. Hermans (The Netherlands), Lijuan Hua (China), Tamzin Palmer (United Kingdom), Brodie Pearson (United States of America/ United Kingdom)

This Chapter should be cited as:

Fox-Kemper, B., H. T. Hewitt, C. Xiao, G. Aðalgeirsdóttir, S. S. Drijfhout, T. L. Edwards, N. R. Golledge, M. Hemer, R. E. Kopp, G. Krinner, A. Mix, D. Notz, S. Nowicki, I. S. Nurhati, L. Ruiz, J-B. Sallée, A. B. A. Slangen, Y. Yu, 2021, Ocean, Cryosphere and Sea Level Change. In: *Climate Change 2021: The Physical Science Basis. Contribution of Working Group I to the Sixth Assessment Report of the Intergovernmental Panel on Climate Change* [Masson-Delmotte, V., P. Zhai, A. Pirani, S. L. Connors, C. Péan, S. Berger, N. Caud, Y. Chen, L. Goldfarb, M. I. Gomis, M. Huang, K. Leitzell, E. Lonnoy, J.B.R. Matthews, T. K. Maycock, T. Waterfield, O. Yelekçi, R. Yu and B. Zhou (eds.)]. Cambridge University Press. In Press.

Date: August 2021

This document is subject to copy-editing, corrigenda and trickle backs.

ACCEPTED VERSION
SUBJECT TO FINAL EDITING

1	Table of Contents	
2	Executive Summary	5
3	9.1 Introduction	11
4	BOX 9.1: Key processes driving sea level change	12
5	9.2 Oceans	14
6	9.2.1 Ocean surface	14
7	9.2.1.1 Sea Surface Temperature (SST)	14
8	9.2.1.2 Air-sea fluxes	16
9	9.2.1.3 Upper Ocean Stratification and Surface Mixed Layers	18
10	BOX 9.2: Marine Heatwaves	20
11	9.2.2 Changes in Heat and Salinity	21
12	9.2.2.1 Ocean Heat Content and Heat Transport	21
13	9.2.2.2 Ocean Salinity	26
14	9.2.2.3 Water Masses	28
15	9.2.3 Regional Ocean Circulation	30
16	9.2.3.1 Atlantic Meridional Overturning Circulation	30
17	9.2.3.2 Southern Ocean	33
18	9.2.3.3 Tropical Oceans	36
19	9.2.3.4 Gyres, Western Boundary Currents, and Inter-Basin Exchanges	36
20	9.2.3.5 Eastern Boundary Upwelling Systems	39
21	9.2.3.6 Coastal Systems and Marginal Seas	40
22	9.2.4 Steric and dynamic sea-level change	41
23	9.2.4.1 Global mean thermosteric sea-level change	41
24	9.2.4.2 Ocean dynamic sea-level change	42
25	9.3 Sea ice	44
26	9.3.1 Arctic Sea Ice	44
27	9.3.1.1 Arctic Sea-Ice Coverage	44
28	9.3.1.2 Arctic Sea-Ice volume and thickness	48
29	9.3.2 Antarctic Sea Ice	49
30	9.3.2.1 Antarctic sea-ice coverage	49
31	9.3.2.2 Antarctic sea-ice thickness	51
32	9.4 Ice Sheets	52

1	9.4.1 Greenland Ice Sheet	52
2	9.4.1.1 Recent observed changes.....	52
3	9.4.1.2 Model evaluation.....	56
4	9.4.1.3 Projections to 2100.....	57
5	9.4.1.4 Projections beyond 2100.....	61
6	BOX 9.3: Insights into land ice evolution from model intercomparison projects.....	62
7	9.4.2 Antarctic Ice Sheet	64
8	9.4.2.1 Recent observed changes.....	64
9	9.4.2.2 Model evaluation.....	67
10	9.4.2.3 Drivers of future Antarctic ice sheet change	69
11	9.4.2.4 Ice sheet instabilities	71
12	9.4.2.5 Projections to 2100.....	72
13	9.4.2.6 Projections beyond 2100.....	76
14	9.5 Glaciers, permafrost and seasonal snow cover.....	78
15	9.5.1 Glaciers	78
16	9.5.1.1 Observed and reconstructed glacier extent and mass changes.....	78
17	9.5.1.2 Model evaluation.....	82
18	9.5.1.3 Projections.....	83
19	9.5.2 Permafrost	85
20	9.5.2.1 Observed and reconstructed changes.....	85
21	9.5.2.2 Evaluation of permafrost in climate models.....	87
22	9.5.2.3 Projected permafrost changes	89
23	9.5.3 Seasonal snow cover.....	89
24	9.5.3.1 Observed changes of seasonal snow cover	90
25	9.5.3.2 Evaluation of seasonal snow in climate models.....	92
26	9.5.3.3 Projected snow cover changes	94
27	9.6 Sea Level Change	94
28	9.6.1 Global and regional sea-level change in the instrumental era	94
29	9.6.1.1 Global mean sea-level change budget in the pre-satellite era	94
30	9.6.1.2 Global mean sea-level change budget in the satellite era	96
31	9.6.1.3 Regional sea-level change in the satellite era.....	98
32	9.6.1.4 Attribution and time of emergence of regional sea-level change.....	99

1 **Executive Summary**

2
3 This chapter assesses past and projected changes in the ocean, cryosphere and sea level using paleo-
4 reconstructions, instrumental observations and model simulations. In the following summary, we update and
5 expand the related assessments from the IPCC Fifth Assessment Report (AR5), the Special Report on Global
6 Warming of 1.5°C (SR1.5) and the Special Report on Ocean and Cryosphere in a Changing Climate
7 (SROCC). Major advances in this chapter since the SROCC include the synthesis of extended and new
8 observations, which allows for improved assessment of past change, processes and budgets for the last
9 century, and the use of a hierarchy of models and emulators, which provide improved projections and
10 uncertainty estimates of future change. In addition, the systematic use of model emulators makes our
11 projections of ocean heat content, land-ice loss and sea level rise fully consistent both with each other and
12 with the assessed equilibrium climate sensitivity and projections of global surface air temperature across the
13 entire report. In this executive summary, uncertainty ranges are reported as *very likely* ranges and expressed
14 by square brackets, unless otherwise noted.

15 **Ocean Heat and Salinity**

16
17
18 **At the ocean surface, temperature has on average increased by 0.88 [0.68–1.01] °C from 1850-1900 to**
19 **2011-2020, with 0.60 [0.44–0.74] °C of this warming having occurred since 1980. The ocean surface**
20 **temperature is projected to increase from 1995–2014 to 2081–2100 on average by 0.86 [0.43–1.47,**
21 **likely range] °C in SSP1-2.6 and by 2.89 [2.01–4.07, likely range] °C in SSP5-8.5.** Since the 1950s, the
22 fastest surface warming has occurred in the Indian Ocean and in Western Boundary Currents, while ocean
23 circulation has caused slow warming or surface cooling in the Southern Ocean, equatorial Pacific, North
24 Atlantic, and coastal upwelling systems (*very high confidence*). At least 83% of the ocean surface will *very*
25 *likely* warm over the 21st century in all SSP scenarios. {2.3.3, 9.2.1}

26
27 **The heat content of the global ocean has increased since at least 1970 and will continue to increase**
28 **over the 21st century (*virtually certain*). The associated warming will likely continue until at least 2300**
29 **even for low-emission scenarios because of the slow circulation of the deep ocean.** Ocean heat content
30 has increased from 1971 to 2018 by [0.28–0.55] yottajoules and will *likely* increase until 2100 by 2 to 4
31 times that amount under SSP1-2.6 and 4 to 8 times that amount under SSP5-8.5. The long time scale also
32 implies that the amount of deep-ocean warming will only become scenario-dependent after about 2040 and
33 that the warming is irreversible over centuries to millennia (*medium confidence*). On annual to decadal time
34 scales, the redistribution of heat by the ocean circulation dominates spatial patterns of temperature change
35 (*high confidence*). At longer time scales, the spatial patterns are dominated by additional heat primarily
36 stored in water-masses formed in the Southern Ocean, and by weaker warming in the North Atlantic where
37 heat redistribution caused by changing circulation counteracts the additional heat input through the surface
38 (*high confidence*). {9.2.2, 9.2.4, 9.6.1, Cross-Chapter Box 9.1}

39
40 **Marine heatwaves – sustained periods of anomalously high near-surface temperatures that can lead to**
41 **severe and persistent impacts on marine ecosystems – have become more frequent over the 20th**
42 **century (*high confidence*). Since the 1980s, they have approximately doubled in frequency (*high***
43 ***confidence*) and have become more intense and longer (*medium confidence*).** This trend will continue,
44 with marine heatwaves at global scale becoming 4 [2–9, *likely range*] times more frequent in 2081–2100
45 compared to 1995–2014 under SSP1-2.6, and 8 [3–15, *likely range*] times more frequent under SSP5-8.5.
46 The largest changes will occur in the tropical ocean and the Arctic (*medium confidence*). {Box 9.2}

47
48 **The upper ocean has become more stably stratified since at least 1970 over the vast majority of the**
49 **globe (*virtually certain*), primarily due to surface-intensified warming and high-latitude surface**
50 **freshening (*very high confidence*).** Changes in ocean stability affect vertical exchanges of surface waters
51 with the deep ocean and large-scale ocean circulation. Based on recent refined analyses of the available

1 observations, the global 0–200 m stratification is now assessed to have increased about twice as much as
2 reported by the SROCC, with a $4.9 \pm 1.5\%$ increase from 1970 to 2018 (*high confidence*) and even higher
3 increases at the base of the surface mixed layer. Upper-ocean stratification will continue to increase
4 throughout the 21st century (*virtually certain*). {9.2.1}

6 Ocean Circulation

7
8 **The Atlantic Meridional Overturning Circulation (AMOC) will *very likely* decline over the 21st**
9 **century for all SSP scenarios. There is *medium confidence* that the decline will not involve an abrupt**
10 **collapse before 2100.** For the 20th century, there is *low confidence* in reconstructed and modelled AMOC
11 changes because of their *low agreement* in quantitative trends. The *low confidence* also arises from new
12 observations that indicate missing key processes in both models and measurements used for formulating
13 proxies and from new evaluations of modelled AMOC variability. This results in *low confidence* in
14 quantitative projections of AMOC decline in the 21st century, despite the *high confidence* in the future
15 decline as a qualitative feature based on process understanding. {9.2.3}

16
17 **Southern Ocean circulation and associated temperature changes in Antarctic ice-shelf cavities are**
18 **sensitive to changes in wind patterns and increased ice-shelf melt (*high confidence*).** However,
19 limitations in understanding feedback mechanisms involving the ocean, atmosphere and cryosphere, which
20 are not fully represented in the current generation of climate models, generally limit our confidence in future
21 projections of the Southern Ocean and of its forcing on Antarctic sea ice and ice shelves. {9.2.3, 9.3.2, 9.4.2}

22
23 **Many ocean currents will change in the 21st century as a response to changes in wind stress associated**
24 **with anthropogenic warming (*high confidence*).** Western boundary currents have shifted poleward since
25 1993 (*medium confidence*), consistent with a poleward shift of the subtropical gyres. Of the four eastern
26 boundary upwelling systems, only the California current system has experienced some large-scale
27 upwelling-favourable wind intensification since the 1980s (*medium confidence*). In the 21st century,
28 consistent with projected changes in the surface winds, the East Australian Current Extension and Agulhas
29 Current Extension will intensify, while the Gulf Stream and Indonesian Throughflow will weaken (*medium*
30 *confidence*). Eastern boundary upwelling systems will change, with a dipole spatial pattern within each
31 system of reduction at low latitude and enhancement at high latitude (*high confidence*). {9.2.1, 9.2.3}

33 Sea Ice

34
35 **The Arctic Ocean will *likely* become practically sea ice-free¹ during the seasonal sea ice minimum for**
36 **the first time before 2050 in all considered SSP scenarios. There is no tipping point for this loss of**
37 **Arctic summer sea ice (*high confidence*).** The practically ice-free state is projected to occur more often
38 with higher greenhouse gas concentrations and will become the new normal for high-emission scenarios by
39 the end of this century (*high confidence*). Based on observational evidence, Coupled Model Intercomparison
40 Project Phase 6 (CMIP6) models and conceptual understanding, the substantial satellite-observed decrease of
41 Arctic sea ice area over the period 1979–2019 is well described as a linear function of global mean surface
42 temperature, and thus of cumulative anthropogenic CO₂ emissions, with superimposed internal variability
43 (*high confidence*). According to both process understanding and CMIP6 simulations, a practically sea ice-
44 free state will *likely* be observed in some years before additional (post-2020) cumulative anthropogenic CO₂
45 emissions reach 1000 GtCO₂. {4.3.2, 9.3.1}

¹ sea ice area below 1 million km²

1 **For Antarctic sea ice, regionally opposing trends and large interannual variability result in no**
2 **significant trend in satellite-observed sea ice area from 1979 to 2020 in both winter and summer (*high***
3 ***confidence*).** The regionally opposing trends result primarily from changing regional wind forcing (*medium*
4 *confidence*). There is *low confidence* in model simulations of past and future Antarctic sea ice evolution due
5 to deficiencies of process representation, in particular at the regional level. {2.3.2, 9.2.3, 9.3.2}

6 7 **Ice Sheets**

8
9 **The Greenland Ice Sheet has lost 4890 [4140–5640] Gt mass over the period 1992–2020, equivalent to**
10 **13.5 [11.4–15.6] mm global mean sea level rise. The mass-loss rate was on average 39 [–3 to 80] Gt yr^{–1}**
11 **over the period 1992–1999, 175 [131 to 220] Gt yr^{–1} over the period 2000–2009 and 243 [197 to 290] Gt**
12 **yr^{–1} over the period 2010–2019.** This mass loss is driven by both discharge and surface melt, with the latter
13 increasingly becoming the dominating component of mass loss with high interannual variability in the last
14 decade (*high confidence*). The largest mass losses occurred in the Northwest and the Southeast of Greenland
15 (*high confidence*). {2.3.2, 9.4.1}

16
17 **The Antarctic Ice Sheet has lost 2670 [1800–3540] Gt mass over the period 1992–2020, equivalent to**
18 **7.4 [5.0–9.8] mm global mean sea level rise. The mass-loss rate was on average 49 [–2 to 100] Gt yr^{–1}**
19 **over the period 1992–1999, 70 [22 to 119] Gt yr^{–1} over the period 2000–2009 and 148 [94 to 202] Gt yr^{–1}**
20 **over the period 2010–2019.** Mass losses from West Antarctic outlet glaciers outpaced mass gain from
21 increased snow accumulation on the continent and dominated the ice sheet mass losses since 1992 (*very high*
22 *confidence*). These mass losses from the West Antarctic outlet glaciers were mainly induced by ice shelf
23 basal melt (*high confidence*) and locally by ice shelf disintegration preceded by strong surface melt (*high*
24 *confidence*). Parts of the East Antarctic Ice Sheet have lost mass in the last two decades (*high confidence*).
25 {2.3.2, 9.4.2, Atlas.11.1}

26
27 **Both the Greenland Ice Sheet (*virtually certain*) and the Antarctic Ice Sheet (*likely*) will continue to lose**
28 **mass throughout this century under all considered SSP scenarios. The related contribution to global**
29 **mean sea level rise until 2100 from the Greenland Ice Sheet will *likely* be 0.01–0.10 m under SSP 1-2.6,**
30 **0.04–0.13 m under SSP2-4.5 and 0.09–0.18 m under SSP5-8.5, while the Antarctic Ice Sheet will *likely***
31 **contribute 0.03–0.27 m under SSP1-2.6, 0.03–0.29 m under SSP2-4.5 and 0.03–0.34 m under SSP5-8.5.**
32 The loss of ice from Greenland will become increasingly dominated by surface melt, as marine margins
33 retreat and the ocean-forced dynamic response of ice-sheet margins diminishes (*high confidence*). In the
34 Antarctic, dynamic losses driven by ocean warming and ice shelf disintegration will *likely* continue to
35 outpace increasing snowfall this century (*medium confidence*). Beyond 2100, total mass loss from both ice
36 sheets will be greater under high-emission scenarios than under low-emission scenarios (*high confidence*).
37 The assessed *likely* ranges consider those ice-sheet processes in whose representation in current models we
38 have at least *medium confidence*, including surface mass balance and grounding-line retreat in the absence of
39 instabilities. Under high-emission scenarios, poorly understood processes related to Marine Ice Sheet
40 Instability and Marine Ice Cliff Instability, characterized by deep uncertainty, have the potential to strongly
41 increase Antarctic mass loss on century to multi-century time scales. {9.4.1, 9.4.2, 9.6.3, Box 9.3, Box 9.4}

42 43 **Glaciers**

44
45 **Glaciers lost 6200 [4600–7800] Gt of mass (17.1 [12.7–21.5] mm global mean sea level equivalent) over**
46 **the period 1993 to 2019 and will continue losing mass under all SSP scenarios (*very high confidence*).**
47 **During the decade 2010 to 2019, glaciers lost more mass than in any other decade since the beginning**
48 **of the observational record (*very high confidence*).** For all regions with long-term observations, glacier
49 mass in the decade 2010 to 2019 is the smallest since at least the beginning of the 20th century (*medium*
50 *confidence*). Because of their lagged response, glaciers will continue to lose mass at least for several decades
51 even if global temperature is stabilized (*very high confidence*). Glaciers will lose 29,000 [9,000–49,000] Gt

1 and 58,000 [28,000–88,000] Gt over the period 2015–2100 for RCP2.6 and RCP8.5, respectively (*medium*
2 *confidence*), which represents 18 [5–31] % and 36 [16–56] % of their early-21st-century mass, respectively.
3 {2.3.2, 9.5.1, 9.6.1, 9.6.3, 12.4}

5 Permafrost

6
7 **Increases in permafrost temperature have been observed over the past three to four decades**
8 **throughout the permafrost regions (*high confidence*), and further global warming will lead to near-**
9 **surface permafrost volume loss (*high confidence*).** Complete permafrost thaw in recent decades is a
10 common phenomenon in discontinuous and sporadic permafrost regions (*medium confidence*). Permafrost
11 warmed globally by 0.29 [0.17–0.41, *likely range*] °C between 2007 and 2016 (*medium confidence*). An
12 increase in the active layer thickness is a pan-Arctic phenomenon (*medium confidence*), subject to strong
13 heterogeneity in surface conditions. The volume of perennially frozen soil within the upper 3 m of the
14 ground will decrease by about 25% per 1°C of global surface air temperature change (up to 4°C above pre-
15 industrial temperature) (*medium confidence*). {9.5.2}

17 Snow

18
19 **Northern Hemisphere spring snow cover extent has been decreasing since 1978 (*very high confidence*),**
20 **and there is *high confidence* that this trend extends back to 1950. Further decrease of Northern**
21 **Hemisphere seasonal snow cover extent is *virtually certain* under further global warming.** The observed
22 sensitivity of Northern Hemisphere snow cover extent to Northern Hemisphere land surface air temperature
23 for 1981–2010 is –1.9 [–2.8 to –1.0, *likely range*] million km² per 1°C throughout the snow season. It is
24 *virtually certain* that Northern Hemisphere snow cover extent will continue to decrease as global climate
25 continues to warm, and process understanding strongly suggests that this also applies to Southern
26 Hemisphere seasonal snow cover (*high confidence*). Northern Hemisphere spring snow cover extent will
27 decrease by about 8% per 1°C of global surface air temperature change (up to 4°C above pre-industrial
28 temperature) (*medium confidence*). {9.5.3}

30 Sea Level

31
32 **Global mean sea level (GMSL) rose faster in the 20th century than in any prior century over the last**
33 **three millennia (*high confidence*), with a 0.20 [0.15–0.25] m rise over the period 1901 to 2018 (*high***
34 ***confidence*).** GMSL rise has accelerated since the late 1960s, with an average rate of 2.3 [1.6–3.1] mm
35 yr⁻¹ over the period 1971–2018 increasing to 3.7 [3.2–4.2] mm yr⁻¹ over the period 2006–2018 (*high*
36 *confidence*). New observation-based estimates published since SROCC lead to an assessed sea level rise
37 over the period 1901 to 2018 that is consistent with the sum of individual components. While ocean thermal
38 expansion (38%) and mass loss from glaciers (41%) dominate the total change from 1901 to 2018, ice sheet
39 mass loss has increased and accounts for about 35% of the sea level increase during the period 2006–2018
40 (*high confidence*). {2.3.3, 9.6.1, 9.6.2, Cross-Chapter Box 9.1, Box 7.2}

41
42 **At the basin scale, sea levels rose fastest in the Western Pacific and slowest in the Eastern Pacific over**
43 **the period 1993–2018 (*medium confidence*).** Regional differences in sea level arise from ocean dynamics;
44 changes in Earth gravity, rotation and deformation due to land-ice and land-water changes; and vertical land
45 motion. Temporal variability in ocean dynamics dominates regional patterns on annual to decadal time scales
46 (*high confidence*). The anthropogenic signal in regional sea level change will emerge in most regions by
47 2100 (*medium confidence*). {9.2.4, 9.6.1}

48
49 **Regional sea level change has been the main driver of changes in extreme still water levels across the**
50 **quasi-global tide gauge network over the 20th century (*high confidence*) and will be the main driver of**

1 **a substantial increase in the frequency of extreme still water levels over the next century (*medium***
2 ***confidence*)**. Observations show that high tide flooding events that occurred five times per year during the
3 period 1960–1980 occurred on average more than eight times per year during the period 1995–2014 (*high*
4 *confidence*). Under the assumption that other contributors to extreme sea levels remain constant (e.g.,
5 stationary tides, storm-surge, and wave climate), extreme sea levels that occurred once per century in the
6 recent past will occur annually or more frequently at about 19–31% of tide gauges by 2050 and at about 60%
7 (SSP1-2.6) to 82% (SSP5-8.5) of tide gauges by 2100 (*medium confidence*). In total, such extreme sea levels
8 will occur about 20 to 30 times more frequently by 2050 and 160 to 530 times more frequently by 2100
9 compared to the recent past, as inferred from the median amplification factors for SSP1-2.6, SSP2-4.5, and
10 SSP5-8.5 (*medium confidence*). Over the 21st century, the majority of coastal locations will experience a
11 median projected regional sea level rise within +/- 20% of the median projected GMSL change (*medium*
12 *confidence*). {9.6.4}

13
14 **It is *virtually certain* that global mean sea level will continue to rise through 2100, because all assessed**
15 **contributors to global mean sea level are *likely* to *virtually certain* to continue contributing throughout**
16 **this century. Considering only processes for which projections can be made with at least *medium***
17 ***confidence*, relative to the period 1995–2014 GMSL will rise by 2050 between 0.18 [0.15–0.23, *likely***
18 **range] m (SSP1-1.9) and 0.23 [0.20–0.30, *likely* range] m (SSP5-8.5), and by 2100 between 0.38 [0.28–**
19 **0.55, *likely* range] m (SSP1-1.9) and 0.77 [0.63–1.02, *likely* range] m (SSP5-8.5). This GMSL rise is**
20 **primarily caused by thermal expansion and mass loss from glaciers and ice sheets, with minor contributions**
21 **from changes in land-water storage. These *likely* range projections do not include those ice-sheet-related**
22 **processes that are characterized by deep uncertainty. {9.6.3}**

23
24 **Higher amounts of GMSL rise before 2100 could be caused by earlier-than-projected disintegration of**
25 **marine ice shelves, the abrupt, widespread onset of Marine Ice Sheet Instability and Marine Ice Cliff**
26 **Instability around Antarctica, and faster-than-projected changes in the surface mass balance and**
27 **discharge from Greenland. These processes are characterised by deep uncertainty arising from limited**
28 **process understanding, limited availability of evaluation data, uncertainties in their external forcing and high**
29 **sensitivity to uncertain boundary conditions and parameters. In a low-likelihood, high-impact storyline,**
30 **under high emissions such processes could in combination contribute more than one additional meter of sea**
31 **level rise by 2100. {9.6.3, Box 9.4}**

32
33 **Beyond 2100, GMSL will continue to rise for centuries due to continuing deep ocean heat uptake and**
34 **mass loss of the Greenland and Antarctic Ice Sheets, and will remain elevated for thousands of years**
35 **(*high confidence*)**. Considering only processes for which projections can be made with at least *medium*
36 *confidence* and assuming no increase in ice-mass flux after 2100, relative to the period 1995–2014, by 2150,
37 GMSL will rise between 0.6 [0.4–0.9, *likely* range] m (SSP1-1.9) and 1.4 [1.0–1.9, *likely* range] m (SSP5-
38 8.5). By 2300, GMSL will rise between 0.3 m and 3.1 m under SSP1-2.6, between 1.7 m and 6.8 m under
39 SSP5-8.5 in the absence of Marine Ice Cliff Instability, and by up to 16 m under SSP5-8.5 considering
40 Marine Ice Cliff Instability (*low confidence*). {9.6.3}

41 42 **Cryospheric Changes and Sea Level Rise at Specific Levels of Global Warming**

43
44 **At sustained warming levels between 1.5°C and 2°C, the Arctic Ocean will become practically sea ice–**
45 **free in September in some years (*medium confidence*); the ice sheets will continue to lose mass (*high***
46 ***confidence*), but will not fully disintegrate on time scales of multiple centuries (*medium confidence*); there is**
47 ***limited evidence* that the Greenland and West Antarctic Ice Sheets will be lost almost completely and**
48 **irreversibly over multiple millennia; about 50–60% of current glacier mass excluding the two ice sheets and**
49 **the glaciers peripheral to the Antarctic Ice Sheet will remain, predominantly in the polar regions (*low***
50 ***confidence*); Northern hemisphere spring snow cover extent will decrease by up to 20% relative to 1995–**
51 **2014 (*medium confidence*); the permafrost volume in the top 3 m will decrease by up to 50% relative to**

1 1995–2014 (*medium confidence*). Committed GMSL rise over 2000 years will be about 2–6 m with 2°C of
2 peak warming (*medium agreement, limited evidence*). {9.3.1, 9.4.1, 9.4.2, 9.5.1, 9.5.2, 9.5.3, 9.6.3}

3
4 **At sustained warming levels between 2°C and 3°C**, the Arctic Ocean will be practically sea ice-free
5 throughout September in most years (*medium confidence*); there is *limited evidence* that the Greenland and
6 West Antarctic Ice Sheets will be lost almost completely and irreversibly over multiple millennia; both the
7 probability of their complete loss and the rate of mass loss will increase with higher temperatures (*high*
8 *confidence*); about 50–60% of current glacier mass outside Antarctica will be lost (*low confidence*); Northern
9 hemisphere spring snow cover extent will decrease by up to 30% relative to 1995–2014 (*medium*
10 *confidence*); permafrost volume in the top 3 m will decrease by up to 75% relative to 1995–2014 (*medium*
11 *confidence*). Committed GMSL rise over 2000 years will be about 4–10 m with 3°C of peak warming
12 (*medium agreement, limited evidence*). {9.3.1, 9.4.1, 9.4.2, 9.5.1, 9.5.2, 9.5.3, 9.6.3}

13
14 **At sustained warming levels between 3°C and 5°C**, the Arctic Ocean will become practically sea ice-free
15 throughout several months in most years (*high confidence*); near-complete loss of the Greenland Ice Sheet
16 and complete loss of the West Antarctic Ice Sheet will occur irreversibly over multiple millennia (*medium*
17 *confidence*); substantial parts or all of Wilkes Subglacial Basin in East Antarctica will be lost over multiple
18 millennia (*low confidence*); 60–75% of current glacier mass outside Antarctica will disappear (*low*
19 *confidence*); nearly all glacier mass in low latitudes, Central Europe, Caucasus, Western Canada and USA,
20 North Asia, Scandinavia and New Zealand will *likely* disappear; Northern Hemisphere spring snow cover
21 extent will decrease by up to 50% relative to 1995–2014 (*medium confidence*); permafrost volume in the top
22 3 m will decrease by up to 90% compared to 1995–2014 (*medium confidence*). Committed GMSL rise over
23 2000 years will be about 12–16 m with 4°C of peak warming and 19–22 m with 5°C of peak warming
24 (*medium agreement, limited evidence*). {9.3.1, 9.4.1, 9.4.2, 9.5.1, 9.5.2, 9.5.3, 9.6.3}

25

9.1 Introduction

This chapter provides a holistic assessment of the physical processes underlying global and regional changes in the ocean, cryosphere and sea level, as well as improved understanding of observed, attributed and projected future changes since the AR5 and the SROCC (see outline in Figure 9.1). The ocean and cryosphere (defined as the frozen components of the Earth system such as sea ice, ice sheets, glaciers, permafrost and snow) exchange heat and freshwater with the atmosphere and each other (Figure 9.2). In a warming climate, the combined effects of thermal expansion of seawater and melting of the terrestrial cryosphere result in global mean sea-level rise (Box 9.1).

[START FIGURE 9.1 HERE]

Figure 9.1: Visual guide to chapter 9 with relevant chapter numbers indicated in red.

[END FIGURE 9.1 HERE]

Ocean acidification and deoxygenation are covered in Chapter 5 and regional changes to the ocean and cryosphere are covered in Chapter 12 and the Atlas. Ecosystem range shifts and climate risk for marine biodiversity associated with ocean change are assessed in AR6 Working Group II. The notion of “climate velocity” often used in impact studies, which is defined as the speed and direction at which a climate variable moves across a corresponding spatial field is underpinned by the assessment of changes in the physical characteristics of the ocean provided in this chapter.

There are two major advances of this chapter compared with the AR5 and the SROCC facilitated by community efforts. The first is the temporal and spatial increase in observations of both the ocean and the cryosphere (Section 1.5.1.1). In particular, extended observations have allowed improved assessment of past change and closure of both the energy and sea-level budget in a consistent way (Cross-Chapter Box 9.1) and the sea level budget for the last century (Section 9.6.1.1). Higher resolution observations have revealed the details of the Atlantic meridional overturning circulation (Section 9.2.3.1) and globally resolved glacier changes for the first time (Section 9.5.1.1). Improved methodology has resulted in a doubling of the assessed level of observed increase in global ocean 0–200 m stratification compared to the SROCC assessment (Section 9.2.1.3).

The second advance is the use of a hierarchy of models and emulators to update projections of oceanic, cryospheric and sea-level change arising from CMIP6 and related projects (Section 1.5.4.3; Table 1.3, Annex II).² CMIP6 included an ice sheet modelling intercomparison for the first time. Particular modelling advances relevant to this chapter are the increase in ocean resolution in the HighResMIP and OMIP2 experiments (Section 1.5.3.1; Section 9.2), projections of future glacier (GlacierMIP) and ice sheet (ISMIP6 and LARMIP-2) response from multi-model studies (Sections 9.5.1, 9.4; Box 9.3), and new methods to synthesize ocean and cryosphere models into sea level projections for all SSPs (Section 1.6.1; Cross-Chapter Box 1.4; Sections 9.4.1.3, 9.4.2.5, 9.6.3) and warming levels (Sections 9.6.3; 1.6.2; Cross-Chapter Box 11.1). In particular, sea level projections and the individual contributions (Section 9.6.3.3) are consistent with equilibrium climate sensitivity and surface temperature assessments across this report (Box 4.1, Cross-Chapter Box 7.1).

There are other advances in scientific understanding. In the cryosphere, this chapter assesses how fast-responding elements (sea ice, permafrost and snow (Sections 9.3 9.5.2; 9.5.3) track warming levels across observations and projections independent of scenario, process understanding of uncertainty in Antarctic ice

² In particular, this range of tools leads to advance in evaluation of confidence in projections. When CMIP6 models are used without additional evidence, the 5-95% confidence range of projections is assigned to a *likely* range to acknowledge that there are uncertainty sources not reflected by model spread, consistent with Chapter 4.

1 sheet projections (Section 9.4.2; Box 9.4) and new insight into thresholds for Arctic sea ice (Section 9.3.1.1)
 2 and Greenland and West Antarctic ice sheets (Section 9.4.1.4; 9.4.2.6). In the ocean, process understanding
 3 of ocean heat uptake (Section 9.2.2.1; Cross-chapter Box 5.3) and observed changes in ocean stratification
 4 (Section 9.2.1.3) have implications for ocean biogeochemistry are also important.
 5
 6

7 **[START FIGURE 9.2 HERE]**
 8

9 **Figure 9.2: Components of ocean, cryosphere and sea level assessed in this chapter.** (a) Schematic of processes
 10 (mCDW=modified Circumpolar Deep Water, GIA=Glacial Isostatic Adjustment). White arrows indicate
 11 ocean circulation. Pinning points indicate where the grounding line is most stable and ice sheet retreat
 12 will slow. (b) Geographic distribution of ocean and cryosphere components (numbers indicate (RGI
 13 Consortium, 2017) glacierized regions, see Figures 9.20 and 9.21 for labels). Sea ice shaded to indicate
 14 the annual mean concentration. Green ocean colours indicate larger surface current speed. Further details
 15 on data sources and processing are available in the chapter data table (Table 9.SM.9).
 16

17 **[END FIGURE 9.2 HERE]**
 18

19
 20 **[START BOX 9.1 HERE]**
 21

22 **BOX 9.1: Key processes driving sea level change**

23
 24 Sea-level change arises from processes acting on a range of spatial and temporal scales, in the ocean,
 25 cryosphere, solid Earth, atmosphere and on land (Figure 9.2). **Relative sea-level change** is the change in
 26 local mean sea surface height relative to the sea floor, as measured by instruments that are fixed to the
 27 Earth's surface (e.g., tide gauges). This reference frame is used when considering coastal impacts, hazards
 28 and adaptation needs. In contrast, **geocentric sea-level change** is the change in local mean sea surface height
 29 with respect to the terrestrial reference frame and is the sea-level change observed with instruments from
 30 space. This box provides a brief summary of sea-level processes using standard terminology (Gregory et al.,
 31 2019).
 32

33 **Global processes**

34
 35 **Global mean sea-level change** (Sections 9.6, 2.3.3.3) is the change in volume of the ocean divided by the
 36 ocean surface area. It is the sum of changes in ocean density (*global mean thermosteric sea-level change*)
 37 and changes in the ocean mass as a result of changes in the cryosphere or land water storage (*barystatic sea-*
 38 *level change*).
 39

40 **Steric sea-level change** is caused by changes in the ocean density and is composed of *thermosteric sea-level*
 41 *change* and *halosteric sea-level change*. **Thermosteric sea-level change** (also referred to as *thermal*
 42 *expansion*) occurs as a result of changes in ocean temperature: increasing temperature reduces ocean density
 43 and increases the volume per unit of mass. **Halosteric sea-level change** occurs as a result of salinity
 44 variations: higher salinity leads to higher density and decreases the volume per unit of mass. Although both
 45 processes can be relevant on regional to local scales, thermosteric changes contribute to global mean sea-
 46 level change, whereas global mean halosteric change is negligible (Gregory et al., 2019). There is *high*
 47 *confidence* in the understanding of processes causing thermosteric sea-level change (Section 9.2.4.1).
 48

49 **The Greenland and Antarctic ice sheets** are the largest reservoirs of frozen freshwater and therefore
 50 potentially the largest contributors to sea-level rise. Fluctuations in ice sheet volume arise from the
 51 imbalance between accumulation (either at the ice sheet surface or on the underside of ice shelves) and loss
 52 from sublimation, surface and basal melting, and iceberg calving. Ice sheets discharge the majority of their
 53 mass through marine-terminating ice streams that are in some cases buttressed by floating ice shelves.
 54 Changes in the thickness and extent of the ice shelves due to melt from below, calving, or disintegration, as a
 55 result of surface meltwater penetrating crevasses, can affect the flow of the inland ice streams. There is
 56 *medium confidence* in ice sheet processes but *low confidence* in their forcing (ocean changes and ice shelf

collapse) and in instability processes (Sections 9.4.1, 9.4.2).³

Glaciers contribute to sea-level change via an imbalance between mass gain and mass loss processes, which leads to adjustments in the glacier geometry over an extended period of time, called the response time. The response time may range from a few years to a few hundred years. The glacial meltwater does not all flow immediately into the ocean: it can refreeze, feed rivers (where it may be extracted for domestic use), evaporate, or be stored in (proglacial) lakes or closed basins. There is *medium to high confidence* in the understanding of processes leading to sea level contributions from glaciers (Section 9.5.1).

Land water storage includes surface water, soil moisture, groundwater storage and snow, but excludes water stored in glaciers and ice sheets. Changes in land water storage can be caused either by direct human intervention in the water cycle (e.g., storage of water in reservoirs by building dams in rivers, groundwater extraction for consumption and irrigation, or deforestation) or by climate variations (e.g., changes in the amount of water in internally drained lakes and wetlands, the canopy, the soil, the permafrost and the snowpack). Land water storage changes caused by climate variations may be indirectly affected by anthropogenic influences. It is difficult to assign a single confidence level to land water storage as understanding can vary from *low confidence* in groundwater recharge processes to *high confidence* in water storage via snowpack changes (Sections 8.2.3, 8.3.1.7).

Regional and local processes

Ocean dynamic sea-level change refers to the change in mean sea level relative to the geoid and is associated with the circulation and density-driven changes in the ocean. Ocean dynamic sea-level change varies regionally but by definition has a zero global mean. It includes the depression of the sea surface by atmospheric pressure. There is *medium confidence* in the understanding of ocean processes leading to dynamic sea-level change (Section 9.2.4.2).

Changes in Earth Gravity, Earth Rotation and viscoelastic solid Earth Deformation (GRD) result from the redistribution of mass between terrestrial ice and water reservoirs and the ocean. Contemporary terrestrial mass loss leads to elastic solid Earth uplift and a nearby relative sea-level fall (for a single source of terrestrial mass loss this is within ~2000 km, for multiple sources the distance depends on the interaction of the different relative sea-level patterns). Farther away (more than ~7000 km for a single source of terrestrial mass loss), relative sea level rises more than the global average, due, to first order, to gravitational effects. Earth deformation associated with adding water to the ocean and a shift of the Earth's rotation axis towards the source of terrestrial mass loss leads to second-order effects that increase spatial variability of the pattern globally. GRD effects due to the redistribution of ocean water within the ocean itself are referred to as *self-attraction and loading effects*. There is *high confidence* in the understanding of GRD processes.

Glacial Isostatic Adjustment is ongoing GRD in response to past changes in the distribution of ice and water on Earth's surface. On a timescale of decades to tens of millennia following mass redistribution, Earth's mantle flows viscously as it evolves toward isostatic equilibrium, causing solid Earth movement and geoid changes, which can result in regional to local sea-level variations. There is *medium confidence* in the understanding of glacial isostatic adjustment processes.

Vertical land motion is the change in height of the land surface or the sea floor and can have several causes in addition to elastic deformation associated with contemporary GRD and viscoelastic deformation associated with glacial isostatic adjustment. Subsidence (sinking of the land surface or sea floor) can occur through compaction of alluvial sediments in deltaic regions, removal of fluids such as gas, oil, and water, or drainage of peatlands. Tectonic deformation of the Earth's crust can occur as a result of earthquakes and volcanic eruptions. There is *medium confidence* in the understanding of vertical land motion processes.

³ The conversion of land ice mass loss to global mean sea-level rise used in this report (the Sea Level Equivalent, SLE) is 362.5 gigatons (Gt) of ice loss for 1 mm of sea-level rise

Extreme sea level is an exceptionally low or high local sea-surface height arising from combined short-term phenomena (e.g. storm surges, tides and waves). Relative sea-level changes affect extreme sea levels directly by shifting the mean water levels and indirectly by modulating the depth for propagation of tides, waves and/or surges. Extreme sea levels can be influenced by changes in the frequency, tracks, or strength of weather systems, or anthropogenic changes such as dredging. **Extreme Still Water Level** refers to the combined contribution of relative sea-level change, tides and storm surges. Wind-waves also contribute to coastal sea level. **Extreme Total Water Level** is the extreme still water level plus wave setup (time-mean sea-level elevation due to wave energy dissipation). When considering coastal impacts, swash (vertical displacement up the shore-face induced by individual waves) is also important and included in **Extreme Coastal Water Level**. There is *low to medium confidence* in the understanding of extreme sea level processes (Sections 9.6.4, 12.4).

[END BOX 9.1 HERE]

9.2 Oceans

9.2.1 Ocean surface

9.2.1.1 Sea Surface Temperature (SST)

The AR5 (Hartmann et al., 2013) assessed that it is certain that global sea-surface temperature (SST) has increased since the beginning of the 20th century (*very high confidence*). The SROCC did not assess past SST change. Since the AR5, improvements in the understanding of recent SST biases in the observational records, especially extending ship-based observations with buoy-based observations and improved treatment of sea ice, have had important consequences for key climate change indicators such as global mean surface temperature (GMST), global mean surface air temperature (GSAT), and SST (Cross-Chapter Box 2.3). The AR5 assessment is confirmed, and it is now *very likely* that global mean SST changed by 0.88°C [0.68–1.01°C] from 1850–1900 to 2011–2020, and 0.60°C [0.44–0.74°C] from 1980 to 2020 (Figure 9.3, Table 2.4).

Regions vary in the rate of SST warming, with slight cooling in some regions (Figure 9.3). The SROCC (Collins et al., 2019) and Section 7.4.4 assess SST changes over specific regions, which are consistent with the changes reported here. The tropical ocean has been warming faster than other regions since 1950, with the fastest warming in regions of the tropical Indian and western Pacific Oceans (Figure 9.3), due to a combination of local atmosphere-ocean coupling, the Indonesian Throughflow (Section 9.2.3.4; Figure 9.11), and trends in the Walker circulation (Section 2.3.1.4.1; Section 3.3.3.1; Figure 3.16). The Western Boundary Currents of the subtropical gyres have warmed faster than the global mean over the past century. There remains *low agreement* in the changes of both the location and the dynamical changes in western boundary current extensions (Sections 2.3.3.4.2, 9.2.3.4, Figure 9.3). In the Arctic, the mean SST increase over the last two decades is similar to or only slightly higher than the global average (Chen et al., 2019b). In contrast, the eastern Pacific Ocean, subpolar North Atlantic Ocean and Southern Ocean have warmed more slowly than the global average or cooled. (Figure 9.3). Surface warming in the subpolar Southern Ocean has been slower than the global average since the 1950s, and this pattern is consistent with the upwelling around Antarctica renewing surface water with pre-industrial, deeper water-masses (Section 9.2.3.2) (Frölicher et al., 2015; Marshall et al., 2015b; Armour et al., 2016). New evidence since the SROCC (Meredith et al., 2019) confirms slight cooling since the 1980s around the subpolar Southern Ocean, contrasting with marked warming directly northward of it (Section 9.2.3.2) (Haumann et al., 2020; Rye et al., 2020; Auger et al., 2021). In Eastern Boundary Upwelling Systems, the SROCC (Bindoff et al., 2019) reported *low agreement* between SST trends in recent decades, due to varying spatio-temporal resolution and interannual to multi-decadal variability. Satellite evidence not included in SROCC show that 92% of these regions warmed more slowly than neighbouring offshore locations between 1982–2015, so upwelling may buffer the near shore from warming (Varela et al., 2018) (Section 9.2.3.5). Coupled ocean-atmospheric modes of variability strongly affect regional SST (Cross-Chapter Box 3.1, Annex IV). In summary, a positive SST trend since 1950 is evident globally, but there is *very high confidence* that the Indian Ocean, western equatorial Pacific

1 Ocean, and western boundary currents have warmed faster than the global average, while the Southern
2 Ocean, the eastern equatorial Pacific, and the North Atlantic Ocean have warmed more slowly or slightly
3 cooled.

4
5
6 **[START FIGURE 9.3 HERE]**

7
8 **Figure 9.3: Sea Surface Temperature (SST) and its changes with time.** (a) Time series of global mean SST
9 anomaly relative to 1950-1980 climatology. Shown are observational reanalyses (HadISST) and multi-
10 model means from the CMIP historical, CMIP projections, and HighResMIP experiment. (b) Map of
11 observed SST (1995-2014 climatology HadISST), (e) bias of CMIP and (h) bias of HighResMIP (bottom
12 left) over 1995-2014. Also shown are 1950-2014 c) historical SST changes from observations, (f) CMIP
13 and (i) HighResMIP, and (d) 2005-2100 SST change rate, (g) 2005-2050 change rate for SSP5-8.5 for the
14 CMIP ensemble, and (j) 2005-2050 change rate for SSP5-8.5 for the HighResMIP ensemble. No overlay
15 indicates regions with high model agreement, where $\geq 80\%$ of models agree on sign of change; diagonal
16 lines indicate regions with low model agreement, where $< 80\%$ of models agree on sign of change (see
17 Cross-Chapter Box Atlas.1 for more information). Further details on data sources and processing are
18 available in the chapter data table (Table 9.SM.9).

19
20 **[END FIGURE 9.3 HERE]**

21
22
23 In the AR5 (Flato et al., 2013), a marginal improvement in CMIP5 climate model SST biases was noted
24 compared to CMIP3 models in the AR4, with a reduction in the magnitude of biases. The AR5 noted that in
25 several regions large SST biases are symptomatic of errors in the representation of important processes, such
26 as dynamics in the equatorial Pacific and North Atlantic, and Southern Ocean. Common regional biases in
27 SST or historical SST trends are not exclusively linked to the representation of the ocean (*high confidence*),
28 but can have multiple causes, including errors in the representation of long term historical trends in
29 equatorial winds (Section 9.2.1.2); misrepresentation of the forced equatorial ocean response (Karnauskas et
30 al., 2012; Kohyama et al., 2017; Coats and Karnauskas, 2018); thermocline depth errors (Linz et al., 2014);
31 errors in atmospheric model cloud-related short-wave radiation (Hyder et al., 2018); biases in ocean
32 circulation variability (Wang et al., 2014a); and deficiencies in upper ocean (Li et al., 2019b) and
33 atmospheric (Bates et al., 2012) boundary layer parameterizations. In CMIP6, the mid-latitude biases in the
34 northern hemisphere are improved in the multi-model mean and the inter-model standard deviation of the
35 zonal mean SST error is significantly decreased in the northern Hemisphere south of 50°N compared to
36 CMIP5, though biases in equatorial regions remains essentially unchanged (Section 3.5.1.1; Figures 3.23,
37 3.24, 9.3). Some longstanding ocean model biases have been reduced through increases in model resolution
38 in CMIP6 (Bock et al., 2020) and improved parameterizations (Fox-Kemper et al., 2011; Li et al., 2016a;
39 Qiao et al., 2016; Reichl and Hallberg, 2018). The high resolution HighResMIP ensemble (Figure 9.3) has
40 smaller cold biases in the North Atlantic and the tropical Pacific, and smaller warm biases in the upwelling
41 regions off the western coasts of Africa, North and South America (Roberts et al., 2018, 2019; Caldwell et
42 al., 2019; Docquier et al., 2019). In summary, CMIP6 models show persistent regional biases in representing
43 the climatological SST state (*very high confidence*), but higher resolution reduces some biases particularly in
44 the North Atlantic and Eastern Boundary Upwelling Systems (Figure 9.3; *high confidence*).

45
46 CMIP6 models represent the observed trends in SST patterns with greater fidelity than CMIP5, with the
47 ocean area that is inconsistent with the observed trends decreasing by about three quarters from CMIP5 to
48 CMIP6 (Olonscheck et al., 2020). In some regions, the direction of SST changes in observations are
49 consistent with CMIP6 only when including internal variability (Olonscheck et al., 2020). This is notably the
50 case in the equatorial Pacific, North Atlantic, and Southern Ocean, which are regions where SST is of known
51 importance in controlling heat uptake (Section 9.2.2.1) and the global radiative feedback parameter (Section
52 7.4.4.3). Overall, despite some persistent regional biases, CMIP6 coupled climate models reproduce the
53 observed SST trends or high internal variability over the past century over a range of different multidecadal
54 periods (Olonscheck et al., 2020; Watanabe et al., 2021) (Figure 9.3), highlighting their skill to inform future
55 large-scale SST changes at regional scale. Warming is projected at varying rates in all regions by 2050,
56 except the North Atlantic Subpolar Region, the equatorial Pacific, and the Southern Ocean where models

1 disagree (*high confidence*).

2
3 It is *virtually certain* that SST will continue to increase in the 21st century at a rate depending on future
4 emission scenario. The future global mean SST increase projected by CMIP6 models for the period 1995-
5 2014 to 2081-2100 is 0.86°C (5-95% range: 0.43-1.47°C) under SSP1-2.6, 1.51 °C [1.02-2.19°C] under
6 SSP2-4.5, 2.19°C (1.56-3.30°C) under SSP3-7.0, and 2.89°C (2.01-4.07°C) under SSP5-8.5 (Figure 9.3).
7 While under SSP1-2.6, the CMIP6 ensemble consistently projects that it is *very likely* at least 83% of the
8 world ocean surface will have warmed by 2100, under SSP5-8.5, at least 98% of the world ocean surface
9 will have warmed. The spatial pattern of future change is consistent with observed SST change over the 20th
10 century, though with notable regional differences (Figure 9.3). Long-term change in SST patterns is
11 important for regional impacts but also affects radiative feedbacks, and therefore long-term change in
12 climate sensitivity (Section 7.4.4.3). In the Southern Ocean, CMIP6 models project that SSTs will eventually
13 consistently increase in the 21st century at a rate dependent on future scenario (Bracegirdle et al., 2020)
14 (Figure 9.3, Section 9.2.3.2). Yet, there is only *low confidence* that this Southern Ocean warming will
15 emerge by the end of the century (Section 7.4.4.1), due the inconsistent historical and near-term simulations
16 and observations over the 20th century (Figure 9.3). Furthermore, the equilibrium SST pattern from proxy
17 records or simulated by climate models under CO₂ forcing stand in contrast with the cooling trends in the
18 Southern Ocean observed over the past decades (Section 7.4.4.1.2). Similarly, the SST change pattern
19 observed in the tropical Pacific Ocean will transition on centennial timescales to a mean pattern resembling
20 the El Niño pattern (*medium confidence*, Annex IV). However, it is difficult to delineate a climate change
21 trend resembling an El Niño pattern and El Niño variability (Wittenberg, 2009; Collins et al., 2010) without
22 large ensembles (Kay et al., 2015). Several Pliocene SST reconstructions indicate enhanced warming in the
23 centre of the eastern Pacific equatorial cold tongue upwelling region, consistent with reconstruction of
24 enhanced subsurface warming and enhanced warming in coastal upwelling regions (Section 7.4.4.2.2). The
25 North Atlantic subpolar gyre is projected to continue to warm more slowly than surrounding regions (Suo et
26 al., 2017), as the Gulf Stream concurrently warms rapidly (Cheng et al., 2013) (Figure 9.3) and the Atlantic
27 Meridional Overturning Circulation further declines under greenhouse gas forcing although models disagree
28 about the rate of change (Figure 9.3, Section 9.2.3.1). In summary, CMIP6 models show a future pattern of
29 SST change comparable to historical trends with intensity depending on future emission scenario, and some
30 of the observed cooling trends over the 20th century will eventually transition to a warming SST on
31 centennial timescales, in particular in the Southern Ocean (*high confidence*) and in the equatorial Pacific
32 (*medium confidence*), while the North Atlantic subpolar gyre will continue to warm more slowly than the
33 global average (*high confidence*).

34 35 36 9.2.1.2 Air-sea fluxes

37
38 Air-sea fluxes of energy, freshwater, and momentum (wind stresses) are difficult to observe directly (Cronin
39 et al., 2019), so estimates of the global mean net air-sea heat flux are inferred from observed ocean warming
40 (Section 2.3.3.1, Box 7.2, and Cross-Chapter Box 9.1). Air-Sea heat fluxes resemble the warming patterns of
41 CMIP3 (Domingues et al., 2008; Levitus et al., 2012) and are consistent with the ensemble mean warming
42 rate of CMIP5 (Cheng et al., 2017, 2019) and CMIP6 models (Section 3.5.1.3). Regional air-sea fluxes in
43 models remain a key driver of uncertainty (Huber and Zanna, 2017; Tsujino et al., 2020). A substantial part
44 of the upper 700 m energy increase is *very likely* attributed to anthropogenic forcing via increasing radiative
45 forcing (Sections 3.5.1.3, 7.2, 7.3).

46
47 The SROCC (Abram et al., 2019) and AR5 (Rhein et al., 2013) assessed that observations of air-sea fluxes
48 had not yet reached the density or accuracy to directly detect trends beyond the noise. New evidence since
49 SROCC confirms that direct heat and freshwater flux trends have not emerged yet as spatial (Figure 9.4),
50 annual (Yu, 2019), and decadal (Zanna et al., 2019a) variability overwhelm detection. Since the AR5,
51 comprehensive comparisons (Bentamy et al., 2017; Valdivieso et al., 2017; Yu et al., 2017) have used
52 updated and new surface flux products to improve surface flux uncertainty estimates, and these comparisons
53 note that implied global energy imbalances often exceed the observed ocean warming. Flux estimates using
54 top of atmosphere observations and atmospheric fluxes from reanalysis have improved over past products
55 (Trenberth and Fasullo, 2018) but require consistency adjustments (Trenberth et al., 2019) as the energy

1 budget is not closed. Adjustments are needed for all flux products, and they remain less accurate than direct
 2 ocean heat content change measurements (Cheng et al., 2017). Some regional changes are *likely* robust in
 3 both satellite observations and projections (Figure 9.4). Recent satellite-based surface flux products with
 4 improved retrieval algorithms and new satellites, e.g., J-OFURO3 (Tomita et al., 2019) and OAFflux-HR
 5 (Yu, 2019), provide a complete suite of turbulent fluxes including heat, moisture, and momentum. When
 6 combined with satellite-based surface radiation from CERES EBAF (Kato et al., 2018) and precipitation
 7 from GPCP (Adler et al., 2003), full ocean-surface forcing is available since 1987 (Figure 9.4). These
 8 products agree with sparse buoy and ship observations within 30 W m^{-2} (Bentamy et al., 2017; Cronin et al.,
 9 2019). While patterns agree between models and satellites in net fluxes (Figure 9.4), the trend magnitudes
 10 are substantially weaker in models. The fluxes tending to warm the North Atlantic and Southern Ocean are
 11 consistent with the largest changes observed in the surface properties and water-masses (Sections 9.2.1.1,
 12 9.2.2.1, 9.2.2.3). The observed trend toward a saltier Atlantic Ocean and a fresher Indian Ocean as well as
 13 trends in evaporation minus precipitation (E-P) patterns in the equatorial Pacific (see also Section 8.3.1)
 14 enhance the present mean pattern of wetting and drying. Elsewhere patterns are less clear with only partial,
 15 large-scale agreement with the wet gets wetter simplification (Sections 3.3.2.2, 4.4.1, 4.5.1). In summary,
 16 globally-integrated and large-scale fluxes are more reliably inferred from heat content and salinity change,
 17 while regional trends are rarely robust in observations and where robust tend to be underestimated or in
 18 disagreement in models (*very high confidence*).

19
 20
 21 **[START FIGURE 9.4 HERE]**

22
 23 **Figure 9.4:** Global maps of observed mean fluxes (a, d, g), the observed trends in these fluxes (b, e, h) and the
 24 projected rate of change in these fluxes from SSP5-8.5 (c, f, i). Shown are the freshwater flux (a, b, c),
 25 net heat flux (d, e, f), and momentum flux or wind stress magnitude (g, h, i), with positive numbers
 26 indicating ocean freshening, warming, and accelerating respectively. The means and observed trends are
 27 calculated between 1995-2014 (freshwater and wind stress) or 2001-2014 (heat) and the SSP5-8.5
 28 projected rates are between 1995-2100 using 20-year averages at each end of the time period.
 29 Observations show objective interpolation from CERES EBAF v4 (Kato et al., 2018), OAFflux-HR (Yu,
 30 2019), and GPCP (Adler et al., 2003) of fluxes and flux trends. (b, e, h) Observed trends with no overlay
 31 indicates regions where the trends are significant at $p = 0.34$ level. Crosses indicate regions where trends
 32 are not significant. For (c, f, i) projections, no overlay indicates regions with high model agreement,
 33 where $\geq 80\%$ of models agree on the sign of change; diagonal lines indicate regions with low model
 34 agreement, where $< 80\%$ of models agree on the sign of change (see Cross-Chapter Box Atlas.1 for more
 35 information). Further details on data sources and processing are available in the chapter data table (Table
 36 9.SM.9).

37
 38 **[END FIGURE 9.4 HERE]**

39
 40
 41 There is *low confidence* in long-term wind stress trends in most regions, but a few locations have *likely*
 42 trends over the scatterometer era and in projections, as shown in Figure 9.4 (Desbiolles et al., 2017; Young
 43 and Ribal, 2019; Yu, 2019). The AR5 (Rhein et al., 2013) assessed with *medium confidence* that zonal wind
 44 stress over the Southern Ocean increased from the early 1980s to the 1990s (Figure 9.4, *medium confidence*).
 45 Over 1995-2014, the zonal wind stress over the Southern Ocean continued to increase, westerly winds in the
 46 North Pacific and North Atlantic weakened while the easterly equatorial Pacific winds of the Walker
 47 circulation strengthened (Figure 9.4). In historical simulations, CMIP5 models projected annular modes
 48 (Annex IV) to move poleward and strengthen in both hemispheres (Yang et al., 2016a), while in CMIP6
 49 models westerlies only strengthen over the Southern Ocean, with a weaker trend than recently observed
 50 (Figure 9.4, Sections 4.5.1, 4.5.3). In the tropical Pacific Ocean, a weakening trend in easterly winds and
 51 Walker circulation in the 20th century has been inferred based on observed sea level pressure data (Vecchi et
 52 al., 2006; Vecchi and Soden, 2007) and coral proxies (Carilli et al., 2014) and is projected to continue by
 53 CMIP6 models (Figure 9.4), yet over 1995-2014 observed winds have strengthened (Figure 9.4). The
 54 observed strengthening may have been influenced by a combination of factors (Section 7.4.4.2.1), but there
 55 is *low confidence* in the attribution of this signal to anthropogenic warming (Section 3.3.3.1) and *medium*
 56 *confidence* that it reflects internal variability (Section 8.3.2.3). Near-term projected changes over the

1 Southern Ocean result from ozone recovery and greenhouse gases (Sections 4.3.3, 4.4.3). Overall, there is
 2 only *low confidence* in observed and projected wind stress trends in most regions because trends in oceanic
 3 wind stresses during the satellite era have not emerged or are inconsistent with historical simulated changes.
 4

5 Air-sea flux biases result from common causes in most models, many are the same as during AR5 (Rhein et
 6 al., 2013). Important currents (e.g., Gulf Stream, Kuroshio, Antarctic Circum-polar Current patterns) are
 7 often found in erroneous locations in models, affecting SST and flux signatures (Bates et al., 2012; Beadling
 8 et al., 2020; Li et al., 2020b), but their locations are improved in high-resolution ocean models (Chassignet et
 9 al., 2017, 2020; Hewitt et al., 2020), and high-resolution coupled models reduce the mean air-sea flux biases
 10 (Delworth et al., 2012; Sakamoto et al., 2012; Small et al., 2014a; Haarsma et al., 2016; Caldwell et al.,
 11 2019; Jackson et al., 2020a). Oceanic variability stems either from internal chaotic variability or atmospheric
 12 forcing (Hasselmann, 1976; Sérazin et al., 2016, 2017). Large scale variability in the ocean tends to follow
 13 atmospheric forcing in low resolution models, while in high-resolution coupled models ocean variability
 14 drives atmospheric variability on small scales (Bishop et al., 2017; Small et al., 2019), allowing these high-
 15 resolution models to mimic the coupling with clouds, precipitation, and atmospheric and oceanic boundary
 16 layers apparent in observations (Chelton and Xie, 2010; Frenger et al., 2013). Even coarse resolution models,
 17 such as the ocean and sea-ice components used in CMIP6, show significant sensitivity in the mean and
 18 variability of SST and sea ice to modest changes in flux forcing (Tsujino et al., 2020). Finally, there is still
 19 considerable disagreement between different parameterizations of air-sea fluxes used in models and strong
 20 scatter in direct observations (Renault et al., 2016; Brodeau et al., 2017). In summary, there is *very high*
 21 *confidence* that air-sea heat flux and stress biases are reduced in coupled models with high ocean resolution
 22 over coarse resolution models, although the effect on trends remain unclear.
 23
 24

25 9.2.1.3 Upper Ocean Stratification and Surface Mixed Layers

26
 27 The density difference from surface to deep ocean is the upper-ocean stratification. The AR5 (Rhein et al.,
 28 2013) assessed that it is *very likely* that the thermal contribution to stratification over the fixed 0-200 m layer
 29 increased by about 1% per decade between 1971 and 2010 (based on linear trend consistently across reports).
 30 The SROCC (Bindoff et al., 2019) found it *very likely* that density stratification increased by 0.46-0.51% per
 31 decade between 60°S and 60°N from 1970 to 2017). New published estimates based on a variety of different
 32 interpolated observations show that the SROCC assessed rate is too low, even using the same data and
 33 methods (Li et al., 2020a). The 1960-2018 stratification increase is estimated at $1.2 \pm 0.1\%$ per decade from
 34 the IAP product, $1.2 \pm 0.4\%$ per decade from the Ishii product, $0.7 \pm 0.5\%$ per decade from the EN4 product,
 35 $0.9 \pm 0.5\%$ per decade from the ORAS4 product, and $1.2 \pm 0.3\%$ per decade from the NCEI product (Li et al.,
 36 2020a). The improved methodology of computing stratification change on individual profiles before gridding
 37 yields a global annual mean increase of 0-200 m stratification change of $0.8 \pm 0.2\%$ per decade between 1960
 38 and 2018 (Yamaguchi and Suga, 2019) and a global summer mean increase of 0-200 m stratification change
 39 of $1.3 \pm 0.3\%$ per decade between 1970 and 2018 (Sallée et al., 2021) is of a similar magnitude to the long
 40 term trend (Yamaguchi and Suga, 2019; Li et al., 2020a). In summary, there is *limited evidence* that focusing
 41 on changes over a fixed depth range might hide larger increases occurring at the seasonally and regionally
 42 variable pycnocline depth. There is also *limited evidence* that summer stratification change within the
 43 pycnocline has occurred at a rate of $8.9 \pm 2.7\%$ per decade from 1970 to 2018, and *limited evidence* of a
 44 winter pycnocline stratification increase (Cummins and Ross, 2020a; Sallée et al., 2021).
 45
 46
 47

48 **[START FIGURE 9.5 HERE]**

49
 50 **Figure 9.5: Mixed layer depth in (a-d) winter and (e-h) summer.** (a, e) Observed climatological mean mixed layer
 51 depth (based on density threshold) from the Argo Mixed Layer Depth (Holte et al., 2017) observations
 52 2000-2019. (b, f) Bias between the observation-based estimate (2000-2019) and the 1995-2014 CMIP6
 53 climatological mean mixed layer depth. (c, d, g, h) Projected MLD change from 1995-2014 to 2081-2100
 54 under (c, g) SSP1-2.6 and (d, h) SSP5-8.5 scenarios. The (a, b, c, d) Winter row shows DJF in the
 55 Northern Hemisphere and JJA in the Southern Hemisphere, and the (e, f, g, h) Summer row shows JJA in
 56 the Northern Hemisphere and DJF in the Southern Hemisphere. The mixed layer depth is the depth where

1 the potential density is 0.03 kg m^{-3} denser than at 10m. No overlay indicates regions with high model
2 agreement, where $\geq 80\%$ of models agree on the sign of change; diagonal lines indicate regions with low
3 model agreement, where $< 80\%$ of models agree on the sign of change (see Cross-Chapter Box Atlas.1 for
4 more information). Further details on data sources and processing are available in the chapter data table
5 (Table 9.SM.9).
6

7 **[END FIGURE 9.5 HERE]**
8
9

10 While AR5 and the SROCC did not assess change in mixed-layer depth, the reported changes in
11 stratification can modulate the surface mixed layer depth, which is set by a balance between fluxes and
12 dynamical mixing (winds, tides, waves, convection) acting against the background stratification and
13 restratification processes (solar and dynamical). Despite the large stratification increase observed at a global
14 scale, new evidence shows that summer mixed-layer depth deepened consistently over the globe at a rate of
15 $2.9 \pm 0.5\%$ per decade from 1970 to 2018, with the largest deepening observed in the Southern Ocean,
16 corresponding to overall deepening from 3-15 m per decade depending on region (Somavilla et al., 2017;
17 Sallée et al., 2021). While the shorter observational record in winter than in summer does not allow global
18 winter mixed-layer trends to be reliably assessed (Sallée et al., 2021), winter mixed-layer depths deepening
19 at rates of 10 m per decade have been reported at individual long-term mid-latitude monitoring sites
20 (Somavilla et al., 2017). Projections agree that shoaling of mixed layer depth is expected in the 21st century,
21 but only for strong emissions scenarios and only in some regions (Figure 9.5). In summary, there is *limited*
22 observational *evidence* that the mixed layer is globally deepening, while models show no emergence of a
23 trend until later in the 21st century under strong emissions.
24

25 The SROCC assessed that upper ocean stratification will continue to increase in the 21st century under
26 increased radiative forcing (*high confidence*), due to increased surface temperature and high-latitude surface
27 freshening (Bindoff et al., 2019). New climate model simulations concur with the SROCC assessment of a
28 future increase of the 0-200 m stratification under increased radiative forcing in all regions of the world
29 ocean (Kwiatkowski et al., 2020). In addition, CMIP6 climate models project a shallowing of the mixed-
30 layer both in summer and winter by the end of the century under increased radiative forcing (Kwiatkowski et
31 al., 2020) (Figure 9.5), with the exception of the Arctic showing deepening of the mixed-layer as a result of
32 sea-ice retreat (Lique et al., 2018a) (Figure 9.5). The regions of largest shallowing are associated with the
33 deepest climatological mixed layer both in winter and summer, particularly affecting the North Atlantic and
34 the Southern Ocean basins (Figure 9.5). While CMIP6 models tend to project shallowing mixed-layers under
35 a warming climate, except at high latitudes (Figure 9.5) (Lique et al., 2018b; Kwiatkowski et al., 2020), a
36 deepening in the summer mixed-layer depth by intensification of the surface winds and storms may explain
37 inconsistency among models in many regions (Figure 9.5) (Young and Ribal, 2019), although model mixed
38 layer biases are large in the summertime in the Southern Ocean (Belcher et al., 2012; Sallée et al., 2013a; Li
39 et al., 2016a; Tsujino et al., 2020). Lack of observed ocean turbulence and climate model limitations do not
40 allow for direct assessment of ocean surface turbulence change and limit confidence in past and future
41 mixed-layer change. Understanding of turbulent processes, its representation in ocean and climate models,
42 and its effect on mixed layer biases have been an active and rapidly evolving topic of research since AR5
43 (Buckingham et al., 2019; Li et al., 2019b). Small-scale mixed layer processes are not resolved in climate
44 models (D'Asaro, 2014; Buckingham et al., 2019; McWilliams, 2019) and despite significant improvements
45 in their parameterisation over the last decade (Fox-Kemper et al., 2011; Jochum et al., 2013; Li et al., 2016a;
46 Qiao et al., 2016; Li et al., 2019b) and significant improvement in some models (Li and Fox-Kemper, 2017;
47 Dunne et al., 2020), biases in mixed-layer representation generally persist (Heuzé, 2017; Williams et al.,
48 2018; Cherchi et al., 2019; Golaz et al., 2019; Voldoire et al., 2019; Yukimoto et al., 2019; Boucher et al.,
49 2020; Danabasoglu et al., 2020; Dunne et al., 2020; Kelley et al., 2020). In summary, the representation of
50 upper ocean stratification and mixed layers has improved in CMIP6 compared to CMIP5. While it is
51 *virtually certain* that the global mean upper ocean will continue to stratify in the 21st century, there is only
52 *low confidence* in the future evolution of mixed-layer depth, which is projected to mostly shoal under high
53 emissions scenarios except in high latitude regions where sea-ice retreats.
54
55

1 [START BOX 9.2 HERE]

2
3 **BOX 9.2: Marine Heatwaves**

4
5 Marine heatwaves (MHW) are periods of extreme high sea temperature relative to the long-term mean
6 seasonal cycle (Hobday et al., 2016). Studies since the SROCC (Collins et al., 2019) confirm the assessment
7 that MHW can lead to severe and persistent impacts on marine ecosystems, from mass mortality of benthic
8 communities including coral bleaching, changes in phytoplankton blooms, shifts in species composition and
9 geographical distribution, toxic algal blooms to decline in fisheries catch and mariculture (Smale et al., 2019;
10 Cheung and Frölicher, 2020; Hayashida et al., 2020a; Piatt et al., 2020). Unlike synoptic atmospheric
11 heatwaves (Section 11.3), MHWs can extend for millions of square kilometres, persist for weeks to months,
12 and occur at subsurface (Bond et al., 2015; Schaeffer and Roughtan, 2017; Perkins-Kirkpatrick et al., 2018;
13 Laufkötter et al., 2020).

14
15 The SROCC established that MHWs have occurred in all basins over the last decades. Additional evidence
16 documenting widespread occurrence of marine heat waves in all basins and marginal seas continues to
17 accumulate (Li et al., 2019c; Yao et al., 2020). The SROCC highlighted the role of large-scale climate modes
18 of variability in amplifying or suppressing MHW occurrences, which has since been further corroborated,
19 increasing confidence in climate modes as important drivers of MHWs (Holbrook et al., 2019; Sen Gupta et
20 al., 2020). More generally, understanding of processes leading to MHWs has increased since the SROCC,
21 including air-sea heat flux (Section 9.2.1.2), increased horizontal heat advection, shoaling of the mixed layer
22 and suppressed mixing processes (Section 9.2.1.3), reduced coastal upwelling and Ekman pumping (Section
23 9.2.3.5), changes in eddy activities and planetary waves, and the re-emergence of warm subsurface
24 anomalies (Holbrook et al., 2020; Sen Gupta et al., 2020).

25
26 The SROCC reported with *high confidence* that MHWs (defined as days exceeding the 99th percentile in SST
27 from 1982 to 2016) have *very likely* doubled in frequency between 1982 and 2016. Additional observation-
28 based evidence and acquisition of longer observation time-series since the SROCC have confirmed and
29 expanded on this assessment: since the 1980s MHWs have also become more intense and longer (Frölicher
30 and Laufkötter, 2018; Smale et al., 2019; Laufkötter et al. 2020). Satellite observations and reanalyses of
31 SST show increase in intensity of 0.04°C per decade from 1982 to 2016, an increase in spatial extent of 19 %
32 per decade from 1982 to 2016, and an increase in annual MHW days of 54 % between the 1987-2016 period
33 compared to 1925-1954 (Frölicher et al., 2018; Oliver, 2019). The SROCC assessed that 84-90% of all
34 MHWs that occurred between 2006 and 2015 are *very likely* caused by anthropogenic warming. There is new
35 evidence since SROCC that the frequency of the most impactful marine heatwaves over the last few decades
36 has increased more than 20-fold because of anthropogenic global warming (Laufkötter et al., 2020). In
37 summary, there is *high confidence* that MHWs have increased in frequency over the 20th century, with an
38 approximate doubling from 1982-2016, and *medium confidence* that they have become more intense and
39 longer since the 1980s.

40
41
42 [START BOX 9.2, FIGURE 1 HERE]

43
44 **Box 9.2, Figure 1: Observed and simulated regional probability ratio of marine heatwaves (MHWs) for the 1985-**
45 **2014 period and for the end of the 21st century under two different greenhouse gas emissions**
46 **scenarios.** The probability ratio is the proportion by which the number of MHW days per year has
47 increased relative to pre-industrial times. A MHW is defined as a deviation beyond the daily 99th
48 percentile (11-day window) in the deseasonalized sea surface temperature. (a) The MHW
49 probability ratio from satellite observations (NOAA OISST V2.1; (Huang et al., 2021) during 1985-
50 2014. The mean warming pattern (difference in ERSST5 (Huang et al., 2017) sea surface
51 temperature between the 1985-2014 and 1854-1900 periods) has been added to the satellite
52 observations to calculate the probability ratio. (b-d) CMIP6 simulated multi-model mean probability
53 ratio of the (b) 1985-2014 period, and 2081-2100 period in the (c) SSP1 2.6 and (d) SSP5 8.5
54 scenarios. The areas with grey diagonal lines in (d) indicate permanent MHWs (> 360 heatwave
55 days per year). These 14 CMIP6 models are included in the analysis: ACCESS-CM2, CESM2,
56 CESM2-WACCM, CMCCM2-SR5, CNRM-CM6-1, CNRM-ESM2-1, CanESM5, EC-Earth3,

1 IPSL-CM6A-LR, MIROC6, MRI-ESM2-0, NESM3, NorESM2-LM, NorESM2-MM. Further
2 details on data sources and processing are available in the chapter data table (Table 9.SM.9).

3
4 **[END BOX 9.2, FIGURE 1 HERE]**

5
6
7 Consistent with the SROCC, future MHWs are defined with reference to the historical climate conditions.
8 The SROCC assessed that MHWs will *very likely* further increase in frequency, duration, spatial extent and
9 intensity under future global warming in the 21st century. CMIP6 projections allow us to confirm this
10 assessment and quantify future change based on global mean probability ratio change (Box 9.2, Figure 1):
11 they project MHWs will become 4 (5-95% range: 2-9) times more frequent in 2081-2100 compared to 1995-
12 2014 under SSP1-2.6, or 8 (3-15) times more frequent under SSP5-8.5. The SROCC highlighted that future
13 change of MHWs will not be globally uniform, with the largest changes in the frequency of marine
14 heatwaves being projected to occur in the western tropical Pacific and the Arctic Ocean (*medium*
15 *confidence*). New evidence from the latest generation of climate models confirms and complements the
16 SROCC assessment (Box 9.2, Figure 1). Moderate increases are projected for mid-latitudes, and only small
17 increases are projected for the Southern Ocean (*medium confidence*) (Hayashida et al., 2020b). While under
18 the SSP5-8.5 scenario, permanent MHWs (more than 360 days per year) are projected to occur in the 21st
19 century in parts of the tropical ocean, the Arctic Ocean and around 45°S, the occurrence of such permanent
20 MHWs can largely be avoided under the SSP1-2.6 scenario (Frölicher et al., 2018; Oliver et al., 2019; Plecha
21 and Soares, 2020). The resolution of current climate models (CMIP5 and CMIP6) capture the broad features
22 of MHWs, but they may have a bias towards weaker and longer MHWs in the historical period (*medium*
23 *confidence*) (Frölicher et al., 2018; Pilo et al., 2019; Plecha and Soares, 2020) and greater intensification in
24 western boundary current regions (Hayashida et al., 2020b).

25
26
27 **[END BOX 9.2 HERE]**

28
29
30 **9.2.2 Changes in Heat and Salinity**

31
32 **9.2.2.1 Ocean Heat Content and Heat Transport**

33
34 Ocean warming, i.e., changing ocean heat content, is an important aspect of energy on Earth: the SROCC
35 (Bindoff et al., 2019) reported that there is *high confidence* that ocean warming during 1971-2010 dominated
36 the increase in the Earth's energy inventory, which is confirmed by the Box 7.2 assessment that the ocean
37 has stored 91% of the total energy gained from 1971 to 2018. As reported in Sections 2.3.3.1, 3.5.1.3 and
38 7.2.2.2, Box 7.2 and Cross-Chapter Box 9.1, confidence in the assessment of global ocean heat content
39 (OHC) change since 1971 is strengthened compared to previous reports and extended backward to include
40 *likely* warming since 1871. Table 7.1 updates the estimates of total ocean heat gains from 1971 to 2018, 1993
41 to 2018 and 2006 to 2018. Section 3.5.1.3 assesses that it is *extremely likely* that anthropogenic forcing was
42 the main driver of the OHC increase over the historical period. Section 2.3.3.1 reports that current
43 multidecadal to centennial rates of OHC gain are greater than at any point since the last deglaciation
44 (*medium confidence*).

45
46 Ocean warming is not uniform with depth. The AR5 (Rhein et al., 2013) assessed that since 1971 ocean
47 warming was *virtually certain* for the upper 700 m and *likely* for the 700-2000 m layer. Both the AR5 and
48 the SROCC (Bindoff et al., 2019) assessed that the deep ocean below 2000 m had *likely* warmed since 1992,
49 especially in the Southern Ocean. Section 2.3.3.1 provides an updated assessment of ocean temperature
50 change for different depth layers, different time periods and different observation-based reconstructions
51 (Table 2.7). Section 2.3.3.1 confirms the previous assessment that it is *virtually certain* that the upper ocean
52 (0-700m) has warmed since 1971, that ocean warming at intermediate depths (700-2000 m) is *very likely*
53 since 2006, and that it is *likely* that ocean warming has occurred below 2000 m since 1992. Section 3.5.1.3
54 assessed that it is *extremely likely* that human influence was the main driver of the ocean heat content
55 increase observed since the 1970s, which extends into the deeper ocean (*very high confidence*), and shows

1 that biases in potential temperature have a complex pattern (Figure 3.25). In the present section, we assess
2 the regional patterns of this warming and associated processes driving regional ocean warming.
3

4 The rate of ocean warming varies regionally, with some regions having experienced slight cooling (Figure
5 9.6). The SROCC (Bindoff et al., 2019) assessed that ocean warming in the 0-700 m is globally widespread,
6 with slower than global average warming in the subpolar North Atlantic. The SROCC (Meredith et al., 2019)
7 also estimated that the Southern Ocean accounted for ~75% of global ocean heat uptake during 1870–1995
8 and that 35-43% of the upper 2000 m global ocean warming occurred in the Southern Ocean over 1970-2017
9 (45-62% for 2005-2017). The SROCC noted that this interhemispheric asymmetry might at least partially be
10 explained by high concentrations of aerosols in the northern hemisphere. Here, we confirm these
11 assessments, bring new evidence attributing these regional trends, and discuss the role of decadal ocean
12 circulation variability in redistributing heat, driving interhemispheric asymmetry of the recent rate of ocean
13 warming (Rathore et al., 2020; Wang et al., 2021b). Since the SROCC, one new study shows that the
14 subpolar North Atlantic “warming hole” observed since the 1980s has emerged from internal climate
15 variability and can be attributed to greenhouse gas emissions (Chemke et al., 2020). A new analysis of a
16 suite of climate models (Hobbs et al., 2020) confirms the SROCC assessment, based on one paper (Swart et
17 al., 2018), attributing the observed Southern Ocean warming to anthropogenic forcing. Given the large
18 fraction of global ocean warming in the Southern Ocean and the sparse observations there before 2005, there
19 is *limited evidence* that global OHC increase since 1971 might have been underestimated (Cheng and Zhu,
20 2014; Durack et al., 2014). Cross-Chapter Box 9.1 accounts for an increased error before 2005 in global
21 OHC change. In summary, in the upper 2000 m since the 1970s, the subpolar North Atlantic has been slowly
22 warming, and the Southern Ocean has stored a disproportionately large amount of anthropogenic heat
23 (*medium confidence*).
24

25
26 [START FIGURE 9.6 HERE]

27
28 **Figure 9.6: Ocean heat content (OHC) and its changes with time.** (a) Time series of global ocean heat content
29 anomaly relative to a 2005-2014 climatology in the upper 2000m of the ocean. Shown are observations
30 (Ishii et al., 2017; Baggenstos et al., 2019; Shackleton et al., 2020), model-observation hybrids (Cheng et
31 al., 2019; Zanna et al., 2019a), and multi-model means from the CMIP6 historical (29 models) and SSP
32 scenarios (label subscripts indicate number of models per SSP). (b-g) Maps of Ocean Heat Content across
33 different time periods, in different layers, and from different data sets/experiments. Maps show the
34 CMIP6 ensemble bias and observed (Ishii et al., 2017) trends of OHC for (b, c) 0-700m for the period
35 1971-2014, and (e, f) 0-2000m for the period 2005-2017. CMIP6 ensemble mean maps show projected
36 rate of change 2015-2100 for (d) SSP5-8.5 and (g) SSP1-2.6 scenarios. Also shown are the projected
37 changes in 0-700m OHC for (d) SSP1-2.6 and (g) SSP5-8.5 in the CMIP6 ensembles, for the period
38 2091-2100 versus 2005-2014. No overlay indicates regions with high model agreement, where $\geq 80\%$ of
39 models agree on the sign of change; diagonal lines indicate regions with low model agreement, where
40 $< 80\%$ of models agree on the sign of change (see Cross-Chapter Box Atlas.1 for more information).
41 Further details on data sources and processing are available in the chapter data table (Table 9.SM.9).
42

43 [END FIGURE 9.6 HERE]

44
45
46 Below 2000 m, direct observations of full-depth ocean temperature change are limited to ship-based, high-
47 quality deep ocean temperature measurements. Such high quality full-depth ship-based sampling has
48 improved from 1990 to the present due to the World Ocean Circulation Experiment (WOCE) and the Global
49 Ocean Ship-based Hydrographic Investigations Program (GO-SHIP) (Sloyan et al., 2019). The SROCC
50 (Bindoff et al., 2019) assessed that the *likely* warming of the ocean since the 1990s below 2000 m is
51 associated with a marked regional pattern, with larger warming in the Southern Ocean. In the deep North
52 Atlantic, warming has reversed to cooling over the past decade, possibly due to internal variability fed by
53 North Atlantic Deep Water (Section 9.2.2.3). Over the past decade, the warming rate of Antarctic Bottom
54 Water (AABW, Section 9.2.2.3) has been dependent on origin: slower from the Weddell Sea and faster from
55 the Ross Sea and Adélie Land. One new study (Purkey et al., 2019a) strengthens confidence in AABW
56 warming: below 4000 m a monotonic, basin-wide, and multidecadal temperature change is found in the

1 southern Pacific basin, with larger warming rates near the bottom water formation sites than further
 2 downstream. New analysis of one model provides *limited evidence* that the sparse observational record may
 3 underestimate the rate of deep ocean warming over 1990-2010 by about 20% (Garry et al., 2019) which is
 4 included in the assessed OHC error (Cross-Chapter Box 9.1). There is still *low agreement* in deep ocean
 5 changes from ocean data-assimilation reanalyses (Palmer et al., 2017) and *low confidence* in such inferences.
 6 In summary, while observational coverage below 2000 m is sparser than in the upper 2000 m, there is *high*
 7 *confidence* that deep ocean warming below 2000 m has been larger in the Southern Ocean than in other
 8 ocean basins due to widespread AABW warming.

9
 10
 11 **[START FIGURE 9.7 HERE]**

12
 13 **Figure 9.7: Meridional-depth profiles of zonal-mean potential temperature in the ocean and its rate of change**
 14 **in the upper 2000m of the Global, Pacific, Atlantic, and Indian Oceans.** Shown are (a, e, i, m)
 15 observed temperature (Argo climatology 2005-2014), (b, f, j, n) bias of the CMIP6 ensemble over this
 16 period, and future changes under (c, g, k, o) SSP1-2.6 and (d, h, l, p) SSP5-8.5. No overlay indicates
 17 regions with high model agreement, where $\geq 80\%$ of models agree on the sign of change; diagonal lines
 18 indicate regions with low model agreement, where $< 80\%$ of models agree on the sign of change (see
 19 Cross-Chapter Box Atlas.1 for more information). Further details on data sources and processing are
 20 available in the chapter data table (Table 9.SM.9).

21
 22 **[END FIGURE 9.7 HERE]**

23
 24
 25 Different processes drive OHC patterns over a range of timescales. Recent literature has highlighted the role
 26 of ocean circulation variability in driving OHC patterns by decomposing the global pattern of OHC change
 27 into a combination of added heat due to climate change taken up under fixed ocean circulation (“added
 28 heat”), and redistribution of heat associated with changing ocean currents (“redistributed heat”) (Gregory et
 29 al., 2016; Bronselaer and Zanna, 2020; Couldrey et al., 2020). Redistributed heat alters regional patterns of
 30 heat storage (and carbon storage; Cross-Chapter Box 5.3) (Bronselaer and Zanna, 2020; Couldrey et al.,
 31 2020; Todd et al., 2020) but does not affect the global OHC. There is *medium confidence* that decadal
 32 variability of the ocean circulation strengthened the rate of ocean warming in the Southern Hemisphere
 33 compared to the Northern Hemisphere in the decade from 2005 (Rathore et al., 2020; Wang et al., 2020; Zika
 34 et al., 2021). More generally, since 2005, the OHC pattern observed is predominantly due to heat
 35 redistribution with regions of both warming and cooling (Zika et al., 2021) (Figure 9.6) but extending
 36 analysis back to 1972 shows the importance of added heat setting a large-scale warming pattern with mid-
 37 latitude maxima consistent with subduction of water masses, particularly in Southern Hemisphere Mode
 38 Waters (Section 9.2.2.3; Figures 9.6, 9.8) (Bronselaer and Zanna, 2020). The longer the analysis window, the
 39 more added heat dominates over redistributed heat. This translates into more ocean area with statistically
 40 significant warming trends and less area with statistically significant cooling trends (Johnson and Lyman,
 41 2020). The region where added heat is most compensated for by redistributed cooling is in the northern
 42 North Atlantic basin, where changes in the subpolar gyre circulation and AMOC result in cooling (Section
 43 9.2.3.1) (Williams et al., 2015b; Piecuch et al., 2017; Zanna et al., 2019a; Bronselaer and Zanna, 2020). In
 44 summary, and strengthening the SROCC assessment, ocean warming is not globally uniform due to patterns
 45 of uptake predominantly along known water mass pathways, and due to changing ocean circulation
 46 redistributing heat within the ocean (*high confidence*).

47
 48
 49 **[START FIGURE 9.8 HERE]**

50
 51 **Figure 9.8: Decomposition of ocean simulated ocean heat content and northward heat transport.** (a, c, e) Total
 52 ocean heat content (0-2000 m) warming rate as observed and simulated by CMIP5 models over the
 53 historical period (1951-2011) and under the RCP8.5 future (2011-2060) versus the associated
 54 decomposed (b, d, f) added heat contribution (neglecting changes in ocean circulation) to the total
 55 (Bronselaer and Zanna, 2020). (g) Relationship between northward heat transport and Atlantic Meridional
 56 Overturning Circulation in HighResMIP models (1950-2050) and observations during the RAPID period

1 (2004-2018). Further details on data sources and processing are available in the chapter data table (Table
2 9.SM.9).

3
4 **[END FIGURE 9.8 HERE]**

5
6
7 While heat redistribution reflects changes in ocean circulation and is a useful concept to understand the
8 underlying processes driving OHC patterns, change in ocean heat transport (OHT) arises due to changes in
9 both ocean circulation and ocean temperature and affects regional OHC change. The AR5 did not assess
10 change in OHT and the SROCC (Meredith et al., 2019) only assessed projected OHT increases into the
11 Nordic Seas and the Arctic Ocean. New evidence of increasing northward OHT into the Arctic has been
12 observed in recent decades (Mulwijk et al., 2018; Wang et al., 2019b; Tsubouchi et al., 2021), similar to the
13 SROCC assessment, and consistent with observed increase in OHC in the ice free Arctic ocean (Mayer et al.,
14 2019). It is estimated that an increase of 0.021 PW of OHT occurred after 2001 into the Arctic, which is
15 sufficient to account for the recent OHC change in the northern seas (Tsubouchi et al., 2021). However,
16 these trends cannot yet be attributed to anthropogenic forcing due to potential internal variability (Mulwijk
17 et al., 2018; Wang et al., 2019b). New evidence strengthens the case that ENSO and the Northern Annular
18 Mode affect interannual OHT variability (Trenberth et al., 2019) and shows that a slowing AMOC reduces
19 northward OHT in the Atlantic at 26.5°N (Bryden et al., 2020) (Section 9.2.3.1, Figure 9.8). Despite a
20 decrease of AMOC northward heat (0.17 PW) and mass (2.5 Sv) transport, OHT has increased toward the
21 Arctic through increased upper northern North Atlantic temperatures and stronger wind-driven gyres
22 (*medium confidence*) (Section 9.2.3.4, Figure 9.11) (Singh et al., 2017; Oldenburg et al., 2018a). In
23 summary, OHT has increased toward the Arctic in recent decades, which at least partially explains the recent
24 OHC change in the Arctic (*medium confidence*).

25
26 Major volcanic eruptions have caused interannual to decadal cooling phases within the marked long-term
27 increase in global OHC (Agung in 1963, El Chichón in 1982 and Pinatubo in 1991; Cross-Chapter Box 4.1)
28 (Church et al., 2005; Fasullo et al., 2016; Stevenson et al., 2016; Fasullo and Nerem, 2018). In the first few
29 years following an eruption, heat exchange with the subsurface ocean allows atmospheric cooling to be
30 sequestered into the seasonal thermocline, therefore reducing the magnitude of the peak atmospheric
31 temperature anomaly (Gupta and Marshall, 2018). However, while explosive volcanic eruptions only disturb
32 the Earth's radiative budget and surface fluxes for a few years, the ocean preserves an anomaly in OHC in
33 the upper 500m (also affecting thermosteric sea level) many years after the eruption (Gupta and Marshall,
34 2018; Bilbao et al., 2019). The anomaly affects the atmosphere through air-sea heat fluxes with surface
35 conditions returning to normal only after several decades (Gupta and Marshall, 2018; Bilbao et al., 2019), or
36 on centennial time-scales in the case of repeated eruptions (Miller et al., 2012a; Atwood et al., 2016; Gupta
37 and Marshall, 2018). In summary, there is *medium confidence* that oceanic mechanisms buffer the
38 atmospheric response to volcanic eruptions on annual timescales by storing volcanic cooling in the
39 subsurface ocean, affecting ocean heat content and thermosteric sea level on decadal to centennial
40 timescales.

41
42 CMIP5 and CMIP6 models simulate OHC changes that are consistent with the updated observational and
43 improved estimates of OHC over the period 1960 to 2018 (Figures 9.6, 9.7, 9.8), and they replicate the
44 vertical partitioning of OHC change for the industrial era, although with a tendency to underestimate OHC
45 gain shallower than 2000 m and overestimate it deeper than 2000 m (Section 3.5.1.3). The AR5 (Flato et al.,
46 2013) assessed that climate models transport heat downward more than the real ocean. Since the AR5,
47 studies have shown that increasing the horizontal resolution of ocean models tends to increase agreement of
48 vertical heat transport with observations as the dependency on ad-hoc choices of eddy parameterizations is
49 relaxed (Griffies et al., 2015; Chassignet et al., 2020). The magnitude of the AMOC and Indonesian
50 Throughflow affect future OHC change, e.g. through overestimated modelled downward heat pumping
51 (Kostov et al., 2014), and there are indications of greater model consistency in these transports at higher
52 resolution (Chassignet et al., 2020; Jackson et al., 2020a) (Figure 9.10). Climate models tend to reproduce
53 the observed added heat, but redistributed heat is less well represented (Figure 9.8) (Bronseleer and Zanna,
54 2020; Dias et al., 2020; Couldrey et al., 2021). Since redistributed heat dominates historical OHC change,
55 historical simulations poorly reproduce regional patterns, but as future OHC change will become dominated

1 by added heat, more skill in future modelled OHC patterns is expected (Bronse laer and Zanna, 2020). In
2 summary, climate models have more skill in representing OHC change from added heat than from ocean
3 circulation change (*high confidence*). Since added heat dominates over redistributed heat on a centennial
4 scale (especially under high emissions scenarios) confidence in future modelled OHC patterns at the end of
5 the 21st century is greater than at decadal scale.
6

7 The SROCC (Bindoff et al., 2019) assessed that the ocean will continue to take up heat in the coming
8 decades for all plausible scenarios, and here this assessment is confirmed with *very high confidence*. The
9 SROCC reported that compared with the observed changes since the 1970s, the warming of the ocean by
10 2100 would *very likely* double to quadruple for low emissions scenarios (RCP2.6) and increase 5 to 7 times
11 for high emissions scenarios (RCP8.5). The SROCC also concluded with *high confidence* that the overall
12 warming of the ocean would continue this century even after radiative forcing and mean surface
13 temperatures stabilize, and SROCC projected that ocean heat content in the 0–2000 m layer will increase
14 from 2017 to 2100 by 0.900 ± 0.345 YJ under RCP2.6 and 2.150 ± 0.540 YJ under RCP8.5. Updating the
15 SROCC estimates with CMIP6 projections gives heat content increases and 17–83% ranges in the 0–2000 m
16 layer from 1995–2014 to 2081–2100 of 1.06 (0.80 – 1.31) YJ, 1.35 (1.08 – 1.67) YJ, 1.62 (1.37 – 1.91) YJ,
17 1.89 (1.60 – 2.29) YJ under scenarios SSP1-2.6, SSP2-4.5, SSP3-7.0, and SSP5-8.5, respectively (Figure 9.6,
18 Table 9.1). The two-layer model used here to calculate thermosteric sea level rise (9.SM.4) and tuned for
19 AR6-assessed ECS (Section 7.SM.2), provides consistent 17–83% ranges of 1.18 (0.99 – 1.42) YJ, 1.56 (1.33
20 – 1.86) YJ, 1.90 (1.63 – 2.21) YJ, 2.23 (1.92 – 2.64) YJ under scenarios SSP1-2.6, SSP2-4.5, SSP3-7.0, and
21 SSP5- 8.5, respectively (Table 9.1). Based on both CMIP6 models and the two-layer model, it is *likely* that,
22 from 1995–2014 to 2081–2100, OHC will increase 2 to 5 times the amount of the 1971–2018 OHC increase
23 under SSP1-2.6, and 4 to 8 times that amount under SSP5-8.5. CMIP6 models show that the dependence of
24 OHC on scenarios begins only after about 2040 (Figure 9.6).
25

26 The patterns of OHC projected by CMIP6 models (Figures 9.6, 9.7) are similar to the CMIP5 projections
27 assessed in the SROCC (Bindoff et al., 2019): faster warming in all water mass subduction regions (e.g.,
28 subtropical cells and Mode waters); deeper penetration in the centre of subtropical gyres; slower northern
29 North Atlantic warming due to slowing AMOC; and slower subpolar Southern Ocean warming due upwelled
30 pre-industrial water masses. Decreased aerosol forcing will allow Northern Hemisphere ocean warming to be
31 faster and less dominated by Southern Hemisphere change (Shi et al., 2018; Irving et al., 2019). Since the
32 SROCC, distinguishing between added and redistributed heat has aided in understanding projections
33 (Bronse laer and Zanna, 2020; Couldrey et al., 2020; Dias et al., 2020). The near-term decades will feature
34 patterns strongly influenced by heat redistribution and internal variability (Rathore et al., 2020).
35 Strengthening Southern Hemisphere westerlies are projected except for stringent mitigation scenarios
36 (Bracegirdle et al., 2020) and will cause a northward and downward OHT. There is *low agreement* in future
37 Southern Ocean warming across model results due to uncertainties in the magnitude of westerly wind
38 changes (Figure 9.4) (Liu et al., 2018; He et al., 2019; Dias et al., 2020; Lyu et al., 2020b) and the degree of
39 eddy compensation of overturning across different parameterisations and resolutions (9.2.3.2) (Beal and
40 Elipot, 2016; Mak et al., 2017; Roberts et al., 2020a). By 2100 however, the OHC change will be dominated
41 by the added heat response, particularly for strong warming scenarios (Garuba and Klinger, 2018; Bronse laer
42 and Zanna, 2020) with added heat following unperturbed water mass pathways in the North Atlantic and
43 Southern Ocean (Couldrey et al., 2020; Dias et al., 2020) (Figure 9.8). There is *high confidence* that
44 projected weakening of the AMOC (Section 9.2.3.1) will cause a decrease in northward OHT in the northern
45 hemisphere mid-latitudes (Figure 9.8; Sections 9.2.3.1, 4.3.2.3; Weijer et al., 2020) associated with a dipole
46 pattern of Atlantic OHC redistributed from northern to low latitudes that may override added heating in the
47 northern North Atlantic (Figures 9.6, 9.7, 9.8). Variations in the degree of AMOC redistributed heat
48 (Menary and Wood, 2018) causes large intermodel spread in SST (Figure 9.3) and OHC (Figure 9.6) change
49 (Kostov et al., 2014; Bronse laer and Zanna, 2020; Couldrey et al., 2020; Todd et al., 2020). In the 700–
50 2000m depth range, CMIP5 and CMIP6 models project the largest warming to be in the North Atlantic Deep
51 Water and Antarctic Intermediate Water (Figure 9.7) while below 2000 m, the North Atlantic cools in many
52 models, and Antarctic Bottom Waters warm (Sallée et al., 2013b; Heuzé et al., 2015). In summary, on
53 decadal timescales, redistribution will dominate regional patterns of OHC change without affecting the
54 globally integrated OHC, but by 2100, particularly under strong warming scenarios, there is *high confidence*
55 that regional patterns of OHC change will be dominated by added heat entering the sea surface primarily in

1 water-mass formation regions in the subtropics, with reduced aerosols increasing the relative rate of
 2 Northern Hemisphere heat uptake (*medium confidence*).

3
 4 The SROCC assessed that the warming of the deep ocean is slow to manifest, with multi-century or longer
 5 response times, so global OHC (and global mean thermosteric sea level) will continue to rise for centuries
 6 (Figures 9.9, 9.30). New studies show that this continuation persists even after cessation of greenhouse gas
 7 emissions (Ehlert and Zickfeld, 2018a). Ocean warming will continue even after emissions reach zero
 8 because of slow ocean circulation (Larson et al., 2020). Ocean heat content will increase until at least 2300
 9 even for low emission scenarios, but with a scenario-dependent rate (Nauels et al., 2017; Palmer et al., 2018)
 10 and depends not only on cumulative CO₂ emissions, but also on the time profile of emissions (Bouttes et al.,
 11 2013). Past long-term changes in total OHC illustrate adjustment relevant to expected future changes (Figure
 12 9.9). Observational data (Figure 9.9) from ice core rare gas elemental and isotopic ratios document a rise in
 13 global OHC relative to the Last Glacial Maximum of >17,000 ZJ (change in mean ocean temperature
 14 >3.1°C) (Bereiter et al., 2018; Baggenstos et al., 2019; Shackleton et al., 2019, 2020). This temperature
 15 increase is significantly larger than the modelled OHC changes associated with collapse of AMOC alone and
 16 tracks rising Southern Ocean SST (Uemura et al., 2018), strengthening of the deep abyssal overturning cell
 17 (Du et al., 2020) and increased North Atlantic water in the Southern Ocean (Wilson et al., 2020),
 18 underscoring the importance of Antarctic abyssal ventilation on long-term oceanic heat budgets (Section
 19 9.2.3.2). An ensemble of four intermediate-complexity models project 10,000-year future responses to CO₂
 20 emissions (Clark et al., 2016) with SST change peaking around 2300 with varying scenario-dependent
 21 magnitude approaching the scale of glacial-to-interglacial changes in paleodata (Figure 9.9). Long-term
 22 OHC commitments relative 1850-1900 conditions are 2.6, 9.7, 15.2, 21.6, and 28.0 YJ (with mean ocean
 23 temperature change as much as 5.1°C) for emissions of 0, 1280, 2560, and 3840 and 5120 Gt after 2000 CE
 24 respectively, with OHC peaking near 4000 CE reflecting whole-ocean warming lagging SST by thousands of
 25 years. The exact timing is uncertain subject to rates of high-latitude meltwater input (Van Breedam et al.,
 26 2020) and circulation time (Gebbie and Huybers, 2019). In summary, there is *high confidence* that there is a
 27 long-term commitment to increased OHC in response to anthropogenic CO₂ emissions, which is essentially
 28 irreversible on human timescales.

29
 30
 31 [START FIGURE 9.9 HERE]

32
 33 **Figure 9.9: Long-term trends of ocean heat content and surface temperature.** (a, b) Ice-core rare gas estimates of
 34 past mean ocean heat content OHC (ZJ), scaled to global mean ocean temperature (°C) and to steric
 35 GMSL (m) (red dashed line) are compared to surface temperatures (black solid line, gold solid line; °C
 36 rightmost axis). Southern Ocean SST from multiple proxies in 11 sediment cores and from ice core
 37 deuterium excess (Uemura et al., 2018). a) Penultimate glacial interval to last interglacial, 150,000-
 38 100,000 yr B2K (Shackleton et al., 2020). b) Last glacial interval to modern interglacial, 40,000-0 yr B2K
 39 (Baggenstos et al., 2019; Shackleton et al., 2019). Changes in OHC (dashed lines) track changes in
 40 Southern Ocean SST (solid lines). c) Long-term projected (2000 to 12000 CE) changes of OHC (dashed
 41 lines) in response to four greenhouse gas emissions scenarios (Clark et al., 2016) scale similarly to large-
 42 scale paleo changes but lag projected global mean SST (solid lines). d) model simulated 1500-1999 OHC
 43 (Gregory et al., 2006) and 1955-2019 observations (Levitus et al., 2012) updated by NOAA NODC. All
 44 data expressed as anomalies relative to pre-industrial time. Further details on data sources and processing
 45 are available in the chapter data table (Table 9.SM.9).

46
 47 [END FIGURE 9.9 HERE]

48 49 9.2.2.2 Ocean Salinity

50
 51
 52 The AR5 (Rhein et al., 2013) assessed that it was *very likely* that subsurface salinity changes reflect surface
 53 salinity change, and that basin-scale regions of high salinity and evaporation had trended more saline, while
 54 regions of low salinity and more precipitation had trended fresher since the 1950s. The SROCC (Bindoff et
 55 al., 2019) assessment was consistent with the AR5. Section 2.3.3.2 strengthens evidence that subsurface
 56 salinity trends are connected to surface trends (*very likely*), which are in turn linked to an intensifying

1 hydrological cycle (*medium confidence*) and increasing evidence from updated observational records
2 indicates it is now *virtually certain* that surface salinity contrasts are increasing. At basin scale, Section
3 2.3.3.2 and the AR5 concur that it is *very likely* that the Pacific and Southern Ocean have freshened, and the
4 Atlantic has become more saline. Figures 3.25 and 3.27 compare CMIP6 models to salinity observations.
5

6 Globally the mean salinity contrast at near-surface between high- and low- salinity regions increased 0.14
7 [0.07 to 0.20] from 1950 to 2019 (Section 2.3.3.2). At regional scale, the SROCC (Meredith et al., 2019)
8 assessed an Arctic liquid freshwater trend of $600 \pm 300 \text{ km}^3 \text{ yr}^{-1}$ ($600 \pm 200 \text{ Gt yr}^{-1}$) between 1992 and 2012,
9 reflecting changes associated with continental freshwater imports that affect ocean mass (land ice, rivers) as
10 well as changes in sea ice volume. Since the AR5, regional observation-based analyses not assessed in the
11 SROCC further confirm the long-term, large-scale and regional patterns of salinity change, both at the ocean
12 surface and in the subsurface ocean, including almost 120 years of changes in the North Atlantic (Friedman
13 et al., 2017) and 60 years of monitoring in the subpolar North Pacific (Cummins and Ross, 2020b). These
14 longer time-series also provide context to detect large multi-annual change, from 2012 to 2016 in the
15 subpolar North Atlantic, unprecedented over the centennial record (Holliday et al., 2020). In summary, there
16 is *high confidence* that salinity trends have extended for more than 60-100 years in the regions with long
17 historical observation records such as the North Pacific and the North Atlantic basin.
18

19 While there is *low confidence* in direct estimates of trends in surface freshwater fluxes (Sections 2.3.1.3.5,
20 8.3.1.1, 9.2.1.2), as discussed in the SROCC (Meredith et al., 2019), observational studies coupled with
21 modelling studies suggest that surface flux changes drive many observed near-surface salinity changes, on
22 top of changes specific to polar regions. Advances in salinity observations (e.g., the Argo program (Riser et
23 al., 2016); SMOS, Aquarius and SMAP (Supply et al., 2018; Vinogradova et al., 2019)), combined with
24 process-studies (SPURS-1/2; (Lindstrom et al., 2015; SPURS-2 Planning Group 2015)) and methodological
25 and numerical advances, have increased understanding of how subsurface salinity anomalies link to surface
26 fluxes, and thus increase confidence that near-surface and subsurface salinity pattern changes since the 1950s
27 are linked to changing surface freshwater fluxes (Zika et al., 2018; Cheng et al., 2020) with an additional
28 contribution from changes in sea-ice and land-ice discharge at high latitudes (Haumann et al., 2016; Purich et
29 al., 2018; Dukhovskoy et al., 2019a; Rye et al., 2020). There is therefore *medium confidence* in the processes
30 linking surface fluxes to surface and subsurface salinity change.
31

32 Ocean circulation changes also affect salinity, largely on annual to decadal timescales (Du et al., 2019; Liu et
33 al., 2019; Holliday et al., 2020). For instance, in the subpolar North Atlantic, increasing northward transport
34 of “Atlantic waters” entering the subpolar gyre from the South have compensated the salinity decrease
35 expected from increased Greenland meltwater flux since the early 1990s (Dukhovskoy et al., 2016, 2019b;
36 Stendardo et al., 2020). After the mid-2010s the trend reversed towards a broad freshening, the largest in 120
37 years, in the North Atlantic (Holliday et al., 2020). The long term freshening in the Pacific Ocean has also
38 been subject to decadal variability, such as a marked salinification since 2005 associated with increased
39 surface fluxes (Li et al., 2019a). Local salinity anomalies forced by water cycle intensification can be
40 weakened by rapid exchange between basins with opposing trends, such as by water-mass exchange in
41 shallow wind-driven cells between the tropics and the subtropics (Levang and Schmitt, 2020). Similarly,
42 eddy exchanges between neighbouring gyres can partly counterbalance decadal time scale long-term
43 subpolar freshening and affect deep convection (Levang and Schmitt, 2020). There is *high confidence* that, at
44 annual to decadal timescales, regional salinity changes are driven by ocean circulation change superimposed
45 on longer term trends.
46

47 CMIP5 historical simulations have patterns similar to, but greater spatial variability than, observed estimates
48 and correspondingly smaller amplitudes in the multi-model mean (Durack, 2015; Cheng et al., 2020; Silvy et
49 al., 2020a). Section 3.5.2.1 reports, however, that the fidelity of ocean salinity simulation has improved in
50 CMIP6, and near-surface and subsurface biases have been reduced (*medium confidence*), though the
51 structure of the biases strongly reflects those of CMIP5. At regional scale, salinity biases are at least partially
52 a result of inaccurate ocean dynamics (Levang and Schmitt, 2020). Despite the regional limitations, Section
53 3.5.2.2 assesses that at the global scale it is *extremely likely* that human influence has contributed to observed
54 surface and subsurface salinity changes since the mid-20th century (strengthened from the *very likely* AR5
55 assessment).

1
2 The SROCC (Bindoff et al., 2019) assessed that projected salinity changes in the subsurface ocean reflect
3 changes in the rates of formation of water masses or their newly formed properties. Additional consistent
4 newer evidence based on CMIP5 and regional climate models confirms that 21st century projections adhere
5 to the fresh gets fresher, salty gets saltier paradigm, through subduction of freshening high latitude waters
6 into the ventilated water-masses in both hemispheres in the Pacific, Indian and Southern Ocean, especially
7 the Arctic and upper Southern Ocean, and saltier subtropical and Mediterranean surface waters lead to saltier
8 pycnoclines and North Atlantic mode water (Metzner et al., 2020; Parras-Berrocal et al., 2020; Silvy et al.,
9 2020a; Soto-Navarro et al., 2020). Overall, projections confirm the SROCC assessment that fresh ocean
10 regions will continue to get fresher and salty ocean regions will continue to get saltier in the 21st century
11 (*medium confidence*).

12 13 14 9.2.2.3 Water Masses

15
16 Water masses refer to connected bodies of ocean water, formed at the ocean surface with identifiable
17 properties (temperature, salinity, density, chemical tracers) resulting from the unique formation conditions of
18 the overlying atmosphere and/or ice, before being transferred (subducted) to the deeper ocean below the
19 surface turbulent layer. As water masses subduct, they ventilate the subsurface ocean, transferring
20 characteristics acquired at the ocean surface to the subsurface. By integrating surface flux changes, water
21 masses provide higher signal-to-noise ratios for detecting and monitoring climate change than surface fluxes
22 (Bindoff and McDougall, 2000; Durack and Wijffels, 2010; Silvy et al., 2020b).

23
24 SubTropical Mode Waters (STMW) ventilate the main thermocline of the ocean at mid- to low-latitudes and
25 have circulation timescales away from the surface of the order of years to decades. The SROCC (Bindoff et
26 al., 2019) reported that warming in the subtropical gyres penetrates deeper than in other gyres, following the
27 density surfaces in these gyres. Consistently, we assess that STMW have deepened worldwide, with greatest
28 deepening in the Southern Hemisphere (*high confidence*) (Häkkinen et al., 2016; Desbruyères et al., 2017).
29 Subsurface warming in the Northern Hemisphere STMW is larger than at the surface (Sugimoto et al., 2017)
30 because they are formed in wintertime western boundary current extensions, where surface warming is larger
31 than the global average (Section 9.2.1.1). Variability in STMW thickness or temperature has a large imprint
32 on ocean heat content (Section 9.2.2.1) (Kolodziejczyk et al., 2019). STMW are observed to be freshening in
33 the North Pacific and to be associated with increased salinity in the North Atlantic (Oka et al., 2017; Silvy et
34 al., 2020a), with large decadal variability (Oka et al., 2019; Wu et al., 2020). Anthropogenic temperature and
35 salinity changes in the STMW layer are projected to intensify in the future, with emergence from natural
36 variability around 2020 to 2040 (Silvy et al., 2020a).

37
38 SubAntarctic Mode Water (SAMW) and Antarctic Intermediate Waters (AAIW) form at the Southern Ocean
39 surface directly north of the Antarctic Circumpolar Current and ventilate the upper 1000 m of the Southern
40 Hemisphere subtropics. The SROCC (Meredith et al., 2019) reported a freshening of these water masses
41 between 1950 and 2018, and they are projected to have the largest subsurface temperature increase of the
42 Southern Hemisphere oceans, along with a continued freshening, in the 21st century. The SROCC connected
43 SAMW and AAIW to Southern Ocean temperature changes as the large Southern Ocean surface heat uptake
44 is circulated and mixed along with these water masses (*high confidence*). Close to its formation region,
45 SAMW is predominantly affected by air-sea flux changes, while further northward it is influenced by wind-
46 forced changes (Meredith et al., 2019). New evidence shows that a change in SAMW heat content over the
47 last decade is primarily attributable to its thickening (Kolodziejczyk et al., 2019). Over the past decade, the
48 SAMW and AAIW volumes have changed by thickening of the lighter and thinning of the denser parts of
49 SAMW and AAIW, leading to lightening of these ventilated ocean layers overall (Hong et al., 2020; Portela
50 et al., 2020). Over the last decade, there is *limited evidence* of increased subduction of SAMW due to
51 deepening mixed layers in the SAMW formation region (9.2.1.3) (Qu et al., 2020). Climate models from
52 CMIP3 to CMIP5 generally simulated shallower and lighter SAMW and AAIW than is observed (Flato et
53 al., 2013). New analysis of CMIP5 models suggests that the freshening of these water masses is one of the
54 most prominent projected salinity changes in the world ocean, and that this freshening emerged from internal
55 variability as early as the 1980–1990s (Silvy et al., 2020b).

1 Trends in North Atlantic Deep Water (NADW) are obscured by decadal variability (Rhein et al., 2013;
2 Bindoff et al., 2019). The AR5 (Rhein et al., 2013) assessed that it is *very likely* that the temperature, salinity,
3 and formation rate of the Upper NADW (formed by deep convection in the Labrador and Irminger Seas) is
4 dominated by strong decadal variability related to the North Atlantic Oscillation (NAO) and it is *likely* that
5 Lower NADW (formed in the Nordic Seas and supplied to the North Atlantic by deep overflows over the
6 sills between Scotland and Greenland) cooled from 1955 to 2005. New insights from observations have
7 emphasized the stability of the deep overflows associated with Lower NADW (Hansen et al., 2016;
8 Jochumsen et al., 2017; Østerhus et al., 2019) and even slight warming in the Faroe Bank Channel (Hansen
9 et al., 2016). As a result, the AR5 assessment that Lower NADW *likely* cooled between 1955 and 2005 is
10 revised to: it is *likely* that any observed changes in temperature, salinity, and formation rate of the Lower
11 NADW are dominated by decadal variability. For CMIP5 models it was shown that AMOC variability is
12 linked to variability in NADW formation (Heuzé, 2017) and projected AMOC decline to decreased NADW
13 formation (both Lower NADW and Upper NADW) (Heuzé et al., 2015). For CMIP6 models, projected
14 AMOC decline is also associated with a decline in NADW formation (Reintges et al., 2017; Weijer et al.,
15 2020). The link between AMOC and NADW formation appears insensitive to the large range in model bias
16 in NADW water mass characteristics (Heuzé, 2017). Many models may overestimate deep water formation
17 in the Labrador Sea, but at least one new model is consistent with recent OSNAP observations showing very
18 weak overturning in the western subpolar gyre, where Labrador Sea Water is formed (Menary et al., 2020a).
19 CMIP6 models show a reduced bias in NADW properties compared to CMIP5 models, but still feature
20 varying locations of deep convection in the subpolar gyre: some convect only in the Labrador Sea (6/35
21 models), most in both the Labrador and Irminger Seas (26/35 models; as is observed), and some only in the
22 Irminger Sea (3/35 models), but in general the area where deep convection takes place has expanded relative
23 to CMIP5, which appears unrealistic (Heuzé, 2021). Models with most deep convection in the subpolar gyre
24 feature the smallest bias in NADW characteristics, partly associated with NADW formed in the Nordic Seas
25 (as observed) being largely unable to leave the area (Heuzé, 2021) due to inaccurate overflows (Danabasoglu
26 et al., 2010; Deshayes et al., 2014; Wang et al., 2015b). Despite the wide range in model bias, it remains *very*
27 *likely* that any long-term (multi-decadal or longer) decrease in AMOC is accompanied by a decline in
28 NADW formation, associated with lighter densities in the northern North Atlantic and Arctic basins.

29
30 The SROCC (Meredith et al., 2019) assessed that the global volume of Antarctic Bottom Water (AABW)
31 had decreased and warmed since the 1980s, most noticeably near Antarctica. The SROCC also noted
32 freshening in the Indian and Pacific sectors of the Southern Ocean and a higher rate of freshening in the
33 Indian Sector from the 2000s to 2010s than from the 1990s to 2000s (*low confidence*). Since the SROCC,
34 freshening of Indian Ocean AABW from 1974 to 2016 has been revealed (Aoki et al., 2020). Additionally,
35 interannual to decadal variability in AABW has been quantified to be larger than previously thought in terms
36 of temperature, salinity and thickness, and in volume transport (Abrahamsen et al., 2019; Purkey et al.,
37 2019b; Gordon et al., 2020; Silvano et al., 2020). Multidecadal-to-centennial modes of variability could have
38 driven the observed trends of the lower cell over the past decades via the opening of a Weddell Sea polynya
39 (Zhang et al., 2019b), although other studies find it contributed minimally to the observed abyssal warming
40 (Zanowski et al., 2015; Zanowski and Hallberg, 2017). Therefore, there is *limited evidence* and *low*
41 *agreement* in the role of open ocean polynyas in driving past decadal observed trends of AABW. Beyond
42 variability, all observational, theoretical, and numerical evidence supports the SROCC assessment that
43 formation and export of AABW will continue to decrease due to warming and freshening of surface source
44 waters near the Antarctic continent. Consistent with Section 9.2.3.2, confidence in this assessment is
45 increased to *medium confidence* compared to the SROCC.

46
47 Circumpolar Deep Water (CDW) lies in the Southern Ocean and forms by mixing of North Atlantic Deep
48 Water and Antarctic Bottom Water (Talley, 2013). The SROCC (Meredith et al., 2019) assessed with *low*
49 *confidence* that mean southward and upward CDW transport is linked to decadal wind variability (Section
50 9.2.3.2), and that CDW has warmed south of the Antarctic Circumpolar Current (ACC) in the past decades.
51 New evidence reinforces the SROCC assessment: changes in Southern Ocean wind stress have been
52 confirmed to drive variability and increase the large-scale southward CDW transport (Waugh et al., 2019). In
53 addition, growing evidence suggests that the upper ocean stratification increase in the subpolar Southern
54 Ocean since the 1970s (Section 9.2.1.3) has reduced the volume of CDW that is mixed to the surface,
55 causing subsurface CDW warming (Bronselaeer et al., 2020; Haumann et al., 2020; Jeong et al., 2020;

1 Moorman et al., 2020). Large regions of the Antarctic shelves are currently isolated from warm CDW
2 (Thompson et al., 2018; Jourdain et al., 2020). The SROCC (Meredith et al., 2019) assessed that subsurface
3 warming extends close to Antarctica and has co-occurred with shoaling of the CDW since the 1980s,
4 influencing the continental shelf most in the Amundsen-Bellinghshausen Seas, Wilkes Land, and the Antarctic
5 Peninsula. New evidence since the SROCC reinforces confidence in the importance of the role of winds in
6 transporting heat associated with CDW to continental shelves and ice cavities in the Amundsen-
7 Bellinghshausen Seas (Dotto et al., 2019) and via variable small-scale undercurrents to the Shirase Glacier
8 Tongue in East Antarctica (Hirano et al., 2020; Kusahara et al., 2021). There is *limited evidence* that
9 increased greenhouse gas forcing has caused a slight mean change of the local winds from 1920-2018
10 facilitating CDW heat intrusion onto the Amundsen-Bellinghshausen continental shelf and ice-shelf melt
11 (Holland et al., 2019). Multiple lines of observational, numerical, theoretical, and paleo evidence provide
12 *high confidence* that changes in wind pattern (Spence et al., 2014; Dotto et al., 2019; Holland et al., 2019),
13 increased ice-shelf melt (Golledge et al., 2019a; Moorman et al., 2020), reduction in sea-ice
14 production (Timmermann and Hellmer, 2013; Obase et al., 2017), and eddies (Stewart and Thompson, 2015;
15 Thompson et al., 2018) can facilitate access of CDW to the sub-ice-shelf cavities (9.4.2.1). However, there is
16 *low confidence* in the quantification, importance and the ability of present models, especially at coarse
17 resolution, to project changes in each of these processes (9.4.2.2). Some studies have projected a possible
18 shift from cold to warm sub-ice shelf cavities causing a sudden flush of warm water underneath ice shelves,
19 but there is *low confidence* both in the driving processes and the threshold to trigger the shift (Box 9.4)
20 (Hellmer et al., 2012, 2017; Silvano et al., 2018; Hazel and Stewart, 2020).

23 9.2.3 Regional Ocean Circulation

25 9.2.3.1 Atlantic Meridional Overturning Circulation

27 The Atlantic meridional overturning circulation (AMOC) is the main overturning current system in the South
28 and North Atlantic Oceans. It transports warm upper-ocean water northwards, and cold, deep water
29 southwards, as part of the global ocean circulation system (Section 2.3.3.4.1). AMOC changes influence
30 global ocean heat content and transport (Section 9.2.2.1); global ocean anthropogenic carbon uptake changes
31 and climate sensitivity (Cross-Chapter Box 5.3); and dynamical sea level (Section 9.2.4). Since the
32 AR5/SROCC, confidence in modelled and reconstructed AMOC has decreased due to new observations and
33 model disagreement. Confidence in modelled AMOC evolution during the 20th century, the magnitude of
34 21st century AMOC decline, and the possibility of an abrupt collapse before 2100 have been revisited.

36 The AR5 (Flato et al., 2013) found that the mean AMOC strength in CMIP5 models ranges from 15 to 30 Sv
37 for the historical period. The multi-model mean overturning at 26°N in CMIP5 and CMIP6 is comparable to
38 the RAPID measurements (Reintges et al., 2017), but the inter-model spread in CMIP6 is as large (10-31 Sv)
39 as in CMIP5 ((Weijer et al., 2020); Section 3.5.4). Biases in simulations of the present day AMOC and
40 associated deep convection in the subpolar gyre and Nordic Seas were large in CMIP5 models with many
41 models exhibiting ocean convection that is too deep, over too large an area, too far south and occurring too
42 frequently (Heuzé, 2017) (Section 9.2.1.3; Figure 9.5) related to biases in sea-ice extent, overflows, and
43 freshwater forcing (Deshayes et al., 2014; Wang, Legg and Hallberg, 2015). As a result, the AMOC in
44 CMIP5 was nearly always too shallow, with too weak a temperature contrast between the northward and
45 southward flowing branches. Deep convection errors are still large in CMIP6 and the shallow bias in AMOC
46 persists (Weijer et al., 2020; Heuzé, 2021). Since the AR5, there is emerging evidence that enhancing
47 horizontal resolution can reduce longstanding climate model biases in AMOC strength, where the magnitude
48 and profile of northward heat transport at 26°N become more comparable to observations (Chassignet et al.,
49 2020; Roberts et al., 2020a). The sensitivity of the AMOC to ocean resolution, however, is model-dependent
50 and can be positive as well as negative (Roberts et al., 2020b). An increase in AMOC strength at 26°N with
51 higher resolution in the ocean component has been associated with too strong (deep) convection in the
52 subpolar gyre and too deep winter mixed layers (Jackson et al., 2020a), which occurs in most CMIP6 models
53 that are unable to overflow deep water formed in the Nordic Seas across the Greenland-Iceland-Scotland
54 Ridge. Thus models with a correct AMOC strength may do so by compensating a lack of deep water outflow
55 from the Nordic Seas through too much deep convection and deep-water formation in the Labrador and

1 Irminger Seas (Heuzé, 2021).

2
3 Models and paleo-reconstructions have often assumed a close relation between the AMOC and deep
4 convection in the Labrador Sea, and Labrador Sea convection variability has been interpreted as connecting
5 to AMOC variability. Observational studies have been inconclusive on whether this relation exists (Buckley
6 and Marshall, 2016). New insight from observed overturning in the eastern and western subpolar gyre in the
7 North Atlantic in OSNAP (Lozier et al., 2019; Petit et al., 2020) reveal that 15.6 ± 3.1 Sv takes place north of
8 the OSNAP array between Greenland and Scotland, with only 2.1 ± 0.9 Sv of overturning occurring across the
9 Labrador Sea as found with the OSNAP 53°N array spanning the mouth, explicitly questioning the validity
10 of the Labrador Sea convection-AMOC link (Lozier et al., 2019). Although their results are derived from
11 only the first 21 months of data of monitoring since 2014, hydrographic observations during 1990-1997
12 previously found small overturning (1-2 Sv) in the Labrador Sea (Pickart and Spall, 2007). On the other
13 hand, previous estimates of Labrador Sea Water formation (obtained with different techniques) suggest
14 larger overturning (Haine et al., 2008). Part of this controversy could be explained if a large fraction of
15 newly formed Labrador Sea Water is not exported from the Labrador Sea. The OSNAP observations are
16 supported by previous hydrographic measurements in showing strong east-west symmetry in isopycnal slope
17 in the Labrador Sea in periods of both strong and weak convection, implying compensating northward and
18 southward transport above and below the potential density surface that separates the upper and lower
19 overturning limbs (Lozier et al., 2019), despite large deep convection variability (Yashayaev, 2007;
20 Yashayaev and Loder, 2016). New observations of deep winter mixing in the Irminger Basin (de Jong et al.,
21 2018; Josey et al., 2019) support the assertion that the Irminger Sea, in addition to the Nordic Seas (Chafik
22 and Rossby, 2019), are the main sources of overturning in the eastern subpolar gyre, consistent with OSNAP
23 (Petit et al., 2020). It is unclear to what extent models are in disagreement with this view of overturning in
24 the subpolar gyre, as a direct comparison with OSNAP in terms of partitioning the overturning in a western
25 and eastern part is lacking for most models, with a notable exception (Menary et al., 2020a). The analysis of
26 water mass formation in CMIP6 models (Heuzé, 2021); the analysis between Labrador Sea water formation
27 and AMOC in a suite of ocean-only models (Danabasoglu et al., 2014); the fact that when the OSNAP
28 observing system design was tested in an eddy-permitting ocean model, almost equal amounts of overturning
29 in the western and eastern subpolar gyre were found (Lozier et al., 2017), give rise to considerable
30 uncertainty over the models' veracity in simulating the overturning partitioning between east and west and
31 the role of various drivers of AMOC variability. Disagreement between models and OSNAP observations
32 may decrease in higher-resolution models (Menary et al., 2020a). In summary, multiple lines of evidence
33 provide *medium agreement* between models and observations on drivers of change and variability in the
34 AMOC and in particular the role of Labrador Sea deep convection in constituting AMOC variability.

35
36 The AMOC is a potential driver of Atlantic Multidecadal Variability (AMV), but there is new evidence that
37 anthropogenic aerosol changes have contributed to observed AMV changes, and that underestimation of the
38 magnitude and duration of AMV changes in CMIP5 is tempered in CMIP6 (Section 3.7.7, Annex IV.2.7).
39 Comparison of observed AMOC variability at the RAPID section with modelled variability reveals that
40 CMIP5 models appear to largely underestimate the interannual and decadal timescale variability (Roberts et
41 al., 2014; Yan et al., 2018), and similar results are found when analysing CMIP6 models (Section 3.5.4.1).
42 By underestimating the multi-decadal AMOC-AMV link and other low-frequency AMOC variability climate
43 models also underestimate internal variability in subpolar SSTs that feedback on the North Atlantic
44 Oscillation (NAO), causing the NAO to lack variability on multidecadal timescales (Kim et al., 2018).
45 Despite the role of the AMOC in generating AMV through subsurface temperatures in antiphase with SST
46 and downward heat fluxes into the ocean that anticorrelate with SSTs (Zhang et al., 2019d), it is generally
47 accepted that AMOC forcing of SST variability exists alongside stochastic wind forcing and external forcing
48 by aerosols (Bellomo et al., 2018; Hausteine et al., 2019; O'Reilly et al., 2019; Wills et al., 2019).

49
50 The SROCC (Collins et al., 2019) assessed that in situ observations (2004–2017) and sea surface
51 temperature reconstructions indicate that the AMOC has weakened relative to 1850–1900 (*medium*
52 *confidence*). However, the SROCC also assessed that there is insufficient data to quantify the magnitude of
53 the weakening, or to properly attribute it to anthropogenic forcing, due to the limited length of the
54 observational record. Here, this assessment is adjusted to *low confidence* in the weakening as also discussed
55 in Sections 2.3.3.4.1 and 3.5.4.1. The CMIP5 multi-model mean showed no 20th century trend in the AMOC

(Cheng et al., 2013). The CMIP6 multi-model mean even slightly opposes the reconstructed decline due to a strong increase in the 1940-1985 period (Menary et al., 2020c; Weijer et al., 2020), thought to be in response to aerosol forcing (Section 3.5.4.1), followed by a smaller decline since the nineties. Also, agreement between different proxy-based reconstructions is weak in many details (Moffa-Sánchez et al., 2019) and questions can be raised regarding various proxies used in reconstructions (Section 2.3.3.4.1). For instance, SST-based proxies can be influenced by atmospheric and other processes acting on different timescales (Moffa-Sánchez et al., 2019; Jackson and Wood, 2020). In addition, many proxies are indirect and based on AMOC-related processes assumed to be similar as found in models, such as the link between AMOC and Labrador Sea convection, which has been questioned recently (see above). In addition, the subpolar gyre from which many AMOC-proxies are taken may vary independently of the AMOC with rather similar patterns in SST and ocean heat content driven by wind variability (Williams et al., 2014; Piecuch et al., 2017). Finally, a new dynamic reconstruction of the Atlantic inflow to the Nordic Seas suggest no slowdown over the past 70-100 years (Rossby et al., 2020), in contrast to a new compilation of proxy reconstructions which suggests that the AMOC is presently in its weakest state in the last millennium (Caesar et al., 2021), reinforcing the evidence that motivated the previous SROCC assessment. Section 3.5.4.1 also questions the veracity of the models' forced AMOC response during the twentieth century. Given the large discrepancy between modelled and reconstructed AMOC in the twentieth century and the uncertainty over the realism of the 20th century modelled AMOC response (Section 3.5.4.1), we have *low confidence* in both.

The strength of the AMOC has been measured directly since 2004 using the RAPID Array (Smeed et al., 2018) (Section 2.3.3.4.1). RAPID-based estimates show a large amount of variability compared to CMIP models (Roberts et al., 2014). Observed changes since 2004 are too short for the evaluation of a long-term trend given the decadal scale internal variability (Section 2.3.3.4.1). Nevertheless, Smeed et al. (2018) argue that between 2007 and 2011 the AMOC shifted to a state of reduced overturning; decreasing from 18.8 Sv between 2004 and 2008 to 16.1 Sv after 2008. A shift in AMOC strength of this magnitude is not captured by CMIP5 and CMIP6 models, which generally underestimate interannual to decadal AMOC variability (Section 3.5.4.1). Additional evidence since SROCC also raises the inconsistency between the RAPID weakening in the 3000-5000 m depth range and the relative constancy of deep overflows from the Arctic (Østerhus et al., 2019), implying that the recent decrease in AMOC at 26.5°N (Smeed et al., 2018) is not caused by overflow weakening or reduced overturning in the Nordic Seas, although the weakening occurred almost exclusively in the 3000 – 5000 m depth range associated with a reduction of Lower NADW (Section 9.2.2.3). It is unclear what causes a weakening of the deepest limb of the AMOC at 26.5°N, if the main sources for this flow farther north remain constant. Various estimates of AMOC and associated heat transport suggest an increase since the 1940s with a subsequent decrease since the 1990s (Section 2.3.3.4.1), supported by ocean reanalysis (Jackson et al., 2019), forced ocean model simulations (Robson et al., 2012; Danabasoglu et al., 2016) and CMIP6 simulations (Menary et al., 2020b). This suggests that the observed AMOC-shift between 2007 and 2011 may be part of a longer-term decrease (*medium confidence*), which has been attributed to be part of multiannual variability (Rhein et al., 2019).

[START FIGURE 9.10 HERE]

Figure 9.10: AMOC strength in simulations and sensitivity to resolution and forcing. (Top left) AMOC magnitude in PMIP experiments. (Top right) Time series of AMOC from CMIP5 and CMIP6 based on (Menary et al., 2020c). (Bottom left) Percent change in AMOC strength per year at different resolutions over the 1950-2050 period with colours for model families (Roberts et al., 2020b). (Bottom right) A compilation (Jackson and Wood, 2018) of percentage changes in the simulated AMOC after applying an additional freshwater flux in the subpolar North Atlantic at the surface for a limited time (de Vries and Weber, 2005; Stouffer et al., 2006; Yin and Stouffer, 2007; Jackson, 2013; Liu and Liu, 2013; Jackson and Wood, 2018; Haskins et al., 2019). Symbols indicate whether the AMOC recovers within 200 years (circles), is starting to recover (upwards arrow) or does not recover within 200 years (downwards arrow). Symbol size indicates rate of freshwater input. Further details on data sources and processing are available in the chapter data table (Table 9.SM.9).

[END FIGURE 9.10 HERE]

1 The SROCC (Collins et al., 2019) found that the AMOC will *very likely* weaken over the 21st century. In
2 CMIP6 projections, the modelled decline starting in the 1990s continues in all future projections, almost
3 independent of the forcing scenario until about 2060, after which low emission scenarios show stabilization,
4 while high-emission scenarios continue to exhibit AMOC decline (Figure 9.10) (Menary et al., 2020b,
5 Weijer et al., 2020). Despite differences in overall AMOC strength, location and latitude of deep convection,
6 sea-ice and SST bias and representation of deep overflows, the model projections are qualitatively similar.
7 This agreement suggests that AMOC decline may be governed by large-scale constraints independent of the
8 details of the models. In theoretical models of the thermohaline circulation, the circulation strength is
9 proportional to a density or pressure difference between the subpolar North Atlantic and subtropical South
10 Atlantic (Kuhlbrodt et al., 2007; Weijer et al., 2019). In all models, the north-south pressure gradient
11 decreases in the 21st century, as subpolar waters warm faster than subtropical waters and an enhanced
12 hydrological cycle drives freshening at subpolar latitudes, while subtropical latitudes feature more
13 evaporation and salinification (Section 9.2.1). As a result, surface waters at subpolar latitudes become more
14 buoyant and more stable, so that deep water formation driving the AMOC declines (Section 9.2.1.3).
15 Projected AMOC decline by 2100 ranges from 24% (4-46%) in SSP1-2.6 to 39% (17-55%) in SSP5-8.5
16 (*medium confidence*; Section 4.3.2.3). Note that these ranges are based on ensemble means of individual
17 models, largely smoothing out internal variability. If single realisations are considered the ranges become
18 larger, lowering especially the low end of the range (Section 4.3.2.3). In summary, it is *very likely* that
19 AMOC will decline in the 21st century, but there is *low confidence* in the models' projected timing and
20 magnitude. In addition, freshwater from the melting of the Greenland ice sheet (Sections 9.4.1.3, 9.4.1.4)
21 could further enhance the future weakening of the AMOC in the 21st century (Collins et al., 2019; Golledge
22 et al., 2019).

23
24 Both the AR5 (Collins et al., 2013) and the SROCC (Collins et al., 2019) assessed that an abrupt collapse of
25 the AMOC before 2100 was *very unlikely*, but the SROCC added that by 2300 an AMOC collapse was *as*
26 *likely as not* for high-emission scenarios. The SROCC also assessed that model-bias may considerably affect
27 the sensitivity of the modelled AMOC to freshwater forcing. Tuning towards stability and model biases
28 (Valdes, 2011; Liu et al., 2017; Mecking et al., 2017; Weijer et al., 2019) provides CMIP models a tendency
29 toward unrealistic stability (*medium confidence*). By correcting for existing salinity biases, Liu et al. (2017)
30 demonstrated that AMOC behaviour may change dramatically on centennial to millennial timescales and that
31 the probability of a collapsed state increases. None of the CMIP6 models features an abrupt AMOC collapse
32 in the 21st century, but they neglect meltwater release from the Greenland ice sheet and a recent process
33 study reveals that a collapse of the AMOC can be induced even by small-amplitude changes in freshwater
34 forcing (Lohmann and Ditlevsen, 2021). As a result, we change the assessment of an abrupt collapse before
35 2100 to *medium confidence* that it will not occur.

36 37 38 9.2.3.2 Southern Ocean

39
40 The changing Southern Ocean circulation system exerts a strong influence on the global climate by
41 modulating (i) global ocean heat content (Section 9.2.2.1); (ii) global ocean anthropogenic carbon uptake
42 (Cross-chapter Box 5.3); global ocean overturning circulation (Section 9.2.3.1); climate sensitivity (Section
43 7.4.4 and Cross-chapter Box 5.3); (iii) sea level through basal melt of ice shelves (9.4.2); and Southern
44 Hemisphere sea-ice cover (Section 9.3.2).

45
46 The SROCC (Meredith et al., 2019) had *low confidence* in all CMIP5-based model projections due to their
47 inability to explicitly resolve eddy processes and their inability to properly consider future meltwater change
48 from the Antarctic Ice Sheet. These limitations of climate models to represent the Southern Ocean persist
49 due to most CMIP6 models still using parameterized mesoscale eddy processes that are limited in projecting
50 the future response of the horizontal and vertical circulation under climate warming, and due to the
51 continued absence of active ice shelf and ice sheet coupling in the CMIP6 model suite, therefore ignoring
52 basal meltwater and calving feedback on the circulation (Meredith et al., 2019). In addition, two important
53 limitations of CMIP6 models of the Southern Ocean involve processes that were not assessed in the SROCC.
54 First, the poor representation of dense overflows causes most of the Antarctic Bottom Water (AABW) to be
55 formed by spurious open ocean convection rather than by dense overflows from the Antarctic continental

1 shelves that feed the lower overturning cell (Snow et al., 2015; Dufour et al., 2017; Heuzé, 2021). Second,
2 Antarctic continental shelf waters are poorly simulated because potentially important controlling
3 mechanisms tend to be too small and transient to observe and resolve in CMIP ocean models. These small
4 processes include the heterogeneity of observed sub-ice shelf melt with warm water driving narrow basal
5 channels that cut underneath the ice (Drews, 2015; Alley et al., 2016; Marsh et al., 2016; Milillo et al.,
6 2019); eddies and tides (Stewart et al., 2018; Jourdain et al., 2019; Hausmann et al., 2020), which can drive
7 Circumpolar Deep Water (CDW) onto the continental shelves or dynamically increase melting (Section
8 9.2.3.6); and feedback mechanisms between ocean, atmosphere and cryosphere that can weaken or amplify
9 initial perturbations (Donat-Magnin et al., 2017; Spence et al., 2017; Turner et al., 2017; Silvano et al., 2018;
10 Webber et al., 2019; Hazel and Stewart, 2020). In addition, the Southern Ocean in CMIP5 and CMIP6
11 models exhibit surface temperature biases (Section 9.2.1.1), which have been linked in CMIP5 model to
12 errors in atmospheric model cloud-related short-wave radiation (Hyder et al., 2018) and are somewhat
13 improved in HighResMIP models (Figure 9.3). In summary, there is *high confidence* that future change in
14 the subpolar Southern Ocean region including sea-ice cover and ocean temperature change on Antarctic
15 continental shelves depends on feedback mechanisms involving the ocean, atmosphere and cryosphere that
16 are poorly understood and not represented in the current generation of climate models. This results in large
17 uncertainty and *low confidence* in the future sea-ice cover (Section 9.3.2) and in ocean temperature change
18 on the Antarctic continental shelf (Section 9.4.2.3).

19
20 Despite these challenges, the CMIP6 ensemble does represent the main Southern Ocean circulation
21 characteristics; the simulated Antarctic Circumpolar Current (ACC) transport is generally lower than
22 observation-based values but consistent when considering ensemble spread and the inter-model spread in
23 ACC transport has greatly reduced from previous generations of climate models from CMIP3 to CMIP6
24 (Beadling et al., 2019, 2020). The structure (but not the magnitude) of the two-cell zonally-averaged
25 overturning is captured by most CMIP6 models (Russell et al., 2018; Beadling et al., 2019). In addition,
26 while issues remain, CMIP6 climate models show clear improvements in their representation of AABW
27 compared to CMIP5: several models correctly represent or parameterise Antarctic shelf processes, fewer
28 models exhibit Southern Ocean deep convection, bottom density biases are reduced, and abyssal overturning
29 is more realistic (Heuzé, 2021). In terms of atmospheric wind forcing, CMIP6 models show an improvement
30 compared to CMIP5 models with an overall reduction in the equatorward bias of the annual mean westerly
31 jet from 1.9° in CMIP5 to 0.4° in CMIP6, but in contrast they show no such overall improvements for their
32 representation of the Amundsen Sea Low (Bracegirdle et al., 2020; Lyu et al., 2020a), which can be critical
33 in driving variability of water-masses on the Antarctic continental shelf in west Antarctica, the Weddell Sea
34 or the Ross Sea (Holland et al., 2019; Silvano et al., 2020).

35
36 The SROCC (Meredith et al., 2019) established that while trends in the atmospheric forcing of the Southern
37 Ocean have been dominated by a strengthening of the southern hemisphere westerly winds in recent decades,
38 there is *medium confidence* that ACC transport is weakly sensitive to changes in winds. It also reported that
39 instead of increasing the mean ACC transport, additional energy input associated with increased wind stress
40 cascades into the eddy field (*medium confidence*). In contrast with the AR5 assessment (Rhein et al., 2013),
41 the SROCC evaluated that it was *unlikely* that there has been a net southward migration of the mean ACC
42 position over the past 20 years. There is no additional evidence to revisit the SROCC assessment on wind
43 sensitivity. However, new evidence does suggest that air-sea buoyancy forcing associated with idealised
44 4xCO₂ forcing leads to an increase in ACC transport (Shi et al., 2020) (*limited evidence*). The SROCC noted
45 that if the general strengthening in westerly winds is sustained, then it is *very likely* that the eddy field will
46 continue to increase in intensity, and that is *likely* that the mean position and strength of the ACC will remain
47 only weakly sensitive to winds. In the future, the strength of the Southern Hemisphere westerly wind jet
48 results from a competition between decrease due to ozone hole recovery and increase due to increased
49 radiative forcing (Section 4.3.3.1). This competition results in an increased atmospheric jet by 2100
50 compared to present day under SSP2-4.5, SSP3-7.0, and SSP5-8.5, but a decreased jet by 2100 under SSP1-
51 2.6 (Bracegirdle et al., 2020). There is little inter-model spread in the CMIP6 future response of the
52 atmospheric westerly jet, providing *high confidence* in this assessment (in contrast, CMIP6 models show no
53 consistency in their future projection of easterly wind change along the Antarctic continental shelf break)
54 (Bracegirdle et al., 2020). Paleo-oceanographic evidence suggests that ACC flow through Drake Passage was
55 consistently stronger during warm intervals of the past (both during interstadials and interglacials), but with

1 relatively little change and no consensus on the sign of change in other regions (Lamy et al., 2015; Toyos et
2 al., 2020). In summary, additional evidence since the SROCC confirms that there is *medium confidence* that
3 the ACC has been weakly sensitive to Southern Hemisphere atmospheric jet increase in the past decades.
4 New evidence since the SROCC suggests that there is *high confidence* that the Southern Hemisphere
5 atmospheric jet will increase in the 21st century for all scenarios (except for SSP1-1.9 and SSP1-2.6; Section
6 4.3.3.1) with a greater increase for larger radiative forcing. An increase in westerly winds will *very likely*
7 force an increase of the eddy field in the ACC, and while there is *medium confidence* that the ACC is weakly
8 sensitive to wind change, new advances since the SROCC provide *limited evidence* that the ACC transport
9 will nevertheless increase in response to wind and buoyancy fluxes.

10
11 For the upper cell overturning circulation, the SROCC concluded that its transport has experienced
12 significant inter-decadal variability in response to wind forcing since the 1990s, and that there is *low*
13 *confidence* in the assessments of a long-term increase in upper ocean overturning. Consistent with the
14 SROCC, the importance of both eddy processes and winds in driving long-term change and variability have
15 been reinforced, with a potential fast wind response partially counteracted by a slower eddy response
16 (Doddrige et al., 2019; Waugh et al., 2019; Stewart et al., 2020). Eddy parameterizations affect the strength
17 of overturning, its sensitivity to winds and the ACC transport (Mak et al., 2017). Even in eddy resolving
18 simulations sub-gridscale dissipation affects the overturning and ACC (Pearson et al., 2017). In addition,
19 there has been progress in understanding the importance of Antarctic Ice Shelf meltwater and sea-ice, in
20 driving the observed changes in the near surface and in the upper overturning cell over the past decades, on
21 top of changes induced by winds and eddies (Bronselaeer et al., 2020; Haumann et al., 2020; Jeong et al.,
22 2020; Rye et al., 2020). In particular, increased stratification caused by increased freshwater flux to the
23 surface ocean (Section 9.2.1.3) can cause a shoaling and warming of the Circumpolar Deep Water layer, and
24 create a positive feedback enhancing basal melt of the Antarctic Ice Sheet (Section 9.4.2.1) (Bronselaeer et
25 al., 2018; Golledge et al., 2019a; Schloesser et al., 2019; Sadai et al., 2020). There is *medium confidence* in
26 the existence of this feedback mechanism but *low agreement* on the magnitude of the feedback. The SROCC
27 reported that CMIP5 models project that the overall transport of upper ocean overturning cell will increase
28 by up to 20% in the 21st century, and no new studies alter that assessment.

29
30 For the lower cell overturning circulation, the SROCC assessed that a slowdown of its transport is consistent
31 with the observed decrease in volume (*medium confidence*) of AABW in the global ocean (Section 9.2.2.3).
32 Additional evidence since the SROCC, strengthens confidence that increased glacial meltwater flux will
33 reduce the density of bottom waters during the 21st century, eventually reaching a point where deep
34 convection will be curtailed and shelf water will become too buoyant to sink to the ocean interior, thereby
35 slowing the lower cell overturning circulation (Bronselaeer et al., 2018; Golledge et al., 2019a; Lago and
36 England, 2019; Moorman et al., 2020). While such changes are consistent with the observed freshening and
37 volume decrease of the AABW layer reported in the SROCC, as discussed in Section 9.2.2.3, new
38 observation-based studies have highlighted how the lower cell overturning can episodically increase as a
39 response to climate anomalies, temporally counteracting the tendency for melt to reduce AABW formation
40 (Abrahamsen et al., 2019; Castagno et al., 2019; Gordon et al., 2020; Silvano et al., 2020). In addition, while
41 the opening of open ocean polynyas can affect the lower cell on decadal to centennial time-scales, there is
42 *limited evidence* and *low agreement* in the role of open ocean polynyas in driving observed trends of the
43 lower cell in the last decade (Section 9.2.2.3). Based on CMIP5 models, the SROCC reported with *low*
44 *confidence* that formation and export of AABW associated with the lower overturning cell will decrease in
45 the 21st century, and there is no new evidence to revisit that assessment from climate models. However,
46 additional paleo evidence from marine sediments suggest that AABW formation/ventilation was vulnerable
47 to freshwater fluxes during past interglacials (Hayes et al., 2014; Huang et al., 2020; Turney et al., 2020) and
48 that AABW formation was strongly reduced (Skinner et al., 2010; Gottschalk et al., 2016; Jaccard et al.,
49 2016) or possibly totally curtailed (Huang et al., 2020) during the LGM and transient cold intervals of MIS 2
50 & 3. Specifically, sedimentary reconstructions show a transient reduction in AABW ventilation in the
51 Atlantic sector of the Southern Ocean during MIS5e, which is assessed to have been warmer than modern
52 climate (Thomas et al., 2020). However, long multi-centennial or millennial model runs under higher-than-
53 pre-industrial CO₂ concentrations show that after 500 -1000 years, ventilation in the Southern Ocean
54 resumes, and even possibly overshoots with enhanced convection in the Weddell and Ross seas leading to
55 enhanced bottom water ventilation globally (Yamamoto et al., 2015; Frölicher et al., 2020). AABW

1 ventilation increased at the onset of the last deglacial transition, promoting the release of previously
2 sequestered CO₂ to the atmosphere on centennial to millennial timescales (Bauska et al., 2016; Jaccard et al.,
3 2016; Rae et al., 2018), concomitant with a southward shift of the SH westerly wind belt (Denton et al.,
4 2010; Jaccard et al., 2016) and reduced sea-ice cover (Ferrari et al., 2014; Stein et al., 2020). In summary,
5 the combination of observational, numerical and paleoclimate evidence provides us with *medium confidence*
6 that the lower cell will continue decreasing in the 21st century as a result of increased basal melt from the
7 Antarctic Ice Sheet.

10 9.2.3.3 Tropical Oceans

11
12 The tropics are a tightly coupled ocean-atmosphere system with tightly interconnected basins (Cai et al.,
13 2019). The zonal atmospheric Walker Circulation and the Indonesian Throughflow (ITF, Figure 9.11) are
14 key connections between the Pacific and Indian Oceans, and variations in the Walker and Hadley
15 Circulations are tightly linked to the tropical Pacific SST and currents. The tropics have a profound influence
16 on the climate system through the multiple modes of variability they host, which have widespread global
17 influence at seasonal to annual timescale (Annex IV).

18
19 The effect of tropical modes of variability on climate and their long-term changes are reviewed in detail in
20 Annex IV, while changes to the tropical ocean are assessed throughout the report and briefly summarized
21 here. Section 2.4 concludes that a sustained shift beyond multi-centennial variability has not been observed
22 for ENSO (*medium confidence*) and that there is *limited evidence* and *limited agreement* about the long-term
23 behaviour of other tropical modes. Section 3.7 assesses with *high confidence* that human influence has not
24 affected the principal tropical modes of interannual climate variability and their associated regional
25 teleconnections beyond the range of internal variability. Section 4.3.3.2 assesses with *medium confidence*
26 that there is no consensus from models for a systematic change in the amplitude of El Niño–Southern
27 Oscillation sea surface temperature variability over the 21st century. The related change in tropical SSTs is
28 covered in Section 9.2.1.1. The projected changes in SST have implications for marine heat wave
29 characteristics, which are assessed in Box 9.2. SST changes in the tropics are related to changes in the
30 atmospheric circulation, including surface equatorial easterly trade winds and Walker Circulation (Section
31 4.5.3.2), and the weakening Indonesian Throughflow and strengthening Agulhas Extension and leakage
32 (Section 9.2.3.4). Weakening trade winds under climate change (Vecchi and Soden, 2007) will tend to
33 decrease upwelling, along isopycnals in the eastern Pacific and diapycnal upwelling in the central Pacific and
34 thus the meridional temperature gradients that drive Tropical Instability Waves (Terada et al., 2020), along
35 with a weakening, flattening and shoaling of the tropical thermocline and equatorial undercurrent (Luo and
36 Rothstein, 2011). A weak or absent Equatorial Undercurrent (Kuntz and Schrag, 2020) and a too diffuse and
37 incorrectly sloped tropical thermocline (Zhu et al., 2020) remain issues in most CMIP6 models. In summary,
38 while future changes in tropical modes of variability remain unclear, change in atmospheric and ocean
39 circulation will drive continued change in tropical ocean temperature in the 21st century (*medium*
40 *confidence*), with part of the region experiencing drastic marine heat wave conditions (*high confidence*).

43 9.2.3.4 Gyres, Western Boundary Currents, and Inter-Basin Exchanges

44
45 The AR5 (Rhein et al., 2013) assessed with *medium to high confidence* that the North Pacific subpolar gyre,
46 the South Pacific subtropical gyre, and the subtropical cells have intensified. They also reported that the
47 North Pacific subtropical gyre had expanded since the 1990s, and that overall the changes in gyre systems
48 were *likely* predominantly due to interannual-to-decadal variability. The SROCC (Meredith et al., 2019)
49 complemented the AR5 assessment by reporting that the polar Beaufort Gyre in the Arctic expanded to the
50 northwest between 2003 and 2014, contemporaneous with changes in its freshwater accumulation and
51 alterations in wind forcing. Consistent with the reported change over the gyres, both the AR5 and the
52 SROCC (Bindoff et al., 2019; Collins et al., 2019) reported that Western Boundary Currents (WBCs) have
53 intensified (Figure 9.11), and expanded poleward, except for the Gulf Stream and the Kuroshio. Section
54 2.3.3.4 provides an overall assessment of gyres and WBCs including an assessment of change from
55 paleoclimate archives. Section 2.3.3.4 assesses that while WBC strength is highly variable at multidecadal

1 scale (*high confidence*), WBCs and subtropical gyres have shifted poleward since 1993 (*medium*
2 *confidence*), at a rate on the order of 0.04-0.1 degree per decade during 1993-2018. Figure 9.11 shows that
3 CMIP5 and CMIP6 models agree in projecting a weaker Gulf Stream and Gulf Stream Extension, while the
4 Kuroshio changes less (Sen Gupta et al., 2016).

5
6 Although the observed wind stress curl shows systematic poleward shift in each basin as a result of
7 anthropogenic warming (Section 2.3.1.4) (Chen and Wu, 2012; Wu et al., 2012; Zhai et al., 2014), which has
8 caused a systematic shift of the WBCs and subtropical gyres since 1993 (Wu et al., 2012; Yang et al., 2016b,
9 2020), the response of current strength is more complex and inconsistent across regions (Sloyan and O’Kane,
10 2015; Wang et al., 2016c; Elipot and Beal, 2018; McCarthy et al., 2018; Wang and Wu, 2018; Dong et al.,
11 2019). The strength of WBCs and gyres exhibit inconsistent responses because they are not only dependent
12 on wind stress forcing, but multi-scale interaction and air-sea interaction have an important role in their long-
13 term trends and variability (Zhang et al., 2020). Observed changes in gyre circulation are dominated by
14 interannual and decadal modes of variability globally (Qiu and Chen, 2012; Melzer and Subrahmanyam,
15 2017; McCarthy et al., 2018; Hu et al., 2020). The North Atlantic subpolar gyre is strongly modulated by
16 variability associated with the NAO and AMV (Robson et al., 2016) (Annex IV). Subpolar gyre systems can
17 change abruptly due to a positive feedback between convective mixing and salinity transport (Born et al.,
18 2013, 2016) and air-sea interaction (Moffa-Sánchez et al., 2014; Moreno-Chamarro et al., 2017) within the
19 gyre. In the Arctic, both the Beaufort gyre and mesoscale eddies strengthened between 2003 and 2014
20 (Armitage et al., 2017), which might be partly due to increased wind stress (Oldenburg et al., 2018b) or
21 reduced sea-ice thickness and changes in sea-ice pack morphology (van der Linden et al., 2019). Presently,
22 there is *limited evidence* in attributing causality to these changes for any of the proposed mechanisms. In the
23 North Pacific, there has been an increasing trend in the Alaska Gyre from 1993 to 2017 (Cummins and
24 Masson, 2018), which might be attributed to PDO (Hristova et al., 2019) (*low confidence*). In the Southern
25 Ocean, *limited evidence* indicates that the subpolar gyres respond to Southern Hemisphere atmospheric
26 modes of variability at interannual time-scale (Armitage et al., 2018; Dotto et al., 2018).

27
28 All climate models reproduce WBCs and gyres, but eddy-present or eddy-rich models (roughly 10-25 km
29 and ~10 km resolution, respectively) represent these currents more realistically than eddy-parameterized
30 models (Small et al., 2014a; Griffies et al., 2015; Chassignet et al., 2017; Hewitt et al., 2017; Roberts et al.,
31 2018; Chassignet et al., 2020; Hewitt et al., 2020) (*very high confidence*). Compared to observations or to
32 eddy-present and eddy-rich models, the eddy-parameterized models from CMIP5 and CMIP6 simulate
33 weaker and wider WBCs as well as less realistic locations of subtropical and subpolar gyre boundaries
34 (Figure 9.11). Increased resolution not only admits mesoscale eddies, but also improves simulation of the
35 strength and position of WBCs such as the Kuroshio Current, Gulf Stream, and East Australian Current
36 (Sasaki et al., 2004; Chassignet and Marshall, 2008; Delworth et al., 2012; Yu et al., 2012; Small et al.,
37 2014b; Haarsma et al., 2016; Chassignet et al., 2017, 2020; Hewitt et al., 2020) (*very high confidence*).
38 Improved boundary current location relates to improved recirculation regions (Jayne et al., 2009), mean path
39 and variability and existence of multiple stable paths (Qiu et al., 2005; Delman et al., 2015), air-sea fluxes
40 (Small et al., 2014a), and related coastal weather patterns (Kaspi and Schneider, 2011). The wind-current
41 feedback, implemented by considering relative velocity of currents and wind, realistically dampens
42 mesoscale eddies and WBCs, through mesoscale air-sea interaction (Ma et al., 2016; Renault et al., 2016,
43 2019), even though sub-mesoscale wind-current damping feedback is missing in these models (Zhang et al.,
44 2016c) (*medium confidence*). As eddies potentially play a role in determining the strength of gyre
45 circulations and their low-frequency variability (Fox-Kemper and Pedlosky, 2004; Berloff et al., 2007), it is
46 expected that eddy-present and eddy-rich models will differ in their decadal variability and sensitivity to
47 changes in wind stress of gyres from eddy-parameterized models (*medium confidence*). Nonetheless,
48 important aspects of gyre strength depend primarily on forcing and not resolution, allowing long term
49 changes in gyre strength to be investigated with low resolution climate models (Hughes and de Cuevas,
50 2001; Yeager, 2015).

51
52 Under future scenarios RCP4.5 and RCP8.5, the AR5 (Collins et al., 2013) assessed an intensification and
53 poleward extension of the southern Hemisphere subtropical gyres in the 21st century. New evidence since the
54 AR5 further reinforce their conclusions which are now extended to all subtropical gyre systems, in both the
55 northern and southern hemispheres (Yang et al., 2016a, 2020). CMIP6 models project changes in WBCs that

1 are consistent with projected changes in the surface winds. Under strong radiative forcing, in scenario SSP5-
 2 8.5, CMIP6 models project that the East Australian Current Extension and Agulhas Current Extension will
 3 intensify in the 21st century, while the Gulf Stream and Brazil Current will weaken (Figure 9.11). Although
 4 CMIP5/CMIP6 are limited in resolution, *medium confidence* is given to changes in western boundary
 5 currents due to consistency across generations of climate models, including CMIP6, despite changes in
 6 model structure, resolution and parameterisations.

7
 8
 9 **[START FIGURE 9.11 HERE]**

10
 11 **Figure 9.11: Simulated barotropic streamfunction, surface speed and major current transport in CMIP5 and**
 12 **CMIP6.** (a) Mean barotropic streamfunction (Sv) 1995-2014 and projected barotropic streamfunction
 13 change (Sv, 2018-2100 vs. 1995-2014) under (b) SSP5-8.5. (d) Mean surface (0-100 m) speed (m/s) and
 14 projected surface speed change (m/s, 2018-2100) versus 1995-2014 under (e) SSP5-8.5. (c, f) Median and
 15 likely range of 1995-2014 and 2081-2100 transport of 3 currents with the largest transport change and 4
 16 with the largest fractional change (Sen Gupta et al., 2016). (c) Deep currents: Agulhas Extension (ACx),
 17 Gulf Stream (GS), Gulf Stream Extension (GSx), Tasman Leakage (TASL), East Australia Current
 18 Extension (EACx), Indonesian Throughflow (ITF), and Brazil Current (BC). (f) Shallow currents: as for
 19 deep but with New Guinea Current (NGC), and without ACx. No overlay indicates regions with high
 20 model agreement, where $\geq 80\%$ of models agree on the sign of change; diagonal lines indicate regions
 21 with low model agreement, where $< 80\%$ of models agree on the sign of change (see Cross-Chapter Box
 22 Atlas.1 for more information). Further details on data sources and processing are available in the chapter
 23 data table (Table 9.SM.9).

24
 25 **[END FIGURE 9.11 HERE]**

26
 27
 28 The SROCC (Collins et al., 2019) concluded with *high confidence* that ITF transport from the Pacific to Indian
 29 ocean has increased in the past two decades, as a result (*medium confidence*) of an unprecedented
 30 intensification of the equatorial Pacific trade wind system. Section 2.3.3.4 assesses that there is *high confidence*
 31 that the increase in the ITF over the past two decades is linked to multi-decadal scale variability rather than a
 32 longer-term trend. Consistently, in the future, as winds change under increased radiative forcing, most models
 33 project a decline of the ITF on the centennial timescale (Figure 9.11). Indeed, one of the clearest changes of
 34 ocean current transport simulated by climate models is a weakening of the Indonesian Throughflow projected
 35 in CMIP5 simulations under RCP4.5 and RCP8.5 scenarios (Sen Gupta et al., 2016; Stellema et al., 2019), as
 36 well as in CMIP6 simulations under the SSP5-8.5 scenario (*high confidence*, Figure 9.11).

37
 38 The SROCC reports with *high confidence* that the Agulhas leakage from the Indian to the Atlantic ocean has
 39 increased in the past two decades (Collins et al., 2019), and there is no additional evidence since then allowing
 40 to revisit this assessment (Biastoch et al., 2015; Loveday et al., 2015; Lübbecke et al., 2015). There is *low*
 41 *confidence* in future projections of Agulhas leakage because most CMIP models cannot directly simulate it,
 42 due to coarse resolution. However, there is *medium evidence* that the strength of the Southern Hemisphere
 43 westerlies controls Agulhas leakage (Durgadoo et al., 2013; Biastoch et al., 2015; Loveday et al., 2015), and
 44 *high confidence* that the strength of the Southern Hemisphere westerlies will increase under increased radiative
 45 forcing except in lower warming scenarios (SSP1-1.9, SSP1.2-6; Section 4.3.3.1) (Bracegirdle et al., 2020).
 46 There is also evidence that increasing Agulhas leakage is consistent with observed change of the temperature
 47 and salinity structure in the Atlantic ocean, and with variability of the AMOC (Section 9.2.3.1) (Biastoch et
 48 al., 2015). This range of indirect evidence provides *medium confidence* that the Agulhas leakage will increase
 49 in the 21st century, except for the strongest mitigation scenario (Figure 9.11).

50
 51 The SROCC assessed that the annual Bering Strait volume transport from the Pacific to the Arctic Ocean
 52 increased from 2001–2014, consistent with an estimated increased northward heat transport of about 60% from
 53 2001–2014, and an increased freshwater transport of $30 \pm 20 \text{ km}^3 \text{ yr}^{-1}$ from 1991 to 2015 (Meredith et al., 2019).
 54 Section 2.3.3.4 assesses that volume transport from the Pacific to the Arctic has increased since the 1990s from
 55 0.8 Sv to 1.0 Sv over 1990–2015. Realistic representation of the Bering Strait transport in the current generation
 56 of climate models is challenging because the strait is narrow compared to the resolution of climate models

1 (Clement Kinney et al., 2014; Aksenov et al., 2016). For the Atlantic to Arctic transport, Section 2.3.3.4 reports
2 that the major branches of Atlantic Water inflow across the Greenland-Scotland Ridge have remained stable,
3 with only the smaller pathway of Atlantic Water north of Iceland showing a strengthening trend during 1993-
4 2018. Section 2.3.3.4 also assesses that the Arctic outflow remained stable from the mid 1990s to the mid
5 2010s. Future changes in these currents have not yet been studied in CMIP6 models.
6
7

8 9.2.3.5 Eastern Boundary Upwelling Systems 9

10 Eastern boundary upwelling systems (EBUS) exist where trade winds draw cold and generally low-pH/low-
11 oxygen waters upward. Coastal upwelling plays a key role in supplying the food chain with nutrients, hence
12 the richness and productivity of EBUS (Bindoff et al., 2019). The SROCC (Bindoff et al., 2019) assessed
13 with *high confidence* that three out of the four major EBUS have experienced large-scale wind
14 intensification in the past 60 years (only the trend for the Canary current is considered uncertain). However,
15 it also emphasized that various processes can also modulate or even reverse wind trends locally (Bindoff et
16 al., 2019). Here we revisit the SROCC (Bindoff et al., 2019) assessment based on evidence showing *low*
17 *agreement* between studies that have investigated trends over past decades of upwelling-favourable winds
18 (Varela et al., 2015). This *low agreement* has been related to differences in wind products, season of interest,
19 and length of the considered time series (Varela et al., 2015). Based on this, we assess that only the
20 California current system has experienced large-scale upwelling-favorable wind intensification over the
21 period 1982-2010 albeit with regional differences (García-Reyes and Largier, 2010; Seo et al., 2012). In the
22 Benguela, Canary, and Humboldt systems, large-scale, upwelling-favourable wind trends are ambiguous,
23 owing to *low confidence* in long-term in situ marine wind data (Cardone et al., 1990; Bakun et al., 2010) and
24 *low agreement* among available studies (Narayan et al., 2010; Sydeman et al., 2014; Varela et al., 2015). Our
25 assessment confirms the SROCC (Bindoff et al., 2019) in that high natural variability of EBUS and their
26 inadequate representation by most climate models gives *low confidence* in attribution of observed changes,
27 while anthropogenic changes are projected to emerge primarily in the second half of the 21st century (*limited*
28 *evidence*: one model and one study) (Brady et al., 2017).
29

30 Under increased radiative forcing, the SROCC (Bindoff et al., 2019) assessed that climate models project, in
31 the 21st century, a reduction of wind and upwelling intensity in EBUS at low latitudes and enhancement at
32 high latitudes under scenario RCP8.5, with an overall reduction in either upwelling intensity or extension. It
33 also highlighted that coastal warming and wind intensification may lead to variable countervailing responses
34 to upwelling intensification at local scales. Despite differences among EBUS (Wang et al., 2015a), there is
35 growing evidence since the SROCC in this pattern of change. While it has long been hypothesized that for
36 upwelling winds, change is linked to air temperature contrast between ocean and land (Bakun, 1990), this
37 hypothesis has increasingly been challenged. Changes in sea level pressure and wind fields in EBUS appear
38 to be primarily tied to those affecting subtropical highs (García-Reyes et al., 2013). Poleward expansion of
39 the Hadley cell (Section 2.3.1.4.1) (Staten et al., 2018) and the related poleward migration of subtropical
40 highs (He et al., 2017; Cherchi et al., 2018), produce robust patterns of changes of reduced upwelling at low
41 latitude and enhanced upwelling at high latitude (Echevin et al., 2012; Belmadani et al., 2014; Bettencourt et
42 al., 2015; Rykaczewski et al., 2015; Sousa et al., 2017; Lamont et al., 2018; Sylla et al., 2019). These
43 patterns are most apparent in summer in both hemispheres. Synoptic variability of upwelling winds,
44 important to the functioning of upwelling ecosystems (García-Reyes et al., 2014), may also be affected by
45 climate change (Aguirre et al., 2019). However, coarse resolution model projections of winds in upwelling
46 regions may be more consistent than higher-resolution projections as these regions are highly sensitive to
47 resolution (Small et al., 2015).
48

49 Projected future annual cumulative upwelling wind changes at most locations and seasons remain
50 within ± 10 -20% of present-day values in the 21st century, even in the context of high-end emission scenarios
51 (4xCO₂ or RCP8.5) (*medium confidence*). Changes due to wind stress curl and alongshore pressure gradients
52 do tend to agree with alongshore wind changes (Oerder et al., 2015a; Sylla et al., 2019). Direct estimation of
53 oceanic upward transport (Oyarzún and Brierley, 2019; Sylla et al., 2019) and nutrient flux into the euphotic
54 layer (Jacox et al., 2018) provide a meaningful estimator of upwelling, integrating all relevant processes,
55 including changes in wind stress curl. However, there is *limited evidence* from vertical velocity of climate

1 models and missing processes in coarse-resolution climate models that presently limit this approach. Change
2 in upper ocean stratification (Section 9.2.1.3) is projected to increase confinement of upwelling vertical
3 velocities to near the ocean surface (Oerder et al., 2015a; Oyarzún and Brierley, 2019) (*high confidence*).

4
5 In summary, the SROCC and we conclude that the California current system has experienced some
6 upwelling-favourable wind intensification since the 1980s (*high confidence*), while *low agreement* among
7 reported wind changes in the Benguela, Canary, and Humboldt systems prevents a similar assessment. As in
8 the SROCC, there is *low confidence* in attribution of observed changes to anthropogenic or natural causes.
9 New evidence reinforces our confidence in the SROCC assessment that under increased radiative forcing,
10 EBUS winds will change with a dipole spatial pattern within each EBUS of reduction (weaker and/or
11 shorter) at low latitude, and enhancement (stronger and/or longer) at high latitude (*high confidence*). There is
12 *medium confidence* that, across all scenarios, upwelling wind changes in EBUS will remain moderate in the
13 21st century, within ± 10 -20% from present-day values.

14 15 16 9.2.3.6 Coastal Systems and Marginal Seas

17
18 Beyond the world's coastlines lie the shoreline, shallow estuaries, continental shelves, and deeper fjords and
19 slopes, where depths increase rapidly from the shelves to the deep ocean floor. It is more difficult to
20 transport fluid across the shelf-break or slope than along (Brink, 2016), and estuaries and shelves have
21 complex circulations and mixing leading to indirect connections between the inner shelves and coastlines
22 and offshore conditions. Coastal processes link to both large-scale metrics of climate and regional effects,
23 from changing rivers and estuaries, melt and runoff to deep water, to how changes offshore affect regional
24 and coastal conditions.

25
26 Shelf-deep ocean exchanges involve eddying, tidal, or turbulent motions and small-scale topography such as
27 submarine canyons; high resolution observations and models are needed to capture these effects (Greenberg
28 et al., 2007; Capet et al., 2008; Allen and Durrieu de Madron, 2009; Colas et al., 2012; Trotta et al., 2017).
29 Example coastal processes that introduce uncertainty into large-scale projections are exchange of CDW
30 across the Antarctic shelf-break, which affects AABW formation and Antarctic ice shelf-ocean interaction
31 (Sections 9.2.2.3, 9.2.3.2) (Stewart and Thompson, 2013, 2015), river and estuarine plumes and their
32 responses to water level and hydrology change (Banas et al., 2009; Sun et al., 2017), fjord dynamics linked
33 to glacial outflows (Straneo and Cenedese, 2015; Torsvik et al., 2019), and changing formation of water
34 masses in marginal seas (Kim et al., 2001; Greene and Pershing, 2007; Giorgi and Lionello, 2008; Renner et
35 al., 2009). Downscaling projections to the local level allows process detail (Foreman et al., 2013; Mathis and
36 Pohlmann, 2014; Meier, 2015; Tinker et al., 2016). Some processes can only be simulated when coastal
37 models are forced by larger-scale models of the atmosphere, cryosphere, or hydrosphere (Seo et al., 2007,
38 2008; Somot et al., 2008; Oerder et al., 2015b; Renault et al., 2016; Zhang et al., 2016a; Wåhlin et al., 2020),
39 including the addition of tides (Janeković and Powell, 2012; Timko et al., 2013; Tinker et al., 2015;
40 Pickering et al., 2017; Hausmann et al., 2020). Due to coastal process complexity and small scale, linking the
41 effects of coastal ocean changes to global ocean changes requires high resolution modelling (Holt et al.,
42 2017, 2018), two-way nesting, or local mesh refinement (Fringer et al., 2006; Zhang and Baptista, 2008;
43 Mason et al., 2010; Dietrich et al., 2012; Hellmer et al., 2012; Ringler et al., 2013; Wang et al., 2014b; Zängl
44 et al., 2015; Zhang et al., 2016b; Soto-Navarro et al., 2020). Coarse climate models and even HighResMIP
45 models do not represent some coastal phenomena such as cross-shelf exchanges and sub-mesoscale eddies
46 which require 1km or finer resolution. Thus, there is *low confidence* in projecting centennial scale coastal
47 climate change where regional downscaling or refinement is lacking. There is *high confidence* in the ability
48 of regional coupled models to improve coastal climate change process understanding and provide regional
49 information (Section 12.4), but many sites globally await such projections.

9.2.4 Steric and dynamic sea-level change

9.2.4.1 Global mean thermosteric sea-level change

Changes in globally averaged ocean heat content (OHC) cause global mean thermosteric sea-level (GMTSL) change (Box 9.1). The observed increased OHC for 1971–2018 of 325 to 546 ZJ (*very likely* range, Section 7.2, Box 7.2) has led to a GMTSL rise of 0.03 to 0.06 m out of a total GMSL of 0.07 to 0.15 m (*very likely* range, Section 2.3.3.3, Table 2.7, Table 9.5, Cross-Chapter Box 9.1).

Projections of GMTSL rise in the AR5 (Church et al., 2013a) and the SROCC (Oppenheimer et al., 2019) were derived from the CMIP5 ensemble, after removing drift estimated based on pre-industrial control simulations. Differences between removing a linear and a quadratic drift are small (Hermans et al. 2021) (Hobbs et al., 2016b; Hermans et al., 2021). These prior assessments filled in projections for models that did not provide GMTSL rise for all scenarios, by calculating the heat content of the climate system from global surface air temperature and net radiative flux, then converting this to GMTSL rise using each model's diagnosed expansion efficiency coefficient. In the AR5, the associated uncertainties were derived by assuming a normal distribution, with the 5th–95th percentile CMIP5 ensemble range taken as the *likely* range (± 1 standard deviation).

In this report, global surface air temperature projections are not derived directly from the CMIP6 ensemble (Box 4.1). Therefore, in order to produce projections of OHC and GMTSL rise that are consistent with the report's assessment of equilibrium climate sensitivity and transient climate response (Section 7.5.2.2), this chapter employs a two-layer energy budget emulator (Supplementary Materials 7.SM.2, 9.SM.4.3). Since the AR5, climate model emulators have been increasingly used to predict GMTSL (Kostov et al., 2014; Palmer et al., 2018, 2020; Nauels et al., 2019) (Cross-Chapter Box 7.1). The expansion efficiency coefficient that relates GMTSL and OHC for the two-layer emulator has a mean and standard deviation of 0.113 ± 0.013 m/YJ (Supplementary Material 9.SM.4.3). This approach yields a *likely* thermosteric contribution between 1995 to 2014 and 2100 that represents a minimal change from the AR5 and the SROCC (Table 9.8). The two-layer emulator GMTSL projected median and 17th–83rd percentile, or *likely*, range is 0.12 (0.09–0.15) m for SSP1-1.9, 0.14 (0.11–0.18) m for SSP1-2.6, 0.20 (0.16–0.24) m for SSP2-4.5, 0.25 (0.21–0.30) m for SSP3-7.0, and 0.30 (0.24–0.36) m for SSP5-8.5 by 2100 (Section 9.6.3.2; Tables 9.1, 9.8, 9.9). The two-layer model heat content increases slightly faster than that of the total depth CMIP6 ensemble, which is related to its role in the assessed energy balance (Section 7.SM.2), but with a similar ensemble spread (Table 9.1). Projecting the *likely* factor by which 1995–2014 to 2081–2100 ocean heat content change exceeds change over 1971 to 2018 in CMIP6 yields 3 to 5 for SSP1-2.6, 4 to 6 for SSP2-4.5, 5 to 7 for SSP3-7.0, and 5 to 8 for SSP5-8.5. The two-layer model *likely* equivalents are 2 to 3 for SSP1-2.6, 3 to 4 for SSP2-4.5, 4 to 5 for SSP3-7.0, and 4 to 6 for SSP5-8.5.

For reconstructions, the expansion efficiency coefficient is required for the conversion between ocean temperature and steric sea level over a specific time scale. Combining the assessed sea level and energy data over 1995 to 2014 (drawn from the analysis in Cross-Chapter Box 9.1) results in a coefficient of 0.1210 ± 0.0014 m/YJ, or 0.6607 ± 0.0076 m/°C in terms of mean ocean temperature. The two-layer emulator assessment used in AR6 results in 0.113 ± 0.013 m/YJ, or 0.617 ± 0.071 m/°C (Appendices 7.SM.2, 9.SM.4). Both of these estimates are in line with an independent estimate of 0.70 m/°C (Hieronimus, 2019) and other estimates, e.g., 0.116 ± 0.011 m/YJ (Kuhlbrodt and Gregory, 2012), but are significantly larger than the temperature to sea level conversion used in the AR5 (0.42 m/°C based on SST and the estimated range from (Levermann et al., 2013)). The expansion coefficient is not fixed across models nor in time, as it varies depending on which water masses are storing the added heat and the commitment time scale (Hallberg et al., 2013). For paleoclimate, a scaling for sea surface temperature (0.6 m/°C) or GSAT (see Cross-Chapter Box 2.3) can be estimated, but mean ocean temperature is in phase with steric sea-level change while sea surface temperatures are not (Shakun et al., 2012; Tierney et al., 2020) (Figure 9.9). Thus, while conversions between OHC, mean ocean temperature and GMTSL across applications are within uncertainty ranges (*medium confidence*, Table 9.1), little consistency is found when correlating these variables to SST or GSAT which may vary independently.

Short-lived climate forcers (Sections 6.3, 6.6.3) are associated with a sea-level commitment, due to an ocean heat content and mean ocean temperature response that lasts substantially longer than their atmospheric forcing and SST response, although not as long as the sea-level commitment associated with CO₂ emissions (Sections 9.2.1.1, 4.4.4). For example, Zickfeld et al., (2017) find that about 70% of the thermosteric sea-level rise associated with methane forcing would persist 100 years after the elimination of methane emissions and 40% would persist for over 500 years.

In summary, consistent relationships between OHC (Section 9.2.2.1), mean ocean temperature and GMTSL are found using two-layer emulators, CMIP6 models, and modern and paleo observations to provide *medium confidence* in the 0.113 ± 0.013 m/YJ, or 0.617 ± 0.071 m/°C *likely* ranges of assessed conversion values. It is possible to estimate relationships between SST or GSAT change and GMTSL rise, but conversions are not generally applicable and depend on time scale and application.

[START TABLE 9.1 HERE]

Table 9.1: Projected contributions to median and 17-83% (parentheses) and 5-95% (square brackets) ranges of thermosteric sea level from AR5 (Church et al., 2013), CMIP6 (Jevrejeva et al., 2020; Hermans et al., 2021) and the two-layer energy balance model (described in Sections 7.SM.2, 9.SM.4 and Box 4.1) averaged over 2081-2100, with respect to a baseline of 1995-2014. Note that AR5 and SROCC interpret 5-95% range as the *likely* range, while in this table square brackets are used for consistency.

Study	RCP2.6/SSP1-2.6	RCP4.5/SSP2-4.5	RCP8.5/SSP5-8.5
IPCC AR5 and SROCC GMTSL (Oppenheimer et al., 2019) (Church et al., 2013a)	0.13 [0.09 – 0.17] m	0.18 [0.13 – 0.22] m	0.26 [0.20 – 0.32] m
CMIP6 5-95% GMTSL (Hermans et al. 2021)	0.14 [0.08 – 0.17] m	0.18 [0.11 – 0.23] m	0.26 [0.17 – 0.33] m
CMIP6 5-95% GMTSL (Jevrejeva et al., 2020)	–	0.19 [0.13 – 0.24] m	0.27 [0.19 – 0.35] m
Assessed GMTSL based on two-layer model 17-83% and 5-95% (Sections 7.SM.2, 9.SM.4)	0.13 (0.11 – 0.16) [0.09 – 0.19] m	0.17 (0.14 – 0.21) [0.12 – 0.25] m	0.25 (0.20 – 0.30) [0.18 – 0.35] m
Total OHC 17-83% and 5-95% from assessed two-layer model (Sections 7.SM.2, 9.SM.4)	1.18 (0.99 – 1.42) [0.86 – 1.65] YJ	1.56 (1.33 – 1.86) [1.19 – 2.12] YJ	2.23 (1.92 – 2.64) [1.71 – 3.00] YJ
0-2000m OHC 17-83% and 5-95% from CMIP6 (Figure 9.6)	1.06 (0.80 – 1.31) [0.66 – 1.64] YJ	1.35 (1.08 – 1.67) [0.90 – 1.84] YJ	1.89 (1.60 – 2.29) [1.28 – 2.58] YJ

[END TABLE 9.1]

9.2.4.2 Ocean dynamic sea-level change

Projections of ocean dynamic sea-level change (Box 9.1) on multiannual timescales resemble the patterns of steric sea-level change in the open ocean (Figures 9.11 and 9.12) (Lowe and Gregory, 2006; Pardaens et al.,

2011; Couldrey et al., 2020). On shorter timescales, especially in extratropical coastal areas, there may be an important barotropic component (also called bottom pressure change) due mostly to changes in wind-driven circulation and eddies apparent in the variance of ocean dynamic sea level (Figure 9.12, (Roberts et al., 2016; Hughes et al., 2018). This component is highly sensitive to ocean model resolution (Chassignet et al., 2020). Steric sea-level change is associated with local changes in temperature and salinity, which come about through changes in surface fluxes of heat and freshwater (Section 9.2.1.2) and through redistribution of existing water masses by changed ocean circulation and mixing processes (Figure 9.12, Sections 9.2.2.1, 9.2.3). Redistribution of water masses often involves anticorrelated thermosteric and halosteric changes (Figure 9.12), especially in the Atlantic (Pardaens et al., 2011; Bouttes et al., 2014; Durack et al., 2014; Griffies et al., 2014; Han et al., 2017).

[START FIGURE 9.12 HERE]

Figure 9.12: (a-f) CMIP6 multi-model mean projected change contributions to relative sea level change in (a,d) steric sea level anomaly, (b, e) thermosteric sea level anomaly, and (c, f) halosteric sea level anomaly between 1995-2014 and 2081-2100 using a method that does not require a reference level (Landerer et al., 2007). Global mean change has been removed from these figures, consistent with the methods in Sections 9.6.3 and 9.SM.4.3 and the definitions of (Gregory et al., 2019). See Figure 9.27 for GMSL. (g-i) Standard deviation of ocean dynamic sea-level change from (g) Aviso observations (10 day highpass filter), (h) 5-day mean of high-resolution OMIP-2 models forced with observed fluxes, and (i) 5-day mean of low-resolution OMIP-2 models which are comparable in resolution to the models in (a-f). No overlay indicates regions with high model agreement, where $\geq 80\%$ of models agree on the sign of change; diagonal lines indicate regions with low model agreement, where $< 80\%$ of models agree on the sign of change (see Cross-Chapter Box Atlas.1 for more information). Further details on data sources and processing are available in the chapter data table (Table 9.SM.9).

[END FIGURE 9.12 HERE]

Ocean dynamic sea-level change is strongly affected by internal variability (Section 9.6.1.4), partly from interannual to decadal coupled atmosphere-ocean modes of variability via wind-driven redistribution (Annex IV; Griffies et al., 2014; Han et al., 2017) and partly from intrinsic ocean variability, particularly in higher resolution simulations (such as HighResMIP), which statistically resemble observations, even on short timescales (Figure 9.12, Griffies et al., 2014; Sérazin et al., 2016; Llovel et al., 2018; Chassignet et al., 2020). High-resolution simulations are not used in relative sea level projections (Section 9.6.3) due to the limited range of forcing scenarios. The most marked feature of long-term regional sea-level change in the continuous satellite altimetry record, beginning in 1992, is the east-west dipole in the Pacific Ocean (rising more rapidly in the east, see also Section 9.6.1.3), which persisted until 2015 and can be explained by anomalously strong trade winds (Merrifield et al., 2012; England et al., 2014; Griffies et al., 2014; Takahashi and Watanabe, 2016; Han et al., 2017) together with associated changes in surface heat flux (Piecuch et al., 2019). The most notable features of sub-annual variability in altimetry are eddies and tides, which are directly simulated only in high resolution models (Haigh et al., 2019; Chassignet et al., 2020).

Projections of the pattern and amplitude of regional ocean dynamic sea-level change in CMIP6 and previous model generations show a large model spread, of a similar size to the geographical spread (Figure 9.12). The model spread derives from model dependence of changes both in surface fluxes (Section 9.2.1.2) and in the ocean response (Section 9.2.2). The spread is similar in CMIP6 and CMIP5, and is largest in regions with large projected variations in ensemble-mean ocean dynamic sea-level change (Lyu et al., 2020a), such as the Southern Ocean dipole with an ocean dynamic sea-level rise north of the ACC and a fall to the south, the Atlantic dipole with a sea-level rise north of 40°N and a fall in 20-40°N, the north-west Pacific dipole, and the large sea-level rise in the Arctic (Church et al., 2013a; Slangen et al., 2014b; Bilbao et al., 2015; Slangen et al., 2015; Gregory et al., 2016; Chen et al., 2019a; Couldrey et al., 2020; Lyu et al., 2020a). Patterns of change are consistent between model simulations and observations (*medium confidence*). The major model ensemble-mean features resemble thermosteric sea level change, as expected from altered input of heat to the ocean without changing circulation, while model spread results from the diversity in redistribution of the heat content of the unperturbed ocean (Section 9.2.2.1; (Bouttes and Gregory, 2014; Gregory et al., 2016;

1 Huber and Zanna, 2017; Couldrey et al., 2020; Lyu et al., 2020b; Todd et al., 2020)).

2
3 The Southern Ocean meridional dipole is driven by a northward advection of excess heat (from changes in
4 surface fluxes) by the wind-driven circulation followed by subduction or diffusive uptake in mid-latitudes,
5 northward redistribution of existing heat by the strengthening of that circulation, and the meridional contrast
6 in thermal expansivity due to its temperature-dependence (Armour et al., 2016; Gregory et al., 2016;
7 Couldrey et al., 2020; Lyu et al., 2020b; Todd et al., 2020).

8
9 The positive Arctic ocean dynamic sea-level change is driven by increased freshwater input (Couldrey et al.,
10 2020). The north-west Pacific dipole is driven by the intensification of the Kuroshio current in response to
11 reduced heat loss and in some models to wind stress change (Chen et al., 2019a; Couldrey et al., 2020).

12
13 The North Atlantic sea-level change dipole is forced by a reduction in heat loss from the ocean north of 40°N
14 (i.e., net heat uptake), which in all Earth system models leads to a weakening of the AMOC, although the
15 magnitude has a large model spread (Gregory et al., 2016; Huber and Zanna, 2017, Section 9.2.3.1). The
16 reduced northward transport of warm, salty water (Section 9.2.2) causes further ocean dynamic sea-level
17 change, whose details are model-dependent. North of 40°N, this redistribution leads to a sea-level rise,
18 predominantly halosteric, reinforcing the thermosteric effect of heat uptake (Couldrey et al., 2020).
19 Comparison of observed Atlantic ocean heat content for 1955-2017 with a reconstruction assuming no
20 change in circulation indicates that the thermosteric sea-level change resulting from southward redistribution
21 of heat may be detectable (Zanna et al., 2019a). This redistribution causes a tendency for SST cooling north
22 of 40°N and anomalous heat input from the atmosphere, and thus a positive feedback on AMOC weakening
23 (Winton et al., 2013; Gregory et al., 2016; Couldrey et al., 2020; Todd et al., 2020). Many climate and ocean
24 models agree that the AMOC weakening is associated with pronounced thermosteric sea-level rise along the
25 American coast around 40°N (Figures 9.12, 9.26), leading to a relatively large ocean dynamic sea-level rise
26 in this region (Yin, 2012; Bouttes et al., 2014; Slangen et al., 2014a; Little et al., 2019; Lyu et al., 2020a).

27
28 In summary, ocean dynamic sea-level change involves changes to temperature and salinity and responses of
29 currents to changing forcing, with significant variability driven by unforced oceanic variability. Projections
30 of dynamic sea-level variability require fully three-dimensional ocean models and only high-resolution ocean
31 models are statistically consistent on short timescales with satellite altimeter observations (*very high*
32 *confidence*).

33 34 35 **9.3 Sea ice**

36 37 **9.3.1 Arctic Sea Ice**

38 39 **9.3.1.1 Arctic Sea-Ice Coverage**

40
41 The observed decrease of Arctic sea-ice area is a key indicator of large-scale climate change (Section
42 2.3.2.1.1, Cross-Chapter Box 2.2). The SROCC (Meredith et al., 2019) assesses that sea-ice extent, which is
43 the total area of all grid cells with at least 15% sea-ice concentration, has declined since 1979 in each month
44 of the year (*very high confidence*). In contrast to the SROCC, we assess changes in sea-ice area (the actual
45 area of the ocean covered by sea ice) rather than sea-ice extent, because sea-ice area is geophysically more
46 relevant and not grid-dependent (Notz, 2014; Ivanova et al., 2016; Notz et al., 2016; Notz and SIMIP
47 Community, 2020). Arctic sea-ice area is calculated based on measurements by passive microwave satellite
48 sensors that provide near-continuous measurements of gridded, pan-Arctic sea-ice concentration from 1979
49 onwards. Irreducible uncertainties in the conversion of thermal microwave brightness temperature to sea-ice
50 concentration and choices in algorithm design cause uncertainties in observed Arctic sea-ice area, which are,
51 though, far smaller than the observed sea-ice loss (e.g., Comiso et al., 2017b; Niederdrenk and Notz, 2018;
52 Alekseeva et al., 2019; Kern et al., 2019; Meier and Stewart, 2019). Sea-ice area has decreased from 1979 to
53 the present in every month of the year (*very high confidence*, Figure 9.13). The absolute and the relative ice
54 losses are highest in late summer-early autumn (*high confidence*, Figure 9.13). Averaged over the decade
55 2010-2019, monthly-average Arctic sea-ice area in August, September and October has been around 2

1 million km² (or about 25%) smaller than that during 1979-1988 (*high confidence*, Figure 9.13).

2
3
4 **[START FIGURE 9.13 HERE]**

5
6 **Figure 9.13: Arctic sea-ice historical records and CMIP6 projections.** Left: Absolute anomaly of monthly-mean
7 Arctic sea-ice area during the period 1979 to 2019 relative to the average monthly-mean Arctic sea-ice
8 area during the period 1979 to 2008. Right: Sea-ice concentration in the Arctic for March and September,
9 which usually are the months of maximum and minimum sea-ice area, respectively. First column:
10 Satellite-retrieved mean sea-ice concentration during the decade 1979-1988. Second column: Satellite-
11 retrieved mean sea-ice concentration during the decade 2010-2019. Third column: Absolute change in
12 sea-ice concentration between these two decades, with grid lines indicating non-significant differences.
13 Fourth column: number of available CMIP6 models that simulate a mean sea-ice concentration above 15
14 % for the decade 2045-2054. The average observational record of sea-ice area is derived from the UHH
15 sea-ice area product (Doerr et al., 2021), based on the average sea-ice concentration of OSISAF/CCI
16 (OSI-450 for 1979-2015, OSI-430b for 2016-2019)(Lavergne et al., 2019), NASA Team (version 1,
17 1979-2019)(Cavalieri et al., 1996) and Bootstrap (version 3, 1979-2019)(Comiso, 2017) that is also used
18 for the figure panels showing observed sea-ice concentration. Further details on data sources and
19 processing are available in the chapter data table (Table 9.SM.9).

20
21 **[END FIGURE 9.13 HERE]**

22
23
24 The SROCC discussed the regional distribution of Arctic sea-ice loss and their findings remain valid for the
25 updated time series covering 2019 (Figure 9.13). Sea-ice loss in winter is strongest in the Barents Sea, while
26 summer losses occur primarily at the summer sea-ice region margins, in particular in the East Siberian,
27 Chukchi, Kara and Beaufort Seas (Frey et al., 2015; Chen et al., 2016; Onarheim et al., 2018; Peng and
28 Meier, 2018; Maksym, 2019). In the Bering Sea, expanding winter sea-ice cover was observed until 2017
29 (Frey et al., 2015; Onarheim et al., 2018; Peng and Meier, 2018), but a marked reduction in sea-ice
30 concentration has occurred since then (Stabeno and Bell, 2019) (*high confidence*).

31
32 With respect to seasonal changes in the sea-ice cover, the winter sea-ice loss causes a decrease in the average
33 sea-ice age and fraction of multi-year ice as assessed by the SROCC (*very high confidence*), and also of the
34 ocean area covered intermittently by sea ice (Bliss et al., 2019). In contrast, the seasonal ice zone (covered
35 by sea ice in winter but not in summer) has expanded regionally (Bliss et al., 2019) and over the whole
36 Arctic (Steele and Ermold, 2015), because the loss of summer sea-ice area is larger than the loss of winter
37 sea-ice area. Arctic sea ice retreat includes an earlier onset of surface melt in spring and a later freeze up in
38 fall, lengthening the open-water season in the seasonal sea-ice zone (Stroeve and Notz, 2018). However,
39 there is *low agreement* in quantification of regional trends of melt and freeze onset between different
40 observational products (Bliss et al., 2017; Smith and Jahn, 2019).

41
42 Reconstructions of Arctic sea-ice coverage put the satellite period changes into centennial context. Direct
43 observational data coverage (Walsh et al., 2017) and model reconstructions (Brennan et al., 2020) warrant
44 *high confidence* that the low Arctic sea-ice area of summer 2012 is unprecedented since 1850, and that the
45 summer sea-ice loss is significant in all Arctic regions except for the Central Arctic (Cai et al., 2021). Direct
46 wintertime observational data coverage before 1953 is too sparse to reliably assess Arctic sea-ice area. Since
47 1953, the years 2015 to 2018 had the four lowest values of maximum Arctic sea-ice area, which usually
48 occurs in March (Figure 2.20) (*high confidence*). Reconstructions of Arctic sea-ice area before 1850 remain
49 sparse, and as in the SROCC, there remains *medium confidence* that the current sea-ice levels in late summer
50 are unique during the past 1 kyr (Kinnard et al., 2011; De Vernal et al., 2013b). (Section 2.3.2.1.1)

51
52 The observed fluctuations and trends of the Arctic sea-ice cover arise from a combination of changes in
53 natural external forcing and anthropogenic forcing, internal variability and internal feedbacks (e.g., Notz and
54 Stroeve, 2018; Halloran et al., 2020). New paleo-proxy techniques indicate regional sea-ice changes over
55 epochs and millennia and allow possible drivers to be assessed. Biomarker IP25 (Belt et al., 2007) together
56 with other sedimentary biomarkers (Belt, 2018) provides local temporal information on seasonal sea-ice

1 coverage, permanent sea-ice coverage and ice-free waters with occasional ambiguous contrasting results
2 (Belt, 2019). These records and other proposed paleo proxies including bromine in ice cores (Spolaor et al.,
3 2016), dinocyst assemblages (e.g., De Vernal et al., 2013b) and driftwood (e.g., Funder et al., 2011) provide
4 evidence of sea-ice fluctuations that exceed internal variability (*high confidence*).

5
6 The inferred sea-ice fluctuations over millennia can be related to Northern-hemisphere temperature evolution
7 and give rise to Arctic-wide fluctuations in sea-ice coverage in the paleo record (Section 2.3.2.1.1). On a
8 regional scale, fluctuations include decreased sea-ice cover during the Allerød warm period (14.7-12.9 ka) in
9 the Laptev (Hörner et al., 2016) and Bering Sea (Méheust et al., 2018); an extensive sea-ice cover during the
10 Younger Dryas (~12 ka) in the Bering (Méheust et al., 2018), Kara (Hörner et al., 2018), Laptev (Hörner et
11 al., 2016) and Barents (Belt et al., 2015) Seas and at the Yermak Plateau (Kremer et al., 2018); little sea ice
12 during the early Holocene, when Northern hemisphere summer insolation was higher than today (8000 to
13 9000 years before present), in the North Icelandic Shelf area (Cabedo-Sanz et al., 2016; Xiao et al., 2017),
14 Sea of Okhotsk (Lo et al., 2018), Canadian Arctic (Spolaor et al., 2016), Barents (Berben et al., 2017),
15 Bering (Méheust et al., 2018), and Chukchi (Stein et al., 2017) Seas, at the Yermak Plateau (Kremer et al.,
16 2018) and north of Greenland (Funder et al., 2011); increasing sea-ice cover throughout much of the middle
17 and late Holocene around Svalbard (Knies et al., 2017), in the North Icelandic Shelf area (Cabedo-Sanz et
18 al., 2016; Harning et al., 2019; Halloran et al., 2020), north of Greenland (Funder et al., 2011), and in the
19 Western Greenland (Kolling et al., 2018), Barents (Belt et al., 2015; Berben et al., 2017), Chukchi (De
20 Vernal et al., 2013a; Stein et al., 2017) and Laptev (Hörner et al., 2016) Seas. The consistent, Arctic-wide
21 changes give *high confidence* in millennial-scale co-variability of the sea-ice cover with temperature
22 fluctuation.

23
24 The SROCC assessed that approximately half of the satellite-observed Arctic summer sea ice loss is driven
25 by increased concentrations of atmospheric greenhouse gases (*medium confidence*). Recent attribution
26 studies now allow the strengthened assessment that it is *very likely* that more than half of the observed Arctic
27 sea-ice loss in summer is anthropogenic (Section 3.4.1.1). This assessment is confirmed by process-based
28 analyses of Arctic sea-ice loss not assessed by the SROCC. Similar to the paleo record, the satellite record of
29 Arctic sea-ice area from 1979 onwards is strongly linearly correlated with global mean temperature on
30 decadal and longer time scales (Figure 9.14a,e) (e.g., Gregory et al., 2002; Rosenblum and Eisenman, 2017).
31 The correlation holds across all months with R^2 ranging from 0.61 to 0.81 (Niederdrenk and Notz, 2018).
32 However, in contrast to paleo-records, sea-ice fluctuations during the satellite period are only weakly
33 correlated with Northern Hemisphere insolation (Notz and Marotzke, 2012); modern Northern Hemisphere
34 sea-ice area is more strongly correlated with atmospheric CO₂ concentration (Johannessen, 2008; Notz and
35 Marotzke, 2012) and cumulative anthropogenic CO₂ emissions (Figure 9.14b,f) (Zickfeld et al., 2012;
36 Herrington and Zickfeld, 2014; Notz and Stroeve, 2016). R^2 values of the correlation between sea-ice area
37 and cumulative CO₂ emissions range across all months from 0.76 to 0.92 (Stroeve and Notz, 2018). In
38 summary, there is *high confidence* that satellite-observed Arctic sea-ice area is strongly correlated with
39 global mean temperature, CO₂ concentration and cumulative anthropogenic CO₂ emissions.

40
41 In addition to changes in the external forcing, internal variability substantially affects Arctic sea ice,
42 evidenced from both paleo records (e.g., (Chan et al., 2017; Hörner et al., 2017; Kolling et al., 2018)) and
43 satellites after 1979 (e.g., Notz and Stroeve, 2018; Roberts et al., 2020) (*high confidence*). Most of the
44 internal variability on annual time scales is related to atmospheric temperature fluctuations, for example
45 linked to cyclone activities (Wernli and Papritz, 2018; Olonscheck et al., 2019), while multidecadal internal
46 variability is primarily related to changes in oceanic heat transport (Zhang, 2015; Halloran et al., 2020).
47 These mechanisms are represented in current climate models (Olonscheck et al., 2019; Halloran et al., 2020),
48 but the resulting internal variability of September sea-ice area in CMIP5 and CMIP6 models, as given by the
49 ensemble mean standard deviation $s_{SIA, Sep}=0.5$ million km² (Olonscheck and Notz, 2017; Notz and SIMIP
50 Community, 2020), exceeds the estimated internal variability for the period 1850 to 1979 from both
51 reanalyses ($s_{SIA, Sep}=0.3$ million km²) and direct observational reconstructions ($s_{SIA, Sep}=0.2$ million km²)
52 (Brennan et al., 2020) (*medium confidence* because of limited reliability of longer-term sea-ice
53 reconstructions). Internal variability has been estimated to have contributed 30 to 50% of the observed Arctic
54 summer sea-ice loss since 1979 (Kay et al., 2011; Stroeve et al., 2012; Ding et al., 2017, 2019; England et
55 al., 2019). However, this estimate from models might be biased towards internal over forced variability

1 because of the models' high internal variability and because the CMIP5 simulated September sea-ice
2 sensitivity to forcing is lower than observed, even if internal variability is taken into account (Notz and
3 Stroeve, 2016; Rosenblum and Eisenman, 2017). Most CMIP6 models fail to simulate the observed
4 sensitivity of sea-ice loss to CO₂ emissions (as a proxy for time) and to temperature simultaneously.
5 However, they better capture the observed sensitivity of sea-ice loss to CO₂ emissions than CMIP5 models
6 (Section 3.4.1, Figure 9.14h; (Notz and SIMIP Community, 2020)).
7

8 The SROCC examined the different atmospheric and oceanic processes that caused the observed sea-ice loss,
9 with recent studies providing new evidence for the importance of variations in air temperature (Olonscheck
10 et al., 2019; Dahlke et al., 2020), wind patterns (Graham et al., 2019), oceanic heat flux (Docquier et al.,
11 2021) and riverine heat influx (Park et al., 2020). As in the SROCC, the relative contribution of each
12 physical cause to the sea-ice loss cannot be robustly quantified because of disagreement among models
13 (Burgard and Notz, 2017), sparse observations and limited understanding of the variation of each factor with
14 global mean temperature. This is addressed by new diagnostics available from CMIP6 simulations, which
15 now allow for more detailed analyses of the drivers of sea-ice loss at a process level (Keen et al., 2021).
16

17 In examining temperature thresholds for the loss of Arctic summer sea ice, the SR1.5 (Hoegh-Guldberg et
18 al., 2018) and the SROCC assess that a reduction of September-mean sea-ice area to below 1 million km²,
19 practically a sea-ice-free Arctic Ocean, is more probable for a global mean warming of 2°C compared to
20 global mean warming of 1.5°C (*high confidence*). Analyses of CMIP6 simulations (Notz and SIMIP
21 Community, 2020) confirm this result, as they show that on decadal and longer time scales, Arctic summer
22 sea ice area will remain highly correlated with global mean temperature until the summer sea ice has
23 vanished (Figure 9.14a,e). Quantitatively, existing studies (Screen and Williamson, 2017; Jahn, 2018; Ridley
24 and Blockley, 2018; Sigmond et al., 2018; Notz and SIMIP Community, 2020) additionally show that for a
25 warming between 1.5 and 2 °C, the Arctic will only be practically sea-ice free in September in some years,
26 while at 3 °C warming the Arctic is practically sea-ice free in September in most years, with longer
27 practically sea-ice-free periods at higher warming levels (*medium confidence*). However, because of the
28 CMIP5 and CMIP6 models' generally too low sensitivity of sea-ice loss to global warming, there is only *low*
29 *confidence* regarding the specific warming level at which the Arctic Ocean first becomes practically sea-ice
30 free (Notz and SIMIP Community, 2020). (Section 4.3.2.1)
31

32
33 [START FIGURE 9.14 HERE]

34
35 **Figure 9.14: Monthly mean March (a-d) and September (e-h) sea-ice area as a function of global surface air**
36 **temperature (GSAT) anomaly (a,e); cumulative anthropogenic CO₂ emissions (b,f); year (c,g) in**
37 **CMIP6 model simulations (shading, ensemble mean as bold line) and in observations (black dots).**
38 Panels d and h show the sensitivity of sea-ice loss to anthropogenic CO₂ emissions as a function of the
39 modelled sensitivity of GSAT to anthropogenic CO₂ emissions. In panels d and h, the black dot denotes
40 the observed sensitivity, while the shading around it denotes internal variability as inferred from CMIP6
41 simulations (after Notz and SIMIP Community, 2020). Further details on data sources and processing are
42 available in the chapter data table (Table 9.SM.9).
43

44 [END FIGURE 9.14 HERE]

45
46
47 In contrast, CMIP6 models capture the observed sensitivity of Arctic sea ice area to cumulative
48 anthropogenic CO₂ emissions well, providing *high confidence* that the Arctic Ocean will *likely* become
49 practically sea-ice free in the September mean for the first time for future CO₂ emissions of less than 1000 Gt
50 and before the year 2050 in all SSP scenarios (Notz and SIMIP Community, 2020). This new assessment is
51 consistent with an observation-based projection of a practically sea-ice free Arctic Ocean in September for
52 additional anthropogenic CO₂ emissions of 800± 330 GtCO₂ beyond the year 2018 (Notz and Stroeve, 2018;
53 Stroeve and Notz, 2018). This estimate may, however, be too high due to neglecting possible future
54 reduction in atmospheric aerosol load that would cause additional warming (Gagné et al., 2015a; Wang et al.,
55 2018) and is subject to the same constraints as the carbon budget analysis for global mean temperature (see
56 section 5.5 for details). Based on CMIP6 simulations, it is *very likely* that the Arctic Ocean will remain sea-

1 ice covered in winter in all scenarios throughout this century (Sections 4.3.2, 4.4.2).

2
3 There is indication that CMIP6 simulations of Arctic sea ice have improved relative to CMIP5 (Section
4 3.4.1.1), but detailed evaluation studies exist mainly for CMIP5 models. These studies found that CMIP5
5 model projections and reanalyses show a large spread of simulated regional Arctic sea-ice concentration
6 (Laliberté et al., 2016; Chevallier et al., 2017), which remains true for CMIP6 models (Shu et al., 2020; Wei
7 et al., 2020). In addition, both CMIP5 and CMIP6 models show a large spread in the simulated seasonal
8 cycle of Arctic sea-ice area, with too high a sea-ice area in March in the ensemble mean (Notz and SIMIP
9 Community, 2020). CMIP5 models also have been found to have difficulty simulating realistic landfast sea
10 ice (Laliberté et al., 2018). These findings imply that both CMIP5 and CMIP6 models do not realistically
11 capture the regional and seasonal processes governing observed Arctic sea-ice evolution, causing *low*
12 *confidence* in the models' projections of future regional sea-ice evolution, including updated projections for
13 shipping routes across the Northern Sea Route and Northwest Passage (Wei et al., 2020).

14
15 CMIP5 models also have issues with capturing the seasonal cycle of observed changes in Arctic sea-ice drift
16 speed, which affects their simulation of regional sea-ice concentration patterns. Direct measurements of
17 Arctic sea ice from drift buoys and satellites show that drift speed of Arctic sea ice has increased over the
18 satellite period in all seasons (e.g., Rampal et al., 2009; Docquier et al., 2017). In summer, CMIP5 models
19 show a slowdown of Arctic sea-ice drift rather than the observed acceleration (Tandon et al., 2018). In
20 winter, CMIP5 models generally capture the observed acceleration of Arctic drift speed. The drift
21 acceleration is primarily caused by the decrease in concentration and thickness, both in the observational
22 record (Rampal et al., 2009; Spreen et al., 2011; Olason and Notz, 2014; Docquier et al., 2017) and, for
23 winter, in CMIP5 models (Tandon et al., 2018). Changes in wind speed are less important for the observed
24 large-scale changes (Spreen et al., 2011; Vihma et al., 2012; Olason and Notz, 2014; Docquier et al., 2017;
25 Tandon et al., 2018). In summary, there is *high confidence* that Arctic sea-ice drift has accelerated because of
26 the decrease in sea ice concentration and thickness.

27
28 The SR1.5 assessed with *high confidence* that there is no hysteresis in the loss of Arctic summer sea ice. In
29 addition, there is no tipping point or critical threshold in global mean temperature beyond which the loss of
30 summer sea ice becomes self-accelerating and irreversible (*high confidence*). This is because stabilizing
31 feedbacks during winter related to increased heat loss through thin ice and thin snow, and increased emission
32 of longwave radiation from open water, dominate over the amplifying ice-albedo feedback (e.g., Eisenman,
33 2012; Wagner and Eisenman, 2015; Notz and Stroeve, 2018) (see section 7.4.2 for details on the individual
34 feedbacks). Observed and modelled Arctic summer sea ice and global mean temperature are linked with little
35 temporal delay, and the summer sea-ice loss is reversible on decadal time scales (Armour et al., 2011; Ridley
36 et al., 2012; Li et al., 2013; Jahn, 2018). The loss of winter sea ice is reversible as well, but the loss of winter
37 sea-ice area per degree of warming in CMIP5 and CMIP6 projections increases as the ice retreats from the
38 continental shore lines, because these limit the possible areal fluctuations (e.g., Bathiany et al., 2016, 2020;
39 Meccia et al., 2020) (*high confidence*) (Section 4.3.2.1).

40 41 42 9.3.1.2 Arctic Sea-Ice volume and thickness

43
44 The SROCC assessed with *very high confidence* that Arctic sea ice has become thinner over the satellite
45 period from 1979 onwards, and this assessment is confirmed for the updated time series (section 2.3.2.1.1).
46 Sea-ice area has also decreased substantially over this period (section 9.3.1.1), leading to the assessment that
47 Arctic sea-ice volume has also decreased with *very high confidence* over the satellite period since 1979.
48 There is, however, only *low confidence* in quantitative estimates of the sea-ice volume loss over this period
49 because of a lack of reliable, long-term, pan-Arctic observations and substantial spread in available
50 reanalyses (Chevallier et al., 2017). Current best estimates from reanalyses suggest a reduction of September
51 Arctic sea ice volume of 55 to 65 % over the period 1979 to 2010, and of about 72 % over the period 1979 to
52 2016, with the latter deemed a conservative estimate (Schweiger et al., 2019).

53
54 For the more recent past, ice-thickness can be directly estimated from satellite estimates of sea-ice freeboard
55 (Kwok and Cunningham, 2015; Kwok, 2018). Based on these retrievals, there is *medium confidence* that

1 Arctic sea-ice volume has decreased since 2003. There is *low confidence* in the amount of decrease over this
2 period and over the CryoSat-2 period from 2011 onwards primarily because of snow-induced uncertainties in
3 the retrieval algorithms, the shortness of the record, and the small identified trend (e.g., (Bunzel et al., 2018;
4 Petty et al., 2018, 2020)).

5
6 Observations of regional changes in sea-ice thickness vary in quality. Analysis of submarine data in the
7 central Arctic Ocean suggests that sea ice there has thinned by about 75 cm compared to the mid-1970s
8 (Section 2.3.2.1.1). For smaller regions, data are too sparse to allow for quantitative estimates of long-term
9 trends (King et al., 2017; Rösel et al., 2018), but a clear thinning signal over 10 to 20 years has been found
10 for sea ice in Fram Strait (Spren et al., 2020), north of Canada (Haas et al., 2017) and for landfast ice in
11 Kongsfjorden/Svalbard (Pavlova et al., 2019). CMIP5 models and reanalyses fail to capture the observed
12 distribution (Stroeve et al., 2014; Shu et al., 2015) and evolution (Chevallier et al., 2017) of Arctic sea-ice
13 thickness. Most CMIP6 models do not capture the observed spatial distribution of sea-ice thickness
14 realistically (Wei et al., 2020). This leads to *low confidence* in estimates of thickness from reanalyses and
15 from CMIP5 and CMIP6 models, and in these models' projections of sea-ice volume.

18 9.3.2 Antarctic Sea Ice

19 9.3.2.1 Antarctic sea-ice coverage

20
21
22 The SROCC (Meredith et al., 2019) assessed that there was no significant trend in annual mean Antarctic
23 sea-ice area over the period of reliable satellite retrievals starting in 1979 (*high confidence*). The updated
24 time series is consistent with this assessment. It includes a maximum sea-ice area in 2014, a substantial
25 decline from then until the minimum sea-ice area in 2017, and an increase in sea-ice area since then
26 (Schlosser et al., 2018; Maksym, 2019; Parkinson, 2019) (Figure 9.15, Figure 2.20). As assessed in Section
27 2.3.2.1.2, the possible significance of the increase in mean Antarctic sea-ice area over the shorter period
28 1979 to 2014 (Figure 2.20) (Simmonds, 2015; Comiso et al., 2017a) is unclear. This is because of
29 observational uncertainty (see section 9.3.1.1), large year-to-year fluctuations in all months (Figure 9.15),
30 and limited understanding of the processes and reliability of year-to-year correlation of Antarctic sea-ice area
31 (Yuan et al., 2017).

32
33 As assessed by the SROCC, the evolution of mean Antarctic sea-ice area is the result of opposing regional
34 trends (*high confidence*), with slightly decreasing sea-ice cover during the period 1979 to 2019 in the
35 Amundsen Sea and the Bellingshausen Sea, particularly during summer, and slightly increasing sea-ice cover
36 in the eastern parts of the Weddell Sea and the Ross Sea (Figure 9.15). With the exception of the Ross Sea,
37 these trends are not significant considering the large variability of the time series (Yuan et al., 2017).

38
39 The SROCC assessed that the regional trends are closely related to meridional wind trends (*high confidence*).
40 This is the case as the regional trends in the maximum northward extent of the ice cover (Figure 9.15) are
41 determined by the balance between the northward advection of the ice that is formed in polynyas near the
42 continental margin, and the lateral and subsurface melting through oceanic heat fluxes. The advection of the
43 sea ice is strongly correlated with winds and cyclones (Schemm, 2018; Vichi et al., 2019; Alberello et al.,
44 2020). Accordingly, the increasing sea-ice area in the Ross Sea can be linked to a strengthening of the
45 Amundsen Sea low (e.g., (Holland et al., 2017b, 2018)), while other regional sea-ice trends in the austral fall
46 can be linked to changes in westerly winds, cyclone activity and the Southern Annular Mode (SAM) in
47 summer and spring (Doddridge and Marshall, 2017; Holland et al., 2017a; Schemm, 2018). In addition to the
48 wind-driven changes, increased near-surface ocean stratification (Section 9.2.1.3) has contributed to the
49 observed increase in sea-ice coverage (e.g., (Purich et al., 2018; Zhang et al., 2019b)) as it tends to cool the
50 surface ocean (Sections 9.2.1.1, 9.2.3.2). The changes in stratification result partly from surface freshening
51 (De Lavergne et al., 2014) (associated with increased northward sea-ice advection (Haumann et al., 2020)
52 and/or melting of the Antarctic ice sheet (e.g., (Haumann et al., 2020; Jeong et al., 2020; Mackie et al.,
53 2020)) (*medium confidence*)) and are amplified by local ice-ocean feedbacks (Goosse and Zunz, 2014;
54 Lecomte et al., 2017; Goosse et al., 2018). In the Amundsen Sea, strong ice-shelf melting can cause local
55 sea-ice melt next to the ice-shelf front by entraining warm Circumpolar Deep Water to the ice-shelf cavity

1 and surface ocean (*medium confidence*) (Sections 9.2.3.2, 9.4.2.2) (Jourdain et al., 2017; Merino et al.,
 2 2018). It has also been suggested that the observed regional increase in sea ice coverage since 1979 results
 3 from a long-term Southern Ocean surface cooling trend (e.g., (Kusahara et al., 2019; Jeong et al., 2020)) but
 4 the importance of this mechanism for the observed sea-ice evolution is unclear owing to intricate feedbacks
 5 between sea-ice change and surface cooling (Haumann et al., 2020). The importance of changing wave
 6 activity (Section 9.6.4.2; Kohout et al., 2014; Bennetts et al., 2017; Roach et al., 2018b) on sea ice is unclear
 7 due to limited process understanding. In summary, there is *high confidence* that regional Antarctic trends are
 8 primarily caused by changes in sea-ice drift and decay, with *medium confidence* in a dominating role of
 9 changing wind pattern. The precise relative contribution of individual drivers remains uncertain because of
 10 limited observations, disagreement between models, unresolved processes, and temporal and spatial remote
 11 linkages caused by sea-ice drift (Section 9.2.3.2, (Pope et al., 2017)).

12
 13 Recent research has confirmed the SROCC assessment of atmospheric and oceanic drivers of the sea-ice
 14 decline from 2014 to 2017, which can be linked to changes in both subsurface ocean heat flux (Meehl et al.,
 15 2019; Purich and England, 2019) and atmospheric circulation, with the latter partly related to teleconnections
 16 with the tropics (Meehl et al., 2019; Purich and England, 2019; Wang et al., 2019a). In the Weddell Sea,
 17 these changes caused in 2017 the re-emergence of the largest polynya over the Maud Rise since the 1970s
 18 (Campbell et al., 2019; Jena et al., 2019; Turner et al., 2020) (Section 9.2.3.2).

19
 20
 21 **[START FIGURE 9.15 HERE]**

22
 23 **Figure 9.15: Antarctic sea-ice historical records and CMIP6 projections.** Left: Absolute anomaly of observed
 24 monthly-mean Antarctic sea-ice area during the period 1979 to 2019 relative to the average monthly-
 25 mean Antarctic sea-ice area during the period 1979 to 2008. Right: Sea-ice coverage in the Antarctic as
 26 given by the average of the three most widely used satellite-based estimates for September and February,
 27 which usually are the months of maximum and minimum sea-ice coverage, respectively. First column:
 28 Mean sea-ice coverage during the decade 1979-1988. Second column: Mean sea-ice coverage during the
 29 decade 2010-2019. Third column: Absolute change in sea-ice concentration between these two decades,
 30 with grid lines indicating non-significant differences. Fourth column: number of available CMIP6 models
 31 that simulate a mean sea-ice concentration above 15 % for the decade 2045-2054. The average
 32 observational record of sea-ice area is derived from the UHH sea-ice area product (Doerr et al., 2021),
 33 based on the average sea-ice concentration of OSISAF/CCI (OSI-450 for 1979-2015, OSI-430b for 2016-
 34 2019)(Lavergne et al., 2019), NASA Team (version 1, 1979-2019)(Cavalieri et al., 1996) and Bootstrap
 35 (version 3, 1979-2019)(Comiso, 2017) that is also used for the figure panels showing observed sea-ice
 36 concentration. Further details on data sources and processing are available in the chapter data table (Table
 37 9.SM.9).

38
 39 **[END FIGURE 9.15 HERE]**

40
 41
 42 The AR5 (Collins et al., 2013) and the SROCC found *low confidence* in future projections of Antarctic sea
 43 ice. This includes the projected mitigation of the sea-ice loss by stratospheric ozone recovery (Smith et al.,
 44 2012) and by an increased freshwater input from melting of the Antarctic ice sheet (Bronselaeer et al., 2018).
 45 Compared to the interannual variability during the satellite record from 1979 onwards, models simulate too
 46 much variability both in CMIP5 (Zunz et al., 2013) and in CMIP6 (Roach et al., 2020). The seasonal cycle in
 47 sea-ice coverage is misrepresented in most CMIP5 (e.g., (Holmes et al., 2019)) and CMIP6 models (Roach et
 48 al., 2020), but the multi-model mean seasonal cycle in CMIP5 and CMIP6 agrees well with observations
 49 (Shu et al., 2015; Roach et al., 2020). Most CMIP5 models do not realistically simulate the evolution of
 50 Antarctic sea-ice volume (Shu et al., 2015) and consistently overestimate the amount of low concentration
 51 sea ice and underestimate the amount of high concentration sea ice (Roach et al., 2018a). CMIP6 models, in
 52 contrast, simulate a more realistic distribution of regional sea-ice coverage (Roach et al., 2020). Most CMIP5
 53 models poorly represent Antarctic sea-ice drift (e.g., (Schroeter et al., 2018; Holmes et al., 2019)), affecting
 54 simulated historical trends, with models that simulate a strong sea-ice motion showing more variability in
 55 sea-ice coverage than models with weaker sea-ice motion (Schroeter et al., 2018). Owing to *limited*
 56 *agreement* between model simulations and observations, limited reliable observations on a process level and

1 a lack of process understanding of the substantial spread in CMIP5 and CMIP6 model simulations, there
2 remains *low confidence* in existing future projections of Antarctic sea-ice evolution.

3
4 The discrepancy between the modelled and observed evolution of Antarctic sea ice has been related by the
5 SROCC to deficiencies in stratification, freshening by ice shelf melt water, clouds, and other wind and ocean
6 driven processes. Recent studies highlight the possible mis-representation of freshwater fluxes from ice
7 shelves (Jeong et al., 2020), and the possible effect of the low resolution of most models (Sidorenko et al.,
8 2019), even though lower-resolution models are in principle capable of a realistic simulation of the seasonal
9 sea-ice budgets in the Southern Ocean (Holmes et al., 2019). The relative importance of these possible
10 reasons for model-shortcomings remains unclear (see section 3.4.1.2 for details).

11
12 The analysis and understanding of the long-term evolution of the Antarctic sea-ice cover is hindered by the
13 scarcity of observational records before the satellite period and the scarcity of paleo records (see section
14 2.3.2.1.2 for further details). Such long records are particularly relevant given that the Southern Ocean
15 response to external forcing takes longer than the length of the available direct observational record (Goosse
16 and Renssen, 2001; Armour et al., 2016). There is only *limited evidence* for large-scale decadal fluctuations
17 in sea-ice coverage caused by large-scale temperature and wind forcing. Sparse direct pre-satellite
18 observations suggest a decrease in sea-ice coverage from the 1950s to the 1970s (Fan et al., 2014). Paleo-
19 proxy data indicate that, on multi-decadal to multi-centennial time scales, sea-ice coverage of the Southern
20 Ocean follows large-scale temperature trends (e.g., (Crosta et al., 2018; Chadwick et al., 2020; Lamping et
21 al., 2020)), for example linked to fluctuations in the El Niño Southern Oscillation and Southern Annular
22 Mode (Crosta et al., 2021), and that during the Last Glacial Maximum Antarctic sea ice extended to about
23 the polar front latitude in most regions during winter, whereas the extent during summer is less well
24 understood (e.g., (Benz et al., 2016; Xiao et al., 2016; Nair et al., 2019)).

25
26 Regionally, proxy data from ice cores consistently indicate that the increase of sea-ice area in the Ross Sea
27 and the decrease of sea-ice area in the Bellingshausen Sea are part of longer centennial trends and exceed
28 internal variability on multi-decadal time-scales (e.g., (Thomas et al., 2019; Tesi et al., 2020)) (*medium*
29 *confidence*). These centennial trends are consistent with simulations from CMIP5 models (Hobbs et al.,
30 2016a; Jones et al., 2016b; Kimura et al., 2017).

31
32 There is *low confidence* in the attribution of the observed changes in Antarctic sea-ice area (Section 3.4.1.2).
33 Based on the available evidence, the lack of a negative trend of Antarctic sea-ice area despite substantial
34 global warming in recent decades has been attributed to internal variability in analyses of the observational
35 record (Meier et al., 2013; Gallaher et al., 2014; Gagné et al., 2015b), reconstructions from early
36 observations (Fan et al., 2014; Edinburgh and Day, 2016) and proxy data (Hobbs et al., 2016a), and model
37 simulations (Turner et al., 2013; Zunz et al., 2013; Zhang et al., 2019c). Nonetheless, without accurate
38 simulations of observed changes, the possible contribution of anthropogenic forcing to the regional changes
39 in sea-ice area remains unclear (Hosking et al., 2013; Turner et al., 2013; Haumann et al., 2014; Zhang et al.,
40 2019c)

41
42 The attribution of the observed trends in atmospheric and oceanic forcing is also uncertain because of limited
43 observational records and discrepancies between modelled and observed evolution of the sea-ice cover. More
44 specifically, there is contrasting evidence for a direct role of stratospheric ozone depletion on the observed
45 changes in atmospheric circulation (Haumann et al., 2014; England et al., 2016; Landrum et al., 2017). In
46 contrast, there is *high confidence* that multi-decadal variations in the tropical Pacific and in the Atlantic
47 affect the Amundsen Sea low (Li et al., 2014; Kwok et al., 2016; Meehl et al., 2016; Purich et al., 2016;
48 Simpkins et al., 2016), while other modes of climate variability (Annex IV) affect, for example, Southern
49 Ocean cyclone activity (Simpkins et al., 2012; Cerrone et al., 2017; Schemm, 2018).

50 51 52 9.3.2.2 *Antarctic sea-ice thickness*

53
54 The SROCC assessed that observations are too sparse to reliably estimate long-term trends in Antarctic sea-
55 ice thickness. This remains true, and only qualitative statements on prevailing thicknesses are possible. Data

1 from ICESat-1 laser altimetry (Kurtz and Markus, 2012), from Operation IceBridge (Kwok and Kacimi,
2 2018), and long-term ship-board observations collected in the ASPeCt data set (Worby et al., 2008) suggest
3 that sea ice thicker than 1 m prevails in regions of multi-year ice along the eastern coast of the Antarctic
4 Peninsula in the Weddell Sea, in the high-latitude embayment of the Weddell Sea, and along the coast of the
5 Amundsen Sea, with remaining regions dominated by thinner first year sea ice (*high confidence*). Regional
6 patterns in ice thickness are affected by large snow deposition and resulting snow-ice formation (Massom et
7 al., 2001; Maksym and Markus, 2008), and deformation, ridging, and rafting that regionally cause formation
8 of very thick sea ice (Massom et al., 2006; Williams et al., 2015a). In addition, near ice shelves a sub-ice
9 platelet layer from supercooled water can significantly increase sea-ice thickness (Hoppmann et al., 2020;
10 Haas et al., 2021). Regarding snow thickness, observations are too sparse in space and time to reliably
11 estimate changes across Southern Ocean sea ice (Webster et al., 2018).

12
13 There is *low confidence* in the long-term trend of Antarctic sea-ice thickness. Both ASPeCt and ICESat-1
14 measurements are biased low in regions with thick ice (Kern and Spreen, 2015), compared to results from
15 reanalyses (Massonnet et al., 2013; Haumann et al., 2016) and observations with autonomous vehicles under
16 sea ice (Williams et al., 2015a). Estimates of sea-ice thickness from Cryosat-2 do not substantially reduce
17 uncertainty, primarily because of the unknown snow thickness and radar scattering above the snow-ice
18 interface (Bunzel et al., 2018; Kwok and Kacimi, 2018; Kacimi and Kwok, 2020). Isolated in-situ time series
19 show no clear long-term trend in landfast ice thickness in the Weddell Sea (Arndt et al., 2020). Reanalyses
20 suggest overall increasing sea-ice thickness and volume between 1980 and 2010 (Holland et al., 2014;
21 Zhang, 2014; Massonnet et al., 2015), while CMIP5 (Shu et al., 2015; Schroeter et al., 2018) and CMIP6
22 models simulate a decrease in Antarctic sea-ice volume over the historical period. Because of this
23 discrepancy, and the unclear reliability of the reanalyses (Uotila et al., 2019), there is *low confidence* in
24 CMIP5 and CMIP6 simulated future Antarctic sea-ice thickness.

25 26 27 **9.4 Ice Sheets**

28 29 **9.4.1 Greenland Ice Sheet**

30 31 **9.4.1.1 Recent observed changes**

32
33 In this section we present regional mass change time series for the Greenland Ice Sheet and assess the
34 different processes causing the increase in mass loss. The vast increase in observational products from
35 various platforms (e.g. GRACE, PROMICE, ESA-CCI, NASA MEaSUREs) provide a consistent and clear
36 picture of a shrinking Greenland Ice Sheet (Colgan et al., 2019; Mottram et al., 2019; Mouginit et al., 2019;
37 King et al., 2020; Mankoff et al., 2020; Moon et al., 2020; Sasgen et al., 2020; The IMBIE Team, 2020;
38 Velicogna et al., 2020). Section 2.3.2.4.1 provides an updated estimate of the total Greenland Ice Sheet mass
39 change in a global context (Figure 2.24). A paleo perspective on Greenland Ice Sheet evolution is presented
40 in Section 9.6.2 with estimated ice sheet extent at different times shown in Figure 9.17.

41
42 For the 20th century, the SROCC (Meredith et al., 2019) presented one reconstruction for 1900-1983 and
43 estimated mass change for the Greenland Ice Sheet and its peripheral glaciers for the period 1901-1990.
44 Since the SROCC, a comprehensive new study has extended the satellite record back to 1972 (Mouginit et
45 al., 2019, Figure 9.16). The rate of change of ice sheet mass was positive (i.e., it gained mass) in 1972-1980
46 (47 ± 21 Gt yr⁻¹) and then negative (i.e., it lost mass) (-51 ± 17 Gt yr⁻¹ and -41 ± 17 Gt yr⁻¹) in 1980-1990 and
47 1990-2000, respectively. Other ice discharge time series starting in 1985 (King et al., 2018, 2020, Mankoff et
48 al., 2019, 2020) agree with (Mouginit et al., 2019, Figure 9.16). There is *limited evidence* of temporally and
49 spatially heterogeneous Greenland outlet glacier evolution during 20th century (Lea et al., 2014; Lüthi et al.,
50 2016; Andresen et al., 2017; Khan et al., 2020; Vermassen et al., 2020). Historical photographs (Khan et al.,
51 2020) show large mass losses of Jakobshavn and Kangerlussuaq glaciers in West Greenland from 1880 until
52 the 1940s, exceeding their 21st century mass loss, whereas the Helheim Glacier in East Greenland remained
53 stable, gained mass in the 1990s then rapidly lost mass after 2000. Together, these 3 large outlet glaciers,
54 draining ~12% of the ice sheet surface area, have lost 22 ± 3 Gt yr⁻¹ in the period 1880-2012 (Khan et al.,
55 2020). Overall, these studies provide a variable picture of the Greenland Ice Sheet mass change in the 20th

1 century. The updated mass loss of Greenland Ice Sheet including peripheral glaciers for period 1901-1990 is
2 120 [70–170] Gt yr⁻¹ (see Table 9.5 and Figures 9.16, 9.17).

3
4 Post-1992, the SROCC stated that it is *extremely likely* that the rate of mass change of Greenland Ice Sheet
5 was more negative during 2012-2016 than during 1992-2001, with *very high confidence* that summer melting
6 has increased since the 1990s to a level unprecedented over at least the last 350 years. Since the SROCC, the
7 updated synthesis of satellite observations by the Ice Sheet Mass Balance Intercomparison Exercise (The
8 IMBIE Team, 2020) and the GRACE Follow-On (GRACE-FO) Mission (Abich et al., 2019; Kornfeld et al.,
9 2019), have confirmed the mass change record and the record has been extended to 2020 (The IMBIE team,
10 2021) as presented in 2.3.2.4.. The Greenland Ice Sheet lost 4890 [4140–5640] Gt of ice between 1992 and
11 2020, causing sea level to rise by 13.5 [11.4–15.6] mm (The IMBIE Team, 2021) (Section 2.3.2.4.1; Figure
12 9.16, Table 9.5). The IMBIE Team (2020) estimates are consistent with other post-AR5 reviews (Figure
13 9.17, Table 9.SM.1) (Bamber et al., 2018a; Cazenave et al., 2018; Mouginit et al., 2019; Slater et al., 2021).
14 Recent GRACE-FO data (Sasgen et al., 2020; Velicogna et al., 2020) show that after two cold summers in
15 2017 and 2018, with relatively moderate mass change of about -100 Gt yr⁻¹, the 2019 mass change (-532 ±
16 58 Gt yr⁻¹) was the largest annual mass loss in the record. The *high agreement* across a variety of methods
17 confirms the SROCC and Chapter 2 assessments. The mass-loss rate was on average 39 [-3 to 80] Gt yr⁻¹
18 over the period 1992–1999, 175 [131 to 220] Gt yr⁻¹ over the period 2000–2009 and 243 [197 to 290] Gt yr⁻¹
19 over the period 2010–2019 (see Table 9.SM.1).

20
21
22 **[START FIGURE 9.16 HERE]**

23
24 **Figure 9.16: Mass changes and mass change rates for Greenland and Antarctic ice sheet regions.** (Upper Left)
25 Time series of mass changes in Greenland for each of the major drainage basins shown in the inset figure
26 (Bamber et al., 2018b; Mouginit et al., 2019) for the periods 1972 – 2018 and 1992-2018. (Upper Right)
27 Time series of mass changes for three portions of Antarctica (Bamber et al., 2018b) for the period 1992 –
28 2018. (Lower rows) Estimates of mass change rates of surface mass balance, discharge and mass balance in
29 seven Greenland regions (Bamber et al., 2018b; Mankoff et al., 2019; Mouginit et al., 2019; King et
30 al., 2020). Estimates of mass change rates of surface mass balance, discharge and mass balance for three
31 regions of Antarctica (Bamber et al., 2018b; The IMBIE Team et al., 2018; Rignot et al., 2019). Further
32 details on data sources and processing are available in the chapter data table (Table 9.SM.9).

33
34 **[END FIGURE 9.16 HERE]**

35
36
37 The SROCC assessed with *high confidence* that surface mass balance (SMB), rather than discharge, has
38 started to dominate the mass loss of the Greenland Ice Sheet (due to increased surface melting and runoff),
39 increasing from 42% of the total mass loss for 2000–2005 to 68% for 2009–2012. While these estimates
40 have been confirmed since the SROCC (Mouginit et al., 2019), the new longer record, as well as further
41 comprehensive studies (Khan et al., 2015; Colgan et al., 2019; Mottram et al., 2019; The IMBIE Team,
42 2020) and detailed discharge records (King et al., 2020; Mankoff et al., 2020) reveal a more complex picture
43 than the continuous trajectory this statement may have implied. Discharge was relatively constant from
44 1972-1999, varying by around 6% for the whole ice sheet, while SMB varied by over a factor of two
45 interannually, leading to either mass gain or loss in a given year (Figure 9.16). During 2000-2005, the rate of
46 discharge increased by 18%, then remained fairly constant again (increasing by 6% from 2006-2018). After
47 2000, SMB decreased more rapidly than discharge increased. In summary, the consistent temporal pattern in
48 these longer datasets leads to *high confidence* that the Greenland Ice Sheet mass losses are increasingly
49 dominated by SMB, but there is *high confidence* that mass loss varies strongly, due to large interannual
50 variability in SMB.

51
52 On a regional scale, the surface elevation is lowering in all regions, and widespread terminus and calving
53 front retreats have been observed (with no glaciers advancing) (Mottram et al., 2019; Moon et al., 2020). The
54 largest mass losses have occurred along the west coast and in southeast Greenland (Figure 9.16),
55 concentrated at a few major outlet glaciers (Mouginit et al., 2019; Khan et al., 2020). This regional pattern is
56 consistent with independent Global Navigation Satellite System (GNSS) observations from the Greenland

1 GPS network which show elastic bedrock uplift of tens of centimetres between 2007-2019 as a result of
 2 ongoing ice mass loss (Bevis et al., 2019). The regional time series (Figures 9.16, Atlas.30) show that SMB
 3 has been gradually decreasing in all regions while the increase in discharge in the southeast, central east,
 4 northwest and central west has been linked to retreating tidewater glaciers (Figure 9.16). In summary, the
 5 detailed regional records show an increase in mass loss in all regions after the 1980s, caused by both
 6 increases in discharge and decreases in SMB (*high confidence*), although the timing and patterns vary
 7 between regions. The largest mass loss occurred in the northwest and the southeast of Greenland (*high*
 8 *confidence*).

9
 10
 11 **[START FIGURE 9.17 HERE]**

12
 13 **Figure 9.17: Greenland Ice Sheet cumulative mass change and equivalent sea level contribution.** (a) A p-box
 14 (Section 9.6.3.2) based estimate of the range of values of paleo Greenland ice sheet mass and sea level
 15 equivalents relative to present day and the median over all central estimates (Simpson et al., 2009; Argus
 16 and Peltier, 2010; Fyke et al., 2011; Robinson et al., 2011; Colville et al., 2011; Dolan et al., 2011; Born
 17 and Nisancioglu, 2012; Miller et al., 2012b; Helsen et al., 2013; Nick et al., 2013; Quiquet et al., 2013;
 18 Stone et al., 2013; Dahl-Jensen et al., 2013; Lecavalier et al., 2014; Robinson and Goelzer, 2014;
 19 Colleoni et al., 2014; Koenig et al., 2015; Peltier et al., 2015; Calov et al., 2015; Stuhne and Peltier, 2015;
 20 Vizcaino et al., 2015; Calov et al., 2018; Dutton et al., 2015; Goelzer et al., 2016; Khan et al., 2016; Yau
 21 et al., 2016; de Boer et al., 2017; Simms et al., 2019); and (b) cumulative mass loss (and sea level
 22 equivalent) from 1972 (Mouginot et al., 2019) and 1992 (Bamber et al., 2018b; The IMBIE Team, 2019),
 23 the estimated mass loss from 1840 (Box and Colgan, 2013; Kjeldsen et al., 2015) indicated with a shaded
 24 box and projections from ISMIP6 by 2100 under RCP8.5/SSP5-8.5 and RCP2.6/SSP1-2.6 scenarios (thin
 25 lines from (Goelzer et al., 2020; Edwards et al., 2021; Payne et al., 2021) and *likely* and *very likely* range
 26 of the ISMIP6 emulation (shades and bold line (Edwards et al., 2021)) are shown as a timeseries.
 27 Schematic interpretations of individual reconstructions (Lecavalier et al., 2014; Goelzer et al., 2016;
 28 Berends et al., 2019) of the spatial extent of the Greenland ice sheet are shown for the (c) mid-Pliocene
 29 Warm Period, (d) the Last Interglacial and (e) the Last Glacial Maximum: grey shading shows extent of
 30 grounded ice. Maps of mean elevation changes (f) 2010–2017 derived from CryoSat 2 radar altimetry
 31 (Bamber et al., 2018b) and (g) ISMIP6 model mean (2093–2100) projected changes for the MIROC5
 32 climate model under the RCP8.5 scenario (Goelzer et al., 2020). Further details on data sources and
 33 processing are available in the chapter data table (Table 9.SM.9).

34
 35 **[END FIGURE 9.17 HERE]**

36
 37
 38 The SROCC stated with *high confidence* that variability in large-scale atmospheric circulation is an
 39 important driver of short-term SMB changes for the Greenland Ice Sheet. This effect of atmospheric
 40 circulation variability on both precipitation and melt rates (and the SROCC assessment) is confirmed by
 41 more recent publications (Välisuo et al., 2018; Zhang et al., 2019a; Velicogna et al., 2020). The strong mass
 42 loss in 2019 (Cullather et al., 2020; Hanna et al., 2020; Tedesco and Fettweis, 2020) was driven by highly
 43 anomalous atmospheric circulation patterns, both on daily (Cullather et al., 2020) and seasonal timescales
 44 (Tedesco and Fettweis, 2020). Although surface melt is anticorrelated with the summer North Atlantic
 45 Oscillation index (Välisuo et al., 2018; Ruan et al., 2019; Sherman et al., 2020), especially in West
 46 Greenland (Bevis et al., 2019), Greenland Ice Sheet melt is more strongly correlated with the Greenland
 47 Blocking Index (Hanna et al., 2016, 2018) than with the summer North Atlantic Oscillation index (Huai et
 48 al., 2020).

49
 50 The SROCC did not assess the role of cloud changes in detail. Studies since the AR5 have shown that higher
 51 incident shortwave radiation in conjunction with reduced cloud cover leads to increased melt rates,
 52 particularly over the low albedo ablation zone in the southern part of the Greenland Ice Sheet (Hofer et al.,
 53 2017; Niwano et al., 2019; Ruan et al., 2019). Conversely, an increase in cloud cover over the high-albedo
 54 central parts of the ice sheet, leading to higher downwelling longwave radiation, was shown to lead either to
 55 increased melt (Bennartz et al., 2013) or reduced refreezing of meltwater (van Tricht et al., 2016). The
 56 elevation dependence of the cloud radiative effect and its control on surface meltwater generation and
 57 refreezing (Wang et al., 2019c; Hahn et al., 2020) can induce a spatially consistent response of the integrated

1 Greenland Ice Sheet melt to dominant patterns of cloud and atmospheric variability. The short- and longwave
2 radiation effects on surface melt by clouds have been shown to compensate for each other during events of
3 strong atmospheric rivers and the increase in melt is caused by increased sensible heat fluxes during such
4 events (Mattingly et al., 2020). In summary, there is *medium confidence* that cloud cover changes are an
5 important driver of the increasing melt rates in the southern and western part of the Greenland Ice Sheet.
6

7 The SROCC stated with *high confidence* that positive albedo feedbacks contributed substantially to the post-
8 1990s Greenland Ice Sheet melt increase. Several, mostly positive, feedbacks involving surface albedo
9 operate on ice sheets (e.g., Fyke et al., 2018). Melt amplification by the observed increase of bare ice
10 exposure through snowline migration to higher parts of the ice sheet since 2000 (Shimada et al., 2016; Ryan
11 et al., 2019) was five times stronger than the effect of hydrological and biological processes that lead to
12 reduced bare ice albedo (Ryan et al., 2019). Impurities, in part biologically active (Ryan et al., 2018), have
13 been observed to lead to albedo reduction (Stibal et al., 2017) and are estimated to have increased runoff
14 from bare ice in the south-western sector of the Greenland Ice Sheet by about 10% (Cook et al., 2020). In
15 summary, new studies confirm that there is *high confidence* that the Greenland Ice Sheet melt increase since
16 about 2000 has been amplified by positive albedo feedbacks, with the expansion of bare-ice extent being the
17 dominant factor, and albedo in the bare-ice zone being primarily controlled by distributed biologically active
18 impurities (see also Section 7.3.4.3).
19

20 The SROCC reported with *medium confidence* that around half of the 1960-2014 Greenland Ice Sheet
21 surface meltwater ran off, while most of the remainder infiltrated firn and snow, where it either refroze or
22 accumulated in firn aquifers. Studies since SROCC show a decrease of firn air content between 1998-2008
23 and 2010-2017 (Vandecrux et al., 2019) in the low-accumulation percolation area of western Greenland,
24 reducing meltwater retention capacity. Moreover, meltwater infiltration into firn can be strongly limited by
25 low-permeability ice slabs created by refreezing of infiltrated meltwater (Machguth et al., 2016). Recent
26 observations and modelling efforts indicate that rapidly expanding low-permeability layers have led to an
27 increase in runoff area since 2001 (MacFerrin et al., 2019). In summary, there is *medium confidence* that
28 meltwater storage and refreezing can temporarily buffer a large-scale melt increase but limiting factors have
29 been identified.
30

31 The SROCC reported that there was *medium confidence* that ocean temperatures near the grounding zone of
32 tidewater glaciers are critically important to their calving rate, but there was *low confidence* in understanding
33 their response to ocean forcing. The increase in ice discharge in the late 1990s and early 2000s (Mouginot et
34 al., 2019; King et al., 2020; Mankoff et al., 2020) has been associated with a period of widespread tidewater
35 glacier retreat (Murray et al., 2015; Wood et al., 2021) and speed up (Moon et al., 2020). Since the SROCC,
36 new studies provide strong evidence for rapid submarine melting at tidewater glaciers (Sutherland et al.,
37 2019; Wagner et al., 2019; Bunce et al., 2020; Jackson et al., 2020b). Changes in submarine melting and
38 subglacial meltwater discharge can trigger increased ice discharge by reducing the buttressing to ice flow
39 and promoting calving (Benn et al., 2017; Todd et al., 2018; Ma and Bassis, 2019; Mercenier et al., 2020);
40 through undercutting (Rignot et al., 2015; Slater et al., 2017b; Wood et al., 2018; Fried et al., 2019) and
41 frontal incision (Cowton et al., 2019). Warming ocean waters have been implicated in the recent thinning
42 and breakup of floating ice tongues in northeastern and northwestern Greenland (Mouginot et al., 2015;
43 Wilson et al., 2017; Mayer et al., 2018; Washam et al., 2018; An et al., 2021; Wood et al., 2021). On decadal
44 timescales, tidewater glacier terminus position correlates with submarine melting (Slater et al., 2019). Over
45 shorter timescales, individual glaciers or clusters of glaciers can behave differently and asynchronously
46 (Bunce et al., 2018; Vijay et al., 2019; An et al., 2021), and there are not always clear associations between
47 water temperature and glacier calving rates (Motyka et al., 2017), retreat or speedup (Joughin et al., 2020;
48 Solgaard et al., 2020). Variations in ice mélange at the front of a glacier, associated with changes in ocean
49 and air temperature, have also emerged as a plausible control on calving (Burton et al., 2018; Xie et al.,
50 2019; Joughin et al., 2020). In summary, there is *high confidence* that warmer ocean waters and increased
51 subglacial discharge of surface melt at the margins of marine-terminating glaciers increase submarine melt,
52 which leads to increased ice discharge, and *medium confidence* that this contributed to the increased rate of
53 mass loss from Greenland particularly in the period 2000-2010 when increased discharge was observed in
54 the southeast and northwest.
55

1 The SROCC reported that accurate bedrock topography is required for understanding and projecting the
2 glacier response to ocean forcing. Accurate bathymetry is essential for both establishing which water masses
3 enter glacial fjords and for reliable estimates of the submarine melt rates experienced by tidewater glaciers
4 (Schaffer et al., 2020; Slater et al., 2020b; Wood et al., 2021). Subglacial and lateral topography is known to
5 strongly modulate tidewater glacier dynamics and the sensitivity of tidewater glaciers to climatic forcing
6 (Enderlin et al., 2013; Catania et al., 2018). Bathymetric mapping around the ice sheet has greatly improved
7 with direct and gravimetric surveys (Millan et al., 2018; An et al., 2019a, 2019b; Jakobsson et al., 2020)
8 leading to the improvement of Greenland-wide bathymetric and topographic mapping (e.g., Morlighem et al.,
9 2017). However, large uncertainties in ice thickness remain for around half of the outlet glaciers (Mouginot
10 et al., 2019; Wood et al., 2021) and sea-ice covered and iceberg-packed regions remain poorly sampled near
11 glacier termini (Morlighem et al., 2017). There is *high confidence* that bathymetry (governing the water
12 masses that flow into fjord cavities) and fjord geometry and bedrock topography (controlling ice dynamics)
13 modulate the response of individual glaciers to climate forcing.

14
15 The AR5 assessed that it is *likely* that anthropogenic forcing contributed to the surface melting of Greenland
16 since 1993 (Bindoff et al., 2013). Section 3.4.3.2 assesses that it is *very likely* that human influence has
17 contributed to the observed surface melting of the Greenland Ice Sheet over the past two decades, and there
18 is *medium confidence* of an anthropogenic contribution to recent mass loss from Greenland.

21 9.4.1.2 Model evaluation

22
23 The SROCC (Oppenheimer et al., 2019) stated that substantial challenges remained for modelling of both the
24 Greenland surface mass balance and the dynamical ice sheet. Since the SROCC, further insights into
25 modelling of the Greenland ice sheet has come from model intercomparison studies of both the surface mass
26 balance (Fettweis et al., 2020) and dynamical ice sheets (Goelzer et al., 2020). Further aspects relevant to the
27 forcing of the ice sheet from large scale global climate models and regional climate models are discussed in
28 Box 9.3 and Section Atlas.11.2.

29
30 The SROCC stated that climate model simulations of Greenland surface mass balance (SMB) had improved
31 since the AR5 giving *medium confidence* in the ability of climate models to simulate changes in Greenland
32 SMB. Since the SROCC, a multi-model intercomparison study (Fettweis et al., 2020) of regional and global
33 climate models has shown that the greatest inter-model spread occurs in the ablation zone, due to
34 deficiencies in an accurate model representation of the ablation zone extent and processes related to surface
35 melt and runoff, confirming the SROCC statement that bare-ice model uncertainty is large (Ryan et al.,
36 2019). This intercomparison showed that simple, well-tuned SMB models using positive degree-day melt
37 schemes can perform as well as more complex physically-based models (Figure Atlas.30). Furthermore, the
38 ensemble-mean of the models produced the best estimate of the present-day SMB relative to observations
39 (particularly in the ablation zone). Further assessment of Greenland ice sheet regional SMB can be found in
40 Section Atlas 11.2.3. Recent progress confirms the SROCC assessment that there is *medium confidence* in
41 the ability of climate models to simulate changes in Greenland SMB.

42
43 The SROCC noted increased use of coupled climate-ice sheet models for simulating the Greenland ice sheet,
44 but also that remaining deficiencies in coupling between models of climate and ice sheets (e.g., low spatial
45 resolution) limited the adequate representation of the feedbacks between them. Some Earth System Models
46 now incorporate multi-layer snow models and full energy balance models (Punge et al., 2012; Cullather et
47 al., 2014; van Kampenhout et al., 2017; Alexander et al., 2019a; van Kampenhout et al., 2020) or use
48 elevation classes to compensate for their coarser resolution (Lipscomb et al., 2013; Sellevold et al., 2019;
49 Muntjewerf et al., 2020a, 2020b; Gregory et al., 2020). Resulting SMB simulations compare better with
50 Regional Climate Models and observations (Alexander et al., 2019b; van Kampenhout et al., 2020), but
51 remaining shortcomings lead to problems reproducing a present-day ice sheet state close to observations. In
52 summary, there is *medium confidence* in quantitative simulations of the present-day state of the Greenland
53 ice sheet in ESMs.

54
55 The SROCC (Meredith et al., 2019) stated that there is *low confidence* in understanding coastal glacier

1 response to ocean forcing because submarine melt rates, calving rates, bed and fjord geometry and the roles
2 of ice mélange and subglacial discharge are poorly understood. Ice-ocean interactions remain poorly
3 understood and difficult to model, with parameterizations often used for calving of marine-terminating
4 glaciers (Mercenier et al., 2018) and submarine and plume-driven melt (Beckmann et al., 2019). Due to the
5 difficulties of modelling the large number of marine-terminating glaciers and limited availability of high-
6 resolution bedrock data, the majority of recent modelling work on Greenland outlet glaciers is focused on
7 individual or a limited number of glaciers (Krug et al., 2014; Bondzio et al., 2016; Morlighem et al., 2016a;
8 Muresan et al., 2016; Bondzio et al., 2017; Choi et al., 2017; Beckmann et al., 2019), or a specific region
9 (Morlighem et al., 2019). Since the SROCC, using a flowline model that includes calving and submarine
10 melting, Beckmann et al. (2019) concluded that the AR5 upscaling of contributions from four of the largest
11 glaciers (Nick et al., 2013) overestimated the total glacier contribution from the Greenland ice sheet, due to
12 differences in response between large and small glaciers. The regional study of Morlighem et al. (2019)
13 confirms that ice-ocean interactions have the potential to trigger extensive glacier retreat over decadal
14 timescales as indicated by observations (Section 9.4.1.1). A focus in continental ice sheet models has been
15 the improved treatment of marine-terminating glaciers via inclusion of calving processes and freely moving
16 calving fronts (Aschwanden et al., 2019; Choi et al., 2021). An improved bedrock topographic dataset
17 (Morlighem et al., 2017) allows for ice discharge to be better captured for outlet glaciers in continental ice
18 sheet models and simulations indicate that bedrock topography controls the magnitude and rate of retreat
19 (Aschwanden et al., 2019; Rückamp et al., 2020). Overall, although there is *high confidence* that the dynamic
20 response of Greenland outlet glaciers is controlled by bedrock topography, there is *low confidence* in
21 quantification of future mass loss from Greenland triggered by warming ocean conditions due to limitations
22 in current understanding of ice-ocean interactions, its implementation in ice sheet models, and knowledge of
23 bedrock topography.

24
25 The SROCC (Oppenheimer et al., 2019) noted the progress made in Greenland Ice Sheet models since the
26 AR5. New since the SROCC is a focus on improved representation of the present-day state of the ice sheet
27 (Goelzer et al., 2018, 2020) (Box 9.3). Improvements are closely linked to the growing number and quality
28 of observations (Section 9.4.1.1), new techniques to generate internally consistent input data sets
29 (Morlighem et al., 2014, 2016b), wider use of data assimilation techniques (Larour et al., 2014, 2016; Perego
30 et al., 2014; Goldberg et al., 2015; Lee et al., 2015; Schlegel et al., 2015; Mosbeux et al., 2016), increased
31 model resolution (Aschwanden et al., 2016) and tuning of key processes such as calving (Choi et al., 2021).
32 A remaining challenge is *low confidence* in reproducing historical mass changes of the Greenland Ice Sheet
33 (Box 9.3). However, there is *medium confidence* in ice sheet models reproducing the present state of the
34 Greenland Ice Sheet leading to *medium confidence* in current ability to accurately project its future evolution.

35 36 37 9.4.1.3 Projections to 2100

38
39 The AR5 and the SROCC projected that changes in Greenland surface mass balance (SMB) will contribute
40 to sea level in 2100 by 0.03 (0.01 to 0.07) m SLE under RCP2.6 and 0.07 (0.03 to 0.16) m SLE under
41 RCP8.5. New since the SROCC are projections of SMB obtained by an Earth system model, two regional
42 climate models, and reconstructions based on temperature from the CMIP5 and CMIP6 ensembles (Hofer et
43 al., 2020; Noël et al., 2021). The range of sea level contribution from Greenland surface mass balance in
44 Noël et al. (2021) are comparable to the AR5 assessment when either CMIP5 or CMIP6 models are used
45 while Hofer et al., (2020) find a greater mass loss across all CMIP6 emission scenarios when compared to
46 CMIP5 scenarios. Using SSP5-8.5 instead of RCP8.5 increases the mean projected sea level from 2005-2100
47 by up to 0.06 m in the regional climate model simulations of Hofer et al., (2020) who attribute the difference
48 mainly to a greater Arctic amplification and associated cloud and sea ice feedbacks in the CMIP6 SSP5-8.5
49 simulations. In summary, these new projections with fixed ice sheet topography do not provide sufficient
50 evidence to change the AR5 and SROCC assessment.

51
52 Reviewing modelling studies since the AR5 (Church et al., 2013a), the SROCC (Oppenheimer et al., 2019)
53 assessed Greenland's contribution to future sea level to be relatively similar to the AR5 (Table 9.2). The
54 baseline for projections has shifted from 1986-2005, in the SROCC, to 1995-2014 in this report. Adjusted to
55 the new 1995-2014 baseline by subtracting 0.01 m, the SROCC projected a *likely* contribution of 0.07 (0.03

1 – 0.11) m SLE under RCP2.6 and 0.14 (0.08 – 0.27) m SLE under RCP8.5 by 2100. Since the SROCC, new
2 projections for the 21st century have included dynamic ice sheets coupled to Earth system models
3 (Muntjewerf et al., 2020a; Van Breedam et al., 2020) or regional atmospheric models (Le clec’h et al., 2019)
4 (Table 9.2). The coupled ESM-ice sheet CESM2-CISM2 model projects a sea level rise of 0.109 m in 2100
5 relative to 2015 under SSP5-8.5 (Muntjewerf et al., 2020a) and a similar contribution under the idealized 1%
6 yr⁻¹ increase in CO₂ scenario (Muntjewerf et al., 2020b). The CESM2-CISM2 simulations include ice sheet-
7 atmosphere interactions and ice sheet surface meltwater is routed to the ocean. The coupled regional
8 atmospheric model and ice sheet model (MAR-GRISLI) projects a sea level rise of 0.079 m in 2100 relative
9 to 2000 under RCP8.5 (Le clec’h et al., 2019). An Earth System model of lower complexity coupled to an
10 ice sheet model gives a sea level contribution of 0.025 to 0.064 m under RCP2.6 and 0.056 to 0.12 m under
11 RCP8.5 (the range is due to four simulations with different parameter sets for the atmosphere model) (Van
12 Breedam et al., 2020). Van Breedam et al., (2020) identify a simulation with a preferred parameter set, that
13 projects 0.034 m for RCP2.6 and 0.073 m for RCP8.5. Although the ocean does not directly force the ice sheet
14 models in these simulations, the new coupled models allow for interactions between ice sheet dynamics,
15 surface mass balance and local climate. The coupled projections fall within the lower bounds of the AR5 and
16 the SROCC, and as these studies do not prescribe ocean forcing directly, it is possible that the dynamic
17 response is underestimated.

18
19 Since the SROCC, projections of the Greenland Ice Sheet are also now available from ISMIP6 (Nowicki et
20 al., 2016, 2020a; Box 9.3; Annex II; Figure 9.17). The ISMIP6 multi-model projections are corrected with an
21 assessment of the historical dynamical response to pre-2015 climate forcing (Box 9.3). For the period 2015-
22 2100, the ISMIP6 uncorrected multi-model ensemble projects a sea level contributions ranging from 0.01 to
23 0.05 m under RCP2.6, 0.04 to 0.14 m under RCP8.5 (Goelzer et al., 2020), 0.02 to 0.06 m under SSP1-2.6
24 and 0.08 to 0.25 m under SSP5-8.5 (Payne et al., 2021)(Table 9.2). The higher mass loss in the SSPs is
25 attributed to a larger decrease in SMB due to the high climate sensitivity of the models used (Payne et al.,
26 2021). This finding is confirmed by (Choi et al., 2021), where CMIP6 SSP5-8.5 SMB leads to larger ice loss
27 than CMIP5 RCP8.5 while ice discharge is similar. As the ISMIP6 framework considers a subset of the
28 RCPs/SSPs and CMIP models, SSP-based projections have been inferred from multiple approaches. First,
29 the ISMIP6 CMIP5-forced (Goelzer et al., 2020) and CMIP6-forced (Payne et al., 2021) combined ensemble
30 projections were corrected with the historical trend (Box 9.3) using bootstrapping. Second, an emulator of
31 the ISMIP6 projections (Edwards et al., 1998, Box 9.3) is forced by distributions of global surface air
32 temperature for each SSP from a two-layer energy budget emulator (Supplementary Material 7.SM.2) and
33 then corrected with the historical trend in the same way. These two approaches result in projections that are
34 similar in their median values to the AR5 and SROCC projections (Table 9.2), but differ in their range.
35 Similar results are obtained when the AR5 parametric fit is applied to the ISMIP6 models (Table 9.2,
36 Supplementary Material 9.SM.4.4), which is used to estimate rates of change and post-2100 projections
37 (Sections 9.4.1.4, 9.6.3.2).

38
39 The SROCC noted that the study by Aschwanden et al., (2019) projects a significantly higher Greenland
40 contribution to sea level than the assessed *likely* range in the AR5 and the SROCC. Under RCP8.5,
41 Aschwanden et al., (2019) found that Greenland could contribute up to 0.33 m to sea level by 2100 relative
42 to 2000 (the ensemble member that best reproduces 2000-2015 mean surface mass balance from a regional
43 climate model projects Greenland mass losses of 0.08 m SLE under RCP2.6 and 0.18 m SLE under RCP8.5.)
44 The SROCC noted that the potentially high sea level in this study could be due to the assumption of spatially
45 uniform warming which can overestimate surface melt rates. However, it also reflects the *deep uncertainty*
46 surrounding atmospheric forcing, surface processes, submarine melt, calving and ice dynamics. Goelzer et
47 al., (2020) ascribe 40% of the ISMIP6 multi-model ensemble spread to ice sheet model uncertainty, 40% to
48 climate model uncertainty and 20% to ocean forcing uncertainty. We note that this finding reflects the
49 current challenges associated with the representation of ice-ocean interactions in models, and the uncertainty
50 in basal conditions (Section 9.4.1.2). However, this finding is consistent with the work of Aschwanden et al.,
51 (2019) and thus, there is *medium confidence* that uncertainty in mass loss from the Greenland Ice Sheet is
52 dominated by uncertainty in climate scenario and surface processes, whereas uncertainty in calving and
53 frontal melt play a minor role.

54
55 The SROCC stated that surface processes, rather than ice discharged into the ocean, will dominate Greenland

1 ice loss over the 21st century, regardless of the emissions scenario (*high confidence*). This is confirmed by
 2 the ISMIP6 projections (Goelzer et al., 2020; Payne et al., 2021). The projected mass loss of Greenland is
 3 predominantly due to increased surface meltwater and loss in refreezing capacity resulting in decreasing
 4 SMB (*high confidence*), concurrent with rising temperatures and darkening of the ice sheet surface (Fettweis
 5 et al., 2013; Vizcaino et al., 2015; Le clec'h et al., 2019; Muntjewerf et al., 2020b, 2020a; Sellevold and
 6 Vizcaíno, 2020). Mass changes due to SMB and outlet glacier dynamics are linked (Goelzer et al., 2013;
 7 Fürst et al., 2015; Rückamp et al., 2020) as mass loss by one process decreases mass loss by the other (for
 8 example, SMB removes ice before it can reach the marine glacier terminus). There is *medium confidence* that
 9 the mass loss through ice discharge will decrease in the future (Fürst et al., 2015; Aschwanden et al., 2019;
 10 Golledge et al., 2019a), because an increase in mass loss (via increased discharge or surface runoff) leads, in
 11 most areas, to a retreat of the glacier margin onto land above sea level, isolating the ice sheet from marine
 12 influence.

13
 14 In summary, it is *virtually certain* that the Greenland Ice Sheet will continue to lose mass this century under
 15 all emissions scenarios and *high confidence* that total mass loss by 2100 will increase with cumulative
 16 emissions. The sea level assessment (Section 9.6.3.3) is based on the emulated ISMIP6 projections allowing
 17 a more consistent approach to a wider range of climate and ocean forcings. The Greenland ice sheet is *likely*
 18 to contribute 0.06 (0.01 to 0.10) m under SSP1-2.6 and 0.13 (0.09 to 0.18) m under SSP5-8.5 by 2100
 19 relative to 1995-2014. These projections (as well as those of AR5 and SROCC) are lower than the study of
 20 (Aschwanden et al., 2019) (or the range of possible sea level changes resulting from structured expert
 21 judgement (Bamber et al., 2019); Section 9.6.3.2), contributing to the *deep uncertainty* in projected sea level
 22 (Box 9.4). There is however *high confidence* that the loss from Greenland will become increasingly
 23 dominated by SMB and surface melt, as the ocean-forced dynamic response of glaciers will diminish as
 24 marine margins retreat to higher grounds.

25
 26
 27 **[START TABLE 9.2 HERE]**

28
 29 **Table 9.2:** Projected sea level contributions in meters from the Greenland ice sheet by 2100 relative to 1995-2014,
 30 unless otherwise stated, for selected RCP and SSP scenarios. Italics denote partial contributions.
 31 Historical dynamic response omitted from ISMIP6 simulations is estimated to be $0.19 \pm 0.10 \text{ mm yr}^{-1}$
 32 ($0.02 \text{ m} \pm 0.01 \text{ m}$ in 2100 relative to 2015). The climate forcing is described in Appendix 7.SM.2.
 33

Representative Concentration Pathways (RCPs)				
Study	RCP2.6	RCP4.5	RCP8.5	Notes
IPCC AR5 and SROCC (Oppenheimer et al., 2019)	0.07 (0.03 to 0.11)	0.08 (0.04 to 0.15)	0.14 (0.08 to 0.27)	Median and <i>likely</i> (66% range) contributions in 2100 relative to 1995-2014. Median of multiple studies.
<i>ISMIP6 CMIP5-forced (Goelzer et al., 2020); excludes historical dynamic response</i>	<i>0.01 to 0.05</i>	---	<i>0.04 to 0.14</i>	<i>Range of multi-model contributions in 2100 relative to 2015 from 1 ESM for RCP2.6 and 6 ESMs for RCP8.5. (see caption).</i>
Coupled regional atmosphere-ice sheet model (Le clec'h et al.,	---	---	0.079	Contribution in 2100 relative to 2000 from MAR-GRISLI model.

2019)				
Coupled Earth system model of lower complexity-ice sheet model (Van Breedam et al., 2020)	0.034 (0.025 to 0.064)		0.073 (0.056 to 0.12)	Contribution in 2100 relative to 2000 from LOVECLIM-AGISM model. Preferred parameter set and range from 4 simulations with different parameters for atmosphere model.
Shared Socioeconomic Pathways (SSPs)				
Study	SSP1-2.6	SSP2-4.5	SSP5-8.5	Notes
Coupled Earth system model-ice sheet model (Muntjewerf et al., 2020, a)	---	---	0.109	Contribution in 2100 relative to 2015 from coupled CESM2-CISM2.
ISMIP6 CMIP6-forced (Payne et al., 2021); excludes historical dynamic response	0.02 to 0.06	---	0.08 to 0.25	Range of multi-model contributions in 2100 relative to 2015 from 1 ESM for SSP1-2.6 and 4 ESMs for SSP5-8.5.
ISMIP6 CMIP5 and CMIP6 forced ensemble including historical dynamic response	0.06 (0.05 to 0.07) [0.04 to 0.08]	---	0.11 (0.09 to 0.14) [0.07 to 0.17]	Median (66% range) [90% range] contribution from ISMIP6 CMIP5- and CMIP6-forced multi-model ensembles
ISMIP6 with AR5 parametric fit: used to estimate rates (Supplementary Material 9.SM.4.4) including historical dynamic response.	0.08 (0.06 to 0.10) [0.05 to 0.12]	0.10 (0.08 to 0.13) [0.07 to 0.15]	0.14 (0.11 to 0.18) [0.10 to 0.22]	Median (66% range) [90% range] contribution from AR5 parametric fit to ISMIP6 ensemble, relative to 1995-2014.
Emulated ISMIP6; excludes historical dynamic response (Edwards et al.,	0.03 (-0.01 to 0.08) [-0.04 to 0.12]	0.06 (0.01 to 0.10) [-0.02 to 0.15]	0.11 (0.06 to 0.16) [0.03 to 0.21]	Median (66% range) [90% range] contribution in 2100 relative to 2015 from emulator of ISMIP6 used with

2021)				<i>chapter 7 climate forcing.</i>
This assessment: emulated ISMIP6 total	0.06 (0.01 to 0.10) [-0.02 to 0.15]	0.08 (0.04 to 0.13) [0.01 to 0.18]	0.13 (0.09 to 0.18) [0.05 to 0.23]	As above, but relative to 1995-2014 and including historical dynamic response.

[END TABLE 9.2 HERE]

9.4.1.4 Projections beyond 2100

The AR5 (Church et al., 2013a) assessed the contribution from Greenland to sea level projections in 2300 as 0.15 m SLE in low emissions scenarios (~RCP2.6) and 0.31-1.19 m in high scenarios (~RCP6.0/RCP8.5). The SROCC (Oppenheimer et al., 2019) did not update the AR5 estimates given *limited evidence* and *low agreement* from three new studies (Vizcaino et al., 2015; Calov et al., 2018; Aschwanden et al., 2019). Since the SROCC, a new study gives a sea level contribution of 0.11 to 0.20 m in low- and 0.61 to 1.29 m in high-emissions scenarios (Van Breedam et al., 2020). The low emissions projections by Van Breedam et al., (2020) encompass the AR5 assessed contribution, while the high emissions are higher than that from the AR5. The ‘optimal’ ensemble member of Aschwanden et al., (2019) (Section 9.4.1.3) indicates that Greenland could contribute 0.25 m under RCP2.6 and 1.74 m under RCP8.5. Structured expert judgement (Bamber et al., 2019) projects Greenland losses of 0.54 (0.28-1.28) m under 2°C warming and 0.97 (0.4-2.23) m under 5°C warming. These studies therefore agree that the AR5 and SROCC assessments are at the low end of the range of projections. In addition, observations suggest that Greenland Ice Sheet losses are tracking the upper range of AR5 projections (Slater et al., 2020b). Therefore, we update the *likely* range for the contribution of the Greenland Ice Sheet to GMSL by 2300 to 0.11-0.25 m under RCP2.6 and 0.31-1.74 m under RCP8.5. However, given the uncertainty in climatic drivers used to project ice sheet change over the 21st century (Goelzer et al., 2020; Hofer et al., 2020; Noël et al., 2021) and the large range in simulations since AR5 extending beyond 2100, we only have *low confidence* in the contribution to GMSL by 2300 and beyond.

The role of the elevation-mass feedback for future projections of Greenland can be assessed from paleo simulations. Ice sheet model simulations of the Laurentide (Gomez et al., 2015; Gregoire et al., 2016) and Eurasian (Alvarez-Solas et al., 2019) ice sheets invoke at least some contribution to last glacial termination mass loss from SMB reduction, as a consequence of an elevation-mass balance feedback (Levermann and Winkelmann, 2016). In a model spanning Meltwater Pulse 1A this mechanism increased mass loss by approximately 66% (Gregoire et al., 2016) but in Last Interglacial simulations the effect of this feedback is shown to depend on the surface scheme of the climate model employed (Plach et al., 2019). Given the agreement between theoretical analyses and paleo-ice sheet model experiments there is *high confidence* that the elevation-mass balance feedback is most relevant at multi-centennial and millennial timescales, consistent with future-focused studies (Gregory et al., 2020, Aschwanden et al. 2019, Le clec’h et al., 2019).

The SROCC adopted the AR5 assessment that complete loss of Greenland ice, contributing about 7 m to sea level, over a millennium or more would occur for a sustained GMST between 1°C (*low confidence*) and 4°C (*medium confidence*) above pre-industrial levels. New studies since the SROCC (Gregory et al., 2020; Van Breedam et al., 2020) confirm this assessment (see also Figure 9.30). Clark et al., (2016) estimate a complete loss to take about 8000 years at 5.5°C and about 3000 years at 8.6°C. Based on agreement between new and previous studies there is therefore *high confidence* that the rate at which Greenland ice sheet commitment is realized depends upon the amount of warming.

Accounting for more detailed feedbacks between the atmosphere and the ice sheet (Gregory et al., 2020) found a gradual relationship between sustained global mean warming and the corresponding near-

1 equilibrium ice sheet volume, in contrast to a sharp threshold as found by (Robinson et al., 2012). Rather
2 than a climatically-controlled tipping point for irreversible loss of the Greenland Ice Sheet, (Gregory et al.,
3 2020) found a threshold of irreversibility linked to ice sheet size, similar to previous work (Ridley et al.,
4 2010). The results of Gregory et al., (2020) show that if the ice sheet loses mass equivalent to about 3-3.5 m
5 of sea-level rise, it would not regrow to its present state, and 2m of the sea-level rise would be irreversible.
6 At which point in time the current ice sheet might reach this critical volume depends on oceanic and
7 atmospheric conditions, ice dynamics, and climate-ice sheet feedbacks (Gregory et al., 2020; Van Breedam
8 et al., 2020), so projections differ in the magnitude and rate of temperature change to cross the threshold for
9 irreversible loss. Projections from a large ensemble indicate that the mass threshold may be reached as early
10 as in 400 years, if warming reaches as high as $>10^{\circ}\text{C}$ above present under extended RCP8.5 (Aschwanden et
11 al., 2019). In summary, there is *high confidence* in the existence of threshold behaviour of the Greenland Ice
12 Sheet in a warmer climate, however there is *low agreement* on the nature of the thresholds and the associated
13 tipping points.

14
15
16 [START BOX 9.3 HERE]

18 **BOX 9.3: Insights into land ice evolution from model intercomparison projects**

19
20 Projections of ice sheets and glaciers in the AR5 (Church et al., 2013a) and the SROCC (Oppenheimer et al.,
21 2019) were assessed by collecting single model studies (with the exception of glaciers in SROCC (Hock et
22 al., 2019b)). Community benchmark experiments (ISMIP-HOM; (Pattyn et al., 2008) or Marine Ice Sheet
23 Model Intercomparison Projects (MISMIP, (Pattyn et al., 2012); MISMIP3d, (Pattyn and Durand, 2013);
24 MISMIP+ (Asay-Davis et al., 2016; Cornford et al., 2020)) have substantially advanced ice sheet modelling
25 since the AR5. Model Intercomparison Projects (MIPs) now inform projections of both ice sheets and
26 glaciers: the Ice Sheet MIP for CMIP6 (ISMIP6) (Section 9.4.1.3; 9.4.2.5), the Linear Antarctic Response
27 MIP (LARMIP-2; Section 9.4.2.5) and GlacierMIP (Section 9.5.1.3).

29 **Regional forcing for land ice intercomparison projects**

30 Simulations of ice sheets and glaciers are dependent on forcing provided by atmosphere and ocean
31 models. Despite progress in representing processes, reducing biases and increasing resolution, regional and
32 global models still have difficulties reproducing observed regional air temperature, surface mass balance and
33 ocean changes (Section 9.4.1.2, 9.4.2.2, Atlas.11). Assessment of CMIP5 and CMIP6 climate models, as
34 forcing for land ice models, has been undertaken (Walsh et al., 2018; Barthel et al., 2020a; Marzeion et al.,
35 2020; Nowicki et al., 2020b) with the aim of selecting the best available historical forcings and sampling
36 potential regional future climate changes. Despite improvement in simulation of atmospheric forcing,
37 persistent biases remain in CMIP5/6, which reduces the fidelity of historical and future simulations of land
38 ice.

40 **ISMIP6 initial state intercomparison projects (initMIP)**

41 The ISMIP6 initial state intercomparison projects (initMIP) for the Greenland (Goelzer et al., 2018) and
42 Antarctic (Seroussi et al., 2019) ice sheets were designed to understand the uncertainty in sea level
43 projections resulting from the choice of initialization procedures used for projections of sea level (Nowicki et
44 al., 2016). Participating modelling groups (Annex II) were free to decide on the initialization method used to
45 bring ice sheet models to a present-day state with the effect of these choices captured in a control simulation
46 (starting from the present day state, with no further climate forcing applied), which measures intrinsic model
47 drift. Compared to the earlier SeaRISE intercomparison project (Bindschadler et al., 2013; Nowicki et al.,
48 2013), the modelled present day ice sheets are in closer agreement with observations and the model drift has
49 been reduced (Goelzer et al., 2018; Seroussi et al., 2019). Nonetheless, historical simulations remain
50 challenging for ice sheet models, due to limited ice sheet observations prior to the satellite era and biases in
51 the historical atmospheric and oceanic forcings from climate models (Nowicki and Seroussi, 2018). ISMIP6
52 and LARMIP-2 therefore did not provide a protocol for the historical runs used to bring the ice sheets to
53 present-day, nor criteria for sub-selecting models from the multi-model ensemble based on ability to
54 reproduce historical changes (Levermann et al., 2020a; Nowicki et al., 2020a).

ISMIP6 projections for the Greenland and Antarctic ice sheets

The ISMIP6 projection protocol (Nowicki et al., 2016, 2020a) was designed to sample the uncertainty in future sea level due to climate scenarios (via the use of high and low emission scenarios and multiple climate models), ice-ocean interactions and inland response to ice shelf collapse, and ice sheet model diversity. The participating ice sheet models are listed in Annex II. For each ice sheet, forcing was selected (Barthel et al., 2020b) from the CMIP5 (Taylor et al., 2012) and CMIP6 (Eyring et al., 2016) models. Atmospheric forcing fields consisted of anomalies in surface mass balance and surface air temperatures generated directly from the CMIP models for the Antarctic ice sheet and downscaled using the MAR regional climate model for the Greenland ice sheet (Hofer et al., 2020). To sample the uncertainty due to ocean forcings, models used either a model-specific scheme using the ISMIP6-provided oceanic dataset or a standard ISMIP6 approach. For the Greenland ice sheet, the oceanic dataset consists of thermal forcing (temperature minus freezing temperature) extrapolated into fjords and subglacial runoff. The standard approach uses timelines of tidewater glacier retreat (Slater et al., 2019, 2020a). For the Antarctic ice sheet, the oceanic dataset consists of salinity, thermal forcing and temperature added to an observationally derived climatology and extrapolated under ice shelves. The standard approach is a basal melt rate that depends quadratically on thermal forcing, adapted from Favier et al., (2019), with two different calibrations (Figure 9.19, Jourdain et al., 2020) that reproduce observed basal melt rates across Antarctica or Pine Island Glacier, respectively (Sections 9.4.2.2, 9.4.2.3). Antarctic ice shelf disintegration datasets (Nowicki et al., 2020a) assume that ice shelves disintegrate when annual surface melt reaches a threshold (Trusel et al., 2015).

The ISMIP6 projections (Goelzer et al., 2020; Seroussi et al., 2020; Payne et al., 2021) are reported as experiment minus control and represent the sea level resulting from future climate change only. The control simulation, which has constant climate conditions starting in 2015 from the historical run, captures drift associated with the choices made for the initialization method and historical run. Subtraction of this control removes any long-term dynamic response of the ice sheet to pre-2015 climate change. This response has been assessed using dynamic discharge derived from observations over the last 40 years (Mouginot et al., 2019; Rignot et al., 2019), under an assumption that it persists at the past rate until 2100 rather than diminishing. The dynamic response to historical forcing is estimated as $0.19 \pm 0.10 \text{ mm yr}^{-1}$ for the Greenland ice sheet (Section 9.4.1.3) and $0.33 \pm 0.16 \text{ mm yr}^{-1}$ for the Antarctic ice sheet (Section 9.4.2.5). Over the period 2015-2100, this leads to an additional sea level contribution of 1.7 cm for Greenland and 2.8 cm for Antarctica.

LARMIP-2 projections for the Antarctic ice sheet

LARMIP-2 is focused on the uncertainty in the ocean forcing and associated ice shelf melting (Levermann et al., 2014, 2020a) with the majority of the models also participating in ISMIP6 (Annex II). The experiments start from present day and impose an additional basal ice shelf melting of 8 m yr^{-1} at the beginning of the 100 yr simulation. A control run is used to remove drift resulting from initialization. The time derivative of the ice sheet response yields a linear response function, which is then convoluted with a forcing of basal shelf melt time series for five Antarctic regions. The forcing time series for RCP2.6, 4.5, 6.0 and 8.5 were obtained from a random combination of global mean temperature for each RCP from MAGICC-6.0 (Meinshausen et al., 2011), a scaling factor and time delay for the relationship between global surface air temperature and subsurface ocean warming in a given sector of the Southern Ocean from one of 19 CMIP5 models (Taylor et al., 2012) and a basal melting sensitivity from the interval $[7, -16] \text{ m yr}^{-1} \text{ }^{\circ}\text{C}^{-1}$ to convert the regional subsurface warming into basal ice shelf melting. This process is repeated 20,000 times to obtain a probability distribution of the sea level contribution for five Antarctic sectors. The linear response framework captures complex temporal responses of the ice sheets resulting from an increase in basal ice shelf melting, but neglects the response to surface mass balance and any self-dampening or self-amplifying processes, such as MISI. The LARMIP-2 method is applied to temperature projections for the SSPs (Supplementary Material 7.SM.2) and an estimate of surface mass balance change from the AR5 parametric Antarctic ice sheet surface mass balance model (Church et al., 2013a) is added to the results (Sections 9.4.2.4, 9.4.2.5, 9.6.3.2). It is not necessary to add a long-term dynamic response to the LARMIP-2 projections, as this is incorporated in the basal melt time series.

GlacierMIP projections

GlacierMIP (Marzeion et al., 2020) was designed to estimate the glacier contribution to sea level rise,

1 including from peripheral glaciers in Greenland and Antarctica that can be considered to be dynamically
2 decoupled, or entirely separate, from the ice sheets. Glacier models are described in Annex II. Initial
3 conditions were based on version 6 of the Randolph Glacier Inventory (RGI Consortium, 2017) and initial
4 ice thickness and volume were provided from an update of Huss and Farinotti, (2012) (although some glacier
5 models used their own estimates). Forcings were taken from ten different CMIP5 GCMs, selected based on
6 availability of multiple RCPs, the choice in a previous model intercomparison (Hock et al., 2019a), and
7 performance in glacier-covered regions according to Walsh et al., (2018). In addition, two global glacier
8 models performed the same experiment with thirteen CMIP6 models (Section 9.5.1.3).

9 Use of an emulator with ISMIP6 and GlacierMIP projections

11 The ISMIP6 and GlacierMIP projections are primarily based on a limited number of CMIP5 RCPs and
12 CMIP6 SSPs, and a limited sampling of ice-ocean interaction parameters and ice shelf collapse simulations.
13 Emulators provide a method for expanding these projections to a range of SSPs with more comprehensive
14 sampling of climate, ice sheet and glacier modelling uncertainties. Sections 9.4.1.3, 9.4.2.5 and 9.5.1.3 show
15 estimates from the emulator of (Edwards et al., 2021). This is a Gaussian Process (rather than physically-
16 based: Cross-Chapter Box 7.1) model derived from the ISMIP6 and GlacierMIP simulations; projections use
17 distributions of GSAT from the two-layer emulator (Supplementary Material 7.SM.2) and ice sheet
18 parameters as inputs, and include estimates of the emulator uncertainty. Probability intervals are therefore
19 not inflated by a further factor, as is often the case for multi-model ensemble projections, to account for
20 missing uncertainties (Section 9.6.3.2). The emulator is used in Section 9.6.3 to provide projections of the
21 land-ice contribution to sea level that are fully consistent with each other, ocean heat content, and the
22 assessed equilibrium climate sensitivity and projections of GSAT across the entire report.

23
24 **[END BOX 9.3 HERE]**

27 9.4.2 Antarctic Ice Sheet

29 9.4.2.1 Recent observed changes

31 As stated in Section 2.3.2.4, satellite observations by IMBIE combining multi-team estimates based on
32 altimetry, gravity anomalies (GRACE) and the input-output method, already presented in the SROCC
33 (Meredith et al., 2019), is updated and extended to 2020 (The IMBIE team, 2021). The Antarctic ice sheet
34 (AIS) lost 2670 [1800–3540] Gt mass over the period 1992–2020, equivalent to 7.4 [5.0–9.8] mm global
35 mean sea level rise (see Table 9.5 for contribution to sea-level budget and Figures 9.16, 9.18). Within
36 uncertainties, this estimate agrees with a review of post-AR5 studies up to 2016 (Bamber et al., 2018b) and
37 is consistent with recent single studies based on satellite laser altimetry (Smith et al., 2020), the input-output
38 method (Rignot et al., 2019) and gravimetry (Velicogna et al., 2020). The mass-loss rate was on average 49
39 [-2 to 100] Gt yr⁻¹ over the period 1992–1999, 70 [22 to 119] Gt yr⁻¹ over the period 2000–2009 and 148 [94
40 to 202] Gt yr⁻¹ over the period 2010–2016 (see Figures 9.16, 9.18 and Table 9.SM.1). However, recent work
41 suggests that the mass loss has not further increased since 2016 because of regional mass gains in Dronning
42 Maud Land (Velicogna et al., 2020). Mass loss of the West Antarctic and Antarctic Peninsula Ice Sheets has
43 increased since about 2000 (*very high confidence*), essentially due to increased ice discharge (Harig and
44 Simons, 2015; Paolo et al., 2015; Forsberg et al., 2017; Bamber et al., 2018b; Gardner et al., 2018; The
45 IMBIE Team et al., 2018; Rignot et al., 2019)

47 The SROCC reported with *very high confidence* that the acceleration, retreat and thinning of the principal
48 West Antarctic outlet glaciers has dominated the observed Antarctic mass loss over the last decades, and
49 stated with *high confidence* that these losses were driven by melting of ice shelves by warm ocean waters.
50 The average West Antarctic Ice Sheet (WAIS) mass loss of 82 ± 9 Gt yr⁻¹ between 1992 and 2017 (The
51 IMBIE Team et al., 2021) leads to substantial observed surface lowering (e.g., Schröder et al., 2019;
52 Shepherd et al., 2019), particularly in coastal regions (Figure 9.18). Recent studies using satellite altimetry
53 (Schröder et al., 2019) and the input-output method (Rignot et al., 2019) consistently show mass loss in these
54 coastal regions since the late 1970s (Figure 9.16). Because of consistent multiple lines of evidence, there is
55 *high confidence* in mass loss of the Totten Glacier in East Antarctica (Miles et al., 2013; Li et al., 2016b;

1 Mohajerani et al., 2018; Rignot et al., 2019; Schröder et al., 2019; Shepherd et al., 2019) since about 2000,
2 dominated by changes in coastal ice dynamics (Li et al., 2016b). It is currently unclear whether mass loss of
3 the East Antarctic Ice Sheet (EAIS) over the last three decades has been significant (Rignot et al., 2019) or,
4 at $5 \pm 46 \text{ Gt yr}^{-1}$ between 1992 and 2017, essentially zero within uncertainties (The IMBIE Team et al.,
5 2018). In summary, WAIS losses, through acceleration, retreat and thinning of the principal outlet glaciers,
6 dominated the AIS mass losses over the last decades (*very high confidence*) and there is *high confidence* that
7 this is the case since the late 1970s. Furthermore, parts of the EAIS have lost mass in the last two decades
8 (*high confidence*).

9
10 As stated in the SROCC, snowfall and glacier flow are the largest components determining AIS mass
11 changes, with glacier flow acceleration (dynamic thinning) on the WAIS and the Antarctic Peninsula driving
12 total loss trends in recent decades (*very high confidence*), and a partial offset of the dominating dynamic-
13 thinning losses by increased snowfall (*high confidence*). The SROCC attributed *medium confidence* to
14 estimates of 20th-century snowfall increases equivalent to a sea level change of $-7.7 \pm 4.0 \text{ mm}$ on the EAIS
15 and $-2.8 \pm 1.7 \text{ mm}$ on the WAIS, respectively (Medley and Thomas, 2019). Loss of buttressing, which can be
16 caused by ice shelf thinning, gradual ice shelf front retreat or ice shelf disintegration, has been linked to
17 instantaneous ice velocity increases and thus dynamic thinning since the early 1990s. This link is clearly
18 evident in the Amundsen and, to a lesser degree, Bellingshausen sectors (Gudmundsson et al., 2019), where
19 passive shelf ice (ice that can be removed without major effects on the ice shelf dynamics) is very limited or
20 absent (Fürst et al., 2016). Surface mass balance (SMB) changes, dominated by snowfall, exhibit strong
21 regional and temporal variability, for example with multidecadal increases in the Antarctic Peninsula
22 inferred since the 1930s (Medley and Thomas, 2019), and dominate the interannual to decadal variability of
23 the AIS mass balance (Rignot et al., 2019). However, no significant continent-wide SMB trend is inferred
24 since 1979 (The IMBIE Team et al., 2018; Medley and Thomas, 2019) (regional changes of Antarctic SMB
25 are assessed further in Atlas Section 11.1). In summary, there is *very high confidence* that the observed AIS
26 mass loss since the early 1990s is primarily linked to ice shelf changes.

27
28
29 **[START FIGURE 9.18 HERE]**

30
31 **Figure 9.18:** (a) A p-box (Section 9.6.3.2) based estimate of the range of values of paleo Antarctic ice sheet mass and
32 sea level equivalents relative to present day and the median over all central estimates (Bamber et al.,
33 2009; Argus and Peltier, 2010; Dolan et al., 2011; Mackintosh et al., 2011; Golledge et al., 2012; Miller
34 et al., 2012b; Whitehouse et al., 2012; Golledge et al., 2013; Ivins et al., 2013; Argus et al., 2014; Briggs
35 et al., 2014; Golledge et al., 2014; Maris et al., 2014; De Boer et al., 2015; Dutton et al., 2015; Golledge
36 et al., 2015; Pollard et al., 2015; DeConto and Pollard, 2016; Gasson et al., 2016; Goelzer et al., 2016;
37 Yan et al., 2016; de Boer et al., 2017; Golledge et al., 2017b; Kopp et al., 2017; Simms et al., 2019) ; and
38 cumulative mass loss (and sea level equivalent) since 2015, with satellite observations shown from 1993
39 (Bamber et al., 2018a; The IMBIE Team et al., 2018; WCRP Global Sea Level Budget Group, 2018a)
40 and observations from 1979 (Rignot et al., 2019), ISMIP6 projected changes by 2100 under
41 RCP8.5/SSP5-8.5 and RCP2.6/SSP1-2.6 scenarios (thin lines from (Seroussi et al., 2020; Edwards et al.,
42 2021; Payne et al., 2021) and 17th to 83rd, 5th to 95th percentile ranges of the ISMIP6 emulation (shaded
43 line, (Edwards et al., 2021)). Right, 17th to 83rd, 5th to 95th percentile ranges for ISMIP6, emulator, and
44 LARMIP-2 including SMB at 2100. Schematic interpretations of individual reconstructions (Anderson et
45 al., 2002; Bentley et al., 2014; De Boer et al., 2015; Goelzer et al., 2016) of the spatial extent of the
46 Antarctic ice sheet are shown for the (b) mid-Pliocene Warm Period, (c) the Last Interglacial and (d) the
47 Last Glacial Maximum (Fretwell et al., 2013): grey shading shows extent of grounded ice. Maps of mean
48 elevation changes (e) 1978-2017 derived from multi-mission satellite altimetry (Schröder et al., 2019) and
49 (f) ISMIP6 (2061-2100) projected changes for an ensemble using the NorESM1-M climate model under
50 the RCP8.5 scenario (Seroussi et al., 2020). Further details on data sources and processing are available
51 in the chapter data table (Table 9.SM.9).

52
53 **[END FIGURE 9.18 HERE]**

54
55
56 The SROCC stated with *high confidence* that melting of ice shelves by warm ocean waters, leading to
57 reduction of ice shelf buttressing, has driven the observed ongoing thinning of major WAIS outlet glaciers.

1 Since the SROCC, digitized radar measurements have shown that the eastern ice shelf of Thwaites Glacier in
2 the Amundsen Sea Embayment thinned between 10 and 33% during the three decades after 1978 (Schroeder
3 et al., 2019), and the role of basal ice shelf melting has been emphasized (Smith et al., 2020). Strong surface
4 meltwater production has been noted as a precursor of ice shelf disintegration in and since the SROCC (Bell
5 et al., 2018), and recent work placed strong meltwater production events (Lenaerts et al., 2017; Nicolas et al.,
6 2017; Wille et al., 2019) and seasons (Robel and Banwell, 2019) in this context. Antarctic ice shelf basal
7 meltwater flux varied between about $1100 \pm 150 \text{ Gt yr}^{-1}$ in the mid-1990s and about $1570 \pm 140 \text{ Gt yr}^{-1}$ in the
8 late 2000s before decreasing to $1160 \pm 150 \text{ Gt yr}^{-1}$ in 2018, and basal melt rates strongly vary with
9 geographical position and depth, as a function of the surrounding water temperature (Adusumilli et al.,
10 2020). Section 9.2.2.3 assesses that the intrusion of warm Circumpolar Deep Water, which has warmed and
11 shoaled since the 1980s, has been at least partially controlled by forcing with significant decadal variability.
12 *Limited evidence* suggests that beyond strong internal decadal wind variability, increased greenhouse gas
13 forcing has slightly modified the mean local winds between 1920 and 2018, facilitating intrusion of
14 Circumpolar Deep Water heat on the Amundsen-Bellingshausen continental shelf and increased ice-shelf
15 melt (Section 9.2.2.3). However, theoretical understanding is still incomplete and in situ measurements
16 within the ice-ocean boundary layer are sparse (Wåhlin et al., 2020). Moreover, modelling and therefore
17 attribution of ice-shelf basal melt remains challenging because of insufficient process understanding,
18 required spatial resolution, the paucity of in-situ observations (Dinniman et al., 2016; Asay-Davis et al.,
19 2017; Turner et al., 2017), and uncertainties of bathymetric datasets under ice shelf cavities (Goldberg et al.,
20 2019, 2020; Morlighem et al., 2020). In summary, ice shelf thinning, mainly driven by basal melt, is
21 widespread around the Antarctic coast and particularly strong around the WAIS (*high confidence*), although
22 basal melt rates show substantial spatio-temporal variability.

23
24 Satellite observations suggest that changes in sea ice coverage and thickness can modulate iceberg calving,
25 ice-shelf flow and glacier terminus position around Antarctica (Miles et al., 2013, 2016, 2017; Massom et al.,
26 2015; Greene et al., 2018; Bevan et al., 2019), either through mechanical coupling or via changes to ocean
27 stratification, influencing basal melting. A combined observational and modelling study (Massom et al.,
28 2018) showed that regional loss of a protective sea-ice buffer played a role in the rapid disintegration events
29 of the Larsen A and B and Wilkins ice shelves in the Antarctic Peninsula between 1995 and 2009, by
30 exposing damaged (rifted) outer ice-shelf margins to enhanced flexure by storm-generated ocean swells. One
31 observational study (Sun et al., 2019) suggests that the absence of sea ice in front of ice shelves, which leads
32 to strengthened topographic waves, favours ice shelf basal melt rates by increasing the baroclinic (depth
33 varying) ocean heat flux which can enter the cavity (Wåhlin et al., 2020). Paleo evidence for sea ice control
34 on ice sheets is lacking, but geologic evidence shows a concordance between periods of ice sheet growth and
35 the expansion of sea ice (Patterson et al., 2014; Levy et al., 2019), both being favoured by reduced sea
36 surface temperatures. Modelling confirms that sea ice controls the strength of ice mélange (Robel, 2017;
37 Schlemm and Levermann, 2021) and thus influences ice shelf flexure and calving rates and stability of
38 floating ice margins, but one model shows this had negligible effect on AIS retreat rates during past warm
39 periods (Pollard et al., 2018). Loss of ice shelf-proximal sea ice is also associated with increased solar
40 heating of surface waters and increased sub-shelf melting (Bendtsen et al., 2017; Stewart et al., 2019). In
41 summary, although in some cases sea-ice decrease and glacier and ice shelf flow and terminus position
42 changes can have the same common cause, there is *medium confidence* that sea ice decrease ultimately
43 favours the mass loss of nearby ice shelves through a variety of processes.

44
45 The SROCC stated with *high confidence* that ice shelf disintegration has driven dynamic thinning in the
46 northern Antarctic Peninsula over recent decades and expressed *high confidence* in currently ongoing mass
47 loss from glaciers that fed now disintegrated ice shelves, although the mass loss rate has decreased in the 20
48 years since the immediate speed-up following ice shelf disintegration in 1995 and 2002. Observed flow
49 speed of these tributary glaciers is still 26% higher than before the ice-shelf disintegration (Seehaus et al.,
50 2018). Conversely, flow speed increase of the tributary glaciers of the Scar Inlet Ice Shelf has been
51 interpreted as a sign of evolving instability of the currently intact ice shelf in one study (Qiao et al., 2020).

52
53 Ongoing grounding line retreat, indicating dynamic thinning, is observed with *high confidence* in many areas
54 of Antarctica and particularly on the WAIS, with the highest rates being in the Amundsen and
55 Bellingshausen Sea areas, and around Totten Glacier in East Antarctica, as stated in the SROCC. Research

1 published since the SROCC has evidenced grounding line retreat of the West Antarctic Berry Glacier on
2 Getz Coast (Millan et al., 2020) and on the East Antarctic Denman Glacier (Brancato et al., 2020), both since
3 1996. Furthermore observed grounding line retreat in excess of 1.5 km between 2003 and 2015 has been
4 reported for parts of Marie Byrd Land (Christie et al., 2018). In summary, there is *high confidence* that
5 grounding lines of marine-terminating glaciers are currently retreating in many areas around Antarctica, and
6 particularly around the WAIS, and additional areas of grounding line retreat have been evidenced since the
7 SROCC.

8
9 The SROCC stated with *medium confidence* that sustained mass losses of several major glaciers in the
10 Amundsen Sea Embayment (ASE) are compatible with the onset of Marine Ice Sheet Instability (MISI), but
11 that whether unstable WAIS retreat had begun or was imminent remained a critical uncertainty. New
12 publications since the SROCC have not substantially clarified this question. On the one hand, a study
13 combining satellite measurements with a numerical model with prescribed ice shelf thinning (Gudmundsson
14 et al., 2019) suggests that MISI is not required to explain the observed current mass loss rates of the WAIS,
15 because they are consistent with external climate drivers. Furthermore, the fast grounding-line retreat of the
16 Pine Island Glacier in the ASE, which was triggered in the 1940s (Smith et al., 2017), observed after 1992
17 (Rignot et al., 2014) and previously interpreted as a sign of MISI (Favier et al., 2014), seems to have
18 stabilized recently (Milillo et al., 2017; Konrad et al., 2018), and its current flow patterns do not suggest
19 ongoing or imminent MISI (Bamber and Dawson, 2020). On the other hand, sustained fast grounding line
20 retreat has been observed for Smith Glacier in the ASE (Scheuchl et al., 2016), and an analysis of flow
21 patterns and grounding line retreat of the ASE Thwaites Glacier between 1992 and 2017 (Milillo et al., 2019)
22 showed sustained, albeit spatially heterogeneous, grounding line retreat, highlighting ice-ocean interactions
23 that lead to increased basal melt. In addition, Denman Glacier in East Antarctica was shown to hold potential
24 for unstable retreat (Brancato et al., 2020). In summary, the observed evolution of the ASE glaciers is
25 compatible with, but not unequivocally indicating an ongoing MISI (*medium confidence*).

26
27 The SROCC reported *limited evidence* and *medium agreement* for anthropogenic forcing of the observed
28 AIS mass balance changes. As stated in Section 3.4.3.2, there remains *low confidence* in attributing the
29 causes of the observed mass of loss from the Antarctic ice sheet since 1993 in spite of some additional
30 process-based evidence to support attribution to anthropogenic forcing.

31 32 33 9.4.2.2 Model evaluation

34
35 The AR5 (Church et al., 2013a; Flato et al., 2013) stated that regional climate models and global models with
36 bias-corrected SST and sea ice concentration tended to produce more accurate simulations of Antarctic
37 surface mass balance (SMB) than coupled climate models, and also noted strong climate model temperature
38 biases over the Antarctic, though the latter may reflect known biases in the reanalysis used (Fréville et al.,
39 2014). Section Atlas.11.1 assesses that there is *medium confidence* in the capacity of climate models to
40 simulate Antarctic climatology and surface mass balance changes.

41
42 Section 9.2.3.2 assesses that there is *low confidence* in simulations of Southern Ocean temperature. Few
43 ocean models resolve ice shelf cavities, and biases in present-day melt rates can be substantial in some
44 sectors, including the key region of the Amundsen Sea (FESOM: Figure 9.19) (Naughten et al., 2018). An
45 increasing number of observational studies from which basal melt rates are calculated (Huhn et al., 2018;
46 Adusumilli et al., 2020; Das et al., 2020; Hirano et al., 2020; Stevens et al., 2020), combined with improved
47 understanding of water-mass-specific influences and modes of melting or dissolving (Silvano et al., 2018;
48 Adusumilli et al., 2020; Malyarenko et al., 2020; Wåhlin et al., 2020), may help to refine these models in the
49 future. However, given the limited number of available models and their biases, there is currently *low*
50 *confidence* in the sub-shelf melt rates simulated by ocean models.

51
52 Improvements in the representation of grounding line evolution in ice sheet models since the AR5 (such as
53 sub-grid schemes for basal friction and ice shelf melt, and local grid refinement) means that most of the
54 model simulations presented in the SROCC were dominated by physical processes. Since then, these
55 advances have been applied in several model intercomparison projects (MISMIP+: Cornford et al., (2020);

1 ABUMIP: Sun et al., (2020); ISMIP6 and LARMIP-2: Box 9.3). All models participating in ISMIP6 and
2 LARMIP-2, for example, simulate ice shelf and grounding line evolution, and include subshelf melt
3 parameterisation, which was not the case in the SeaRISE intercomparison (Bindschadler et al., 2013;
4 Nowicki et al., 2013). Simulations of grounding line evolution (Seroussi et al., 2017, 2020) have benefited
5 from improved bedrock topography (Morlighem et al., 2020). Treatment of subshelf melting, however,
6 remains one of the causes of large differences in Antarctic ice sheet models, particularly for partially floating
7 grid cells in models with coarse resolution (Levermann et al., 2020a; Edwards et al., 2021). Due to the
8 limitations in resolving cavities in ocean models, as described above, basal melt rates are generally
9 parameterized at the ice-shelf base, based on ocean model simulations of temperatures and salinity instead
10 (Nowicki et al., 2020b; Seroussi et al., 2020). While this has the advantage of connecting melt rates to
11 emission scenarios, a large variety of melt parameterisations exist (DeConto and Pollard, 2016; Lazeroms et
12 al., 2018; Reese et al., 2018; Hoffman et al., 2019; Pelle et al., 2019; Jourdain et al., 2020), and there is *low*
13 *agreement* due to limited observational constraints (ocean temperature, salinity, velocity, and ice shelf
14 draft)(Jourdain et al., 2020), uncertainty in the physics of parameterized processes, missing processes (e.g.,
15 tides), and uncertainty in the treatment of ice-sheet–climate feedbacks (Donat-Magnin et al., 2017;
16 Bronselaer et al., 2018; Gолledge et al., 2019a). Parameterisations are usually calibrated to present-day melt
17 rates, but can respond differently to projected ocean warming (Favier et al., 2019; Jourdain et al., 2020). Two
18 different calibrations were used in ISMIP6 (Jourdain et al., 2020; Nowicki et al., 2020b; Box 9.3): one
19 reproducing melt rates averaged around the whole continent (MeanAnt: Figure 9.19), and the other
20 reproducing melt rates near the grounding line of Pine Island Glacier (PIGL: Figure 9.19), leading to large
21 differences in melt rates. Evaluation with observations and two cavity-resolving models suggests that the
22 MeanAnt parameterisation better reproduces observed melt rates and projected increases in both the warm
23 Amundsen Sea Embayment and cold Ronne-Filchner shelf cavity, as well as total Antarctic melting
24 (Jourdain et al., 2020). The PIGL calibration represents the upper end for increased basal melt sensitivity that
25 would be caused by continent-wide changes to ocean water properties and circulation under strong future
26 forcing (Jourdain et al., 2020). The basal sliding law also has a strong influence on grounding line retreat and
27 glacier acceleration in response to perturbations, and varies spatially (Sun et al., 2020). Sliding laws (Joughin
28 et al., 2019) can only be constrained with observations in regions experiencing significant change and with
29 sufficiently long observational records.

30
31
32 **[START FIGURE 9.19 HERE]**

33
34 **Figure 9.19: Ice shelf basal melt rates for present-day (upper panels) and changes from present-day to**
35 **the end of the 21st century under the RCP8.5 scenario (lower panels).** Present-day melt
36 rates were estimated through: the input-output method constrained by satellite observations and
37 atmosphere/snow simulations (Rignot et al., 2013) and representative of 2003-2008 (upper left);
38 the non-local-PIGL parameterization constrained by observation-based ocean properties
39 (Jourdain et al., 2020) and representative of 1995-2014 (upper centre); the Finite Element Sea-
40 ice/ice-shelf Ocean Model (FESOM) simulation over 2006-2015, forced by atmospheric
41 conditions from a CMIP5 multi-model mean (MMM) under the RCP8.5 scenario ((Naughten et
42 al., 2018) upper right). Future anomalies are calculated as 2081-2100 minus present-day using
43 the ISMIP6 non-local-MeanAnt and non-local-PIGL parameterizations (Jourdain et al., 2020)
44 lower left and centre respectively) based on projections from the NorESM1-M CMIP5 model,
45 and the FESOM-MMM projection (lower right). Note the symmetric-log colour bar (linear
46 around zero, logarithmic for stronger negative and positive values). Inset highlights the
47 Amundsen Sea Region. Further details on data sources and processing are available in the chapter data
48 table (Table 9.SM.9).

49
50 **[END FIGURE 9.19 HERE]**

51
52
53 The SROCC noted that Antarctic ice sheet simulations are increasingly evaluated or formally calibrated with
54 modern observations and/or paleodata – to obtain more realistic initial conditions (ice sheet geometry,
55 velocity and forcing) and to constrain uncertainty in probabilistic projections. This trend continues (Nias et

1 al., 2019; Gilford et al., 2020; Hamlington et al., 2020b; Wernecke et al., 2020). However, while the large-
2 scale characteristics of the initial ice sheet state have improved significantly (Box 9.3), capturing the smaller-
3 scale rates of change, including mass trends, remains challenging for many models (Goldberg et al., 2015;
4 Reese et al., 2020; Seroussi et al., 2020; Siegert et al., 2020). This increases uncertainty in projections,
5 especially for the 21st century (Section 9.4.2.5). Uncertainties in ice sheet model simulations have been,
6 however, much better quantified since the AR5, through model intercomparison projects (in particular,
7 ISMIP6 and LARMIP-2: Box 9.3), perturbed parameter ensembles, and increasing use of statistical
8 emulation (Gilford et al., 2020; Levermann et al., 2020a; Wernecke et al., 2020; DeConto et al., 2021;
9 Edwards et al., 2021) to better sample the parameter space. By exploring uncertainties more fully, these
10 methods have the potential to identify better simulations of the historical period.

11
12 An important difficulty is how to evaluate simulations of processes that are not currently observed, or rare,
13 or indirectly deduced: in particular, the ice shelf disintegrations and cliff failures that would drive the
14 proposed Marine Ice Cliff Instability (MICI: Section 9.4.2.4 and Box 9.4)(DeConto and Pollard, 2016;
15 DeConto et al., 2021). Models of ice cliff failure can only be indirectly and partially evaluated, using
16 existing (i.e., static) cliffs and laboratory experiments (Clerc et al., 2019). The SROCC stated that there was
17 *low agreement* on the exact MICI mechanism and *limited evidence* of its occurrence in the present or the
18 past, and that the validity of MICI remains unproven. Only one ice sheet model represents MICI (Pollard et
19 al., 2015; DeConto and Pollard, 2016; DeConto et al., 2021). The mechanism has not been found to be
20 essential for reproducing Mid Pliocene Warm Period and Last Interglacial reconstructions or satellite
21 observations, though Last Interglacial data slightly favours it in this model (Edwards et al., 2019a; Gilford et
22 al., 2020; DeConto et al., 2021).

23
24 In summary, there is now *medium confidence* in many ice sheet processes in ice sheet models, including
25 grounding line evolution. However, there remains *low confidence* in the ocean forcing affecting the basal
26 melt rates and *low confidence* in simulating mechanisms that have the potential to cause widespread,
27 sustained and very rapid ice loss from Antarctica through MICI.

28 29 30 9.4.2.3 Drivers of future Antarctic ice sheet change

31 *Surface mass balance*

32
33 The AR5 projected a negative contribution from Antarctic surface mass balance (SMB) changes to sea level
34 over the 21st century (i.e., mitigating sea-level rise), due to increased snowfall associated with warmer air
35 temperatures. Sensitivity of SMB to Antarctic surface air temperature change varied from 3.7 to 7 % °C⁻¹,
36 and the sea level projections assumed a sensitivity of 5.1 ± 1.5 % °C⁻¹ from CMIP3 era models (Gregory and
37 Huybrechts, 2006) to estimate SMB changes from Antarctic temperatures in the CMIP5 ensemble. Since the
38 AR5, analyses of CMIP5 and CMIP6 models have found Antarctic temperature sensitivity for accumulation
39 (precipitation minus sublimation) of 3.5 to 8.7 % °C⁻¹ (Frieler et al., 2015), for SMB of 6.0 to 9.9 % °C⁻¹
40 (Previdi and Polyani, 2016) and for precipitation of around 4 to 9% °C⁻¹ (Bracegirdle et al., 2020) (± 1 s.d.
41 ranges). An accumulation sensitivity estimate derived from ice core data lies in the middle of the range ~6%
42 °C⁻¹ (Frieler et al., 2015). These are consistent, within uncertainties, with each other and the AR5, under the
43 approximation that SMB is dominated by snowfall.

44
45 The AR5 found that the median and *likely* sea level contributions due to SMB from 1986-2005 to 2100 were
46 -0.05 (-0.09 to -0.02) under RCP8.5 and -0.02 (-0.05 to 0.00) m under RCP2.6. The SROCC did not present
47 a separate SMB contribution, instead showing total Antarctic projections derived from ice sheet models
48 (Section 9.4.2.5). Projections of the SMB contribution to sea level tend to be slightly more negative since the
49 AR5, due at least in part to the higher range in equilibrium climate sensitivity values in CMIP6 (Payne et al.,
50 2021). Mean and ± 1 s.d. ranges for grounded Antarctic ice sheet SMB changes from 2000 to 2100 computed
51 from CMIP5 models are -0.08 (-0.13 to -0.04) m SLE for RCP8.5 and similarly for CMIP6 models are -0.07
52 (-0.11 to -0.03) m for SSP5-8.5 (Gorte et al., 2020). The GCMs used to drive ice sheet models in ISMIP6
53 (Box 9.3) project mean grounded AIS SMB changes from 2005 to 2100 of -0.06 (range -0.08 to -0.03) m
54 SLE under RCP8.5 for the six CMIP5 models (Seroussi et al., 2020) and -0.09 (range -0.10 to -0.07) m SLE
55 under SSP5-8.5 for the four CMIP6 models, which have climate sensitivity values of 4.8-5.3 °C (Payne et al.,

2021). We apply the AR5 parametric AIS SMB model (Section 9.6.3.2) to updated projections of global mean temperature from a two-layer energy budget emulator (Supplementary Material 7.SM.2.), which gives a median -0.05 (5-95% range -0.07 to -0.02) m SLE for SSP5-8.5 (Section 9.4.2.5, Table 9.3), i.e., similar to the AR5 assessment and slightly smaller than the CMIP6 estimate. This estimate is used to augment the LARMIP-2 dynamic projections (Box 9.3) in Sections 9.4.2.5 and 9.4.2.6. Overall, then, CMIP5 and CMIP6 GCM simulations of sea level fall by 2100 due to Antarctic SMB increases are around 2-4 cm greater than estimates derived with the statistical method used in the AR5. Further details about projections of Antarctic temperature, precipitation and SMB are provided in Section Atlas.11.1.4, which assesses that, due to the challenges of model evaluation (Section 9.4.2.2) and the possibility of increased meltwater runoff (Kittel et al., 2021), there is only *medium confidence* that the future contribution of Antarctic SMB to sea level this century will be negative under all greenhouse gas emissions scenarios. Longer timescales are discussed in 9.4.2.6.

Sub-shelf melting

The SROCC highlighted that an important ongoing deficiency in projections of Antarctic sub-shelf melting is the lack of ice-ocean coupling in most continental-scale studies. Increased basal melting is mainly caused by warmer Circumpolar Deep Water (CDW; Section 9.2.2.3) on the continental shelves and warming surface waters intruding under ice shelves (Naughten et al., 2018). Predicting whether or not open ocean water masses will freely penetrate ice-shelf cavities, or will be partially blocked by ocean density gradients, is complex (Wåhlin et al., 2020), and whilst melting related to CDW inflow is currently dominant in the Amundsen Sea Embayment, melt in other embayments is limited by deep inflows of high salinity shelf water or seasonally-warmed shallow incursions of Antarctic Surface Water (Stewart et al., 2019; Adusumilli et al., 2020). There is little consensus regarding future change in CDW (Section 9.2.2.3), and more generally *low confidence* in future change in the temperature of Antarctic ice shelf cavities (Section 9.2.3.2).

The response of sub-shelf melting to ocean warming is also poorly constrained. A key unknown is whether, and when, cold ice shelf cavities might become more similar to the Amundsen Sea Embayment, not only in ocean temperature but also ice-ocean heat exchange, which depends on the cavity geometry and ocean circulation (Little et al., 2009). Only two ocean models with ice shelf cavities have been used to make subshelf basal melting projections for SRES and RCP scenarios (Hellmer et al., 2012; Timmermann and Hellmer, 2013; Timmermann and Goeller, 2017; Naughten et al., 2018). FESOM forced by a CMIP5 multi-model mean under RCP8.5 projects a 90% increase in melting (Figure 9.19), although this could be overestimated due to an underestimation of present day melt rates (Naughten et al., 2018)(Section 9.4.2.2). The temperature-melt relationship was parameterised by ISMIP6 in terms of heat exchange velocity in m a^{-1} , and by LARMIP-2 as basal melt sensitivity in $\text{m a}^{-1} \text{ } ^\circ\text{C}^{-1}$ (Box 9.3; Jourdain et al., 2020; Levermann et al., 2020a; Reese et al., 2020), and both vary widely around the continent depending on cavity type. Median values of ISMIP6 heat exchange velocity vary by a factor of 5-10 when calibrating to either mean Antarctic or high Pine Island Glacier observed melt rates (Section 9.4.2.2; Box 9.3; Jourdain et al., 2020). Basal melt sensitivities near the grounding line estimated by Reese et al., (2020) with a box model of ocean overturning range from $3.9 \text{ m a}^{-1} \text{ } ^\circ\text{C}^{-1}$ for the Weddell Sea to $10.5 \text{ m a}^{-1} \text{ } ^\circ\text{C}^{-1}$ for the Amundsen Sea region, with a continental mean of $5.3 \text{ m a}^{-1} \text{ } ^\circ\text{C}^{-1}$. Similarly high Amundsen Sea sensitivities are estimated in coupled ice-ocean simulations of Thwaites Glacier (mean $9.4 \text{ m a}^{-1} \text{ } ^\circ\text{C}^{-1}$; range 6 to $16 \text{ m a}^{-1} \text{ } ^\circ\text{C}^{-1}$)(Seroussi et al., 2017). These large variations lead to large differences in basal melt rates and projected sea level contributions when applied to the whole ice sheet in ISMIP6 and LARMIP-2 (Box 9.3). Projections of melt rates from the two ISMIP6 calibrations are higher than those from FESOM driven by a CMIP5 multi-model mean (Figure 9.19; Jourdain et al., 2020). The ISMIP6 ensemble mostly uses the mean Antarctic calibration, but includes some simulations with the Pine Island Glacier calibration and the ISMIP6 emulator samples more of these higher values; LARMIP-2 use basal melt sensitivities (7 to $16 \text{ m a}^{-1} \text{ } ^\circ\text{C}^{-1}$) consistent with estimates for the Amundsen Sea Embayment. Due to the limited availability of cavity-resolving ocean models and the wide regional variation in estimates of basal melt sensitivity to ocean temperature, there is therefore only *low confidence* in projected future sub-ice shelf melt rates. The impact of this uncertainty on Antarctic ice sheet model projections to 2100 is discussed in Section 9.4.2.5.

Ice shelf disintegration

Antarctic ice shelves modulate grounded ice flow through buttressing, so their weakening or disintegration is

1 crucial for the timing and magnitude of ice loss and onset of instabilities (Section 9.4.2.4; Box 9.4).
2 Projections of ice shelf disintegration are uncertain in terms of both atmospheric warming and the response
3 of the shelf surface (surface melting, and whether shelves then disintegrate due to hydrofracturing and
4 flexing, or are resilient through refreezing or drainage; (Bell et al., 2018). The SROCC stated it is not
5 expected that widespread ice shelf loss will occur before the end of the 21st century, but this was based on
6 only one study, using a regional climate model forced by five GCMs (Trusel et al., 2015), so there was *low*
7 *confidence* in this assessment. The study of DeConto and Pollard (2016) projected the appearance of
8 extensive surface meltwater several decades earlier than (Trusel et al., 2015) and was therefore assessed to
9 be too uncertain to include in the SROCC projections of the Antarctic ice sheet.

10
11 Since the SROCC, further studies have highlighted the modelling uncertainties in this area. Coastal surface
12 air temperature projections in CMIP6 models show large inter-model differences driven by sea ice retreat,
13 and exhibit more warming relative to global mean temperature under low emissions than high, due to
14 delayed response of the Southern Ocean to stabilised emissions and stratospheric ozone recovery
15 (Bracegirdle et al., 2020). The updated study of DeConto et al., (1998) includes improvements to the climate
16 simulations relative to those in DeConto and Pollard, (2016) and the resulting surface meltwater projections
17 are now consistent with Trusel et al., (2015). However, the net effect of meltwater feedbacks on ice shelves
18 is uncertain. Ice discharge is expected to lead to surface ocean and atmosphere cooling: this increases ocean
19 stratification and sub-shelf melting, but also reduces ice shelf surface melting and delays hydrofracturing
20 (Golledge et al., 2019a; Sadai et al., 2020; DeConto et al., 2021). The new studies are insufficient to change
21 the SROCC *low confidence* assessment on ice shelf loss. The consequence of this uncertainty on projections
22 is discussed in Section 9.4.2.5 and Box 9.4.

23 24 25 9.4.2.4 *Ice sheet instabilities*

26
27 A major uncertainty in future Antarctic mass losses is the possibility of rapid and/or irreversible ice losses
28 through instability of marine parts of the ice sheet, proposed via the mechanisms of Marine Ice Sheet
29 Instability (MISI) and Marine Ice Cliff Instability (MICI), and whether these processes will lead to a collapse
30 of the West Antarctic ice sheet (WAIS).

31
32 MISI is a proposed self-reinforcing mechanism within marine ice sheets that lie on a bed that slopes down
33 towards the interior of the ice sheet, whereby, in the absence of ice shelf buttressing, the position of the
34 grounding line is inherently unstable until reaching an upward sloping bed. The SROCC (Meredith et al.,
35 2019) noted advances in modelling MISI since the AR5, but that 'significant discrepancies' remained in
36 projections due to poor understanding of mechanisms and lack of observational data to constrain the models.
37 Since the SROCC, modelling uncertainties have been more thoroughly explored, rather than constrained.
38 (compatibility of current observations in the Amundsen Sea Embayment with MISI is assessed in Section
39 9.4.2.1). Internal climate variability might either slow (Hoffman et al., 2019) or amplify (Robel et al., 2019)
40 MISI, and stable grounding line positions can be reached on downward sloping beds if ice shelves provide
41 buttressing (Sergienko and Wingham, 2019; Cornford et al., 2020). Ice sheet model simulations that remove
42 all Antarctic ice shelves (and prevent them from reforming) show 2-10 m SLE Antarctic mass loss after 500
43 years due to MISI, of which WAIS collapse contributes 2-5 m (Sun et al., 2020), with the majority of the
44 mass loss in the first one to two centuries. Much of the multi-model variation is due to the sliding law
45 (Section 9.4.2.2). However, it is not expected that widespread ice shelf loss will occur before the end of the
46 21st century (Section 9.4.2.3; Box 9.4). A recent update of bed topography that has unveiled large and
47 overdeepened subglacial troughs in East Antarctica potentially vulnerable to MISI (Morlighem et al., 2020)
48 has only been used by a few models (Seroussi et al., 2020; Sun et al., 2020), so current projections could
49 underestimate vulnerability in these regions. The sea level rise contribution of the Antarctic ice sheet
50 therefore crucially depends on the behaviour of individual ice shelves and outlet glacier systems and whether
51 they enter MISI for a given level of warming (Pattyn and Morlighem, 2020, Box 9.4). As for Antarctic
52 simulations generally (Sections 9.4.2.2, 9.4.2.3), there is *medium confidence* in simulating MISI but *low*
53 *confidence* in projecting the subshelf melting and ice shelf disintegration that drive it.

54
55 The SROCC noted *limited evidence* from geological records and ice sheet modelling suggesting that parts of

1 the AIS experienced rapid (centennial) retreat *likely* due to MISI between 20,000 and 9,000 years ago, and
2 also described more uncertain evidence for the LIG and MPWP. Recent support for past MISI is provided by
3 model simulations of the WAIS during the LIG (Clark et al., 2020), the British Ice Sheet during the last
4 termination (Gandy et al., 2018) and the Laurentide Ice Sheet during the Younger Dryas (Pico et al., 2019),
5 which show progressive retreat despite declining temperatures, indicative of a true (ice dynamic) instability.
6 Direct observational evidence of rapid paleo-ice sheet grounding-line retreat is rare, but on the Larsen
7 continental shelf retreat rates of $>10 \text{ km yr}^{-1}$ during the deglaciation have been estimated (Dowdeswell et al.,
8 2020). MISI has also been inferred from sedimentological evidence of ice loss from Wilkes Subglacial
9 Basin, East Antarctica (Bertram et al., 2018; Wilson et al., 2018; Blackburn et al., 2020) but these
10 reconstructions cannot unambiguously identify unstable from progressive retreat. Therefore there is *limited*
11 *evidence* to identify the operation of instability mechanisms such as MISI in paleo-ice sheet retreat.

12
13 The SROCC assessed that ice-sheet interactions with the solid Earth are not expected to substantially slow
14 sea-level rise from marine-based ice in Antarctica over the 21st century (*medium confidence*), but that these
15 processes could become important on multi-century and longer time scales. More recent modelling of
16 deglaciation of the Ross Embayment by (Lowry et al., 2020) is consistent with this assessment. However,
17 new projections for Pine Island Glacier (Kachuck et al., 2020) support previous work (Barletta et al., 2018)
18 suggesting lower mantle viscosity in this region leads to a negative feedback on decadal time scales.
19 Grounding-line stabilisation by the solid Earth response may therefore occur over the 21st century in the
20 Amundsen Sea Embayment, where most mass loss is occurring (Section 9.4.2.1), but more generally occurs
21 over multi-centennial to millennial timescales (*medium confidence*).

22
23 The MICI hypothesis describes rapid, unmitigated calving triggered by ice shelf collapse (Pollard et al.,
24 2015). The SROCC noted that the MICI mechanism led one model (DeConto and Pollard, 2016) to lose
25 mass far more rapidly, but excluded the mechanism from its projections due to uncertainty in the timing of
26 the ice shelf disintegration (Section 9.4.2.3). They stated that MICI could lead to sea level contributions
27 beyond 2100 considerably higher than the *likely* range projected by other models, but given the *low*
28 *agreement* on the exact MICI mechanism and *limited evidence* of its occurrence in the present or the past
29 (Section 9.4.2.2), its potential to affect future sea level rise was very uncertain. Since the SROCC, new
30 simulations show later ice shelf disintegration, in agreement with other models (DeConto et al., 9998;
31 Section 9.4.2.3), and therefore lower projections at 2100 (Section 9.4.2.5). New theoretical evidence
32 suggests that ice cliff collapse may only occur after very rapid ice shelf disintegration caused by unusually
33 high meltwater production (Clerc et al., 2019; Robel and Banwell, 2019), and that the subsequent rate of
34 retreat depends on the terminus geometry (Bassis and Ultee, 2019). As SROCC noted, only Crane Glacier on
35 the Peninsula has shown retreat consistent with MICI, after the Larsen B ice shelf collapsed, and MICI-style
36 behaviour at Jakobshavn and Helheim glaciers in Greenland might not be representative of wider Antarctic
37 glaciers. Observations from Greenland show that steep cliffs commonly evolve into short floating
38 extensions, rather than collapsing catastrophically (Joughin et al., 2020). As assessed in Section 9.4.2.2 and
39 9.4.2.3, there is therefore *low confidence* in simulating mechanisms that have the potential to cause
40 widespread, sustained and very rapid ice loss from Antarctica this century through MICI, and *low confidence*
41 in projecting the driver of ice shelf disintegration.

42
43 In summary, poorly understood processes of instabilities, characterized by *deep uncertainty*, have the
44 potential to strongly increase Antarctic mass loss under high greenhouse gas emissions on century to
45 multicentury timescales (Box 9.4). These instabilities are therefore considered separately in assessments of
46 the future contribution to GMSL (Sections 9.4.2.5, 9.4.2.6, 9.6.3.2, 9.6.3.5).

47 48 49 9.4.2.5 Projections to 2100

50
51 The AR5 assessed the median and *likely* (66-100% probability) sea level contributions of the Antarctic ice
52 sheet (AIS) in 2100 relative to 1986-2005 to be 0.06 (-0.04 to 0.16) m SLE under RCP2.6 and 0.04 (-0.08 to
53 0.14) m SLE under RCP8.5 (Table 9.3; no change when using the AR6 baseline). The AR5 stated that only
54 the collapse of the marine-based sectors of the AIS, if initiated, could cause global mean sea level to rise
55 substantially above the *likely* range during the 21st century, with *medium confidence* this would not exceed

1 several tenths of a metre during this period. The assessment of the dynamical contribution had no
2 dependence on emissions scenario, due to the lack of literature, so the decrease in sea level contribution in
3 the higher emissions scenario was solely due to increased SMB (Section 9.4.2.3). The SROCC
4 (Oppenheimer et al., 2019) assessed the total contribution based on five new ice sheet modelling studies that
5 incorporated marine ice sheet dynamics, combining their estimates and interpreting the 5-95th percentile
6 range of the resulting distribution as the *likely* range (17-83% probability interval, i.e., not open-ended as in
7 the AR5). The median and *likely* range contributions by 2100 were 0.04 (0.01–0.11) m under RCP2.6 and
8 0.12 (0.03-0.28) m under RCP8.5 (Table 9.3). The positive scenario-dependence in the SROCC - where
9 increases in dynamic losses driven by ocean warming and ice shelf disintegration under higher emissions
10 (Section 9.4.2.3) dominate over increases in surface mass balance - arose from a combination of physical
11 processes and model limitations. Modelling improvements in these studies included improved
12 representations of grounding line response to drivers, more extensive exploration of uncertainties, and
13 inclusion of a positive feedback of meltwater on climate (Golledge et al., 2019b). However, two of the
14 projections did not include surface mass balance changes that would offset dynamic losses (Levermann et
15 al., 2014; Ritz et al., 2015), and the scenario dependence may have been further amplified by highly sensitive
16 subshelf melt parameterisations and use of simplified surface mass balance schemes (Golledge et al., 2015,
17 2019b; Bulthuis et al., 2019; Oppenheimer et al., 2019).

18
19 Since the SROCC, new projections have arisen from multi-model intercomparison projects ISMIP6 and
20 LARMIP-2 (Box 9.3), with one model including MICI (Section 9.4.2.4) (DeConto et al., 2021)(Table 9.3).
21 Corrections are added to allow comparison: all ISMIP6-derived projections have an estimate of the historical
22 dynamical response to pre-2015 climate forcing added, which increases contributions (Box 9.3; Figure 9.18);
23 the LARMIP-2 dynamic projections are combined with an estimate of surface mass balance, which decreases
24 contributions (Sections 9.4.2.3, 9.6.3.2); and the ISMIP6 emulated and LARMIP-2 projections were re-
25 estimated using the global surface air temperature distributions from the two-layer energy budget emulator
26 described in Supplementary Material 7.SM.2. The majority of the new projections indicate that the AIS will
27 overall lose mass and contribute to sea level rise, under all emissions scenarios. Most thinning occurs in the
28 Amundsen Sea sector in WAIS and Totten Glacier in EAIS (Figure 9.18). The most negative contribution is
29 -0.02 m (5th percentile of ISMIP6 combined RCP8.5 and SSP5-8.5 projections after correction) and the
30 largest contribution is 0.57 m SLE (95th percentile; (Levermann et al., 2020b)), or 0.63 m SLE with MICI
31 (95th percentile; (DeConto et al., 2021)). ISMIP6 ensemble ranges are wider for the high scenarios
32 (RCP8.5/SSP5-8.5) than the low (RCP2.6/SSP1-2.6), in part because more simulations were available. The
33 ISMIP6 simulations that apply an ice shelf collapse scenario based on exceedance of a surface meltwater
34 threshold (Trusel et al., 2015) driven by CMIP5 models show only a small increase in mass loss (~0-0.04 m),
35 mostly from the Peninsula, due in part to the small number of ice shelves predicted to collapse this century
36 (Seroussi et al., 2020). Simulations driven by the CMIP5 model HadGEM2-ES, which has unusually extreme
37 warming in the Ross Sea (Barthel et al., 2020b), show a larger mass loss (up to ~0.05 m) in East Antarctica
38 under ice shelf collapse (Edwards et al., 2021). The ISMIP6 projections do not include the efficient
39 meltwater drainage or atmospheric feedbacks that could reduce mass loss further (Seroussi et al., 2020).

40
41 The relationship between emissions scenario and AIS response varies across the studies, with emulated
42 ISMIP6 projections showing a slight negative scenario-dependence in the median (-0.01 m) from SSP1-2.6
43 to SSP5-8.5, and LARMIP-2-based projections showing a slight positive scenario-dependence in the median
44 (0.02 m) (Table 9.3). A lack of clear scenario-dependence in the median masks large individual variations
45 across climate and ice sheet models, whereby the net AIS contribution response to emissions scenario
46 depends on the relative magnitudes of the atmosphere, ocean and ice sheet responses (Barthel et al., 2020b;
47 Seroussi et al., 2020; Edwards et al., 2021). Climate and ice sheet models do not project that the AIS
48 response will be the same under high or low greenhouse gas emissions in 2100, but rather there is no
49 consensus on the sign of the change. In contrast, strong scenario dependence is seen from RCP4.5 to RCP8.5
50 in projections that allow MICI (Section 9.4.2.4;(DeConto et al., 2021), though less so than earlier projections
51 (DeConto and Pollard, 2016) due to later ice shelf disintegrations. A negative or positive scenario-
52 dependence of the AIS response this century cannot be deduced from recent observations, because there is
53 still *low confidence* in attributing the causes of observed mass loss (Section 9.4.2.1), and neither regional
54 mass increases by surface mass balance nor regional mass losses by ice flow have a linear relationship with
55 global mean temperature (Sections 9.4.2.1, 9.4.2.2, 9.4.2.3). There is therefore *low agreement* on the

1 relationship between emissions scenario and AIS response. However, in the longer-term, mass loss is
2 expected to dominate (Section 9.4.2.6).

3
4 The LARMIP-2 median projections are higher than those of the ISMIP6 emulator (by 0.04-0.07 m), and the
5 95th percentiles are two to three times higher. Two possible reasons for the differences between the emulated
6 ISMIP6 and LARMIP-2 projections are assessed: the set of ice sheet models (Annex II) and the parameter
7 values determining subshelf melt sensitivity to ocean temperature (Section 9.4.2.3; Box 9.3). Using only the
8 thirteen ice sheet models common to ISMIP6 and LARMIP-2 reduces the LARMIP-2 median projections by
9 0.02-0.03 m SLE and the 95th percentiles by 0.04-0.08m SLE (Table 9.3), approximately halving the
10 difference in medians but having relatively small effect on the upper end. Subshelf melt sensitivity has a
11 larger effect, due to the wide variation of estimates from different regions and methods. Using only the Pine
12 Island Glacier subshelf melt distribution (Sections 9.4.2.2, 9.4.2.3) in the ISMIP6 emulator gives a median
13 Antarctic projection of ~0.08 m in 2100 in all scenarios before historical correction, compared with ~0 m
14 using only the mean Antarctic distribution; the published projections use a joint distribution (Edwards et al.,
15 2021). Reese et al., (2020) find that using the basal melt sensitivities of LARMIP-2 yield an order of
16 magnitude greater mass loss under RCP8.5 than with the ISMIP6 mean Antarctic values. Halving the basal
17 melt sensitivity parameter range (i.e., in line with a continental mean estimate: Section 9.4.2.3) would lead to
18 a halving of the LARMIP-2 dynamic contribution. This would reconcile the LARMIP-2 and ISMIP6
19 emulator median and 95th percentile projections using the common subset of models within ~0.02-0.05 m.
20 There is therefore *limited evidence* that the ISMIP6 and LARMIP-2 projections could be reconciled by using
21 common ice sheet models and basal melt sensitivity values.

22
23 It is not possible to distinguish which of ISMIP6 and LARMIP-2 is more realistic due to limitations in
24 historical simulations (Box 9.3) and understanding of basal melting (Section 9.4.3), so the projections are
25 combined using a 'p-box' approach (Section 9.6.3.2). The mean of the ISMIP6 emulated and LARMIP-2
26 medians gives the assessed median projections, and the outer edges of the 17-83% ranges give the outer
27 edges of the assessed *likely* (17-83%) ranges, i.e., encompassing the structural and parametric uncertainties
28 of both methods, giving *medium confidence* in their combined projections. The main difference between this
29 assessment and the SROCC is to increase the medians of the lower scenarios by 0.05-0.07 m, so that all SSPs
30 are similar to the SROCC assessment of RCP8.5, and to substantially increase the upper ends of the *likely*
31 ranges: by 0.14-0.16 m for RCP2.6/SSP1-2.6 and RCP4.5/SSP2-4.5, and 0.06 m for RCP8.5/SSP5-8.5. The
32 increase relative to the SROCC is partly due to the increase in LARMIP-2 projections relative to the original
33 LARMIP study (Levermann et al., 2014), arising from the larger number of participating ice sheet models
34 (Levermann et al., 2020b). The historical dynamic response to pre-2015 climate forcing applied to the
35 ISMIP6 emulator could be overestimated, due to the assumption of a constant future rate (Box 9.3). This
36 assessment encompasses the SROCC and all projections since, except the 83rd percentiles of projections that
37 allow MICI under RCP8.5 (DeConto et al., 2021) and the structured expert judgement under 5°C shown in
38 the SROCC (Bamber et al., 2019). Both are used in further p-box estimates to give the outer limits of *low*
39 *confidence* assessments (Section 9.6.3.2).

40
41 In summary, it is *likely* that the Antarctic ice sheet will continue to lose mass throughout this century under
42 all emissions scenarios, i.e., that dynamic losses driven by ocean warming and ice shelf disintegration will
43 *likely* continue to outpace increasing snowfall (*medium confidence*). The upper end of projections is not well
44 constrained, due to different assumptions about the future sensitivity of subshelf basal melting to ocean
45 warming and the proposed Marine Ice Cliff Instability triggered by ice shelf disintegration (Sections 9.4.2.3
46 and 9.4.2.4; Box 9.4).

47
48
49 **[START TABLE 9.3 HERE]**

50
51 **Table 9.3:** Projected sea level contributions in meters from the Antarctic ice sheet in 2100 relative to 1995-2014,
52 unless otherwise stated, for selected RCP and SSP scenarios. Italics denote partial contributions. The
53 historical dynamic response omitted from ISMIP6 simulations is estimated to be $0.33 \pm 0.16 \text{ mm yr}^{-1}$
54 ($0.03 \text{ m} \pm 0.01 \text{ m}$ in 2100 relative to 2015; Box 9.3). The climate forcing is described in Supplementary
55 Material 7.SM.2.

1

Representative Concentration Pathways (RCPs)				
Study	RCP2.6	RCP4.5	RCP8.5	Notes
IPCC AR5 (Church et al., 2013a)	0.06 (-0.04 to 0.16)	0.05 (-0.05 to 0.15)	0.04 (-0.08 to 0.14)	Median and <i>likely</i> (>= 66% range) contribution.
IPCC SROCC (Oppenheimer et al., 2019)	0.04 (0.01 to 0.11)	0.06 (0.01 to 0.15)	0.12 (0.03 to 0.28)	Median and <i>likely</i> (66% range) contribution. Combination of five studies.
<i>ISMIP6 CMIP5-forced (Seroussi et al., 2020); excludes historical dynamic response</i>	<i>-0.01 to 0.16</i>	<i>---</i>	<i>-0.08 to 0.30</i>	<i>Range of ISMIP6 multi-model contributions in 2100 relative to 2015 from 2 ESMs for RCP2.6 and 6 ESMs for RCP8.5.</i>
<i>LARMIP-2; excludes surface mass balance (Levermann et al., 2020b)</i>	<i>0.13 (0.07 to 0.24) [0.04 to 0.37]</i>	<i>0.14 (0.07 to 0.28) [0.05 to 0.44]</i>	<i>0.17 (0.09 to 0.36) [0.06 to 0.58]</i>	<i>Median (67% range) [90% range] LARMIP-2 multi-model dynamic contribution in 2100 relative to 1900.</i>
MICI (DeConato et al., 2021)	0.08 (0.06 to 0.12) [0.06 to 0.15]	0.09 (0.07 to 0.11) [0.07 to 0.15]	0.34 (0.19 to 0.53) [0.11 to 0.63]	Median (66% range) [90% range]
Shared Socioeconomic Pathways (SSPs)				
Study	SSP1-2.6	SSP2-4.5	SSP5-8.5	
<i>Multi-model ensemble projections</i>				
<i>ISMIP6 CMIP6-forced (Payne et al., 2021); excludes historical dynamic response</i>	<i>-0.05 to 0.01</i>	<i>---</i>	<i>-0.09 to 0.11</i>	<i>Range of ISMIP6 multi-model contributions in 2100 relative to 2015 from 1 ESM for SSP1-2.6 and 4 ESMs for SSP5-8.5.</i>
ISMIP6 all (CMIP5 and CMIP6-forced) including historical dynamic response	0.05 (0.04 to 0.08) [0.03 to 0.11]	<i>---</i>	0.04 (0.00 to 0.12) [-0.02 to 0.23]	Median (66% range) [90% range] contribution from ISMIP6 CMIP5- and CMIP5-forced multi-model ensembles, (see caption).
<i>Emulated ISMIP6; excludes historical dynamic response (Edwards et al., 2021)</i>	<i>0.04 (-0.01 to 0.10) [-0.05 to 0.14]</i>	<i>0.04 (-0.02 to 0.10) [-0.06 to 0.14]</i>	<i>0.04 (-0.01 to 0.09) [-0.05 to 0.14]</i>	<i>Median (66% range) [90% range] contribution in 2100 relative to 2015 from emulator of ISMIP6 used with Chapter 7 climate forcing.</i>

Emulated ISMIP6 total	0.09 (0.03 to 0.14) [-0.01 to 0.19]	0.09 (0.03 to 0.14) [-0.01 to 0.18]	0.08 (0.03 to 0.14) [0.00 to 0.18]	Emulated ISMIP6, but relative to 1995-2014 and including historical dynamic response (see caption)
<i>Surface mass balance</i>	-0.02 (-0.03 to -0.01)	-0.03 (-0.04 to -0.02)	-0.05 (-0.07 to -0.03)	Median (66% range) [90% range] surface mass balance estimated for the AR5, used to correct LARMIP-2 below.
<i>LARMIP-2; excludes surface mass balance</i>	0.15 (0.08 to 0.29) [0.05 to 0.44]	0.17 (0.09 to 0.33) [0.06 to 0.49]	0.20 (0.10 to 0.39) [0.07 to 0.61]	Median (66% range) [90% range] dynamic contribution from LARMIP-2 multi-model method used with Chapter 7 climate forcing.
<i>LARMIP-2 subset of models; excludes surface mass balance</i>	0.14 (0.08 to 0.26) [0.05 to 0.39]	0.15 (0.08 to 0.29) [0.05 to 0.45]	0.17 (0.10 to 0.35) [0.06 to 0.54]	As above, but using only the 13 of 16 ice sheet models common to both ISMIP6 and LARMIP-2.
<i>LARMIP-2 subset of models; includes surface mass balance</i>	0.11 (0.05 to 0.24) [0.03 to 0.37]	0.12 (0.05 to 0.26) [0.02 to 0.42]	0.12 (0.05 to 0.30) [0.01 to 0.49]	As above, but including the surface mass balance estimate.
LARMIP-2 total	0.13 (0.06 to 0.27) [0.03 to 0.41]	0.14 (0.06 to 0.29) [0.02 to 0.46]	0.15 (0.05 to 0.34) [0.01 to 0.57]	Median (66% range) [90% range] dynamic contribution from LARMIP-2 multi-model method used with Chapter 7 climate forcing, including the surface mass balance estimate.
This assessment: combination of emulated ISMIP6 and LARMIP-2	0.11 (0.03 to 0.27) [-0.01 to 0.41]	0.11 (0.03 to 0.29) [-0.01 to 0.46]	0.12 (0.03 to 0.34) [0.00 to 0.57]	Median (66% range) [90% range] assessment combining emulated ISMIP6 and LARMIP-2.

[END TABLE 9.3 HERE]

9.4.2.6 Projections beyond 2100

The SROCC assessed the median and *likely* range of Antarctic sea level equivalent contributions at 2300 as 0.16 (0.07 – 0.37) m under RCP2.6 and 1.46 (0.60 – 2.89) m under RCP8.5, based on three studies. It was noted that *deep uncertainty* remained beyond 2100: whilst solid Earth feedbacks could reduce ice loss over

1 multi-century timescales, Marine Ice Cliff Instability (MICI; Section 9.4.2.4) might give contributions higher
2 than the *likely* ranges. The SROCC also presented structured expert judgement (SEJ) projections for
3 comparison (Bamber et al., 2019), which give higher values. Since the SROCC, three studies have made
4 projections to 2300. Rodehacke et al., (2020) assessed two methods for implementing precipitation changes
5 (based on repeating 2071-2100 forcings beyond 2100), which both gave negative projections at 2300
6 because the dynamic response was very small (-0.11 to -0.01 m SLE for RCP2.6; -0.25 to -0.07 m for
7 RCP8.5 forcing). In contrast, simulations forced by 2081-2100 ocean-only projections under RCP8.5/SSP-
8 8.5 beyond 2100, using two implementations of the ISMIP6 'non-local' basal melt parameterisations (Box
9 9.3; Section 9.4.2.2) and two sliding laws, are all positive (0.08 m to 0.96 m SLE by 2300), though these do
10 not include the negative contribution from surface mass balance changes (Lipscomb et al., 2021). Finally,
11 DeConto et al., (9998) update projections for the MICI hypothesis (Section 9.4.2.4) using the extensions of
12 the RCPs to 2300, and obtain far higher contributions: median (17-83%) ranges of 1.09 (0.71 to 1.35) m SLE
13 under RCP2.6 and 9.60 (6.87 to 13.54) m SLE under RCP8.5. These are larger than previous estimates
14 (DeConto and Pollard, 2016), particularly at the upper end: 0.68 (0.29 to 1.13) m SLE for RCP2.6 and 8.40
15 (7.47 to 9.76) m for RCP8.5 (Edwards et al., 2019b), which can largely be explained by the higher maximum
16 ice-cliff calving rate. LARMIP-2 dynamic projections (Box 9.3) are also estimated under the extended SSPs
17 and corrected with surface mass balance (as in Section 9.4.2.5), giving median (17-83%) ranges of 0.40
18 (0.18–0.78) m SLE at 2300 under SSP1-2.6 and 1.57 (0.68–3.14) m under SSP5-8.5. The longer timescale
19 may invalidate the linear response assumption of LARMIP-2, which neglects any self-dampening or self-
20 amplifying processes. The ranges of projections for 2300 without MICI (Golledge et al., 2015; Bulthuis et
21 al., 2019; Levermann et al., 2020a; Rodehacke et al., 2020; Lipscomb et al., 2021); 'assessed ice-sheet
22 contributions' in Section 9.6.3.5) are -0.14 to 0.78 m SLE under RCP2.6/SSP1-2.6, and -0.27 to 3.14 m SLE
23 under RCP8.5/SSP5-8.5. The lower bounds are the 5th percentile of (Bulthuis et al., 2019) and the lowest
24 mean/median from (Rodehacke et al., 2020), respectively; the upper bounds are the 83% percentiles of the
25 LARMIP-2 estimates. These ranges are wider than the SROCC *likely* ranges, and more consistent with the
26 SEJ (Bamber et al., 2019). However, projections in which Antarctica contributes much more than the
27 assessed ranges under sustained very high greenhouse gas emissions, i.e., around 7–14 m to GMSL by 2300
28 (DeConto et al., 2021), cannot be ruled out and are taken as a sensitivity case (Section 9.6.3.5; Table 9.11).
29 In summary, there is *high confidence* that Antarctic mass loss will be greater beyond 2100 under high
30 greenhouse gas emissions than low, but the large range of projections mean we have only *low confidence* in
31 the likely AIS contribution to GMSL by 2300 for a given scenario. *Deep uncertainty* remains in the role of
32 Antarctic ice sheet instabilities under very high emissions.

33
34 The West and East Antarctic ice sheets are considered to be tipping elements, i.e., susceptible to critical
35 thresholds. The SR1.5 (Hoegh-Guldberg et al., 2018) assessed that a threshold for WAIS instability may be
36 close to 1.5–2°C (*medium confidence*), as only RCP2.6 led to long-term projections of less than 1 m
37 (Golledge et al., 2015; DeConto and Pollard, 2016). Based on the agreement of a further study (Bulthuis et
38 al., 2019), the SROCC confirmed that low emissions would limit Antarctic ice loss over multi-century
39 timescales (*high confidence*), but it was not possible to determine whether this was sufficient to prevent
40 substantial ice loss (*medium confidence*). Since the SROCC, new studies have revisited this topic (Garbe et
41 al., 2020; Rodehacke et al., 2020; Van Breedam et al., 2020; DeConto et al., 2021; Lipscomb et al., 2021),
42 allowing a more complete assessment along with other studies (Feldmann and Levermann, 2015; Clark et al.,
43 2016; Golledge et al., 2017a; Edwards et al., 2019b) and the extension to LARMIP-2 above. The majority
44 project 0–1.3 m SLE on multi-century timescales under scenarios of 1–2°C warming. Projections can
45 increase up to 2 m SLE under high basal melt sensitivity to ocean warming (Section 9.4.2.3)(Lipscomb et al.,
46 2021) or MICI (Section 9.4.2.4). On multi-millennial timescales ($\geq 2,000$ years), many projections remain
47 below 1.6 m SLE under 1–2°C warming, i.e. less than about half of the West Antarctic ice sheet in sea level
48 equivalent (see also Section 9.6.3.5 and Figure 9.30). Other studies project majority or total loss of WAIS
49 under 1–2°C warming, exceeding 2 m SLE, under the higher end of the warming range ($\geq 1.5^\circ\text{C}$), or high
50 ocean warming ($\geq 0.5^\circ\text{C}$) and/or high basal melting around WAIS, or MICI. All but two of these multi-
51 millennial studies use variants of the same ice sheet model, though different modelling choices mean they
52 can be considered quasi-independent. Simulations of previous interglacial periods often show near or total
53 WAIS disintegration, with mass loss exceeding 3 m SLE (e.g. Figure 9.18), although limitations of these
54 studies or inferences that can be drawn under different forcings limit confidence in the robustness of these as
55 quantitative analogues (Sections 9.4.2.4, 9.6.2). Overall, increased evidence and agreement on the timescales

1 and drivers of mass loss confirm the SR1.5 assessment that a threshold for WAIS instability may be close to
2 1.5–2°C (*medium confidence*), and that the probability of passing a threshold is larger for 2°C warming than
3 for 1.5°C (*medium confidence*), particularly under strong ocean warming. New projections agree with
4 previous studies that only part of WAIS would be lost on multi-century timescales if warming remains less
5 than 2°C (*medium confidence*). There is *limited agreement* about whether complete disintegration would
6 eventually occur at this level of warming, but *medium confidence* this would take millennia.
7

8 Under ~2–3°C peak warming, complete or near-complete loss of the West Antarctic ice sheet is projected in
9 most studies after multiple millennia (*low confidence*), with continent-wide mass losses of ~2–5 m SLE or
10 more; this could occur on multi-century timescales under very high basal melting (Lipscomb et al., 2021) or
11 widespread ice shelf loss and/or MICI (Sun et al., 2020; DeConto et al., 2021) (*low confidence*). Mass losses
12 under ~2–3°C warming could be less than 2 m SLE, particularly for multi-century timescales, low basal
13 melting, or less responsive sliding laws. If warming exceeds ~3°C above pre-industrial, part of the East
14 Antarctic ice sheet (typically the Wilkes Subglacial Basin) is projected to be lost on multi-millennial
15 timescales (*low confidence*), with total AIS mass loss equivalent to around 6–12 m or more sea level rise;
16 mass loss could be much smaller if the dynamic response is small (Bulthuis et al., 2019; Rodehacke et al.,
17 2020), or much faster under widespread ice shelf loss and/or MICI (Sun et al., 2020; DeConto et al., 2021).
18 A new study by Garbe et al., (2020) suggests that 6°C sustained warming and associated mass loss of ~12 m
19 SLE may be a critical threshold beyond which the ice sheet re-organises to a new state, leading to large
20 losses from East Antarctica (including the Aurora Subglacial Basin) and leading to a further 10 m sea level
21 contribution per degree of warming; other studies also show much higher mass loss per °C at higher levels of
22 warming (Van Breedam et al., 2020; DeConto et al., 2021) (Section 9.6.3.5; Figure 9.30).
23

24 The SROCC (Meredith et al., 2019; Oppenheimer et al., 2019) assessed that Antarctic mass losses could be
25 irreversible over decades to millennia (*low confidence*). Garbe et al., (2020) show that the Antarctic ice sheet
26 is always volumetrically smaller when regrowing under a given warming level than when it retreats under
27 the same forcing, and that even if retreat followed by regrowth results in a net zero change in volume, the
28 spatial distribution of mass may be altered, especially in parts of West Antarctica vulnerable to MISI.
29 Projections that start reducing CO₂ concentrations from 2030 onwards, reaching pre-industrial levels around
30 2300, show sea level contributions exceeding 1 m by 2500 when including MICI (DeConto et al., 2021).
31 New research therefore confirms the SROCC assessment that mass loss from the AIS is irreversible on
32 decadal to millennial timescales (*low confidence*) (FAQ 9.1), and suggests that reducing atmospheric CO₂
33 concentrations or temperatures to pre-industrial levels may not be sufficient to prevent or reverse substantial
34 Antarctic mass losses (*low confidence*).
35
36

37 9.5 Glaciers, permafrost and seasonal snow cover

38 9.5.1 Glaciers

39 9.5.1.1 Observed and reconstructed glacier extent and mass changes

40 *Global glacier contribution*

41 The AR5 (Vaughan et al., 2013) assessed glacier changes from studies based on the regions defined in the
42 Randolph Glacier Inventory (RGI; version 2.0): a satellite observation-based, global inventory of glacier
43 outlines for the year 2000. Following the SROCC (Hock et al., 2019b; Meredith et al., 2019), we report
44 studies based on RGI version 6.0 (RGI Consortium, 2017). Increased volume of satellite observations and
45 the inclusion of detailed regional glacier inventories has resulted in an improved inventory (RGI Consortium,
46 2017). A new consensus estimate for the ice thickness distribution of all glaciers in RGI 6.0 was obtained
47 from an ensemble of five numerical models (although only one out of five models covered all regions
48 (Farinotti et al., 2019)) calibrated and validated with the worldwide Glacier Thickness Database (GlaThiDa
49 3.0; (GlaThiDa Consortium, 2019; Welty et al., 2020)) where possible. The updated inventory shows
50 decreases in estimated glacier volume in the Arctic, High Mountain Asia and Southern Andes, partially
51 compensated by increases in Antarctica. 15% of the total glacier volume is estimated to be below sea level
52 and would not contribute to sea-level rise if melted (Farinotti et al., 2019). Supplementary Material Table
53
54
55

1 9.SM.2 shows the inventory glacier area and mass for each region in the year 2000.

2
3 The SROCC found a globally coherent trend of glacier decline in the last decades despite large annual
4 variability and regional differences (*very high confidence*). Section 2.3.2.3 assesses the global glacier mass
5 changes for the whole 20th century (see Table 9.5 for contribution to the sea-level budget, note that the
6 peripheral glaciers in Greenland and Antarctica are added to the ice sheets for the budget). The AR6
7 assessment is based on Marzeion et al., (2015), using glacier-length reconstructions (Leclercq et al., 2011)
8 and a glacier model forced by gridded climate observations (Marzeion et al., 2012), and not considering the
9 estimated mass loss of uncharted glaciers ($100 \pm 50 \text{ Gt yr}^{-1}$) (Parkes and Marzeion, 2018). The time series are
10 assumed independent resulting in larger uncertainty than presented in the SROCC (see also Section 9.6.1).
11 The rate of global glacier mass loss (excluding the periphery of ice sheets) for the period 1901-1990 is
12 estimated to be *very likely* $210 \pm 90 \text{ Gt yr}^{-1}$, representing 16 [28 to 7]% of the glacier mass in 1901, in
13 agreement with the SROCC within uncertainty estimates.

14
15 Since the SROCC, new regional estimates for the Andes (Dussaillant et al., 2019), High Mountain Asia
16 (Shean et al., 2020), Iceland (Aðalgeirsdóttir et al., 2020), the European Alps (Davaze et al., 2020; Sommer
17 et al., 2020) and Svalbard (Schuler et al., 2020), two new global (Ciraci et al., 2020; Hugonnet et al., 2021)
18 and an ad-hoc estimate for the latest glaciological observations (Zemp et al., 2020) have extended the glacier
19 mass change time series up to 2018/2019 (Figure 9.21 and Supplementary Material Table 9.SM.3). A
20 reconciled global estimate for the period 1962 to 2019 has been compiled by Slater et al., (2021). However,
21 in contrast to Slater et al., (2021), after 2000 this assessment is based on the first globally complete and
22 consistent estimate of 21st-century glacier mass change from differencing of digital elevation models
23 (Hugonnet et al., 2021) covering 94.7% of glacier area with glacier mass change for each glacier in the
24 inventory produced with unprecedented accuracy. The estimates from (Hugonnet et al., 2021) agree within
25 uncertainties with new and previous estimates at global (Hock et al., 2019b; Wouters et al., 2019; Zemp et
26 al., 2019; Ciraci et al., 2020; Slater et al., 2021) and regional scale (Dussaillant et al., 2019; Aðalgeirsdóttir
27 et al., 2020; Schuler et al., 2020; Shean et al., 2020). Excluding peripheral glaciers of ice sheets (RGI regions
28 5 and 19), glacier mass loss rate was *very likely* $170 \pm 80 \text{ Gt yr}^{-1}$ for the period 1971 to 2019 (8 [14 - 4]% of
29 1971 glacier mass), $210 \pm 50 \text{ Gt yr}^{-1}$ over the period 1993 to 2019 (6 [8 - 4]% of 1993 glacier mass) and 240
30 $\pm 40 \text{ Gt yr}^{-1}$ over the period 2006-2019 (3 [4 - 2]% of 2006 glacier mass) (Sections 2.3.2.3, 9.6.1; Table 9.5⁴;
31 Cross-Chapter Box 9.1). Including the peripheral glaciers of the ice sheets, the global glacier mass loss rate
32 in the period 2000-2019 is *very likely* $266 \pm 16 \text{ Gt yr}^{-1}$ (4 [6 - 3]% of glacier mass in 2000) with an increase in
33 the mass loss rate from $240 \pm 9 \text{ Gt yr}^{-1}$ in 2000-2009 to $290 \pm 10 \text{ Gt yr}^{-1}$ in 2010-2019 (*high confidence*).
34 These estimates are in agreement with the SROCC estimate and extend the period to 2018/19. In summary,
35 new evidence published since the SROCC shows that during the decade 2010 to 2019 glaciers lost more
36 mass than in any other decade since the beginning of the observational record (*very high confidence*; Figure
37 9.20; Section 8.3.1.7.1).

38
39
40 [START FIGURE 9.20 HERE]

41
42 **Figure 9.20: Global and regional glacier mass change rate between 1960 and 2019.** The time series of annual and
43 decadal mean mass change are based on glaciological and geodetic balances (Zemp et al. (2019) and
44 Zemp et al. (2020)). Superimposed are the 2002-2019 average rates by (Ciraci et al., 2020) based on the
45 Gravity Recovery and Climate Experiment (GRACE), 2006-2015 estimated rates as assessed in SROCC
46 and the new decadal averages (2000-2009 and 2010-2019) by Hugonnet et al. (2021). (*) New regional
47 estimates for the Andes (Dussaillant et al., 2019), High Mountain Asia (Shean et al., 2020), Iceland
48 (Aðalgeirsdóttir et al., 2020), Central Europe (Sommer et al., 2020) and Svalbard (Schuler et al., 2020)
49 are also shown. The uncertainty reported in each study is shown. See Figure 9.2 for the location of each
50 region. Further details on data sources and processing are available in the chapter data table (Table
51 9.SM.9).

52 [END FIGURE 9.20 HERE]

⁴ The periods in Table 9.5 end in 2018 leading to a slight difference in the values

1 *Regional glacier changes*

2 A major advance since the SROCC is the availability of high accuracy mass loss estimates for individual
3 glaciers (Hugonnet et al., 2021). These results show that during the last 20 years, the highest regional mass
4 loss rates ($>720 \text{ kg m}^{-2} \text{ yr}^{-1}$) were observed in the Southern Andes, New Zealand, Alaska, Central Europe,
5 and Iceland. Meanwhile, the lowest regional mass loss rates ($<250 \text{ kg m}^{-2} \text{ yr}^{-1}$) were observed in High
6 Mountain Asia, the Russian Arctic, and the periphery of Antarctica. Glacier mass loss in Alaska (25% of
7 2000-2019 total mass loss), the periphery of Greenland (13%), Arctic Canada North (11%), Arctic Canada
8 South (10%), the periphery of Antarctica (8%), the Southern Andes (8%) and High Mountain Asia (8%),
9 represent the majority (83%) of the total glacier mass loss during the last 20 years (2000-2019).

10
11 The glacier mass loss rate from geodetic mass balance assessments in the Southern Andes during 2006-2015
12 was smaller ($720 \pm 70 \text{ kg m}^{-2} \text{ yr}^{-1}$) (Braun et al., 2019; Dussailant et al., 2019; Hugonnet et al., 2021) than
13 previously assessed in the SROCC ($860 \pm 160 \text{ kg m}^{-2} \text{ yr}^{-1}$), though within uncertainties. In the Central and
14 Desert regions of the Southern Andes, an increase in mass loss from 2000-2009 to 2010-2018, and a high
15 loss rate in Patagonia for the whole period, are observed (Dussailant et al., 2019). Records of glacier mass
16 loss in Peru (Seehaus et al., 2019a) and Bolivia (Seehaus et al., 2019b) in the period 2000-2016 show an
17 increase in mass loss towards the end of the observation period. In Western North America, outside of
18 Alaska and western Yukon, there was a fourfold increase in mass loss for 2009-2018 ($860 \pm 320 \text{ kg m}^{-2} \text{ yr}^{-1}$)
19 compared to 2000-2009 ($203 \pm 214 \text{ kg m}^{-2} \text{ yr}^{-1}$) (Menounos et al., 2019), and in the Canadian Arctic there
20 was a doubling of mass loss in the last two decades compared with pre-1996 (Noël et al., 2018; Cook et al.,
21 2019). The peripheral glaciers in NE Greenland experienced a 23% increase in mass loss in 1980-2014
22 compared to the period 1910-1978/87 (Carrivick et al., 2019). In Iceland, $16 \pm 4 \%$ of the ~ 1890 glacier mass
23 has been lost; about half of that loss occurred in the period 1994-2019 (Aðalgeirsdóttir et al., 2020). Glacier
24 records starting in 1960 in Norway show that half of the observed glaciers advanced in the 1990s but all have
25 retreated since 2000 (Andreassen et al., 2020). In Svalbard, glaciers have been losing mass since the 1960s
26 with a tendency towards more negative mass balance since 2000 (Deschamps-Berger et al., 2019; Van Pelt et
27 al., 2019; Morris et al., 2020; Noël et al., 2020; Schuler et al., 2020). A similar increase in mass loss has been
28 observed for Franz Josef Land in the Russian Arctic (Zheng et al., 2018). Rapid retreat and downwasting
29 throughout the European Alps in the early 21st century is reported (Sommer et al., 2020) and long term
30 records, although limited, indicate sustained glacier mass loss in High Mountain Asia since ~ 1850 , with
31 increased mass loss in recent decades (Shean et al., 2020). In summary, although interannual variability is
32 high in many regions, glacier mass records throughout the world show with *very high confidence* that the
33 loss rate has been increasing in the last two decades (see also Section 8.3.1.7.1 and 12.4 for regional glacier
34 assessment).

35
36 Section 2.3.2.3 assesses that the rate and global character of glacier retreat in the latter part of 20th century
37 and finds the first decades of the 21st century appear to be unusual in the context of the Holocene (*medium*
38 *confidence*) and the global glacier recession in the beginning of the 21st century to be unprecedented in the
39 last 2000 years (*medium confidence*). These assessments are supported by regional evidence. New
40 reconstructions of the Patagonian Ice Sheet suggest that 20th-century glacial recession occurred faster than at
41 any time during the Holocene (Davies et al., 2020). The reconstructions of glacier variations show that the
42 glaciers in some regions are now smaller than previously recorded: since the mid-16th century in the Mont
43 Blanc and Grindelwald regions of the European Alps (Nussbaumer and Zumbühl, 2012), since the 9th
44 century in Norway (Nesje et al., 2012), and for the past 1800 years in NW Iceland (Harning et al., 2016,
45 2018). In Arctic Canada and Svalbard, many glaciers are now smaller than they have been in at least 4000
46 years (Lowell et al., 2013; Miller et al., 2013, 2017, Schweinsberg et al., 2017, 2018) and more than 40,000
47 years in Baffin Island (Pendleton et al., 2019). Although the millennial glacier length variation records are
48 incomplete and discontinuous, and glacier fluctuations depend on multiple factors (e.g. temperature,
49 precipitation, topography, internal glacial dynamics), there is a coherent relationship between rising
50 temperatures, negative mass balance and glacier retreat on centennial timescales across most of the world.
51 Glaciological and geodetic observations show that the rates of early 21st-century mass loss are the highest
52 since 1850 (Zemp et al., 2015). For all regions with long-term observations, glacier mass in the decade 2010
53 to 2019 was the smallest since at least the beginning of the 20th century (*medium confidence*).

54
55 In contrast to the global glacier mass decline (Figure 9.21, Supplementary Material 9.SM.2, Table 9.5), a few

1 glaciers have gained mass or advanced due to internal glacier dynamics or locally restricted climatic causes.
2 The SROCC discusses the “Karakoram anomaly” (centred on the western Kunlun range (at about
3 80°E/35°N), but also covering part of the Pamir and Karakoram ranges), where glaciers have been close to
4 balance since at least the 1970s and had a slightly positive mass balance since the 2000s. Since the SROCC,
5 new evidence suggests that this anomaly is related to a combination of low-temperature sensitivity of debris-
6 covered glaciers, a decrease of summer air temperatures (Cross-Chapter Box 10.3), and an increase in
7 snowfall possibly caused by increases in evapotranspiration from irrigated agriculture (Bonekamp et al.,
8 2019; de Kok et al., 2020; Farinotti et al., 2020; Shean et al., 2020). However, a recent geodetic mass
9 balance estimate suggests substantially increased thinning rates of High Mountain Asian glaciers after about
10 2010 (Hugonnet et al., 2021). There is *limited evidence* to assess whether the “Karakoram Anomaly” will
11 persist in coming decades, but due to the projected increase in air temperature throughout the region its long-
12 term persistence is *unlikely (high confidence)* (Kraaijenbrink et al., 2017; de Kok et al., 2020; Farinotti et al.,
13 2020; Cross-Chapter Box 10.3).

14 15 16 *Drivers of glacier change*

17 The AR5 (Masson-Delmotte et al., 2013) noted that early-to-mid-Holocene glacier minima could be
18 attributed to high summer insolation (*high confidence*), unlike the current situation. Since the AR5, new and
19 improved chronologies of glacier size variations from the end of the last glacial period and the Holocene
20 (e.g., Solomina et al., 2015, 2016; Eaves et al., 2019; Hall et al., 2019; Marcott et al., 2019; Bohleber et al.,
21 2020; Davies et al., 2020; Palacios et al., 2020) confirm the dominant role of orbital forcing for millennial-
22 scale glacier fluctuations but emphasize the role of other forcings – solar and volcanic activity, ocean
23 circulation, sea ice and internal climate variability – in explaining the regional variability of glacier
24 fluctuations at shorter time scales. Shakun et al., (2015) demonstrated that during the last deglacial transition
25 (18-11 ka), the mid-to-low-latitude glacier retreat was driven by an increase in atmospheric CO₂ and global
26 temperature.

27
28 In the Northern Hemisphere, where summer insolation decreased during the Holocene (Section 2.2.1),
29 glaciers generally waxed (Briner et al., 2016; Kaufman et al., 2016; Lecavalier et al., 2017; Zhang et al.,
30 2017; Axford et al., 2019; Geirsdóttir et al., 2019; Larsen et al., 2019; Luckman et al., 2020). Conversely, in
31 the Southern Hemisphere, where summer insolation increased during the Holocene, glaciers generally waned
32 (Solomina et al., 2015; Kaplan et al., 2016; Reynhout et al., 2019). However, these general global trends
33 were modulated by regional climate variations in temperature and precipitation (Murari et al., 2014; Kaplan
34 et al., 2016; Batbaatar et al., 2018; Saha et al., 2018) and there are a number of examples of this. A
35 precipitation increase led to a local early Holocene (7-8 ka) glacier maximum in arid Mongolia (Gichginii
36 Range). Glacier advances at ~9 ka in Southwest Greenland have been suggested to be a consequence of the
37 freshwater pulse from the Laurentide Ice Sheet, which led to cooling in the Baffin Bay area (Schweinsberg et
38 al., 2018). Lake sediments indicate that the glaciers in the region were smaller than today or absent between
39 8.6 and 1.4 ka BP (Larocca et al., 2020). Glaciers on the Antarctic Peninsula and in Patagonia during the
40 Holocene were strongly affected by the Southern Westerly Winds, sea ice extent, and ocean circulation
41 (García et al., 2020). Recent studies indicate that explosive volcanism can drive glacier advances (Solomina
42 et al., 2015, 2016; Schweinsberg et al., 2018; Brönnimann et al., 2019). In summary, on millennial time
43 scales over the Holocene, there is *high confidence* orbital forcing drove hemispheric-scale glacier variations,
44 but new studies provide a nuanced picture of responses to a variety of regional-scale forcings.

45
46 Section 3.4.3.1 assesses new attribution studies for glaciers and finds that human influence is *very likely* the
47 main driver of the global, near-universal retreat of glaciers since the 1990s. The SROCC assessed that it is
48 *very likely* that atmospheric warming is the primary driver for the global glacier recession. Since the
49 SROCC, a study of glaciers in New Zealand used event attribution to confirm a connection between extreme
50 glacier mass loss years and anthropogenic warming (Vargo et al., 2020).

51
52 The SROCC stated with *high confidence* that besides temperature, other factors, such as precipitation
53 changes or internal glacier dynamics, have modified the temperature-induced glacier response in some
54 regions. Deposition of a thin layer (<2 cm) of light-absorbing particles (e.g., black carbon, brown carbon,
55 algae, mineral dust or volcanic ash) can exert an important control on glacier mass balance, by decreasing

1 surface albedo and thus increasing absorbed shortwave radiation and melt (see also section 7.3.4.3. The
2 SROCC found *limited evidence* and *low agreement* that this process has had a significant effect on observed
3 long-term glacier changes. Several studies have shown melt increases due to the deposition of light-
4 absorbing particles (Schmale et al., 2017; Wittmann et al., 2017; Sigl et al., 2018; Di Mauro et al., 2019,
5 2020; Magalhães et al., 2019; Constantin et al., 2020). Conversely, increasingly thick debris cover (>2-5 cm)
6 on retreating glaciers can slow down glacier melt (Pratap et al., 2015; Brun et al., 2016). Although debris
7 covers only about 4-7% of the total glacier area globally (Scherler et al., 2018; Herreid and Pellicciotti,
8 2020), many glaciers are heavily debris-covered in their lower reaches, especially in High Mountain Asia,
9 the Caucasus, the European Alps, Southern Andes and Alaska, resulting in different responses to warming
10 than similar clean-ice glaciers. A shift in regional meteorological conditions driven by the location and
11 strength of the upper level zonal wind has been found to have forced recent high mass loss rates in Western
12 North America (Menounos et al., 2019). High geothermal heat flux areas underneath glaciers and high
13 energy dissipation in the flow of water and ice causes additional mass loss of the glaciers in Iceland
14 (Jóhannesson et al., 2020), accounting for 20% of the mass loss since 1994 (Aðalgeirsdóttir et al., 2020).
15 Glacier lake volume, in front of retreating glaciers, has increased globally by around 48% between 1990 and
16 2018 (Shugar et al., 2020), which can increase both subaqueous melt and calving. In summary, there is *high*
17 *confidence* that non-climatic drivers have and will continue to modulate the first-order temperature response
18 of glaciers in some regions.

19
20
21 **[START FIGURE 9.21 HERE]**

22
23 **Figure 9.21: Global and regional glacier mass evolution between 1901 and 2100 relative to glacier mass in 2015.**
24 Reconstructed glacier mass change through the 20th century (Marzeion et al., 2015) and observed during
25 1961-2016 (Zemp et al., 2019). Projected (2015-2100) glacier mass evolution is based on the median of
26 three Representative Concentration Pathways (RCPs) emission scenarios (Marzeion et al., 2020).
27 Uncertainties are in all cases the 90% confidence interval. For a better comparison between regions, the
28 maximum relative mass change was set to 200%, although for three regions, the volume changes between
29 1901 and 2015 exceeded that value. For the Low Latitude, New Zealand, and High Mountain Asia
30 glaciers, the changes were larger than 1000%, 350%, and 250%, respectively. See Figure 9.2 for the
31 location of each region. Further details on data sources and processing are available in the chapter data
32 table (Table 9.SM.9).

33
34 **[END FIGURE 9.21 HERE]**

35 36 37 9.5.1.2 Model evaluation

38
39 Since the AR5, glacier mass projections have been coordinated by the Glacier Model Intercomparison
40 Project (GlacierMIP) (Hock et al., 2019a; Marzeion et al., 2020). The SROCC (Hock et al., 2019b) relied on
41 six global-scale glacier models based on previously published glacier model projections (Hock et al., 2019a),
42 and found with *high confidence* that glaciers will lose substantial mass by the end of the century but assigned
43 *medium confidence* to the magnitude and timing of the projected glacier mass loss, because of the simplicity
44 of the models, the limited observations in some regions to calibrate them and the diverging initial glacier
45 volumes.

46
47 Since the SROCC, (Marzeion et al., 2020) projected 21st century global-scale glacier mass changes based on
48 seven global-scale and four regional-scale glacier models (Annex II). All models used the same initial and
49 boundary conditions, forming a more coherent ensemble of projections compared to the SROCC.
50 Nevertheless, challenges remain because of scarcity of glacier thickness, surface mass balance and frontal
51 ablation data for model calibration, but also due to uncertainties in glacier outlines, surface elevations and ice
52 velocities. The global surface mass balance models are of varying complexity, including mass balance
53 sensitivity approaches (van de Wal and Wild, 2001), temperature-index methods (Anderson and Mackintosh,
54 2012; Marzeion et al., 2012; Radić et al., 2014; Huss and Hock, 2015; Kraaijenbrink et al., 2017; Maussion
55 et al., 2019a; Zekollari et al., 2019; Rounce et al., 2020) and simplified energy balance calculations (Sakai
56 and Fujita, 2017; Shannon et al., 2019). Compared to simpler, empirical parameterizations, full energy-

1 balance models are not necessarily the most appropriate choice for simulating future glacier response to
2 climate change, even at the local scale (Réveillet et al., 2017, 2018), because of parameter and forcing
3 uncertainties. All models account for glacier retreat and advance but only two models (Anderson and
4 Mackintosh, 2012; Huss and Hock, 2015) include frontal ablation.

5
6 Secondary processes such as debris-cover thickening (e.g., Herreid and Pellicciotti, 2020), albedo changes
7 due to light-absorbing particles (e.g., Magalhães et al., 2019; Williamson et al., 2019), trends of refreezing
8 and water storage in firn (e.g., Ochwat et al., 2021), dynamic instabilities such as surges (e.g., Thøgersen et
9 al., 2019) or glacier collapse (e.g., Kääb et al., 2018), are not represented in global glacier models, resulting
10 in both underestimated and overestimated sensitivity to warming that is currently not possible to quantify.
11 Furthermore, challenges for future projections are caused by the low resolution and high spatial variability at
12 subgrid scale of the precipitation amount provided by GCMs, which requires downscaling to the spatial scale
13 of a glacier (Maussion et al., 2019a; Zekollari et al., 2019; Marzeion et al., 2020). In summary, in agreement
14 with the SROCC, progress in global scale glacier modelling efforts allows *medium confidence* in the
15 capability of current-generation glacier models to simulate the magnitude and timing of glacier mass changes
16 as a response to the climatic forcing.

17 18 19 9.5.1.3 Projections

20
21 The AR5 (Vaughan et al., 2013) and the SROCC (Hock et al., 2019b) stated with *high confidence* that the
22 world's glaciers are presently in imbalance due to the warming of recent decades. The observed retreat of
23 glaciers is only a partial response to the already realized warming (Christian et al., 2018), and they are
24 committed to losing considerable mass in the future, even without further change in air temperature (Mernild
25 et al., 2013; Trüssel et al., 2013; Zekollari and Huybrechts, 2015; Huss and Fischer, 2016; Marzeion et al.,
26 2018; Jouvét and Huss, 2019). One model estimates that $36 \pm 8\%$ of global glacier mass is already
27 committed to be lost due to past greenhouse gas emissions (Marzeion et al., 2018). Although accumulation
28 and ablation instantly determine the surface mass balance, the glacier geometries adjust to changed
29 atmospheric conditions over a longer time (Zekollari et al., 2020). The adjustment time, often referred to as
30 the response time, is variable from one glacier to another, depending on the glacier geometry (thickness and
31 steepness), surface mass balance and gradient (e.g., Jóhannesson et al., 1989; Harrison et al., 2001; Lüthi,
32 2009; Zekollari et al., 2020). Response time is variable: years for smaller and steeper glaciers (Beedle et al.,
33 2009; Lüthi and Bauder, 2010; Rabatel et al., 2013), up to tens or hundreds of years for larger and gentle-
34 sloped glaciers (e.g., Burgess and Sharp, 2004; Lüthi et al., 2010; Zekollari et al., 2020). The models
35 indicate that the disequilibrium between the glaciers and present atmospheric conditions (1995 to 2014)
36 reduces and then disappears at around year 2070 (Marzeion et al., 2020). There is therefore *very high*
37 *confidence* that the disequilibrium of glaciers will persist as warming continues and that glaciers will
38 continue to lose mass for at least several decades because of their lagged response even if global temperature
39 is stabilized.

40
41 The SROCC assessed that global glacier mass loss by 2100, relative to 2015 will be 18% [*likely* range 11 to
42 25%] for scenario RCP2.6 and 36% [*likely* range 26 to 47%] for RCP8.5, and that many glaciers will
43 disappear regardless of the emission scenario (*very high confidence*). Since the SROCC, new results from
44 (Marzeion et al., 2020) have been published (Box 9.3; Figure 9.21, Table 9.4, including peripheral glaciers in
45 Greenland and Antarctica). Glaciers will lose 29,000 [9,000 to 49,000] Gt and 58,000 [28,000 to 88,000] Gt
46 over the period 2015-2100 for RCP2.6 and RCP8.5, respectively (*medium confidence*), which represents 18
47 [5 to 31] % and 36 [16 to 56] % of their early 21st century mass, respectively (Table 9.4). Within
48 uncertainties, these agree with the SROCC estimates, although with a slightly smaller mass loss due to the
49 inclusion of models with lower sensitivity to changing climate conditions (Marzeion et al., 2020). The
50 greatest source of uncertainty in glacier mass loss until the middle of the 21st century is the disagreement
51 between glacier models, with emissions scenario becoming the dominant cause of uncertainty by the end of
52 the 21st century (Marzeion et al., 2020).

53
54 Although the GlacierMIP projections (Hock et al., 2019a; Marzeion et al., 2020) were forced by RCP
55 scenarios, two global glacier models (Huss and Hock, 2015; Maussion et al., 2019b) were also run with 13

1 GCMs and SSP scenarios (Table 9.4). These results show increased mass loss compared to the RCP forced
 2 simulations, although with fewer global glacier models. To enable the glacier contribution to future sea level
 3 rise to be estimated under the full range of SSP scenarios (Section 9.6.3.3), the GlacierMIP results are
 4 emulated using a Gaussian Process model (Edwards et al., 2021) (Box 9.3, Table 9.4). The emulated
 5 projections show a narrower range than the roughly equivalent RCP projections, which may be explained by
 6 not accounting for covariance in the regional uncertainties (Marzeion et al., 2020) and by the fact that the
 7 emulator caps sea level contribution for each region at the volume above floatation estimated by (Farinotti et
 8 al., 2019) (Table 9.SM.2). Comparison of simulated and emulated regional sea level contributions support
 9 this explanation. Rates of change and post-2100 projections for the sea level projections are estimated with
 10 the AR5 parametric fit (Supplementary Material 9.SM.4.5;(Church et al., 2013a)) applied to the GlacierMIP
 11 results (Marzeion et al., 2020), and these are also shown in Table 9.4 for comparison.

12
13
14 **[START TABLE 9.4]**

15
16 **Table 9.4:** Projected sea level contributions in meters from global glaciers (including peripheral glaciers in
 17 Greenland and Antarctica) by 2100 relative to 2015, for selected RCP and SSP scenarios.
18

Representative Concentration Pathways (RCPs)				
Study	RCP2.6	RCP4.5	RCP8.5	Notes
IPCC AR5 and SROCC (Church et al., 2013a; Oppenheimer et al., 2019)	0.10 (0.04 – 0.16)	0.12 (0.06 – 0.19)	0.17 (0.09 – 0.25)	Median and <i>likely</i> (66% range) contributions in 2100 relative to 1995-2014
GlacierMIP Hock et al. (2019a)	0.094 (0.069 – 0.119)	0.142 (107 – 177)	0.200 (0.156 – 0.240)	Mean (\pm 1 s.d. range) contributions
GlacierMIP Marzeion et al., (2020)	0.079 [0.023 – 0.135]	0.119 [0.053 – 0.185]	0.159 [0.073 – 0.245]	Median [90% range]
Shared Socioeconomic Pathways (SSPs)				
Study	SSP1-2.6	SSP2-4.5	SSP5-8.5	Notes
GlacierMIP experimental protocol (Marzeion et al., 2020) with CMIP6 forcing	0.111 (0.077 to 0.145) [0.05 to 0.167]	0.136 (0.096 to 0.176) [0.07 to 0.201]	0.190 (0.133 to 0.247) [0.09 to 0.283]	Mean (66% range) [90% range] using 13 GCMs and 2 glacier models ¹
GlacierMIP (Marzeion et al., 2020) with AR5 parametric fit: used for rates and post-2100 projections (Supplementary Material 9.SM.4.5)	0.102 (0.076 to 0.134) [0.059 to 0.154]	0.128 (0.095 to 0.167) [0.076 to 0.192]	0.171 (0.124 to 0.224) [0.098 to 0.259]	Median (66% range) [90% range] contribution from AR5 parametric fit to GlacierMIP ensemble, relative to 1995- 2014
Emulated (Marzeion et al., 2020); (Edwards et al., 2021)	0.080 (0.059 to 0.101) [0.046 to 0.116]	0.115 (0.093 to 0.137) [0.077 to 0.155]	0.170 (0.144 to 0.196) [0.124 to 0.218]	Median (66% range) [90% range] contribution in 2100 relative to

2015 from
emulator of
GlacierMIP6
used with
Chapter 7 climate
forcing

¹ OGGM (Maussion et al., 2019a) and GloGEM (Huss and Hock, 2015)

[END TABLE 9.4]

The mass loss rates vary between regions and there are distinctively different patterns between scenarios (Marzeion et al., 2020). The global models agree that regions characterized by relatively little glacier-covered area (Low Latitude, Central Europe, Caucasus, Western Canada and US, North Asia, Scandinavia and New Zealand) will lose nearly all (>80%) glacier mass by 2100 in the RCP 8.5 scenario, but their corresponding contribution to sea-level rise will be small. A study using detailed ice dynamics for the largest glacier of the European Alps, Great Aletsch Glacier, projects 60% of present ice volume will be lost by 2100 in RCP2.6 and an almost complete wastage of the ice in RCP8.5 (Jouvet and Huss, 2019). Due to their larger mass, the largest contribution to sea level rise comes from glaciers in the Arctic and Antarctic regions (Antarctic, Arctic Canada, Alaska, Greenland, Svalbard and Russian Arctic), in spite of having the smallest relative mass loss, and it is expected that they will continue to contribute to sea level rise beyond 2100. The regions with intermediate glacier mass (Southern Andes, High Mountain Asia and Iceland) show decreasing mass loss rates for RCP2.6 throughout the 21st century, and increasing rates for RCP8.5 that peak in the mid to late 21st century (Figure 9.21). The peak in mass loss rate followed by reduction is due to both decreasing glacier volume and stabilizing mass balance (Marzeion et al., 2020). Vatnajökull, the largest glacier in Iceland, is projected to lose about 50% of its mass by 2300 in extended RCP4.5 and 80-100% in extended RCP8.5 scenarios (Schmidt et al., 2019). In summary, both global and regional studies agree that glacier mass loss will continue in all regions, with larger mass loss for high emission scenarios (*high confidence*) (see also Section 8.4.1.7.1).

In the AR5 and the SROCC, glacier mass loss beyond 2100 was calculated employing a parametric fit to available model simulations. In section 9.6.3.5, that same parametric fit is applied to (Marzeion et al., 2020) projections resulting in complete glacier mass loss at year 2300 under SSP5-8.5 and 40-100% mass loss under SSP1-2.6. (Clark et al., 2016) simulate glacier mass evolution, not including glaciers peripheral to the Antarctic ice sheet, for different warming levels for the next ten thousand years. There is *limited evidence* and *low confidence* that at sustained warming levels between 1.5 and 2°C, about 50-60% of glacier mass will remain, predominantly in the polar regions. At sustained warming levels between 2 and 3°C, about 50-60% of glacier mass outside Antarctica will be lost and at sustained warming levels between 3 and 5 °C, 60-75% of glacier mass outside Antarctica will disappear. Based on (Marzeion et al., 2020), there is *medium confidence* that nearly all glacier mass in low latitudes, Central Europe, the Caucasus, Western Canada and the US, North Asia, Scandinavia and New Zealand will disappear at this high warming level.

9.5.2 Permafrost

This section focuses on the physical aspects of permafrost (perennially frozen ground) as an element of the climate system, drawing on the assessment of observed global permafrost changes provided in Section 2.3.2.5, and treating more specifically model evaluation and projections. The permafrost carbon feedback is assessed in Box 5.1. Section 12.4 of this report provides permafrost information relevant to impacts and risk on regional scales.

9.5.2.1 Observed and reconstructed changes

The current extent of the global permafrost region is about $22 \pm 3 \times 10^6$ km² (Gruber, 2012). Permafrost underlies about 15% of Northern Hemisphere land and more than 50% of the unglacierized land north of

1 60°N (Zhang et al., 1999; Gruber, 2012; Obu et al., 2019). It is also found in high-altitude areas of mountain
2 ranges in both hemispheres (estimated in the SROCC (Hock et al., 2019b) as representing about 27-29% of
3 the global permafrost area (*medium confidence*) and most unglacierized areas in Antarctica (Vieira et al.,
4 2010; Obu et al., 2020)). Ground ice volume in permafrost is variable, reaching up to 90% in syngenetic
5 permafrost deposits (Kanevskiy et al., 2013; Gilbert et al., 2016). The SROCC (Meredith et al., 2019)
6 reported *medium confidence* in the estimation that Earth's total perennial ground ice volume is equivalent to
7 2-10 cm of global sea level (Zhang et al., 2000). There is no evidence suggesting that a large part of this
8 volume, if melted, would run off and contribute to global sea level. Therefore, and because of the modest
9 total volume of mobilizable water, the contribution of permafrost thaw to past and future sea-level budgets is
10 usually neglected (see section 9.6.3.2).

11
12 Permafrost changes mostly refer to changes in extent, temperature and active layer thickness. The SROCC
13 (Hock et al., 2019b; Meredith et al., 2019) reported with *very high confidence* that record high permafrost
14 temperatures at the depth of the zero annual amplitude (the depth about 10 to 20 m below the surface where
15 the seasonal soil temperature cycle vanishes) were attained in recent decades in the Northern circumpolar
16 permafrost region, *high confidence* that permafrost has warmed over recent decades in many mountain
17 ranges, and overall *very high confidence* that global warming over the last decades has led to widespread
18 permafrost warming. As reported in the SROCC, the global (polar and mountain) permafrost temperature has
19 increased at $0.29 \pm 0.12^{\circ}\text{C}$ near the depth of zero annual amplitude between 2007 and 2016 (Biskaborn et al.,
20 2019). Stronger warming has been observed in the continuous permafrost zone ($0.39 \pm 0.15^{\circ}\text{C}$) compared to
21 the discontinuous zone ($0.20 \pm 0.10^{\circ}\text{C}$), consistent with the fact that near the melting point, a large amount of
22 energy is required for melting the ice (Figure 9.22), and because of the reduced effect of Arctic amplification
23 in more southerly locations (Romanovsky et al., 2017). This is consistent with longer-term Arctic trends
24 from deep boreholes shown in Figure 2.22. Mountain permafrost temperature trends are heterogeneous,
25 reflecting variations in local conditions such as topography, surface type, soil texture and snow cover, but
26 again, generally weaker warming rates are observed in warmer permafrost at temperatures close to 0°C ,
27 particularly when ice content is high (e.g., Mollaret et al., 2019; Noetzli et al., 2019; PERMOS, 2019). In
28 summary, strong variability in recent permafrost temperature trends is linked to local conditions, regionally
29 varying temperature trends and the thermal state of permafrost itself, but as discussed in Section 2.3.2.5,
30 there is overall *high confidence* in the observed increases in permafrost temperature over the past 3 to 4
31 decades throughout the permafrost regions.

32
33 Closer to the surface, the active layer undergoes annual cycles of freeze and thaw. The SROCC reported
34 *medium confidence* in active layer thickness (ALT) increase as a pan-Arctic phenomenon. Recent evidence
35 presented in Section 2.3.2.5 shows pervasive ALT increase in the European and Russian Arctic in the 21st
36 century and in high elevation areas in Europe and Asia since the mid-1990s. Emergence of a clearer global
37 picture is hampered by (1) uneven distribution of observing sites, (2) substantial variability among the
38 existing sites, strongly influenced by local conditions (soil constituents and moisture, snow cover,
39 vegetation); (3) interannual variability, and (4) thaw settlement in ice-rich terrain (Streletskiy et al., 2017;
40 O'Neill et al., 2019). In summary, in agreement with the SROCC and recent evidence presented in Section
41 2.3.2.5, there is *medium confidence* that ALT increase is a pan-Arctic phenomenon.

42
43 There is *medium confidence* that the observed acceleration and destabilization of rock glaciers is related to
44 warming temperatures and increase in water content at the permafrost table in recent decades (Deline et al.,
45 2015; Cicoira et al., 2019; Marcer et al., 2019; PERMOS, 2019; Kenner et al., 2020). There is also *medium*
46 *confidence* that observed increases in size and frequency of rock avalanches are linked to permafrost
47 degradation in rock walls (Ravanel et al., 2017; Patton et al., 2019; Tapia Baldis and Trombotto Liaudat,
48 2019). In summary, there is *medium confidence* that mountain permafrost degradation at high altitude has
49 increased the instability of mountain slopes in the past decade.

50
51 The SROCC assessed with *high confidence* that the extent of subsea permafrost, formed before submersion
52 on Arctic continental shelves during the last deglaciation, is much reduced compared to older studies that
53 had estimated the entire formerly exposed Arctic shelf area to be underlain by permafrost. This is supported
54 by observations (Shakhova et al., 2017) that show rapid thaw of recently submerged permafrost on the East
55 Siberian Shelf. A modelling study (Overduin et al., 2019) estimates that 97% of permafrost under Arctic

1 shelves is currently thinning.

2
3 Based on multiple studies, there is *medium confidence* that widespread retreat of coastal permafrost is
4 accelerating in the Arctic (Günther et al., 2015; Cunliffe et al., 2019; Isaev et al., 2019). There is also
5 consistent evidence of complete permafrost thaw in areas of discontinuous and sporadic permafrost since
6 about 1980 (Camill, 2005; Kirpotin et al., 2011; James et al., 2013; Jones et al., 2016a; Borge et al., 2017;
7 Chasmer and Hopkinson, 2017; Gibson et al., 2018a), but this evidence is geographically scattered. In spite
8 of increasing evidence of landscape changes from site studies and remote sensing, quantifying permafrost
9 extent change remains challenging because it is a subsurface phenomenon that cannot be observed directly
10 (Jorgenson and Grosse, 2016; Trofaier et al., 2017). A modelling study for the Qinghai-Tibet Plateau
11 between the 1960s and the 2000s (Ran et al., 2018) suggests transition from permafrost to seasonally frozen
12 ground over an area of more than 400,000 km². In summary, there is *medium confidence* that complete
13 permafrost thaw in recent decades is a common phenomenon in discontinuous and sporadic permafrost
14 regions. In addition, paleoclimatic evidence presented in Section 2.3.2.5 confirms a long-term sensitivity of
15 permafrost extent to climatic variations, although an analysis of North American speleothem records over the
16 last two glacial cycles indicates that this apparent high sensitivity could be a consequence of regional-scale
17 variability (Batchelor et al., 2019).

18
19 There is a lack of formal studies attributing observed permafrost changes (thaw depth, thermal state) or
20 associated landscape changes to anthropogenic forcing. However, the observed Arctic warming has been
21 attributed to anthropogenic forcing (e.g., Najafi et al., 2015) and an obvious physical link exists between
22 ground temperatures (and thus permafrost) and surface air temperatures. Therefore physically consistent and
23 convergent lines of evidence lead to *medium confidence* in anthropogenic forcing being the dominant cause
24 of the observed pan-Arctic permafrost changes. Added to this, local permafrost change by soil and
25 ecosystem disturbance is induced by increasing human industrial activities in the Arctic (e.g., Reynolds et
26 al., 2014).

27 28 29 9.5.2.2 Evaluation of permafrost in climate models

30
31 As stated in AR5 (Flato et al., 2013), coupled models contributing to CMIP5 showed large inter-model
32 variability of permafrost extent due to deficiencies in reproducing surface characteristics and processes
33 (Koven et al., 2013), particularly thermal properties of the ground and snow. These deficiencies led the
34 SROCC (Meredith et al., 2019) to express only *medium confidence* in the models' capacity to correctly
35 project the magnitude of future permafrost changes, in spite of *high confidence* in the models' projection of a
36 general thaw depth increase and a substantial loss of shallow permafrost. The SROCC further noted that
37 several types of physical "pulse" disturbances, in particular fire and thermokarst formation, are usually not
38 represented in coupled climate models. This has been discussed in detail in the SROCC, which assessed that
39 there is *high confidence* that permafrost degradation through fire (Jones et al., 2015; Gibson et al., 2018b) is
40 currently occurring faster in some well-studied regions than during the first half of the 20th century, and
41 *medium confidence* that thermokarst formation, to which about 20% of the northern permafrost region is
42 vulnerable (Olefeldt et al., 2016), can lead to faster large-scale permafrost degradation in response to climate
43 change.

44
45 Since the SROCC, dedicated modelling of the evolution of ice- and organic-rich permafrost in the northeast
46 Siberian lowlands (Nitzbon et al., 2020) has shown that not representing thermokarst-inducing processes in
47 ice-rich terrain leads to a systematic underestimation of the rapidity and magnitude of permafrost thaw.
48 Simplified inventory-based modelling (Turetsky et al., 2020) points towards similar conclusions. Although
49 these pulse disturbances still need to be represented in CMIP-type models, there have been many new
50 developments to that type of model since CMIP5 and the AR5. Soil freezing and its thermal and hydrological
51 effects are now included in a large number of land-surface modules that are part of the CMIP6 ensemble
52 (Chadburn et al., 2015a; Hagemann et al., 2016; Cuntz and Haverd, 2018; Guimberteau et al., 2018;
53 Yokohata et al., 2020), sometimes allowing for the effects of excess ice (Lee et al., 2014). Improved
54 representation of snow insulation in models has led to more realistic simulated permafrost extents (e.g.,
55 Paquin and Sushama, 2015). In a post-CMIP5 ensemble of land-surface models driven by observed

1 meteorological conditions (McGuire et al., 2016), inter-model spread was substantially reduced when the
2 ensemble was restricted to models that appropriately represented the effect of snow insulation on the
3 underlying soil (Wang et al., 2016b). More detailed descriptions of high-latitude vegetation characteristics,
4 vegetation dynamics, and snow-vegetation interactions have been included in several models (Chadburn et
5 al., 2015b; Porada et al., 2016; Druel et al., 2017) since the AR5.

6
7 A total soil column depth of at least about 10 m is required to adequately represent the dampening effect of
8 seasonal-scale heat exchanges between shallow and deeper ground, and thus to correctly simulate active
9 layer thickness (Lawrence et al., 2008; Ekici et al., 2015). However, many CMIP6 models still have
10 shallower total soil columns (Burke et al., 2020) and the proportion of models with deeper total soil columns
11 has not increased since CMIP5 (Koven et al., 2013). Another recently identified process, usually not
12 represented in the current (CMIP6) generation of climate models (Zhu et al., 2019), is warming-driven
13 decomposition and burning of organic material that provides strong thermal insulation of underlying ground.
14 Decay of the insulating organic material can lead to increased permafrost thaw, creating a positive feedback
15 loop.

16
17 In spite of the aforementioned structural improvements to many models, the simulated current permafrost
18 extent from available CMIP6 models shows no substantial improvement with respect to CMIP5 (see Figure
19 9.22a). The extent of the region where permafrost is simulated within the top 15 m in the Northern
20 Hemisphere for the 1979-1998 period is characterized by very large scatter in the coupled CMIP5 and
21 CMIP6 historical simulations compared to estimates of the present permafrost extent based on multiple
22 observational lines of evidence (Zhang et al., 1999) and models based on satellite observations and
23 reanalyses (Gruber, 2012; Obu et al., 2019). Outliers with very low simulated permafrost extent are models
24 that have only a very shallow soil column (leading to an underestimate of thermal inertia at depth) and do not
25 take into account soil water phase changes. These inadequacies lead to an overestimate of seasonal thaw
26 depth, exceeding the total thickness of the models' soil columns (Burke et al., 2020). Excessive simulated
27 permafrost extent can in several cases be traced to insufficient thermal insulation by the winter snow cover
28 (Burke et al., 2020).

29
30 Figure 9.22a also shows that the corresponding land-atmosphere simulations with prescribed observed sea-
31 surface temperatures and sea-ice concentrations, and the land-only simulations with prescribed reanalysis-
32 based meteorological forcing, do not provide an improved simulation of the current permafrost extent,
33 although, by construction, they can be expected to exhibit lower land surface climate biases. This further
34 points to deficiencies in the land modules as the main reason for biases, consistent with conclusions drawn
35 from the analysis of CMIP5 output (Koven et al., 2013), as reported in the SROCC and the AR5.

36
37 In spite of more realistic description of permafrost-related processes in many coupled climate models, the
38 CMIP6 models thus still produce a very scattered ensemble of estimates of current permafrost extent, and
39 there is *high confidence* that this is strongly linked to deficiencies of the representation of soil processes.
40 Furthermore, current-generation climate models tend to neglect several physical disturbances that can lead to
41 faster permafrost thaw. Because of large uncertainties in the future evolution of these drivers (see SROCC),
42 there is *limited evidence* that these shortcomings lead to an underestimate of permafrost degradation rates in
43 response to climate change in the CMIP6 ensemble. In summary, there is *high confidence* that coupled
44 models correctly simulate the sign of future permafrost changes linked to surface climate changes, but only
45 *medium confidence* in the amplitude and timing of the transient response.

46
47
48 **[START FIGURE 9.22 HERE]**

49
50 **Figure 9.22: Simulated versus observed permafrost extent and permafrost volume change by warming level. a)**
51 Diagnosed Northern Hemisphere permafrost extent (area with perennially frozen ground at 15 m depth, or
52 at the deepest model soil level if this is above 15 m) for 1979-1998, for available CMIP5 and CMIP6
53 models, from the first ensemble member of the historical coupled run, and for CMIP6 AMIP
54 (atmosphere+land surface, prescribed ocean) and land-hist (land only, prescribed atmospheric forcing)
55 runs. Estimates of current permafrost extents based on physical evidence and reanalyses are indicated as
56 black symbols (triangle: Obu et al. (2018); star: Zhang et al. (1999); circle: central value and associated

1 range from Gruber (2012)). b) Simulated global permafrost volume change between the surface and 3 m
2 depth as a function of the simulated GSAT change, from the first ensemble members of a selection of
3 scenarios, for available CMIP6 models. Further details on data sources and processing are available in the
4 chapter data table (Table 9.SM.9).
5

6 **[END FIGURE 9.22 HERE]**
7

9 9.5.2.3 Projected permafrost changes

10 The AR5 (Collins et al., 2013) and the SROCC (Meredith et al., 2019) (based on available CMIP5 output)
11 both expressed *high confidence* that future pan-Arctic thaw depth will increase and near-surface permafrost
12 extent will decrease under future global warming, and *medium confidence* in the magnitude of the simulated
13 changes because of model deficiencies and large spread of the results.
14

15 The equilibrium sensitivity of permafrost extent to stabilized global mean warming has been inferred (by
16 constraining CMIP5 output with diagnosed relationships between the observed present-day spatial
17 distribution of permafrost and air temperature) to be about $4.0 \times 10^6 \text{ km}^2 \text{ }^\circ\text{C}^{-1}$ (Chadburn et al., 2017) for
18 GSAT changes with respect to the present below about $+3^\circ\text{C}$. This equilibrium permafrost sensitivity,
19 relevant for assessing long-term permafrost changes at a stabilized warming level, is about 20% higher than
20 the transient centennial-scale near-surface permafrost extent sensitivity (diagnosed from seasonal thaw down
21 to 3 m depth) suggested by direct analysis of CMIP5 output (Slater and Lawrence, 2013). Compared to these
22 and other studies reported in the AR5 and the SROCC (Koven et al., 2013), the recently suggested
23 equilibrium extent sensitivity to GSAT changes of about $1.5 \times 10^6 \text{ km}^2 \text{ }^\circ\text{C}^{-1}$ based on idealized ground
24 temperature modelling (Liu et al., 2021) appears unrealistically low.
25

26 A strong transient temperature sensitivity of the volume of perennially frozen soil in the top 3 m below the
27 surface is consistently suggested by the available CMIP6 models (Figure 9.22b). Relative to the current
28 volume, the transient sensitivity of the modelled permafrost volume in the top 3 m to GSAT changes (with
29 respect to the 1995-2014 average and up to $+3^\circ\text{C}$ change, that is, about up to $+4^\circ\text{C}$ with respect to pre-
30 industrial levels) is about $25 \pm 5 \% \text{ }^\circ\text{C}^{-1}$ (Burke et al., 2020), but there is only *medium confidence* in this
31 value and 1s.d. uncertainty range because of the model deficiencies discussed in 9.5.2.2. It is important to
32 note that permafrost loss will not be limited to the top 3 m, with delayed response of deeper permafrost. The
33 simulated transient temperature sensitivity of permafrost volume is slightly stronger in the SSP1-2.6 scenario
34 than in other SSPs because subsurface temperature lag increases with higher atmospheric warming rates,
35 particularly when ground ice melting induces additional delays.
36

37 Due to the role of air temperature as a major driver of permafrost change, the SROCC (Hock et al., 2019b)
38 expressed *very high confidence* that permafrost in high-mountain regions is expected to undergo increasing
39 thaw and degradation during the 21st century, with stronger consequences expected for higher greenhouse
40 gas emission scenarios. Recently published studies (e.g., Zhao et al., 2019) support this SROCC assessment.
41

42 In summary, based on *high agreement* across CMIP6 and older model projections, fundamental process
43 understanding, and paleoclimate evidence, it is *virtually certain* that permafrost extent and volume will
44 shrink as global climate warms.
45

46 9.5.3 Seasonal snow cover

47 Mean snow cover extent in January and February, the usual months of maximum extent, covers about 45%
48 of the Northern Hemisphere (NH) land surface (more than 45 million km^2 over the 1967-2014 period
49 (Estilow et al., 2015)). In contrast, maximum seasonal snow cover in South America, the dominant ice-free
50 land mass in the Southern Hemisphere in terms of seasonal snow cover extent, remains well below 1 million
51 km^2 (Foster et al., 2009) or less than 2% of the Southern Hemisphere land surface.
52
53
54
55

1 Terrestrial snow cover is characterized via three variables: (1) areal snow cover extent (SCE), (2) the time
2 period of continuous snow cover (snow cover duration (SCD) which reflects snow-on and snow-off dates)
3 and (3) snow accumulation expressed either as snow depth (SD) or snow water equivalent (SWE; the depth
4 of water stored by the snowpack).

5
6 Observed large-scale snow cover changes, their attribution to human activity and their effects on the
7 hydrological cycle are also discussed in Chapter 2 (Section 2.3.2.2), Chapter 3 (Section 3.4.2) and Chapter 8
8 (Section 8.2.3.1) of this report. The role of snow in the global surface albedo feedback is assessed in Section
9 7.4.2.3. The effect of aerosol deposition on snow albedo and associated climate forcing is assessed in Section
10 7.3.4.3.

11 12 13 9.5.3.1 Observed changes of seasonal snow cover

14
15 The AR5 (Vaughan et al., 2013) reported that NH SCE in June *very likely* decreased by 11.7% [8.8 to 14.6
16 %] per decade over the 1967-2012 period, exceeding the absolute and relative reductions observed in March
17 and April. The AR5 further reported *very high confidence* that NH March and April SCE decreased over the
18 90 years after 1922. The SROCC only assessed snow cover changes for the Arctic and mountain areas. For
19 the Arctic (north of 60°N), the SROCC (Meredith et al., 2019) expressed *high confidence* in SCE decreases
20 of $-3.5 \pm 1.9\%$ per decade in May and $-13.4 \pm 5.4\%$ per decade in June, based on a combination of multiple
21 datasets (Mudryk et al., 2017). Concerning mountain snow cover, the SROCC (Hock et al., 2019b) reported
22 with *high confidence* that mountain snow cover (both in terms of SCE and maximum SWE) has generally
23 declined since the middle of the 20th century at lower elevations. At higher elevations, the SROCC reported
24 *medium confidence* in generally insignificant snow cover trends where these were available. The large-scale
25 assessment provided in Section 2.3.2.2 of this report reports *very high confidence* in substantial reductions of
26 NH snow cover extent (particularly in spring) since 1978, and states that there is *limited evidence* that this
27 decline extends back to the early 20th century.

28
29 Since the SROCC, progress in characterizing seasonal NH snow cover changes has been made through the
30 combined analysis of datasets from multiple sources (surface observations, remote sensing, land surface
31 models and reanalysis products). A recent combined dataset (Mudryk et al., 2020) identified negative NH
32 SCE trends in all months between 1981 and 2018, exceeding $-50 \times 10^3 \text{ km}^2\text{yr}^{-1}$ in November, December,
33 March and May (Figure 9.23a,b). The loss of spring SCE is also reflected in earlier spring snow melt,
34 derived from surface observations (Bulygina et al., 2011; Brown et al., 2017), satellite observations (Wang et
35 al., 2013; Estilow et al., 2015; Anttila et al., 2018), and model-based analyses (Liston and Hiemstra, 2011).
36 There is considerable inter-dataset and regional variability, but the continental-scale trends of spring snow-
37 off dates from these datasets are consistently negative (Brown et al., 2017; Kouki et al., 2019).

38
39 Satellite-derived estimates of NH SCE compiled within the NOAA snow chart Climate Data Record (NOAA
40 CDR) extend back to 1967, providing one of the longest environmental data records from spaceborne
41 measurements (Estilow et al., 2015). Continental trends from these coarse resolution estimates (~200 km)
42 show declining snow cover during the spring period, consistent with surface warming (Hernández-Henríquez
43 et al., 2015; Mudryk et al., 2017). As assessed in Section 2.3.2.2, there is therefore *very high confidence* that
44 the NH spring SCE has been decreasing since 1978.

45
46 Hemispheric reconstructions with simple snow models and in-situ observations have extended the satellite
47 record to 1922 (Brown and Robinson, 2011), putting the satellite era in historical context. This study, also
48 assessed in the AR5, suggests an increase in North American spring (March-April) SCE from 1915 to about
49 1950, followed by a decrease of the same total magnitude afterwards. In Eurasia, a negative trend in April is
50 visible over the entire 1922-2010 period of record, while in March, a step decrease at about 1985 separates
51 two periods with insignificant trends. Overall, combining March and April, consistency between the
52 continental trends since 1950 and agreement in sign with the NOAA satellite record since 1967 provides
53 *high confidence* in Northern Hemisphere spring snow cover decrease since about 1950. Analysis of
54 paleoclimate records (Pederson et al., 2011; Belmecheri et al., 2016) suggests that recent snowpack
55 reductions in western North America are exceptional on a millennial timescale (*medium confidence*).

1
2 Recent remote sensing global-scale studies (Hammond et al., 2018; Notarnicola, 2020) report that since
3 2000, snow cover area and/or duration decreased in 78% of global mountain areas (Notarnicola, 2020). Due
4 to the shortness of these records and high spatial variability, they only provide *limited evidence* in *medium*
5 *agreement* that snow cover area and duration changes over that recent period are more consistently negative
6 at higher (>4000 m) than at lower elevations, and do not alter the *high confidence* in longer-term mountain
7 snow cover decrease at lower elevations since the middle of the 20th century that was already reported in the
8 SROCC.

9
10 As assessed in detail in Chapter 3 (Section 3.4.2), it is *very likely* that anthropogenic influence contributed to
11 the observed reductions in Northern Hemisphere springtime snow cover since the mid-20th century. The
12 reasons for this assessment are: (1) physical consistency of the observed spring snowpack and surface
13 temperature changes both in observations and models, (2) the strong observed hemispheric and regional
14 spring SCE and SWE trends, and (3) the general attribution of hemispheric temperature changes to human
15 influence. Consistent between multiple observational products and historical climate model simulations, the
16 observed NH SCE sensitivity to NH land (>30°N) warming (Mudryk et al., 2017) is approximately $-1.9 \times$
17 $10^6 \text{ km}^2\text{°C}^{-1}$ (95% confidence range of $\pm 0.9 \times 10^6 \text{ km}^2\text{°C}^{-1}$ throughout the snow season.

18
19 Compared to numerous studies on spring SCE changes, less attention has been paid to changes in NH snow
20 cover during the onset period in the autumn, a challenging period to retrieve snow information from optical
21 satellite imagery due to persistent clouds and decreased solar illumination at higher latitudes. Positive trends
22 in October and November SCE in the NOAA-CDR (Hernández-Henríquez et al., 2015) are not replicated in
23 other surface, satellite, and model datasets (Brown and Derksen, 2013; Peng et al., 2013; Hori et al., 2017;
24 Mudryk et al., 2017). The positive trends from the NOAA-CDR are also inconsistent with later autumn
25 snow-on dates since 1980 (-0.6 to -1.4 days per decade), based on historical surface observations, model-
26 derived analyses and independent satellite datasets (updated from Derksen et al., 2017). Furthermore, the
27 SCE trend sensitivity to surface temperature forcing in the NOAA-CDR is anomalous compared to other
28 datasets during October and November (Mudryk et al., 2017). There is therefore *medium confidence* that the
29 NH SCE trend for the 1981-2016 period was also negative during these two months (Mudryk et al., 2020).

30
31 In the low-to-mid latitude (18°S-40°S) South American Andes, a dry-season snow cover decrease of about
32 12% per decade has been reported for the period 1986-2018 (Cordero et al., 2019), linked to ENSO changes
33 dominant in the northern part and an additional influence of poleward migration of the westerly wind zone in
34 the southern part of the study area. Further South, long-term warming has been identified as the dominant
35 cause of observed winter snow cover reduction over the 1972-2016 period at about 53°S in Brunswick
36 Peninsula (Aguirre et al., 2018).

37
38 The AR5 (Hock et al., 2019b) reported on snow water equivalent (SWE) and snow depth (SD) in situ
39 observations mostly from mountain areas, the majority of which showed negative trends over their respective
40 observational periods. However, the AR5 did not provide an assessment of large-scale snow mass changes
41 across the Northern Hemisphere. The SROCC attributed *medium confidence* to reports of negative SWE
42 trends in the Russian Arctic between 1966 and 2014, and stated that seasonal maximum snow depth trends in
43 the North American Arctic were mostly insignificant and of inconsistent sign. It further attributed *medium*
44 *confidence* to gridded products that suggest negative pan-Arctic SWE trends between 1981 and 2016, and
45 *high confidence* in a general decline of mountain snow mass at lower elevations, albeit with regional
46 variations.

47
48 Since the AR5, the number of global or hemispheric-scale gridded SWE products has substantially increased.
49 A validation and intercomparison (Mortimer et al., 2020) of datasets derived from (1) reanalysis-based
50 products, (2) a combined surface observation – passive microwave remote sensing product and (3) stand-
51 alone passive microwave products has led to better understanding of the strengths and limitations of each.
52 These gridded products consistently identify negative trends in maximum pre-melt SWE over the 1981 –
53 2016 period over both Eurasia and North America (Mudryk et al., 2020); (Figure 9.23c and d). To further
54 constrain SWE uncertainty, Pulliainen et al. (2020) implemented a bias correction based on snow course
55 observations which yielded a current best estimate for the average 1980-2018 March SWE over NH non-

1 alpine land north of 40°N of 2938 Gt [*likely* range 2846-3062 Gt]. Using this method, the bias-corrected
2 GlobSnow3.0 dataset suggests a 4.6 Gt yr⁻¹ decrease of March SWE over this 39-year period across North
3 America, and a negligible trend across Eurasia. These SWE trends are consistent with the continental SCE
4 trends over this period as assessed above, but strong regional and temporal variability only allows *medium*
5 *confidence* in the signs and magnitudes of these trends. However, there is *high confidence* in a general
6 decline of NH spring SWE since 1981 (Section 2.3.2.2). In the longer term (see also Section 2.3.2.2), annual
7 maximum snow depth trends from site measurements confirm mostly negative trends in North America
8 (Kunkel et al., 2016) between 1960/61 and 2014/15 and strong spatial variability in Eurasia (Zhong et al.,
9 2018) between 1966 and 2012, with spatial patterns bearing some resemblance to the shorter satellite-based
10 trends reported by Pulliainen et al. (2020). However, over this longer period, the Eurasian measurements
11 (Zhong et al., 2018) exhibit, on average, a positive trend. On the Qinghai–Tibetan Plateau, site
12 measurements between 1961 and 2010 (Xu et al., 2017) suggest a shift from an initial increase of spring
13 snow depth until about 1980 to a decreasing trend afterwards.

14
15
16 [START FIGURE 9.23 HERE]

17
18 **Figure 9.23: Observed monthly Northern Hemisphere (a) snow cover trends and (b) anomalies, and (c) snow**
19 **mass trends and (d) anomalies.** From the observation-based ensemble discussed in the text (Mudryk et
20 al., 2020). Trends and anomalies are calculated over the 1981-2018 period. Further details on data sources
21 and processing are available in the chapter data table (Table 9.SM.9).

22
23 [END FIGURE 9.23 HERE]

24
25
26 Concerning the assessment of SWE trends in mountainous regions, the SROCC noted a need for
27 observations spanning several decades because of very strong temporal variability. Moreover, determining
28 SWE trends in mountain regions is challenging because the coarse resolution (typically 25 to 50 km) of
29 gridded SWE products is inadequate in areas of mountainous terrain (Snauffer et al., 2016). Based on a
30 compilation of a large number of studies of SWE trends in mountain regions, the SROCC noted strong
31 regional variations, but a general consistency in greater reductions in SWE at lower elevations associated
32 with shifts from solid to liquid precipitation. A recent synthesis of snow observations in the European Alps
33 (Matiu et al., 2021) shows a 1971-2019 seasonal (November to May) snow depth trend of -8.4% per decade,
34 along with negative maximum snow depth and seasonal snow cover duration trends. The trends are stronger
35 and more significant during transitional seasons and at transitional (from no snow to snow) altitudes, and
36 exhibit strong regional variations, consistent with earlier reports for the Swiss and Austrian Alps (Schöner et
37 al., 2019) and the Pyrenees (López-Moreno et al., 2020).

38
39 In summary, since the AR5, intercomparison, dataset blending of gridded products, and bias correction using
40 snow course measurements contributed to an improved estimate of the average 1980-2018 March SWE over
41 NH non-alpine land north of 40°N of 2938 Gt [*likely* range 2846-3062 Gt], with *medium confidence* in the
42 magnitudes of continental-scale trends over that period. However, there is *high confidence* in a general
43 decline of NH spring SWE since 1981 (Section 2.3.2.2). In mountain areas, in situ observations tend to
44 suggest that annual maximum SWE reductions are generally stronger at elevation bands where shifts from
45 solid to liquid precipitation affected the snow mass.

46 47 48 9.5.3.2 Evaluation of seasonal snow in climate models

49
50 Building on the AR5 (Flato et al., 2013) and subsequent published work, the SROCC (Meredith et al., 2019)
51 stated that CMIP5 models tended to underestimate the observed decrease of Northern Hemisphere spring
52 snow cover extent due to inappropriate parameterisation of snow processes, misrepresentation of the snow-
53 albedo feedback, underestimated temperature sensitivity, and biased climatological spring snow cover. Since
54 the AR5, progress in the observation, description and understanding of snow microstructure (Kinar and
55 Pomeroy, 2015; Calonne et al., 2017) and its links to physical (thermal and radiative) properties (Löwe et al.,

2013; Calonne et al., 2014) has prompted efforts to represent physical properties as a function of the evolving snow microstructure in models (Carmagnola et al., 2014; Calonne et al., 2015). However, even state-of-the-art snow models intended for meteorological and climate applications still struggle to correctly represent the time evolution of the snow thermal properties, particularly of cold and dry tundra snow (Domine et al., 2016). Moreover, most, if not all, CMIP6 climate models do not explicitly represent the darkening of snow by deposition of BC and other light-absorbing aerosol species that is known to influence snow melt rates (Section 7.3.4.3). Regardless of these shortcomings, snow modules of climate models continue to be improved. Recent progress includes the incorporation of multiple energy balances within the canopy and between subgrid-tiles with different snow heights (Aas et al., 2017; Boone et al., 2017) and inclusion of advanced specific snow models in coupled climate models (Niwano et al., 2018; Voltaire et al., 2019), opening the prospect of future progress in quantifying snow-related feedbacks in a changing climate. Recently developed multi-physics snow models (Essery, 2015; Lafaysse et al., 2017), which are able to emulate the behaviour of a large number of models in a broad range of climates, allow model shortcomings and key parameter uncertainties, for example, concerning snow masking by vegetation or snow thermal conductivity, to be identified. Guidance for future model improvement can be provided by improved diagnostics, such as a concise metric of snow insulation (Slater et al., 2017a), which builds on an observed relation between effective seasonal mean snow depth and the dampening of winter season temperature decrease within the soil, and allows an efficient quantification of inaccuracies in the simulated snow insulation effect.

There is *high confidence* that large inter-model variations in the snow-cover sensitivity to temperature can largely be explained by inaccuracies in the simulated snow albedo feedback (Qu and Hall, 2014); a multi-model sub-ensemble of CMIP5 models that simulate a correct magnitude of this feedback presents a 40% reduced spread in the projected 21st century Northern Hemisphere land warming trend (Thackeray and Fletcher, 2016). Errors of the simulated feedback strength were linked to 1) systematic positive albedo biases over the boreal forest belt, mostly due to unrealistic treatment of vegetation masking (Thackeray and Fletcher, 2016), 2) inaccurate prescribed tree cover fraction and inappropriate parameterization of leaf area index in some models (Lorant et al., 2014; Wang et al., 2016a) and 3) low spatial resolution leading to inaccuracies in the strength of the simulated SAF in mountainous regions (Letcher and Minder, 2015). Although the representation of snow albedo feedback improved in many CMIP5 models over CMIP3, some models deteriorated (Thackeray et al., 2018).

Analysis of the available CMIP6 historical simulations for the 1981-2014 shows that on average, CMIP6 models simulate well the observed SCE (Mudryk et al., 2020), except for outliers and a median low bias during the winter months (Figure 9.24a). This is an improvement over CMIP5 (Mudryk et al., 2020), in which many snow-related biases were linked to inadequacies of the vegetation masking of snow cover over the boreal forests (Thackeray et al., 2015). A comparison between CMIP5 and CMIP6 results (Mudryk et al., 2020) shows that there is no notable progress in the quality of the representation of the observed 1981-2014 monthly snow cover trends.

[START FIGURE 9.24 HERE]

Figure 9.24: Simulated CMIP6 and observed snow cover extent (SCE). a) Simulated CMIP6 and observed (Mudryk et al., 2020) SCE (in millions of km²) for 1981-2014. Boxes and whiskers with outliers represent monthly mean values for the individual CMIP6 models averaged over 1981-2014, with the red bar indicating the median of the CMIP6 multi-model ensemble for that period. The observed interannual distribution over the period is represented in green, with the yellow bar indicating the median. b) Spring (March to May) Northern Hemisphere snow cover extent against GSAT (relative to the 1995-2014 average) for the CMIP6 Tier 1 scenarios (SSP1-2.6, SSP2-4.5, SSP3-7.0 and SSP5-8.5), with linear regressions. Each data point is the mean for one CMIP6 simulation (first ensemble member for each available model) in the corresponding temperature bin. Further details on data sources and processing are available in the chapter data table (Table 9.SM.9).

[END FIGURE 9.24 HERE]

9.5.3.3 Projected snow cover changes

The AR5 (Collins et al., 2013) stated that substantial NH spring snow cover reductions at the end of the 21st century were *very likely* under strong emission scenarios, and expressed *medium confidence* in the projected geographic patterns of annual maximum SWE changes. Based on studies using downscaled CMIP5 or RCM output, either directly or via snowpack models driven by such output, the SROCC (Hock et al., 2019b) reported *likely* snow depth or mass decreases at lower elevations in many mountain ranges over the 21st century and *high confidence* in smaller future changes at higher elevations.

Since the AR5, one study (Brown et al., 2017), applying a method developed by de Elía et al. (2013) to a CMIP5 sub-ensemble, suggested that over most of the Northern Hemisphere, the projected decrease of SCD will exceed natural variability before this will be the case for annual maximum SWE. The same study reports that over large parts of Eastern and Western North America and Europe, forced SCD changes are projected to exceed natural variability in the 2020s both in spring and autumn, while the signals tend to emerge later in the Arctic regions and particularly late, after 2060, in Eastern Siberia under the RCP8.5 scenario. Thackeray and Fletcher (2016) have shown that inter-model spread in projected spring SCE trends could be reduced through improved simulation of spring season warming because of the tight coupling between temperature and SCE linked to the snow albedo feedback (Qu and Hall, 2014; Thackeray and Fletcher, 2015).

Across all emission scenarios and with negligible scenario dependence (Figure 9.24b), CMIP6 models consistently (all models and all months) simulate Northern Hemisphere snow cover decrease in response to future GSAT change over the 21st century (Mudryk et al., 2020). The simulated SCE decrease is close to a linear function of global temperature change for all months (shown in Figure 9.24b for spring, with *medium confidence* in an average sensitivity of about -8% per °C of GSAT increase), except when snow cover vanishes. This occurs at about +2°C of GSAT change above the 1995-2014 level (that is, about +3°C above the pre-industrial level) for the months of July and August, and at about +3°C above the 1995-2014 level for June and September. Possible effects of such changes on the hydrological cycle are assessed in Chapter 8 (Section 8.2.3.1).

In summary, consistent projections from all generations of global climate models, elementary process understanding and strong covariance between snow cover and temperature on several time scales make it *virtually certain* that future Northern Hemisphere snow cover extent and duration will continue to decrease as global climate continues to warm, and process understanding strongly suggests that this also applies to Southern Hemisphere seasonal snow cover (*high confidence*).

Seasonal snow cover, by definition, has a clear annual cycle with usually complete disappearance in spring and summer and re-formation in autumn or winter. Therefore, there is *very high confidence* that the current and projected changes to seasonal snow cover are reversible (Verfaillie et al., 2018). In the case of global or regional cooling, abrupt large-scale snow-cover changes with a transition from seasonal to persistent snow cover due to a strong snow albedo feedback are a typical feature of glacial inceptions (e.g., Baum and Crowley, 2003; Calov et al., 2005), and these can be irreversible on centennial or longer timescales because of this feedback. In summary, based on physical understanding and the absence of occurrence of such events in climate model projections, abrupt future changes of seasonal snow cover on large scales in the absence of concomitant abrupt atmospheric change as a driver appear *very unlikely* in the context of current and projected warming.

9.6 Sea Level Change

9.6.1 Global and regional sea-level change in the instrumental era

9.6.1.1 Global mean sea-level change budget in the pre-satellite era

The SROCC (Oppenheimer et al., 2019) discussed the development and application of new statistical methodologies for reconstructing global mean sea level (GMSL; Box 9.1) from tide-gauge data over the 20th

1 century. Based on an ensemble of tide gauge reconstructions, the SROCC assessed an average rate of GMSL
2 rise of 1.38 mm yr⁻¹ [0.81 to 1.95 *very likely* range] for the period 1901 to 1990. Since the SROCC, two new
3 GMSL reconstructions have been published (Dangendorf et al., 2019; Frederikse et al., 2020b) and are
4 included in an updated ensemble estimate of GMSL change (Palmer et al., 2021, Section 2.3.3.3). Based on
5 these updated data and methods, the GMSL change over the (pre-satellite) period 1901 to 1990 is assessed to
6 be 0.12 m [0.07 to 0.17 *very likely* range] with an average rate of 1.35 mm yr⁻¹ [0.78 to 1.92 *very likely*
7 range] (*high confidence*) (Table 9.5; section 2.3.3.3) in agreement with the SROCC assessment. Both this
8 assessment and SROCC have substantially larger uncertainties than the AR5 assessment, which was based
9 upon a single tide gauge reconstruction and did not account for structural uncertainty (see Palmer et al.,
10 (2021) for a discussion).

11
12 The SROCC found that four of the five available tide gauge reconstructions that extend back to at least 1902
13 showed a robust acceleration (*high confidence*) of GMSL rise over the 20th century, with estimates for the
14 period 1902-2010 (-0.002 to 0.019 mm yr⁻²) that were consistent with the AR5. New tide gauge
15 reconstructions published since the SROCC (Dangendorf et al., 2019; Frederikse et al., 2020b) support this
16 assessment and suggest that increased ocean heat uptake related to changes in Southern Hemisphere winds
17 and increased mass loss from Greenland are the primary physical mechanisms for the acceleration (section
18 2.3.3.3). Therefore, the SROCC assessment on the acceleration of GMSL rise over the 20th century is
19 maintained.

20
21 The evaluation of the sea-level budget presented here, and in section 9.6.1.2, draws on assessments of the
22 individual components (Section 2.3.3.1 and 9.2.4.1 for global-mean thermosteric and sections 9.5.1.1, 9.4.1.1
23 and 9.4.2.1 for ice mass loss contributions to GMSL change from glaciers and ice sheets). Following the
24 approach of the SROCC, the mass loss from ice sheet peripheral glaciers is included in the ice sheet
25 contributions to GMSL change (glacier mass loss from regions 5 and 19 of the Randolph Glacier Inventory
26 6.0 (RGI Consortium, 2017) are added to ice sheet mass loss where applicable, with uncertainties added in
27 quadrature). The total change in GMSL for each component, and their sum, is summarised in Table 9.5
28 (uncertainties added in quadrature). For consistency across the report and to simplify the treatment of
29 uncertainties, all budget calculations are based on the difference between the first and last year in each period
30 (Palmer et al., 2021), rather than a linear fit to the underlying time series as used in SROCC and AR5.

31
32 The sea-level budget in the SROCC included the anthropogenic contribution of land water storage (LWS;
33 Box 9.1) change from a single estimate (Wada, 2016). Since the SROCC, two studies have combined
34 estimates of natural LWS change with anthropogenic LWS changes from reservoir impoundment and
35 groundwater depletion (Cáceres et al., 2020; Frederikse et al., 2020b). For (Cáceres et al., 2020), zero change
36 is assumed for the period 1901-1948, since their LWS change estimates are not available before 1948. Given
37 the large year-to-year changes associated with hydrological variability, the assessed changes in LWS (Table
38 9.5) are based on linear trends for each period, following (Palmer et al., 2021). Structural uncertainty is
39 estimated from the standard deviation of the trends across the two studies and parametric uncertainty is
40 estimated based on the Monte Carlo simulations of (Frederikse et al., 2020b). These two sources of
41 uncertainty are combined in quadrature and the assessed central estimate is taken as the average of the
42 ensemble mean trends. Compared to the SROCC assessed LWS trend of -0.12 mm yr⁻¹ for the period 1901-
43 1990, the updated assessment leads to a more negative trend of -0.16 [-0.35 to 0.04] mm yr⁻¹, although the
44 two are consistent within the estimated uncertainties. Previous studies and the SROCC have highlighted the
45 large uncertainty in estimates of LWS change over the 20th century (Gregory et al., 2013), and therefore the
46 SROCC assessment of *low confidence* in the estimated LWS contribution to GMSL change is maintained.

47
48 Since the SROCC, a new ocean heat content reconstruction (Zanna et al., 2019b) (Section 2.3.3.1) has
49 allowed global thermosteric sea-level change to be estimated over the 20th century. As a result, the sea-level
50 budget for the 20th century can now be assessed for the first time. For the periods 1901 to 1990 and 1901 to
51 2018 the assessed *very likely* range for the sum of components is found to be consistent with the assessed
52 *very likely* range of observed GMSL change (*medium confidence*), in agreement with (Frederikse et al.,
53 2020b) (Table 9.5). This represents a major step forward in the understanding of observed GMSL change
54 over the 20th century, which is dominated by glacier (52%) and Greenland ice sheet mass loss (29%) and the
55 effect of ocean thermal expansion (32%), with a negative contribution from the land water storage change (-

14%). While the combined mass loss for Greenland and glaciers is consistent with the SROCC, updates in the underlying datasets lead to differences in partitioning of the mass loss.

9.6.1.2 Global mean sea-level change budget in the satellite era

The SROCC (Oppenheimer et al., 2019) concluded that GMSL increased at a rate of 3.16 [2.79 to 3.53 *very likely* range] mm yr⁻¹ in the period 1993 to 2015 (the satellite altimetry era) and a rate of 3.58 [3.10 to 4.06 *very likely* range] mm yr⁻¹ in the period 2006 to 2015 (the GRACE/Argo era) (*high confidence*). An updated assessment for the periods 1993 to 2018 and 2006 to 2018 yields values of 3.25 [2.88 to 3.61] and 3.69 [3.21 to 4.17] mm yr⁻¹ (*high confidence*) (Table 9.5), with the slightly larger central estimates consistent with the observed acceleration in GMSL rise since the late 1960s (Dangendorf et al., 2019), given the longer assessment periods. Based on the GMSL assessed time series presented in section 2.3.3.3, GMSL acceleration is estimated as 0.075 [0.066 to 0.080] mm yr⁻² for 1971 to 2018 and 0.094 [0.082–0.115] mm yr⁻² for 1993–2018 (*high confidence*). For the common period of 1993–2010, the assessed rate of GMSL rise based on tide gauge reconstructions (3.19 [1.18 to 5.20] mm yr⁻¹) is consistent with the assessment based on satellite altimetry (2.77 [2.26 to 3.28] mm yr⁻¹), within the estimated uncertainties.

Since the SROCC, two new estimates of the LWS contribution have been published (Cáceres et al., 2020; Frederikse et al., 2020b) (see Section 9.6.1.1). For the early 21st century (the periods 1993 to 2018 and 2006 to 2018) both publications find a positive LWS contribution (Table 9.5), based on the most recent GRACE-derived estimates. This contrasts with the negative LWS contribution presented for the same periods in the SROCC based on (WCRP Global Sea Level Budget Group, 2018b) and reinforces the *low confidence* assessment of the LWS contribution.

For both periods in the satellite era, i.e., 1993 to 2018 and 2006 to 2018, the sum of contributions is consistent with the total observed GMSL change (*high confidence*) (Table 9.5). However, the latter period, which is characterised by improved data quality and coverage associated with satellite and Argo observations, shows much closer agreement in the central estimates. The marginal sea-level budget closure for the period 1993 to 2018 may indicate underestimated uncertainty, which may be structural as well as parametric. The sea-level budget assessments across the various periods in Table 9.5 demonstrate that the acceleration in GMSL rise (Section 2.3.3.3) since the late 1960s is mostly the result of increased ice sheet mass loss. However, all contributions to GMSL rise show their largest rate during 2006 to 2018, with the ice sheets accounting for about 35% of the total change during this period.

[START TABLE 9.5 HERE]

Table 9.5: Observed contributions to global mean sea level (GMSL) change for five different periods. Values are expressed as the total change (Δ) in the annual mean or year mid-point value over each period (mm) along with the equivalent rate (mm yr⁻¹). The *very likely* ranges appear in brackets based on the various section assessments as indicated. Uncertainties for the sum of contributions are added in quadrature, assuming independence. Percentages are based on central estimate contributions compared to the central estimate of the sum of contributions.

Observed contribution to GMSL change		1901-1990 {9.6.1.1}	1971-2018 {CCBox 9.1}	1993-2018 {9.6.1.2}	2006-2018 {9.6.1.2}	1901-2018 {9.6.1.1}
Thermal expansion (Section 2.3.3.1, Table 2.7)	Δ (mm)	31.6 [14.7 to 48.5] (31.9%)	47.5 [34.3 to 60.7] (50.3%)	32.7 [23.8 to 41.6] (45.7%)	16.7 [8.9 to 24.6] (34.4%)	63.2 [47.0 to 79.4] (38.4%)

	mm yr ⁻¹	0.36 [0.17 to 0.54]	1.01 [0.73 to 1.29]	1.31 [0.95 to 1.66]	1.39 [0.74 to 2.05]	0.54 [0.40 to 0.68]
Glaciers (Excl. peripheral glaciers) (Sections 2.3.2.3, 9.5.1.1)	Δ (mm)	51.8 [30.4 to 73.2] (52.3%)	20.9 [10.0 to 31.7] (22.1%)	13.8 [10.0 to 17.6] (19.3%)	7.5 [6.8 to 8.2] (15.4%)	67.2 [41.8 to 92.6] (40.8%)
	mm yr ⁻¹	0.58 [0.34 to 0.82]	0.44 [0.21 to 0.67]	0.55 [0.40 to 0.70]	0.62 [0.57 to 0.68]	0.57 [0.36 to 0.79]
Greenland ice sheet (Incl. peripheral glaciers) (Sections 2.3.2.4.1, 9.4.1.1)	Δ (mm)	29.0 [16.3 to 41.7] (29.3%)	11.9 [7.7 to 16.1] (12.6%)	10.9 [9.0 to 12.8] (15.2%)	10.9 [9.5 to 12.2] (22.3%)	40.4 [27.2 to 53.5] (24.5%)
	mm yr ⁻¹	0.33 [0.18 to 0.47]	0.25 [0.16 to 0.34]	0.44 [0.36 to 0.51]	0.91 [0.79 to 1.02]	0.35 [0.23 to 0.46]
Antarctic ice sheet (Incl. peripheral glaciers) (Sections 2.3.2.4.2, 9.4.2.1)	Δ (mm)	0.4 [-8.8 to 9.6] (0.4%)	6.8 [-3.9 to 17.5] (7.2%)	6.4 [4.3 to 8.5] (9.0%)	6.4 [4.8 to 8.0] (13.1%)	6.9 [-3.8 to 17.5] (4.2%)
	mm yr ⁻¹	0.00 [-0.10 to 0.11]	0.14 [-0.08 to 0.37]	0.26 [0.17 to 0.34]	0.53 [0.40 to 0.66]	0.06 [-0.03 to 0.15]
Land water storage* (Section 9.6.1.1)	Δ (mm)	-13.8 [-31.4 to 3.8] (-13.9%)	7.3 [-2.4 to 16.9] (7.7%)	7.8 [3.3 to 12.2] (10.8%)	7.2 [3.8 to 10.6] (14.8%)	-12.9 [-45.8 to 20.0] (-7.8%)
	mm yr ⁻¹	-0.15 [-0.35 to 0.04]	0.15 [-0.05 to 0.36]	0.31 [0.13 to 0.49]	0.60 [0.32 to 0.88]	-0.11 [-0.39 to 0.17]

Sum of observed contributions	Δ (mm)	99.0 [63.0 to 135.1]	94.4 [71.7 to 117.1]	71.6 [60.5 to 82.6]	48.7 [39.9 to 57.5]	164.8 [117.0 to 212.5]
	mm yr ⁻¹	1.11 [0.71 to 1.52]	2.01 [1.52 to 2.49]	2.86 [2.42 to 3.30]	4.06 [3.32 to 4.79]	1.41 [1.00 to 1.82]
Observed GMSL change (Section 2.3.3.3)	Δ (mm)	120.1^T [69.3 to 170.8]	109.6^{T&A} [72.8 to 146.4]	81.2^A [72.1 to 90.2]	44.3^A [38.6 to 50.0]	201.9^{T&A} [150.3 to 253.5]
	mm yr ⁻¹	1.35^T [0.78 to 1.92]	2.33^{T&A} [1.55 to 3.12]	3.25^A [2.88 to 3.61]	3.69^A [3.21 to 4.17]	1.73^{T&A} [1.28 to 2.17]

^{T, A} and ^{T&A} indicate assessments based on tide gauge reconstructions (T), satellite altimetry (A), or a combination of both (T&A). The assessment uses tide gauge reconstructions before 1993 and satellite altimetry after 1993.

*For the periods 1971-2018, 1993-2018, 2006-2018 and 1901-2018 the Caceres et al. (2020) linear trends are based on the period up to 2016.

[END TABLE 9.5 HERE]

9.6.1.3 Regional sea-level change in the satellite era

Regional sea-level changes are resolved by both tide gauge and satellite altimetry observations (Hamlington et al., 2020a). Altimeters have the advantage of quasi-global coverage but are limited to a period (1993-present) in which the forced trend response is just emerging on regional scales (Section 9.6.1.4). An analysis of the local altimetry error budget to estimate 90% confidence intervals on regional sea-level trends and accelerations reports that 98% of the ocean surface has experienced significant sea-level rise over the satellite era (Prandi et al., 2021). The same study finds that sea-level accelerations display a less uniform pattern, with an east/west dipole in the Pacific, a north/south dipole in the Southern Ocean and in the North Atlantic, and 85% of the ocean surface experiencing significant sea-level acceleration or deceleration, above instrumental and post processing noise. Longer records are available from tide gauges, albeit with variable coverage by basin. Regional departures from GMSL rise are primarily driven by ocean transport divergences that result from wind stress anomalies and spatial variability in atmospheric heat and freshwater fluxes (Section 9.2.4).

The SROCC (Oppenheimer et al., 2019) noted the occurrence of large multiannual sea-level variations in the Pacific, associated with the Pacific Decadal Oscillation (PDO) in particular, and involving the El Niño Southern Oscillation (ENSO), North Pacific Gyre Oscillation (NPGO) and Indian Ocean Dipole (IOD) (Annex IV) (Royston et al., 2018; Hamlington et al., 2020b). There was intensified sea-level rise during the 1990s and 2000s, with 10-year trends exceeding 20 mm yr⁻¹ in the western tropical Pacific Ocean, while sea-level trends were negative on the North American west coast. During the 2010s, the situation reversed, with western Pacific sea level falling at more than 10 mm yr⁻¹ (Hamlington et al., 2020b). For the Atlantic Ocean,

1 the SROCC described regional sea-level variability as being driven primarily by wind and heat flux
2 variations associated with the North Atlantic Oscillation (NAO) and heat transport changes associated with
3 AMOC variability. During periods of subpolar North Atlantic warming, winds along the European coast are
4 predominantly from the south and may communicate steric anomalies onto the continental shelf, driving
5 regional sea-level rise, with the reverse during periods of cooling (Chafik et al., 2019). High rates of sea-
6 level rise in the North Indian Ocean are accompanied by a weakening summer South Asian monsoon
7 circulation (Swapna et al., 2017).

8
9 The Arctic ocean is typically excluded from global sea-level studies, owing to the uncertainties associated
10 with resolving sea-level in ice-covered regions, strong variations in GRD effects, and uncertain GIA
11 estimates (Box 9.1). Spanning 1991-2018, a *very likely* sea-level rise of 1.16-1.81 mm yr⁻¹ is observed (Rose
12 et al., 2019). Since the SROCC, the forced response in regional sea level varies in time with the relative
13 influence of different forcing agents (Fasullo et al., 2020).

14
15 The SROCC estimated regional sea-level changes from combinations of the various contributions to sea-
16 level change from CMIP5 climate model outputs, allowing comparison with satellite altimeter and tide-
17 gauge observations. Closure of the regional sea-level budget is complicated by the fact that regional sea-level
18 variability is larger than GMSL variability and there are more processes that need to be considered, such as
19 vertical land movement and ocean dynamical changes (Box 9.1). A number of observation-based studies
20 have focussed on specific areas, such as the Mediterranean (García et al., 2006), the South China Sea (Feng
21 et al., 2012), the US east coast (Frederikse et al., 2017; Piecuch et al., 2018), the North Atlantic basin
22 (Kleinherenbrink et al., 2016) and the Northwestern European continental shelf seas (Frederikse et al., 2016).
23 Studies using tide gauge data and observation-based estimates of the contributions find that, while local
24 agreement is not yet possible, the observational sea-level budget can be closed on a basin scale (Slangen et
25 al., 2014a; Frederikse et al., 2016, 2018, 2020b). A budget analysis for the GRACE era found that the budget
26 closes in some but not all coastal regions: substantial parts of the sea-level change signal in the North
27 Atlantic could not be explained by steric or barystatic changes (Rietbroek et al., 2016). This is in agreement
28 with other work comparing climate model estimates to 20th century tide gauge observations (Meysignac et
29 al., 2017), where the majority of local spatial variability is determined by the ocean dynamic component.
30 Vertical land movement is another major cause of local spatial variability in sea-level change, and for
31 instance relevant for oceanic islands (Forbes et al., 2013; Martínez-Asensio et al., 2019). In summary, the
32 regional sea-level budget, using either observations or models, can currently only be closed on basin scales
33 (*medium confidence*), with large uncertainties remaining on smaller scales.

34 35 36 9.6.1.4 Attribution and time of emergence of regional sea-level change

37
38 The SROCC (Oppenheimer et al., 2019) attributed anthropogenic forcing to be the dominant cause of GMSL
39 rise since 1970 (see also Section 3.5.3.2), but detection and attribution (Cross-Working Group Box:
40 Attribution in Chapter 1) of 20th century externally forced regional sea-level changes is more challenging, as
41 regional variability is larger (Section 9.6.1.3), and therefore the signal-to-noise ratio is smaller (Richter and
42 Marzeion, 2014; Monselesan et al., 2015; Palanisamy et al., 2015). Whereas SROCC assessed with *high*
43 *confidence* that GMSL rise is attributable to anthropogenic greenhouse gas emissions, they assessed with
44 *medium confidence* that the regional anomalies in ocean basins are a combination of the response to
45 anthropogenic GHG emissions and internal variability.

46
47 The simulated ocean dynamic and thermosteric response to external forcings during 1861-2005 is larger than
48 simulated internal variability only in the Southern Ocean and North Pacific on a 1° grid (Slangen et al.,
49 2015), but on spatial scales exceeding 2000 km a detectable signal is revealed in the last 45 years in 63% of
50 the global ocean area (Richter et al., 2017). The thermosteric change in the upper 700 m in the period 1970-
51 2005 shows similar observed and simulated forced geographical patterns, and anthropogenic forcing
52 accounts for part (North Atlantic, 65%) or all (tropical Pacific, Southern Ocean) of the observed regional-
53 mean (Marcos and Amores, 2014). The influences of greenhouse gases and anthropogenic aerosols can be
54 partially distinguished by considering geographical or vertical ocean temperature variations (Slangen et al.,
55 2015; Bilbao et al., 2019; Fasullo et al., 2020). Zonal-mean forced ocean dynamic sea-level change alone is

1 not detectable but, using spatial correlation, the global geographical pattern during the altimeter period is
2 detectable in sea-level trends (Fasullo and Nerem, 2018). This pattern may already or will soon be detectable
3 in individual years, based on an analysis of CMIP5 climate model simulations (Bilbao et al., 2015).
4 Anthropogenic forcing, dominated by greenhouse gases, has strengthened the meridional sea-level gradient
5 in the Southern Ocean since the 1960s (Slangen et al., 2015; Bilbao et al., 2019; Fasullo et al., 2020). New
6 evidence finds that observed zonal-mean total sea-level trends during 1993 to 2018 in all basins are
7 inconsistent with unforced variability alone and consistent with the modelled response to external forcing
8 (Richter et al., 2020).

9
10 A region that has been studied intensely in the context of sea-level detection and attribution is the tropical
11 Pacific. Observed sea-level trends in the tropical Pacific show a PDO-like (Annex IV) East-West dipole
12 (with a greater rate of rise in the west, see section 9.6.1.3). This dipole does not occur in CMIP5 simulations
13 with the magnitude and duration that was observed in the 1990s and 2000s, neither in response to historical
14 forcing, nor as internal variability after removing the variability associated with the PDO (Bilbao et al.,
15 2015). (Hamlington et al., 2014) did obtain a residual trend pattern for 1993-2010 in the tropical Pacific that
16 may link to anthropogenic warming of the tropical Indian Ocean. Allowing for PDO and ENSO variations,
17 (Royston et al., 2018) describe patches of the Pacific Ocean where the sea-level trend for 1993-2015 is
18 distinguishable from temporally correlated noise. The acceleration in eastern Pacific sea-level rise is largely
19 accounted for by variations resembling PDO and ENSO (Hamlington et al., 2020a).

20
21 In the future, the anthropogenic signal in regional sea-level change from ocean density and dynamics is
22 projected to emerge first in regions with relatively small internal variability, such as the tropical Atlantic
23 Ocean and the tropical Indian Ocean (Jordà, 2014; Lyu et al., 2014; Richter and Marzeion, 2014; Bilbao et
24 al., 2015). The signal is projected to emerge over 50% of the ocean area by the 2040s (Lyu et al., 2014), but
25 in regions where variability is large and projected changes are small, such as the Southern Ocean, the signal
26 will not emerge before late in the century. Adding the projected sea-level change from land ice mass loss and
27 groundwater extraction strengthens and modifies the forced signal, leading to times of emergence 10-20
28 years earlier in most parts of the ocean, except in regions close to sources of mass loss, with emergence over
29 50% of the ocean area by 2020 and nearly everywhere by 2100 (Lyu et al., 2014; Richter et al., 2017)
30 (*medium confidence*).

31
32 In summary, detection of forced regional changes for some ocean areas in recent decades is possible
33 (*medium confidence*), but attribution of regional sea-level change to forcings over longer periods (20th
34 century) and for all ocean basins is not yet possible.

35
36
37 **[START CROSS-CHAPTER BOX 9.1 HERE]**

38 39 **Cross-Chapter Box 9.1: Global energy inventory and sea level budget**

40
41 **Coordinators:** Matthew D. Palmer (UK), Aimée B.A. Slangen (The Netherlands),

42
43 **Contributors:** Guðfinna Aðalgeirsdóttir (Iceland), Fábio Boeira Dias (Finland/Brazil), Catia M. Domingues
44 (Australia/Brazil), Gerhard Krinner (France), Johannes Quaas (Germany), Lucas Ruiz (Argentina)

45
46 Increased atmospheric greenhouse gas emissions since the 19th century have led to a net positive radiative
47 forcing of Earth's climate (Sections 2.2, 7.3) and a corresponding accumulation of energy in the Earth
48 System. Quantification of this energy gain is essential to our understanding of observed climate change and
49 for estimates of climate sensitivity (Section 7.5). The global energy inventory is closely linked to our
50 understanding of observed global sea-level change, through the energy associated with loss of land-based ice
51 and the effect of thermal expansion associated with ocean warming (Box 9.1, Sections 2.3.3.1, 9.6.1; Table
52 9.5).

53
54 The Earth System gained substantial energy over the period 1971-2018 (*high confidence*), with an assessed
55 *very likely* range of 325 to 546 ZJ or 0.43 to 0.72 W m⁻² expressed per unit area of the Earth's surface

(Cross-Chapter Box 9.1, Figure 1a; Section 7.2, Box 7.2). Ocean warming dominates the energy inventory change (*high confidence*), accounting for 91% of the observed energy increase for the period 1971-2018, with upper ocean warming (0-700 m) accounting for 56% (Section 7.2). Much smaller amounts went into melting of ice (3%) and heating of the land (5%) and atmosphere (1%). Overall, the percentage contributions are similar to those reported in IPCC AR5 for the period 1971-2010 (Rhein et al., 2013).

The observed global mean sea-level (GMSL) budget is assessed through comparison of the sum of individual components of GMSL change with independent observations of total GMSL change from tide gauge and satellite altimeter observations (Cross-Chapter Box 9.1, Figure 1b; Sections 2.3.3, 9.6.1; Table 9.5). The assessed sum of the observed components indicates that GMSL *very likely* increased by 72 to 117 mm over the period 1971-2018 (Table 9.5), with the largest contributions from ocean thermal expansion (50%) and melting of ice sheets and glaciers (42%). The assessed total GMSL change (Section 2.3.3) for the period 1971-2018 has a *very likely* range of 73-146 mm and as a result the sea-level budget is closed for this period (Cross-Chapter Box 9.1, Figure 1b, Section 9.6.1, Table 9.5).

The sea-level budget closure demonstrates improved quantification of the processes of observed GMSL change for this period relative to previous IPCC assessments (Church et al., 2013a; Oppenheimer et al., 2019). A related assessment presented in Chapter 7 demonstrates closure of the global energy budget (*high confidence*) (Box 7.2) and strengthens the confidence in scientific understanding of both of these key aspects of climate change.

[START CROSS-CHAPTER BOX 9.1, FIGURE 1 HERE]

Cross-Chapter 9.1, Figure 1: Global Energy Inventory and Sea Level Budget. a) Observed changes in the global energy inventory for 1971-2018 (shaded time series) with component contributions as indicated in the figure legend. Earth System Heating for the whole period and associated uncertainty is indicated to the right of the plot (red bar = central estimate; shading = *very likely* range); b) Observed changes in components of global mean sea-level for 1971-2018 (shaded time series) as indicated in the figure legend. Observed global mean sea-level change from tide gauge reconstructions (1971-1993) and satellite altimeter measurements (1993-2018) is shown for comparison (dashed line) as a 3-year running mean to reduce sampling noise. Closure of the global sea-level budget for the whole period is indicated to the right of the plot (red bar = component sum central estimate; red shading = *very likely* range; black bar = total sea level central estimate; grey shading = *very likely* range). Full details of the datasets and methods used are available in Annex I. Further details on energy and sea-level components are reported in Table 7.1 and Table 9.5.

[END CROSS-CHAPTER BOX 9.1, FIGURE 1 HERE]

[END CROSS-CHAPTER BOX 9.1 HERE]

9.6.2 *Paleo context of global and regional sea-level change*

As the SROCC (Oppenheimer et al., 2019) noted, paleo-sea level records provide information on past ice-sheet changes, and process-based ice sheet models of past warm periods inform equilibrium responses. However, given uncertainties in paleo-sea level and polar paleoclimate and limited temporal resolution of paleo-sea level records, there is *low confidence* in the utility of paleo-sea level records for quantitatively informing near-term GMSL change. Nonetheless the paleo record does contextualise sea level and can test projection models (see also FAQ 1.3). Proxy constraints on GMSL and global ice volume are assessed in Sections 2.3.2.4. and 2.3.3.3 (see also FAQ 9.1). This section updates prior assessments of drivers of past GMSL changes and climatically coherent areas of relative sea-level variability. GMSL changes are framed in terms of GMST but noting that amplified high latitude warming is a robust equilibrium response to elevated CO₂ (Masson-Delmotte et al., 2013): polar air temperatures during past warm periods were up to twice the

1 GMST changes shown in Table 9.6. The SROCC assessment that past multi-metre sea-level changes have
 2 resulted from significant ice sheet changes beyond those presently observed is confirmed (*very high*
 3 *confidence*).

4
 5
 6 **[START TABLE 9.6 HERE]**

7
 8 **Table 9.6:** Reference ranges of age, global mean surface temperature, atmospheric carbon dioxide concentration, and
 9 global mean sea level for the paleo periods discussed in this chapter.
 10

Paleo period	Years CCB 2.1	GMST relative to 1850-1900 Section 2.3.1.1	CO ₂ Sections 2.2.3.1, 2.2.3.2	GMSL Section 2.3.3.3
Early Eocene Climatic Optimum EECO	53 – 49 Ma	+10 to +18°C	1150 – 2500 ppm	+70 to +76m
Mid-Pliocene Warm Period (MPWP)	3.3 – 3.0 Ma	+2.5 to +4°C	360 – 420 ppm	+5 to +25 m
Marine Isotope Stage (MIS) 11	~424 – 395 ka	0.5 ± 1.6 °C ^a	265 – 286 ppm	+6 to +13 m
Last Interglacial (LIG)	~129 – 116 ka	+0.5 to +1.5°C	266 – 282 ppm	+5 to +10 m
Last Glacial Maximum (LGM)	21- 19 ka	-5 to -7°C	188 – 194 ppm	-125 to -134 m
Last Deglacial Transition	18 – 11 ka	–	193 → 271 ppm	-120 → -50 m
Early Holocene	11.65 – 6.5 ka	–	250 – 268 ppm	-50 → -3.5 m
Mid Holocene	6.5 – 5.5 ka	+0.2 to +1.0°C	260 - 268 ppm	-3.5 to +0.5 m
Last Millennium	850 to 1850 CE	-0.14 to +0.24 °C	278 - 285 ppm	-0.05 to +0.03 m

11 ^aBased on one study (Irvali et al., 2020) relative to ~year 2000 SST values

12
 13 **[END TABLE 9.6]**

14
 15
 16 *Mid-Pliocene Warm Period (MPWP)*

17 During the MPWP, GMST was 2.5-4°C warmer than 1850-1900 (*medium confidence*) and GMSL was
 18 between 5 and 25 m higher than today (Table 9.6) (*medium confidence*) (Section 2.3.3.3). The AR5
 19 (Masson-Delmotte et al., 2013) concluded that ice-sheet models consistently produce near-complete
 20 deglaciation of the Greenland and West Antarctic Ice Sheets, and multi-metre loss of the East Antarctic Ice
 21 Sheet in response to MPWP climate conditions. Studies since the AR5 have yielded a consistent but broader
 22 range, due in part to larger ensembles exploring more parameters (DeConto and Pollard, 2016; Yan et al.,
 23 2016; DeConto et al., 2021). Partly on the basis of these studies the SROCC proposed a ‘plausible’ upper
 24 bound on GMSL of 25 m (*low confidence*) with evidence suggesting an Antarctic contribution of anywhere
 25 between 5.4 – 17.8 m.

26
 27 The MPWP climate had substantial polar amplification (up to 8 °C above pre-industrial levels in Arctic
 28 Russia, (Fischer et al., 2018); Section 7.4.4.1). Ice sheet model simulations indicate that Northern
 29 Hemisphere glaciation was limited to high-elevation regions in eastern and southern Greenland (Figure 9.17)
 30 (*medium confidence*)(De Schepper et al., 2014; Yan et al., 2014; Koenig et al., 2015; Dowsett et al., 2016;

Do Not Cite, Quote or Distribute

1 Berends et al., 2019) with Northern Hemisphere glaciation only becoming more widespread from the
2 (cooler) late Pliocene (Bachem et al., 2017; Blake-Mizzen et al., 2019; Knutz et al., 2019; Sánchez-Montes et
3 al., 2020). Southern Hemisphere glaciation was characterised by an Antarctic ice sheet reduced in volume
4 from present (Figure 9.18) (Dowsett et al., 2016; Berends et al., 2019; Grant et al., 2019; Miller et al., 2020)
5 (*medium confidence*) with mountain ice fields in the Andes of South America (De Schepper et al., 2014). Ice
6 sheet models are inconsistent in the magnitude of the sea level contribution from Antarctica (DeConto and
7 Pollard, 2016; Yan et al., 2016; Golledge et al., 2017b; Berends et al., 2019; DeConto et al., 2021) but near-
8 field sedimentological reconstructions support precessionally-modulated and eccentricity-paced multi-metre
9 sea level contributions from the Wilkes Subglacial Basin over 3 – 5 kyr (Patterson et al., 2014; Bertram et
10 al., 2018). In summary, under a past warming level of around 2.5 – 4 °C, ice sheets in both hemispheres were
11 reduced in extent compared to present (*high confidence*). Proxy-based evidence (Section 2.3.3.3) combined
12 with numerical modelling indicates that, on millennial timescales, the GMSL contribution arising from ice
13 sheets was >5 m (*high confidence*) or >10 m (*medium confidence*) (Moucha and Ruetenik, 2017; Berends et
14 al., 2019; Dumitru et al., 2019) (Figures 9.17, 9.18).

15 *Marine Isotope Stage 11 (MIS 11)*

16 The SROCC (Meredith et al., 2019) noted that Greenland may have been ice-free for extensive periods
17 during Pleistocene interglaciations, implying a high sensitivity of the Greenland ice sheet to warming levels
18 close to present day. The AR5 (Church et al., 2013a) assigned *medium confidence* to a MIS 11 GMSL of 6–
19 15 m above present, requiring a loss of much of the Greenland and West Antarctic ice sheets, and a possible
20 contribution from East Antarctica. High-resolution multi-proxy sea surface temperature reconstructions and
21 climate model simulations concur that MIS 11 was an extremely long interglacial that exhibited positive
22 annual (0.5 ± 1.6 °C, (Irvali et al., 2020)) and summer (2.1–3.4 °C, (Robinson et al., 2017)) temperature
23 anomalies (de Wet et al., 2016). GMSL was 6–13 m above present (*medium confidence*, Section 2.3.3.3). The
24 Greenland Ice Sheet lost 4.5–6 m (Reyes et al., 2014)) or ca. 6.1 m (3.9–7 m, 95% confidence) sea-level
25 equivalent by ca. 7 kyr after peak summer warmth (Robinson et al., 2017), with marine-based ice from AIS
26 (Blackburn et al., 2020) contributing 6.4–8.8 m sea-level equivalent at this time (Mas e Braga et al., 2021).
27 Agreement between GMSL and ice-sheet reconstructions gives *high confidence* in identifying a high
28 sensitivity of both ice sheets to the protracted duration of thermal forcing even at low warming levels (Reyes
29 et al., 2014; Robinson et al., 2017; Irvali et al., 2020; Mas e Braga et al., 2021). Modelled mean mass loss
30 rates for the Greenland Ice Sheet of 0.4 m kyr^{-1} during MIS 11 (Robinson et al., 2017) are indistinguishable
31 from recent mass loss rates averaged over 1992–2018 (Section 9.4.1.1). In summary, geological
32 reconstructions and numerical simulations consistently show that past warming levels of <2 °C (GMST) are
33 sufficient to trigger multi-metre mass loss from both the Greenland and Antarctic ice sheets if maintained for
34 millennia (*high confidence*), in agreement with the SROCC findings for comparable warming levels during
35 MIS 5e, the Last Interglacial.

36 *Last Interglacial (LIG)*

37 The AR5 found the LIG GMSL was >5 m (*very high confidence*) but <10 m (*high confidence*). Their best
38 estimate of 6 m was based on two studies (Kopp et al., 2009; Dutton and Lambeck, 2012). The SROCC
39 concluded that during the Last Interglacial the Greenland contribution to the GMSL highstand of 6–9 m
40 increased gradually whereas the Antarctic contribution occurred early, from ca. 129 ka. Due to widely
41 varying reconstructions from model studies (Greenland) and the paucity of direct evidence of ice sheet
42 change (Antarctic), the magnitude of sea-level contributions from both ice sheets was assigned *low*
43 *confidence*.

44 Since the AR5, information about the LIG, when GMST was about 0.5–1.5 °C above 1850–1900 (*medium*
45 *confidence*) (Section 2.3.1.1), has improved. The LIG had higher summer insolation than present and polar
46 amplified sea surface and surface air temperatures that reached >1–4 °C and >3–11 °C in the Arctic
47 respectively (Landais et al., 2016; Capron et al., 2017; Fischer et al., 2018). Mean annual and maximum
48 summer ocean temperatures peaked early (129–125 ka) in the interglacial period, reaching 1.1 ± 0.3 °C
49 above the modern global mean (Shackleton et al., 2020) with summer anomalies of 2.5–3.5 °C in the
50 Southern Ocean (Bianchi and Gersonde, 2002) and spatially variable timing (Chadwick et al., 2020). It is
51 *virtually certain* GMSL was higher than today, *likely* by 5–10 m (*medium confidence*) (Section 2.3.3.3).
52 Global mean thermal expansion peaked at about 0.9 ± 0.3 m early in the LIG (~129 ka), declining to modern
53
54
55

1 levels by about 127 ka (Shackleton et al., 2020). With no more than 0.3 ± 0.1 m of GMSL rise from glaciers
2 (Section 9.5.1), at most 1.0 ± 0.3 m of the GMSL rise originated from sources other than the polar ice sheets.
3

4 Recent LIG ice sheet simulations agree that peak loss from the Greenland Ice sheet occurred late (125–120
5 ka) (Goelzer et al., 2016; Tabone et al., 2018; Plach et al., 2019) when Northern Hemisphere insolation was
6 greater than at present (Capron et al., 2017) (*medium confidence*), consistent with inferences from marine
7 sediment records (Hatfield et al., 2016; Irvah et al., 2020) and far-field GMSL indicators (Rohling et al.,
8 2019). Best estimates of the GMSL contribution from Greenland (Figure 9.17) differ between models: ≤ 1 m
9 (Albrecht et al., 2020; Clark et al., 2020), 1–2 m (Calov et al., 2015; Goelzer et al., 2016; Bradley et al.,
10 2018), up to 3 m (Tabone et al., 2018; Plach et al., 2019), > 5 m (Yau et al., 2016). There is *high confidence*
11 that the response time of the Greenland Ice Sheet to LIG warming was multi-millennial and *high confidence*
12 that it contributed to LIG GMSL change, but *low agreement* in the contribution magnitude.
13

14 Far-field GMSL records suggest that the Antarctic Ice Sheet contributed to LIG sea level from 129.5–125 ka
15 (Figure 9.18) but direct evidence is sparse. Thinning of part of the West Antarctic Ice Sheet is interpreted
16 from a 130 ka–80 ka hiatus in the Patriot Hills horizontal ice core record (Turney et al., 2020). Marine
17 sediment records suggest a dynamic response of the Wilkes Subglacial Basin (WSB) of the East Antarctic Ice
18 Sheet during this period indicating a response timescale of 1000–2500 yr (Wilson et al., 2018), consistent
19 with modelling studies (Mengel and Levermann, 2014; Golledge et al., 2017b; Sutter et al., 2020). Isotopic
20 changes in the Talos Dome ice core are inconsistent with local surface lowering, limiting retreat to 0.4–0.8 m
21 SLE from this sector (Sutter et al., 2020). Ice sheet models forced with unmodified atmosphere–ocean
22 models (Goelzer et al., 2016; Clark et al., 2020) simulate 3–4.4 m sea-level equivalent mass loss, primarily
23 from the West Antarctic Ice Sheet, with no retreat in WSB (e.g., Figure 9.18). Models forced with proxy-
24 based or ad hoc LIG ocean temperature anomalies (DeConto and Pollard, 2016; Sutter et al., 2016) indicate
25 collapse of West Antarctica under 2–3 °C ocean forcing yielding 3–7.5 m sea-level contribution, but modest
26 or no retreat in the WSB. Based on *limited evidence* and *limited agreement* between models, there is *low*
27 *confidence* in both the magnitude and timing of LIG mass loss from the Antarctic Ice Sheet.
28

29 In summary, paleo-environmental and modelling studies both indicate that under past warming of the level
30 achieved during the LIG (ca. 0.5–1.5 °C) it is *likely* that both the Greenland and Antarctic ice sheets
31 responded dynamically over multiple millennia (*high confidence*)
32

33 *Last Glacial Maximum (LGM)*

34 At the LGM geological proxies and GIA models indicate that GMSL was 125–134 m below present (Section
35 2.3.3.3; Figures 9.17, 9.18). New studies have not changed the conclusions of the AR5 regarding the size or
36 timing of the LGM and last glacial termination but have further examined the LGM sea-level budget. Based
37 on a synthesis of multiple prior studies, (Simms et al., 2019) estimated central 67% probability contributions
38 to the LGM lowstand of 76 ± 7 m from the North American Laurentide ice sheet, 18 ± 5 m from the Eurasian
39 ice sheet, 10 ± 2 m from Antarctica, 4 ± 1 m from Greenland, 5.5 ± 0.5 m from glaciers, and 2.4 ± 0.3 m due
40 to an increase in ocean density. Of the residual, up to about 1.4 m may be ascribed to groundwater, leaving a
41 shortfall of 16 ± 10 m yet to be allocated among land ice reservoirs or lakes.
42

43 *Last Deglacial Transition: Meltwater pulse 1A (MWP-1A)*

44 During MWP-1A, GMSL *very likely* (*medium confidence*) rose by 8–15 m (Liu et al., 2016). Consistent with
45 the AR5, the drivers of this rapid rise remain ambiguous. The spatial patterns of relative sea-level change
46 over this interval are inadequately observed to constrain the relative contributions of the North American and
47 Antarctic ice sheets (Liu et al., 2016). Modelling studies of the North American ice sheet permit a 3–6 m
48 (Gregoire et al., 2016) or 6–9 m contribution over the duration of MWP-1A (Tarasov et al., 2012).
49 Sedimentological evidence (Weber et al., 2014; Bart et al., 2018) provides near-field evidence for an
50 Antarctic contribution, consistent with modelling studies (Golledge et al., 2014; Stuhne and Peltier, 2015),
51 but does not constrain the magnitude of the contribution. A recent statistical analysis of Norwegian Sea and
52 Arctic Ocean sediments suggests a 3–7 m contribution from the Eurasian Ice Sheet (Brendryen et al., 2020), a
53 possibility not considered in the AR5 or the meta-analysis of (Liu et al., 2016). In summary, MWP-1A
54 appears to have been driven by a combination of melt in North America (*high confidence*), Eurasia (*low*
55 *confidence*), and Antarctica (*low confidence*), but the budget is not closed.

1 *Holocene*

2 Around half (~50–60 m) of the GMSL rise since the LGM occurred during the early Holocene at a sustained
3 rate of ~15 m kyr⁻¹ from ~11.4–8.2 ka (Lambeck et al., 2014), possibly punctuated by abrupt meltwater
4 pulses (Smith et al., 2011; Carlson and Clark, 2012; Törnqvist and Hijma, 2012; Harrison et al., 2019). An
5 abrupt ~1.1 m sea-level rise at ~8.2 ka was associated with drainage of the pro-glacial lakes Agassiz and
6 Ojibway, attributed to accelerated melt from collapsing Laurentide Ice Sheet ice saddles (Matero et al.,
7 2017). The Laurentide Ice Sheet provided the greatest contribution (27 m) to early Holocene GMSL (Peltier
8 et al., 2015; Roy and Peltier, 2017), the Scandinavian ice sheet contributed ~2 m from the beginning of the
9 Holocene until its demise by ~10.5 ka, (Cuzzone et al., 2016), whilst the Barents Sea ice sheet contributed a
10 small but unknown amount (Patton et al., 2015, 2017; Auriac et al., 2016). The Greenland Ice Sheet
11 contributed ~4 m, consistent with ice thinning rates inferred from the Camp Century ice core (Lecavalier et
12 al., 2017; McFarlin et al., 2018). Recent estimates of Antarctic contributions during the early Holocene vary
13 considerably from ~1.2 m to ~8.5 m (Whitehouse et al., 2012; Ivins et al., 2013; Argus et al., 2014; Briggs et
14 al., 2014; Golledge et al., 2014; Pollard et al., 2016; Roy and Peltier, 2017; Albrecht et al., 2020). In
15 summary, the early Holocene was characterised by steadily rising GMSL as global ice sheets continued to
16 retreat from their LGM extents. This steady rise was punctuated by abrupt pulses during episodes of rapid
17 meltwater discharge.

18
19 In the middle Holocene, GMST peaked at 0.2–1.0°C higher than 1850–1900 temperature between 7 and 6 ka
20 (Section 2.3.1.1.2). GMSL rise slowed coincidentally with final melting of the Laurentide ice sheet by $6.7 \pm$
21 0.4 ka (Ullman et al., 2016), after which only Greenland and Antarctic ice sheets could have contributed
22 significantly. At 6 ka, GMSL was -3.5 to +0.5 m (*medium confidence*) (Section 2.3.3.3). Simulations of the
23 Holocene Thermal Maximum (HTM) give a Greenland ice sheet broadly consistent with geological
24 reconstructions so, despite uncertainties regarding the timing of minimum ice sheet volume and extent, there
25 is *medium confidence* that minima were reached at different times in different areas during the period 8–3 ka
26 BP (Larsen et al., 2015; Young and Briner, 2015; Briner et al., 2016). Geochronological and numerical
27 modelling studies indicate that it is *likely (medium confidence)* that the period of smaller-than-present ice
28 extent in all sectors of Greenland persisted for at least 2000 to 3000 years (Larsen et al., 2015; Young and
29 Briner, 2015; Briner et al., 2016; Nielsen et al., 2018). Based on ice sheet modelling and ¹⁴C dating
30 (Kingslake et al., 2018) suggested that West Antarctic grounding lines retreated prior to ~10 ka BP, followed
31 by a readvance. Other studies from the same region conclude that retreat was fastest from 9 to 8 ka BP
32 (Spector et al., 2017), or from 7.5 to 4.8 ka BP (Venturelli et al., 2020). Marine geological evidence indicates
33 open marine conditions east of Ross Island by 8.6 ± 0.2 ka BP (McKay et al., 2016). In the western Weddell
34 Sea, (Johnson et al., 2019) reported rapid glacier thinning from 7.5 to 6 ka BP. (Hein et al., 2016) concluded
35 that the fastest thinning further south took place from 6.5 to 3.5 ka BP, potentially contributing 1.4–2 m to
36 GMSL. Geophysical data indicate stabilisation or readvance in this area around 6 ± 2 ka BP (Wearing and
37 Kingslake, 2019). In coastal Dronning Maud Land (East Antarctica) rapid thinning occurred 9 to 5 ka BP
38 (Kawamata et al., 2020), whereas glaciers in the Northern Antarctic Peninsula receded during the period 11
39 to 8 ka BP and readvanced to their maximal extents by 7 to 4 ka BP (Kaplan et al., 2020). In summary,
40 higher-than-pre-industrial GMST during the mid Holocene coincided with recession of the Greenland Ice
41 Sheet to a smaller-than-present extent (*high confidence*). Multiple lines of evidence give *high confidence* that
42 thinning or retreat in parts of Antarctica during the Holocene took place at different times in different places,
43 but limited data means there is only *low confidence* in whether or not the ice sheet as a whole was smaller
44 than present during the mid Holocene.

45
46 In summary, both proxies and model simulations indicate that GMSL changes during the early to mid
47 Holocene were the result of episodic pulses, due to drainage of meltwater lakes, superimposed on a trend of
48 steady rise due to continued ice sheet retreat (*high confidence*).

49
50 The combination of tide gauge observations and geological reconstructions indicates that a sustained
51 increase of GMSL began between 1820 and 1860 and led to a 20th century GMSL rise that was *very likely*
52 (*high confidence*) faster than in any preceding century in the last 3000 yr (Section 2.3.3.3). At a regional
53 level, tide gauge and geological data from the North Atlantic and Australasia show inflections in relative sea-
54 level trends between 1895–1935, with an increase of 0.8 to 2.5 mm yr⁻¹ across the inflection (Gehrels and
55 Woodworth, 2013). A statistical meta-analysis of globally distributed geological and tide gauge data (Kopp

1 et al., 2016) found that, in all twenty examined regions with geological records stretching back at least 2000
2 years, the rate of RSL rise in the 20th century was greater than the local average over 0-1700 CE. In four of
3 the twenty regions, all in the North Atlantic (Connecticut, New Jersey, North Carolina, and Iceland), the 19th
4 century rate was also greater than the 0-1700 CE average (90% confidence interval). In summary, rates of
5 RSL rise exceeding the pre-industrial background rate of rise are apparent in parts of the North Atlantic in
6 the nineteenth century (*medium confidence*) and in most of the world in the twentieth century (*high*
7 *confidence*).

10 **9.6.3 Future sea-level changes**

12 This section first assesses sea-level projections since the AR5 (Church et al., 2013a) (and including the
13 SROCC (Oppenheimer et al., 2019)) based on Representative Concentration Pathways (Section 9.6.3.1).
14 Process-level assessments in sections 9.2.4, 9.4.1.3, 9.4.1.4, 9.4.2.5, 9.4.2.6 and 9.5.1.3 are synthesised
15 (Section 9.6.3.2) to produce new global-mean and regional sea-level projections based on the Shared
16 Socioeconomic Pathways up to 2150 (Section 9.6.3.3) and on global warming levels up to 2100 (Section
17 9.6.3.4). Long-term global mean sea-level projections, both at 2300 and on multimillennial timescales, are
18 also assessed (Section 9.6.3.5).

20 In sections 9.6.3.3 and 9.6.3.4, *likely* ranges of the new global-mean sea-level projections are presented,
21 incorporating only processes in whose projections there is at least *medium confidence*, consistent with
22 headline projections in the AR5 and the SROCC. As emphasized by the SROCC, there is a substantial
23 likelihood that sea level rise will be outside the *likely* range. As described in Box 1.1, since the definition of
24 ‘*likely*’ refers to at least 66% probability, there may be as much as a 34% probability that the processes in
25 which there is at least *medium confidence* will generate outcomes outside the *likely* range. Furthermore,
26 additional processes in which there is *low confidence* (Section 9.4.2.4; Box 9.4) may also contribute to sea-
27 level change. The presentation of *likely* sea-level change (Tables 9.8-9.9 and in Figures 9.27, 9.29) is
28 therefore accompanied by a *low confidence* range intended to reflect potential contributions from additional
29 processes under high-emissions scenarios. The *low confidence* range incorporates ice-sheet projections based
30 on both structured expert judgement (i.e., a formal, calibrated method of combining quantified expert
31 assessments that incorporate all potential processes) and projections from an Antarctic ice sheet model that
32 includes the Marine Ice Cliff Instability (a specific uncertain process not generally included in ice sheet
33 models; Section 9.4.2.4).

36 **9.6.3.1 Global mean sea level projections based on the Representative Concentration Pathways**

38 The AR5 (Church et al., 2013a) generated global mean sea level (GMSL) projections for the Representative
39 Concentration Pathways (RCPs) by combining information from CMIP5 climate models with glacier and
40 ice-sheet surface mass balance models and assessments of projected ice-sheet dynamic and land-water
41 storage contributions (Section 9.6.3.2). The SROCC (Oppenheimer et al., 2019) updated the AR5 projections
42 based upon a revised assessment of the Antarctic ice sheet contribution to GMSL rise. The AR5 and the
43 SROCC employ a baseline period of 1986 to 2005, which is updated in this report to a baseline period of
44 1995 to 2014 (Section 1.4.1). Between these two periods, GMSL rose by 3 cm and this correction is applied
45 to projections from previous reports to allow comparison (Table 9.8). Accounting for this shift, the
46 conclusion of the SROCC is that, with *medium confidence*, GMSL will rise between 0.40 m (0.26–0.56 m,
47 *likely* range) (RCP 2.6) and 0.81 m (0.58–1.07 m, *likely* range) (RCP 8.5) by 2100 relative to 1995-2014.
48 The AR5 and the SROCC projections of GMSL for the 2007-2018 period have been shown to be consistent
49 with observed trends in GMSL and regional weighted mean tide gauges (Wang et al., 2021a).

51 Since the AR5, a number of projections of GMSL rise have been published based on the RCPs (Slangen et
52 al., 2014a; Kopp et al., 2014, 2017; Grinsted et al., 2015; Jackson et al., 2016; Mengel et al., 2016; Bakker et
53 al., 2017; Bittermann et al., 2017; Nauels et al., 2017; Wong et al., 2017; Le Bars et al., 2017; Nicholls et al.,
54 2018; Goodwin et al., 2018; Le Cozannet et al., 2019; Palmer et al., 2020)(see (Garner et al., 2018) for a
55 database; Tables 9.SM.5, 9.SM.6). Some studies also produced associated global sets of regional projections

1 (Kopp et al., 2014, 2017; Slangen et al., 2014a; Le Cozannet et al., 2019; Palmer et al., 2020). Since the
 2 SROCC, (Le Cozannet et al., 2019) focussed on the low end of the probability distribution of GMSL rise,
 3 (Palmer et al., 2020) extended projections beyond 2100 using a climate model emulator (Cross-Chapter Box
 4 7.1) and (Horton et al., 2020) conducted a survey of 106 sea-level experts, providing additional context for
 5 interpreting sea-level rise projections for 2100 and 2300.

6
 7 As noted by the SROCC, the largest differences between projections of GMSL in 2100 are due to the ice
 8 sheet projection method, which generally fall into one of three categories: (1) projections from ice sheet
 9 models that represent processes in which there is at least *medium confidence* (Sections 9.4.1.2, 9.4.2.2), (2)
 10 projections from an Antarctic ice-sheet model that incorporates the Marine Ice Cliff Instability (MICI)
 11 (Section 9.4.2.4) (DeConto and Pollard, 2016), or (3) projections based on structured expert judgement (SEJ)
 12 (Sections 9.4.1.3; 9.4.1.4; 9.4.2.5; 9.4.2.6) (Bamber and Aspinall, 2013; Bamber et al., 2019). *Low*
 13 *confidence* is ascribed to projections incorporating MICI because there is *low confidence* in the current
 14 ability to quantify MICI (Section 9.4.2.4). *Low confidence* is also ascribed to projections based on SEJ,
 15 because individual experts participating in the SEJ study may have incorporated processes in whose
 16 quantification there is *low confidence*, and the experts' reasoning has not been examined in detail. In general,
 17 the range of GMSL projections based upon ice-sheet models not incorporating MICI overlaps with but is
 18 lower than projections incorporating MICI or employing SEJ (Figure 9.25).

19
 20 There is *high agreement* across published GMSL projections for 2050 and there is little sensitivity to
 21 emissions scenario (Figure 9.25, left panel). Up to 2050, projections are broadly consistent with
 22 extrapolation of the observed acceleration of GMSL rise (Sections 2.3.3.3, 9.6.1.1, 9.6.1.2). Considering
 23 only projections incorporating ice-sheet processes in whose quantification there is at least *medium*
 24 *confidence*, the GMSL projections for 2050, across all emissions scenarios, fall between 0.1 and 0.4 m (5th—
 25 95th percentile range). Projections incorporating MICI or SEJ do not extend this range under RCP 2.6 or RCP
 26 4.5 and extend the upper part of the range to 0.6 m under RCP 8.5. On the basis of these studies, we
 27 therefore have *high confidence* that GMSL in 2050 will be between 0.1 and 0.4 m higher than in 1995 to
 28 2014 under low and moderate emissions scenarios and between 0.1 and 0.6 m under high emissions
 29 scenarios.

30
 31 Conversely, there is *low agreement* across published GMSL projections for 2100, particularly for higher
 32 emissions scenarios, as well as a higher degree of sensitivity to the choice of emissions scenario (Figure
 33 9.25, right panel). Considering only projections representing processes in whose quantification there is at
 34 least *medium confidence*, the GMSL projections for 2100 fall between 0.2 and 1.0 m (5th—95th percentile
 35 range) under RCP 2.6 and RCP 4.5, and between 0.3 and 1.6 m under RCP 8.5. Considering also projections
 36 incorporating MICI or SEJ (*low confidence*), the projections for 2100 fall between 0.2 and 1.0 m (5th—95th
 37 percentile range) under RCP 2.6, 0.2 and 1.6 m under RCP 4.5, and 0.4 and 2.4 m under RCP 8.5. In
 38 summary, RCP-based projections published since the AR5 show *high agreement* for 2050, but exhibit broad
 39 ranges and *low agreement* for 2100, particularly under RCP 8.5.

40
 41
 42 [START FIGURE 9.25 HERE]

43
 44 **Figure 9.25: Literature global mean sea level (GMSL) projections (m) for 2050 (left) and 2100 (right) since 1995-**
 45 **2014, for RCP 8.5/SSP5-8.5 (top set), RCP 4.5/SSP2-4.5 (middle set), and RCP 2.6/ SSP1-2.6**
 46 **(bottom set).** Projections are standardised to account for minor differences in time periods. Thick bars
 47 span from the 17th-83rd percentile projections, and thin bars span the 5th-95th percentile projections. The
 48 different assessments of ice sheet contributions are indicated by 'MED' (ice sheet projections including
 49 only processes in whose quantification there is *medium confidence*), 'MICI' (ice sheet projections which
 50 incorporate Marine Ice Cliff Instability), and 'SEJ' (structured expert judgement (SEJ) to assess the
 51 central range of the ice-sheet projection distributions). 'Survey' indicates the results of a 2020 survey of
 52 sea-level experts on GMSL rise from all sources (Horton et al., 2020). Projection categories incorporating
 53 processes in which there is *low confidence* ('MICI' and 'SEJ') are lightly shaded. Dispersion among the
 54 different projections represents *deep uncertainty*, which arises as a result of *low agreement* regarding
 55 appropriate conceptual models describing ice sheet behaviour and *low agreement* regarding probability
 56 distributions used to represent key uncertainties. Individual studies are shown in Tables 9.SM.5, 9.SM.6.

Further details on data sources and processing are available in the chapter data table (Table 9.SM.9).

[END FIGURE 9.25 HERE]

9.6.3.2 Drivers of projected sea-level change

This section describes the choices made for the contributions to the updated global mean and regional sea-level projections (Section 9.6.3.3) based on assessments in this report and compares the updated projections to the AR5 (Church et al., 2013a) and the SROCC (Oppenheimer et al., 2019) (Tables 9.7, 9.8). Since there is no single model that can directly compute all of the contributions to sea-level change (Box 9.1), the contributions to sea level are computed separately and then combined (Tables 9.8, 9.9). For consistency with global surface air temperature (GSAT) projections (Section 4.3.1.1) and assessment of equilibrium climate sensitivity (ECS) and transient climate response (TCR) (Section 7.5), temperature-dependent projections (thermal expansion, ice sheets, glaciers) are forced by GSAT projections from a two-layer energy budget emulator (Smith et al., 2018) that is calibrated to be consistent with the assessment of ECS and TCR (Box 7.1, Supplementary Material 7.SM.2). Throughout, *likely* ranges are assessed based upon the combination of uncertainty in the GSAT distribution and uncertainty in the relationships between GSAT and changes to individual components. In general, 17th-83rd percentile results, incorporating both GSAT and sea-level process uncertainty, are interpreted as *likely* ranges. This is distinct from the approach used by the AR5, which interpreted the 5th-95th percentile range of CMIP5 projections and therefore of GMSL projections driven by them as *likely* ranges. The shift in interpretation here is consistent with the use of the emulator for GSAT (Box 4.1, Cross-Chapter Box 7.1). *Very likely* ranges are not assessed because of the potential for processes in whose projections there is currently *low confidence* to substantially augment total projected GMSL change.

[START TABLE 9.7 HERE]

Table 9.7: Methods used to project the drivers of GMSL and RSL change in the SSP- and warming-level-based projections of GMSL, RSL and ESL change. Section numbers indicate location of primary assessment text.

Driver of Global-Mean or Regional Sea-Level change	SROCC Projection Method	AR6 Projection method
Thermal expansion (Section 9.2.4.1)	CMIP5 ensemble drift-corrected <i>zostoga</i> , with surrogates derived from climate system heat content where not available	Two-layer emulator with climate sensitivity calibrated to the AR6 assessment (Supplementary Material 7.SM.2) and expansion coefficients calibrated to emulate CMIP6 models (Supplementary Material 9.SM.4.2, 9.SM.4.3)
Greenland ice sheet (excluding peripheral glaciers) (Section 9.4.1.3; 9.4.1.4)	Surface mass balance: scaled cubic polynomial fit to GMST Dynamics: Quadratic function of time, calibrated based on multimodel assessment	<i>Medium confidence</i> processes up to 2100: Emulated ISMIP6 simulations (Box 9.3) (Edwards et al., 2021) <i>Medium confidence</i> processes after 2100: Parametric model fit to ISMIP6 simulations up to 2100, extrapolated based on either constant post-2100 rates or a quadratic interpolation to the multimodel assessed 2300 range (Supplementary Material 9.SM.4.4) <i>Low confidence</i> processes:

		Structured expert judgement (Bamber et al., 2019)
Antarctic ice sheet (excluding peripheral glaciers ^a) (Section 9.4.2.5; 9.4.2.6)	Multimodel assessment	<p><i>Medium confidence</i> processes up to 2100: p-box including (1) Emulated ISMIP6 simulations (Edwards et al., 2021) and (2) LARMIP-2 simulations (Levermann et al., 2020a) augmented by AR5 surface mass balance model (Box 9.3)</p> <p><i>Medium confidence</i> processes after 2100: p-box including (1) AR5 parametric AIS model and (2) LARMIP-2 simulations augmented by AR5 surface mass balance model, with both methods extrapolated based on either constant post-2100 rates or a quadratic interpolation to the multimodel assessed 2300 range (Section 9.6.3.2)</p> <p><i>Low confidence</i> processes: (1) Single ice-sheet-model ensemble simulations incorporating Marine Ice Cliff Instability (DeConto et al., 2021) and (2) structured expert judgement (Bamber et al., 2019)</p>
Glaciers (including peripheral glaciers) (Section 9.5.1.3)	Power law function of integrated GMST fit to glacier models	<p>Up to 2100: Emulated GlacierMIP (Marzeion et al., 2020; Edwards et al., 2021) simulations (Box 9.3)</p> <p>Beyond 2100: AR5 parametric model re-fit to GlacierMIP (Marzeion et al., 2020) (Supplementary Material 9.SM.4.5)</p>
Land water storage (Section 9.6.3.2)	<p>Groundwater depletion: combination of (1) continuation of early 21st century trends and (2) land-surface hydrology models (Wada et al., 2012)</p> <p>Water impoundment: combination of (1) continuation of historical rate and (2) assumption of no net impoundment after 2010</p>	<p>Groundwater depletion: Population/groundwater depletion relationship calibrated based on (Konikow, 2011; Wada et al., 2012, 2016)</p> <p>Water impoundment: Population/dam impoundment relationship calibrated based on (Chao et al., 2008), adjusted for new construction following (Hawley et al., 2020) for 2020 to 2040</p>
Ocean dynamic sea level (Section 9.2.4.2)	CMIP5 ensemble <i>zos</i> field after polynomial drift removal	Distribution derived from CMIP6 ensemble <i>zos</i> field after linear drift removal (Supplementary Material 9.SM.4.2, 9.SM.4.3)
Gravitational, rotational, and deformational effects (Section 9.6.3.2)	Sea-level equation solver (Slangen et al., 2014a) driven by projections of ice sheet, glacier, and land water storage changes	

Glacial isostatic adjustment and other drivers of vertical land motion (Section 9.6.3.2)	GIA model, with ice history from mean of ANU and ICE-5G	Spatiotemporal statistical model of tide-gauge data (updated from (Kopp et al., 2014)) (Supplementary Material 9.SM.4.6)
--	---	--

^a Ice sheet models include some of the larger islands in the Antarctic periphery, so there is some overlap in the projected glacier contribution and the projected Antarctic contribution, but the effect of this is estimated to be of order 0.5-1 cm or less (Edwards et al., 2021).

[END TABLE 9.7 HERE]

Global Mean Thermosteric Sea-Level Rise

In the AR5 and the SROCC, global mean thermosteric sea-level rise was derived from the 21 members of the CMIP5 ensemble that provided the required variables (Section 9.2.4.1). The AR5 and the SROCC removed drift estimated based on a pointwise polynomial fit to pre-industrial control simulations. They extended projections to scenarios not provided by the models by calculating the heat content of the climate system from global mean surface temperature and net radiative flux, and converting this to global mean thermosteric sea-level rise using each model's diagnosed expansion efficiency coefficient. The AR5 and the SROCC derived the associated uncertainties by assuming a normal distribution, with the 5th-95th percentile CMIP5 ensemble interpreted as the *likely* range. In this report, global mean thermosteric sea-level rise is derived from a two-layer energy budget emulator consistent with the assessment of ECS and TCR (Section 9.2.4.1; Supplementary Material 9.SM.4.2, 9.SM.4.3). Despite the change in methodology, this leads to a *likely* global mean thermosteric contribution (17th-83rd percentile) between 1995 to 2014 and 2100 that represents a minimal change from the AR5 and the SROCC (Table 9.8).

Greenland ice sheet

The AR5 and the SROCC projected the Greenland surface-mass balance using a cubic polynomial fit to a regional climate model as a function of global mean surface temperature (with a log-normal scaling factor reflecting uncertainty in surface-mass balance models, and another scaling factor reflecting the positive feedback of ice-sheet elevation changes on mass loss), and the dynamic contribution was estimated based on a multi-model assessment interpolated as a quadratic function of time.

For processes in whose projections we have at least *medium confidence*, the updated projections use emulated ISMIP6 projections of the Greenland ice sheet (Section 9.4.1.3; Box 9.3; Tables 9.2, 9.7; Figure 9.17). Since the ISMIP6 emulator does not account for temporal correlation, a parametric fit to the ISMIP6 results is employed to calculate rates of change (Supplementary Material 9.SM.4.4). For projections beyond 2100 (when the ISMIP6 simulations end), the polynomial fit is extrapolated based on two alternate approaches: (1) an assumption of constant rates of mass change after 2100, and (2) for SSP1-2.6 and SSP5-8.5, a quadratic function of time extending to 2300 based on the multimodel assessment of contributions under RCP 2.6 and RCP 8.5 at 2300 (Section 9.4.1.4). Differences between the two approaches are small up to 2150, and since the latter approach is not available for all scenarios, only the former (constant rates) is used for time-series projections up to 2150. Both approaches are used for examining uncertainty in the timing of different levels of GMSL rise and to inform projections for the year 2300 (Section 9.4.1.4). For 2100, the ISMIP6 emulator yields the *likely* contribution from the Greenland ice sheet shown in Table 9.2 and Figure 9.17, representing a slight narrowing from the AR5 projections.

Antarctic ice sheet

For the Antarctic ice sheet, the AR5 applied a temperature-based scaling approach for surface mass balance and a quadratic function of time, calibrated to a multimodel assessment, for dynamic contributions. The

1 SROCC used a new assessment based on the results of five process-based studies (Section 9.4.2.5). For
 2 processes in whose projections we have at least *medium confidence*, the *likely range* projections for the
 3 Antarctic ice sheet are based upon 1) the emulated ISMIP6 ensemble and 2) the LARMIP-2 ensemble,
 4 augmented with the AR5 parametric Antarctic surface mass balance model. GMSL projections are produced
 5 with both distributions and combined in a ‘p-box’ (Kriegler and Held, 2005; Le Cozannet et al., 2017),
 6 which represents the upper and lower bounds of the distribution (Section 9.4.2.5, Box 9.3, Table 9.3). A
 7 *likely range* is then identified, spanning the lower of the two 17th percentile projections and the higher of the
 8 two 83rd percentile projections⁵, with the median taken as the mean of the medians of the two projections.
 9 Since the ISMIP6 emulator does not account for temporal correlation, the AR5 parametric AIS model is
 10 substituted for the emulator in the p-box for rates of change. As the AR5 projections are modestly lower than
 11 those from the ISMIP6 emulator, this substitution modestly broadens the *likely range* at the low end for
 12 projections of rate and changes beyond 2100. For projections beyond 2100 (when the ISMIP6 and LARMIP-
 13 2 simulations end), the AIS simulations are extrapolated using the same two approaches as the GrIS
 14 projections (Section 9.2.4.6). The *likely ranges* to 2100 are consistent with the SROCC (Table 9.8).

15 *Low confidence ice sheet projections*

16 To test the possible effect of additional ice-sheet processes for which there is *low confidence* (Sections
 17 9.4.1.3, 9.4.1.4, 9.4.2.5, 9.4.2.6, 9.6.3.1; Box 9.4), two additional approaches are considered. For both the
 18 Greenland and Antarctic ice sheets, we produce sensitivity cases employing the SEJ projections of (Bamber
 19 et al., 2019), mapping 2°C and 5°C stabilization scenarios to SSP1-2.6 and SSP5-8.5, respectively. For the
 20 Antarctic ice sheet, we produce an additional sensitivity case using projections, which incorporate the
 21 Marine Ice Cliff Instability (DeConto et al., 2021), mapping projections for RCP 2.6 and RCP 8.5 to SSP1-
 22 2.6 and SSP5-8.5. For the Greenland ice sheet, the SEJ projections indicate the potential for outcomes
 23 outside the corresponding *likely ranges* (Table 9.8). For the Antarctic ice sheet, there is no evidence from
 24 these studies to suggest an important role under lower emissions scenarios for processes in whose projections
 25 we have *low confidence*. By contrast, for SSP5-8.5, the SEJ and MICI projections exhibit 17th-83rd percentile
 26 ranges of 0.02-0.56 m and 0.19-0.53 m by 2100, consistent with one another but considerably broader than
 27 the *likely contribution* for *medium confidence* processes of 0.03 to 0.34 m. This lower level of agreement for
 28 higher emissions scenarios reflects the *deep uncertainty* in the AIS contribution to GMSL change under
 29 higher emissions scenarios (Box 9.4). This *deep uncertainty* grows after 2100: by 2150, under SSP 5-8.5,
 30 *medium confidence* processes *likely* lead to a -0.1 to 0.7 m AIS contribution, while SEJ and MICI-based
 31 projections indicate 0.0-1.1 m and 1.4-3.7 m, respectively.

32 *Glaciers*

33 In the AR5 and the SROCC, global glacier mass changes were derived from a power law of integrated
 34 global-mean surface temperature change fit to results from four different glacier models. The updated
 35 projections use emulated GlacierMIP projections (Section 9.5.1.3, Box 9.3). Since the GlacierMIP emulator
 36 does not account for temporal correlation and terminates, along with the GlacierMIP simulations, in 2100,
 37 we employ a parametric fit to the GlacierMIP simulations, with a functional form similar to that employed
 38 by the AR5, to calculate rates of change and extrapolate changes beyond 2100 (up to a maximum potential
 39 contribution of 0.32 m) (see Supplementary Material 9.SM.4.5). This approach leads to a median glacier
 40 contribution that is a minimal change (Table 9.8) from the AR5 and the SROCC and a modest narrowing of
 41 *likely ranges* (Section 9.5.1.3). For RCP 2.6, the AR5 projected 0.10 (0.04-0.16, *likely range*) m, compared to
 42 0.09 (0.07-0.11) m projected here for SSP1-2.6. For RCP 8.5, the AR5 projected a *likely contribution* of 0.17
 43 (0.09-0.25) m, compared to 0.18 (0.15-0.21) m projected here.

44 *Land water storage*

45 In the AR5 and the SROCC, the groundwater depletion contribution to GMSL rise was based on combining
 46 results from two approaches, one assuming a continuation of early 21st century trends (Konikow, 2011) and
 47 the other using land-surface hydrology models (Wada et al., 2012). Together, these yielded a range of about
 48 0.02-0.09 m of GMSL rise by 2080-2099. The rate of water impoundment in reservoirs was likewise based
 49
 50
 51

⁵ Note that the use of this approach implies that the *likely ranges* are *likely* in the use of the term to mean 66–100% probable; this is distinct from the usage in the SROCC, where *likely range* was defined to have a precise 66% probability.

on two approaches, one assuming the continuation of the average rate over 1971-2010 (and thus -0.01 to -0.03 m by 2080-2099) (Chao et al., 2008), and the other assuming no net impoundment after 2010 (Lettenmaier and Milly, 2009). Together, these yield a GMSL contribution from groundwater impoundment of -0.03 to 0 m. Combining groundwater depletion and water impoundment led the AR5 and the SROCC to infer a projected range of -0.01 to +0.11 m by 2100.

In the updated projections, a statistical relationship is applied linking historical and future SSP global population to dam impoundment and groundwater extraction (Rahmstorf et al., 2012; Kopp et al., 2014). The population/groundwater depletion relationship is calibrated based on the same studies used in the AR5 (Konikow, 2011; Wada et al., 2012), reduced by ~20% to account for water retained on land (Wada et al., 2016). The population/dam impoundment relationship is calibrated based upon (Chao et al., 2008). However, while historically dam impoundment has been declining with population, recent literature shows that planned dam construction considerably exceeds the historical trend (Zarfl et al., 2015; Hawley et al., 2020). Over 2020-2040, the impoundment contribution to GMSL rise based upon past trends would be about -0.1 mm yr⁻¹, compared to about -0.5 mm yr⁻¹ if all currently planned dams are built (Hawley et al., 2020) and the statistical projection is therefore augmented by an additional -0.4 to 0.0 mm yr⁻¹ over 2020-2040 to account for the possible effects of planned dam construction. As in the AR5 and the SROCC, climatically driven changes to LWS have not been included in published sea-level projections, as they are not well quantified (e.g., (Jensen et al., 2019)) or are considered negligible (e.g., permafrost, Section 9.5.2). This approach yields a *likely* global-mean land water storage contribution (Figure 9.27, Table 9.8) that is slightly lower and narrower than the AR5 and the SROCC *likely* ranges. Since the projections are explicitly population driven, these projections also exhibit a weak scenario dependence, with a ~0.01 m higher contribution under SSP3 than under other scenarios.

[START TABLE 9.8 HERE]

Table 9.8: Global mean sea-level projections between 1995-2014 and 2100 for total change and individual contributions, median values, (*likely*) ranges of the process-based model ensemble, for RCP 2.6 (from the AR5 (Church et al., 2013b) and the SROCC (Oppenheimer et al., 2019)) and SSP1-2.6 (this report), and for RCP 8.5 (from the AR5 (Church et al., 2013b) and the SROCC (Oppenheimer et al., 2019)) and SSP5-8.5 (this report). Values for the AR5 (Church et al., 2013b) and the SROCC (Oppenheimer et al., 2019) are adjusted from the 1986-2005 baseline used in past reports. Only the Antarctic contribution changed between the AR5 (Church et al., 2013b) and the SROCC (Oppenheimer et al., 2019). Unshaded cells represent processes in which there is *medium confidence*; shading indicates the inclusion of processes in which there is *low confidence*. For the MICI and SEJ-based projections, parenthetical numbers represent the 17-83rd percentile of the associated probability distributions, not assessed *likely* ranges.

	RCP 2.6		SSP1-2.6		
	AR5	SROCC	<i>Medium confidence processes</i>	MICI	SEJ
<i>m rel. to 1995-2014</i>					
Thermal expansion (9.2.4.1)	0.14 (0.10-0.19)		0.14 (0.11-0.18)		
Greenland (9.4.1.3)	0.07 (0.03-0.11)		0.06 (0.01-0.10)		0.13 (0.07-0.30)
Antarctica (9.4.2.5)	0.06 (-0.04-0.16)	0.04 (0.01-0.11)	0.11 (0.03-0.27)	0.08 (0.06-0.12)	0.09 (-0.01-0.25)
Glaciers (9.5.1.3)	0.10 (0.04-0.16)		0.09 (0.07-0.11)		
Land water storage (9.6.3.2)	0.05 (-0.01-0.11)		0.03 (0.02-0.04)		

Total (2100)	0.41 (0.25-0.58)	0.40 (0.26-0.56)	0.44 (0.33-0.61)	0.41 (0.35-0.48)	0.53 (0.38-0.80)
Total (2150)	0.29-0.63	0.56 (0.40-0.73)	0.69 (0.46-1.00)	0.74 (0.63-0.91)	0.84 (0.56-1.34)
GMSL rate, 2080-2100 (mm yr⁻¹)	4.4 (2.0-6.8)	4 (2-6)	5.3 (3.3-8.1)	5.2 (4.4-6.2)	6.0 (2.9-1.1)

	RCP 8.5		SSP5-8.5		
<i>m rel. to 1995-2014</i>	AR5	SROCC	Medium confidence processes	MICI	SEJ
Thermal expansion (9.2.4.1)	0.31 (0.24-0.38)		0.30 (0.24-0.36)		
Greenland (9.4.1.3)	0.14 (0.08-0.27)		0.13 (0.09-0.18)		0.23 (0.10-0.59)
Antarctica (9.4.2.5)	0.04 (-0.08-0.14)	0.12 (0.03-0.28)	0.12 (0.03-0.34)	0.34 (0.19-0.53)	0.21 (0.02-0.56)
Glaciers (9.5.1.3)	0.17 (0.09-0.25)		0.18 (0.15-0.21)		
Land water storage (9.6.3.2)	0.05 (-0.01-0.11)		0.03 (0.02-0.04)		
Total (2100)	0.71 (0.49-0.95)	0.81 (0.58-1.07)	0.77 (0.63-1.02)	0.99 (0.82-1.19)	1.01 (0.70-1.61)
Total (2150)	0.34-1.35	1.27 (0.80-1.79)	1.35 (1.02-1.89)	3.48 (2.58-4.83)	1.80 (1.23-2.93)
GMSL rate, 2080-2100 (mm yr⁻¹)	11.2 (7.5-15.7)	15 (10-20)	12.2 (8.8-17.7)	23.2 (17.7-30.2)	16.1 (9.8-29.1)

[END TABLE 9.8 HERE]

Ocean dynamic sea level

In the AR5 and the SROCC, the ocean dynamic sea-level contribution to relative sea-level (RSL) projections was derived from the CMIP5 ensemble, after removing drift estimated based on pre-industrial control simulations. This report uses updated simulations from the CMIP6 ensemble (Section 9.2.4.2; Supplementary Material 9.SM.4.2) to project the ocean dynamic sea-level contribution to relative sea-level change (Figure 9.26; Section 9.2.4.2). To produce ocean dynamic sea-level projections consistent with the global mean thermosteric projections from the two-layer energy budget emulator, we follow the approach of (Kopp et al., 2014), employing a correlation between global-mean thermosteric sea-level change and ocean dynamic sea level derived from the CMIP6 ensemble (Supplementary Material 9.SM.4.3). Since CMIP6 models are of fairly coarse (typically ~100km) resolution, and even the models participating in HighResMIP (near 10km resolution) do not capture all the phenomena that contribute to coastal ocean dynamic sea-level change, there is *low confidence* in the details of ocean dynamic sea-level change along the coast (Section 9.2.3.6) and in semi-enclosed basins, like the Mediterranean, where coarse models can misrepresent key dynamic processes. Regional high-resolution models can improve projections of coastal ocean dynamic sea-level change (Section 12.4) (Hermans et al., 2020), but have not been implemented at a global scale.

Gravitational, rotational, and deformational (GRD) effects

Do Not Cite, Quote or Distribute

1 GRD effects (Box 9.1) lead to distinct variations in the RSL change pattern, which are similar across a range
2 of benchmarked GRD solvers (Martinec et al., 2018; Palmer et al., 2020). There is *high confidence* in the
3 understanding of GRD processes. RSL rise associated with GRD is *very likely* to be largest in the Pacific,
4 due to the combined effects of projected GrIS, AIS and glacier mass loss (*high confidence*) (e.g., Kopp et al.,
5 2014; Slangen et al., 2014a; Larour et al., 2017; Mitrovica et al., 2018). The GRD effect associated with
6 mass loss from an ice sheet is sensitive to the spatial distribution of that mass loss. For example, the GRD
7 contribution to RSL rise in Australia will be larger for Antarctic mass loss sourced from the Antarctic
8 Peninsula than for Antarctic mass loss sourced from Thwaites Glacier. In parts of northeastern North
9 America and northwestern Europe, GRD effects associated with mass loss from southern Greenland will lead
10 to a RSL fall, whereas mass loss from northern Greenland will lead to a RSL rise (*high confidence*) (Larour
11 et al., 2017; Mitrovica et al., 2018) (Figure 9.26). The AR5 and the SROCC computed RSL patterns using a
12 gravitationally self-consistent GRD solver given the amounts, locations and timing of the projected
13 barostatic sea-level changes driven by glaciers, ice sheets and LWS (Church et al., 2013a). A similar GRD
14 solver is used in the updated projections (following (Slangen et al., 2014a)). The Earth model used is based
15 on PREM (Dziewonski and Anderson, 1981), and is elastic, compressible and radially stratified.

16 *Glacial isostatic adjustment and other drivers of vertical land motion*

17 Glacial Isostatic Adjustment (GIA; Box 9.1) leads to vertical land motion (VLM; Box 9.1) and changes in
18 sea-surface height, both of which contribute to RSL change. GIA uncertainty is caused by uncertainty in the
19 rheological structure of the solid Earth, which drives the longer-term viscous Earth deformation, as well as in
20 the modelled global ice history (e.g., Whitehouse, 2018). In the AR5 and the SROCC, GIA contributions to
21 relative sea-level change were calculated using a sea-level equation solver with an ice-sheet history taken as
22 the mean of the ICE5G (Peltier et al., 2015) and ANU (Lambeck et al., 2014) ice sheet models. Since the
23 AR5, new global models are emerging that more rigorously treat ice and Earth structure uncertainty (Caron
24 et al., 2018). However, there is also a growing recognition that lateral variations in Earth structure limit the
25 utility of global models that treat the solid Earth as though it were laterally uniform (Love et al., 2016; Huang
26 et al., 2019; Li et al., 2020c).

27
28
29 As noted by the SROCC, VLM from sources other than GIA – including tectonics and mantle dynamic
30 topography, volcanism, compaction, and anthropogenic subsidence – can be locally important, producing
31 VLM rates comparable to or greater than rates of GMSL change. Complete global projections of these
32 processes are not available because of the small spatial scales, the sensitivity of subsidence to local human
33 activities, and the stochasticity of tectonics (Wöppelmann and Marcos, 2016; Oppenheimer et al., 2019).
34 Integrated RSL projections to date have therefore either included only the component of VLM associated
35 with GIA, as in the AR5 and SROCC, or used a constant long-term background rate of change (including
36 both GIA and other long-term drivers of VLM) estimated from historical tide gauge trends (e.g., (Kopp et al.,
37 2014)). The updated projections use the second approach and extrapolate the field of long-term background
38 rates of RSL change, including long-term VLM derived from tide gauges, to global coverage using a
39 spatiotemporal statistical approach (Kopp et al., 2014) (Supplementary Material 9.SM.4.6). The combined
40 GIA and long-term VLM is assumed to be constant over the projected period and scenario independent. In
41 areas (e.g., the western Gulf of Mexico) where rapid subsidence occurs in a cluster of tide-gauges, the
42 associated rates are interpolated between the tide gauges. In areas where the available tide-gauges exhibit
43 large, tectonically driven VLM that changes considerably in rate over short distances (e.g., Alaska and the
44 Bering Strait) a sizable uncertainty propagates into the RSL projections (Figure 9.26). Rates of RSL rise are
45 likely to be underestimated due to subsidence in shallow strata that are not recorded by tide gauges (Keogh
46 and Törnqvist, 2019) and in some locations may therefore be minimum values, especially if anomalously
47 high subsidence rates associated with fluid extraction (e.g., (Minderhoud et al., 2017)) are also considered.
48 There is therefore, depending on location, *low to medium confidence* in the GIA and VLM projections
49 employed in this report. In many regions, higher fidelity projections would require more detailed regional
50 analysis.

1 [START FIGURE 9.26 HERE]

2
3 **Figure 9.26: Median global mean and regional relative sea-level projections (m) by contribution for the SSP1-2.6 and SSP5-8.5 scenarios.** (upper time series) Global mean contributions to sea-level change as a function of time, relative to 1995-2014. (lower maps) Regional projections of the sea-level contributions in 2100 relative to 1995-2014 for SSP5-8.5 and SSP1-2.6. Vertical land motion is common to both SSPs. Further details on data sources and processing are available in the chapter data table (Table 9.SM.9).

8
9 [END FIGURE 9.26 HERE]

10
11
12 9.6.3.3 *Sea-level projections to 2150 based on SSP scenarios*

13
14 Up to 2050, consistent with the AR5 and the SROCC, GMSL projections exhibit little scenario dependence (Figure 9.27, Table 9.9) (*high confidence*), with *likely (medium confidence)* sea-level rise between the baseline period (1995 to 2014) and 2050 of 0.19 (0.16-0.25) m under SSP1-2.6 and 0.23 (0.20-0.30) m under SSP5-8.5. These projections fall centrally within the range of published projections for RCP 2.6 and RCP 8.5 (Section 9.6.3.1).

15
16
17
18
19
20 Beyond 2050, the scenarios increasingly diverge. Between the baseline period (1995 to 2014) and 2100, processes in whose projection there is *medium confidence* drive *likely* GMSL rise of 0.44 m (0.33-0.61) m and 0.77 (0.63-1.02) m under SSP1-2.6 and SSP5-8.5, respectively (Tables 9.8, 9.9). While derived using substantially updated methods, these projections are broadly consistent with the SROCC, which over this period projected *likely* GMSL rise of 0.41 (0.26-0.56) m and 0.81 (0.58-1.07) m under RCP 2.6 and RCP 8.5, respectively. They are modestly higher than those of the AR5, which projected *likely* GMSL rise of 0.41 (0.25-0.58) m under RCP 2.6 and 0.71 (0.49-0.95) m under RCP 8.5 (Figure 9.25, Table 9.8). They are also broadly consistent with projections produced by driving the AR5 methods with CMIP6 temperature and thermal expansion projections, which leads to 0.44 (0.27-0.61) m under SSP1-2.6 and 0.73 (0.49-1.02) m under SSP5-8.5 (Hermans et al., 2021). The SSP1-2.6 and SSP5-8.5 projections are consistent with the ranges of published projections for RCP 2.6 and RCP 8.5 that do not incorporate MICI or SEJ (Section 9.6.3.1).

21
22
23
24
25
26
27
28
29
30
31
32
33 The *likely* GMSL projections for SSP3-7.0 and SSP5-8.5 are consistent with a continuation of the GMSL satellite-observed rate (*very likely* 3.25 [2.88-3.61] mm yr⁻¹) and acceleration (*very likely* 0.094 [0.082-0.115] mm yr⁻²) of GMSL rise over 1993-2018 (Table 9.5 and Section 2.3.3.3), which would imply a *likely* GMSL rise of 0.24 m (0.23-0.25 m) by 2050 and 0.73 m (0.69-0.77 m) by 2100. This extrapolation would also imply a *likely* rate of GMSL rise of 7.5 (7.4-7.6) mm yr⁻¹ over 2040-2060 and 11.2 (10.6-11.8) mm yr⁻¹ over 2080-2100. Over the satellite period, the observed acceleration has been driven primarily by ice-sheet contributions (Section 9.6.1.2; Table 9.5); in the median projections for SSP3-7.0 and SSP5-8.5, these accelerations are projected to continue at a slightly lower level, while the GMSL acceleration is augmented by an acceleration of thermal expansion and glacier loss associated with rising global temperature. Overall, these extrapolations imply that, under SSP1-1.9, SSP1-2.6, and SSP2-4.5, the GMSL acceleration is projected to decrease from its current level.

34
35
36
37
38
39
40
41
42
43
44
45
46 [START TABLE 9.9 HERE]

47
48 **Table 9.9:** Global mean sea-level projections for 5 SSP scenarios, relative to a baseline of 1995-2014, in meters. Individual contributions are shown for the year 2100. Median values (*likely* ranges) are shown. Average rates for total sea-level change are shown in mm yr⁻¹. Unshaded cells represent processes in whose projections there is *medium confidence*. Shaded cells incorporate a representation of processes in which there is *low confidence*; in particular, the SSP5-8.5 *low confidence* column shows the 17th-83rd percentile range from a p-box including SEJ- and MICI-based projections rather than an assessed *likely* range. Methods are described in 9.6.3.2.

	SSP1-1.9	SSP1-2.6	SSP2-4.5	SSP3-7.0	SSP5-8.5	SSP5-8.5 <i>Low Confidence</i>
Thermal expansion	0.12 (0.09-0.15)	0.14 (0.11-0.18)	0.20 (0.16-0.24)	0.25 (0.21-0.30)	0.30 (0.24-0.36)	0.30 (0.24-0.36)
Greenland	0.05 (0.00-0.09)	0.06 (0.01-0.10)	0.08 (0.04-0.13)	0.11 (0.07-0.16)	0.13 (0.09-0.18)	0.15 (0.09-0.59)
Antarctica	0.10 (0.03-0.25)	0.11 (0.03-0.27)	0.11 (0.03-0.29)	0.11 (0.03-0.32)	0.12 (0.03-0.34)	0.19 (0.02-0.56)
Glaciers	0.08 (0.06-0.10)	0.09 (0.07-0.11)	0.12 (0.10-0.15)	0.16 (0.13-0.18)	0.18 (0.15-0.21)	0.17 (0.12-0.22)
Land Water Storage	0.03 (0.02-0.04)	0.03 (0.02-0.04)	0.03 (0.02-0.04)	0.04 (0.02-0.05)	0.03 (0.02-0.04)	0.03 (0.02-0.04)
Total (2030)	0.09 (0.08-0.12)	0.09 (0.08-0.12)	0.09 (0.08-0.12)	0.10 (0.08-0.12)	0.10 (0.09-0.12)	0.10 (0.09-0.15)
Total (2050)	0.18 (0.15-0.23)	0.19 (0.16-0.25)	0.21 (0.18-0.26)	0.22 (0.19-0.28)	0.23 (0.20-0.30)	0.24 (0.20-0.40)
Total (2090)	0.35 (0.26-0.49)	0.39 (0.30-0.54)	0.48 (0.38-0.65)	0.56 (0.46-0.74)	0.64 (0.52-0.83)	0.71 (0.52-1.31)
Total (2100)	0.38 (0.28-0.55)	0.44 (0.33-0.61)	0.56 (0.44-0.76)	0.68 (0.55-0.90)	0.77 (0.63-1.02)	0.88 (0.63-1.61)
Total (2150)	0.57 (0.37-0.85)	0.69 (0.46-1.00)	0.93 (0.67-1.33)	1.21 (0.92-1.67)	1.35 (1.02-1.89)	1.99 (1.02-4.83)
Rate (2040-2060)	4.2 (2.9-6.1)	4.9 (3.6-6.9)	5.9 (4.5-8.0)	6.5 (5.1-8.7)	7.3 (5.7-9.8)	7.9 (5.7-16.2)
Rate (2080-2100)	4.3 (2.5-6.6)	5.3 (3.3-8.1)	7.8 (5.3-11.5)	10.4 (7.5-14.9)	12.2 (8.8-17.7)	15.9 (8.8-30.2)

[END TABLE 9.9 HERE]

While ice-sheet processes in whose projection there is *low confidence* have little influence up to 2100 on projections under SSP1-1.9 and SSP1-2.6 (Table 9.9), this is not the case under higher emissions scenarios, where they could lead to GMSL rise well above the *likely* range. In particular, under SSP5-8.5, *low-confidence* processes could lead to a total GMSL rise of 0.6-1.6 m over this time period (17th-83rd percentile range of p-box including SEJ- and MICI-based projections), with 5th-95th percentile projections extending to 0.5-2.3 m (*low confidence*). The assessed *low confidence* range is slightly narrower than but broadly consistent with the full 0.4-2.4 m range of published 5th-95th percentile projections for RCP 8.5 since the AR5 (Section 9.6.3.1), including those based on SEJ or incorporating MICI, and highlights the *deep uncertainty* in GMSL rise under the highest emissions scenarios (Box 9.4). The assessment of the potential contribution of processes in which there is *low confidence* to GMSL rise by 2100 is broadly consistent with the assessment of the AR5 (Church et al., 2013a), which concluded that collapse of marine-based sectors of the Antarctic ice sheet could cause several tenths of a meter of global mean sea-level rise above the *likely* range.

While prior assessment reports, starting with the First Assessment Report (Warrick et al., 1990), have focused on projecting GMSL up to the year 2100, time has progressed, and the year 2100 is now within the timeframe of some long-term infrastructure decisions. For this reason, projections up to the year 2150 are also highlighted (Table 9.9). Over this time period, assuming no acceleration in ice-sheet mass fluxes after 2100, processes in which there is *medium confidence* lead to GMSL rise of 0.5-1.0 m under SSP1-2.6 and 1.0-1.9 m under SSP5-8.5. Processes in which there is *low confidence* could drive GMSL rise under SSP5-8.5 to 1.0-4.8 m (17th-83rd percentile) or even 0.9-5.4 m (5th-95th percentile).

1 [START FIGURE 9.27 HERE]

2
3 **Figure 9.27: Projected global mean sea level rise under different SSP scenarios.** *Likely* global mean sea-level change
4 for SSP scenarios resulting from processes in whose projection there is *medium confidence*. Projections and
5 *likely* ranges at 2150 are shown on right. Lightly shaded ranges and thinner lightly shaded ranges on the
6 right show the 17th-83rd and 5th-95th percentile ranges for projections including *low confidence* processes
7 for SSP1-2.6 and SSP5-8.5 only, derived from a p-box including Structured Expert Judgement and Marine
8 Ice Cliff Instability projections. Black lines show historical GMSL change, and thick solid and dash-dotted
9 black lines show the mean and *likely* range extrapolating the 1993-2018 satellite altimeter trend and
10 acceleration. Further details on data sources and processing are available in the chapter data table (Table
11 9.SM.9).

12
13 [END FIGURE 9.27 HERE]

14
15
16 Median projected relative sea-level changes are shown in Figure 9.28, with driving factors highlighted in
17 Figure 9.26. Over the 21st century, the majority of coastal locations have a median projected regional sea-
18 level rise within +/- 20% of the median projected GMSL change (*medium confidence*). Consistent with the
19 AR5, loss of land-ice mass will be an important contributor to spatial patterns in relative sea-level change
20 (*high confidence*), with ocean dynamic sea-level being particularly important as a dipolar contributor in the
21 Northwest Atlantic, a positive contributor in the Arctic Ocean, and a negative contributor in the Southern
22 Ocean south of the ACC (*medium confidence*) (Section 9.2.4.2). As today, vertical land motion will remain a
23 major driver of relative sea-level change (*high confidence*). Uncertainty in relative sea-level projections is
24 greatest in tectonically active areas in which vertical land motion varies over short distances (e.g., Alaska)
25 and in areas potentially subject to large ocean dynamic sea-level change (e.g., the northwestern Atlantic)
26 (*high confidence*).

27
28
29 [START FIGURE 9.28 HERE]

30
31 **Figure 9.28: Regional sea level change at 2100 for different scenarios (with respect to 1995-2014).** Median
32 regional relative sea-level change from 1995 to 2014 up to 2100 for (a) SSP1-1.9, (b) SSP1-2.6, (c) SSP2-
33 4.5, (d) SSP3-7.0, (e) SSP5-8.5, and (f) width of the *likely* range for SSP3-7.0. The high uncertainty in
34 projections around Alaska and the Aleutian Islands arises from the tectonic contribution to vertical land
35 motion, which varies greatly over short distances in this region. Further details on data sources and
36 processing are available in the chapter data table (Table 9.SM.9).

37
38 [END FIGURE 9.28 HERE]

39
40
41 An alternative perspective on uncertainty in future sea-level rise is provided by looking at uncertainty in time
42 rather than elevation; that is, looking at the range of dates when specific thresholds of sea-level rise are
43 projected to be crossed (Figure 9.29). Considering only *medium confidence* processes, GMSL rise is *likely* to
44 exceed 0.5 m between about 2080 and 2170 under SSP1-2.6 and between about 2070 and 2090 under SSP5-
45 8.5. It is *likely* to exceed 1.0 m between about 2150 and some point after 2300 under SSP1-2.6, and between
46 about 2100 and 2150 under SSP5-8.5. It is *unlikely* to exceed 2.0 m until after 2300 under SSP1-2.6, while it
47 is *likely* to do so between about 2160 and 2300 under SSP5-8.5. However, processes in whose projections
48 there is *low confidence* could lead to substantially earlier exceedances under higher emissions scenarios:
49 under SSP5-8.5, 1.0 m could be exceeded by about 2080 and 2.0 m could be exceeded by about 2110 (17th
50 percentile of p-box incorporating projections based on SEJ and MICI), with 5th percentile projections as early
51 as about 2070 for 1.0 m and 2090 for 2.0 m.

52
53
54 [START FIGURE 9.29 HERE]

55
56 **Figure 9.29: Timing of when GMSL thresholds of 0.5, 1.0, 1.5 and 2.0 m are exceeded, based upon four different**
57 **ice-sheet projection methods informing post-2100 projections.** Methods are labelled based on their

1 treatment of ice sheets. “No acceleration” assumes constant rates of mass change after 2100. “Assessed
 2 ice sheet” models post-2100 ice sheet losses using a parametric fit (Supplementary Material 9.SM.4)
 3 extending to 2300 based on a multimodel assessment of contributions under RCP2.6 and RCP8.5 at 2300.
 4 Structured Expert Judgement (SEJ) employs ice-sheet projections from Bamber et al. (2019) Marine Ice
 5 Cliff Instability (MICI) combines the parametric fit (Supplementary Material 9.SM.4) for Greenland with
 6 Antarctic projections based on (DeConto et al., 2021). Circles/thick bars/thin bars represent the 50th, 17th-
 7 83rd, and 5th-95th percentiles of the exceedance timing for the indicated projection method. Further details
 8 on data sources and processing are available in the chapter data table (Table 9.SM.9).
 9

10 **[END FIGURE 9.29 HERE]**

11 9.6.3.4 Sea-level projections up to 2100 based on global warming levels

12
 13 Global warming levels represent a new dimension of integration in the AR6 cycle (Section 1.6.2, Cross-
 14 Chapter Box 11.1). The SR1.5 (Hoegh-Guldberg et al., 2018) concluded that, based upon an assessment of
 15 GMSL projections published for 1.5°C and 2.0°C scenarios, there is *medium agreement* that GMSL in 2100
 16 would be 0.04–0.16 m higher in a 2°C warmer world compared to a 1.5°C warmer world based on the 17–
 17 83% confidence interval (0.00–0.24 m based on the 5–95% confidence interval) with a value of around 0.1
 18 m. The SR1.5 did not attempt to standardize the definition of warming-level scenarios, or to examine
 19 additional warming levels. No new integrated GMSL projections for 1.5°C or 2.0°C scenarios have been
 20 published since the SR1.5.
 21

22
 23 Most of the contributors to GMSL are more closely tied to time-integrated GSAT than instantaneous GSAT
 24 (Hermans et al., 2021), which means that sea level projections by warming level can only be interpreted if
 25 the warming levels are linked to a specific timeframe. Here, the warming level projections are defined based
 26 on the 2081-2100 GSAT anomaly (Supplementary Material 9.SM.4.7). Different pathways in GSAT can be
 27 followed to reach a certain temperature level, which affects the temporal evolution of the different
 28 contributors to sea-level change. For instance, there will be different ice sheet and glacier responses to a fast
 29 increase to a peak warming of 2°C in 2050 followed by a plateau or a decrease, compared to a gradual
 30 increase to the same level of warming in 2100. The sea-level projections presented might include different
 31 pathways to the same warming level in 2100, which is reflected in the uncertainty ranges, and should
 32 therefore be interpreted as an illustration of sea-level scenarios under a certain warming level.
 33

34
 35 Projections of *likely* 21st century GMSL rise along climate trajectories leading to different increases in GSAT
 36 between 1850-1900 and 2081-2100 are shown in Table 9.10, along with the SSPs for which the temperature-
 37 level projections are most closely aligned. For example, considering only processes in which there is *medium*
 38 *confidence*, from the baseline period (1995 to 2014) up to 2100, GMSL in a 2°C scenario is *likely* to rise by
 39 0.40-0.69, which is intermediate between the projections for SSP1-2.6 and SSP2-4.5. GMSL in a 4°C
 40 scenario is *likely* to rise by 0.58-0.91 m, similar to the projection for SSP3-7.0. Consistent with the
 41 discussion in Section 9.6.3.3, there is *deep uncertainty* in the projections for temperature levels above 3°C,
 42 and alternative approaches to projecting ice sheet changes may yield substantially different projections in
 43 4°C and 5°C futures. For example, employing SEJ (Bamber et al., 2019) ice-sheet projections instead of the
 44 projections for *medium confidence* processes only leads to a 17th-83rd percentile rise between the baseline
 45 period (1995-2014) and 2100 of 0.7-1.6 m rather than 0.7-1.1 m in a 5°C scenario.
 46

47
 48 **[START TABLE 9.10 HERE]**

49
 50 **Table 9.10:** Global mean sea-level projections and commitments for exceedance of 5 global warming levels, defined
 51 by sorting GSAT change in 2081-2100 w.r.t. 1850-1900. Median values and (*likely*) ranges are in meters
 52 relative to a 1995-2014 baseline. Rates are in mm yr⁻¹. Unshaded cells represent processes in whose
 53 projections there is *medium confidence*. Shaded cells incorporate a representation of processes in which
 54 there is *low confidence*; in particular, the SSP5-8.5 *low confidence* column shows the 17th-83rd percentile
 55 range from a p-box including SEJ- and MICI-based projections rather than an assessed *likely* range.
 56 Methods are described in 9.6.3.2.

1

	1.5°C	2.0°C	3.0°C	4.0°C	5.0°C	SSP5-8.5 <i>Low Confidence</i>
Closest SSPs	SSP1-2.6	SSP1-2.6/SSP2-4.5	SSP2-4.5/SSP3-7.0	SSP3-7.0	SSP5-8.5	
Total (2050)	0.19 (0.16--0.24)	0.20 (0.17--0.26)	0.21 (0.18--0.27)	0.22 (0.19--0.28)	0.25 (0.22--0.31)	0.24 (0.20--0.40)
Total (2100)	0.44 (0.34--0.59)	0.51 (0.40--0.69)	0.62 (0.50--0.81)	0.70 (0.58--0.91)	0.81 (0.68--1.05)	0.88 (0.63--1.61)
Rate (2040-2060)	4.1 (3.0--5.8)	5.1 (3.8--7.1)	6.0 (4.7--8.2)	6.5 (5.1--8.6)	7.3 (5.8--9.8)	7.9 (5.7--16.2)
Rate (2080-2100)	4.3 (2.6--6.5)	5.5 (3.5--8.3)	7.9 (5.4--11.6)	9.9 (7.2--14.2)	11.8 (8.6--17.0)	15.9 (8.8--30.2)
2000-yr commitment	2-3	2-6	4-10	12-16	19-22	
10000-yr commitment	6-7	8-13	10-24	19-33	28-37	

2

3

[END TABLE 9.10 HERE]

4

5

6

9.6.3.5 Multi-century and multi-millennial sea-level rise

7

8

Neither the AR5 nor the SROCC discussed the sea-level commitment associated with historical emissions.

9

Since the AR5, new evidence has suggested that historical emissions up to 2016 will lead to a *likely* committed sea-level rise (i.e., the rise that would occur in the absence of additional emissions) of 0.7—1.1 m up to 2300, while pledged emissions through 2030 increase the committed rise to 0.8—1.4 m (Nauels et al., 2019).

12

13

14

Between the baseline period (1995 to 2014) and 2300, the AR5 projected a GMSL rise of 0.38-0.82 m under a non-specific low emissions scenario and 0.9-3.6 m under a non-specific high emissions scenario (Table 9.11). The SROCC projected 0.6-1.0 m under RCP 2.6 and 2.3-5.3 m under RCP 8.5 (*low confidence*). RCP-based projections for 2300 published since the AR5 span a broader range, even excluding studies employing SEJ or MICI, with 17-83rd percentile projections ranging from 0.3-2.9 m for RCP 2.6 and 1.7-6.8 m for RCP 8.5 (Kopp et al., 2014, 2017, Nauels et al., 2017, 2019; Bamber et al., 2019; Palmer et al., 2020) (Table 9.SM.8). Conservatively extending the ISMIP6- and LARMIP-2-based projections beyond 2100 by assuming no subsequent change in ice-sheet mass flux rates (an approach similar to that adopted by (Palmer et al., 2020) for the Greenland Ice Sheet and for the Antarctic Ice Sheet dynamics) leads to a GMSL change up to 2300 of 0.8-2.0 m under SSP1-2.6 and 1.9-4.1 m under SSP5-8.5 (17th-83rd percentile), while incorporating the ice-sheet contributions for 2300 assessed in Section 9.4.1.4 and Section 9.4.2.6 leads to 0.6-1.5 m and 2.2-5.9 m, respectively. Incorporating Antarctic results from a model with Marine Ice Cliff Instability (Section 9.4.2.4), using RCP forcing to inform SSP-based projections, leads to 1.4-2.1 m for SSP1-2.6 and 9.5-16.2 m for SSP5-8.5 (DeConto et al., 2021). Incorporating the SEJ-based ice-sheet projections of (Bamber et al., 2019) for 2°C and 5°C stabilization scenarios yields 1.0-3.1 m for SSP1-2.6 and 2.4-6.3 m for SSP5-8.5, though because of the differences in scenarios, the SSP1-2.6 estimates may be overestimated and the SSP5-8.5 may be underestimated. The eight-fold uncertainty range across projection methods under SSP5-8.5 reflects *deep uncertainty* in the multi-century response of ice sheets to strong climate forcing.

32

33

1 Taking into account all these approaches, including published projections for RCP 2.6, under SSP1-2.6
 2 GMSL will rise between 0.3 and 3.1 m by 2300 (*low confidence*). This projection range indicates that, while
 3 the SROCC projections under low emissions to 2300 are consistent with no ice sheet acceleration after 2100,
 4 there is the possibility of a much broader range of outcomes at the high end, reflected in the range of
 5 published GMSL projections. Under SSP5-8.5, GMSL will rise between 1.7 and 6.8 m by 2300 in the
 6 absence of MICI and by up to 16 m considering MICI, a wider range than the AR5 or the SROCC
 7 assessments but consistent with published projections (*low confidence*).
 8
 9

10 **[START TABLE 9.11 HERE]**

11
 12 **Table 9.11:** Global mean sea-level projections between 1995-2014 and 2300 for total change and individual
 13 contributions, for low emissions (from the AR5 (Church et al., 2013b)), RCP 2.6 (from the SROCC
 14 (Oppenheimer et al., 2019), and published projections (Table 9.SM.8)) and SSP1-2.6 (this report), and for
 15 high emissions (from the AR5 (Church et al., 2013b)), RCP 8.5 (from the SROCC (Oppenheimer et al.,
 16 2019), and published projections (Table 9.SM.8)), and SSP5-8.5 (this report). Values for the AR5
 17 (Church et al., 2013b) and the SROCC (Oppenheimer et al., 2019) are adjusted from the 1986-2005
 18 baseline used in past reports. Only total values are shown for published ranges. Only the Antarctic
 19 contribution changed between the AR5 (Church et al., 2013b) and the SROCC (Oppenheimer et al.,
 20 2019). If a range is given it is the 17th–83rd percentile range.
 21
 22

	Low	RCP 2.6		SSP1-2.6			
<i>m rel. to 1995-2014</i>	AR5	SROCC	Post-AR5 Published range	No ice-sheet acceleration after 2100	Assessed ice-sheet contribution	MICI	SEJ
Thermal expansion	0.07-0.46			0.19--0.35			
Greenland	0.14			0.22--0.39	0.11--0.25		0.28-- 1.28
Antarctica	0.21-0.25			-0.07--1.13	-0.14--0.78	0.71-- 1.35	-0.11-- 1.56
Glaciers	–			0.13--0.30			
Land water storage	-0.03	0.07- 0.37		0.05--0.10			
Total (2300)	0.38- 0.82	0.57- 1.04	0.3--2.9	0.8--2.0	0.6--1.5	1.4--2.1	1.0-3.1

	High	RCP 8.5		SSP5-8.5			
<i>m rel. to 1995-2014</i>	AR5	SROCC	Post-AR5 Published range without (with) MICI	No ice-sheet acceleration after 2100	Assessed ice-sheet contribution	MICI	SEJ
Thermal expansion	0.28-1.80			0.91--1.50			
Greenland	0.30-1.18			0.53--0.89	0.32--1.74		0.40-- 2.23
Antarctica	0.02- 0.19	0.60- 2.89		-0.24--1.68	-0.27--3.17	6.87-- 13.54	0.03-- 3.05

Glaciers	0.29-0.39		0.32				
Land water storage	–		0.05--0.10				
Total (2300)	0.89-3.56	2.25-5.34	1.7--6.8 (up to 14.1)	1.9--4.1	2.2--5.9	9.5--16.2	2.4--6.3

[END TABLE 9.11 HERE]

On still longer timescales, the AR5 concluded with *low confidence* that the multi-millennial GMSL commitment sensitivity to warming was about 1 to 3 m°C⁻¹ GSAT increase. Two process-model-based studies since the AR5 (Clark et al., 2016; Van Breedam et al., 2020) indicate higher commitments (Figure 9.30). Ice sheets dominate the multi-millennial sea-level commitment (Sections 9.4.1.4, 9.4.2.6), but the two studies disagree on the relative contribution of the Greenland and Antarctic ice sheets. Notably, processes such as Marine Ice Cliff Instability (Section 9.4.2.4) that are a major factor behind the *deep uncertainty* in century-scale Antarctic ice sheet response do not appear to have a substantial effect on the multimillennial magnitude (DeConto and Pollard, 2016). Only one of the studies of multimillennial GMSL commitments includes scenarios consistent with 1.5°C of peak warming (Clark et al., 2016); this study suggests a 2000-year commitment at 1.5°C of about 2.3-3.1 m, with approximately an additional 1.4-2.3 m commitment between 1.5°C and 2.0°C (i.e., about 3 to 5 m °C⁻¹). Taken together, both studies show a 2000-year GMSL commitment of about 2-6 m for peak warming of about 2°C, 4-10 m for 3°C, 12-16 m for 4°C, and 19-22 m for 5°C (*medium agreement, limited evidence*, Table 9.10). GMSL rise continues after 2000 years, leading to a 10,000-year commitment of about 6-7 m for 1.5°C of peak warming (based on (Clark et al., 2016)), and of about 8-13 m for 2.0°C, 10-24 m for 3.0°C, 19-33 m for 4.0°C, and 28-37 m for 5°C (based on both studies) (*medium agreement, limited evidence*, Table 9.10).

[START FIGURE 9.30 HERE]

Figure 9.30: Global mean sea-level commitment as a function of peak global surface air temperature. From models (Clark et al., 2016; DeConto and Pollard, 2016; Garbe et al., 2020; Van Breedam et al., 2020) and paleo data on 2000-year (lower row) and 10,000 year (upper row) timescales. Columns indicate different contributors to GMSL rise (from left to right: total GMSL change, Antarctic Ice Sheet, Greenland Ice Sheet, global mean thermosteric sea-level rise, and glaciers). Further details on data sources and processing are available in the chapter data table (Table 9.SM.9).

[END FIGURE 9.30 HERE]

An indicative metric for the equilibrium sea-level response can be provided by comparing paleo global surface air temperature and GMSL during past multimillennial warm periods (Sections 2.3.1.1, 2.3.3.3 9.6.2, Figure 9.9). However, caution is needed as the present and past warm periods differ in astronomical and other forcings (Cross-chapter Box 2.1) and in terms of polar amplification. The Last Interglacial (*likely* 5-10 m higher GMSL than today and 0.5-1.5°C warmer than 1850-1900; Section 9.6.2; Table 9.6) is consistent with the (Clark et al., 2016) projections for the 10,000-year commitment associated with 1.5°C of warming. Similarly, the Mid-Pliocene Warm Period (*very likely* 5-25 m higher GMSL than today and *very likely* 2.5-4°C warmer; Section 9.6.2; Table 9.6) is consistent with the range of 10,000 year commitments associated with 2.5-4°C of warming, but GMSL reconstructions provide only a weak, broad constraint on model-based projections. An additional paleo constraint comes from the Early Eocene Climatic Optimum, which indicates that 10-18°C of warming is associated with ice-free conditions and a *likely* GMSL rise of 70-76 m (Section 2.3.3, Section 9.6.2). Together with model-based projections (Clark et al., 2016; Van Breedam et al., 2020), this period suggests that commitment to ice-free conditions would occur for peak warming of about 7 - 13°C (*medium agreement, limited evidence*).

1 On the basis of modeling studies, paleo constraints, single-ice sheet studies finding multimillennial nonlinear
2 responses from both the Greenland and Antarctic ice sheets (Sections 9.4.1.4, 9.4.2.6), and the underlying
3 physics, we conclude that GMSL commitment is nonlinear in peak warming on timescales of both 2,000 and
4 10,000 years (*medium confidence*) and exceeds the AR5 assessment of 1 to 3 m °C⁻¹ (*medium agreement*,
5 *limited evidence*) (Table 9.9). Although thermosteric sea level will start to decline slowly about 2,000 years
6 after emissions cease, the slower responses from the Greenland and Antarctic ice sheets mean that GMSL
7 will continue to rise for 10,000 years under most scenarios (*medium confidence*).

8
9 Since the AR5, a small number of modelling studies have examined the reversibility of the multimillennial
10 sea-level commitment under carbon dioxide removal, solar radiation modification or local ice-shelf
11 engineering. The slow response of the deep ocean to forcing leads to global-mean thermosteric sea-level fall
12 occurring long afterward even if CO₂ levels are restored after a transient increase: global mean thermosteric
13 sea level takes over a millennium to reverse course (Ehlert and Zickfeld, 2018b). Rapid reversion to pre-
14 industrial CO₂ concentrations has been found to be ineffective at fostering regrowth of the Antarctic ice sheet
15 (DeConto et al., 2021) but may reduce the multimillennial sea-level commitment (DeConto and Pollard,
16 2016). Altering sub-ice shelf bathymetry (Wolovick and Moore, 2018) or triggering ice-shelf advance
17 through massive snow deposition (Feldmann et al., 2019) might interrupt Marine Ice Sheet Instability
18 (Section 9.4.2.4) and thus reduce sea-level commitment. A reversion to pre-industrial Greenland ice sheet
19 temperatures with solar radiation modification is projected to stop mass loss in Greenland but leads to
20 minimal regrowth (Applegate and Keller, 2015). Based on *limited evidence*, carbon dioxide removal, solar
21 radiation modification, and local ice-shelf engineering may be effective at reducing the yet-to-be-realized
22 sea-level commitment but ineffective at reversing GMSL rise (*low confidence*).

23
24
25 **[START BOX 9.4 HERE]**

26 **BOX 9.4: High-end storyline of 21st century sea-level rise**

27 In this box, we outline a storyline (Glossary, Box 10.2 (Shepherd et al., 2018)) for high-end sea-level
28 projections for 2100. This storyline considers processes whose quantification is highly uncertain regarding
29 the timing of their possible onset and/or their potential to accelerate sea-level rise. These processes are
30 therefore not considered for the assessed upper bound of *likely* sea-level rise by 2100 in section 9.6.3.3, as
31 the *likely* range includes only processes that can be projected skilfully with at least *medium confidence*
32 (based on *agreement* and *evidence*).

33 As noted by the SROCC, stakeholders with a low risk tolerance (e.g., those planning for coastal safety in
34 cities and long-term investment in critical infrastructure) may wish to consider global-mean sea-level rise
35 above the assessed *likely* range by the year 2100, because “*likely*” implies an assessed likelihood of up to 16
36 % that sea-level rise by 2100 will be higher (see also (Siegert et al., 2020)). Because of our limited
37 understanding of the rate at which some of the governing processes contribute to long-term sea-level rise, we
38 cannot currently robustly quantify the likelihood with which they can cause higher sea-level rise before 2100
39 (Stammer et al., 2019).

40 In light of such *deep uncertainty*, we employ a storyline approach in examining the potential for, and early-
41 warning signals of a high-end sea-level scenario unfolding within this century. In doing so, we note upfront
42 that the main uncertainty related to high-end sea-level rise is “when” rather than “if” it arises: the upper limit
43 of 1.02 m of *likely* sea-level range by 2100 for the SSP 5-8.5 scenario will be exceeded in any future
44 warming scenario on time scales of centuries to millennia (*high confidence*), but it is uncertain how quickly
45 the long-term committed sea level will be reached (Section 9.6.3.5). Hence, global-mean sea level might rise
46 well above the *likely* range before 2100, which is reflected by assessments of ice-sheet contributions based
47 on structured expert judgment (Bamber et al., 2019) leading to a 95th percentile of projected future sea-level
48 rise as high as 2.3 m in 2100 (Section 9.6.3.3).

49 A plausible storyline for such high-end sea-level rise in 2100 assumes a strong warming scenario (Section
50 4.8). The storyline considers faster-than-projected disintegration of marine ice shelves and the abrupt,
51

1 widespread onset of Marine Ice Cliff Instability (MICI) and Marine Ice Sheet Instability (MISI) in Antarctica
2 (Section 9.4.2.4), and faster-than-projected changes in both the surface mass balance and dynamical ice loss
3 in Greenland. While conceptual studies provide *medium evidence* of these processes, substantial
4 uncertainties and *low agreement* in quantifying their future evolution arise from limited process
5 understanding, limited availability of evaluation data, missing or crude representation in model simulations,
6 their high sensitivity to uncertain boundary conditions and parameters, and/or uncertain atmosphere and
7 ocean forcing (Sections 9.4.1.2; 9.4.2.2).

8
9 In Antarctica, high warming might lead to floating ice shelves starting to break up earlier than expected due
10 to processes not yet accounted for in ice-sheet models or in current climate models used to force ice-sheet
11 projections. Such processes include hydrofracturing driven by surface meltwater and increase in ocean
12 thermal forcing driven by ocean circulation changes (Sections 9.2.2.3, 9.2.3.2, 9.4.2.3) (Hellmer et al., 2012,
13 2017; Silvano et al., 2018; Hazel and Stewart, 2020). In particular, the Thwaites and Pine Island Glacier ice
14 shelves could potentially disintegrate this century, which might trigger MICI before 2100 (DeConto and
15 Pollard, 2016; DeConto et al., 2021). MISI could potentially develop earlier and faster than simulated by the
16 majority of models if fast flowing ice streams follow plastic, instead of currently assumed more viscous,
17 sliding laws (Sun et al., 2020). Oceanic feedbacks could drive high-end sea-level rise by changes in the
18 meltwater-driven overturning circulation in ice cavities that cause additional melting (Jeong et al., 2020); by
19 a warming of the ocean water in contact with the ice shelves due to increased stratification and thus reduced
20 vertical mixing (Sections 9.2.2.3, 9.2.3.2) (Golledge et al., 2019b; Moorman et al., 2020; Sadai et al., 2020);
21 or by an increase in sea-ice cover due to increased ocean stratification (Section 9.3.2.1), which could reduce
22 the amount of warm, moist air that reaches the continent and limit the mass gain from snowfall over the ice
23 sheet (Sadai et al., 2020).

24
25 In Greenland, stronger mass loss than currently projected might also occur (Aschwanden et al., 2019; Khan
26 et al., 2020; Slater et al., 2020b). For example, warming-induced dynamical changes in atmospheric
27 circulation could enhance summer blocking and produce more frequent extreme melt events over Greenland
28 similar to the record mass loss of more than 500 Gt in summer 2019 (Section 9.4.1.1) (Delhasse et al., 2018;
29 Sasgen et al., 2020). Cloud processes in polar areas that are not well represented in models could further
30 enhance surface melt (Hofer et al., 2019), as could feedbacks between surface melt and the increasing albedo
31 from meltwater, detritus and pigmented algae (Section 9.4.1.1) (Cook et al., 2020). The same ice dynamical
32 processes associated with basal melt and MISI discussed for Antarctica could also occur in Greenland as
33 long as the ice sheet is in contact with the ocean.

34
35 The strength of all these processes is currently understood to depend strongly on global mean temperature
36 and polar amplification, with additional linkages through feedback from global mean sea-level (Gomez et al.,
37 2020). These dependencies on a joint forcing imply that processes are strongly correlated. Hence, both their
38 uncertainties and their possible cascading contribution to high-end sea-level rise are expected to combine.
39 High-end sea-level rise can therefore occur if one or two processes related to ice-sheet collapse in Antarctica
40 result in an additional sea-level rise at the maximum of their plausible ranges (Sections 9.4.2.5, 9.6.3.3;
41 Table 9.7) or if several of the processes described in this box result in individual contributions to additional
42 sea-level rise at moderate levels. In both cases, global-mean sea-level rise by 2100 would be substantially
43 higher than the assessed *likely* range, as indicated by the projections including *low confidence* processes
44 reaching in 2100 as high as 1.6 m at the 83rd percentile and 2.3 m at the 95th percentile (Section 9.6.3.3).

45
46 Identifying the potential drivers of a high-end sea-level rise allows identification of sites and observables that
47 can provide early warnings of a much faster sea-level rise than the *likely* range of this and previous reports.
48 One potential site for such monitoring is Thwaites Glacier, which is melting faster in some places and slower
49 in others than models simulate. At this glacier, the effect of tides and channelling of warm water flows on the
50 melting is evident (Milillo et al., 2019), making the floating ice shelf potentially vulnerable to breakup from
51 hydrofracturing, driven by surface meltwater, much earlier than expected. In addition, the glacier is
52 retreating towards a zone with deeper bedrock, which at its present rate of retreat would be reached in 30
53 years (Yu et al., 2019). Thwaites Glacier is therefore a strong candidate to experience large-scale MISI
54 and/or MICI (Golledge et al., 2019b; DeConto et al., 2021), making it the ideal site for monitoring early-
55 warning signals of accelerated sea-level-rise from Antarctica. Such signals could possibly be observed within

1 the next few decades (Scambos et al., 2017).

2
3 **[END BOX 9.4 HERE]**
4
5

6 **9.6.4 Extreme sea levels: Tides, surges and waves**

7
8 An extreme sea level (ESL) refers to an occurrence of exceptionally high or low local sea surface height
9 (Box 9.1). This section focusses on oceanographic driven changes in ESL (Box 9.1).

10 11 12 **9.6.4.1 Past changes**

13
14 The AR5 (Church et al., 2013a) concluded that changes in extreme still water levels (ESWL, combining
15 relative sea level, tide and surge as observed by tide gauges: Box 9.1) are *very likely* to be caused by
16 observed increases in relative sea level, but noted *low confidence* in region-specific results owing to the
17 limited number of studies considering localised contributions from storm surge, tide or wave effects.
18 Influences from dominant modes of climate variability, particularly ENSO and NAO (Annex IV), were also
19 noted. Climate modes affect sea level extremes in many regions, as a result of both sea-level anomalies
20 (Sections 9.2.4.2, 9.6.1.3) and changes in storminess (Section 11.7). The SROCC (Oppenheimer et al., 2019)
21 concluded with *high confidence* that inclusion of local processes (wave effects, storm surges, tides plus other
22 regional morphology changes due to erosion, sedimentation and compaction) is essential for estimation of
23 changes in ESL events.

24
25 As in the AR5 and the SROCC, tide gauge observations show that relative sea level rise (Section 9.6.1.3) is
26 the primary driver of changes in ESWL at most locations and, across tide gauges, has led to a median 165%
27 increase in high-tide flooding over 1995-2014 relative to those over 1960-1980 (Figure 9.31) (*high*
28 *confidence*). Some locations exhibit substantial differences between long-term relative sea level trends and
29 ESWL (*high confidence*), particularly given decadal to multidecadal variations of other ESWL contributors
30 (Rashid and Wahl, 2020). Since the SROCC, relative sea level rise has been shown to be the dominant
31 contributor to ESWL rise at most gauge sites along the Chinese coast, but, at some locations, the surge
32 contribution dominates (Feng et al., 2019). Trends in the difference between ESWL and mean relative sea
33 level rise can result from changes (either positive or negative) in the surge or tidal components, and can
34 include non-linear interactions between tide, surge, and relative sea level (Arns et al., 2015; Schindelegger et
35 al., 2018). The positive phase of the 18.6 year nodal cycle of the astronomical tide is a further consideration,
36 contributing to an increased flood hazard relative to the long term average (Talke et al., 2018; Peng et al.,
37 2019; Baranes et al., 2020). Failing to consider the non-linear interactions between tide, surge and relative
38 sea level may overestimate trends in ESWL (Arns et al., 2020) (*low confidence*), and, in some regions,
39 changes in ESWL depend more on changes in surge or tide than on sea level trends.

40
41 Ongoing development of the GESLA tide gauge database (Woodworth et al., 2016) along with data
42 archaeology (Talke and Jay, 2013) extends availability of tide gauge records back to the mid 19th Century (or
43 earlier). Dynamical datasets used to assess trends in ESL at global or regional scales (e.g., tide and surge
44 contributions from the Global Tide and Surge Reanalysis (GTSR) (Muis et al., 2016, 2020), or wave
45 setup/swash contributions from available wave hindcasts/reanalyses (Melet et al., 2018)) have model biases
46 introduced with resolution and parameterisation limitations, incomplete atmospheric data and currently span
47 only a few decades, so they are not yet long or accurate enough to assess long-term trends in ESLs.
48 Therefore, there is *medium confidence* in observed trends in ESWL but only *low confidence* in modelled
49 ESL trends.

50
51 The AR5 indicated that the amplitude and phase of major tidal constituents have exhibited long-term change,
52 but that their effects on ESL were not well understood. The SROCC (Bindoff et al., 2019) reported changes
53 in tides (amplification and dampening) at some locations to be of comparable importance to changes in mean
54 sea level for explaining changes in high water levels, with the sign of change being dependent on stability of
55 shoreline position. Relative sea level rise causes water depth-based alterations to the resonant characteristics

1 of the basin, changes the bottom friction and increases the wave speed (Pickering et al., 2012) and remains
2 the primary hypothesis for observed tidal changes. Other contributing processes include strong localised
3 anthropogenic drivers (e.g., port development, dredging, flood defences, land reclamation), changes in
4 stratification associated with ocean warming (Section 9.2.1.3), and changes in seabed roughness associated
5 with ecological change (e.g., Haigh et al., 2019). Tide gauge data show that, although principal tidal
6 components have varied in amplitude on the order of 2% to 10% per century (Jay, 2009; Ray, 2009),
7 identifying direct causality remains challenging (Haigh et al., 2019). Combined, observations and models
8 indicate relative sea level rise and direct anthropogenic factors are the primary drivers of observed tidal
9 changes at tide gauge stations (*medium confidence*).

10
11 The SROCC (Oppenheimer et al., 2019) reported variations in storm surge not related to changes in relative
12 sea level, and concluded with *high confidence* that consideration of localised storm surge processes was
13 essential to monitor trends in ESL. Storm surge-driven ESL events are a response to tropical and
14 extratropical cyclones. While historical trends in extra-tropical cyclones are less clear (Section 11.7.2.1),
15 there is mounting evidence for an increasing proportion of stronger tropical cyclones globally, with an
16 associated poleward migration (Section 11.7.1.2). These changes are captured in the ESL record, for
17 example, via increasing intensity and poleward shift in the location of typhoon-driven storm surges reported
18 across 64 years (1950–2013) in the western North Pacific (Oey and Chou, 2016). Along the US east coast,
19 there has been an increase in frequency of ESL events due to tropical cyclone changes since 1923 that can be
20 statistically linked to changes in global average temperature (Grinsted et al., 2013), and the signal is
21 projected to emerge around 2030 (Lee et al., 2017). At century and longer timescales, geological proxies
22 such as overwash deposits in coastal lagoons or sinkholes can be used to reconstruct past changes in storm
23 activity (e.g., Brandon et al., 2013; Lin et al., 2014) and put recent events into historical perspective (e.g.,
24 Brandon et al., 2015). However, there is *low confidence* in the current ability to quantitatively compare
25 geological proxies with gauge data. Historical storm surge activity is being increasingly assessed with use of
26 hydrodynamic model simulations and data-driven global reconstructions to supplement tide-gauge
27 observations to investigate historical changes at centennial to millennial time scales (e.g., (Ji et al., 2020;
28 Muis et al., 2020; Tadesse et al., 2020). Large regional variations and limited observational data lead to *low*
29 *confidence* in observed trends in the surge contribution to increasing ESL.

30
31
32 [START FIGURE 9.31 HERE]

33
34 **Figure 9.31: Historical occurrences of minor extreme still water levels.** Defined as the 99th percentile of daily
35 observed water levels over 1995–2014. (a) Percent change in occurrences over 1995–2014 relative to
36 those over 1960–1980. (b–g) Annual mean sea level (blue) and annual occurrences of extreme still water
37 levels over the 1995–2014 99th percentile daily maximum (yellow) at six selected tide gauge locations.
38 Further details on data sources and processing are available in the chapter data table (Table 9.SM.9).

39
40 [END FIGURE 9.31 HERE]

41
42
43 Waves contribute to ESL via wave setup, infra-gravity waves and swash processes (Dodet et al., 2019), with
44 Extreme Total Water Level (ETWL: Box 9.1) used to represent ESL with addition of wave setup, and
45 Extreme Coastal Water Level (ECWL: Box 9.1) also including contributions from swash. The SROCC
46 (Oppenheimer et al., 2019) reported the dependency of these processes on nearshore geomorphology and
47 deep-water wave climate, and thus sensitivity to internal climate variability and climate change. Few long
48 term deployments of in-situ measurements in the very dynamic surf zone means that long term records of
49 ETWL or ECWL are limited to a few sites; tidal gauges are typically located in sheltered locations (e.g.,
50 harbours) where wave contributions are absent (Lambert et al., 2020). Consequently, trends in wave
51 contributions to ESL are typically derived from trends in wave conditions observed offshore. On the basis of
52 satellite altimeter observations, the SROCC reported increasing extreme wave heights in the Southern and
53 North Atlantic Oceans of around 1.0 cm yr⁻¹ and 0.8 cm yr⁻¹ over the period 1985–2018 (*medium confidence*).
54 The SROCC (Collins et al., 2019) also identified sea-ice loss in the Arctic as leading to increased wave
55 heights over the period 1992 to 2014 (*medium confidence*). Since the SROCC, the satellite wave record has

1 been shown to be sensitive to alternate processing techniques, leading to important differences in reported
2 trends (Timmermans et al., 2020). The most common observation platform for surface waves over the past
3 30 years are in-situ buoys. However, evolving biases associated with changing instrument type,
4 configuration and sampling methodology introduce artificial trends (e.g., Gemmrich et al., 2011;
5 Timmermans et al., 2020). Accurate metadata is required to address these issues, and, while available
6 locally, are only beginning to be globally coordinated (Centurioni et al., 2019). Wave reanalysis and hindcast
7 products have also been used to investigate total water level at global scale (Melet et al., 2018; Reguero et
8 al., 2019). Their applicability for trend analysis is limited by inhomogeneous data for assimilation (Stopa et
9 al., 2019), but they inform relationships between seasonal, inter-annual to inter-decadal variability of climate
10 indices and wind-wave characteristics (Marshall et al., 2015a, 2018; Kumar et al., 2016; Stopa et al., 2016).
11 To summarise, satellite era trends in wave heights of order 0.5 cm yr⁻¹ have been reported, most pronounced
12 in the Southern Ocean. However, sensitivity of processing techniques, inadequate spatial distribution of
13 observations, and homogeneity issues in available records limit confidence in reported trends (*medium*
14 *confidence*).

15
16 Only a few studies have attempted to quantify the role of anthropogenic climate change in ESL events (e.g.
17 Mori et al., 2014, Takayabu et al., 2015, Turki et al., 2019). Detection and attribution of the human influence
18 on climatic changes in surges, and waves remains a challenge (Ceres et al., 2017), with *limited evidence* to
19 suggest in some instances (e.g., poleward migration of tropical cyclones in the Western North Pacific:
20 Section 11.7.1.2), changes in surges and waves can be attributed to anthropogenic climate change (*low*
21 *confidence*). With relative sea-level change being considered the primary driver of observed tidal changes,
22 there is *medium confidence* that these changes can be attributed to human influence. The close relationship
23 between local ESL and long-term relative sea level change, combined with the robust attribution of GMSL
24 change (Section 9.6.1.4), implies that observed global changes in ESL can be attributed, at least in part, to
25 human-caused climate change (*medium confidence*), but reconciling regional variation in these changes is
26 not yet possible (Section 9.6.1.4).

27 28 29 9.6.4.2 Future changes

30
31 There are two distinct methods used to project future ESL changes. The static, or mean sea level offset,
32 approach employs historical distributions of tidal, surge and wave components and adjusts future ESL
33 distributions for mean relative sea level rise. The dynamic approach employs hydrodynamic and/or wave
34 models forced with GCM-derived atmospheric fields to project changes in tidal, storm surge and wave
35 distributions, which are then combined with relative sea level projections to project future ESLs. The
36 dynamic approach is computationally expensive. Use of the dynamic approach on large spatial or global
37 scales has only recently been successful to project 21st Century changes in ETWL (Vousdoukas et al., 2017,
38 2018) and ECWL (Melet et al., 2020). (Kirezci et al., 2020) assume stationarity in global wave and storm
39 surge simulations to assess projected 21st century changes in episodic coastal ETWL driven flooding under
40 global sea-level rise scenarios.

41
42 The SROCC (Oppenheimer et al., 2019) presents projections of ESL derived using a static approach. Such
43 projections often quantify changes in ESL event frequency, expressed as “frequency amplification factors”
44 (Hunter, 2010, 2012). Like relative sea level projections, frequency amplification factors increase under
45 higher emission scenarios, and differences between scenarios increase over time. The SROCC concludes that
46 even small to moderate changes in mean relative sea level can lead to hundred- to thousand-fold increases in
47 the frequencies with which certain thresholds are exceeded; e.g., what is currently a 1-in-100 year ESL
48 height (1% annual probability or 0.01 expected annual events) will be expected once or even multiple times
49 per year in future at many locations (Figure 9.32). The SROCC showed that currently rare ESL events (e.g.,
50 with an average return period of 100 years) will occur annually or more frequently at most available
51 locations for RCP4.5 by the end of the century (*high confidence*). Results from these assessments are
52 sensitive to the type of ESL probability distribution assumed (Buchanan et al., 2016; Wahl et al., 2017), as
53 well as the magnitude and uncertainty of projected relative sea level change (Slangen et al., 2017; Wahl et
54 al., 2017; Frederikse et al., 2020a). Frequency amplification factors tend to be largest in tropical regions due
55 in part to higher relative sea level rise projections, but primarily to the relative rarity of high ESLs in areas

1 with little historical exposure to tropical or extratropical cyclones. Alternative representation of changes in
2 ESL, such as presenting changes in exceedances per year (Sweet and Park, 2014), are subject to similar
3 sensitivities, and lead to *medium confidence* in projected changes of event frequency using these methods.
4

5 Employing a similar static approach (fitting a Gumbel distribution between Mean Higher High Water
6 (average of higher high water height of each tidal day) and a threshold following (Buchanan et al., 2016)),
7 this report updates the SROCC projections of ESL with the relative sea level projections from Section
8 9.6.3.3 (see also Supplementary Material 9.SM.4). By 2050, the median increase in frequency amplification
9 factor at 634 tide gauge stations is 19 for SSP1-2.6, 22 for SSP2-4.5 and 30 for SSP5-8.5 (Figure 9.32). This
10 means that by 2050 a historical (1995-2014) 1% annual probability ESL will have increased to an 19-30%
11 annual probability. The 1% historical annual probability event is expected to become an annual event at 19-
12 31% of the 634 stations by 2050, consistent with the SROCC. By 2100, the median frequency amplification
13 factor is projected to be 163 for SSP1-2.6, 325 for SSP2-4.5 and 532 for SSP5-8.5, with respectively 60%,
14 71%, and 82% of the stations experiencing a currently 1% annual probability event at least yearly (Figure
15 9.32) (*medium confidence*).
16

17 In the dynamic approach, the low resolution of the forcing fields arising from GCMs limits the ability to
18 resolve historical and future changes in tropical and extra-tropical storm frequency and intensity, and
19 resolution of local geography and morphology limit ability to represent ECWL (Box 9.1). Not all relevant
20 processes, e.g., river discharge, are included in the dynamic models, and ESL events are typically a
21 combination of multiple contributing processes, which are often not independent (Jevrejeva et al., 2019). In
22 both static and dynamical approaches, global assessment of the performance of modelled storm surge and
23 wave contributions to ESL is limited by poor coverage of observations (limited to tide-gauges for ESWL,
24 (Muis et al., 2020), and unavailable for the wave dependent ETWL and ECWL estimates (Vitousek et al.,
25 2017; Vousdoukas et al., 2018; Kirezci et al., 2020; Lambert et al., 2020; Melet et al., 2020). In studies to
26 date, individual models are used to simulate different contributions to ESL, non-linear interactions are not
27 well captured, and uncertainties associated with downscaling methodology are poorly resolved, leading to
28 *low confidence* in available ESL projections that include these modelled wave and surge contributions.
29

30 Assessment of dynamic ETWL changes for regions is presented in Chapter 12, following the methods of
31 (Vousdoukas et al., 2018) and (Kirezci et al., 2020). Consistent with studies using the static approach,
32 (Vousdoukas et al., 2018) finds that by 2050 the historical 1% average annual probability ETWL will have
33 increased to a 2-50% average annual probability for most high latitude regions, and more often (up to
34 multiple times a year, >100% annual probability) in the tropics, under both RCP 4.5 and RCP 8.5. For 2100,
35 present-day 1% average annual probability extreme sea levels will be exceeded multiple times each year
36 almost everywhere. In summary, despite waves and surges being non-negligible contributors to projected
37 ETWL and ECWL changes (Vousdoukas et al., 2018; Melet et al., 2020), relative sea level change is
38 expected to be the main driver in changes in future ESL return periods in most areas (*medium confidence*).
39

40 The SROCC (Bindoff et al., 2019) concluded that the majority of coastal regions will experience statistically
41 significant changes in tidal amplitudes through the 21st Century. Comprehensive high-resolution (of order
42 10km) numerical modelling studies provide evidence for spatially coherent changes in tidal amplitudes in
43 shelf seas as a result of relative sea level rise (Haigh et al., 2019, and references therein). There is *high*
44 *confidence* that GMSL rise will be the primary driver of global tidal amplitude increases and decreases over
45 the next 100-200 years, changing the baseline tide that ESLs are imposed upon. At local and regional scales,
46 anthropogenic factors such as major land reclamation efforts (e.g., East China Sea, Song et al., 2013) or
47 differing national coastal management strategies (maintaining the present coastline position or managed
48 retreat) will locally modulate the influence of GMSL rise on tidal amplitude (*medium confidence*).
49

50 The SROCC (Oppenheimer et al., 2019) concluded that the intensity of severe tropical cyclones will increase
51 in a warmer climate (Section 11.7.1), but *low confidence* remains in the future frequency of tropical
52 cyclones. Changes in tropical cyclone climatology will contribute to variations in frequency and magnitude
53 of future ESL surge events, although estimates of this contribution range widely (Lin et al., 2012; McInnes et
54 al., 2014, 2016; Little et al., 2015; Garner et al., 2017; Mori et al., 2019; Muis et al., 2020). In the Gulf of
55 Mexico, changes in ESL due to tropical cyclone activity may be as important as SLR in enhancing future

1 flood hazards (Marsooli et al., 2019). For the Korean Peninsula, a maximum change in 100-year return
2 height associated with typhoon-induced storm surges of 10% under 4°C warming is found (Yang et al.,
3 2018). The effects of projected changes in tropical cyclone intensity may be enhanced or offset in different
4 locations by effects of changes in tracks (Garner et al., 2017) (Section 11.7.1). There is *low confidence* in
5 projected changes in ESL driven by changes in tropical cyclone climatology.
6

7 Changes in surface wave conditions occur in response to changes in frequency; intensity and position of
8 forcing winds and storms (Morim et al., 2018, 2019); reduction in sea-ice and associated changes in fetch
9 conditions (Thomson and Rogers, 2014; Casas-Prat and Wang, 2020); and changes in coastal morphology
10 associated with relative sea level rise (Wandres et al., 2017; Storlazzi et al., 2018). A few studies considering
11 the contribution of a non-stationary wave climate on future changes in ESL infer a small but non-negligible
12 contribution (Vousdoukas et al., 2018; Melet et al., 2020). The SROCC presented qualitative assessments of
13 projected changes in wave conditions. Since the SROCC, a quantitative assessment of a community
14 ensemble of global wind-wave projections (Morim et al., 2019) found robust projected changes of ~5-10%
15 (positive or negative, depending on region) in annual mean significant wave height, mean wave period,
16 and/or mean wave directions along ~52% of the world's coastline that exceed internal climate variability
17 under RCP8.5 by 2100. Continued retreat of sea-ice cover in the Arctic will lead to more energetic wind-
18 wave conditions (Casas-Prat and Wang, 2020). Wave climate modelling methods introduce up to ~50% of
19 the ensemble variance in mean wave climate projections (Morim et al., 2019). GCMs do not typically
20 resolve the higher-resolution tropical and extratropical storm features required to accurately determine the
21 contribution of extreme waves to ESLs and individual studies have sought to improve resolution to address
22 these issues (e.g., Timmermans et al., 2017). To date, projections of wave height extremes have been
23 constrained to single wave model configurations (e.g., Timmermans et al., 2017; Meucci et al., 2020). In
24 summary, there is *medium confidence* in projections of changes in mean wave climate but *low confidence* in
25 the projected changes in extreme wave conditions due to *limited evidence*.
26

27 Correlations between changes in sea level-forced (mean sea level and tidal) and atmospherically-forced
28 drivers (ocean surface waves and surges) of ESLs have only been considered in a few studies, although high
29 surge and high waves co-occur along a majority of the world's coastlines (Marcos et al., 2019). Along the
30 US east coast, ocean dynamic sea level change and change in power dissipation index (a proxy for North
31 Atlantic tropical cyclone activity) are correlated across CMIP5 GCMs, resulting in an increase in ESLs
32 relative to analyses assuming independence of these changes (Little et al., 2015). In the Irish Sea,
33 dynamically coupled wave-tide modelling results in high water wave heights up to 20% higher than in an
34 uncoupled analysis (Lewis et al., 2019). In the German Bight, relative sea level rise relaxes the breaking
35 criterion of nearshore waves (assuming no geomorphological response), allowing larger waves to propagate
36 closer to shore, leading to increased wave runup (Arns et al., 2017). In south-western Australia, the influence
37 of projected SLR was found to exceed the influence of projected changes in forcing winds on wave
38 characteristics at the coast (Wandres et al., 2017). Thus, projections of ESL that do not consider correlations
39 between and among sea level-forced and atmospherically-forced drivers can differ strongly from coupled
40 projections (*medium confidence*).
41

42 The SROCC (Collins et al., 2019b) highlighted compound events, or coincident occurrence of multiple
43 hazards, as an example of *deep uncertainty*, and noted that failing to account for multiple factors contributing
44 to extreme events will lead to underestimation of the probabilities of occurrence (*high confidence*). Statistical
45 studies have shown that high rain or streamflow often co-occurs with storm surge as examples of
46 "compound" surge-rain or surge-discharge events (Sections 11.8.1; 12.4.5.6; Wahl and Chambers, 2015;
47 Moftakhari et al., 2017; Ward et al., 2018; Wu et al., 2018; Couasnon et al., 2019). Dynamical modelling
48 studies show co-occurrence of flood drivers raises ESLs at some locations in estuaries (e.g., Rhine Delta,
49 Zhong et al., 2013; the Netherlands, van den Hurk et al., 2015; Taiwan, Chen and Liu, 2016; and the Hudson
50 River, USA Orton et al., 2018), particularly when hydrologic catchments are steep and cause high rainfall
51 near the coast (SW UK, Svensson and Jones, 2004). The compound effect of storm surge and rainfall
52 contributes greater projected flood risk than climate induced amplification (Hsiao et al., 2021). However, at
53 other locations, co-occurrence was unimportant because streamflow timing was not coincident with the
54 coastal peak storm surge (Hudson River, Orton et al., 2012; Rhine delta, Klerk et al., 2015). The SROCC
55 (Oppenheimer et al., 2019) detailed the complexity of interactions in deltaic environments. Direct increases

1 in flooding driven by increasing relative sea levels and by increased storm surge, rain, or correlations
2 between these flood-drivers (e.g., Moftakhari et al., 2017; Orton et al., 2018) are expected to be further
3 accompanied by increases in flooding due to subsidence (vertical land movement) and sedimentation
4 (relative sea level driven blockage of river flows). The probability of concurrent surge, wave and
5 precipitation events has been projected to increase by more than 25% by 2100 compared to present, with
6 high northern latitudes displaying compound flooding becoming more than 2.5 times as frequent, and
7 weakening in the subtropics (Bevacqua et al., 2020). However, the number of studies on compound events is
8 still limited and therefore there is *low confidence* in understanding the extent by which compound surge-rain
9 events will change in response to relative sea level rise and climate change.

10
11
12 **[START FIGURE 9.32 HERE]**

13
14 **Figure 9.32: Projected median frequency amplification factors for the 1% average annual probability extreme**
15 **still water level in 2050 (a, c, e) and 2100 (b, d, f).** Based on a peak-over-threshold (99.7%) method
16 applied to the historical extreme still water levels of GESLA2 following SROCC and additionally fitting
17 a Gumbel distribution between MHHW and the threshold following (Buchanan et al., 2016), using the
18 regional sea-level projections of this chapter (Section 9.6.3.3) for (a, b) SSP5-8.5, (c, d) SSP2-4.5 and (e,
19 f) SSP1-2.6. Further details on data sources and processing are available in the chapter data table (Table
20 9.SM.9).

21
22 **[END FIGURE 9.32 HERE]**

23 24 25 **9.7 Final Remarks**

26
27 The process-based assessment of observed and projected change in the ocean, cryosphere and sea level
28 undertaken here reveals advances and gaps in reconstructions, observations, models and process
29 understanding. Revisiting the updated assessments since the AR5 and the SROCC helps to gauge the
30 robustness of understanding and quantitative assessments. The CMIP6 family of models builds upon the
31 experience of the CMIP5 models, and the projections of ISMIP6, LARMIP2 and GlacierMIP strengthen
32 understanding. Taken together with emulators of these simulations (Box 9.3) and transparent statistical
33 approaches (Section 9.6.3), this chapter provides projections which are consistent with the assessment of
34 Equilibrium Climate Sensitivity in this report and that have improved estimates of uncertainty.

35
36 The largest uncertainties in future sea level and cryosphere change are related to the Greenland and Antarctic
37 ice sheets (Sections 9.4.1.3, 9.4.1.4, 9.4.2.5, 9.4.2.6). While the ISMIP6 and LARMIP2 protocols provide
38 simulations permitting uncertainty estimation and probabilistic inferences, remaining *deep uncertainty*
39 relates both to ice sheet processes and the atmospheric and oceanic conditions simulated by CMIP models in
40 polar regions (Sections 9.4.2.3, 9.4.2.4). ISMIP6 and LARMIP2 have not been simulated beyond 2100,
41 which greatly reduces the amount and variety of state-of-the-art projections available to make ice sheet and
42 sea level projections beyond 2150. After 2150, *limited agreement* causes us to consider all projections as *low*
43 *confidence*. Critically, the uncertainty in ice sheet projections is the leading uncertainty in projections of
44 future global sea level for the second half of this century and beyond (Section 9.6.3).

45
46 Glacier inventory and projection uncertainty has been a significant source of past sea level budget
47 uncertainty and remains a dominant uncertainty until mid-century. Emission scenario becomes the largest
48 source of glacier change uncertainty by 2100 just as the relative importance of glacier loss is projected to
49 decrease (Section 9.5.1).

50
51 New high-resolution climate models show that SST, overturning circulation, ocean heat content change and
52 sea-ice cover are considerably improved in most models when compared to the coarser resolution models.
53 Change in the Southern Ocean and adjacent shelves (Section 9.2.3.2) is intimately linked to the future of the
54 Antarctic ice sheet (Section 9.4.2.3), and projection of the Southern Ocean depends on both oceanic and
55 atmospheric drivers affecting heat (and carbon) uptake and sea ice. However, resolution remains a factor, as
56 most CMIP6 models are far from resolutions that directly represent coastal and regional shallow-water

1 processes such as those beneath Antarctic ice shelves, in Greenland fjords and the eddying convection found
2 by OSNAP.

3
4 Processes that change on long timescales—particularly AMOC, ocean heat content, and ice sheets—require
5 additional projections beyond the CMIP scenarios to explore longer term commitment, post-forcing recovery
6 measured in centuries rather than years or decades, and potential tipping points and thresholds. There were
7 only a few new studies focussed on longer timescales and none based on CMIP6 models.
8
9

ACCEPTED VERSION
SUBJECT TO FINAL EDITING

1 Frequently Asked Questions

2

3 **FAQ 9.1: Can continued melting of the Greenland and Antarctic ice sheets be reversed? How long** 4 **would it take for them to grow back?**

5

6 *Evidence from the distant past shows that some parts of the Earth system might take hundreds to thousands*
7 *of years to fully adjust to changes in climate. This means that some of the consequences of human-induced*
8 *climate change will continue for a very long time, even if atmospheric heat-trapping gas levels and global*
9 *temperatures are stabilized or reduced in the future. This is especially true for the Greenland and Antarctic*
10 *ice sheets, which grow much more slowly than they retreat. If the current melting of these ice sheets*
11 *continues for long enough it becomes effectively irreversible on human timescales, as does the sea level rise*
12 *caused by that melting.*

13

14 Humans are changing the climate and there are mechanisms that amplify the warming in the polar regions
15 (Arctic and Antarctic). The Arctic is already warming faster than anywhere else (see FAQ 4.3). This is
16 significant because these colder high latitudes are home to our two remaining ice sheets: in Antarctica and
17 Greenland. Ice sheets are huge reservoirs of frozen freshwater, built up by tens of thousands of years of
18 snowfall. If they were to completely melt, the water released would raise global sea level by about 65 m.
19 Understanding how these ice sheets are affected by warming of nearby ocean and atmosphere is therefore
20 critically important. The Greenland and Antarctic ice sheets are already slowly responding to recent changes
21 in climate, but it takes a long time for these huge masses of ice to adjust to changes in global temperature.
22 That means that the full effects of a warming climate may take hundreds or thousands of years to play out.
23 An important question is whether these changes can eventually be reversed, once levels of greenhouse gases
24 in the atmosphere are stabilized or reduced by humans and natural processes. Records from the past can help
25 us answer this question.

26

27 For at least the last 800,000 years, the Earth has followed cycles of gradual cooling followed by rapid
28 warming caused by natural processes. During cooling phases, more and more ocean water is gradually
29 deposited as snowfall, causing ice sheets to grow and sea level to slowly decrease. During warming phases,
30 the ice sheets melt more quickly, resulting in more rapid rises in sea level (FAQ 9.1, Figure 1). Ice sheets
31 build up very slowly because growth relies on the steady accumulation of falling snow that eventually
32 compacts into ice. As the climate cools, areas that can accumulate snow expand, reflecting back more
33 sunlight that otherwise would keep the Earth warmer. This means that once started, glacial climates develop
34 rapidly. However, as the climate cools, the amount of moisture that the air can hold tends to decrease. As a
35 result, even though glaciations begin quite quickly, it takes tens of thousands of years for ice sheets to grow
36 to a point where they are in balance with the colder climate.

37

38 Ice sheets retreat more quickly than they grow because of processes that, once triggered, drive self-
39 reinforcing ice loss. For ice sheets that are mostly resting on bedrock *above* sea level – like the Greenland ice
40 sheet – the main self-reinforcing loop that affects them is the ‘elevation–mass balance feedback’ (FAQ 9.1,
41 Figure 1, right). In this situation, the altitude of the ice sheet surface decreases as it melts, exposing the sheet
42 to warmer air. The lowered surface then melts even more, lowering it faster still, until eventually the whole
43 ice sheet disappears. In places where the ice sheet rests instead on bedrock that is *below* sea level and which
44 also deepens inland, including many parts of the Antarctic ice sheet, an important process called ‘marine ice-
45 sheet instability’ is thought to drive rapid retreat (FAQ 9.1, Figure 1, left). This happens when the part of the
46 ice sheet that is surrounded by sea water melts. That leads to additional thinning, which in turn accelerates
47 the motion of the glaciers that feed into these areas. As the ice sheet flows more quickly into the ocean, more
48 melting takes place, leading to more thinning and even faster flow that brings ever-more glacier ice into the
49 ocean, ultimately driving rapid deglaciation of whole ice-sheet drainage basins.

50

51 These (and other) self-reinforcing processes explain why relatively small increases in temperature in the past
52 led to very substantial sea level rise over centuries to millennia, compared to the many tens of thousands of
53 years it takes to grow the ice sheets that lowered the sea level in the first place. These insights from the past
54 imply that if human-induced changes to the Greenland and Antarctic ice sheets continue for the rest of this
55 century, it will take thousands of years to reverse that melting, even if global air temperatures decrease

1 within this or the next century. In this sense, these changes are therefore irreversible, since the ice sheets
2 would take much longer to regrow than the decades or centuries for which modern society is able to plan.
3
4

5 **[START FAQ9.1, FIGURE 1 HERE]**
6

7 **FAQ 9.1, Figure 1: Ice sheets growth and decay.** (Top) Changes in ice-sheet volume modulate sea level variations.
8 The grey line depicts data from a range of physical environmental sea-level recorders such as coral
9 reefs (see Table 9.SM.5) while the blue line is a smoothed version of it. (Bottom, left) Example of
10 destabilisation mechanism in Antarctica. (Bottom, right) Example of destabilisation mechanism in
11 Greenland.
12
13

14 **[END FAQ9.1, FIGURE 1 HERE]**
15
16
17

ACCEPTED VERSION
SUBJECT TO FINAL EDITING

1 FAQ 9.2: How much will sea level rise in the next few decades?

2

3 *As of 2018, global average sea level was about 15–25 cm higher than in 1900 and 7–15 cm higher than in*
4 *1971. Sea level will continue to rise by an additional 10–25 cm by 2050. The major reasons for this ongoing*
5 *rise in sea level are the thermal expansion of seawater as its temperature increases and the melting of*
6 *glaciers and ice sheets. Local sea level changes can be larger or smaller than the global average, with the*
7 *smallest changes in formerly glaciated areas and the largest changes in low-lying river delta regions.*

8

9 Across the globe, sea level is rising, and the rate of increase has accelerated. Sea level increased by about 4
10 mm per year from 2006 to 2018, which was more than double the average rate over the 20th century. Rise
11 during the early 1900s was due to natural factors, such as glaciers catching up to warming that occurred in
12 the Northern Hemisphere during the 1800s. However, since at least 1970, human activities have been the
13 dominant cause of global average sea level rise, and they will continue to be for centuries into the future.

14

15 Sea level rises either through warming of ocean waters or the addition of water from melting ice and bodies
16 of water on land. Expansion due to warming caused about 50% of the rise observed from 1971 to 2018.
17 Melting glaciers contributed about 22% over the same period. Melting of the two large ice sheets in
18 Greenland and Antarctica has contributed about 13% and 7%, respectively, during 1971–2018, but melting
19 has accelerated in the recent decades, increasing their contribution to 22% and 14% since 2016. Another
20 source is changes in land water storage: reservoirs and aquifers on land have reduced, which contributed
21 about a 8% increase in sea level.

22

23 By 2050, sea level is expected to rise an additional 10–25 cm whether or not greenhouse gas emissions are
24 reduced (FAQ 9.2, Figure 1). Beyond 2050, the amount by which sea level will rise is more uncertain. The
25 accumulated total emissions of greenhouse gases over the upcoming decades will play a big role beyond
26 2050, especially in determining where sea level rise and ice sheet changes eventually level off.

27

28 Even if net zero emissions are reached, sea level rise will continue because the deep ocean will continue to
29 warm and ice sheets will take time to catch up to the warming caused by past and present emissions: ocean
30 and ice sheets are slow to respond to environmental changes (see FAQ 5.3). Some projections under low
31 emissions show sea level rise continuing as net zero is approached at a rate comparable to today (3–8 mm
32 per year by 2100 versus 3–4 mm per year in 2015), while others show substantial acceleration to more than
33 five times the present rate by 2100, especially if emissions continue to be high and processes that accelerate
34 retreat of the Antarctic Ice Sheet occur widely (FAQ 9.1).

35

36 Sea level rise will increase the frequency and severity of extreme sea level events at coasts (see FAQ 8.2),,
37 such as storm surges, wave inundation and tidal floods: risk can be increased by even small changes in
38 global average sea level. Scientists project that in some regions, extreme sea level events that were recently
39 expected once in 100 years will occur annually at 20–25% of locations by 2050 regardless of emissions, but
40 by 2100 emissions choice will matter: annually at 60% of locations for low emissions, and at 80% of
41 locations under strong emissions.

42

43 In many places, local sea level change will be larger or smaller than the global average. From year to year
44 and place to place, changes in ocean circulation and wind can lead to local sea level change. In regions
45 where large ice sheets, such as the Fennoscandian in Eurasia and the Laurentide and Cordilleran in North
46 America, covered the land during the last ice age, the land is still slowly rising up now that the extra weight
47 of the ice sheets is gone. This local recovery is compensating for global sea level rise in these regions and
48 can even lead to local decrease in sea level. In regions just beyond where the former ice sheets reached and
49 the Earth bulged upwards, the land is now falling, and as a result local sea level rise is faster than the global
50 rate. In many regions within low-lying delta regions (such as New Orleans and the Ganges–Brahmaputra
51 delta), the land is rapidly subsiding (sinking) because of human activities such as building dams or
52 groundwater and fossil fuel extraction. Further, when an ice sheet melts it has less gravitational pull on the
53 ocean water nearby. This reduction in gravitational attraction causes sea level to fall close to the (now less-
54 massive) ice sheet while causing sea level to rise farther away. Melt from a polar ice sheet therefore raises
55 sea level most in the opposite hemisphere or in low latitudes – amounting to tens of centimetres difference in

1 rise between regions by 2100.
2
3

4 **[START FAQ9.2, FIGURE 1 HERE]**
5

6 **FAQ 9.2, Figure 1: Observed and projected global mean sea level rise and the contributions from its major**
7 **constituents.**
8

9 **[END FAQ9.2, FIGURE 1 HERE]**
10
11

ACCEPTED VERSION
SUBJECT TO FINAL EDITING

FAQ 9.3: Will the Gulf Stream shut down?

The Gulf Stream is part of two circulation patterns in the North Atlantic: the Atlantic Meridional Overturning Circulation (AMOC) and the subtropical gyre. Based on models and theory, scientific studies indicate that, while the AMOC is expected to slow in a warming climate, the Gulf Stream will not change much and would not shut down totally, even if the AMOC did. Most climate models project that the AMOC slows in the later 21st century under most emissions scenarios, with some models showing it slowing even sooner. The Gulf Stream affects the weather and sea level, so if it slows, North America will see higher sea levels and Europe's weather and rate of relative warming will be affected.

The Gulf Stream is the biggest current in the North Atlantic Ocean. It transports about 30 billion kilograms of water per second northward past points on the east coast of North America. It is a warm current, with temperatures 5°C to 15°C warmer than surrounding waters, so it carries warmer water (thermal energy) from its southern origins and releases warmth to the atmosphere and surrounding water.

The Gulf Stream is part of two major circulation patterns, the Atlantic Meridional Overturning Circulation (AMOC) and the North Atlantic Subtropical Gyre (FAQ 9.3, Figure 1). The rotation of the Earth causes the big currents in both circulations to stay on the western side of their basin, which in the Atlantic means the circulations combine to form the Gulf Stream. Other large currents contribute to gyres, such as the Kuroshio in the North Pacific and the East Australian Current in the South Pacific, but the Gulf Stream is special in its dual role. There is no comparable deep overturning circulation in the North Pacific to the AMOC, so the Kuroshio plays only one role as part of a gyre.

The gyres circulate surface waters and result primarily from winds driving the circulation. These winds are not expected to change much and so neither will the gyres, which means the gyre portion of the Gulf Stream and the Kuroshio will continue to transport thermal energy poleward from the equator much as they do now. The gyre contribution to the Gulf Stream is 2 to 10 times larger than the AMOC contribution.

The Gulf Stream's role in the AMOC is supplying surface source water that cools, becomes denser and sinks to form cold, deep waters that travel back equatorward, spilling over features on the ocean floor and mixing with other deep Atlantic waters to form a southward current at a depth of about 1500 metres beneath the Gulf Stream. This overturning flow is the AMOC, with the Gulf Stream in the upper kilometre flowing northward and the colder deep water flowing southward.

The AMOC is expected to slow over the coming centuries. One reason why is freshening of the ocean waters: by meltwater from Greenland, changing Arctic sea ice, and increased precipitation over warmer northern seas. An array of moorings across the Atlantic has been monitoring the AMOC since 2004, with recently expanded capabilities. The monitoring of the AMOC has not been long enough for a trend to emerge from variability and detect long-term changes that may be underway (see FAQ 1.2). Other indirect signs may indicate slowing overturning – for example, slower warming where the Gulf Stream's surface waters sink. Climate models show that this 'cold spot' of slower-than-average warming occurs as the AMOC weakens, and they project that this will continue. Paleoclimate evidence indicates AMOC changed significantly in the past, especially during transitions from colder climates to warmer ones, but indicate it has been stable for 8000 years.

What happens if the AMOC slows in a warming world? The atmosphere adjusts somewhat, compensating partly for the decreases in heat carried by AMOC by carrying more heat. But the 'cold spot' makes parts of Europe warm more slowly. Models indicate that weather patterns in Greenland and around the Atlantic will be affected, with reduced precipitation in the mid-latitudes, changing strong precipitation patterns in the tropics and Europe, and stronger storms in the North Atlantic storm track. The slowing of this current combined with the rotation of the Earth means that sea level along North America rises as the AMOC contribution to the Gulf Stream slows.

The North Atlantic is not the only site of sensitive meridional overturning. Around Antarctica, the world's densest seawater is formed by freezing into sea ice, leaving behind salty, cold water that sinks to the bottom

1 and spreads northward. Recent studies show that melting of the Antarctic Ice Sheet and changing winds over
2 the Southern Ocean can affect this southern meridional overturning, affecting regional weather.
3
4

5 **[START FAQ9.3, FIGURE 1 HERE]**
6

7 **FAQ 9.3, Figure 1: Horizontal (gyre) and vertical (Atlantic Meridional Overturning Circulation - AMOC)**
8 **circulations in the Atlantic today (left) and in a warmer world (right).** The Gulf Stream is a
9 warm current composed of both circulations.

10 **[END FAQ9.3, FIGURE 1 HERE]**
11
12

ACCEPTED VERSION
SUBJECT TO FINAL EDITING

1 Acknowledgements

2

3 We acknowledge the contribution of invited expert reviewers and the IMBIE Team. Their valuable input and
4 advice have significantly improved the chapter. We thank colleagues, institutions and, in particular, our
5 families for their support. Thanks to the TSU and especially Sophie Berger for support.

ACCEPTED VERSION
SUBJECT TO FINAL EDITING

1 **Reference**

- 2
- 3 Aas, K.S., K. Gislén, S. Westermann, and T.K. Berntsen, 2017: A Tiling Approach to Represent Subgrid Snow
4 Variability in Coupled Land Surface-Atmosphere Models. *Journal of Hydrometeorology*, **18**(1), 49–63,
5 doi:[10.1175/jhm-d-16-0026.1](https://doi.org/10.1175/jhm-d-16-0026.1).
- 6 Abich, K. et al., 2019: In-Orbit Performance of the GRACE Follow-on Laser Ranging Interferometer. *Phys. Rev. Lett.*,
7 **123**(3), 31101, doi:[10.1103/physrevlett.123.031101](https://doi.org/10.1103/physrevlett.123.031101).
- 8 Abrahamsen, E.P. et al., 2019: Stabilization of dense Antarctic water supply to the Atlantic Ocean overturning
9 circulation. *Nature Climate Change*, **9**(10), 742–746, doi:[10.1038/s41558-019-0561-2](https://doi.org/10.1038/s41558-019-0561-2).
- 10 Abram, N. et al., 2019: Framing and Context of the Report. In: *IPCC Special Report on the Ocean and Cryosphere in a*
11 *Changing Climate* [Pörtner, H.-O., D.C. Roberts, V. Masson-Delmotte, P. Zhai, M. Tignor, E. Poloczanska, K.
12 Mintenbeck, A. Alegría, M. Nicolai, A. Okem, J. Petzold, B. Rama, and N.M. Weyer (eds.)]. In Press, pp. 73–
13 129.
- 14 Aðalgeirsdóttir, G. et al., 2020: Glacier changes in Iceland from ~1890 to 2019. *Frontiers in Earth Science*, **8**, 520,
15 doi:[10.3389/feart.2020.523646](https://doi.org/10.3389/feart.2020.523646).
- 16 Adler, R.F. et al., 2003: The Version-2 Global Precipitation Climatology Project (GPCP) Monthly Precipitation
17 Analysis (1979–Present). *Journal of Hydrometeorology*, **4**(6), 1147–1167, doi:[10.1175/1525-
18 7541\(2003\)004<1147:tvgpcc>2.0.co;2](https://doi.org/10.1175/1525-7541(2003)004<1147:tvgpcc>2.0.co;2).
- 19 Adusumilli, S., H.A. Fricker, B. Medley, L. Padman, and M.R. Siegfried, 2020: Interannual variations in meltwater
20 input to the Southern Ocean from Antarctic ice shelves. *Nature Geoscience*, **13**, 616–620, doi:[10.1038/s41561-
21 020-0616-z](https://doi.org/10.1038/s41561-020-0616-z).
- 22 Aguirre, C., M. Rojas, R.D. Garreaud, and D.A. Rahn, 2019: Role of synoptic activity on projected changes in
23 upwelling-favourable winds at the ocean’s eastern boundaries. *npj Climate and Atmospheric Science*, **2**(1), 44,
24 doi:[10.1038/s41612-019-0101-9](https://doi.org/10.1038/s41612-019-0101-9).
- 25 Aguirre, F. et al., 2018: Snow Cover Change as a Climate Indicator in Brunswick Peninsula, Patagonia. *Frontiers in*
26 *Earth Science*, **6**, doi:[10.3389/feart.2018.00130](https://doi.org/10.3389/feart.2018.00130).
- 27 Aksenov, Y. et al., 2016: Arctic pathways of Pacific Water: Arctic Ocean Model Intercomparison experiments. *Journal*
28 *of Geophysical Research: Oceans*, **121**(1), 27–59, doi:[10.1002/2015jc011299](https://doi.org/10.1002/2015jc011299).
- 29 Alberello, A. et al., 2020: Drift of Pancake Ice Floes in the Winter Antarctic Marginal Ice Zone During Polar Cyclones.
30 *Journal of Geophysical Research: Oceans*, **125**(3), e2019JC015418, doi:[10.1029/2019jc015418](https://doi.org/10.1029/2019jc015418).
- 31 Albrecht, T., R. Winkelmann, and A. Levermann, 2020: Glacial-cycle simulations of the Antarctic Ice Sheet with the
32 Parallel Ice Sheet Model (PISM)-Part 1: Boundary conditions and climatic forcing. *Cryosphere*, **14**(2), 599–
33 632, doi:[10.5194/tc-14-599-2020](https://doi.org/10.5194/tc-14-599-2020).
- 34 Alekseeva, T. et al., 2019: Comparison of Arctic Sea Ice concentrations from the NASA team, ASI, and VASIA2
35 algorithms with summer and winter ship data. *Remote Sensing*, **11**(21), doi:[10.3390/rs11212481](https://doi.org/10.3390/rs11212481).
- 36 Alexander, P.M. et al., 2019a: Simulated Greenland Surface Mass Balance in the GISS ModelE2 GCM: Role of the Ice
37 Sheet Surface. *Journal of Geophysical Research: Earth Surface*, **124**(3), 750–765, doi:[10.1029/2018jf004772](https://doi.org/10.1029/2018jf004772).
- 38 Alexander, P.M. et al., 2019b: Simulated Greenland Surface Mass Balance in the GISS ModelE2 GCM: Role of the Ice
39 Sheet Surface. *Journal of Geophysical Research: Earth Surface*, **124**(3), 750–765, doi:[10.1029/2018jf004772](https://doi.org/10.1029/2018jf004772).
- 40 Allen, S.E. and X. Durrieu de Madron, 2009: A review of the role of submarine canyons in deep-ocean exchange with
41 the shelf. *Ocean Science*, **5**(4), 607–620, doi:[10.5194/os-5-607-2009](https://doi.org/10.5194/os-5-607-2009).
- 42 Alley, K.E., T.A. Scambos, M.R. Siegfried, and H.A. Fricker, 2016: Impacts of warm water on Antarctic ice shelf
43 stability through basal channel formation. *Nature Geoscience*, doi:[10.1038/ngeo2675](https://doi.org/10.1038/ngeo2675).
- 44 Alvarez-Solas, J., R. Banderas, A. Robinson, and M. Montoya, 2019: Ocean-driven millennial-scale variability of the
45 Eurasian ice sheet during the last glacial period simulated with a hybrid ice-sheet-shelf model. *Climate of the*
46 *Past*, **15**(3), 957–979, doi:[10.5194/cp-15-957-2019](https://doi.org/10.5194/cp-15-957-2019).
- 47 An, L., E. Rignot, R. Millan, K. Tinto, and J. Willis, 2019a: Bathymetry of Northwest Greenland Using “Ocean Melting
48 Greenland” (OMG) High-Resolution Airborne Gravity and Other Data. *Remote Sensing*, **11**(2), 131,
49 doi:[10.3390/rs11020131](https://doi.org/10.3390/rs11020131).
- 50 An, L. et al., 2019b: Bathymetry of Southeast Greenland From Oceans Melting Greenland (OMG) Data. *Geophysical*
51 *Research Letters*, **46**(20), 11197–11205, doi:[10.1029/2019gl083953](https://doi.org/10.1029/2019gl083953).
- 52 An, L. et al., 2021: Ocean melting of the Zachariae Isstrøm and Nioghalvfjærdssjøen glaciers, northeast Greenland.
53 *Proceedings of the National Academy of Sciences*, **118**(2), doi:[10.1073/pnas.2015483118](https://doi.org/10.1073/pnas.2015483118).

- 1 Anderson, B. and A. Mackintosh, 2012: Controls on mass balance sensitivity of maritime glaciers in the Southern Alps,
2 New Zealand: The role of debris cover. *Journal of Geophysical Research: Earth Surface*, **117**(F1),
3 doi:[10.1029/2011jf002064](https://doi.org/10.1029/2011jf002064).
- 4 Anderson, J.B., S.S. Shipp, A.L. Lowe, J.S. Wellner, and A.B. Mosola, 2002: The Antarctic Ice Sheet during the Last
5 Glacial Maximum and its subsequent retreat history: A review. *Quaternary Science Reviews*, **21**(1–3), 49–70,
6 doi:[10.1016/s0277-3791\(01\)00083-x](https://doi.org/10.1016/s0277-3791(01)00083-x).
- 7 Andreassen, L.M., H. Elvehøy, B. Kjølmoen, and J.M.C. Belart, 2020: Glacier change in Norway since the 1960s – an
8 overview of mass balance, area, length and surface elevation changes. *Journal of Glaciology*, **66**(256), 313–
9 328, doi:[10.1017/jog.2020.10](https://doi.org/10.1017/jog.2020.10).
- 10 Andresen, C.S. et al., 2017: Exceptional 20th century glaciological regime of a major SE Greenland outlet glacier.
11 *Scientific Reports*, **7**(1), 13626, doi:[10.1038/s41598-017-13246-x](https://doi.org/10.1038/s41598-017-13246-x).
- 12 Anttila, K., T. Manninen, E. Jääskeläinen, A. Riihelä, and P. Lahtinen, 2018: The role of climate and land use in the
13 changes in surface albedo prior to snow melt and the timing of melt season of seasonal snow in northern land
14 areas of 40°N–80°N during 1982–2015. *Remote Sensing*, **10**(10), doi:[10.3390/rs10101619](https://doi.org/10.3390/rs10101619).
- 15 Aoki, S. et al., 2020: Freshening of Antarctic Bottom Water off Cape Darnley, East Antarctica. *Journal of Geophysical
16 Research: Oceans*, **125**, e2020JC016374, doi:[10.1029/2020jc016374](https://doi.org/10.1029/2020jc016374).
- 17 Applegate, P.J. and K. Keller, 2015: How effective is albedo modification (solar radiation management geoengineering)
18 in preventing sea-level rise from the Greenland Ice Sheet? *Environmental Research Letters*, **10**(8), 84018,
19 doi:[10.1088/1748-9326/10/8/084018](https://doi.org/10.1088/1748-9326/10/8/084018).
- 20 Argus, D.F. and W.R. Peltier, 2010: Constraining models of postglacial rebound using space geodesy: a detailed
21 assessment of model ICE-5G (VM2) and its relatives. *Geophysical Journal International*, **181**(2), 697–723.
- 22 Argus, D.F., W.R. Peltier, R. Drummond, and A.W. Moore, 2014: The Antarctica component of postglacial rebound
23 model ICE-6G_C (VM5a) based on GPS positioning, exposure age dating of ice thicknesses, and relative sea
24 level histories. *Geophysical Journal International*, **198**(1), 537–563.
- 25 Armitage, T.W.K., R. Kwok, A.F. Thompson, and G. Cunningham, 2018: Dynamic Topography and Sea Level
26 Anomalies of the Southern Ocean: Variability and Teleconnections. *Journal of Geophysical Research:
27 Oceans*, **123**(1), 613–630, doi:[10.1002/2017jc013534](https://doi.org/10.1002/2017jc013534).
- 28 Armitage, T.W.K. et al., 2017: Arctic Ocean surface geostrophic circulation 2003–2014. *The Cryosphere*, **11**(4), 1767–
29 1780, doi:[10.5194/tc-11-1767-2017](https://doi.org/10.5194/tc-11-1767-2017).
- 30 Armour, K.C., I. Eisenman, E. Blanchard-Wrigglesworth, K.E. McCusker, and C.M. Bitz, 2011: The reversibility of sea
31 ice loss in a state-of-the-art climate model. *Geophysical Research Letters*, **38**(16), doi:[10.1029/2011gl048739](https://doi.org/10.1029/2011gl048739).
- 32 Armour, K.C., J. Marshall, J.R. Scott, A. Donohoe, and E.R. Newsom, 2016: Southern Ocean warming delayed by
33 circumpolar upwelling and equatorward transport. *Nature Geoscience*, **9**, 549, doi:[10.1038/ngeo2731](https://doi.org/10.1038/ngeo2731).
- 34 Arndt, S., M. Hoppmann, H. Schmithüsen, A.D. Fraser, and M. Nicolaus, 2020: Seasonal and interannual variability of
35 landfast sea ice in Atka Bay, Weddell Sea, Antarctica. *The Cryosphere*, **14**(9), 2775–2793, doi:[10.5194/tc-14-
36 2775-2020](https://doi.org/10.5194/tc-14-2775-2020).
- 37 Arns, A., T. Wahl, I.D. Haigh, and J. Jensen, 2015: Determining return water levels at ungauged coastal sites: a case
38 study for northern Germany. *Ocean Dynamics*, doi:[10.1007/s10236-015-0814-1](https://doi.org/10.1007/s10236-015-0814-1).
- 39 Arns, A. et al., 2017: Sea-level rise induced amplification of coastal protection design heights. *Scientific reports*, **7**(1),
40 40171, doi:[10.1038/srep40171](https://doi.org/10.1038/srep40171).
- 41 Arns, A. et al., 2020: Non-linear interaction modulates global extreme sea levels, coastal flood exposure, and impacts.
42 *Nature Communications*, **11**(1), 1–9, doi:[10.1038/s41467-020-15752-5](https://doi.org/10.1038/s41467-020-15752-5).
- 43 Asay-Davis, X.S., N.C. Jourdain, and Y. Nakayama, 2017: Developments in Simulating and Parameterizing
44 Interactions Between the Southern Ocean and the Antarctic Ice Sheet. *Current Climate Change Reports*, **3**(4),
45 316–329, doi:[10.1007/s40641-017-0071-0](https://doi.org/10.1007/s40641-017-0071-0).
- 46 Asay-Davis, X.S. et al., 2016: Experimental design for three interrelated marine ice sheet and ocean model
47 intercomparison projects: MISMIP v. 3 (MISMIP +), ISOMIP v. 2 (ISOMIP +) and MISOMIP v. 1
48 (MISOMIP1). *Geoscientific Model Development*, **9**(7), 2471–2497, doi:[10.5194/gmd-9-2471-2016](https://doi.org/10.5194/gmd-9-2471-2016).
- 49 Aschwanden, A., M.A. Fahnestock, and M. Truffer, 2016: Complex Greenland outlet glacier flow captured. *Nature
50 Communications*, **7**, 10524, doi:[10.1038/ncomms10524](https://doi.org/10.1038/ncomms10524).
- 51 Aschwanden, A. et al., 2019: Contribution of the Greenland Ice Sheet to sea level over the next millennium. *Science
52 Advances*, **5**(6), doi:[10.1126/sciadv.aav9396](https://doi.org/10.1126/sciadv.aav9396).
- 53 Atwood, A.R., E. Wu, D.M.W. Frierson, D.S. Battisti, and J.P. Sachs, 2016: Quantifying Climate Forcings and
54 Feedbacks over the Last Millennium in the CMIP5?PMIP3 Models. *Journal of Climate*, **29**(3), 1161–1178,
55 doi:[10.1175/jcli-d-15-0063.1](https://doi.org/10.1175/jcli-d-15-0063.1).

- 1 Auger, M., R. Morrow, E. Kestenare, J.-B. Sallée, and R. Cowley, 2021: Southern Ocean in-situ temperature trends
2 over 25 years emerge from interannual variability. *Nature Communications*, **12**(514), doi:[10.1038/s41467-020-
3 20781-1](https://doi.org/10.1038/s41467-020-20781-1).
- 4 Auriac, A. et al., 2016: Glacial isostatic adjustment associated with the Barents Sea ice sheet: A modelling inter-
5 comparison. *Quaternary Science Reviews*, **147**, 122–135, doi:[10.1016/j.quascirev.2016.02.011](https://doi.org/10.1016/j.quascirev.2016.02.011).
- 6 Axford, Y. et al., 2019: Holocene temperature history of northwest Greenland – With new ice cap constraints and
7 chironomid assemblages from Deltasø. *Quaternary Science Reviews*, **215**, 160–172,
8 doi:[10.1016/j.quascirev.2019.05.011](https://doi.org/10.1016/j.quascirev.2019.05.011).
- 9 Bachem, P.E., B. Risebrobakken, S. De Schepper, and E.L. McClumont, 2017: Highly variable Pliocene sea surface
10 conditions in the Norwegian Sea. *Climate of the Past*, **13**(9), 1153–1168, doi:[10.5194/cp-13-1153-2017](https://doi.org/10.5194/cp-13-1153-2017).
- 11 Baggenstos, D. et al., 2019: Earth’s radiative imbalance from the Last Glacial Maximum to the present. *Proceedings of
12 the National Academy of Sciences*, **116**(30), 14881–14886, doi:[10.1073/pnas.1905447116](https://doi.org/10.1073/pnas.1905447116).
- 13 Bakker, A.M.R., T.E. Wong, K.L. Ruckert, and K. Keller, 2017: Sea-level projections representing the deeply uncertain
14 contribution of the West Antarctic ice sheet. *Scientific Reports*, **7**(1), 3880, doi:[10.1038/s41598-017-04134-5](https://doi.org/10.1038/s41598-017-04134-5).
- 15 Bakker, P. et al., 2016: Fate of the Atlantic Meridional Overturning Circulation: Strong decline under continued
16 warming and Greenland melting. *Geophysical Research Letters*, **43**(23), 12,252–12,260,
17 doi:[10.1002/2016gl070457](https://doi.org/10.1002/2016gl070457).
- 18 Bakun, A., 1990: Global climate change and intensification of coastal ocean upwelling. *Science*, **247**(4939), 198–201.
- 19 Bakun, A., D.B. Field, A. Redondo-Rodriguez, and S.J. Weeks, 2010: Greenhouse gas, upwelling-favorable winds, and
20 the future of coastal ocean upwelling ecosystems. *Global Change Biology*, **16**(4), 1213–1228,
21 doi:[10.1111/j.1365-2486.2009.02094.x](https://doi.org/10.1111/j.1365-2486.2009.02094.x).
- 22 Bamber, J.L. and W.P. Aspinall, 2013: An expert judgement assessment of future sea level rise from the ice sheets.
23 *Nature Climate Change*, **3**, 424–427, doi:[10.1038/nclimate1778](https://doi.org/10.1038/nclimate1778).
- 24 Bamber, J.L. and G.J. Dawson, 2020: Complex evolving patterns of mass loss from Antarctica’s largest glacier. *Nature
25 Geoscience*, **13**(2), 127–131, doi:[10.1038/s41561-019-0527-z](https://doi.org/10.1038/s41561-019-0527-z).
- 26 Bamber, J.L., R.E.M. Riva, B.L.A. Vermeersen, and A.M. Le Brocq, 2009: Reassessment of the Potential Sea-Level
27 Rise from a Collapse of the West Antarctic Ice Sheet. *Science*, **324**, 901–903.
- 28 Bamber, J.L., R.M. Westaway, B. Marzeion, and B. Wouters, 2018a: A new synthesis of annual land ice mass trends
29 1992 to 2016. , doi:[10.1594/pangaea.890030](https://doi.org/10.1594/pangaea.890030).
- 30 Bamber, J.L., R.M. Westaway, B. Marzeion, and B. Wouters, 2018b: The land ice contribution to sea level during the
31 satellite era. *Environmental Research Letters*, **13**, 063008, doi:[10.1088/1748-9326/aac2f0](https://doi.org/10.1088/1748-9326/aac2f0).
- 32 Bamber, J.L., M. Oppenheimer, R.E. Kopp, W.P. Aspinall, and R.M. Cooke, 2019: Ice sheet contributions to future sea-
33 level rise from structured expert judgment. *Proceedings of the National Academy of Sciences*, **116**(23), 11195–
34 11200, doi:[10.1073/pnas.1817205116](https://doi.org/10.1073/pnas.1817205116).
- 35 Banas, N.S.S., P. MacCready, and B.M.M. Hickey, 2009: The Columbia River plume as cross-shelf exporter and along-
36 coast barrier. *Continental Shelf Research*, **29**(1), 292–301, doi:[10.1016/j.csr.2008.03.011](https://doi.org/10.1016/j.csr.2008.03.011).
- 37 Baranes, H.E. et al., 2020: Tidally driven interannual variation in extreme sea level frequencies in the Gulf of Maine.
38 *Journal of Geophysical Research: Oceans*, doi:[10.1029/2020jc016291](https://doi.org/10.1029/2020jc016291).
- 39 Barletta, V.R. et al., 2018: Observed rapid bedrock uplift in Amundsen Sea Embayment promotes ice-sheet stability.
40 *Science*, **360**(6395), 1335–1339.
- 41 Bart, P.J., M. DeCesare, B.E. Rosenheim, W. Majewski, and A. McGlannan, 2018: A centuries-long delay between a
42 paleo-ice-shelf collapse and grounding-line retreat in the Whales Deep Basin, eastern Ross Sea, Antarctica.
43 *Scientific Reports*, doi:[10.1038/s41598-018-29911-8](https://doi.org/10.1038/s41598-018-29911-8).
- 44 Barthel, A. et al., 2020a: CMIP5 model selection for ISMIP6 ice sheet model forcing: Greenland and Antarctica. *The
45 Cryosphere*, **14**, 855–879, doi:[10.5194/tc-14-855-2020](https://doi.org/10.5194/tc-14-855-2020).
- 46 Barthel, A. et al., 2020b: CMIP5 model selection for ISMIP6 ice sheet model forcing: Greenland and Antarctica. *The
47 Cryosphere*, **14**, 855–879, doi:[10.5194/tc-14-855-2020](https://doi.org/10.5194/tc-14-855-2020).
- 48 Bassis, J.N. and L. Ultee, 2019: A Thin Film Viscoplastic Theory for Calving Glaciers: Toward a Bound on the Calving
49 Rate of Glaciers. *Journal of Geophysical Research: Earth Surface*, **124**(8), 2036–2055,
50 doi:[10.1029/2019jef0005160](https://doi.org/10.1029/2019jef0005160).
- 51 Batbaatar, J., A. Gillespie, D. Fink, A. Matmon, and T. Fujioka, 2018: Asynchronous glaciations in arid continental
52 climate. *Quaternary Science Reviews*, **182**, 1–19, doi:[10.1016/j.quascirev.2017.12.001](https://doi.org/10.1016/j.quascirev.2017.12.001).
- 53 Batchelor, C.J. et al., 2019: Distinct Permafrost Conditions Across the Last Two Glacial Periods in Midlatitude North
54 America. *Geophysical Research Letters*, **46**, 13318–13326, doi:[10.1029/2019gl083951](https://doi.org/10.1029/2019gl083951).
- 55 Bates, S.C. et al., 2012: Mean biases, variability, and trends in air-sea fluxes and sea surface temperature in the
56 CCSM4. *Journal of Climate*, **25**(22), doi:[10.1175/jcli-d-11-00442.1](https://doi.org/10.1175/jcli-d-11-00442.1).

- 1 Bathiany, S., J. Hidding, and M. Scheffer, 2020: Edge Detection Reveals Abrupt and Extreme Climate Events. *Journal*
2 *of Climate*, **33**(15), 6399–6421, doi:[10.1175/jcli-d-19-0449.1](https://doi.org/10.1175/jcli-d-19-0449.1).
- 3 Bathiany, S., D. Notz, T. Mauritsen, G. Ruedel, and V. Brovkin, 2016: On the potential for abrupt Arctic winter sea-ice
4 loss. *Journal of Climate*, doi:[10.1175/jcli-d-15-0466.1](https://doi.org/10.1175/jcli-d-15-0466.1).
- 5 Baum, S.K. and T.J. Crowley, 2003: The snow/ice instability as a mechanism for rapid climate change: A
6 Neoproterozoic Snowball Earth model example. *Geophysical Research Letters*, **30**(20), 2030,
7 doi:[10.1029/2003gl017333](https://doi.org/10.1029/2003gl017333).
- 8 Bauska, T.K. et al., 2016: Carbon isotopes characterize rapid changes in atmospheric carbon dioxide during the last
9 deglaciation. *Proceedings of the National Academy of Sciences of the United States of America*, **113**(13),
10 3465–3470, doi:[10.1073/pnas.1513868113](https://doi.org/10.1073/pnas.1513868113).
- 11 Beadling, R.L., J.L. Russell, R.J. Stouffer, P.J. Goodman, and M. Mazloff, 2019: Assessing the quality of Southern
12 Ocean circulation in CMIP5 AOGCM and Earth System Model simulations. *Journal of Climate*, **32**, 5915–
13 5940, doi:[10.1175/jcli-d-19-0263.1](https://doi.org/10.1175/jcli-d-19-0263.1).
- 14 Beadling, R.L. et al., 2020: Representation of Southern Ocean properties across Coupled Model Intercomparison
15 Project generations: CMIP3 to CMIP6. *Journal of Climate*, **33**, 6555–6581, doi:[10.1175/jcli-d-19-0970.1](https://doi.org/10.1175/jcli-d-19-0970.1).
- 16 Beal, L.M. and S. Elipot, 2016: Broadening not strengthening of the Agulhas Current since the early 1990s. *Nature*,
17 **540**(7634), 570–573, doi:[10.1038/nature19853](https://doi.org/10.1038/nature19853).
- 18 Beckmann, J. et al., 2019: Modeling the response of Greenland outlet glaciers to global warming using a coupled
19 flowline-plume model. *The Cryosphere*, **13**, 2281–2301, doi:[10.5194/tc-2018-89](https://doi.org/10.5194/tc-2018-89).
- 20 Beedle, M.J., B. Menounos, B.H. Luckman, and R. Wheate, 2009: Annual push moraines as climate proxy.
21 *Geophysical Research Letters*, **36**(20), L20501, doi:[10.1029/2009gl039533](https://doi.org/10.1029/2009gl039533).
- 22 Belcher, S.E. et al., 2012: A global perspective on Langmuir turbulence in the ocean surface boundary layer.
23 *Geophysical Research Letters*, **39**(18), doi:[10.1029/2012gl052932](https://doi.org/10.1029/2012gl052932).
- 24 Bell, R.E., A.F. Banwell, L.D. Trusel, and J. Kingslake, 2018: Antarctic surface hydrology and impacts on ice-sheet
25 mass balance. *Nature Climate Change*, **8**(12), 1044–1052, doi:[10.1038/s41558-018-0326-3](https://doi.org/10.1038/s41558-018-0326-3).
- 26 Bellomo, K., L.N. Murphy, M.A. Cane, A.C. Clement, and L.M. Polvani, 2018: Historical forcings as main drivers of
27 the Atlantic multidecadal variability in the CESM large ensemble. *Climate Dynamics*, **50**(9–10), 3687–3698,
28 doi:[10.1007/s00382-017-3834-3](https://doi.org/10.1007/s00382-017-3834-3).
- 29 Belmadani, A., V. Echevin, F. Codron, K. Takahashi, and C. Junquas, 2014: What dynamics drive future wind
30 scenarios for coastal upwelling off Peru and Chile? *Climate dynamics*, **43**(7–8), 1893–1914.
- 31 Belmecheri, S., F. Babst, E.R. Wahl, D.W. Stahle, and V. Trouet, 2016: Multi-century evaluation of Sierra Nevada
32 snowpack. *Nature Climate Change*, **6**, 2–3, doi:[10.1038/nclimate2809](https://doi.org/10.1038/nclimate2809).
- 33 Belt, S.T., 2018: Source-specific biomarkers as proxies for Arctic and Antarctic sea ice. *Organic Geochemistry*, **125**,
34 277–298, doi:[10.1016/j.orggeochem.2018.10.002](https://doi.org/10.1016/j.orggeochem.2018.10.002).
- 35 Belt, S.T., 2019: What do IP25 and related biomarkers really reveal about sea ice change? *Quaternary Science Reviews*,
36 **204**, 216–219, doi:[10.1016/j.quascirev.2018.11.025](https://doi.org/10.1016/j.quascirev.2018.11.025).
- 37 Belt, S.T. et al., 2007: A novel chemical fossil of palaeo sea ice: IP25. *Organic Geochemistry*, **38**(1), 16–27,
38 doi:[10.1016/j.orggeochem.2006.09.013](https://doi.org/10.1016/j.orggeochem.2006.09.013).
- 39 Belt, S.T. et al., 2015: Identification of paleo Arctic winter sea ice limits and the marginal ice zone: Optimised
40 biomarker-based reconstructions of late Quaternary Arctic sea ice. *Earth and Planetary Science Letters*, **431**,
41 127–139, doi:[10.1016/j.epsl.2015.09.020](https://doi.org/10.1016/j.epsl.2015.09.020).
- 42 Bendtsen, J. et al., 2017: Sea ice breakup and marine melt of a retreating tidewater outlet glacier in northeast Greenland
43 (81°N). *Scientific Reports*, **7**(1), 1–11, doi:[10.1038/s41598-017-05089-3](https://doi.org/10.1038/s41598-017-05089-3).
- 44 Benn, D.I., T. Cowton, J. Todd, and A. Luckman, 2017: Glacier Calving in Greenland. *Current Climate Change*
45 *Reports*, **3**(4), 282–290, doi:[10.1007/s40641-017-0070-1](https://doi.org/10.1007/s40641-017-0070-1).
- 46 Bennartz, R. et al., 2013: July 2012 Greenland melt extent enhanced by low-level liquid clouds. *Nature*, **496**, 83–86,
47 doi:[10.1038/nature12002](https://doi.org/10.1038/nature12002).
- 48 Bennetts, L.G., S. O'Farrell, and P. Uotila, 2017: Brief communication: Impacts of ocean-wave-induced breakup of
49 Antarctic sea ice via thermodynamics in a stand-alone version of the CICE sea-ice model. *The Cryosphere*,
50 **11**(3), 1035–1040, doi:[10.5194/tc-11-1035-2017](https://doi.org/10.5194/tc-11-1035-2017).
- 51 Bentamy, A. et al., 2017: Review and assessment of latent and sensible heat flux accuracy over the global oceans.
52 *Remote Sensing of Environment*, **201**, 196–218, doi:[10.1016/j.rse.2017.08.016](https://doi.org/10.1016/j.rse.2017.08.016).
- 53 Bentley, M.J. et al., 2014: A community-based geological reconstruction of Antarctic Ice Sheet deglaciation since the
54 Last Glacial Maximum. *Quaternary Science Reviews*, **100**, 1–9, doi:[10.1016/j.quascirev.2014.06.025](https://doi.org/10.1016/j.quascirev.2014.06.025).

- 1 Benz, V., O. Esper, R. Gersonde, F. Lamy, and R. Tiedemann, 2016: Last Glacial Maximum sea surface temperature
2 and sea-ice extent in the Pacific sector of the Southern Ocean. *Quaternary Science Reviews*, **146**, 216–237,
3 doi:[10.1016/j.quascirev.2016.06.006](https://doi.org/10.1016/j.quascirev.2016.06.006).
- 4 Berben, S.M.P., K. Husum, A. Navarro-Rodriguez, S.T. Belt, and S. Aagaard-Sørensen, 2017: Semi-quantitative
5 reconstruction of early to late Holocene spring and summer sea ice conditions in the northern Barents Sea.
6 *Journal of Quaternary Science*, **32(5)**, 587–603, doi:[10.1002/jqs.2953](https://doi.org/10.1002/jqs.2953).
- 7 Bereiter, B., S. Shackleton, D. Baggenstos, K. Kawamura, and J. Severinghaus, 2018: Mean global ocean temperatures
8 during the last glacial transition. *Nature*, **553(7686)**, 39–44, doi:[10.1038/nature25152](https://doi.org/10.1038/nature25152).
- 9 Berends, C.J., B. de Boer, A.M. Dolan, D.J. Hill, and R.S.W. van de Wal, 2019: Modelling ice sheet evolution and
10 atmospheric CO₂ during the Late Pliocene. *Climate of the Past*, **15**, 1603–1619, doi:[10.5194/cp-2019-34](https://doi.org/10.5194/cp-2019-34).
- 11 Berloff, P. et al., 2007: The Turbulent Oscillator: A Mechanism of Low-Frequency Variability of the Wind-Driven
12 Ocean Gyres. *Journal of Physical Oceanography*, **37(9)**, 2363–2386, doi:[10.1175/jpo3118.1](https://doi.org/10.1175/jpo3118.1).
- 13 Bertram, R.A. et al., 2018: Pliocene deglacial event timelines and the biogeochemical response offshore Wilkes
14 Subglacial Basin, East Antarctica. *Earth and Planetary Science Letters*, **494**, 109–116,
15 doi:[10.1016/j.epsl.2018.04.054](https://doi.org/10.1016/j.epsl.2018.04.054).
- 16 Bettencourt, J.H. et al., 2015: Boundaries of the Peruvian oxygen minimum zone shaped by coherent mesoscale
17 dynamics. *Nature Geoscience*, **8(12)**, 937.
- 18 Bevacqua, E. et al., 2020: More meteorological events that drive compound coastal flooding are projected under climate
19 change. *Communications Earth & Environment*, **1(1)**, 1–11, doi:[10.1038/s43247-020-00044-z](https://doi.org/10.1038/s43247-020-00044-z).
- 20 Bevan, S.L., A.J. Luckman, D.I. Benn, T. Cowton, and J. Todd, 2019: Impact of warming shelf waters on ice mélange
21 and terminus retreat at a large SE Greenland glacier. *Cryosphere*, **13(9)**, 2303–2315, doi:[10.5194/tc-13-2303-](https://doi.org/10.5194/tc-13-2303-2019)
22 [2019](https://doi.org/10.5194/tc-13-2303-2019).
- 23 Bevis, M. et al., 2019: Accelerating changes in ice mass within Greenland, and the ice sheet's sensitivity to atmospheric
24 forcing. *Proceedings of the National Academy of Sciences of the United States of America*, **116(6)**, 1934–1939,
25 doi:[10.1073/pnas.1806562116](https://doi.org/10.1073/pnas.1806562116).
- 26 Bianchi, C. and R. Gersonde, 2002: The Southern Ocean surface between Marine Isotope Stages 6 and 5d: Shape and
27 timing of climate changes. *Palaeogeography, Palaeoclimatology, Palaeoecology*, **187(1–2)**, 151–177,
28 doi:[10.1016/s0031-0182\(02\)00516-3](https://doi.org/10.1016/s0031-0182(02)00516-3).
- 29 Biastoch, A. et al., 2015: Atlantic multi-decadal oscillation covaries with Agulhas leakage. *Nature Communications*,
30 **6(1)**, 10082, doi:[10.1038/ncomms10082](https://doi.org/10.1038/ncomms10082).
- 31 Bilbao, R.A.F., J.M. Gregory, and N. Bouttes, 2015: Analysis of the regional pattern of sea level change due to ocean
32 dynamics and density change for 1993–2099 in observations and CMIP5 AOGCM's. *Climate Dynamics*,
33 doi:[10.1007/s00382-015-2499-z](https://doi.org/10.1007/s00382-015-2499-z).
- 34 Bilbao, R.A.F., J.M. Gregory, N. Bouttes, M.D. Palmer, and P. Stott, 2019: Attribution of ocean temperature change to
35 anthropogenic and natural forcings using the temporal, vertical and geographical structure. *Climate Dynamics*,
36 **53(9)**, 5389–5413, doi:[10.1007/s00382-019-04910-1](https://doi.org/10.1007/s00382-019-04910-1).
- 37 Bindoff, N.L. and T.J. McDougall, 2000: Decadal Changes along an Indian Ocean Section at 32°S and Their
38 Interpretation. *Journal of Physical Oceanography*, **30(6)**, 1207–1222, doi:[10.1175/1520-](https://doi.org/10.1175/1520-0485(2000)030<1207:dcaio>2.0.co;2)
39 [0485\(2000\)030<1207:dcaio>2.0.co;2](https://doi.org/10.1175/1520-0485(2000)030<1207:dcaio>2.0.co;2).
- 40 Bindoff, N.L. et al., 2013: Detection and Attribution of Climate Change: from Global to Regional. In: *Climate Change*
41 *2013: The Physical Science Basis. Contribution of Working Group I to the Fifth Assessment Report of the*
42 *IPCC* [Stocker, T.F., D. Qin, G.-K. Plattner, M. Tignor, S.K. Allen, J. Boschung, A. Nauels, Y. Xia, V. Bex,
43 and P.M. Midgley (eds.)]. Cambridge University Press, pp. 867–952, doi:[10.1017/cbo9781107415324.022](https://doi.org/10.1017/cbo9781107415324.022).
- 44 Bindoff, N.L. et al., 2019: Changing Ocean, Marine Ecosystems, and Dependent Communities. In: *IPCC Special*
45 *Report on the Ocean and Cryosphere in a Changing Climate* [Pörtner, H.-O., D.C. Roberts, V. Masson-
46 Delmotte, P. Zhai, M. Tignor, E. Poloczanska, K. Mintenbeck, M. Nicolai, A. Okem, J. Petzold, B. Rama, and
47 N. Weyer (eds.)]. In Press, pp. 447–588.
- 48 Bindschadler, R.A. et al., 2013: Ice-sheet model sensitivities to environmental forcing and their use in projecting future
49 sea level (the SeaRISE project). *Journal of Glaciology*, **59(214)**, 195–224, doi:[10.3189/2013jog12j125](https://doi.org/10.3189/2013jog12j125).
- 50 Bishop, S.P. et al., 2017: Scale Dependence of Midlatitude Air–Sea Interaction. *Journal of Climate*, **30(20)**, 8207–8221,
51 doi:[10.1175/jcli-d-17-0159.1](https://doi.org/10.1175/jcli-d-17-0159.1).
- 52 Biskaborn, B.K. et al., 2019: Permafrost is warming at a global scale. *Nature Communications*, **10(1)**, 264,
53 doi:[10.1038/s41467-018-08240-4](https://doi.org/10.1038/s41467-018-08240-4).
- 54 Bittermann, K., S. Rahmstorf, R.E. Kopp, and A.C. Kemp, 2017: Global mean sea-level rise in a world agreed upon in
55 Paris. *Environmental Research Letters*, **12(12)**, doi:[10.1088/1748-9326/aa9def](https://doi.org/10.1088/1748-9326/aa9def).

- 1 Blackburn, T. et al., 2020: Ice retreat in Wilkes Basin of East Antarctica during a warm interglacial. *Nature*, **583(7817)**,
2 554–559, doi:[10.1038/s41586-020-2484-5](https://doi.org/10.1038/s41586-020-2484-5).
- 3 Blake-Mizen, K. et al., 2019: Southern Greenland glaciation and Western Boundary Undercurrent evolution recorded
4 on Eirik Drift during the late Pliocene intensification of Northern Hemisphere glaciation. *Quaternary Science*
5 *Reviews*, **209**, 40–51, doi:[10.1016/j.quascirev.2019.01.015](https://doi.org/10.1016/j.quascirev.2019.01.015).
- 6 Bliss, A.C., J.A. Miller, and W.N. Meier, 2017: Comparison of passive microwave-derived early melt onset records on
7 Arctic sea ice. *Remote Sensing*, doi:[10.3390/rs9030199](https://doi.org/10.3390/rs9030199).
- 8 Bliss, A.C., M. Steele, G. Peng, W.N. Meier, and S. Dickinson, 2019: Regional variability of Arctic sea ice seasonal
9 change climate indicators from a passive microwave climate data record. *Environmental Research Letters*,
10 **14(4)**, doi:[10.1088/1748-9326/aafb84](https://doi.org/10.1088/1748-9326/aafb84).
- 11 Bock, L. et al., 2020: Quantifying progress across different CMIP phases with the ESMValTool. *J. Geophys. Res.*,
12 **submitted**.
- 13 Bohleber, P., M. Schwikowski, M. Stocker-Waldhuber, L. Fang, and A. Fischer, 2020: New glacier evidence for ice-
14 free summits during the life of the Tyrolean Iceman. *Scientific Reports*, **10(1)**, 20513, doi:[10.1038/s41598-
15 020-77518-9](https://doi.org/10.1038/s41598-020-77518-9).
- 16 Bond, N.A., M.F. Cronin, H. Freeland, and N. Mantua, 2015: Causes and impacts of the 2014 warm anomaly in the NE
17 Pacific. *Geophysical Research Letters*, **42**, 3414–3420, doi:[10.1002/2015gl063306](https://doi.org/10.1002/2015gl063306).
- 18 Bondzio, J.H. et al., 2016: Modelling calving front dynamics using a level-set method: application to Jakobshavn Isbræ,
19 West Greenland. *The Cryosphere*, **10(2)**, 497–510, doi:[10.5194/tc-10-497-2016](https://doi.org/10.5194/tc-10-497-2016).
- 20 Bondzio, J.H. et al., 2017: The mechanisms behind Jakobshavn Isbræ's acceleration and mass loss: A 3-D
21 thermomechanical model study. *Geophysical Research Letters*, **44(12)**, 6252–6260,
22 doi:[10.1002/2017gl073309](https://doi.org/10.1002/2017gl073309).
- 23 Bonekamp, P.N.J., R.J. de Kok, E. Collier, and W.W. Immerzeel, 2019: Contrasting Meteorological Drivers of the
24 Glacier Mass Balance Between the Karakoram and Central Himalaya. *Frontiers in Earth Science*, **7**, 107,
25 doi:[10.3389/feart.2019.00107](https://doi.org/10.3389/feart.2019.00107).
- 26 Boone, A. et al., 2017: The interactions between soil-biosphere-atmosphere land surface model with a multi-energy
27 balance (ISBA-MEB) option in SURFEXv8-Part 1: Model description. *Geoscientific Model Development*,
28 doi:[10.5194/gmd-10-843-2017](https://doi.org/10.5194/gmd-10-843-2017).
- 29 Borge, A.F., S. Westermann, I. Solheim, and B. Etzelmüller, 2017: Strong degradation of palsas and peat plateaus in
30 northern Norway during the last 60 years. *Cryosphere*, **11(1)**, 1–16, doi:[10.5194/tc-11-1-2017](https://doi.org/10.5194/tc-11-1-2017).
- 31 Born, A. and K.H. Nisancioglu, 2012: Melting of Northern Greenland during the last interglaciation. *The Cryosphere*,
32 **6**, 1239–1250, doi:[10.5194/tc-6-1239-2012](https://doi.org/10.5194/tc-6-1239-2012).
- 33 Born, A., T.F. Stocker, and A.B. Sandø, 2016: Transport of salt and freshwater in the Atlantic Subpolar Gyre. *Ocean*
34 *Dynamics*, **66(9)**, 1051–1064, doi:[10.1007/s10236-016-0970-y](https://doi.org/10.1007/s10236-016-0970-y).
- 35 Born, A., T.F. Stocker, C.C. Raible, and A. Levermann, 2013: Is the Atlantic subpolar gyre bistable in comprehensive
36 coupled climate models? *Climate Dynamics*, **40(11–12)**, 2993–3007, doi:[10.1007/s00382-012-1525-7](https://doi.org/10.1007/s00382-012-1525-7).
- 37 Boucher, O. et al., 2020: Presentation and Evaluation of the IPSL-CM6A-LR Climate Model. *Journal of Advances in*
38 *Modeling Earth Systems*, **12(7)**, e2019MS002010, doi:[10.1029/2019ms002010](https://doi.org/10.1029/2019ms002010).
- 39 Bouttes, N. and J.M. Gregory, 2014: Attribution of the spatial pattern of CO₂-forced sea level change to ocean surface
40 flux changes. *Environmental Research Letters*, **9(3)**, 034004, doi:[10.1088/1748-9326/9/3/034004](https://doi.org/10.1088/1748-9326/9/3/034004).
- 41 Bouttes, N., J.M. Gregory, and J.A. Lowe, 2013: The reversibility of sea level rise. *Journal of Climate*, **26(8)**, 2502–
42 2513, doi:[10.1175/jcli-d-12-00285.1](https://doi.org/10.1175/jcli-d-12-00285.1).
- 43 Bouttes, N., J.M. Gregory, T. Kuhlbrodt, and R.S. Smith, 2014: The drivers of projected North Atlantic sea level
44 change. *Climate Dynamics*, **43(5–6)**, 1531–1544.
- 45 Box, J.E. and W. Colgan, 2013: Greenland Ice Sheet Mass Balance Reconstruction. Part III: Marine Ice Loss and Total
46 Mass Balance (1840–2010). *Journal of Climate*, **26(18)**, 6990–7002, doi:[10.1175/jcli-d-12-00546.1](https://doi.org/10.1175/jcli-d-12-00546.1).
- 47 Bracegirdle, T. et al., 2020: Twenty-first century changes in Antarctic and Southern Ocean surface climate in CMIP6.
48 *Atmospheric Science Letters*, **21(9)**, asl984, doi:[10.1002/asl.984](https://doi.org/10.1002/asl.984).
- 49 Bradley, S.L., T.J. Reerink, R.S.W. Van De Wal, and M.M. Helsen, 2018: Simulation of the Greenland Ice Sheet over
50 two glacial-interglacial cycles: investigating a sub-ice-shelf melt parameterization and relative sea level
51 forcing in an ice-sheet-ice-shelf model. *Climate of the Past*, **14(5)**, 619–635, doi:[10.5194/cp-14-619-2018](https://doi.org/10.5194/cp-14-619-2018).
- 52 Brady, R.X., M.A. Alexander, N.S. Lovenduski, and R.R. Rykaczewski, 2017: Emergent anthropogenic trends in
53 California Current upwelling. *Geophysical Research Letters*, **44(10)**, 5044–5052, doi:[10.1002/2017gl072945](https://doi.org/10.1002/2017gl072945).
- 54 Brancato, V. et al., 2020: Grounding Line Retreat of Denman Glacier, East Antarctica, Measured With COSMO-
55 SkyMed Radar Interferometry Data. *Geophysical Research Letters*, **47(7)**, e2019GL086291,
56 doi:[10.1029/2019gl086291](https://doi.org/10.1029/2019gl086291).

- 1 Brandon, C.M., J.D. Woodruff, D. Lane, and J.P. Donnelly, 2013: Tropical cyclone wind speed constraints from
2 resultant storm surge deposition: A 2500 year reconstruction of hurricane activity from St. Marks, FL.
3 *Geochemistry, Geophysics, Geosystems*, **14**(8), 2993–3008, doi:[10.1002/ggge.20217](https://doi.org/10.1002/ggge.20217).
- 4 Brandon, C.M., J.D. Woodruff, J.P. Donnelly, and R.M. Sullivan, 2015: How Unique was Hurricane Sandy?
5 Sedimentary Reconstructions of Extreme Flooding from New York Harbor. *Scientific Reports*, **4**(1), 7366,
6 doi:[10.1038/srep07366](https://doi.org/10.1038/srep07366).
- 7 Braun, M.H. et al., 2019: Constraining glacier elevation and mass changes in South America. *Nature Climate Change*,
8 **9**(2), 130–136, doi:[10.1038/s41558-018-0375-7](https://doi.org/10.1038/s41558-018-0375-7).
- 9 Brendryen, J., H. Hafliðason, Y. Yokoyama, K.A. Haaga, and B. Hannisdal, 2020: Eurasian Ice Sheet collapse was a
10 major source of Meltwater Pulse 1A 14,600 years ago. *Nature Geoscience*, **13**(5), 363–368,
11 doi:[10.1038/s41561-020-0567-4](https://doi.org/10.1038/s41561-020-0567-4).
- 12 Brennan, M.K., G.J. Hakim, and E. Blanchard-Wrigglesworth, 2020: Arctic Sea-Ice Variability During the Instrumental
13 Era. *Geophysical Research Letters*, **47**(7), e2019GL086843, doi:[10.1029/2019gl086843](https://doi.org/10.1029/2019gl086843).
- 14 Briggs, R.D., D. Pollard, and L. Tarasov, 2014: A data-constrained large ensemble analysis of Antarctic evolution since
15 the Eemian. *Quaternary Science Reviews*, **103**, 91–115, doi:[10.1016/j.quascirev.2014.09.003](https://doi.org/10.1016/j.quascirev.2014.09.003).
- 16 Briner, J.P. et al., 2016: Holocene climate change in Arctic Canada and Greenland. *Quaternary Science Reviews*, **147**,
17 340–364, doi:[10.1016/j.quascirev.2016.02.010](https://doi.org/10.1016/j.quascirev.2016.02.010).
- 18 Brink, K.H., 2016: Cross-shelf exchange. *Annual review of marine science*, **8**, 59–78, doi:[10.1146/annurev-marine-010814-015717](https://doi.org/10.1146/annurev-marine-010814-015717).
- 19 Brodeau, L., B. Barnier, S.K. Gulev, and C. Woods, 2017: Climatologically Significant Effects of Some
20 Approximations in the Bulk Parameterizations of Turbulent Air–Sea Fluxes. *Journal of Physical*
21 *Oceanography*, **47**(1), 5–28, doi:[10.1175/jpo-d-16-0169.1](https://doi.org/10.1175/jpo-d-16-0169.1).
- 22 Brönnimann, S. et al., 2019: Last phase of the Little Ice Age forced by volcanic eruptions. *Nature Geoscience*, **12**(8),
23 650–656, doi:[10.1038/s41561-019-0402-y](https://doi.org/10.1038/s41561-019-0402-y).
- 24 Bronselaer, B. and L. Zanna, 2020: Heat and carbon coupling reveals ocean warming due to circulation changes.
25 *Nature*, **584**, 227–233, doi:[10.1038/s41586-020-2573-5](https://doi.org/10.1038/s41586-020-2573-5).
- 26 Bronselaer, B. et al., 2018: Change in future climate due to Antarctic meltwater. *Nature*, **564**(7734), 53–58,
27 doi:[10.1038/s41586-018-0712-z](https://doi.org/10.1038/s41586-018-0712-z).
- 28 Bronselaer, B. et al., 2020: Importance of wind and meltwater for observed chemical and physical changes in the
29 Southern Ocean. *Nature Geoscience*, **13**, 35–42.
- 30 Brown, R. et al., 2017: Arctic terrestrial snow cover. *Snow, Water, Ice and Permafrost in the Arctic (SWIPA) 2017*, 25–
31 64.
- 32 Brown, R.D. and D.A. Robinson, 2011: Northern Hemisphere spring snow cover variability and change over 1922–2010
33 including an assessment of uncertainty. *The Cryosphere*, **5**(1), 219–229, doi:[10.5194/tc-5-219-2011](https://doi.org/10.5194/tc-5-219-2011).
- 34 Brown, R.D. and C. Derksen, 2013: Is Eurasian October snow cover extent increasing? *Environmental Research*
35 *Letters*, **8**(2), 024006, doi:[10.1088/1748-9326/8/2/024006](https://doi.org/10.1088/1748-9326/8/2/024006).
- 36 Brun, F. et al., 2016: Quantifying volume loss from ice cliffs on debris-covered glaciers using high-resolution terrestrial
37 and aerial photogrammetry. *Journal of Glaciology*, **62**(234), 684–695, doi:[10.1017/jog.2016.54](https://doi.org/10.1017/jog.2016.54).
- 38 Bryden, H.L. et al., 2020: Reduction in ocean heat transport at 26°N since 2008 cools the eastern subpolar gyre of the
39 North Atlantic Ocean. *Journal of Climate*, **33**(5), 1677–1689, doi:[10.1175/jcli-d-19-0323.1](https://doi.org/10.1175/jcli-d-19-0323.1).
- 40 Buchanan, M.K., R.E. Kopp, M. Oppenheimer, and C. Tebaldi, 2016: Allowances for evolving coastal flood risk under
41 uncertain local sea-level rise. *Climatic Change*, **137**(3–4), doi:[10.1007/s10584-016-1664-7](https://doi.org/10.1007/s10584-016-1664-7).
- 42 Buckingham, C.E. et al., 2019: The contribution of surface and submesoscale processes to turbulence in the open ocean
43 surface boundary layer. *Journal of Advances in Modeling Earth Systems*, **n/a**(n/a),
44 doi:[10.1029/2019ms001801](https://doi.org/10.1029/2019ms001801).
- 45 Buckley, M.W. and J. Marshall, 2016: Observations, inferences, and mechanisms of the Atlantic Meridional
46 Overturning Circulation: A review. *Reviews of Geophysics*, **54**(1), 5–63, doi:[10.1002/2015rg000493](https://doi.org/10.1002/2015rg000493).
- 47 Bulthuis, K., M. Arnst, S. Sun, and F. Pattyn, 2019: Uncertainty quantification of the multi-centennial response of the
48 antarctic ice sheet to climate change. *Cryosphere*, **13**, 1349–1380, doi:[10.5194/tc-13-1349-2019](https://doi.org/10.5194/tc-13-1349-2019).
- 49 Bulygina, O.N., P.Y. Groisman, V.N. Razuvaev, and N.N. Korshunova, 2011: Changes in snow cover characteristics
50 over Northern Eurasia since 1966. *Environmental Research Letters*, **6**(4), 0452204, doi:[10.1088/1748-9326/6/4/045204](https://doi.org/10.1088/1748-9326/6/4/045204).
- 51 Bunce, C., J.R. Carr, P.W. Nienow, N. Ross, and R. Killick, 2018: Ice front change of marine-terminating outlet
52 glaciers in northwest and southeast Greenland during the 21st century. *Journal of Glaciology*, **64**(246), 523–
53 535, doi:[10.1017/jog.2018.44](https://doi.org/10.1017/jog.2018.44).

- 1 Bunce, C., P. Nienow, A. Sole, T. Cowton, and B. Davison, 2020: Influence of glacier runoff and near-terminus
2 subglacial hydrology on frontal ablation at a large Greenlandic tidewater glacier. *Journal of Glaciology*, 1–10,
3 doi: [10.1017/jog.2020.109](https://doi.org/10.1017/jog.2020.109).
- 4 Bunzel, F., D. Notz, and L.T. Pedersen, 2018: Retrievals of Arctic Sea-Ice Volume and Its Trend Significantly Affected
5 by Interannual Snow Variability. *Geophysical Research Letters*, **45(21)**, 11,751–11,759,
6 doi: [10.1029/2018gl078867](https://doi.org/10.1029/2018gl078867).
- 7 Burgard, C. and D. Notz, 2017: Drivers of Arctic Ocean warming in CMIP5 models. *Geophysical Research Letters*,
8 **44(9)**, 4263–4271, doi: [10.1002/2016gl072342](https://doi.org/10.1002/2016gl072342).
- 9 Burgess, D.O. and M.J. Sharp, 2004: Recent Changes in Areal Extent of the Devon Ice Cap, Nunavut, Canada. *Arctic,*
10 *Antarctic, and Alpine Research*, **36(2)**, 261–271, doi: [10.1657/1523-0430\(2004\)036\[0261:rciaeo\]2.0.co;2](https://doi.org/10.1657/1523-0430(2004)036[0261:rciaeo]2.0.co;2).
- 11 Burke, E., Y. Zhang, and G. Krinner, 2020: Evaluating permafrost physics in the Coupled Model Intercomparison
12 Project 6 (CMIP6) models and their sensitivity to climate change. *The Cryosphere*, **14**, 3155–3174,
13 doi: [10.5194/tc-14-3155-2020](https://doi.org/10.5194/tc-14-3155-2020).
- 14 Burton, J.C., J.M. Amundson, R. Cassotto, C.-C. Kuo, and M. Dennin, 2018: Quantifying flow and stress in ice
15 mélange, the world’s largest granular material.. *Proceedings of the National Academy of Sciences of the United*
16 *States of America*, **115(20)**, 5105–5110, doi: [10.1073/pnas.1715136115](https://doi.org/10.1073/pnas.1715136115).
- 17 Cabedo-Sanz, P., S.T. Belt, A.E. Jennings, J.T. Andrews, and Geirsdóttir, 2016: Variability in drift ice export from the
18 Arctic Ocean to the North Icelandic Shelf over the last 8000 years: A multi-proxy evaluation. *Quaternary*
19 *Science Reviews*, **146**, 99–115, doi: [10.1016/j.quascirev.2016.06.012](https://doi.org/10.1016/j.quascirev.2016.06.012).
- 20 Cáceres, D. et al., 2020: Assessing global water mass transfers from continents to oceans over the period 1948–2016.
21 *Hydrology and Earth System Sciences*, **24(10)**, 4831–4851, doi: [10.5194/hess-24-4831-2020](https://doi.org/10.5194/hess-24-4831-2020).
- 22 Caesar, L., G.D. McCarthy, D.J.R. Thornalley, N. Cahill, and S. Rahmstorf, 2021: Current Atlantic Meridional
23 Overturning Circulation weakest in last millennium. *Nature Geoscience*, doi: [10.1038/s41561-021-00699-z](https://doi.org/10.1038/s41561-021-00699-z).
- 24 Cai, Q. et al., 2021: Accelerated decline of summer Arctic sea ice during 1850–2017 and the amplified Arctic warming
25 during the recent decades. *Environmental Research Letters*, **16(3)**, 034015, doi: [10.1088/1748-9326/abdb5f](https://doi.org/10.1088/1748-9326/abdb5f).
- 26 Cai, W. et al., 2019: Pantropical climate interactions. *Science*, **363(6430)**, doi: [10.1126/science.aav4236](https://doi.org/10.1126/science.aav4236).
- 27 Caldwell, P.M. et al., 2019: The DOE E3SM Coupled Model Version 1: Description and Results at High Resolution.
28 *Journal of Advances in Modeling Earth Systems*, **11(12)**, 4095–4146, doi: [10.1029/2019ms001870](https://doi.org/10.1029/2019ms001870).
- 29 Calonne, N., C. Geindreau, and F. Flin, 2015: Macroscopic modeling of heat and water vapor transfer with phase
30 change in dry snow based on an upscaling method: Influence of air convection. *Journal of Geophysical*
31 *Research F: Earth Surface*, **120**, 2476–2497, doi: [10.1002/2015jf003605](https://doi.org/10.1002/2015jf003605).
- 32 Calonne, N., M. Montagnat, M. Matzl, and M. Schneebeli, 2017: The layered evolution of fabric and microstructure of
33 snow at Point Barnola, Central East Antarctica. *Earth and Planetary Science Letters*, **460**, 293–301,
34 doi: [10.1016/j.epsl.2016.11.041](https://doi.org/10.1016/j.epsl.2016.11.041).
- 35 Calonne, N., F. Flin, C. Geindreau, B. Lesaffre, and S. Rolland Du Roscoat, 2014: Study of a temperature gradient
36 metamorphism of snow from 3-D images: Time evolution of microstructures, physical properties and their
37 associated anisotropy. *The Cryosphere*, **8**, 2255–2274, doi: [10.5194/tc-8-2255-2014](https://doi.org/10.5194/tc-8-2255-2014).
- 38 Calov, R., A. Robinson, M. Perrette, and A. Ganopolski, 2015: Simulating the Greenland ice sheet under present-dat
39 and palaeo constraints including a new discharge parameterization.. *The Cryosphere*, **9(1)**, 179–196.
- 40 Calov, R., A. Ganopolski, M. Claussen, V. Petoukhov, and R. Greve, 2005: Transient simulation of the last glacial
41 inception. Part I: Glacial inception as a bifurcation in the climate system. *Climate Dynamics*, **24(6)**, 545–561,
42 doi: [10.1007/s00382-005-0007-6](https://doi.org/10.1007/s00382-005-0007-6).
- 43 Calov, R. et al., 2018: Simulation of the future sea level contribution of Greenland with a new glacial system model.
44 *The Cryosphere*, **12(10)**, 3097–3121, doi: [10.5194/tc-12-3097-2018](https://doi.org/10.5194/tc-12-3097-2018).
- 45 Camill, P., 2005: Permafrost thaw accelerates in boreal peatlands during late-20th century climate warming. *Climatic*
46 *Change*, **68**, 135–152, doi: [10.1007/s10584-005-4785-y](https://doi.org/10.1007/s10584-005-4785-y).
- 47 Campbell, E.C. et al., 2019: Antarctic offshore polynyas linked to Southern Hemisphere climate anomalies. *Nature*,
48 **570(7761)**, 319–325, doi: [10.1038/s41586-019-1294-0](https://doi.org/10.1038/s41586-019-1294-0).
- 49 Capet, X., E.J. Campos, and A.M. Paiva, 2008: Submesoscale activity over the Argentinian shelf. *Geophysical*
50 *Research Letters*, **35(15)**, L15605, doi: [10.1029/2008gl034736](https://doi.org/10.1029/2008gl034736).
- 51 Capron, E., A. Govin, R. Feng, B.L. Otto-Bliesner, and E.W. Wolff, 2017: Critical evaluation of climate syntheses to
52 benchmark CMIP6/PMIP4 127 ka Last Interglacial simulations in the high-latitude regions. *Quaternary*
53 *Science Reviews*, doi: [10.1016/j.quascirev.2017.04.019](https://doi.org/10.1016/j.quascirev.2017.04.019).
- 54 Cardone, V.J., J.G. Greenwood, and M.A. Cane, 1990: On Trends in Historical Marine Wind Data. *Journal of Climate*,
55 **3(1)**, 113–127, doi: [10.1175/1520-0442\(1990\)003<0113:otihmw>2.0.co;2](https://doi.org/10.1175/1520-0442(1990)003<0113:otihmw>2.0.co;2).

- 1 Carilli, J.E. et al., 2014: Equatorial Pacific coral geochemical records show recent weakening of the Walker Circulation.
2 *Paleoceanography*, **29**(11), 1031–1045, doi:[10.1002/2014pa002683](https://doi.org/10.1002/2014pa002683).
- 3 Carlson, A.E. and P.U. Clark, 2012: Ice sheet sources of sea level rise and freshwater discharge during the last
4 deglaciation. *Reviews of Geophysics*, doi:[10.1029/2011rg000371](https://doi.org/10.1029/2011rg000371).
- 5 Carmagnola, C.M. et al., 2014: Implementation and evaluation of prognostic representations of the optical diameter of
6 snow in the SURFEX/ISBA-Crocus detailed snowpack model. *The Cryosphere*, **8**(2), 417–437, doi:[10.5194/tc-
7 8-417-2014](https://doi.org/10.5194/tc-8-417-2014).
- 8 Caron, L. et al., 2018: GIA Model Statistics for GRACE Hydrology, Cryosphere, and Ocean Science. *Geophysical
9 Research Letters*, doi:[10.1002/2017gl076644](https://doi.org/10.1002/2017gl076644).
- 10 Carrivick, J.L. et al., 2019: Accelerated Volume Loss in Glacier Ablation Zones of NE Greenland, Little Ice Age to
11 Present. *Geophysical Research Letters*, **46**(3), 1476–1484, doi:[10.1029/2018gl081383](https://doi.org/10.1029/2018gl081383).
- 12 Casas-Prat, M. and X.L. Wang, 2020: Projections of extreme ocean waves in the Arctic and potential implications for
13 coastal inundation and erosion. *Journal of Geophysical Research: Oceans*, doi:[10.1029/2019jc015745](https://doi.org/10.1029/2019jc015745).
- 14 Castagno, P. et al., 2019: Rebound of shelf water salinity in the Ross Sea. *Nature Communications*, **10**(1), 5441,
15 doi:[10.1038/s41467-019-13083-8](https://doi.org/10.1038/s41467-019-13083-8).
- 16 Catania, G.A. et al., 2018: Geometric Controls on Tidewater Glacier Retreat in Central Western Greenland. *Journal of
17 Geophysical Research: Earth Surface*, **123**(8), 2024–2038, doi:[10.1029/2017jf004499](https://doi.org/10.1029/2017jf004499).
- 18 Cavalieri, D.J., C.L. Parkinson, P. Gloersen, and H.J. Zwally, 1996: Sea Ice Concentrations from Nimbus-7 SMMR and
19 DMSP SSM/I-SSMIS Passive Microwave Data, Version 1. NASA National Snow and Ice Data Center
20 Distributed Active Archive Center, Boulder, CO, USA. Retrieved from: <https://nsidc.org/data/nsidc-0051>.
- 21 Cazenave, A. et al., 2018: Global sea-level budget 1993-present. *Earth System Science Data*, doi:[10.5194/essd-10-
22 1551-2018](https://doi.org/10.5194/essd-10-1551-2018).
- 23 Centurioni, L.R. et al., 2019: Global in-situ observations of essential climate and ocean variables at the air-sea interface.
24 *Frontiers in Marine Science*, **6**(JUL), 419, doi:[10.3389/fmars.2019.00419](https://doi.org/10.3389/fmars.2019.00419).
- 25 Ceres, R.L., C.E. Forest, and K. Keller, 2017: Understanding the detectability of potential changes to the 100-year peak
26 storm surge. *Climatic Change*, **145**(1–2), 221–235, doi:[10.1007/s10584-017-2075-0](https://doi.org/10.1007/s10584-017-2075-0).
- 27 Cerrone, D., G. Fusco, I. Simmonds, G. Aulicino, and G. Budillon, 2017: Dominant covarying climate signals in the
28 southern ocean and antarctic sea ice influence during the last three decades. *Journal of Climate*, **30**(8), 3055–
29 3072, doi:[10.1175/jcli-d-16-0439.1](https://doi.org/10.1175/jcli-d-16-0439.1).
- 30 Chadburn, S. et al., 2015: An improved representation of physical permafrost dynamics in the JULES land-surface
31 model. *Geoscientific Model Development*, **8**(5), 1493–1508, doi:[10.5194/gmd-8-1493-2015](https://doi.org/10.5194/gmd-8-1493-2015).
- 32 Chadburn, S.E. et al., 2015: Impact of model developments on present and future simulations of permafrost in a global
33 land-surface model. *The Cryosphere*, **9**(4), 1505–1521, doi:[10.5194/tc-9-1505-2015](https://doi.org/10.5194/tc-9-1505-2015).
- 34 Chadburn, S.E. et al., 2017: An observation-based constraint on permafrost loss as a function of global warming.
35 *Nature Climate Change*, **7**(5), 340–344, doi:[10.1038/nclimate3262](https://doi.org/10.1038/nclimate3262).
- 36 Chadwick, M., C.S. Allen, L.C. Sime, and C.D. Hillenbrand, 2020: Analysing the timing of peak warming and
37 minimum winter sea-ice extent in the Southern Ocean during MIS 5e. *Quaternary Science Reviews*, **229**,
38 106134, doi:[10.1016/j.quascirev.2019.106134](https://doi.org/10.1016/j.quascirev.2019.106134).
- 39 Chafik, L. and T. Rossby, 2019: Volume, Heat, and Freshwater Divergences in the Subpolar North Atlantic Suggest the
40 Nordic Seas as Key to the State of the Meridional Overturning Circulation. *Geophysical Research Letters*,
41 **46**(9), 4799–4808, doi:[10.1029/2019gl082110](https://doi.org/10.1029/2019gl082110).
- 42 Chafik, L., J.E. Nilsen, S. Dangendorf, G. Reverdin, and T. Frederikse, 2019: North Atlantic Ocean Circulation and
43 Decadal Sea Level Change During the Altimetry Era. *Scientific Reports*, **9**(1), 1041, doi:[10.1038/s41598-018-
44 37603-6](https://doi.org/10.1038/s41598-018-37603-6).
- 45 Chan, P. et al., 2017: Multicentennial record of Labrador Sea primary productivity and sea-ice variability archived in
46 coralline algal barium. *Nature Communications*, **8**, 15543, doi:[10.1038/ncomms15543](https://doi.org/10.1038/ncomms15543).
- 47 Chao, B.F., Y.H. Wu, and Y.S. Li, 2008: Impact of artificial reservoir water impoundment on global sea level.. *Science
48 (New York, N.Y.)*, **320**(5873), 212–4, doi:[10.1126/science.1154580](https://doi.org/10.1126/science.1154580).
- 49 Chasmer, L. and C. Hopkinson, 2017: Threshold loss of discontinuous permafrost and landscape evolution. *Global
50 Change Biology*, **23**, 2672–2686, doi:[10.1111/gcb.13537](https://doi.org/10.1111/gcb.13537).
- 51 Chassignet, E.P. and D.P. Marshall, 2008: Gulf Stream separation in numerical ocean models. In: *Ocean Modeling in
52 an Eddy Regime, Volume 177* [Hecht, M.W. and H. Hasumi (eds.)]. American Geophysical Union (AGU),
53 Washington, DC, USA, pp. 39–61, doi:[10.1029/177gm05](https://doi.org/10.1029/177gm05).
- 54 Chassignet, E.P., X. Xu, E.P. Chassignet, and X. Xu, 2017: Impact of Horizontal Resolution (1/12° to 1/50°) on Gulf
55 Stream Separation, Penetration, and Variability. *Journal of Physical Oceanography*, **47**(8), 1999–2021,
56 doi:[10.1175/jpo-d-17-0031.1](https://doi.org/10.1175/jpo-d-17-0031.1).

- 1 Chassignet, E.P. et al., 2020: Impact of horizontal resolution on global ocean–sea ice model simulations based on the
2 experimental protocols of the Ocean Model Intercomparison Project phase 2 (OMIP-2). *Geoscientific Model*
3 *Development*, **13(9)**, 4595–4637, doi:[10.5194/gmd-13-4595-2020](https://doi.org/10.5194/gmd-13-4595-2020).
- 4 Chelton, D.B. and S.-P. Xie, 2010: Coupled Ocean-Atmosphere Interaction at Oceanic Mesoscales. *Oceanography*, **23**,
5 52–69, doi:[10.2307/24860862](https://doi.org/10.2307/24860862).
- 6 Chemke, R., L. Zanna, and L.M. Polvani, 2020: Identifying a human signal in the North Atlantic warming hole. *Nature*
7 *Communications*, **11(1)**, 1540, doi:[10.1038/s41467-020-15285-x](https://doi.org/10.1038/s41467-020-15285-x).
- 8 Chen, C., W. Liu, and G. Wang, 2019: Understanding the Uncertainty in the 21st Century Dynamic Sea Level
9 Projections: The Role of the AMOC. *Geophysical Research Letters*, **46(1)**, 210–217,
10 doi:[10.1029/2018gl080676](https://doi.org/10.1029/2018gl080676).
- 11 Chen, H.W., R.B. Alley, and F. Zhang, 2016: Interannual Arctic sea ice variability and associated winter weather
12 patterns: A regional perspective for 1979–2014. *Journal of Geophysical Research*, **121(24)**, 14433–14455,
13 doi:[10.1002/2016jd024769](https://doi.org/10.1002/2016jd024769).
- 14 Chen, J.-L., S.-C. Kang, X.-H. Meng, and Q.-L. You, 2019: Assessments of the Arctic amplification and the changes in
15 the Arctic sea surface. *Advances in Climate Change Research*, **10(4)**, 193–202,
16 doi:[10.1016/j.accr.2020.03.002](https://doi.org/10.1016/j.accr.2020.03.002).
- 17 Chen, W.-B. and W.-C. Liu, 2016: Assessment of storm surge inundation and potential hazard maps for the southern
18 coast of Taiwan. *Natural Hazards*, **82(1)**, 591–616.
- 19 Chen, Z. and L. Wu, 2012: Long-term change of the Pacific North Equatorial Current bifurcation in SODA. *Journal of*
20 *Geophysical Research: Oceans*, **117(C6)**, n/a–n/a, doi:[10.1029/2011jc007814](https://doi.org/10.1029/2011jc007814).
- 21 Cheng, L. and J. Zhu, 2014: Artifacts in variations of ocean heat content induced by the observation system changes.
22 *Geophysical Research Letters*, **41(20)**, 7276–7283, doi:[10.1002/2014gl061881](https://doi.org/10.1002/2014gl061881).
- 23 Cheng, L., J. Abraham, Z. Hausfather, and K.E. Trenberth, 2019: How fast are the oceans warming? *Science*,
24 **363(6423)**, 128–129, doi:[10.1126/science.aav7619](https://doi.org/10.1126/science.aav7619).
- 25 Cheng, L. et al., 2017: Improved estimates of ocean heat content from 1960 to 2015. *Science Advances*, **3(3)**, e1601545,
26 doi:[10.1126/sciadv.1601545](https://doi.org/10.1126/sciadv.1601545).
- 27 Cheng, L. et al., 2020: Improved Estimates of Changes in Upper Ocean Salinity and the Hydrological Cycle. *Journal of*
28 *Climate*, **33(23)**, 10357–10381.
- 29 Cheng, W., J.C.H.H. Chiang, and D. Zhang, 2013: Atlantic Meridional Overturning Circulation (AMOC) in CMIP5
30 Models: RCP and Historical Simulations. *Journal of Climate*, **26(18)**, 7187–7197, doi:[10.1175/jcli-d-12-00496.1](https://doi.org/10.1175/jcli-d-12-00496.1).
- 31
- 32 Cherchi, A. et al., 2018: The response of subtropical highs to climate change. *Current Climate Change Reports*, **4(4)**,
33 371–382.
- 34 Cherchi, A. et al., 2019: Global Mean Climate and Main Patterns of Variability in the CMCC-CM2 Coupled Model.
35 *Journal of Advances in Modeling Earth Systems*, **11(1)**, 185–209, doi:[10.1029/2018ms001369](https://doi.org/10.1029/2018ms001369).
- 36 Cheung, W.W.L. and T.L. Frölicher, 2020: Marine heatwaves exacerbate climate change impacts for fisheries in the
37 northeast Pacific. *Scientific Reports*, **10(1)**, 6678, doi:[10.1038/s41598-020-63650-z](https://doi.org/10.1038/s41598-020-63650-z).
- 38 Chevallier, M. et al., 2017: Intercomparison of the Arctic sea ice cover in global ocean–sea ice reanalyses from the
39 ORA-IP project. *Climate Dynamics*, **49(3)**, 1107–1136, doi:[10.1007/s00382-016-2985-y](https://doi.org/10.1007/s00382-016-2985-y).
- 40 Choi, Y., M. Morlighem, E. Rignot, and M. Wood, 2021: Ice dynamics will remain a primary driver of Greenland ice
41 sheet mass loss over the next century. *Communications Earth & Environment*, **2(1)**, 26, doi:[10.1038/s43247-021-00092-z](https://doi.org/10.1038/s43247-021-00092-z).
- 42
- 43 Choi, Y., M. Morlighem, E. Rignot, J. Mouginot, and M. Wood, 2017: Modeling the Response of
44 Nioghalvfjærdsfjorden and Zachariae Isstrøm Glaciers, Greenland, to Ocean Forcing Over the Next Century.
45 *Geophysical Research Letters*, **44(21)**, 11,11–71,79, doi:[10.1002/2017gl075174](https://doi.org/10.1002/2017gl075174).
- 46 Christian, J.E., M. Koutnik, and G. Roe, 2018: Committed retreat: controls on glacier disequilibrium in a warming
47 climate. *Journal of Glaciology*, **64(246)**, 675–688, doi:[10.1017/jog.2018.57](https://doi.org/10.1017/jog.2018.57).
- 48 Christie, F.D.W. et al., 2018: Glacier change along West Antarctica’s Marie Byrd Land Sector and links to inter-
49 decadal atmosphere-ocean variability. *The Cryosphere*, **12**, 2461–2479, doi:[10.5194/tc-12-2461-2018](https://doi.org/10.5194/tc-12-2461-2018).
- 50 Church, J.A., N.J. White, and J.M. Arblaster, 2005: Significant decadal-scale impact of volcanic eruptions on sea level
51 and ocean heat content. *Nature*, **438(7064)**, 74–77, doi:[10.1038/nature04237](https://doi.org/10.1038/nature04237).
- 52 Church, J.A., D. Monselesan, J.M. Gregory, and B. Marzeion, 2013: Evaluating the ability of process based models to
53 project sea-level change. *Environmental Research Letters*, **8(1)**, 14051, doi:[10.1088/1748-9326/8/1/014051](https://doi.org/10.1088/1748-9326/8/1/014051).
- 54 Church, J.A.A. et al., 2013: Sea Level Change. In: *Climate Change 2013: The Physical Science Basis. Contribution of*
55 *Working Group I to the Fifth Assessment Report of the Intergovernmental Panel on Climate Change* [Stocker,
56 T.F., D. Qin, G.-K. Plattner, M. Tignor, S.K. Allen, J. Boschung, A. Nauels, Y. Xia, V. Bex, and P.M. Midgley

- 1 (eds.]. Cambridge University Press, Cambridge, United Kingdom and New York, NY, USA, pp. 1137–1216,
2 doi:[10.1017/cbo9781107415324.026](https://doi.org/10.1017/cbo9781107415324.026).
- 3 Cicoira, A., J. Beutel, J. Faillettaz, and A. Vieli, 2019: Water controls the seasonal rhythm of rock glacier flow. *Earth*
4 *and Planetary Science Letters*, **528**, doi:[10.1016/j.epsl.2019.115844](https://doi.org/10.1016/j.epsl.2019.115844).
- 5 Ciraci, E., I. Velicogna, and S. Swenson, 2020: Continuity of the Mass Loss of the World's Glaciers and Ice Caps From
6 the GRACE and GRACE Follow-On Missions. *Geophysical Research Letters*, **47(9)**, e2019GL086926,
7 doi:[10.1029/2019g1086926](https://doi.org/10.1029/2019g1086926).
- 8 Clark, P.U. et al., 2016: Consequences of twenty-first-century policy for multi-millennial climate and sea-level change.
9 *Nature Climate Change*, **6(4)**, 360–369, doi:[10.1038/nclimate2923](https://doi.org/10.1038/nclimate2923).
- 10 Clark, P.U. et al., 2020: Oceanic forcing of penultimate deglacial and last interglacial sea-level rise. *Nature*, **577**, 660–
11 664, doi:[10.1038/s41586-020-1931-7](https://doi.org/10.1038/s41586-020-1931-7).
- 12 Clement Kinney, J. et al., 2014: On the Flow Through Bering Strait: A Synthesis of Model Results and Observations.
13 In: *The Pacific Arctic Region: Ecosystem Status and Trends in a Rapidly Changing Environment* [Grebmeier,
14 J.M. and W. Maslowski (eds.)]. Springer, Dordrecht, The Netherlands, pp. 167–198, doi:[10.1007/978-94-017-
15 8863-2_7](https://doi.org/10.1007/978-94-017-8863-2_7).
- 16 Clerc, F., B.M. Minchew, and M.D. Behn, 2019: Marine Ice Cliff Instability Mitigated by Slow Removal of Ice
17 Shelves. *Geophysical Research Letters*, doi: 10.1029/2019GL084183.
- 18 Coats, S. and K.B. Karnauskas, 2018: A role for the equatorial undercurrent in the ocean dynamical thermostat. *Journal*
19 *of Climate*, doi:[10.1175/jcli-d-17-0513.1](https://doi.org/10.1175/jcli-d-17-0513.1).
- 20 Colas, F., J.C. McWilliams, X. Capet, and J. Kurian, 2012: Heat balance and eddies in the Peru-Chile current system.
21 *Climate Dynamics*, **39(1–2)**, 509–529, doi:[10.1007/s00382-011-1170-6](https://doi.org/10.1007/s00382-011-1170-6).
- 22 Colgan, W. et al., 2019: Programme for monitoring of the Greenland ice sheet (PROMICE): Ice sheet mass balance
23 (1995-2015). Dataset published via Geological Survey of Denmark and Greenland.
- 24 Colleoni, F. et al., 2014: Modeling Northern Hemisphere ice-sheet distribution during MIS 5 and MIS 7 glacial
25 inception. *Climate of the Past*, **10(1)**, 269–291, doi:[10.5194/cp-10-269-2014](https://doi.org/10.5194/cp-10-269-2014).
- 26 Collins, M. et al., 2010: The impact of global warming on the tropical Pacific Ocean and El Niño. *Nature Geoscience*,
27 doi:[10.1038/ngeo868](https://doi.org/10.1038/ngeo868).
- 28 Collins, M. et al., 2013: Long-term Climate Change: Projections, Commitments and Irreversibility. In: *Climate Change*
29 *2013: The Physical Science Basis. Contribution of Working Group I to the Fifth Assessment Report of the*
30 *Intergovernmental Panel on Climate Change* [Stocker, T.F., D. Qin, G.-K. Plattner, M. Tignor, S.K. Allen, J.
31 Boschung, A. Nauels, Y. Xia, V. Bex, and P.M. Midgley (eds.)]. Cambridge University Press, Cambridge,
32 United Kingdom and New York, USA, pp. 1029–1136, doi:[10.1017/cbo9781107415324.024](https://doi.org/10.1017/cbo9781107415324.024).
- 33 Collins, M. et al., 2019: Extremes, Abrupt Changes and Managing Risks. In: *IPCC Special Report on the Ocean and*
34 *Cryosphere in a Changing Climate* [Pörtner, H.-O., D.C. Roberts, V. Masson-Delmotte, P. Zhai, M. Tignor, E.
35 Poloczanska, K. Mintenbeck, M. Nicolai, A. Okem, J. Petzold, B. Rama, and N. Weyer (eds.)]. In Press, pp.
36 589-655.
- 37 Colville, E.J. et al., 2011: Sr-Nd-Pb isotope evidence for ice-sheet presence on southern Greenland during the Last
38 Interglacial. *Science*, **333(6042)**, 620–623.
- 39 Comiso, J.C., 2017: Bootstrap Sea Ice Concentrations from Nimbus-7 SMMR and DMSP SSM/I-SSMIS, Version 3.
40 NASA National Snow and Ice Data Center Distributed Active Archive Center, Boulder, CO, USA. Retrieved
41 from: <https://nsidc.org/data/nsidc-0079>.
- 42 Comiso, J.C., W.N. Meier, and R. Gersten, 2017a: Variability and trends in the Arctic Sea ice cover: Results from
43 different techniques. *Journal of Geophysical Research: Oceans*, **122(8)**, 6883–6900,
44 doi:[10.1002/2017jc012768](https://doi.org/10.1002/2017jc012768).
- 45 Comiso, J.C. et al., 2017b: Positive Trend in the Antarctic Sea Ice Cover and Associated Changes in Surface
46 Temperature. *Journal of Climate*, **30(6)**, 2251–2267, doi:[10.1175/jcli-d-16-0408.1](https://doi.org/10.1175/jcli-d-16-0408.1).
- 47 Constantin, J.G. et al., 2020: Measurements and modeling of snow albedo at Alerce Glacier, Argentina: Effects of
48 volcanic ash, snow grain size, and cloudiness. *Cryosphere*, **14(12)**, 4581–4601, doi:[10.5194/tc-14-4581-2020](https://doi.org/10.5194/tc-14-4581-2020).
- 49 Cook, A.J. et al., 2019: Atmospheric forcing of rapid marine-terminating glacier retreat in the Canadian Arctic
50 Archipelago. *Science Advances*, **5(3)**, eaau8507, doi:[10.1126/sciadv.aau8507](https://doi.org/10.1126/sciadv.aau8507).
- 51 Cook, J.M. et al., 2020: Glacier algae accelerate melt rates on the south-western Greenland Ice Sheet. *The Cryosphere*,
52 **14**, 309–330, doi:[10.5194/tc-14-309-2020](https://doi.org/10.5194/tc-14-309-2020).
- 53 Cordero, R.R. et al., 2019: Dry-Season Snow Cover Losses in the Andes (18°–40°S) driven by Changes in Large-Scale
54 Climate Modes. *Scientific Reports*, **9**, 16945, doi:[10.1038/s41598-019-53486-7](https://doi.org/10.1038/s41598-019-53486-7).
- 55 Cornford, S.L. et al., 2020: Results of the third Marine Ice Sheet Model Intercomparison Project (MISMIP+). *The*
56 *Cryosphere*, **14(7)**, 2283–2301, doi:[10.5194/tc-14-2283-2020](https://doi.org/10.5194/tc-14-2283-2020).

- 1 Couasnon, A. et al., 2020: Measuring compound flood potential from river discharge and storm surge extremes at the
2 global scale and its implications for flood hazard. *Natural Hazards and Earth System Sciences*, **20**, 489–504,
3 doi:[10.5194/nhess-20-489-2020](https://doi.org/10.5194/nhess-20-489-2020).
- 4 Couldrey, M.P. et al., 2020: What causes the spread of model projections of ocean dynamic sea level change in
5 response to greenhouse gas forcing? *Climate Dynamics*, doi:[10.1007/s00382-020-05471-4](https://doi.org/10.1007/s00382-020-05471-4).
- 6 Couldrey, M.P. et al., 2021: What causes the spread of model projections of ocean dynamic sea-level change in
7 response to greenhouse gas forcing? *Climate Dynamics*, **56**(1–2), 155–187, doi:[10.1007/s00382-020-05471-4](https://doi.org/10.1007/s00382-020-05471-4).
- 8 Cowton, T.R., J.A. Todd, and D.I. Benn, 2019: Sensitivity of Tidewater Glaciers to Submarine Melting Governed by
9 Plume Locations. *Geophysical Research Letters*, **46**, 11219–11227, doi:[10.1029/2019gl084215](https://doi.org/10.1029/2019gl084215).
- 10 Cronin, M.F. et al., 2019: Air-sea fluxes with a focus on heat and momentum. *Frontiers in Marine Science*, **6**(JUL),
11 430, doi:[10.3389/fmars.2019.00430](https://doi.org/10.3389/fmars.2019.00430).
- 12 Crosta, X. et al., 2018: Ocean as the main driver of Antarctic ice sheet retreat during the Holocene. *Global and
13 Planetary Change*, **166**, 62–74, doi:[10.1016/j.gloplacha.2018.04.007](https://doi.org/10.1016/j.gloplacha.2018.04.007).
- 14 Crosta, X. et al., 2021: Multi-decadal trends in Antarctic sea-ice extent driven by ENSO–SAM over the last 2,000 years.
15 *Nature Geoscience*, doi:[10.1038/s41561-021-00697-1](https://doi.org/10.1038/s41561-021-00697-1).
- 16 Cullather, R.I., S.M.J. Nowicki, B. Zhao, and M.J. Suarez, 2014: Evaluation of the Surface Representation of the
17 Greenland Ice Sheet in a General Circulation Model. *Journal of Climate*, **27**(13), 4835–4856, doi:[10.1175/jcli-d-13-00635.1](https://doi.org/10.1175/jcli-d-13-00635.1).
- 18 Cullather, R.I. et al., 2020: Anomalous Circulation in July 2019 Resulting in Mass Loss on the Greenland Ice Sheet.
19 *Geophysical Research Letters*, **47**, e2020GL087263, doi:[10.1029/2020gl087263](https://doi.org/10.1029/2020gl087263).
- 20 Cummins, P.F. and D. Masson, 2018: Low-frequency isopycnal variability in the Alaska Gyre from Argo. *Progress in
21 Oceanography*, **168**, 310–324, doi:[10.1016/j.pocean.2018.09.014](https://doi.org/10.1016/j.pocean.2018.09.014).
- 22 Cummins, P.F. and T. Ross, 2020a: Secular trends in water properties at Station P in the northeast Pacific: an updated
23 analysis. *Progress in Oceanography*, 102329, doi:[10.1016/j.pocean.2020.102329](https://doi.org/10.1016/j.pocean.2020.102329).
- 24 Cummins, P.F. and T. Ross, 2020b: Secular trends in water properties at Station P in the northeast Pacific: an updated
25 analysis. *Progress in Oceanography*, 102329, doi:[10.1016/j.pocean.2020.102329](https://doi.org/10.1016/j.pocean.2020.102329).
- 26 Cunliffe, A. et al., 2019: Rapid retreat of permafrost coastline observed with aerial drone photogrammetry. *Cryosphere*,
27 **13**(5), 1513–1528, doi:[10.5194/tc-13-1513-2019](https://doi.org/10.5194/tc-13-1513-2019).
- 28 Cuntz, M. and V. Haverd, 2018: Physically Accurate Soil Freeze-Thaw Processes in a Global Land Surface Scheme.
29 *Journal of Advances in Modeling Earth Systems*, **10**(1), 54–77, doi:[10.1002/2017ms001100](https://doi.org/10.1002/2017ms001100).
- 30 Cuzzone, J.K. et al., 2016: Final deglaciation of the Scandinavian Ice Sheet and implications for the Holocene global
31 sea-level budget. *Earth and Planetary Science Letters*, **448**, 34–41, doi:[10.1016/j.epsl.2016.05.019](https://doi.org/10.1016/j.epsl.2016.05.019).
- 32 D’Asaro, E.A., 2014: Turbulence in the Upper-Ocean Mixed Layer. *Annual Review of Marine Science*, **6**(1), 101–115,
33 doi:[10.1146/annurev-marine-010213-135138](https://doi.org/10.1146/annurev-marine-010213-135138).
- 34 Dahl-Jensen, D. et al., 2013: Eemian interglacial reconstructed from a Greenland folded ice core. *Nature*, **493**(7433),
35 489–494, doi:[10.1038/nature11789](https://doi.org/10.1038/nature11789).
- 36 Dahlke, S. et al., 2020: The observed recent surface air temperature development across Svalbard and concurring
37 footprints in local sea ice cover. *International Journal of Climatology*, **n/a**(n/a), doi:[10.1002/joc.6517](https://doi.org/10.1002/joc.6517).
- 38 Danabasoglu, G., W.G. Large, and B.P. Briegleb, 2010: Climate impacts of parameterized Nordic Sea overflows.
39 *Journal of Geophysical Research*, **115**(C11), C11005, doi:[10.1029/2010jc006243](https://doi.org/10.1029/2010jc006243).
- 40 Danabasoglu, G. et al., 2014: North Atlantic Simulations in Coordinated Ocean-ice Reference Experiments phase 2
41 (CORE-II). Part 1: Mean States. *Ocean Modelling*, **73**, 76–107, doi:[10.1016/j.ocemod.2013.10.005](https://doi.org/10.1016/j.ocemod.2013.10.005).
- 42 Danabasoglu, G. et al., 2016: North Atlantic simulations in Coordinated Ocean-ice Reference Experiments phase II
43 (CORE-II). Part II: Inter-annual to decadal variability. *Ocean Modelling*, **97**, 65–90,
44 doi:[10.1016/j.ocemod.2015.11.007](https://doi.org/10.1016/j.ocemod.2015.11.007).
- 45 Danabasoglu, G. et al., 2020: The Community Earth System Model Version 2 (CESM2). *Journal of Advances in
46 Modeling Earth Systems*, **12**(2), e2019MS001916, doi:[10.1029/2019ms001916](https://doi.org/10.1029/2019ms001916).
- 47 Dangendorf, S. et al., 2019: Persistent acceleration in global sea-level rise since the 1960s. *Nature Climate Change*,
48 **9**(9), 705–710, doi:[10.1038/s41558-019-0531-8](https://doi.org/10.1038/s41558-019-0531-8).
- 49 Das, I. et al., 2020: Multidecadal Basal Melt Rates and Structure of the Ross Ice Shelf, Antarctica, Using Airborne Ice
50 Penetrating Radar. *Journal of Geophysical Research: Earth Surface*, **125**(3), doi:[10.1029/2019jf005241](https://doi.org/10.1029/2019jf005241).
- 51 Davaze, L., A. Rabatel, A. Dufour, R. Hugonnet, and Y. Arnaud, 2020: Region-Wide Annual Glacier Surface Mass
52 Balance for the European Alps From 2000 to 2016. *Frontiers in Earth Science*, **8**, 149,
53 doi:[10.3389/feart.2020.00149](https://doi.org/10.3389/feart.2020.00149).
- 54 Davies, B.J. et al., 2020: The evolution of the Patagonian Ice Sheet from 35 ka to the present day (PATICE). *Earth-
55 Science Reviews*, **204**, 103152, doi:[10.1016/j.earscirev.2020.103152](https://doi.org/10.1016/j.earscirev.2020.103152).
- 56

- 1 de Boer, B., A.M. Haywood, A.M. Dolan, S.J. Hunter, and C.L. Prescott, 2017: The transient response of ice volume to
2 orbital forcing during the warm late Pliocene. *Geophysical Research Letters*, **44**(20), 10–486,
3 doi:[10.1002/2017g1073535](https://doi.org/10.1002/2017g1073535).
- 4 De Boer, B. et al., 2015: Simulating the Antarctic ice sheet in the late-Pliocene warm period: PLISMIP-ANT, an ice-
5 sheet model intercomparison project. *Cryosphere*, **9**(3), 881–903, doi:[10.5194/tc-9-881-2015](https://doi.org/10.5194/tc-9-881-2015).
- 6 de Elía, R., S. Biner, and A. Frigon, 2013: Interannual variability and expected regional climate change over North
7 America. *Climate Dynamics*, **41**(5–6), 1245–1267, doi:[10.1007/s00382-013-1717-9](https://doi.org/10.1007/s00382-013-1717-9).
- 8 de Jong, M.F., M. Oltmanns, J. Karstensen, and L. de Steur, 2018: Deep Convection in the Irminger Sea Observed with
9 a Dense Mooring Array. *Oceanography*, **31**(1), 50–59, doi:[10.5670/oceanog.2018.109](https://doi.org/10.5670/oceanog.2018.109).
- 10 de Kok, R.J., P.D.A. Kraaijenbrink, O.A. Tuinenburg, P.N.J. Bonekamp, and W.W. Immerzeel, 2020: Towards
11 understanding the pattern of glacier mass balances in High Mountain Asia using regional climatic modelling.
12 *The Cryosphere*, **14**(9), 3215–3234, doi:[10.5194/tc-14-3215-2020](https://doi.org/10.5194/tc-14-3215-2020).
- 13 De Lavergne, C., J.B. Palter, E.D. Galbraith, R. Bernardello, and I. Marinov, 2014: Cessation of deep convection in the
14 open Southern Ocean under anthropogenic climate change. *Nature Climate Change*, **4**, 278,
15 doi:[10.1038/nclimate2132](https://doi.org/10.1038/nclimate2132).
- 16 De Schepper, S., P.L. Gibbard, U. Salzmann, and J. Ehlers, 2014: A global synthesis of the marine and terrestrial
17 evidence for glaciation during the Pliocene Epoch. *Earth-Science Reviews*, **135**, 83–102,
18 doi:[10.1016/j.earscirev.2014.04.003](https://doi.org/10.1016/j.earscirev.2014.04.003).
- 19 De Vernal, A., R. Gersonde, H. Goosse, M.S. Seidenkrantz, and E.W. Wolff, 2013a: Sea ice in the paleoclimate system:
20 The challenge of reconstructing sea ice from proxies - an introduction. *Quaternary Science Reviews*, **79**, 1–8,
21 doi:[10.1016/j.quascirev.2013.08.009](https://doi.org/10.1016/j.quascirev.2013.08.009).
- 22 De Vernal, A. et al., 2013b: Dinocyst-based reconstructions of sea ice cover concentration during the Holocene in the
23 Arctic Ocean, the northern North Atlantic Ocean and its adjacent seas. *Quaternary Science Reviews*, **79**, 111–
24 121, doi:[10.1016/j.quascirev.2013.07.006](https://doi.org/10.1016/j.quascirev.2013.07.006).
- 25 de Vries, P. and S.L. Weber, 2005: The Atlantic freshwater budget as a diagnostic for the existence of a stable shut
26 down of the meridional overturning circulation. *Geophysical Research Letters*, **32**(9),
27 doi:[10.1029/2004g1021450](https://doi.org/10.1029/2004g1021450).
- 28 de Wet, G.A., I.S. Castañeda, R.M. DeConto, and J. Brigham-Grette, 2016: A high-resolution mid-Pleistocene
29 temperature record from Arctic Lake El'gygytyn: A 50 kyr super interglacial from MIS 33 to MIS 31? *Earth
30 and Planetary Science Letters*, **436**, 56–63, doi:[10.1016/j.epsl.2015.12.021](https://doi.org/10.1016/j.epsl.2015.12.021).
- 31 DeConto, R.M. and D. Pollard, 2016: Contribution of Antarctica to past and future sea-level rise. *Nature*, **531**(7596),
32 591–597, doi:[10.1038/nature17145](https://doi.org/10.1038/nature17145).
- 33 DeConto, R.M. et al., 2021: The Paris Climate Agreement and future sea-level rise from Antarctica. *Nature*, **in press**.
- 34 Delhasse, A., X. Fettweis, C. Kittel, C. Amory, and C. Agosta, 2018: Brief communication: Impact of the recent
35 atmospheric circulation change in summer on the future surface mass balance of the Greenland Ice Sheet. *The
36 Cryosphere*, **12**(11), 3409–3418, doi:[10.5194/tc-12-3409-2018](https://doi.org/10.5194/tc-12-3409-2018).
- 37 Deline, P. et al., 2015: Ice Loss and Slope Stability in High-Mountain Regions. In: *Snow and Ice-Related Hazards,
38 Risks, and Disasters* [John F. Shroder, W. Haeberli, and C. Whiteman (eds.)]. Academic Press, pp. 521–561,
39 doi:[10.1016/b978-0-12-394849-6.00015-9](https://doi.org/10.1016/b978-0-12-394849-6.00015-9).
- 40 Delman, A.S. et al., 2015: Effects of Eddy Vorticity Forcing on the Mean State of the Kuroshio Extension. *Journal of
41 Physical Oceanography*, **45**(5), 1356–1375, doi:[10.1175/jpo-d-13-0259.1](https://doi.org/10.1175/jpo-d-13-0259.1).
- 42 Delworth, T.L. et al., 2012: Simulated Climate and Climate Change in the GFDL CM2.5 High-Resolution Coupled
43 Climate Model. *Journal of Climate*, **25**(8), 2755–2781, doi:[10.1175/jcli-d-11-00316.1](https://doi.org/10.1175/jcli-d-11-00316.1).
- 44 Denton, G.H. et al., 2010: The Last Glacial Termination. *Science*, **328**(5986), 1652–1656,
45 doi:[10.1126/science.1184119](https://doi.org/10.1126/science.1184119).
- 46 Derksen, C., R. Brown, L. Mudryk, and K. Luoju, 2017: Terrestrial snow cover. *State of the Climate in 2016. Bulletin
47 of the American Meteorological Society*. 98 (8), **98**(8), S143–S145, doi:[10.1175/2017bamsstateofthecclimate.1](https://doi.org/10.1175/2017bamsstateofthecclimate.1).
- 48 Desbiolles, F. et al., 2017: Two decades [1992–2012] of surface wind analyses based on satellite scatterometer
49 observations. *Journal of Marine Systems*, **168**, 38–56, doi:[10.1016/j.jmarsys.2017.01.003](https://doi.org/10.1016/j.jmarsys.2017.01.003).
- 50 Desbruyères, D., E.L. McDonagh, B.A. King, and V. Thierry, 2017: Global and Full-Depth Ocean Temperature Trends
51 during the Early Twenty-First Century from Argo and Repeat Hydrography. *Journal of Climate*, **30**(6), 1985–
52 1997, doi:[10.1175/jcli-d-16-0396.1](https://doi.org/10.1175/jcli-d-16-0396.1).
- 53 Deschamps-Berger, C. et al., 2019: Closing the mass budget of a tidewater glacier: The example of Kronebreen,
54 Svalbard. *Journal of Glaciology*, **65**(249), 136–148, doi:[10.1017/jog.2018.98](https://doi.org/10.1017/jog.2018.98).
- 55 Deshayes, J. et al., 2014: CMIP5 Model Intercomparison of Freshwater Budget and Circulation in the North Atlantic.
56 *Journal of Climate*, **27**(9), 3298–3317, doi:[10.1175/jcli-d-12-00700.1](https://doi.org/10.1175/jcli-d-12-00700.1).

- 1 Di Mauro, B. et al., 2019: Saharan dust events in the European Alps: role in snowmelt and geochemical
2 characterization. *The Cryosphere*, **13**(4), 1147–1165, doi:[10.5194/tc-13-1147-2019](https://doi.org/10.5194/tc-13-1147-2019).
- 3 Di Mauro, B. et al., 2020: Glacier algae foster ice-albedo feedback in the European Alps. *Scientific Reports*, **10**(1),
4 4739, doi:[10.1038/s41598-020-61762-0](https://doi.org/10.1038/s41598-020-61762-0).
- 5 Dias, F.B. et al., 2020: Ocean heat uptake driven by redistribution of heat in response to ocean circulation changes.
6 *Journal of Climate*, **33**(21), 9065–9082.
- 7 Dietrich, J.C. et al., 2012: Performance of the Unstructured-Mesh, SWAN+ADCIRC Model in Computing Hurricane
8 Waves and Surge. *Journal of Scientific Computing*, **52**(2), 468–497, doi:[10.1007/s10915-011-9555-6](https://doi.org/10.1007/s10915-011-9555-6).
- 9 Ding, Q. et al., 2017: Influence of high-latitude atmospheric circulation changes on summertime Arctic sea ice. *Nature*
10 *Climate Change*, **7**(4), 289–295, doi:[10.1038/nclimate3241](https://doi.org/10.1038/nclimate3241).
- 11 Ding, Q. et al., 2019: Fingerprints of internal drivers of Arctic sea ice loss in observations and model simulations.
12 *Nature Geoscience*, **12**(1), 28, doi:[10.1038/s41561-018-0256-8](https://doi.org/10.1038/s41561-018-0256-8).
- 13 Dinniman, M. et al., 2016: Modeling Ice Shelf/Ocean Interaction in Antarctica: A Review. *Oceanography*, **29**(4), 144–
14 153, doi:[10.5670/oceanog.2016.106](https://doi.org/10.5670/oceanog.2016.106).
- 15 Docquier, D., T. Koenigk, R. Fuentes-Franco, M.P. Karami, and Y. Ruprich-Robert, 2021: Impact of ocean heat
16 transport on the Arctic sea-ice decline: a model study with EC-Earth3. *Climate Dynamics*,
17 doi:[10.1007/s00382-020-05540-8](https://doi.org/10.1007/s00382-020-05540-8).
- 18 Docquier, D. et al., 2017: Relationships between Arctic sea ice drift and strength modelled by NEMO-LIM3.6. *The*
19 *Cryosphere*, **11**(6), 2829–2846, doi:[10.5194/tc-11-2829-2017](https://doi.org/10.5194/tc-11-2829-2017).
- 20 Docquier, D. et al., 2019: Impact of model resolution on Arctic sea ice and North Atlantic Ocean heat transport. *Climate*
21 *Dynamics*, **53**(7), 4989–5017, doi:[10.1007/s00382-019-04840-y](https://doi.org/10.1007/s00382-019-04840-y).
- 22 Doddridge, E.W. and J. Marshall, 2017: Modulation of the Seasonal Cycle of Antarctic Sea Ice Extent Related to the
23 Southern Annular Mode. *Geophysical Research Letters*, **44**(19), 9761–9768, doi:[10.1002/2017gl074319](https://doi.org/10.1002/2017gl074319).
- 24 Doddridge, E.W. et al., 2019: Eddy Compensation Dampens Southern Ocean Sea Surface Temperature Response to
25 Westerly Wind Trends. *Geophysical Research Letters*, **46**(8), 4365–4377, doi:[10.1029/2019gl082758](https://doi.org/10.1029/2019gl082758).
- 26 Dodet, G. et al., 2019: The Contribution of Wind-Generated Waves to Coastal Sea-Level Changes. *Surveys in*
27 *Geophysics*, **40**(6), 1563–1601, doi:[10.1007/s10712-019-09557-5](https://doi.org/10.1007/s10712-019-09557-5).
- 28 Doerr, J., D. Notz, and S. Kern, 2021: UHH sea-ice area product, 1850–2019. University of Hamburg, Hamburg,
29 Germany.
- 30 Dolan, A.M. et al., 2011: Sensitivity of Pliocene ice sheets to orbital forcing. *Palaeogeography, Palaeoclimatology,*
31 *Palaeoecology*, **309**(1–2), 98–110, doi:[10.1016/j.palaeo.2011.03.030](https://doi.org/10.1016/j.palaeo.2011.03.030).
- 32 Domine, F., M. Barrere, and D. Sarrazin, 2016: Seasonal evolution of the effective thermal conductivity of the snow
33 and the soil in high Arctic herb tundra at Bylot Island, Canada. *The Cryosphere*, **10**(6), 2573–2588,
34 doi:[10.5194/tc-10-2573-2016](https://doi.org/10.5194/tc-10-2573-2016).
- 35 Domingues, C.M. et al., 2008: Improved estimates of upper-ocean warming and multi-decadal sea-level rise. *Nature*,
36 **453**(7198), 1090–1093, doi:[10.1038/nature07080](https://doi.org/10.1038/nature07080).
- 37 Donat-Magnin, M. et al., 2017: Ice-Shelf Melt Response to Changing Winds and Glacier Dynamics in the Amundsen
38 Sea Sector, Antarctica. *Journal of Geophysical Research: Oceans*, **122**(12), 10206–10224,
39 doi:[10.1002/2017jc013059](https://doi.org/10.1002/2017jc013059).
- 40 Dong, S., M.O. Baringer, and G.J. Goni, 2019: Slow Down of the Gulf Stream during 1993–2016. *Scientific Reports*,
41 **9**(1), 6672, doi:[10.1038/s41598-019-42820-8](https://doi.org/10.1038/s41598-019-42820-8).
- 42 Dotto, T.S. et al., 2018: Variability of the Ross Gyre, Southern Ocean: Drivers and Responses Revealed by Satellite
43 Altimetry. *Geophysical Research Letters*, **45**(12), 6195–6204, doi:[10.1029/2018gl078607](https://doi.org/10.1029/2018gl078607).
- 44 Dotto, T.S. et al., 2019: Wind-Driven Processes Controlling Oceanic Heat Delivery to the Amundsen Sea, Antarctica.
45 *Journal of Physical Oceanography*, **49**(11), 2829–2849, doi:[10.1175/jpo-d-19-0064.1](https://doi.org/10.1175/jpo-d-19-0064.1).
- 46 Dowdeswell, J.A. et al., 2020: Delicate seafloor landforms reveal past Antarctic grounding-line retreat of kilometers per
47 year. *Science*, **368**(6494), 1020–1024, doi:[10.1126/science.aaz3059](https://doi.org/10.1126/science.aaz3059).
- 48 Dowsett, H. et al., 2016: The PRISM4 (mid-Piacenzian) palaeoenvironmental reconstruction. *Climate of the Past*, **12**,
49 1519–1538.
- 50 Drews, R., 2015: Evolution of ice-shelf channels in Antarctic ice shelves. *The Cryosphere*, **9**(3), 1169–1181,
51 doi:[10.5194/tc-9-1169-2015](https://doi.org/10.5194/tc-9-1169-2015).
- 52 Druel, A. et al., 2017: Towards a more detailed representation of high-latitude vegetation in the global land surface
53 model ORCHIDEE (ORC-HL-VEGv1.0). *Geoscientific Model Development*, **10**(12), 4693–4722,
54 doi:[10.5194/gmd-10-4693-2017](https://doi.org/10.5194/gmd-10-4693-2017).

- 1 Du, J., B.A. Haley, and A.C. Mix, 2020: Evolution of the Global Overturning Circulation since the Last Glacial
2 Maximum based on marine authigenic neodymium isotopes. *Quaternary Science Reviews*, **241**, 106396,
3 doi:[10.1016/j.quascirev.2020.106396](https://doi.org/10.1016/j.quascirev.2020.106396).
- 4 Du, Y., Y. Zhang, and J. Shi, 2019: Relationship between sea surface salinity and ocean circulation and climate change.
5 *Science China Earth Sciences*, **62(5)**, 771–782, doi:[10.1007/s11430-018-9276-6](https://doi.org/10.1007/s11430-018-9276-6).
- 6 Dufour, C.O. et al., 2017: Preconditioning of the Weddell Sea Polynya by the Ocean Mesoscale and Dense Water
7 Overflows. *Journal of Climate*, **30(19)**, 7719–7737, doi:[10.1175/jcli-d-16-0586.1](https://doi.org/10.1175/jcli-d-16-0586.1).
- 8 Dukhovskoy, D.S. et al., 2016: Greenland freshwater pathways in the sub-Arctic Seas from model experiments with
9 passive tracers. *Journal of Geophysical Research: Oceans*, **121(1)**, 877–907, doi:[10.1002/2015jc011290](https://doi.org/10.1002/2015jc011290).
- 10 Dukhovskoy, D.S. et al., 2019a: Role of Greenland Freshwater Anomaly in the Recent Freshening of the Subpolar
11 North Atlantic. *Journal of Geophysical Research: Oceans*, **124(5)**, 3333–3360, doi:[10.1029/2018jc014686](https://doi.org/10.1029/2018jc014686).
- 12 Dukhovskoy, D.S. et al., 2019b: Role of Greenland Freshwater Anomaly in the Recent Freshening of the Subpolar
13 North Atlantic. *Journal of Geophysical Research: Oceans*, **124(5)**, 3333–3360, doi:[10.1029/2018jc014686](https://doi.org/10.1029/2018jc014686).
- 14 Dumitru, O.A. et al., 2019: Constraints on global mean sea level during Pliocene warmth. *Nature*, **574(7777)**, 233–236,
15 doi:[10.1038/s41586-019-1543-2](https://doi.org/10.1038/s41586-019-1543-2).
- 16 Dunne, J.P. et al., 2020: The GFDL Earth System Model Version 4.1 (GFDL-ESM 4.1): Overall Coupled Model
17 Description and Simulation Characteristics. *Journal of Advances in Modeling Earth Systems*, **12(11)**,
18 e2019MS002015, doi:[10.1029/2019ms002015](https://doi.org/10.1029/2019ms002015).
- 19 Durack, P., 2015: Ocean Salinity and the Global Water Cycle. *Oceanography*, **28(1)**, 20–31,
20 doi:[10.5670/oceanog.2015.03](https://doi.org/10.5670/oceanog.2015.03).
- 21 Durack, P.J. and S.E. Wijffels, 2010: Fifty-Year trends in global ocean salinities and their relationship to broad-scale
22 warming. *Journal of Climate*, doi:[10.1175/2010jcli3377.1](https://doi.org/10.1175/2010jcli3377.1).
- 23 Durack, P.J., S.E. Wijffels, and P.J. Gleckler, 2014: Long-term sea-level change revisited: The role of salinity.
24 *Environmental Research Letters*, **9(11)**, doi:[10.1088/1748-9326/9/11/114017](https://doi.org/10.1088/1748-9326/9/11/114017).
- 25 Durgadoo, J., B.R. Loveday, C.J.C. Reason, P. Penven, and A. Biastoch, 2013: Agulhas Leakage Predominantly
26 Responds to the Southern Hemisphere Westerlies. *Journal of Physical Oceanography*, **43(10)**, 2113–2131,
27 doi:[10.1175/jpo-d-13-047.1](https://doi.org/10.1175/jpo-d-13-047.1).
- 28 Dussaillant, I. et al., 2019: Two decades of glacier mass loss along the Andes. *Nature Geoscience*, **12(10)**, 802–808,
29 doi:[10.1038/s41561-019-0432-5](https://doi.org/10.1038/s41561-019-0432-5).
- 30 Dutton, A. and K. Lambeck, 2012: Ice Volume and Sea Level During the Last Interglacial. *Science*, **337(6091)**, 216–
31 219, doi:[10.1126/science.1205749](https://doi.org/10.1126/science.1205749).
- 32 Dutton, A., J.M. Webster, D. Zwartz, K. Lambeck, and B. Wohlfarth, 2015: Tropical tales of polar ice: evidence of Last
33 Interglacial polar ice sheet retreat recorded by fossil reefs of the granitic Seychelles islands. *Quaternary
34 Science Reviews*, **107**, 182–196.
- 35 Dziewonski, A.M. and D.L. Anderson, 1981: Preliminary reference Earth model (PREM). *Physics of the Earth and
36 Planetary Interiors*, **25(4)**, 297–356, doi:[10.1016/0031-9201\(81\)90046-7](https://doi.org/10.1016/0031-9201(81)90046-7).
- 37 Eaves, S.R. et al., 2019: Late-glacial and Holocene glacier fluctuations in North Island, New Zealand. *Quaternary
38 Science Reviews*, **223**, 105914, doi:[10.1016/j.quascirev.2019.105914](https://doi.org/10.1016/j.quascirev.2019.105914).
- 39 Echevin, V., K. Goubanova, A. Belmadani, and B. Dewitte, 2012: Sensitivity of the Humboldt Current system to global
40 warming: a downscaling experiment of the IPSL-CM4 model. *Climate Dynamics*, **38(3–4)**, 761–774.
- 41 Edinburgh, T. and J.J. Day, 2016: Estimating the extent of Antarctic summer sea ice during the Heroic Age of Antarctic
42 Exploration. *The Cryosphere*, **10(6)**, 2721–2730, doi:[10.5194/tc-10-2721-2016](https://doi.org/10.5194/tc-10-2721-2016).
- 43 Edwards, T.L. et al., 2019a: Revisiting Antarctic ice loss due to marine ice cliff instability. *Nature*, **566(7742)**.
- 44 Edwards, T.L. et al., 2019b: Revisiting Antarctic ice loss due to marine ice-cliff instability. *Nature*, **566(7742)**, 58–64,
45 doi:[10.1038/s41586-019-0901-4](https://doi.org/10.1038/s41586-019-0901-4).
- 46 Edwards, T.T.L. et al., 2021: Projecting the land ice contribution to sea level rise this century. *Nature*, **in press**.
- 47 Ehlert, D. and K. Zickfeld, 2018a: Irreversible ocean thermal expansion under carbon dioxide removal. *Earth System
48 Dynamics*, **9**, 197–210, doi:[10.5194/esd-9-197-2018](https://doi.org/10.5194/esd-9-197-2018).
- 49 Ehlert, D. and K. Zickfeld, 2018b: Irreversible ocean thermal expansion under carbon dioxide removal. *Earth System
50 Dynamics*, **9**, 197–210, doi:[10.5194/esd-9-197-2018](https://doi.org/10.5194/esd-9-197-2018).
- 51 Eisenman, I., 2012: Factors controlling the bifurcation structure of sea ice retreat. *Journal of Geophysical Research
52 Atmospheres*, **117(1)**, doi:[10.1029/2011jd016164](https://doi.org/10.1029/2011jd016164).
- 53 Ekici, A. et al., 2015: Site-level model intercomparison of high latitude and high altitude soil thermal dynamics in
54 tundra and barren landscapes. *Cryosphere*, **9(4)**, 1343–1361, doi:[10.5194/tc-9-1343-2015](https://doi.org/10.5194/tc-9-1343-2015).
- 55 Elipot, S. and L.M. Beal, 2018: Observed Agulhas Current sensitivity to interannual and long-term trend atmospheric
56 forcings. *Journal of Climate*, JCLI-D-17-0597.1, doi:[10.1175/jcli-d-17-0597.1](https://doi.org/10.1175/jcli-d-17-0597.1).

- 1 Enderlin, E.M., I.M. Howat, and A. Vieli, 2013: High sensitivity of tidewater outlet glacier dynamics to shape. *The*
2 *Cryosphere*, **7(3)**, 1007–1015.
- 3 England, M., A. Jahn, and L. Polvani, 2019: Nonuniform Contribution of Internal Variability to Recent Arctic Sea Ice
4 Loss. *Journal of Climate*, **32(13)**, 4039–4053, doi:[10.1175/jcli-d-18-0864.1](https://doi.org/10.1175/jcli-d-18-0864.1).
- 5 England, M.H. et al., 2014: Recent intensification of wind-driven circulation in the Pacific and the ongoing warming
6 hiatus. *Nature Climate Change*, doi:[10.1038/nclimate2106](https://doi.org/10.1038/nclimate2106).
- 7 England, M.R., L.M. Polvani, K.L. Smith, L. Landrum, and M.M. Holland, 2016: Robust response of the Amundsen
8 Sea Low to stratospheric ozone depletion. *Geophysical Research Letters*, **43(15)**, 8207–8213,
9 doi:[10.1002/2016gl070055](https://doi.org/10.1002/2016gl070055).
- 10 Essery, R., 2015: A factorial snowpack model (FSM 1.0). *Geoscientific Model Development*, **8(12)**, 3867–3876,
11 doi:[10.5194/gmd-8-3867-2015](https://doi.org/10.5194/gmd-8-3867-2015).
- 12 Estilow, T.W., A.H. Young, and D.A. Robinson, 2015: A long-term Northern Hemisphere snow cover extent data
13 record for climate studies and monitoring. *Earth System Science Data*, **7(1)**, 137–142, doi:[10.5194/essd-7-137-](https://doi.org/10.5194/essd-7-137-2015)
14 [2015](https://doi.org/10.5194/essd-7-137-2015).
- 15 Eyring, V. et al., 2016: Overview of the Coupled Model Intercomparison Project Phase 6 (CMIP6) experimental design
16 and organization. *Geoscientific Model Development*, **9(5)**, 1937–1958, doi:[10.5194/gmd-9-1937-2016](https://doi.org/10.5194/gmd-9-1937-2016).
- 17 Fan, T., C. Deser, and D.P. Schneider, 2014: Recent Antarctic sea ice trends in the context of Southern Ocean surface
18 climate variations since 1950. *Geophysical Research Letters*, **41(7)**, 2419–2426, doi:[10.1002/2014gl059239](https://doi.org/10.1002/2014gl059239).
- 19 Farinotti, D., W.W. Immerzeel, R.J. Kok, D.J. Quincey, and A. Dehecq, 2020: Manifestations and mechanisms of the
20 Karakoram glacier Anomaly. *Nature Geoscience*, **13**, 8–16, doi:[10.1038/s41561-019-0513-5](https://doi.org/10.1038/s41561-019-0513-5).
- 21 Farinotti, D. et al., 2019: A consensus estimate for the ice thickness distribution of all glaciers on Earth. *Nature*
22 *Geoscience* 2019, 1, doi:[10.1038/s41561-019-0300-3](https://doi.org/10.1038/s41561-019-0300-3).
- 23 Fasullo, J.T. and R.S. Nerem, 2018: Altimeter-era emergence of the patterns of forced sea-level rise in climate models
24 and implications for the future. *Proceedings of the National Academy of Sciences*, **115(51)**, 12944–12949,
25 doi:[10.1073/pnas.1813233115](https://doi.org/10.1073/pnas.1813233115).
- 26 Fasullo, J.T., R.S. Nerem, and B. Hamlington, 2016: Is the detection of accelerated sea level rise imminent? *Scientific*
27 *Reports*, **6(1)**, 31245, doi:[10.1038/srep31245](https://doi.org/10.1038/srep31245).
- 28 Fasullo, J.T., P.R. Gent, and R. Steven Nerem, 2020: Sea level rise in the CESM large ensemble: The role of individual
29 climate forcings and consequences for the coming decades. *Journal of Climate*, **33(16)**, 6911–6927,
30 doi:[10.1175/jcli-d-19-1001.1](https://doi.org/10.1175/jcli-d-19-1001.1).
- 31 Favier, L. et al., 2014: Retreat of Pine Island Glacier controlled by marine ice-sheet instability. *Nature Climate Change*,
32 **5(2)**, 117–121, doi:[10.1038/nclimate2094](https://doi.org/10.1038/nclimate2094).
- 33 Favier, L. et al., 2019: Assessment of Sub-Shelf Melting Parameterisations Using the Ocean-Ice Sheet Coupled Model
34 NEMO(v3.6)-Elmer/Ice(v8.3). *Geoscientific Model Development*, **12**, 2255–2283, doi:[10.5194/gmd-2019-26](https://doi.org/10.5194/gmd-2019-26).
- 35 Feldmann, J. and A. Levermann, 2015: Collapse of the West Antarctic Ice Sheet after local destabilization of the
36 Amundsen Basin. *Proceedings of the National Academy of Sciences*, **112(46)**, 14191–14196,
37 doi:[10.1073/pnas.1512482112](https://doi.org/10.1073/pnas.1512482112).
- 38 Feldmann, J., A. Levermann, and M. Mengel, 2019: Stabilizing the West Antarctic Ice Sheet by surface mass
39 deposition. *Science advances*, **5(7)**, eaaw4132, doi:[10.1126/sciadv.aaw4132](https://doi.org/10.1126/sciadv.aaw4132).
- 40 Feng, J. et al., 2019: Acceleration of the Extreme Sea Level Rise Along the Chinese Coast. *Earth and Space Science*,
41 **6(10)**, 1942–1956, doi:[10.1029/2019ea000653](https://doi.org/10.1029/2019ea000653).
- 42 Feng, W., M. Zhong, and H.Z. Xu, 2012: Sea level variations in the South China Sea inferred from satellite gravity,
43 altimetry, and oceanographic data. *Science China Earth Sciences*, doi:[10.1007/s11430-012-4394-3](https://doi.org/10.1007/s11430-012-4394-3).
- 44 Ferrari, R. et al., 2014: Antarctic sea ice control on ocean circulation in present and glacial climates. *Proceedings of the*
45 *National Academy of Sciences*, **111(24)**, 8753–8758, doi:[10.1073/pnas.1323922111](https://doi.org/10.1073/pnas.1323922111).
- 46 Fettweis, X. et al., 2013: Estimating the Greenland ice sheet surface mass balance contribution to future sea level rise
47 using the regional atmospheric climate model MAR. *The Cryosphere*, **7(2)**, 469–489, doi:[10.5194/tc-7-469-](https://doi.org/10.5194/tc-7-469-2013)
48 [2013](https://doi.org/10.5194/tc-7-469-2013).
- 49 Fettweis, X. et al., 2020: GrSMBMIP: Intercomparison of the modelled 1980–2012 surface mass balance over the
50 Greenland Ice sheet. *The Cryosphere*, **14**, 3935–3958, doi:[10.5194/tc-14-3935-2020](https://doi.org/10.5194/tc-14-3935-2020).
- 51 Fischer, H. et al., 2018: Palaeoclimate constraints on the impact of 2°C anthropogenic warming and beyond. *Nature*
52 *Geoscience*, **11(7)**, 474–485, doi:[10.1038/s41561-018-0146-0](https://doi.org/10.1038/s41561-018-0146-0).
- 53 Flato, G. et al., 2013: Evaluation of Climate Models. In: *Climate Change 2013: The Physical Science Basis.*
54 *Contribution of Working Group I to the Fifth Assessment Report of the IPCC* [Stocker, T.F., D. Qin, G.-K.
55 Plattner, M. Tignor, S.K. Allen, J. Boschung, A. Nauels, Y. Xia, V. Bex, and P.M. Midgley (eds.)]. Cambridge

- 1 University Press, Cambridge, United Kingdom and New York, USA, pp. 741–866,
2 doi:[10.1017/cbo9781107415324.020](https://doi.org/10.1017/cbo9781107415324.020).
- 3 Forbes, D.L., T.S. James, M. Sutherland, and S.E. Nichols, 2013: Physical basis of coastal adaptation on tropical small
4 islands. *Sustainability Science*, **8**(3), 327–344, doi:[10.1007/s11625-013-0218-4](https://doi.org/10.1007/s11625-013-0218-4).
- 5 Foreman, M.G.G., W. Callendar, D. Masson, J. Morrison, and I. Fine, 2013: A Model Simulation of Future Oceanic
6 Conditions along the British Columbia Continental Shelf. Part II: Results and Analyses. ,
7 doi:[10.1080/07055900.2013.873014](https://doi.org/10.1080/07055900.2013.873014).
- 8 Forsberg, R., L. Sørensen, and S. Simonsen, 2017: Greenland and Antarctica Ice Sheet Mass Changes and Effects on
9 Global Sea Level. *Surveys in Geophysics*, **38**(1), 89–104, doi:[10.1007/s10712-016-9398-7](https://doi.org/10.1007/s10712-016-9398-7).
- 10 Foster, J.L., D.K. Hall, R.E.J. Kelly, and L. Chiu, 2009: Seasonal snow extent and snow mass in South America using
11 SMMR and SSM/I passive microwave data (1979–2006). *Remote Sensing of Environment*, **113**, 291–305,
12 doi:[10.1016/j.rse.2008.09.010](https://doi.org/10.1016/j.rse.2008.09.010).
- 13 Fox-Kemper, B. and J. Pedlosky, 2004: Wind-driven barotropic gyre I: Circulation control by eddy vorticity fluxes to
14 an enhanced removal region. *Journal of Marine Research*, **62**(2), 169–193,
15 doi:[10.1357/002224004774201681](https://doi.org/10.1357/002224004774201681).
- 16 Fox-Kemper, B. et al., 2011: Parameterization of mixed layer eddies. III: Implementation and impact in global ocean
17 climate simulations. *Ocean Modelling*, **39**(1), 61–78, doi:[10.1016/j.ocemod.2010.09.002](https://doi.org/10.1016/j.ocemod.2010.09.002).
- 18 Frederikse, T., K. Simon, C.A. Katsman, and R. Riva, 2017: The sea-level budget along the Northwest Atlantic coast:
19 GIA , mass changes, and large-scale ocean dynamics. *Journal of Geophysical Research: Oceans*, **122**(7),
20 5486–5501, doi:[10.1002/2017jc012699](https://doi.org/10.1002/2017jc012699).
- 21 Frederikse, T. et al., 2016: Closing the sea level budget on a regional scale: Trends and variability on the Northwestern
22 European continental shelf. *Geophysical Research Letters*, **43**(20), 10,864–10,872, doi:[10.1002/2016gl070750](https://doi.org/10.1002/2016gl070750).
- 23 Frederikse, T. et al., 2018: A Consistent Sea-Level Reconstruction and Its Budget on Basin and Global Scales over
24 1958–2014. *Journal of Climate*, **31**(3), 1267–1280, doi:[10.1175/jcli-d-17-0502.1](https://doi.org/10.1175/jcli-d-17-0502.1).
- 25 Frederikse, T. et al., 2020a: Antarctic Ice Sheet and emission scenario controls on 21st-century extreme sea-level
26 changes. *Nature Communications*, **11**(1), 1–11, doi:[10.1038/s41467-019-14049-6](https://doi.org/10.1038/s41467-019-14049-6).
- 27 Frederikse, T. et al., 2020b: The causes of sea-level rise since 1900. *Nature*, **584**(7821), 393–397, doi:[10.1038/s41586-020-2591-3](https://doi.org/10.1038/s41586-020-2591-3).
- 29 Frenger, I., N. Gruber, R. Knutti, and M. Münnich, 2013: Imprint of Southern Ocean eddies on winds, clouds and
30 rainfall. *Nature Geoscience*, **6**(8), 608–612, doi:[10.1038/ngeo1863](https://doi.org/10.1038/ngeo1863).
- 31 Fretwell, P. et al., 2013: Bedmap2: improved ice bed, surface and thickness datasets for Antarctica. *Cryosphere*, **7**(1),
32 375–393, doi:[10.5194/tc-7-375-2013](https://doi.org/10.5194/tc-7-375-2013).
- 33 Fréville, H. et al., 2014: Using MODIS land surface temperatures and the Crocus snow model to understand the warm
34 bias of ERA-Interim reanalyses at the surface in Antarctica. *The Cryosphere*, **8**(4), 1361–1373, doi:[10.5194/tc-8-1361-2014](https://doi.org/10.5194/tc-8-1361-2014).
- 36 Frey, K.E., G.W.K. Moore, L.W. Cooper, and J.M. Grebmeier, 2015: Divergent patterns of recent sea ice cover across
37 the Bering, Chukchi, and Beaufort seas of the Pacific Arctic Region. *Progress in Oceanography*, **136**, 32–49,
38 doi:[10.1016/j.pocean.2015.05.009](https://doi.org/10.1016/j.pocean.2015.05.009).
- 39 Fried, M.J. et al., 2019: Distinct Frontal Ablation Processes Drive Heterogeneous Submarine Terminus Morphology.
40 *Geophysical Research Letters*, **46**, 12083–12091, doi:[10.1029/2019gl083980](https://doi.org/10.1029/2019gl083980).
- 41 Friedman, A.R., G. Reverdin, M. Khodri, and G. Gastineau, 2017: A new record of Atlantic sea surface salinity from
42 1896 to 2013 reveals the signatures of climate variability and long-term trends. *Geophysical Research Letters*,
43 **44**(4), 1866–1876, doi:[10.1002/2017gl072582](https://doi.org/10.1002/2017gl072582).
- 44 Frieler, K. et al., 2015: Consistent evidence of increasing Antarctic accumulation with warming. *Nature Climate
45 Change*, **5**(4), 348–352, doi:[10.1038/nclimate2574](https://doi.org/10.1038/nclimate2574).
- 46 Fringer, O.B., M. Gerritsen, and R.L. Street, 2006: An unstructured-grid, finite-volume, nonhydrostatic, parallel coastal
47 ocean simulator. *Ocean Modelling*, **14**(3–4), 139–173, doi:[10.1016/j.ocemod.2006.03.006](https://doi.org/10.1016/j.ocemod.2006.03.006).
- 48 Frölicher, T.L. and C. Laufkötter, 2018: Emerging risks from marine heat waves. *Nature Communications*, **9**(1), 650,
49 doi:[10.1038/s41467-018-03163-6](https://doi.org/10.1038/s41467-018-03163-6).
- 50 Frölicher, T.L., E.M. Fischer, and N. Gruber, 2018: Marine heatwaves under global warming. *Nature*, **560**(7718), 360–
51 364, doi:[10.1038/s41586-018-0383-9](https://doi.org/10.1038/s41586-018-0383-9).
- 52 Frölicher, T.L. et al., 2015: Dominance of the Southern Ocean in Anthropogenic Carbon and Heat Uptake in CMIP5
53 Models. *Journal of Climate*, **28**(2), 862–886, doi:[10.1175/jcli-d-14-00117.1](https://doi.org/10.1175/jcli-d-14-00117.1).
- 54 Frölicher, T.L. et al., 2020: Contrasting Upper and Deep Ocean Oxygen Response to Protracted Global Warming.
55 *Global Biogeochemical Cycles*, **34**(8), e2020GB006601, doi:[10.1029/2020gb006601](https://doi.org/10.1029/2020gb006601).

- 1 Funder, S. et al., 2011: A 10,000-year record of Arctic Ocean Sea-ice variability – View from the beach. *Science*,
2 **333(6043)**, 747–750, doi:[10.1126/science.1202760](https://doi.org/10.1126/science.1202760).
- 3 Fürst, J.J., H. Goelzer, and P. Huybrechts, 2015: Ice-dynamic projections of the Greenland ice sheet in response to
4 atmospheric and oceanic warming. *The Cryosphere*, **9**, 1039–1062.
- 5 Fürst, J.J. et al., 2016: The safety band of Antarctic ice shelves. *Nature Climate Change*, **6(5)**, 479–482,
6 doi:[10.1038/nclimate2912](https://doi.org/10.1038/nclimate2912).
- 7 Fyke, J., O. Sergienko, M. Löfverström, S. Price, and J.T.M. Lenaerts, 2018: An Overview of Interactions and
8 Feedbacks Between Ice Sheets and the Earth System. *Reviews of Geophysics*, **56**.
- 9 Fyke, J.G. et al., 2011: A new coupled ice sheet/climate model: description and sensitivity to model physics under
10 Eemian, Last Glacial Maximum, late Holocene and modern climate conditions. *Geoscientific Model
11 Development*, **4(1)**, 117–136.
- 12 Gagné, M., N.P. Gillett, and J.C. Fyfe, 2015a: Impact of aerosol emission controls on future Arctic sea ice cover.
13 *Geophysical Research Letters*, **42(20)**, 8481–8488, doi:[10.1002/2015gl065504](https://doi.org/10.1002/2015gl065504).
- 14 Gagné, M., N.P. Gillett, and J.C. Fyfe, 2015b: Observed and simulated changes in Antarctic sea ice extent over the past
15 50 years. *Geophysical Research Letters*, **42(1)**, 90–95, doi:[10.1002/2014gl062231](https://doi.org/10.1002/2014gl062231).
- 16 Gallaher, D.W., G.G. Campbell, and W.N. Meier, 2014: Anomalous Variability in Antarctic Sea Ice Extents During the
17 1960s With the Use of Nimbus Data. *IEEE Journal of Selected Topics in Applied Earth Observations and
18 Remote Sensing*, **7(3)**, 881–887, doi:[10.1109/jstars.2013.2264391](https://doi.org/10.1109/jstars.2013.2264391).
- 19 Gandy, N. et al., 2018: Marine Ice Sheet Instability and Ice Shelf Buttressing Influenced Deglaciation of the Minch Ice
20 Stream, Northwest Scotland. *The Cryosphere*, **12(11)**, 3635–3651, doi:[10.5194/tc-12-3635-2018](https://doi.org/10.5194/tc-12-3635-2018).
- 21 Garbe, J., T. Albrecht, A. Levermann, J.F. Donges, and R. Winkelmann, 2020: The hysteresis of the Antarctic Ice
22 Sheet. *Nature*, **585(7826)**, 538–544, doi:[10.1038/s41586-020-2727-5](https://doi.org/10.1038/s41586-020-2727-5).
- 23 García, D., B.F. Chao, J. Del Río, I. Vigo, and J. García-Lafuente, 2006: On the steric and mass-induced contributions
24 to the annual sea level variations in the Mediterranean Sea. *Journal of Geophysical Research*, **111(C9)**,
25 C09030, doi:[10.1029/2005jc002956](https://doi.org/10.1029/2005jc002956).
- 26 García, J.-L. et al., 2020: 14C and 10Be dated Late Holocene fluctuations of Patagonian glaciers in Torres del Paine
27 (Chile, 51°S) and connections to Antarctic climate change. *Quaternary Science Reviews*, **246**, 106541,
28 doi:[10.1016/j.quascirev.2020.106541](https://doi.org/10.1016/j.quascirev.2020.106541).
- 29 García-Reyes, M. and J. Largier, 2010: Observations of increased wind-driven coastal upwelling off central California.
30 *Journal of Geophysical Research: Oceans*, **115(C4)**, doi:[10.1029/2009jc005576](https://doi.org/10.1029/2009jc005576).
- 31 García-Reyes, M., J.L. Largier, and W.J. Sydeman, 2014: Synoptic-scale upwelling indices and predictions of phyto-
32 and zooplankton populations. *Progress in Oceanography*, **120**, 177–188, doi:[10.1016/j.pocean.2013.08.004](https://doi.org/10.1016/j.pocean.2013.08.004).
- 33 García-Reyes, M. et al., 2013: Relative influence of oceanic and terrestrial pressure systems in driving upwelling-
34 favorable winds. *Geophysical Research Letters*, **40(19)**, 5311–5315, doi:[10.1002/2013gl057729](https://doi.org/10.1002/2013gl057729).
- 35 Gardner, A.S. et al., 2018: Increased West Antarctic and unchanged East Antarctic ice discharge over the last 7 years.
36 *Cryosphere*, **12**, 521–547, doi:[10.5194/tc-12-521-2018](https://doi.org/10.5194/tc-12-521-2018).
- 37 Garner, A.J. et al., 2017: Impact of climate change on New York City’s coastal flood hazard: Increasing flood heights
38 from the preindustrial to 2300 CE. *Proceedings of the National Academy of Sciences of the United States of
39 America*, **114(45)**, doi:[10.1073/pnas.1703568114](https://doi.org/10.1073/pnas.1703568114).
- 40 Garner, A.J. et al., 2018: Evolution of 21 st Century Sea-level Rise Projections. *Earth’s Future*, **6(11)**, 1603–1615,
41 doi:[10.1029/2018ef000991](https://doi.org/10.1029/2018ef000991).
- 42 Garry, F.K. et al., 2019: Model-Derived Uncertainties in Deep Ocean Temperature Trends Between 1990 and 2010.
43 *Journal of Geophysical Research: Oceans*, **124(2)**, 1155–1169, doi:[10.1029/2018jc014225](https://doi.org/10.1029/2018jc014225).
- 44 Garuba, O.A. and B.A. Klinger, 2018: The Role of Individual Surface Flux Components in the Passive and Active
45 Ocean Heat Uptake. *Journal of Climate*, **31(15)**, 6157–6173, doi:[10.1175/jcli-d-17-0452.1](https://doi.org/10.1175/jcli-d-17-0452.1).
- 46 Gasson, E., R.M.R.M. DeConto, D.P.- Geology, U. 2016, and D. Pollard, 2016: Modeling the oxygen isotope
47 composition of the Antarctic ice sheet and its significance to Pliocene sea level. *Geology*, **44(10)**, 827–830,
48 doi:[10.1130/g38104.1](https://doi.org/10.1130/g38104.1).
- 49 Gebbie, G. and P. Huybers, 2019: The Little Ice Age and 20th Century Deep Pacific Cooling. *Science*, **363(6422)**, 70–
50 74, doi:[10.1126/science.aar8413](https://doi.org/10.1126/science.aar8413).
- 51 Gehrels, W.R. and P.L. Woodworth, 2013: When did modern rates of sea-level rise start? *Global and Planetary
52 Change*, **100**, 263–277, doi:[10.1016/j.gloplacha.2012.10.020](https://doi.org/10.1016/j.gloplacha.2012.10.020).
- 53 Geirsdóttir et al., 2019: The onset of neoglaciation in Iceland and the 4.2\,ka event. *Climate of the Past*, **15(1)**, 25–40,
54 doi:[10.5194/cp-15-25-2019](https://doi.org/10.5194/cp-15-25-2019).
- 55 Gemmrich, J., B. Thomas, and R. Bouchard, 2011: Observational changes and trends in northeast Pacific wave records.
56 *Geophysical Research Letters*, doi:[10.1029/2011gl049518](https://doi.org/10.1029/2011gl049518).

- 1 Gibson, C.M. et al., 2018a: Wildfire as a major driver of recent permafrost thaw in boreal peatlands. *Nature*
2 *Communications*, **9**(1), 3041, doi:[10.1038/s41467-018-05457-1](https://doi.org/10.1038/s41467-018-05457-1).
- 3 Gibson, C.M. et al., 2018b: Wildfire as a major driver of recent permafrost thaw in boreal peatlands. *Nature*
4 *Communications*, **9**(1), 3041, doi:[10.1038/s41467-018-05457-1](https://doi.org/10.1038/s41467-018-05457-1).
- 5 Gilbert, G.L., M. Kanevskiy, and J.B. Murton, 2016: Recent Advances (2008–2015) in the Study of Ground Ice and
6 Cryostratigraphy. *Permafrost and Periglacial Processes*, **27**(4), 377–389, doi:[10.1002/ppp.1912](https://doi.org/10.1002/ppp.1912).
- 7 Gilford, D.M. et al., 2020: Could the Last Interglacial Constrain Projections of Future Antarctic Ice Mass Loss and Sea-
8 Level Rise? *Journal of Geophysical Research: Earth Surface*, **125**(10), e2019JF005418,
9 doi:[10.1029/2019jf005418](https://doi.org/10.1029/2019jf005418).
- 10 Giorgi, F. and P. Lionello, 2008: Climate change projections for the Mediterranean region. *Global and Planetary*
11 *Change*, **63**(2–3), 90–104, doi:[10.1016/j.gloplacha.2007.09.005](https://doi.org/10.1016/j.gloplacha.2007.09.005).
- 12 GlaThiDa Consortium, 2019: Glacier Thickness Database 3.0.1. World Glacier Monitoring Service, Zurich,
13 Switzerland.
- 14 Goelzer, H., P. Huybrechts, M.-F.M.-F. Loutre, and T. Fichetef, 2016: Last Interglacial climate and sea-level evolution
15 from a coupled ice sheet-climate model. *Climate of the Past*, **12**(12), 2195–2213, doi:[10.5194/cp-12-2195-](https://doi.org/10.5194/cp-12-2195-2016)
16 [2016](https://doi.org/10.5194/cp-12-2195-2016).
- 17 Goelzer, H. et al., 2013: Sensitivity of Greenland ice sheet projections to model formulations. *Journal of Glaciology*,
18 **59**(216), doi:[10.3189/2013jog12j182](https://doi.org/10.3189/2013jog12j182).
- 19 Goelzer, H. et al., 2018: Design and results of the ice sheet model initialisation experiments initMIP-Greenland: an
20 ISMIP6 intercomparison. *The Cryosphere*, **12**(4), 1433–1460, doi:[10.5194/tc-12-1433-2018](https://doi.org/10.5194/tc-12-1433-2018).
- 21 Goelzer, H. et al., 2020: The future sea-level contribution of the Greenland ice sheet: a multi-model ensemble study of
22 ISMIP6. *The Cryosphere*, **14**, 3071–3096.
- 23 Golaz, J.-C. et al., 2019: The DOE E3SM Coupled Model Version 1: Overview and Evaluation at Standard Resolution.
24 *Journal of Advances in Modeling Earth Systems*, **11**(7), 2089–2129, doi:[10.1029/2018ms001603](https://doi.org/10.1029/2018ms001603).
- 25 Goldberg, D.N., P. Heimbach, I. Joughin, and B. Smith, 2015: Committed retreat of Smith, Pope, and Kohler Glaciers
26 over the next 30 years inferred by transient model calibration. *The Cryosphere*, **9**(6), 2429–2446,
27 doi:[10.5194/tc-9-2429-2015](https://doi.org/10.5194/tc-9-2429-2015).
- 28 Goldberg, D.N., T.A. Smith, S.H.K. Narayanan, and P. Heimbach, 2020: Bathymetric influences on Antarctic ice-shelf
29 melt rates. *Journal of Geophysical Research: Oceans*, 1–39, doi:[10.1029/2020jc016370](https://doi.org/10.1029/2020jc016370).
- 30 Goldberg, D.N., N. Gourmelen, S. Kimura, R. Millan, and K. Snow, 2019: How Accurately Should We Model Ice Shelf
31 Melt Rates? *Geophysical Research Letters*, **46**(1), 189–199, doi:[10.1029/2018gl080383](https://doi.org/10.1029/2018gl080383).
- 32 Golledge, N.R., C.J. Fogwill, A.N. Mackintosh, and K.M. Buckley, 2012: Dynamics of the last glacial maximum
33 Antarctic ice-sheet and its response to ocean forcing. *Proceedings of the National Academy of Sciences of the*
34 *United States of America*, **109**(40), doi:[10.1073/pnas.1205385109](https://doi.org/10.1073/pnas.1205385109).
- 35 Golledge, N.R., R.H. Levy, R.M. McKay, and T.R. Naish, 2017a: East Antarctic ice sheet most vulnerable to Weddell
36 Sea warming. *Geophysical Research Letters*, **44**(5), 2343–2351, doi:[10.1002/2016gl072422](https://doi.org/10.1002/2016gl072422).
- 37 Golledge, N.R. et al., 2013: Glaciology and geological signature of the Last Glacial Maximum Antarctic ice sheet.
38 *Quaternary Science Reviews*, **78**, doi:[10.1016/j.quascirev.2013.08.011](https://doi.org/10.1016/j.quascirev.2013.08.011).
- 39 Golledge, N.R. et al., 2014: Antarctic contribution to meltwater pulse 1A from reduced Southern Ocean overturning.
40 *Nature Communications*, **5**, doi:[10.1038/ncomms6107](https://doi.org/10.1038/ncomms6107).
- 41 Golledge, N.R. et al., 2015: The multi-millennial Antarctic commitment to future sea-level rise. *Nature*, **526**(7573),
42 doi:[10.1038/nature15706](https://doi.org/10.1038/nature15706).
- 43 Golledge, N.R. et al., 2017b: Antarctic climate and ice-sheet configuration during the early Pliocene interglacial at 4.23
44 Ma. *Climate of the Past*, **13**(7), doi:[10.5194/cp-13-959-2017](https://doi.org/10.5194/cp-13-959-2017).
- 45 Golledge, N.R. et al., 2019a: Global environmental consequences of twenty-first-century ice-sheet melt. *Nature*,
46 **566**(7742), doi:[10.1038/s41586-019-0889-9](https://doi.org/10.1038/s41586-019-0889-9).
- 47 Golledge, N.R. et al., 2019b: Global environmental consequences of twenty-first-century ice-sheet melt. *Nature*,
48 **566**(7742), doi:[10.1038/s41586-019-0889-9](https://doi.org/10.1038/s41586-019-0889-9).
- 49 Gomez, N., D. Pollard, and D. Holland, 2015: Sea-level feedback lowers projections of future Antarctic Ice-Sheet mass
50 loss. *Nature Communications*, **6**, 8798.
- 51 Gomez, N., M.E. Weber, P.U. Clark, J.X. Mitrovica, and H.K. Han, 2020: Antarctic ice dynamics amplified by
52 Northern Hemisphere sea-level forcing. *Nature*, **587**(7835), 600–604, doi:[10.1038/s41586-020-2916-2](https://doi.org/10.1038/s41586-020-2916-2).
- 53 Goodwin, P., S. Brown, I.D. Haigh, R.J. Nicholls, and J.M. Matter, 2018: Adjusting Mitigation Pathways to Stabilize
54 Climate at 1.5°C and 2.0°C Rise in Global Temperatures to Year 2300. *Earth's Future*,
55 doi:[10.1002/2017ef000732](https://doi.org/10.1002/2017ef000732).

- 1 Goosse, H. and H. Renssen, 2001: A two-phase response of the Southern Ocean to an increase in greenhouse gas
2 concentrations. *Geophysical Research Letters*, **28(18)**, 3469–3472, doi:[10.1029/2001gl013525](https://doi.org/10.1029/2001gl013525).
- 3 Goosse, H. and V. Zunz, 2014: Decadal trends in the Antarctic sea ice extent ultimately controlled by ice-ocean
4 feedback. *The Cryosphere*, **8(2)**, 453–470, doi:[10.5194/tc-8-453-2014](https://doi.org/10.5194/tc-8-453-2014).
- 5 Goosse, H. et al., 2018: Quantifying climate feedbacks in polar regions. *Nature Communications*, **9(1)**, 1919,
6 doi:[10.1038/s41467-018-04173-0](https://doi.org/10.1038/s41467-018-04173-0).
- 7 Gordon, A.L., B.A. Huber, and E.P. Abrahamsen, 2020: Interannual Variability of the Outflow of Weddell Sea Bottom
8 Water. *Geophysical Research Letters*, **47(4)**, e2020GL087014, doi:[10.1029/2020gl087014](https://doi.org/10.1029/2020gl087014).
- 9 Gorte, T., J.T.M. Lenaerts, and B. Medley, 2020: Scoring Antarctic surface mass balance in climate models to refine
10 future projections. *The Cryosphere*, **14**, 4719–4733, doi:[10.5194/tc-14-4719-2020](https://doi.org/10.5194/tc-14-4719-2020).
- 11 Gottschalk, J. et al., 2016: Biological and physical controls in the Southern Ocean on past millennial-scale atmospheric
12 CO₂ changes. *Nature Communications*, **7**, 11539, doi:[10.1038/ncomms11539](https://doi.org/10.1038/ncomms11539).
- 13 Graham, R.M. et al., 2019: Winter storms accelerate the demise of sea ice in the Atlantic sector of the Arctic Ocean.
14 *Scientific Reports*, **9(1)**, doi:[10.1038/s41598-019-45574-5](https://doi.org/10.1038/s41598-019-45574-5).
- 15 Grant, G.R. et al., 2019: The amplitude and origin of sea-level variability during the Pliocene epoch. *Nature*,
16 doi:[10.1038/s41586-019-1619-z](https://doi.org/10.1038/s41586-019-1619-z).
- 17 Greenberg, D.A., F. Dupont, F.H. Lyard, D.R. Lynch, and F.E. Werner, 2007: Resolution issues in numerical models of
18 oceanic and coastal circulation. *Continental Shelf Research*, **27(9)**, 1317–1343, doi:[10.1016/j.csr.2007.01.023](https://doi.org/10.1016/j.csr.2007.01.023).
- 19 Greene, C.A., D.A. Young, D.E. Gwyther, B.K. Galton-Fenzi, and D.D. Blankenship, 2018: Seasonal dynamics of
20 Totten Ice Shelf controlled by sea ice buttressing. *The Cryosphere*, **12**, 2869–2882, doi:[10.5194/tc-12-2869-](https://doi.org/10.5194/tc-12-2869-2018)
21 [2018](https://doi.org/10.5194/tc-12-2869-2018).
- 22 Greene, C.H. and A.J. Pershing, 2007: Climate Drives Sea Change. *Science*, **315(5815)**, 1084–1085,
23 doi:[10.1126/science.1136495](https://doi.org/10.1126/science.1136495).
- 24 Gregoire, L.J., B. Otto-Bliesner, P.J. Valdes, and R. Ivanovic, 2016: Abrupt Bølling warming and ice saddle collapse
25 contributions to the Meltwater Pulse 1a rapid sea level rise. *Geophysical research letters*, **43(17)**, 9130–9137.
- 26 Gregory, J., S. George, and R. Smith, 2020: Large and irreversible future decline of the Greenland ice-sheet. *The*
27 *Cryosphere*, **14**, 4299–4322, doi:[10.5194/tc-2020-89](https://doi.org/10.5194/tc-2020-89).
- 28 Gregory, J.M. and P. Huybrechts, 2006: Ice-sheet contributions to future sea-level change. *Philosophical Transactions*
29 *of the Royal Society of London, Series A*, **364(1844)**, 1709–1731, doi:[10.1098/rsta.2006.1796](https://doi.org/10.1098/rsta.2006.1796).
- 30 Gregory, J.M., J.A. Lowe, and S.F.B. Tett, 2006: Simulated Global-Mean Sea Level Changes over the Last Half-
31 Millennium. *Journal of Climate*, **19(18)**, 4576–4591, doi:[10.1175/jcli3881.1](https://doi.org/10.1175/jcli3881.1).
- 32 Gregory, J.M. et al., 2002: Recent and future changes in Arctic sea ice simulated by the HadCM3 AOGCM.
33 *Geophysical Research Letters*, **29(24)**, 28–1–28–4, doi:[10.1029/2001gl014575](https://doi.org/10.1029/2001gl014575).
- 34 Gregory, J.M. et al., 2013: Twentieth-century global-mean sea level rise: Is the whole greater than the sum of the parts?
35 *Journal of Climate*, **26(13)**, 4476–4499, doi:[10.1175/jcli-d-12-00319.1](https://doi.org/10.1175/jcli-d-12-00319.1).
- 36 Gregory, J.M. et al., 2016: The Flux-Anomaly-Forced Model Intercomparison Project (FAFMIP) contribution to
37 CMIP6: investigation of sea-level and ocean climate change in response to CO₂ forcing. *Geoscientific Model*
38 *Development*, **9(11)**, 3993–4017, doi:[10.5194/gmd-9-3993-2016](https://doi.org/10.5194/gmd-9-3993-2016).
- 39 Gregory, J.M. et al., 2019: Concepts and Terminology for Sea Level: Mean, Variability and Change, Both Local and
40 Global. *Surveys in Geophysics*, **40(6)**, 1251–1289, doi:[10.1007/s10712-019-09525-z](https://doi.org/10.1007/s10712-019-09525-z).
- 41 Griffies, S.M. et al., 2014: An assessment of global and regional sea level for years 1993–2007 in a suite of interannual
42 CORE-II simulations. *Ocean Modelling*, **78**, 35–89, doi:[10.1016/j.ocemod.2014.03.004](https://doi.org/10.1016/j.ocemod.2014.03.004).
- 43 Griffies, S.M. et al., 2015: Impacts on ocean heat from transient mesoscale eddies in a hierarchy of climate models.
44 *Journal of Climate*, **28(3)**, 952–977, doi:[10.1175/jcli-d-14-00353.1](https://doi.org/10.1175/jcli-d-14-00353.1).
- 45 Grinsted, A., J.C. Moore, and S. Jevrejeva, 2013: Projected Atlantic hurricane surge threat from rising temperatures.
46 *Proceedings of the National Academy of Sciences*, **110(14)**, 5369–5373, doi:[10.1073/pnas.1209980110](https://doi.org/10.1073/pnas.1209980110).
- 47 Grinsted, A., S. Jevrejeva, R.E.M. Riva, and D. Dahl-Jensen, 2015: Sea level rise projections for Northern Europe under
48 RCP8.5. *Climate Research*, **64(1)**, 2015, doi:[10.3354/cr01309](https://doi.org/10.3354/cr01309).
- 49 Gruber, S., 2012: Derivation and analysis of a high-resolution estimate of global permafrost zonation. *The Cryosphere*,
50 **6**, 221–233, doi:[10.5194/tc-6-221-2012](https://doi.org/10.5194/tc-6-221-2012).
- 51 Gudmundsson, G.H., F.S. Paolo, S. Adusumilli, and H.A. Fricker, 2019: Instantaneous Antarctic ice sheet mass loss
52 driven by thinning ice shelves. *Geophysical Research Letters*, **46(23)**, 13903–13909,
53 doi:[10.1029/2019gl085027](https://doi.org/10.1029/2019gl085027).
- 54 Guimberteau, M. et al., 2018: ORCHIDEE-MICT (v8.4.1), a land surface model for the high latitudes: model
55 description and validation. *Geoscientific Model Development*, **11**, 121–163, doi:[10.5194/gmd-11-121-2018](https://doi.org/10.5194/gmd-11-121-2018).

- 1 Günther, F. et al., 2015: Observing Muostakh disappear: Permafrost thaw subsidence and erosion of a ground-ice-rich
2 Island in response to arctic summer warming and sea ice reduction. *Cryosphere*, **9**(1), 151–178,
3 doi:[10.5194/tc-9-151-2015](https://doi.org/10.5194/tc-9-151-2015).
- 4 Gupta, M. and J. Marshall, 2018: The Climate Response to Multiple Volcanic Eruptions Mediated by Ocean Heat
5 Uptake: Damping Processes and Accumulation Potential. *Journal of Climate*, **31**(21), 8669–8687,
6 doi:[10.1175/jcli-d-17-0703.1](https://doi.org/10.1175/jcli-d-17-0703.1).
- 7 Haarsma, R.J. et al., 2016: High Resolution Model Intercomparison Project (HighResMIP v1.0) for CMIP6.
8 *Geoscientific Model Development*, **9**(11), 4185–4208, doi:[10.5194/gmd-9-4185-2016](https://doi.org/10.5194/gmd-9-4185-2016).
- 9 Haas, C. et al., 2017: Ice and Snow Thickness Variability and Change in the High Arctic Ocean Observed by In Situ
10 Measurements. *Geophysical Research Letters*, doi:[10.1002/2017gl075434](https://doi.org/10.1002/2017gl075434).
- 11 Haas, C. et al., 2021: Airborne mapping of the sub-ice platelet layer under fast ice in McMurdo Sound, Antarctica. *The
12 Cryosphere*, **15**(1), 247–264, doi:[10.5194/tc-15-247-2021](https://doi.org/10.5194/tc-15-247-2021).
- 13 Hagemann, S., T. Blome, A. Ekici, and C. Beer, 2016: Soil-frost-enabled soil-moisture-precipitation feedback over
14 northern high latitudes. *Earth System Dynamics*, **7**(3), 611–625, doi:[10.5194/esd-7-611-2016](https://doi.org/10.5194/esd-7-611-2016).
- 15 Hahn, L.C., T. Storelmo, S. Hofer, R. Parfitt, and C.C. Ummenhofer, 2020: Importance of orography for Greenland
16 cloud and melt response to atmospheric blocking. *Journal of Climate*, **33**(10), 4187–4206, doi:[10.1175/jcli-d-
17 19-0527.1](https://doi.org/10.1175/jcli-d-19-0527.1).
- 18 Haigh, I.D. et al., 2019: The Tides They Are a-Changin’: A comprehensive review of past and future non-astronomical
19 changes in tides, their driving mechanisms and future implications. *Reviews of Geophysics*, 2018RG000636,
20 doi:[10.1029/2018rg000636](https://doi.org/10.1029/2018rg000636).
- 21 Haine, T. et al., 2008: North Atlantic Deep Water Formation in the Labrador Sea, Recirculation Through the Subpolar
22 Gyre, and Discharge to the Subtropics. In: *Arctic–Subarctic Ocean Fluxes* [Dickson, R.R., J. Meincke, and P.
23 Rhines (eds.)]. Springer, Dordrecht, The Netherlands, pp. 653–701, doi:[10.1007/978-1-4020-6774-7_28](https://doi.org/10.1007/978-1-4020-6774-7_28).
- 24 Häkkinen, S., P.B. Rhines, and D.L. Worthen, 2016: Warming of the Global Ocean: Spatial Structure and Water-Mass
25 Trends. *Journal of Climate*, **29**(13), 4949–4963, doi:[10.1175/jcli-d-15-0607.1](https://doi.org/10.1175/jcli-d-15-0607.1).
- 26 Hall, B.L., T. Lowell, G.R.M. Bromley, G.H. Denton, and A.E. Putnam, 2019: Holocene glacier fluctuations on the
27 northern flank of Cordillera Darwin, southernmost South America. *Quaternary Science Reviews*, **222**, 105904,
28 doi:[10.1016/j.quascirev.2019.105904](https://doi.org/10.1016/j.quascirev.2019.105904).
- 29 Hallberg, R., A. Adcroft, J.P. Dunne, J.P. Krasting, and R.J. Stouffer, 2013: Sensitivity of Twenty-First-Century
30 Global-Mean Steric Sea Level Rise to Ocean Model Formulation. *Journal of Climate*, **26**(9), 2947–2956,
31 doi:[10.1175/jcli-d-12-00506.1](https://doi.org/10.1175/jcli-d-12-00506.1).
- 32 Halloran, P.R. et al., 2020: Natural drivers of multidecadal Arctic sea ice variability over the last millennium. *Scientific
33 Reports*, **10**(1), 688, doi:[10.1038/s41598-020-57472-2](https://doi.org/10.1038/s41598-020-57472-2).
- 34 Hamlington, B.D., T. Frederikse, R.S. Nerem, J.T. Fasullo, and S. Adhikari, 2020a: Investigating the Acceleration of
35 Regional Sea Level Rise During the Satellite Altimeter Era. *Geophysical Research Letters*, **47**(5),
36 e2019GL086528, doi:[10.1029/2019gl086528](https://doi.org/10.1029/2019gl086528).
- 37 Hamlington, B.D. et al., 2014: Uncovering an anthropogenic sea-level rise signal in the Pacific Ocean. *Nature Clim
38 Change*, **4**(9), 782–785, doi:[10.1038/nclimate2307](https://doi.org/10.1038/nclimate2307).
- 39 Hamlington, B.D. et al., 2020b: Understanding of Contemporary Regional Sea-Level Change and the Implications for
40 the Future. *Reviews of Geophysics*, **58**(3), doi:[10.1029/2019rg000672](https://doi.org/10.1029/2019rg000672).
- 41 Hammond, J.C., F.A. Saavedra, and S.K. Kampf, 2018: Global snow zone maps and trends in snow persistence 2001–
42 2016. *International Journal of Climatology*, **38**, 4369–4383, doi:[10.1002/joc.5674](https://doi.org/10.1002/joc.5674).
- 43 Han, W. et al., 2017: Spatial Patterns of Sea Level Variability Associated with Natural Internal Climate Modes. *Surveys
44 in Geophysics*, **38**(1), 217–250, doi:[10.1007/s10712-016-9386-y](https://doi.org/10.1007/s10712-016-9386-y).
- 45 Hanna, E., X. Fettweis, and R.J. Hall, 2018: Brief communication: Recent changes in summer Greenland blocking
46 captured by none of the CMIP5 models. *The Cryosphere*, **12**(10), 3287–3292, doi:[10.5194/tc-12-3287-2018](https://doi.org/10.5194/tc-12-3287-2018).
- 47 Hanna, E., T.E. Cropper, R.J. Hall, and J. Cappelen, 2016: Greenland Blocking Index 1851–2015: a regional climate
48 change signal. *International Journal of Climatology*, **36**(15), 4847–4861, doi:[10.1002/joc.4673](https://doi.org/10.1002/joc.4673).
- 49 Hanna, E. et al., 2020: Greenland surface air temperature changes from 1981 to 2019 and implications for ice-sheet melt
50 and mass-balance change. *International Journal of Climatology*, 1–17, doi:[10.1002/joc.6771](https://doi.org/10.1002/joc.6771).
- 51 Hansen, B., K.M. Húsgarð Larsen, H. Hátún, and S. Østerhus, 2016: A stable Faroe Bank Channel overflow 1995–
52 2015. *Ocean Science*, **12**(6), 1205–1220, doi:[10.5194/os-12-1205-2016](https://doi.org/10.5194/os-12-1205-2016).
- 53 Harig, C. and F.J. Simons, 2015: Accelerated West Antarctic ice mass loss continues to outpace East Antarctic gains.
54 *Earth and Planetary Science Letters*, **415**, 134–141, doi:[10.1016/j.epsl.2015.01.029](https://doi.org/10.1016/j.epsl.2015.01.029).

- 1 Harning, D.J., Geirsdóttir, and G.H. Miller, 2018: Punctuated Holocene climate of Vestfirðir, Iceland, linked to
2 internal/external variables and oceanographic conditions. *Quaternary Science Reviews*, **189**, 31–42,
3 doi:[10.1016/j.quascirev.2018.04.009](https://doi.org/10.1016/j.quascirev.2018.04.009).
- 4 Harning, D.J., Geirsdóttir, G.H. Miller, and L. Anderson, 2016: Episodic expansion of Drangajökull, Vestfirðir, Iceland,
5 over the last 3 ka culminating in its maximum dimension during the Little Ice Age. *Quaternary Science
6 Reviews*, **152**, 118–131, doi:[10.1016/j.quascirev.2016.10.001](https://doi.org/10.1016/j.quascirev.2016.10.001).
- 7 Harning, D.J. et al., 2019: Sea Ice Control on Winter Subsurface Temperatures of the North Iceland Shelf During the
8 Little Ice Age: A TEX86 Calibration Case Study. *Paleoceanography and Paleoclimatology*, **34(6)**, 1006–1021,
9 doi:[10.1029/2018pa003523](https://doi.org/10.1029/2018pa003523).
- 10 Harrison, S., D.E. Smith, and N.F. Glasser, 2019: Late Quaternary meltwater pulses and sea level change. *Journal of
11 Quaternary Science*, **34(1)**, 1–15, doi:[10.1002/jqs.3070](https://doi.org/10.1002/jqs.3070).
- 12 Harrison, W.D., D.H. Elsberg, K.A. Echelmeyer, and R.M. Krimmel, 2001: On the characterization of glacier response
13 by a single time-scale. *Journal of Glaciology*, **47(159)**, 659–664, doi:[10.3189/172756501781831837](https://doi.org/10.3189/172756501781831837).
- 14 Hartmann, D.L. et al., 2013: Observations: Atmosphere and Surface. In: *Climate Change 2013: the Physical Science
15 Basis. Contribution of Working Group I to the Fifth Assessment Report of the Intergovernmental Panel on
16 Climate Change* [Stocker, T.F., D. Qin, G.-K. Plattner, M. Tignor, S.K. Allen, A. J. Boschung, Nauels, Y. Xia,
17 V. Bex, and P.M. Midgley (eds.)]. Cambridge University Press, Cambridge, United Kingdom and New York,
18 NY, USA, pp. 159–254, doi:[10.1017/cbo9781107415324.008](https://doi.org/10.1017/cbo9781107415324.008).
- 19 Haskins, R.K., K.I.C. Oliver, L.C. Jackson, S.S. Drijfhout, and R.A. Wood, 2019: Explaining asymmetry between
20 weakening and recovery of the AMOC in a coupled climate model. *Climate Dynamics*, **53(1)**, 67–79,
21 doi:[10.1007/s00382-018-4570-z](https://doi.org/10.1007/s00382-018-4570-z).
- 22 Hasselmann, K., 1976: Stochastic climate models Part I. Theory. *Tellus*, **28(6)**, 473–485, doi:[10.1111/j.2153-
23 3490.1976.tb00696.x](https://doi.org/10.1111/j.2153-3490.1976.tb00696.x).
- 24 Hatfield, R.G. et al., 2016: Interglacial responses of the southern Greenland ice sheet over the last 430,000 years
25 determined using particle-size specific magnetic and isotopic tracers. *Earth and Planetary Science Letters*,
26 **454**, 225–236, doi:[10.1016/j.epsl.2016.09.014](https://doi.org/10.1016/j.epsl.2016.09.014).
- 27 Haumann, F.A., D. Notz, and H. Schmidt, 2014: Anthropogenic influence on recent circulation-driven Antarctic sea ice
28 changes. *Geophysical Research Letters*, **41(23)**, 8429–8437, doi:[10.1002/2014gl061659](https://doi.org/10.1002/2014gl061659).
- 29 Haumann, F.A., N. Gruber, and M. Münnich, 2020: Sea-Ice Induced Southern Ocean Subsurface Warming and Surface
30 Cooling in a Warming Climate. *AGU Advances*, **1(2)**, e2019AV000132, doi:[10.1029/2019av000132](https://doi.org/10.1029/2019av000132).
- 31 Haumann, F.A., N. Gruber, M. Münnich, I. Frenger, and S. Kern, 2016: Sea-ice transport driving Southern Ocean
32 salinity and its recent trends. *Nature*, **537(7618)**, 89–92, doi:[10.1038/nature19101](https://doi.org/10.1038/nature19101).
- 33 Hausmann, U. et al., 2020: The Role of Tides in Ocean–Ice Shelf Interactions in the Southwestern Weddell Sea. *Journal
34 of Geophysical Research: Oceans*, **125(6)**, e2019JC015847, doi:[10.1029/2019jc015847](https://doi.org/10.1029/2019jc015847).
- 35 Haustein, K. et al., 2019: A Limited Role for Unforced Internal Variability in Twentieth-Century Warming. *Journal of
36 Climate*, **32(16)**, 4893–4917, doi:[10.1175/jcli-d-18-0555.1](https://doi.org/10.1175/jcli-d-18-0555.1).
- 37 Hawley, W.B., C.C. Hay, J.X. Mitrovica, and R.E. Kopp, 2020: A Spatially Variable Time Series of Sea Level Change
38 Due to Artificial Water Impoundment. *Earth's Future*, e2020EF001497.
- 39 Hayashida, H., R.J. Matear, P.G. Strutton, and X. Zhang, 2020a: Insights into projected changes in marine heatwaves
40 from a high-resolution ocean circulation model. *Nature Communications*, **11(1)**, 4352, doi:[10.1038/s41467-
41 020-18241-x](https://doi.org/10.1038/s41467-020-18241-x).
- 42 Hayashida, H., R.J. Matear, P.G. Strutton, and X. Zhang, 2020b: Insights into projected changes in marine heatwaves
43 from a high-resolution ocean circulation model. *Nature Communications*, **11(1)**, 4352, doi:[10.1038/s41467-
44 020-18241-x](https://doi.org/10.1038/s41467-020-18241-x).
- 45 Hayes, C.T. et al., 2014: A stagnation event in the deep South Atlantic during the last interglacial period. *Science*,
46 **346(6216)**, 1514–1517, doi:[10.1126/science.1256620](https://doi.org/10.1126/science.1256620).
- 47 Hazel, J.E. and A.L. Stewart, 2020: Bistability of the Filchner-Ronne Ice Shelf Cavity Circulation and Basal Melt.
48 *Journal of Geophysical Research: Oceans*, **125(4)**, e2019JC015848, doi:[10.1029/2019jc015848](https://doi.org/10.1029/2019jc015848).
- 49 He, C., Z. Liu, and A. Hu, 2019: The transient response of atmospheric and oceanic heat transports to anthropogenic
50 warming. *Nature Climate Change*, **9(3)**, 222–226, doi:[10.1038/s41558-018-0387-3](https://doi.org/10.1038/s41558-018-0387-3).
- 51 He, C., B. Wu, L. Zou, and T. Zhou, 2017: Responses of the summertime subtropical anticyclones to global warming.
52 *Journal of Climate*, **30(16)**, 6465–6479.
- 53 Hein, A.S. et al., 2016: Mid-Holocene pulse of thinning in the Weddell Sea sector of the West Antarctic ice sheet.
54 *Nature Communications*, **7**, 1–8, doi:[10.1038/ncomms12511](https://doi.org/10.1038/ncomms12511).
- 55 Hellmer, H.H., F. Kauker, R. Timmermann, and T. Hattermann, 2017: The fate of the Southern Weddell sea continental
56 shelf in a warming climate. *Journal of Climate*, **30(12)**, 4337–4350, doi:[10.1175/jcli-d-16-0420.1](https://doi.org/10.1175/jcli-d-16-0420.1).

- 1 Hellmer, H.H., F. Kauker, R. Timmermann, J. Determann, and J. Rae, 2012: Twenty-first-century warming of a large
2 Antarctic ice-shelf cavity by a redirected coastal current. *Nature*, **485(7397)**, 225, doi:[10.1038/nature11064](https://doi.org/10.1038/nature11064).
- 3 Helsen, M.M., W.J. Van De Berg, R.S.W. van de Wal, M.R. van den Broeke, and J. Oerlemans, 2013: Coupled regional
4 climate-ice-sheet simulation shows limited Greenland ice loss during the Eemian. *Climate of the Past*, **9(4)**,
5 1773–1788, doi:[10.5194/cp-9-1773-2013](https://doi.org/10.5194/cp-9-1773-2013).
- 6 Hermans, T.H.J. et al., 2020: Improving sea-level projections on the Northwestern European shelf using dynamical
7 downscaling. *Climate Dynamics*, **54(3)**, 1987–2011, doi:[10.1007/s00382-019-05104-5](https://doi.org/10.1007/s00382-019-05104-5).
- 8 Hermans, T.H.J. et al., 2021: Projecting Global Mean Sea-Level Change Using CMIP6 Models. *Geophysical Research*
9 *Letters*, **48(5)**, doi:[10.1029/2020gl092064](https://doi.org/10.1029/2020gl092064).
- 10 Hernández-Henríquez, M.A., S.J. Déry, and C. Derksen, 2015: Polar amplification and elevation-dependence in trends
11 of Northern Hemisphere snow cover extent, 1971–2014. *Environmental Research Letters*, **10(4)**, 044010,
12 doi:[10.1088/1748-9326/10/4/044010](https://doi.org/10.1088/1748-9326/10/4/044010).
- 13 Herreid, S. and F. Pellicciotti, 2020: The state of rock debris covering Earth’s glaciers. *Nature Geoscience*, **13(9)**, 621–
14 627, doi:[10.1038/s41561-020-0615-0](https://doi.org/10.1038/s41561-020-0615-0).
- 15 Herrington, T. and K. Zickfeld, 2014: Path independence of climate and carbon cycle response over a broad range of
16 cumulative carbon emissions. *Earth System Dynamics*, **5(2)**, 409–422, doi:[10.5194/esd-5-409-2014](https://doi.org/10.5194/esd-5-409-2014).
- 17 Heuzé, C., 2017: North Atlantic deep water formation and AMOC in CMIP5 models. *Ocean Science*, **13(4)**, 609–622,
18 doi:[10.5194/os-13-609-2017](https://doi.org/10.5194/os-13-609-2017).
- 19 Heuzé, C., 2021: Antarctic Bottom Water and North Atlantic Deep Water in CMIP6 models. *Ocean Science*, **17(1)**, 59–
20 90, doi:[10.5194/os-17-59-2021](https://doi.org/10.5194/os-17-59-2021).
- 21 Heuzé, C., K.J. Heywood, D.P. Stevens, and J.K. Ridley, 2015: Changes in Global Ocean Bottom Properties and
22 Volume Transports in CMIP5 Models under Climate Change Scenarios. *Journal of Climate*, **28(8)**, 2917–
23 2944, doi:[10.1175/jcli-d-14-00381.1](https://doi.org/10.1175/jcli-d-14-00381.1).
- 24 Hewitt, H.T. et al., 2017: Will high-resolution global ocean models benefit coupled predictions on short-range to
25 climate timescales? *Ocean Modelling*, **120**, doi:[10.1016/j.ocemod.2017.11.002](https://doi.org/10.1016/j.ocemod.2017.11.002).
- 26 Hewitt, H.T. et al., 2020: Resolving and Parameterising the Ocean Mesoscale in Earth System Models. *Current Climate*
27 *Change Reports*, doi:[10.1007/s40641-020-00164-w](https://doi.org/10.1007/s40641-020-00164-w).
- 28 Hieronymus, M., 2019: An update on the thermosteric sea level rise commitment to global warming. *Environmental*
29 *Research Letters*, **14(5)**, 054018, doi:[10.1088/1748-9326/ab1e31](https://doi.org/10.1088/1748-9326/ab1e31).
- 30 Hirano, D. et al., 2020: Strong ice-ocean interaction beneath Shirase Glacier Tongue in East Antarctica. *Nature*
31 *Communications*, **11(1)**, 4221, doi:[10.1038/s41467-020-17527-4](https://doi.org/10.1038/s41467-020-17527-4).
- 32 Hobbs, W., M.D. Palmer, and D. Monselesan, 2016a: An Energy Conservation Analysis of Ocean Drift in the CMIP5
33 Global Coupled Models. *Journal of Climate*, **29(5)**, 1639–1653, doi:[10.1175/jcli-d-15-0477.1](https://doi.org/10.1175/jcli-d-15-0477.1).
- 34 Hobbs, W., M. Curran, N. Abram, and E.R. Thomas, 2016b: Century-scale perspectives on observed and simulated
35 Southern Ocean sea ice trends from proxy reconstructions. *JOURNAL OF GEOPHYSICAL RESEARCH-*
36 *OCEANS*, **121(10)**, 7804–7818, doi:[10.1002/2016jc012111](https://doi.org/10.1002/2016jc012111).
- 37 Hobbs, W.R., C. Roach, T. Roy, S. Jean-Baptiste, and N. Bindoff, 2020: Anthropogenic temperature and salinity
38 changes in the Southern Ocean. *Journal of Climate*, 1–37, doi:[10.1175/jcli-d-20-0454.1](https://doi.org/10.1175/jcli-d-20-0454.1).
- 39 Hobday, A.J. et al., 2016: A hierarchical approach to defining marine heatwaves. *Progress in Oceanography*, **141**, 227–
40 238, doi:[10.1016/j.pocean.2015.12.014](https://doi.org/10.1016/j.pocean.2015.12.014).
- 41 Hock, R. et al., 2019a: GlacierMIP - A model intercomparison of global-scale glacier mass-balance models and
42 projections. *Journal of Glaciology*, **65(251)**, 453–467.
- 43 Hock, R. et al., 2019b: High Mountain Areas. In: *IPCC Special Report on the Ocean and Cryosphere in a Changing*
44 *Climate* [Pörtner, H.-O., D.C. Roberts, V. Masson-Delmotte, P. Zhai, M. Tignor, E. Poloczanska, K.
45 Mintenbeck, A. Alegría, M. Nicolai, A. Okem, J. Petzold, B. Rama, and N.M. Weyer (eds.)]. In Press, pp.
46 131–202.
- 47 Hoegh-Guldberg, O. et al., 2018: Impacts of 1.5°C Global Warming on Natural and Human Systems. In: *Global*
48 *Warming of 1.5°C. An IPCC Special Report on the impacts of global warming of 1.5°C above pre-industrial*
49 *levels and related global greenhouse gas emission pathways, in the context of strengthening the global*
50 *response to the threat of climate change*, [Masson-Delmotte, V., P. Zhai, H.-O. Pörtner, D. Roberts, J. Skea,
51 P.R. Shukla, A. Pirani, W. Moufouma-Okia, C. Péan, R. Pidcock, S. Connors, J.B.R. Matthews, Y. Chen, X.
52 Zhou, M.I. Gomis, E. Lonnoy, T. Maycock, M. Tignor, and T. Waterfield (eds.)]. In Press, pp. 175–311.
- 53 Hofer, S., A.J. Tedstone, X. Fettweis, and J.L. Bamber, 2017: Decreasing cloud cover drives the recent mass loss on the
54 Greenland Ice Sheet. *Science Advances*, **3(6)**, doi:[10.1126/sciadv.1700584](https://doi.org/10.1126/sciadv.1700584).
- 55 Hofer, S., A.J. Tedstone, X. Fettweis, and J.L. Bamber, 2019: Cloud microphysics and circulation anomalies control
56 differences in future Greenland melt. *Nature Climate Change*, **9(7)**, 523–528, doi:[10.1038/s41558-019-0507-8](https://doi.org/10.1038/s41558-019-0507-8).

- 1 Hofer, S. et al., 2020: Greater Greenland Ice Sheet contribution to global sea level rise in CMIP6. *Nature*
2 *Communications*, **11**(1), 6289, doi:[10.1038/s41467-020-20011-8](https://doi.org/10.1038/s41467-020-20011-8).
- 3 Hoffman, M.J., X. Asay-Davis, S.F. Price, J. Fyke, and M. Perego, 2019: Effect of Subshelf Melt Variability on Sea
4 Level Rise Contribution From Thwaites Glacier, Antarctica. *Journal of Geophysical Research: Earth Surface*,
5 **124**(12), 2798–2822, doi:[10.1029/2019jf005155](https://doi.org/10.1029/2019jf005155).
- 6 Holbrook, N.J. et al., 2019: A global assessment of marine heatwaves and their drivers. *Nature Communications*, **10**(1),
7 2624, doi:[10.1038/s41467-019-10206-z](https://doi.org/10.1038/s41467-019-10206-z).
- 8 Holbrook, N.J. et al., 2020: Keeping pace with marine heatwaves. *Nature Reviews Earth & Environment*, **1**(9), 482–
9 493, doi:[10.1038/s43017-020-0068-4](https://doi.org/10.1038/s43017-020-0068-4).
- 10 Holland, M.M., L. Landrum, Y. Kostov, and J. Marshall, 2017a: Sensitivity of Antarctic sea ice to the Southern
11 Annular Mode in coupled climate models. *CLIMATE DYNAMICS*, **49**(5–6), 1813–1831, doi:[10.1007/s00382-
12 016-3424-9](https://doi.org/10.1007/s00382-016-3424-9).
- 13 Holland, M.M., L. Landrum, M. Raphael, and S. Stammerjohn, 2017b: Springtime winds drive Ross Sea ice variability
14 and change in the following autumn. *NATURE COMMUNICATIONS*, **8**, doi:[10.1038/s41467-017-00820-0](https://doi.org/10.1038/s41467-017-00820-0).
- 15 Holland, M.M., L. Landrum, M.N. Raphael, and R. Kwok, 2018: The regional, seasonal, and lagged influence of the
16 Amundsen Sea Low on Antarctic Sea Ice. *Geophysical Research Letters*, doi:[10.1029/2018gl080140](https://doi.org/10.1029/2018gl080140).
- 17 Holland, P.R., T.J. Bracegirdle, P. Dutrieux, A. Jenkins, and E.J. Steig, 2019: West Antarctic ice loss influenced by
18 internal climate variability and anthropogenic forcing. *Nature Geoscience*, **12**(9), 718–724,
19 doi:[10.1038/s41561-019-0420-9](https://doi.org/10.1038/s41561-019-0420-9).
- 20 Holland, P.R. et al., 2014: Modeled trends in Antarctic sea ice thickness. *Journal of Climate*, **27**(10), 3784–3801,
21 doi:[10.1175/jcli-d-13-00301.1](https://doi.org/10.1175/jcli-d-13-00301.1).
- 22 Holliday, N.P. et al., 2020: Ocean circulation causes the largest freshening event for 120 years in eastern subpolar North
23 Atlantic. *Nature Communications*, **11**(1), 585, doi:[10.1038/s41467-020-14474-y](https://doi.org/10.1038/s41467-020-14474-y).
- 24 Holmes, C.R., P.R. Holland, and T.J. Bracegirdle, 2019: Compensating biases and a noteworthy success in the CMIP5
25 representation of Antarctic sea ice processes. *Geophysical Research Letters*, doi:[10.1029/2018gl081796](https://doi.org/10.1029/2018gl081796).
- 26 Holt, J. et al., 2017: Prospects for improving the representation of coastal and shelf seas in global ocean models.
27 *Geoscientific Model Development*, **10**(1), 499–523, doi:[10.5194/gmd-10-499-2017](https://doi.org/10.5194/gmd-10-499-2017).
- 28 Holt, J. et al., 2018: Climate-Driven Change in the North Atlantic and Arctic Oceans Can Greatly Reduce the
29 Circulation of the North Sea. *Geophysical Research Letters*, **45**(21), 11,827–11,836,
30 doi:[10.1029/2018gl078878](https://doi.org/10.1029/2018gl078878).
- 31 Holte, J., L.D. Talley, J. Gilson, and D. Roemmich, 2017: An Argo mixed layer climatology and database. *Geophysical*
32 *Research Letters*, **44**(11), 5618–5626, doi:[10.1002/2017gl073426](https://doi.org/10.1002/2017gl073426).
- 33 Hong, Y., Y. Du, T. Qu, Y. Zhang, and W. Cai, 2020: Variability of the Subantarctic Mode Water Volume in the South
34 Indian Ocean During 2004–2018. *Geophysical Research Letters*, **47**(10), e2020GL087830,
35 doi:[10.1029/2020gl087830](https://doi.org/10.1029/2020gl087830).
- 36 Hoppmann, M. et al., 2020: Platelet ice, the Southern Ocean’s hidden ice: a review. *Annals of Glaciology*, 1–28, doi:
37 [10.1017/aog.2020.54](https://doi.org/10.1017/aog.2020.54).
- 38 Hori, M. et al., 2017: A 38-year (1978–2015) Northern Hemisphere daily snow cover extent product derived using
39 consistent objective criteria from satellite-borne optical sensors. *Remote Sensing of Environment*, **191**, 402–
40 418, doi:[10.1016/j.rse.2017.01.023](https://doi.org/10.1016/j.rse.2017.01.023).
- 41 Hörner, T., R. Stein, and K. Fahl, 2017: Evidence for Holocene centennial variability in sea ice cover based on
42 IP25 biomarker reconstruction in the southern Kara Sea (Arctic Ocean). *Geo-Marine Letters*, **37**(5), 515–526,
43 doi:[10.1007/s00367-017-0501-y](https://doi.org/10.1007/s00367-017-0501-y).
- 44 Hörner, T., R. Stein, and K. Fahl, 2018: Paleo-sea ice distribution and polynya variability on the Kara Sea shelf during
45 the last 12 ka. *Arktos*, **4**(1), 6, doi:[10.1007/s41063-018-0040-4](https://doi.org/10.1007/s41063-018-0040-4).
- 46 Hörner, T., R. Stein, K. Fahl, and D. Birgel, 2016: Post-glacial variability of sea ice cover, river run-off and biological
47 production in the western Laptev Sea (Arctic Ocean) – A high-resolution biomarker study. *Quaternary Science*
48 *Reviews*, **143**, 133–149, doi:[10.1016/j.quascirev.2016.04.011](https://doi.org/10.1016/j.quascirev.2016.04.011).
- 49 Horton, B.P. et al., 2020: Estimating global mean sea-level rise and its uncertainties by 2100 and 2300 from an expert
50 survey. *npj Climate and Atmospheric Science*, **3**(1), 18, doi:[10.1038/s41612-020-0121-5](https://doi.org/10.1038/s41612-020-0121-5).
- 51 Hosking, J.S., A. Orr, G.J. Marshall, J. Turner, and T. Phillips, 2013: The influence of the Amundsen-Bellinghshausen
52 Aas low on the climate of West Antarctica and its representation in coupled climate model simulations.
53 *Journal of Climate*, **26**(17), 6633–6648, doi:[10.1175/jcli-d-12-00813.1](https://doi.org/10.1175/jcli-d-12-00813.1).
- 54 Hristova, H.G., C. Ladd, and P.J. Stabeno, 2019: Variability and Trends of the Alaska Gyre From Argo and Satellite
55 Altimetry. *Journal of Geophysical Research: Oceans*, **124**(8), 5870–5887, doi:[10.1029/2019jc015231](https://doi.org/10.1029/2019jc015231).

- 1 Hsiao, S.C. et al., 2021: Flood risk influenced by the compound effect of storm surge and rainfall under climate change
2 for low-lying coastal areas. *Science of the Total Environment*, **764**, 144439,
3 doi:[10.1016/j.scitotenv.2020.144439](https://doi.org/10.1016/j.scitotenv.2020.144439).
- 4 Hu, S. et al., 2020: Deep-reaching acceleration of global mean ocean circulation over the past two decades. *Science*
5 *Advances*, **6(6)**, eaax7727, doi:[10.1126/sciadv.aax7727](https://doi.org/10.1126/sciadv.aax7727).
- 6 Huai, B., M.R. van den Broeke, and C.H. Reijmer, 2020: Long-term surface energy balance of the western Greenland
7 ice sheet and the role of large-scale circulation variability. *The Cryosphere*, **14**, 4181–4199, doi:[10.5194/tc-14-4181-2020](https://doi.org/10.5194/tc-14-4181-2020).
- 8
- 9 Huang, B. et al., 2021: Improvements of the Daily Optimum Interpolation Sea Surface Temperature (DOISST) Version
10 2.1. *Journal of Climate*, **34(8)**, 2923–2939, doi:[10.1175/jcli-d-20-0166.1](https://doi.org/10.1175/jcli-d-20-0166.1).
- 11 Huang, H., M. Gutjahr, A. Eisenhauer, and G. Kuhn, 2020: No detectable Weddell Sea Antarctic Bottom Water export
12 during the Last and Penultimate Glacial Maximum. *Nature Communications*, **11(1)**, 424, doi:[10.1038/s41467-020-14302-3](https://doi.org/10.1038/s41467-020-14302-3).
- 13
- 14 Huang, P.P., P. Wu, and H. Steffen, 2019: In search of an ice history that is consistent with composite rheology in
15 Glacial Isostatic Adjustment modelling. *Earth and Planetary Science Letters*, doi:[10.1016/j.epsl.2019.04.011](https://doi.org/10.1016/j.epsl.2019.04.011).
- 16 Huang, P.-Q., Y.-Z. Lu, and S.-Q. Zhou, 2017: An Objective Method for Determining Ocean Mixed Layer Depth with
17 Applications to WOCE Data. *Journal of Atmospheric and Oceanic Technology*, **35(3)**, 441–458,
18 doi:[10.1175/jtech-d-17-0104.1](https://doi.org/10.1175/jtech-d-17-0104.1).
- 19 Huber, M.B. and L. Zanna, 2017: Drivers of uncertainty in simulated ocean circulation and heat uptake. *Geophysical*
20 *Research Letters*, **44(3)**, 1402–1413, doi:[10.1002/2016gl071587](https://doi.org/10.1002/2016gl071587).
- 21 Hughes, C.W. and B.A. de Cuevas, 2001: Why Western Boundary Currents in Realistic Oceans are Inviscid: A Link
22 between Form Stress and Bottom Pressure Torques. *Journal of Physical Oceanography*, **31(10)**, 2871–2885,
23 doi:[10.1175/1520-0485\(2001\)031<2871:wwbcir>2.0.co;2](https://doi.org/10.1175/1520-0485(2001)031<2871:wwbcir>2.0.co;2).
- 24 Hughes, C.W., J. Williams, A. Blaker, A. Coward, and V. Stepanov, 2018: A window on the deep ocean: The special
25 value of ocean bottom pressure for monitoring the large-scale, deep-ocean circulation. *Progress in*
26 *Oceanography*, **161**, 19–46, doi:[10.1016/j.pocean.2018.01.011](https://doi.org/10.1016/j.pocean.2018.01.011).
- 27 Hugonnet, R. et al., 2021: Accelerating global glacier mass loss in the early twenty-first century. *Nature*, **592**, 726–731,
28 doi: [10.1038/s41586-021-03436-z](https://doi.org/10.1038/s41586-021-03436-z)
- 29 Huhn, O. et al., 2018: Basal Melt and Freezing Rates From First Noble Gas Samples Beneath an Ice Shelf. *Geophysical*
30 *Research Letters*, **45(16)**, doi:[10.1029/2018gl079706](https://doi.org/10.1029/2018gl079706).
- 31 Hunter, J., 2010: Estimating sea-level extremes under conditions of uncertain sea-level rise. *Climatic Change*, **99(3)**,
32 331–350, doi:[10.1007/s10584-009-9671-6](https://doi.org/10.1007/s10584-009-9671-6).
- 33 Hunter, J., 2012: A simple technique for estimating an allowance for uncertain sea-level rise. *Climatic Change*, **113(2)**,
34 239–252, doi:[10.1007/s10584-011-0332-1](https://doi.org/10.1007/s10584-011-0332-1).
- 35 Huss, M. and D. Farinotti, 2012: Distributed ice thickness and volume of all glaciers around the globe. *Journal of*
36 *Geophysical Research: Earth Surface*, **117(F4)**, n/a–n/a, doi:[10.1029/2012jf002523](https://doi.org/10.1029/2012jf002523).
- 37 Huss, M. and R. Hock, 2015: A new model for global glacier change and sea-level rise. *Frontiers in Earth Science*, **3**,
38 doi:[10.3389/feart.2015.00054](https://doi.org/10.3389/feart.2015.00054).
- 39 Huss, M. and M. Fischer, 2016: Sensitivity of Very Small Glaciers in the Swiss Alps to Future Climate Change.
40 *Frontiers in Earth Science*, **4**, doi:[10.3389/feart.2016.00034](https://doi.org/10.3389/feart.2016.00034).
- 41 Hyder, P. et al., 2018: Critical Southern Ocean climate model biases traced to atmospheric model cloud errors. *Nature*
42 *Communications*, **9(1)**, 3625, doi:[10.1038/s41467-018-05634-2](https://doi.org/10.1038/s41467-018-05634-2).
- 43 Irvali, N. et al., 2020: A low climate threshold for south Greenland Ice Sheet demise during the Late Pleistocene.
44 *Proceedings of the National Academy of Sciences of the United States of America*, **117(1)**, 190–195,
45 doi:[10.1073/pnas.1911902116](https://doi.org/10.1073/pnas.1911902116).
- 46 Irving, D.B., S. Wijffels, and J.A. Church, 2019: Anthropogenic Aerosols, Greenhouse Gases, and the Uptake,
47 Transport, and Storage of Excess Heat in the Climate System. *Geophysical Research Letters*, **46(9)**, 4894–
48 4903, doi:[10.1029/2019gl082015](https://doi.org/10.1029/2019gl082015).
- 49 Isaev, V.S. et al., 2019: Cliff retreat of permafrost coast in south-west Baydaratskaya Bay, Kara Sea, during 2005–2016.
50 *Permafrost and Periglacial Processes*, **30(1)**, 35–47, doi:[10.1002/ppp.1993](https://doi.org/10.1002/ppp.1993).
- 51 Ishii, M. et al., 2017: Accuracy of Global Upper Ocean Heat Content Estimation Expected from Present Observational
52 Data Sets. *SOLA*, **13(0)**, 163–167, doi:[10.2151/sola.2017-030](https://doi.org/10.2151/sola.2017-030).
- 53 Ivanova, D.P., P.J. Gleckler, K.E. Taylor, P.J. Durack, and K.D. Marvel, 2016: Moving beyond the total sea ice extent
54 in gauging model biases. *Journal of Climate*, doi:[10.1175/jcli-d-16-0026.1](https://doi.org/10.1175/jcli-d-16-0026.1).
- 55 Ivins, E.R. et al., 2013: Antarctic contribution to sea level rise observed by GRACE with improved GIA correction.
56 *Journal of Geophysical Research: Solid Earth*, **118(6)**, 3126–3141, doi:[10.1002/jgrb.50208](https://doi.org/10.1002/jgrb.50208).

- 1 Jaccard, S.L., E.D. Galbraith, A. Martínez-García, and R.F. Anderson, 2016: Covariation of deep Southern Ocean
2 oxygenation and atmospheric CO₂ through the last ice age. *Nature*, **530**, 207.
- 3 Jackson, L.C., 2013: Shutdown and recovery of the AMOC in a coupled global climate model: The role of the advective
4 feedback. *Geophysical Research Letters*, **40(6)**, 1182–1188, doi:[10.1002/grl.50289](https://doi.org/10.1002/grl.50289).
- 5 Jackson, L.C. and R.A. Wood, 2018: Timescales of AMOC decline in response to fresh water forcing. *Climate
6 Dynamics*, doi:[10.1007/s00382-017-3957-6](https://doi.org/10.1007/s00382-017-3957-6).
- 7 Jackson, L.C. and R.A. Wood, 2020: Fingerprints for Early Detection of Changes in the AMOC. *Journal of Climate*,
8 **33(16)**, 7027–7044, doi:[10.1175/jcli-d-20-0034.1](https://doi.org/10.1175/jcli-d-20-0034.1).
- 9 Jackson, L.C., K.A. Peterson, C.D. Roberts, and R.A. Wood, 2016: Recent slowing of Atlantic overturning circulation
10 as a recovery from earlier strengthening. *Nature Geoscience*, **9(7)**, 518–522, doi:[10.1038/ngeo2715](https://doi.org/10.1038/ngeo2715).
- 11 Jackson, L.C. et al., 2019: The Mean State and Variability of the North Atlantic Circulation: A Perspective From Ocean
12 Reanalyses. *Journal of Geophysical Research: Oceans*, **124(12)**, 9141–9170, doi:[10.1029/2019jc015210](https://doi.org/10.1029/2019jc015210).
- 13 Jackson, L.C. et al., 2020: Impact of ocean resolution and mean state on the rate of AMOC weakening. *Climate
14 Dynamics*, doi:[10.1007/s00382-020-05345-9](https://doi.org/10.1007/s00382-020-05345-9).
- 15 Jackson, R.H. et al., 2020: Meltwater Intrusions Reveal Mechanisms for Rapid Submarine Melt at a Tidewater Glacier.
16 *Geophysical Research Letters*, **47(2)**, doi:[10.1029/2019gl085335](https://doi.org/10.1029/2019gl085335).
- 17 Jacox, M.G., C.A. Edwards, E.L. Hazen, and S.J. Bograd, 2018: Coastal Upwelling Revisited: Ekman, Bakun, and
18 Improved Upwelling Indices for the U.S. West Coast. *Journal of Geophysical Research: Oceans*, **123(10)**,
19 7332–7350, doi:[10.1029/2018jc014187](https://doi.org/10.1029/2018jc014187).
- 20 Jahn, A., 2018: Reduced probability of ice-free summers for 1.5°C compared to 2°C warming. *Nature Climate Change*,
21 **8(5)**, 409–413, doi:[10.1038/s41558-018-0127-8](https://doi.org/10.1038/s41558-018-0127-8).
- 22 Jakobsson, M. et al., 2020: The International Bathymetric Chart of the Arctic Ocean Version 4.0. *Scientific Data*, **7(1)**,
23 176, doi:[10.1038/s41597-020-0520-9](https://doi.org/10.1038/s41597-020-0520-9).
- 24 James, M., A.G. Lewkowicz, S.L. Smith, and C.M. Miceli, 2013: Multi-decadal degradation and persistence of
25 permafrost in the Alaska Highway corridor, northwest Canada. *Environmental Research Letters*, **8(4)**, 045013,
26 doi:[10.1088/1748-9326/8/4/045013](https://doi.org/10.1088/1748-9326/8/4/045013).
- 27 Janeković, I. and B. Powell, 2012: Analysis of imposing tidal dynamics to nested numerical models. *Continental Shelf
28 Research*, **34**, 30–40, doi:[10.1016/j.csr.2011.11.017](https://doi.org/10.1016/j.csr.2011.11.017).
- 29 Jay, D.A., 2009: Evolution of tidal amplitudes in the eastern Pacific Ocean. *Geophysical Research Letters*,
30 doi:[10.1029/2008gl036185](https://doi.org/10.1029/2008gl036185).
- 31 Jayne, S.R. et al., 2009: The Kuroshio Extension and its recirculation gyres. *Deep Sea Research Part I: Oceanographic
32 Research Papers*, **56(12)**, 2088–2099, doi:[10.1016/j.dsr.2009.08.006](https://doi.org/10.1016/j.dsr.2009.08.006).
- 33 Jena, B., M. Ravichandran, and J. Turner, 2019: Recent Reoccurrence of Large Open-Ocean Polynya on the Maud Rise
34 Seamount. *Geophysical Research Letters*, **46(8)**, 4320–4329, doi:[10.1029/2018gl081482](https://doi.org/10.1029/2018gl081482).
- 35 Jensen, L., A. Eicker, H. Dobsław, T. Stacke, and V. Humphrey, 2019: Long-term wetting and drying trends in land
36 water storage derived from GRACE and CMIP5 models. *Journal of Geophysical Research: Atmospheres*,
37 **124(17–18)**, 9808–9823, doi:[10.1029/2018jd029989](https://doi.org/10.1029/2018jd029989).
- 38 Jeong, H. et al., 2020: Impacts of Ice-Shelf Melting on Water-Mass Transformation in the Southern Ocean from E3SM
39 Simulations. *Journal of Climate*, **33(13)**, 5787–5807, doi:[10.1175/jcli-d-19-0683.1](https://doi.org/10.1175/jcli-d-19-0683.1).
- 40 Jevrejeva, S., H. Palanisamy, and L.P. Jackson, 2020: Global mean thermosteric sea level projections by 2100 in
41 CMIP6 climate models. *Environmental Research Letters*, **16(1)**, 14028, doi:[10.1088/1748-9326/abceea](https://doi.org/10.1088/1748-9326/abceea).
- 42 Jevrejeva, S. et al., 2019: Probabilistic Sea Level Projections at the Coast by 2100. *Surveys in Geophysics*, **40(6)**, 1673–
43 1696, doi:[10.1007/s10712-019-09550-y](https://doi.org/10.1007/s10712-019-09550-y).
- 44 Ji, T., G. Li, and R. Liu, 2020: Historical Reconstruction of Storm Surge Activity in the Southeastern Coastal Area of
45 China for the Past 60 Years. *Earth and Space Science*, **7(8)**, doi:[10.1029/2019ea001056](https://doi.org/10.1029/2019ea001056).
- 46 Jochum, M. et al., 2013: The Impact of Oceanic Near-Inertial Waves on Climate. *Journal of Climate*, **26(9)**, 2833–
47 2844, doi:[10.1175/jcli-d-12-00181.1](https://doi.org/10.1175/jcli-d-12-00181.1).
- 48 Jochumsen, K. et al., 2017: Revised transport estimates of the Denmark Strait overflow. *Journal of Geophysical
49 Research: Oceans*, **122(4)**, 3434–3450, doi:[10.1002/2017jc012803](https://doi.org/10.1002/2017jc012803).
- 50 Johannessen, O.M., 2008: Decreasing Arctic Sea Ice Mirrors Increasing CO₂ on Decadal Time Scale. *Atmospheric and
51 Oceanic Science Letters*, **1(1)**, 51–56, doi:[10.1080/16742834.2008.11446766](https://doi.org/10.1080/16742834.2008.11446766).
- 52 Jóhannesson, T., C. Raymond, and E. Waddington, 1989: Time-Scale for Adjustment of Glaciers to Changes in Mass
53 Balance. *Journal of Glaciology*, **35(121)**, 355–369, doi:[10.3189/s002214300000928x](https://doi.org/10.3189/s002214300000928x).
- 54 Jóhannesson, T. et al., 2020: Non-surface mass balance of glaciers in Iceland. *Journal of Glaciology*, **66(258)**, 685–697,
55 doi:[10.1017/jog.2020.37](https://doi.org/10.1017/jog.2020.37).

- 1 Johnson, G.C. and J.M. Lyman, 2020: Warming trends increasingly dominate global ocean. *Nature Climate Change*,
2 **10(8)**, 757–761, doi:[10.1038/s41558-020-0822-0](https://doi.org/10.1038/s41558-020-0822-0).
- 3 Johnson, J.S., K.A. Nichols, B.M. Goehring, G. Balco, and J.M. Schaefer, 2019: Abrupt mid-Holocene ice loss in the
4 western Weddell Sea Embayment of Antarctica. *Earth and Planetary Science Letters*, **518**, 127–135,
5 doi:[10.1016/j.epsl.2019.05.002](https://doi.org/10.1016/j.epsl.2019.05.002).
- 6 Jones, B.M. et al., 2015: Recent Arctic tundra fire initiates widespread thermokarst development. *Scientific Reports*,
7 doi:[10.1038/srep15865](https://doi.org/10.1038/srep15865).
- 8 Jones, B.M. et al., 2016: Presence of rapidly degrading permafrost plateaus in south-central Alaska. *The Cryosphere*,
9 **10**, 2673–2692, doi:[10.5194/tc-10-2673-2016](https://doi.org/10.5194/tc-10-2673-2016).
- 10 Jones, J.M. et al., 2016: Assessing recent trends in high-latitude Southern Hemisphere surface climate. *Nature Climate*
11 *Change*, **6**, 917, doi:[10.1038/nclimate3103](https://doi.org/10.1038/nclimate3103).
- 12 Jordà, G., 2014: Detection time for global and regional sea level trends and accelerations. *Journal of Geophysical*
13 *Research: Oceans*, **119(10)**, 7164–7174, doi:[10.1002/2014jc010005](https://doi.org/10.1002/2014jc010005).
- 14 Jorgenson, M.T. and G. Grosse, 2016: Remote Sensing of Landscape Change in Permafrost Regions. *Permafrost and*
15 *Periglacial Processes*, **27(4)**, 324–338, doi:[10.1002/ppp.1914](https://doi.org/10.1002/ppp.1914).
- 16 Josey, S.A., M.F. Jong, M. Oltmanns, G.K. Moore, and R.A. Weller, 2019: Extreme Variability in Irminger Sea Winter
17 Heat Loss Revealed by Ocean Observatories Initiative Mooring and the ERA5 Reanalysis. *Geophysical*
18 *Research Letters*, **46(1)**, 293–302, doi:[10.1029/2018gl080956](https://doi.org/10.1029/2018gl080956).
- 19 Joughin, I., B.E. Smith, and C.G. Schoof, 2019: Regularized Coulomb Friction Laws for Ice Sheet Sliding: Application
20 to Pine Island Glacier, Antarctica. *Geophysical Research Letters*, **46(9)**, 4764–4771,
21 doi:[10.1029/2019gl082526](https://doi.org/10.1029/2019gl082526).
- 22 Joughin, I., D. E. Shean, B. E. Smith, and D. Floricioiu, 2020: A decade of variability on Jakobshavn Isbræ: Ocean
23 temperatures pace speed through influence on mélange rigidity. *Cryosphere*, **14(1)**, 211–227, doi:[10.5194/tc-14-211-2020](https://doi.org/10.5194/tc-14-211-2020).
- 24
25 Jourdain, N.C. et al., 2017: Ocean circulation and sea-ice thinning induced by melting ice shelves in the Amundsen Sea.
26 *JOURNAL OF GEOPHYSICAL RESEARCH-OCEANS*, **122(3)**, 2550–2573, doi:[10.1002/2016jc012509](https://doi.org/10.1002/2016jc012509).
- 27 Jourdain, N.C. et al., 2019: Simulating or prescribing the influence of tides on the Amundsen Sea ice shelves. *Ocean*
28 *Modelling*, **133**, 44–55, doi:[10.1016/j.ocemod.2018.11.001](https://doi.org/10.1016/j.ocemod.2018.11.001).
- 29 Jourdain, N.C. et al., 2020: A protocol for calculating basal melt rates in the ISMIP6 Antarctic ice sheet projections.
30 *The Cryosphere*, **14(9)**, 3111–3134, doi:[10.5194/tc-2019-277](https://doi.org/10.5194/tc-2019-277).
- 31 Jouvett, G. and M. Huss, 2019: Future retreat of Great Aletsch Glacier. *Journal of Glaciology*, **65(253)**, 869–872,
32 doi:[10.1017/jog.2019.52](https://doi.org/10.1017/jog.2019.52).
- 33 Kääb, A. et al., 2018: Massive collapse of two glaciers in western Tibet in 2016 after surge-like instability. *Nature*
34 *Geoscience*, **11(2)**, 114–120, doi:[10.1038/s41561-017-0039-7](https://doi.org/10.1038/s41561-017-0039-7).
- 35 Kachuck, S.B., D.F. Martin, J.N. Bassis, and S.F. Price, 2020: Rapid Viscoelastic Deformation Slows Marine Ice Sheet
36 Instability at Pine Island Glacier. *Geophysical Research Letters*, **47(10)**, 1–12, doi:[10.1029/2019gl086446](https://doi.org/10.1029/2019gl086446).
- 37 Kacimi, S. and R. Kwok, 2020: The Antarctic sea ice cover from ICESat-2 and CryoSat-2: freeboard, snow depth, and
38 ice thickness. *The Cryosphere*, **14(12)**, 4453–4474, doi:[10.5194/tc-14-4453-2020](https://doi.org/10.5194/tc-14-4453-2020).
- 39 Kanevskiy, M. et al., 2013: Ground ice in the upper permafrost of the Beaufort Sea coast of Alaska. *Cold Regions*
40 *Science and Technology*, **85**, 56–70, doi:[10.1016/j.coldregions.2012.08.002](https://doi.org/10.1016/j.coldregions.2012.08.002).
- 41 Kaplan, M.R. et al., 2016: Patagonian and southern South Atlantic view of Holocene climate. *Quaternary Science*
42 *Reviews*, **141**, 112–125, doi:[10.1016/j.quascirev.2016.03.014](https://doi.org/10.1016/j.quascirev.2016.03.014).
- 43 Kaplan, M.R. et al., 2020: Holocene glacier behavior around the northern Antarctic Peninsula and possible causes.
44 *Earth and Planetary Science Letters*, **534**, 116077, doi:[10.1016/j.epsl.2020.116077](https://doi.org/10.1016/j.epsl.2020.116077).
- 45 Karnauskas, K.B., G.C. Johnson, and R. Murtugudde, 2012: An equatorial ocean bottleneck in global climate models.
46 *Journal of Climate*, doi:[10.1175/jcli-d-11-00059.1](https://doi.org/10.1175/jcli-d-11-00059.1).
- 47 Kaspi, Y. and T. Schneider, 2011: Winter cold of eastern continental boundaries induced by warm ocean waters.
48 *Nature*, **471(7340)**, 621–624, doi:[10.1038/nature09924](https://doi.org/10.1038/nature09924).
- 49 Kato, S. et al., 2018: Surface Irradiances of Edition 4.0 Clouds and the Earth’s Radiant Energy System (CERES)
50 Energy Balanced and Filled (EBAF) Data Product. *Journal of Climate*, **31(11)**, 4501–4527, doi:[10.1175/jcli-d-17-0523.1](https://doi.org/10.1175/jcli-d-17-0523.1).
- 51
52 Kaufman, D.S. et al., 2016: Holocene climate changes in eastern Beringia (NW North America) – A systematic review
53 of multi-proxy evidence. *Quaternary Science Reviews*, **147**, 312–339, doi:[10.1016/j.quascirev.2015.10.021](https://doi.org/10.1016/j.quascirev.2015.10.021).
- 54 Kawamata, M. et al., 2020: Abrupt Holocene ice-sheet thinning along the southern Soya Coast, Lützow-Holm Bay, East
55 Antarctica, revealed by glacial geomorphology and surface exposure dating. *Quaternary Science Reviews*, **247**,
56 106540, doi:[10.1016/j.quascirev.2020.106540](https://doi.org/10.1016/j.quascirev.2020.106540).

- 1 Kay, J.E., M.M. Holland, and A. Jahn, 2011: Inter-annual to multi-decadal Arctic sea ice extent trends in a warming
2 world. *Geophysical Research Letters*, **38**(15), doi:[10.1029/2011gl048008](https://doi.org/10.1029/2011gl048008).
- 3 Kay, J.E. et al., 2015: The community earth system model (CESM) large ensemble project: A community resource for
4 studying climate change in the presence of internal climate variability. *Bulletin of the American*
5 *Meteorological Society*, **96**(8), 1333–1349, doi:[10.1175/bams-d-13-00255.1](https://doi.org/10.1175/bams-d-13-00255.1).
- 6 Keen, A. et al., 2021: An inter-comparison of the mass budget of the Arctic sea ice in CMIP6 models. *The Cryosphere*,
7 **15**(2), 951–982, doi:[10.5194/tc-15-951-2021](https://doi.org/10.5194/tc-15-951-2021).
- 8 Kelley, M. et al., 2020: GISS-E2.1: Configurations and Climatology. *Journal of Advances in Modeling Earth Systems*,
9 **12**(8), e2019MS002025, doi:[10.1029/2019ms002025](https://doi.org/10.1029/2019ms002025).
- 10 Kenner, R., L. Pruessner, J. Beutel, P. Limpach, and M. Phillips, 2020: How rock glacier hydrology, deformation
11 velocities and ground temperatures interact: Examples from the Swiss Alps. *Permafrost and Periglacial*
12 *Processes*, **31**(1), 3–14, doi:[10.1002/ppp.2023](https://doi.org/10.1002/ppp.2023).
- 13 Keogh, M.E. and T.E. Törnqvist, 2019: Measuring rates of present-day relative sea-level rise in low-elevation coastal
14 zones: a critical evaluation. *Ocean Science*, **15**(1), 61–73, doi:[10.5194/os-15-61-2019](https://doi.org/10.5194/os-15-61-2019).
- 15 Kern, S. and G. Spreen, 2015: Uncertainties in Antarctic sea-ice thickness retrieval from ICESat. *Annals of Glaciology*,
16 **56**(69), 107–119, doi:[10.3189/2015aog69a736](https://doi.org/10.3189/2015aog69a736).
- 17 Kern, S. et al., 2019: Satellite Passive Microwave Sea-Ice Concentration Data Set Intercomparison: Closed Ice and
18 Ship-Based Observations. *The Cryosphere*, doi:[10.5194/tc-2019-120](https://doi.org/10.5194/tc-2019-120).
- 19 Khan, S.A. et al., 2015: Greenland ice sheet mass balance: a review. *Reports on Progress in Physics*, **78**(4), 46801,
20 doi:[10.1088/0034-4885/78/4/046801](https://doi.org/10.1088/0034-4885/78/4/046801).
- 21 Khan, S.A. et al., 2016: Geodetic measurements reveal similarities between post–Last Glacial Maximum and present-
22 day mass loss from the Greenland ice sheet. *Science Advances*, **2**(9), e1600931, doi:[10.1126/sciadv.1600931](https://doi.org/10.1126/sciadv.1600931).
- 23 Khan, S.A. et al., 2020: Centennial response of Greenland’s three largest outlet glaciers. *Nature Communications*,
24 **11**(1), 5718, doi:[10.1038/s41467-020-19580-5](https://doi.org/10.1038/s41467-020-19580-5).
- 25 Kim, K. et al., 2001: Warming and structural changes in the east (Japan) Sea: A clue to future changes in global oceans?
26 *Geophysical Research Letters*, **28**(17), 3293–3296, doi:[10.1029/2001gl013078](https://doi.org/10.1029/2001gl013078).
- 27 Kim, W.M., S. Yeager, P. Chang, and G. Danabasoglu, 2018: Low-Frequency North Atlantic Climate Variability in the
28 Community Earth System Model Large Ensemble. *Journal of Climate*, **31**(2), 787–813, doi:[10.1175/jcli-d-17-0193.1](https://doi.org/10.1175/jcli-d-17-0193.1).
- 29
30 Kimura, S. et al., 2017: Oceanographic Controls on the Variability of Ice-Shelf Basal Melting and Circulation of
31 Glacial Meltwater in the Amundsen Sea Embayment, Antarctica. *Journal of Geophysical Research: Oceans*,
32 **122**(12), 10131–10155, doi:[10.1002/2017jc012926](https://doi.org/10.1002/2017jc012926).
- 33 Kinar, N.J. and J.W. Pomeroy, 2015: Measurement of the physical properties of the snowpack. *Reviews of Geophysics*,
34 **53**, 481–544, doi:[10.1002/2015rg000481](https://doi.org/10.1002/2015rg000481).
- 35 King, J. et al., 2017: Sea-ice thickness from field measurements in the northwestern Barents Sea. *Journal of*
36 *Geophysical Research: Oceans*, **122**(2), 1497–1512, doi:[10.1002/2016jc012199](https://doi.org/10.1002/2016jc012199).
- 37 King, M.D. et al., 2018: Seasonal to decadal variability in ice discharge from the Greenland Ice Sheet. *The Cryosphere*,
38 **12**(12), 3813–3825, doi:[10.5194/tc-12-3813-2018](https://doi.org/10.5194/tc-12-3813-2018).
- 39 King, M.D. et al., 2020: Dynamic ice loss from the Greenland Ice Sheet driven by sustained glacier retreat.
40 *Communications Earth & Environment*, **1**(1), 1, doi:[10.1038/s43247-020-0001-2](https://doi.org/10.1038/s43247-020-0001-2).
- 41 Kingslake, J. et al., 2018: Extensive retreat and re-advance of the West Antarctic Ice Sheet during the Holocene.
42 *Nature*, **558**(7710), 430–434, doi:[10.1038/s41586-018-0208-x](https://doi.org/10.1038/s41586-018-0208-x).
- 43 Kinnard, C. et al., 2011: Reconstructed changes in Arctic sea ice over the past 1,450 years. *Nature*, **479**(7374), 509–
44 512, doi:[10.1038/nature10581](https://doi.org/10.1038/nature10581).
- 45 Kirezci, E. et al., 2020: Projections of global-scale extreme sea levels and resulting episodic coastal flooding over the
46 21st Century. *Scientific Reports*, **10**(1), 1–12, doi:[10.1038/s41598-020-67736-6](https://doi.org/10.1038/s41598-020-67736-6).
- 47 Kirpotin, S. et al., 2011: West Siberian palsa peatlands: Distribution, typology, cyclic development, present day
48 climate-driven changes, seasonal hydrology and impact on CO₂ cycle. *International Journal of*
49 *Environmental Studies*, **68**(5), 603–623, doi:[10.1080/00207233.2011.593901](https://doi.org/10.1080/00207233.2011.593901).
- 50 Kittel, C. et al., 2021: Diverging future surface mass balance between the Antarctic ice shelves and grounded ice sheet.
51 *The Cryosphere*, **15**(3), 1215–1236, doi:[10.5194/tc-15-1215-2021](https://doi.org/10.5194/tc-15-1215-2021).
- 52 Kjeldsen, K.K. et al., 2015: Spatial and temporal distribution of mass loss from the Greenland Ice Sheet since AD 1900.
53 *Nature*, **528**, 396, doi:[10.1038/nature16183](https://doi.org/10.1038/nature16183).
- 54 Kleinherenbrink, M., R. Riva, and Y. Sun, 2016: Sub-basin-scale sea level budgets from satellite altimetry, Argo floats
55 and satellite gravimetry: A case study in the North Atlantic Ocean. *Ocean Science*, doi:[10.5194/os-12-1179-2016](https://doi.org/10.5194/os-12-1179-2016).
- 56

- 1 Klerk, W.-J., H.C. Winsemius, W.J. Van Verseveld, A.M.R. Bakker, and F.L.M. Diermanse, 2015: The co-occurrence of
2 storm surges and extreme discharges within the Rhine-Meuse Delta. *Environmental Research Letters*, **10**(3),
3 35005.
- 4 Knies, J. et al., 2017: Sea-ice dynamics in an Arctic coastal polynya during the past 6500 years. *Arktos*, **3**(1), 1,
5 doi:[10.1007/s41063-016-0027-y](https://doi.org/10.1007/s41063-016-0027-y).
- 6 Knutz, P.C. et al., 2019: Eleven phases of Greenland Ice Sheet shelf-edge advance over the past 2.7 million years.
7 *Nature Geoscience*, **12**(5), 361–368, doi:[10.1038/s41561-019-0340-8](https://doi.org/10.1038/s41561-019-0340-8).
- 8 Koenig, S.J. et al., 2015: Ice sheet model dependency of the simulated Greenland Ice Sheet in the mid-Pliocene.
9 *Climate of the Past*, **11**, 369–381, doi:[10.5194/cp-11-369-2015](https://doi.org/10.5194/cp-11-369-2015).
- 10 Kohout, A.L., M.J.M. Williams, S.M. Dean, and M.H. Meylan, 2014: Storm-induced sea-ice breakup and the
11 implications for ice extent. *Nature*, **509**(7502), 604–607, doi:[10.1038/nature13262](https://doi.org/10.1038/nature13262).
- 12 Kohyama, T., D.L. Hartmann, and D.S. Battisti, 2017: La Niña-like mean-state response to global warming and
13 potential oceanic roles. *Journal of Climate*, doi:[10.1175/jcli-d-16-0441.1](https://doi.org/10.1175/jcli-d-16-0441.1).
- 14 Kolling, H.M., R. Stein, K. Fahl, K. Perner, and M. Moros, 2018: New insights into sea ice changes over the past 2.2
15 kyr in Disko Bugt, West Greenland. *Arktos*, **4**(1), 11, doi:[10.1007/s41063-018-0045-z](https://doi.org/10.1007/s41063-018-0045-z).
- 16 Kolodziejczyk, N., W. Llovel, and E. Portela, 2019: Interannual Variability of Upper Ocean Water Masses as Inferred
17 From Argo Array. *Journal of Geophysical Research: Oceans*, **124**(8), 6067–6085, doi:[10.1029/2018jc014866](https://doi.org/10.1029/2018jc014866).
- 18 Konikow, L.F., 2011: Contribution of global groundwater depletion since 1900 to sea-level rise. *Geophysical Research
19 Letters*, **38**(17), doi:[10.1029/2011gl048604](https://doi.org/10.1029/2011gl048604).
- 20 Konrad, H. et al., 2018: Net retreat of Antarctic glacier grounding lines. *Nature Geoscience*, **11**(4), 258–262,
21 doi:[10.1038/s41561-018-0082-z](https://doi.org/10.1038/s41561-018-0082-z).
- 22 Kopp, R.E., F.J. Simons, J.X. Mitrovica, A.C. Maloof, and M. Oppenheimer, 2009: Probabilistic assessment of sea
23 level during the last interglacial stage. *Nature*, **462**(7275), doi:[10.1038/nature08686](https://doi.org/10.1038/nature08686).
- 24 Kopp, R.E. et al., 2014: Probabilistic 21st and 22nd century sea-level projections at a global network of tide gauge sites.
25 *Earth's Future*, **2**, 383–406, doi:[10.1002/2014ef000239](https://doi.org/10.1002/2014ef000239).
- 26 Kopp, R.E. et al., 2016: Temperature-driven global sea-level variability in the Common Era. *Proceedings of the
27 National Academy of Sciences*, **113**(11), E1434–E1441, doi:[10.1073/pnas.1517056113](https://doi.org/10.1073/pnas.1517056113).
- 28 Kopp, R.E. et al., 2017: Evolving Understanding of Antarctic Ice-Sheet Physics and Ambiguity in Probabilistic Sea-
29 Level Projections. *Earth's Future*, **5**(12), 1217–1233, doi:[10.1002/2017ef000663](https://doi.org/10.1002/2017ef000663).
- 30 Kornfeld, R.P. et al., 2019: GRACE-FO: The Gravity Recovery and Climate Experiment Follow-On Mission. *Journal
31 of Spacecraft and Rockets*, **56**(3), 931–951, doi:[10.2514/1.a34326](https://doi.org/10.2514/1.a34326).
- 32 Kostov, Y., K.C. Armour, and J. Marshall, 2014: Impact of the Atlantic meridional overturning circulation on ocean
33 heat storage and transient climate change. *Geophysical Research Letters*, **41**(6), 2108–2116,
34 doi:[10.1002/2013gl058998](https://doi.org/10.1002/2013gl058998).
- 35 Kouki, K. et al., 2019: Intercomparison of Snow Melt Onset Date Estimates From Optical and Microwave Satellite
36 Instruments Over the Northern Hemisphere for the Period 1982–2015. *Journal of Geophysical Research:
37 Atmospheres*, **124**(21), 11205–11219, doi:[10.1029/2018jd030197](https://doi.org/10.1029/2018jd030197).
- 38 Koven, C.D., W.J. Riley, and A. Stern, 2013: Analysis of permafrost thermal dynamics and response to climate change
39 in the CMIP5 earth system models. *Journal of Climate*, **26**(6), 1877–1900, doi:[10.1175/jcli-d-12-00228.1](https://doi.org/10.1175/jcli-d-12-00228.1).
- 40 Kraaijenbrink, P.D.A., M.F.P. Bierkens, A.F. Lutz, and W.W. Immerzeel, 2017: Impact of a global temperature rise of
41 1.5 degrees Celsius on Asia's glaciers. *Nature*, **549**(7671), 257–260, doi:[10.1038/nature23878](https://doi.org/10.1038/nature23878).
- 42 Kremer, A. et al., 2018: Changes in sea ice cover and ice sheet extent at the Yermak Plateau during the last 160 ka –
43 Reconstructions from biomarker records. *Quaternary Science Reviews*, **182**, 93–108,
44 doi:[10.1016/j.quascirev.2017.12.016](https://doi.org/10.1016/j.quascirev.2017.12.016).
- 45 Kriegler, E. and H. Held, 2005: Utilizing belief functions for the estimation of future climate change. *International
46 Journal of Approximate Reasoning*, **39**(2), 185–209, doi:[10.1016/j.ijar.2004.10.005](https://doi.org/10.1016/j.ijar.2004.10.005).
- 47 Krug, J., J. Weiss, O. Gagliardini, and G. Durand, 2014: Combining damage and fracture mechanics to model calving.
48 *The Cryosphere*, **8**(6), 2101–2117, doi:[10.5194/tc-8-2101-2014](https://doi.org/10.5194/tc-8-2101-2014).
- 49 Kuhlbrodt, T. and J.M. Gregory, 2012: Ocean heat uptake and its consequences for the magnitude of sea level rise and
50 climate change. *Geophysical Research Letters*, doi:[10.1029/2012gl052952](https://doi.org/10.1029/2012gl052952).
- 51 Kuhlbrodt, T. et al., 2007: On the driving processes of the Atlantic meridional overturning circulation. *Reviews of
52 Geophysics*, **45**(2), RG2001, doi:[10.1029/2004rg000166](https://doi.org/10.1029/2004rg000166).
- 53 Kumar, P., S.K. Min, E. Weller, H. Lee, and X.L. Wang, 2016: Influence of climate variability on extreme ocean
54 surface wave heights assessed from ERA-interim and ERA-20C. *Journal of Climate*, doi:[10.1175/jcli-d-15-0580.1](https://doi.org/10.1175/jcli-d-15-0580.1).
- 55

- 1 Kunkel, K.E. et al., 2016: Trends and Extremes in Northern Hemisphere Snow Characteristics. *Current Climate Change*
2 *Reports*, **2**, 65–73, doi:[10.1007/s40641-016-0036-8](https://doi.org/10.1007/s40641-016-0036-8).
- 3 Kuntz, L.B. and D.P. Schrag, 2020: Representation of the Equatorial Undercurrent in CMIP5 Models. *Journal of*
4 *Physical Oceanography*, **50(10)**, 2997–3007, doi:[10.1175/jpo-d-20-0007.1](https://doi.org/10.1175/jpo-d-20-0007.1).
- 5 Kurtz, N.T. and T. Markus, 2012: Satellite observations of Antarctic sea ice thickness and volume. *Journal of*
6 *Geophysical Research: Oceans*, **117(C8)**, C08025, doi:[10.1029/2012jc008141](https://doi.org/10.1029/2012jc008141).
- 7 Kusahara, K., G.D. Williams, R. Massom, P. Reid, and H. Hasumi, 2019: Spatiotemporal dependence of Antarctic sea
8 ice variability to dynamic and thermodynamic forcing: a coupled ocean–sea ice model study. *Climate*
9 *Dynamics*, **52(7)**, 3791–3807, doi:[10.1007/s00382-018-4348-3](https://doi.org/10.1007/s00382-018-4348-3).
- 10 Kusahara, K., D. Hirano, M. Fujii, A. Fraser, and T. Tamura, 2021: Modeling intensive ocean–cryosphere interactions
11 in Lützow-Holm Bay, East Antarctica. *The Cryosphere*, **in press**, doi:[10.5194/tc-2020-240](https://doi.org/10.5194/tc-2020-240).
- 12 Kwiatkowski, L. et al., 2020: Twenty-first century ocean warming, acidification, deoxygenation, and upper-ocean
13 nutrient and primary production decline from CMIP6 model projections. *Biogeosciences*, **17(13)**, 3439–3470,
14 doi:[10.5194/bg-17-3439-2020](https://doi.org/10.5194/bg-17-3439-2020).
- 15 Kwok, R., 2018: Arctic sea ice thickness, volume, and multiyear ice coverage: Losses and coupled variability (1958–
16 2018). *Environmental Research Letters*, **13(10)**, 105005, doi:[10.1088/1748-9326/aae3ec](https://doi.org/10.1088/1748-9326/aae3ec).
- 17 Kwok, R. and G.F. Cunningham, 2015: Variability of Arctic sea ice thickness and volume from CryoSat-2.
18 *Philosophical Transactions of the Royal Society A: Mathematical, Physical and Engineering Sciences*,
19 **373(2045)**, 20140157, doi:[10.1098/rsta.2014.0157](https://doi.org/10.1098/rsta.2014.0157).
- 20 Kwok, R. and S. Kacimi, 2018: Three years of sea ice freeboard, snow depth, and ice thickness of the weddell sea from
21 operation icebridge and cryosat-2. *Cryosphere*, doi:[10.5194/tc-12-2789-2018](https://doi.org/10.5194/tc-12-2789-2018).
- 22 Kwok, R., J.C. Comiso, T. Lee, and P.R. Holland, 2016: Linked trends in the South Pacific sea ice edge and Southern
23 Oscillation Index. *Geophysical Research Letters*, **43(19)**, 10,210–295,302, doi:[10.1002/2016gl070655](https://doi.org/10.1002/2016gl070655).
- 24 Lafaysse, M. et al., 2017: A multiphysical ensemble system of numerical snow modelling. *The Cryosphere*, **11**, 1173–
25 1198, doi:[10.5194/tc-11-1173-2017](https://doi.org/10.5194/tc-11-1173-2017).
- 26 Lago, V. and M.H. England, 2019: Projected Slowdown of Antarctic Bottom Water Formation in Response to
27 Amplified Meltwater Contributions. *Journal of Climate*, **32(19)**, 6319–6335, doi:[10.1175/jcli-d-18-0622.1](https://doi.org/10.1175/jcli-d-18-0622.1).
- 28 Laliberté, F., S.E.L. Howell, and P.J. Kushner, 2016: Regional variability of a projected sea ice-free Arctic during the
29 summer months. *Geophysical Research Letters*, **43(1)**, 256–263, doi:[10.1002/2015gl066855](https://doi.org/10.1002/2015gl066855).
- 30 Laliberté, F., S.E.L. Howell, J.-F. Lemieux, F. Dupont, and J. Lei, 2018: What historical landfast ice observations tell
31 us about projected ice conditions in Arctic archipelagoes and marginal seas under anthropogenic forcing. *The*
32 *Cryosphere*, **12(11)**, 3577–3588, doi:[10.5194/tc-12-3577-2018](https://doi.org/10.5194/tc-12-3577-2018).
- 33 Lambeck, K., H. Rouby, A. Purcell, Y. Sun, and M. Sambridge, 2014: Sea level and global ice volumes from the Last
34 Glacial Maximum to the Holocene. *Proceedings of the National Academy of Sciences*, 201411762,
35 doi:[10.1073/pnas.1411762111](https://doi.org/10.1073/pnas.1411762111).
- 36 Lambert, E., J. Rohmer, G. Le Cozannet, and R.S.W. van de Wal, 2020: Adaptation time to magnified flood hazards
37 underestimated when derived from tide gauge records. *Environmental Research Letters*, **15(7)**, 074015,
38 doi:[10.1088/1748-9326/ab8336](https://doi.org/10.1088/1748-9326/ab8336).
- 39 Lamont, T., M. García-Reyes, S.J. Bograd, C.D. van der Lingen, and W.J. Sydeman, 2018: Upwelling indices for
40 comparative ecosystem studies: Variability in the Benguela Upwelling System. *Journal of Marine Systems*,
41 **188**, 3–16, doi:[10.1016/j.jmarsys.2017.05.007](https://doi.org/10.1016/j.jmarsys.2017.05.007).
- 42 Lamping, N. et al., 2020: Highly branched isoprenoids reveal onset of deglaciation followed by dynamic sea-ice
43 conditions in the western Amundsen Sea, Antarctica. *Quaternary Science Reviews*, **228**, 106103,
44 doi:[10.1016/j.quascirev.2019.106103](https://doi.org/10.1016/j.quascirev.2019.106103).
- 45 Lamy, F. et al., 2015: Glacial reduction and millennial-scale variations in Drake Passage throughflow. *Proceedings of*
46 *the National Academy of Sciences*, **112(44)**, 13496–13501, doi:[10.1073/pnas.1509203112](https://doi.org/10.1073/pnas.1509203112).
- 47 Landais, A. et al., 2016: How warm was Greenland during the last interglacial period? *Climate of the Past*, **12(9)**, 1933–
48 1948, doi:[10.5194/cp-12-1933-2016](https://doi.org/10.5194/cp-12-1933-2016).
- 49 Landerer, F.W., J.H. Jungclauss, and J. Marotzke, 2007: Regional Dynamic and Steric Sea Level Change in Response to
50 the IPCC-A1B Scenario. *Journal of Physical Oceanography*, **37(2)**, 296–312, doi:[10.1175/jpo3013.1](https://doi.org/10.1175/jpo3013.1).
- 51 Landrum, L.L., M.M. Holland, M.N. Raphael, and L.M. Polvani, 2017: Stratospheric Ozone Depletion: An Unlikely
52 Driver of the Regional Trends in Antarctic Sea Ice in Austral Fall in the Late Twentieth Century. *Geophysical*
53 *Research Letters*, **44(21)**, 11,062–11,070, doi:[10.1002/2017gl075618](https://doi.org/10.1002/2017gl075618).
- 54 Larocca, L.J., Y. Axford, S.A. Woodroffe, G.E. Lasher, and B. Gawin, 2020: Holocene glacier and ice cap fluctuations
55 in southwest Greenland inferred from two lake records. *Quaternary Science Reviews*, **246**, 106529,
56 doi:[10.1016/j.quascirev.2020.106529](https://doi.org/10.1016/j.quascirev.2020.106529).

- 1 Larour, E., E.R. Ivins, and S. Adhikari, 2017: Should coastal planners have concern over where land ice is melting?
2 *Science Advances*, **3(11)**, e1700537, doi:[10.1126/sciadv.1700537](https://doi.org/10.1126/sciadv.1700537).
- 3 Larour, E., J. Utke, A. Bovin, M. Morlighem, and G. Perez, 2016: An approach to computing discrete adjoints for MPI-
4 parallelized models applied to Ice Sheet System Model 4.11. *Geoscientific Model Development*, **9(11)**, 3907–
5 3918, doi:[10.5194/gmd-9-3907-2016](https://doi.org/10.5194/gmd-9-3907-2016).
- 6 Larour, E. et al., 2014: Inferred basal friction and surface mass balance of the Northeast Greenland Ice Stream using
7 data assimilation of ICESat (Ice Cloud and land Elevation Satellite) surface altimetry and ISSM (Ice Sheet
8 System Model). *The Cryosphere*, **8(6)**, 2335–2351, doi:[10.5194/tc-8-2335-2014](https://doi.org/10.5194/tc-8-2335-2014).
- 9 Larsen, N.K. et al., 2015: The response of the southern Greenland ice sheet to the Holocene thermal maximum.
10 *Geology*, **43(4)**, 291–294.
- 11 Larsen, N.K. et al., 2019: Local ice caps in Finderup Land, North Greenland, survived the Holocene Thermal
12 Maximum. *Boreas*, **48(3)**, 551–562, doi:[10.1111/bor.12384](https://doi.org/10.1111/bor.12384).
- 13 Larson, E.J.L., R.W. Portmann, S. Solomon, and D.M. Murphy, 2020: Decadal Attribution of Historic Temperature and
14 Ocean Heat Content Change to Anthropogenic Emissions. *Geophysical Research Letters*, **47(3)**,
15 e2019GL085905, doi:[10.1029/2019gl085905](https://doi.org/10.1029/2019gl085905).
- 16 Laufkötter, C., J. Zscheischler, and T.L. Frölicher, 2020: High-impact marine heatwaves attributable to human-induced
17 global warming. *Science*, **369(6511)**, 1621–1625, doi:[10.1126/science.aba0690](https://doi.org/10.1126/science.aba0690).
- 18 Laverge, T. et al., 2019: Version 2 of the EUMETSAT OSI SAF and ESA CCI sea-ice concentration climate data
19 records. *The Cryosphere*, **13(1)**, 49–78, doi:[10.5194/tc-13-49-2019](https://doi.org/10.5194/tc-13-49-2019).
- 20 Lawrence, D.M., A.G. Slater, V.E. Romanovsky, and D.J. Nicolsky, 2008: Sensitivity of a model projection of near-
21 surface permafrost degradation to soil column depth and representation of soil organic matter. *Journal of*
22 *Geophysical Research: Earth Surface*, **113(2)**, doi:[10.1029/2007jf000883](https://doi.org/10.1029/2007jf000883).
- 23 Lazeroms, W.M.J., A. Jenkins, G. Hilmar Gudmundsson, and R.S.W. Van De Wal, 2018: Modelling present-day basal
24 melt rates for Antarctic ice shelves using a parametrization of buoyant meltwater plumes. *Cryosphere*,
25 doi:[10.5194/tc-12-49-2018](https://doi.org/10.5194/tc-12-49-2018).
- 26 Le Bars, D., S. Drijfhout, and H. De Vries, 2017: A high-end sea level rise probabilistic projection including rapid
27 Antarctic ice sheet mass loss. *Environmental Research Letters*, **12(4)**, doi:[10.1088/1748-9326/aa6512](https://doi.org/10.1088/1748-9326/aa6512).
- 28 Le clec'h, S. et al., 2019: Assessment of the Greenland ice sheet–atmosphere feedbacks for the next century with a
29 regional atmospheric model coupled to an ice sheet model. *The Cryosphere*, **13(1)**, 373–395, doi:[10.5194/tc-13-373-2019](https://doi.org/10.5194/tc-13-373-2019).
- 31 Le Cozannet, G., J.C. Manceau, and J. Rohmer, 2017: Bounding probabilistic sea-level projections within the
32 framework of the possibility theory. *Environmental Research Letters*, doi:[10.1088/1748-9326/aa5528](https://doi.org/10.1088/1748-9326/aa5528).
- 33 Le Cozannet, G. et al., 2019: Quantifying uncertainties of sandy shoreline change projections as sea level rises.
34 *Scientific Reports*, **9(1)**, 42, doi:[10.1038/s41598-018-37017-4](https://doi.org/10.1038/s41598-018-37017-4).
- 35 Lea, J.M. et al., 2014: Terminus-driven retreat of a major southwest Greenland tidewater glacier during the early 19th
36 century: insights from glacier reconstructions and numerical modelling. *Journal of Glaciology*, **60(220)**, 333–
37 344, doi:[10.3189/2014jog13j163](https://doi.org/10.3189/2014jog13j163).
- 38 Lecavalier, B.S. et al., 2014: A model of Greenland ice sheet deglaciation constrained by observations of relative sea
39 level and ice extent. *Quaternary Science Reviews*, **102**, 54–84, doi:[10.1016/j.quascirev.2014.07.018](https://doi.org/10.1016/j.quascirev.2014.07.018).
- 40 Lecavalier, B.S. et al., 2017: High Arctic Holocene temperature record from the Agassiz ice cap and Greenland ice
41 sheet evolution. *Proceedings of the National Academy of Sciences*, doi:[10.1016/j.phpro.2012.10.059](https://doi.org/10.1016/j.phpro.2012.10.059).
- 42 Leclercq, P.W., J. Oerlemans, and J.G. Cogley, 2011: Estimating the Glacier Contribution to Sea-Level Rise for the
43 Period 1800–2005. *Surveys in Geophysics*, **32(4–5)**, 519–535, doi:[10.1007/s10712-011-9121-7](https://doi.org/10.1007/s10712-011-9121-7).
- 44 Lecomte, O. et al., 2017: Vertical ocean heat redistribution sustaining sea-ice concentration trends in the Ross Sea.
45 *NATURE COMMUNICATIONS*, **8**, doi:[10.1038/s41467-017-00347-4](https://doi.org/10.1038/s41467-017-00347-4).
- 46 Lee, B.S., M. Haran, and K. Keller, 2017: Multidecadal Scale Detection Time for Potentially Increasing Atlantic Storm
47 Surges in a Warming Climate. *Geophysical Research Letters*, **44(20)**, 6106–6117, doi:[10.1002/2017gl074606](https://doi.org/10.1002/2017gl074606).
- 48 Lee, H., S.C. Swenson, A.G. Slater, and D.M. Lawrence, 2014: Effects of excess ground ice on projections of
49 permafrost in a warming climate. *Environmental Research Letters*, **9(12)**, 124006, doi:[10.1088/1748-9326/9/12/124006](https://doi.org/10.1088/1748-9326/9/12/124006).
- 50 Lee, V., S.L. Cornford, and A.J. Payne, 2015: Initialization of an ice-sheet model for present-day Greenland. *Annals of*
51 *Glaciology*, **56(70)**, 129–140, doi:[10.3189/2015aog70a121](https://doi.org/10.3189/2015aog70a121).
- 52 Lenaerts, J.T.M. et al., 2015: Representing Greenland ice sheet freshwater fluxes in climate models. *Geophysical*
53 *Research Letters*, **42**, 6373–6381, doi:[10.1002/2015gl064738](https://doi.org/10.1002/2015gl064738).

- 1 Lenaerts, J.T.M. et al., 2017: Meltwater produced by wind-albedo interaction stored in an East Antarctic ice shelf.
2 *Nature Climate Change*, **7**(1), 58–62, doi:[10.1038/nclimate3180](https://doi.org/10.1038/nclimate3180).
- 3 Letcher, T.W. and J.R. Minder, 2015: Characterization of the simulated regional snow albedo feedback using a regional
4 climate model over complex terrain. *Journal of Climate*, **28**(19), 7576–7595, doi:[10.1175/jcli-d-15-0166.1](https://doi.org/10.1175/jcli-d-15-0166.1).
- 5 Lettenmaier, D.P. and P.C.D. Milly, 2009: Land waters and sea level. *Nature Geoscience*, doi:[10.1038/ngeo567](https://doi.org/10.1038/ngeo567).
- 6 Levang, S.J. and R.W. Schmitt, 2020: Intergyre Salt Transport in the Climate Warming Response. *Journal of Physical
7 Oceanography*, **50**(1), 255–268, doi:[10.1175/jpo-d-19-0166.1](https://doi.org/10.1175/jpo-d-19-0166.1).
- 8 Levermann, A. and R. Winkelmann, 2016: A simple equation for the melt elevation feedback of ice sheets. *Cryosphere*,
9 **10**(4), 1799–1807, doi:[10.5194/tc-10-1799-2016](https://doi.org/10.5194/tc-10-1799-2016).
- 10 Levermann, A. et al., 2013: The multimillennial sea-level commitment of global warming.. *Proceedings of the National
11 Academy of Sciences of the United States of America*, **110**(34), 13745–50, doi:[10.1073/pnas.1219414110](https://doi.org/10.1073/pnas.1219414110).
- 12 Levermann, A. et al., 2014: Projecting Antarctic ice discharge using response functions from SeaRISE ice-sheet
13 models. *Earth System Dynamics*, **5**(2), 271–293, doi:[10.5194/esd-5-271-2014](https://doi.org/10.5194/esd-5-271-2014).
- 14 Levermann, A. et al., 2020a: Projecting Antarctica’s contribution to future sea level rise from basal ice shelf melt using
15 linear response functions of 16 ice sheet models (LARMIP-2). *Earth System Dynamics*, **11**(1), 35–76,
16 doi:[10.5194/esd-11-35-2020](https://doi.org/10.5194/esd-11-35-2020).
- 17 Levermann, A. et al., 2020b: Projecting Antarctica’s contribution to future sea level rise from basal ice shelf melt using
18 linear response functions of 16 ice sheet models (LARMIP-2). *Earth System Dynamics*, **11**, 35–76,
19 doi:[10.5194/esd-11-35-2020](https://doi.org/10.5194/esd-11-35-2020).
- 20 Levitus, S. et al., 2012: World ocean heat content and thermosteric sea level change (0–2000 m), 1955–2010.
21 *Geophysical Research Letters*, **39**(10), n/a–n/a, doi:[10.1029/2012gl051106](https://doi.org/10.1029/2012gl051106).
- 22 Levy, R.H. et al., 2019: Antarctic ice-sheet sensitivity to obliquity forcing enhanced through ocean connections. *Nature
23 Geoscience*, **12**(2), 132–137, doi:[10.1038/s41561-018-0284-4](https://doi.org/10.1038/s41561-018-0284-4).
- 24 Lewis, M.J. et al., 2019: Wave-tide interaction modulates nearshore wave height. *Ocean Dynamics*,
25 doi:[10.1007/s10236-018-01245-z](https://doi.org/10.1007/s10236-018-01245-z).
- 26 Li, C., D. Notz, S. Tietsche, and J. Marotzke, 2013: The transient versus the equilibrium response of sea ice to global
27 warming. *Journal of Climate*, **26**(15), 5624–5636, doi:[10.1175/jcli-d-12-00492.1](https://doi.org/10.1175/jcli-d-12-00492.1).
- 28 Li, G. et al., 2019: Examining the salinity change in the upper Pacific Ocean during the Argo period. *Climate
29 Dynamics*, **53**(9), 6055–6074, doi:[10.1007/s00382-019-04912-z](https://doi.org/10.1007/s00382-019-04912-z).
- 30 Li, G. et al., 2020: Increasing ocean stratification over the past half-century. *Nature Climate Change*,
31 doi:[10.1038/s41558-020-00918-2](https://doi.org/10.1038/s41558-020-00918-2).
- 32 Li, J.-L.F. et al., 2020: An Overview of CMIP5 and CMIP6 Simulated Cloud Ice, Radiation Fields, Surface Wind
33 Stress, Sea Surface Temperatures, and Precipitation Over Tropical and Subtropical Oceans. *Journal of
34 Geophysical Research: Atmospheres*, **125**(15), e2020JD032848, doi:[10.1029/2020jd032848](https://doi.org/10.1029/2020jd032848).
- 35 Li, Q. and B. Fox-Kemper, 2017: Assessing the effects of Langmuir turbulence on the entrainment buoyancy flux in the
36 ocean surface boundary layer. *Journal of Physical Oceanography*, **47**(12), 2863–2886, doi:[10.1175/jpo-d-17-0085.1](https://doi.org/10.1175/jpo-d-17-0085.1).
- 37
38 Li, Q. et al., 2016: Langmuir mixing effects on global climate: WAVEWATCH III in CESM. *Ocean Modelling*, **103**,
39 145–160, doi:[10.1016/j.ocemod.2015.07.020](https://doi.org/10.1016/j.ocemod.2015.07.020).
- 40 Li, Q. et al., 2019: Comparing Ocean Surface Boundary Vertical Mixing Schemes Including Langmuir Turbulence.
41 *Journal of Advances in Modeling Earth Systems*, **11**(11), 3545–3592, doi:[10.1029/2019ms001810](https://doi.org/10.1029/2019ms001810).
- 42 Li, T. et al., 2020: Uncertainties of Glacial Isostatic Adjustment Model Predictions in North America Associated With
43 3D Structure. *Geophysical Research Letters*, doi:[10.1029/2020gl087944](https://doi.org/10.1029/2020gl087944).
- 44 Li, X., D.M. Holland, E.P. Gerber, and C. Yoo, 2014: Impacts of the north and tropical Atlantic Ocean on the Antarctic
45 Peninsula and sea ice. *Nature*, **505**(7484), 538–542, doi:[10.1038/nature12945](https://doi.org/10.1038/nature12945).
- 46 Li, X., E. Rignot, J. Mouginot, and B. Scheuchl, 2016: Ice flow dynamics and mass loss of Totten Glacier, East
47 Antarctica, from 1989 to 2015. *Geophysical Research Letters*, **43**(12), 6366–6373, doi:[10.1002/2016gl069173](https://doi.org/10.1002/2016gl069173).
- 48 Li, Y., G. Ren, Q. Wang, and Q. You, 2019: More extreme marine heatwaves in the China Seas during the global
49 warming hiatus. *Environmental Research Letters*, **14**(10), 104010, doi:[10.1088/1748-9326/ab28bc](https://doi.org/10.1088/1748-9326/ab28bc).
- 50 Lin, N., K. Emanuel, M. Oppenheimer, and E. Vanmarcke, 2012: Physically based assessment of hurricane surge threat
51 under climate change. *Nature Climate Change*, **2**(6), 462, doi:[10.1038/nclimate1389](https://doi.org/10.1038/nclimate1389).
- 52 Lin, N., P. Lane, K.A. Emanuel, R.M. Sullivan, and J.P. Donnelly, 2014: Heightened hurricane surge risk in northwest
53 Florida revealed from climatological-hydrodynamic modeling and paleorecord reconstruction. *Journal of
54 Geophysical Research: Atmospheres*, **119**(14), 8606–8623, doi:[10.1002/2014jd021584](https://doi.org/10.1002/2014jd021584).
- 55 Lindstrom, E., F. Bryan, and R. Schmitt, 2015: SPURS: Salinity Processes in the Upper-ocean Regional Study – The
56 North Atlantic Experiment. *Oceanography*, **28**(1), 14–19, doi:[10.5670/oceanog.2015.01](https://doi.org/10.5670/oceanog.2015.01).

- 1 Linz, M., E. Tziperman, and D.G. MacMartin, 2014: Process-based analysis of climate model ENSO simulations:
2 Intermodel consistency and compensating errors. *Journal of Geophysical Research: Atmospheres*, **119**(12),
3 7396–7409, doi:[10.1002/2013jd021415](https://doi.org/10.1002/2013jd021415).
- 4 Lipscomb, W.H. et al., 2013: Implementation and Initial Evaluation of the Glimmer Community Ice Sheet Model in the
5 Community Earth System Model. *Journal of Climate*, **26**(19), 7352–7371, doi:[10.1175/jcli-d-12-00557.1](https://doi.org/10.1175/jcli-d-12-00557.1).
- 6 Lipscomb, W.H. et al., 2021: ISMIP6-based projections of ocean-forced Antarctic Ice Sheet evolution using the
7 Community Ice Sheet Model. *The Cryosphere*, **15**, 633–661, doi:[10.5194/tc-15-633-2021](https://doi.org/10.5194/tc-15-633-2021).
- 8 Lique, C., H.L. Johnson, and Y. Plancherel, 2018a: Emergence of deep convection in the Arctic Ocean under a warming
9 climate. *Climate Dynamics*, **50**(9), 3833–3847, doi:[10.1007/s00382-017-3849-9](https://doi.org/10.1007/s00382-017-3849-9).
- 10 Lique, C., H.L. Johnson, and Y. Plancherel, 2018b: Emergence of deep convection in the Arctic Ocean under a
11 warming climate. *Climate Dynamics*, **50**(9), 3833–3847, doi:[10.1007/s00382-017-3849-9](https://doi.org/10.1007/s00382-017-3849-9).
- 12 Liston, G.E. and C.A. Hiemstra, 2011: The changing cryosphere: Pan-Arctic snow trends (1979–2009). *Journal of*
13 *Climate*, **24**(21), 5691–5712, doi:[10.1175/jcli-d-11-00081.1](https://doi.org/10.1175/jcli-d-11-00081.1).
- 14 Little, C.M., A. Gnanadesikan, and M. Oppenheimer, 2009: How ice shelf morphology controls basal melting. *Journal*
15 *of Geophysical Research: Oceans*, **114**(C12), doi:[10.1029/2008jc005197](https://doi.org/10.1029/2008jc005197).
- 16 Little, C.M. et al., 2015: Joint projections of US East Coast sea level and storm surge. *Nature Climate Change*,
17 doi:[10.1038/nclimate2801](https://doi.org/10.1038/nclimate2801).
- 18 Little, C.M. et al., 2019: The Relationship Between U.S. East Coast Sea Level and the Atlantic Meridional Overturning
19 Circulation: A Review. *Journal of Geophysical Research: Oceans*, **124**(9), 6435–6458,
20 doi:[10.1029/2019jc015152](https://doi.org/10.1029/2019jc015152).
- 21 Liu, C., X. Liang, R.M. Ponte, N. Vinogradova, and O. Wang, 2019: Vertical redistribution of salt and layered changes
22 in global ocean salinity. *Nature Communications*, **10**(1), 3445, doi:[10.1038/s41467-019-11436-x](https://doi.org/10.1038/s41467-019-11436-x).
- 23 Liu, J., G.A. Milne, R.E. Kopp, P.U. Clark, and I. Shennan, 2016: Sea-level constraints on the amplitude and source
24 distribution of Meltwater Pulse 1A. *Nature Geoscience*, doi:[10.1038/ngeo2616](https://doi.org/10.1038/ngeo2616).
- 25 Liu, L. et al., 2021: Permafrost sensitivity to global warming of 1.5°C and 2°C in the Northern Hemisphere.
26 *Environmental Research Letters*, **16**(3), 034038, doi:[10.1088/1748-9326/abd6a8](https://doi.org/10.1088/1748-9326/abd6a8).
- 27 Liu, W. and Z. Liu, 2013: A Diagnostic Indicator of the Stability of the Atlantic Meridional Overturning Circulation in
28 CCSM3. *J. Climate*, **26**, 1926–1938, doi:[10.1175/jcli-d-11-00681.1](https://doi.org/10.1175/jcli-d-11-00681.1).
- 29 Liu, W., J. Lu, and S.-P. Xie, 2018: Southern Ocean Heat Uptake, Redistribution, and Storage in a Warming Climate:
30 The Role of Meridional Overturning Circulation. *Journal of Climate*, **31**, 4727–4743, doi:[10.1175/jcli-d-17](https://doi.org/10.1175/jcli-d-17).
- 31 Liu, W., S.P. Xie, Z. Liu, and J. Zhu, 2017: Overlooked possibility of a collapsed atlantic meridional overturning
32 circulation in warming climate. *Science Advances*, **3**(1), doi:[10.1126/sciadv.1601666](https://doi.org/10.1126/sciadv.1601666).
- 33 Llovel, W. et al., 2018: Contributions of Atmospheric Forcing and Chaotic Ocean Variability to Regional Sea Level
34 Trends Over 1993–2015. *Geophysical Research Letters*, **45**(24), 13,405–13,413, doi:[10.1029/2018gl080838](https://doi.org/10.1029/2018gl080838).
- 35 Lo, L. et al., 2018: Precession and atmospheric CO2 modulated variability of sea ice in the central Okhotsk Sea since
36 130,000 years ago. *Earth and Planetary Science Letters*, **488**, 36–45, doi:[10.1016/j.epsl.2018.02.005](https://doi.org/10.1016/j.epsl.2018.02.005).
- 37 Lohmann, J. and P.D. Ditlevsen, 2021: Risk of tipping the overturning circulation due to increasing rates of ice melt.
38 *Proceedings of the National Academy of Sciences*, **118**(9), e2017989118, doi:[10.1073/pnas.2017989118](https://doi.org/10.1073/pnas.2017989118).
- 39 López-Moreno, J.I. et al., 2020: Long-term trends (1958–2017) in snow cover duration and depth in the Pyrenees.
40 *International Journal of Climatology*, doi:[10.1002/joc.6571](https://doi.org/10.1002/joc.6571).
- 41 Loranty, M.M., L.T. Berner, S.J. Goetz, Y. Jin, and J.T. Randerson, 2014: Vegetation controls on northern high latitude
42 snow-albedo feedback: Observations and CMIP5 model simulations. *Global Change Biology*, **20**(2), 594–606,
43 doi:[10.1111/gcb.12391](https://doi.org/10.1111/gcb.12391).
- 44 Love, R. et al., 2016: The contribution of glacial isostatic adjustment to projections of sea-level change along the
45 Atlantic and Gulf coasts of North America. *Earth's Future*, **4**(10), 440–464, doi:[10.1002/2016ef000363](https://doi.org/10.1002/2016ef000363).
- 46 Loveday, B.R., P. Penven, and C.J.C. Reason, 2015: Southern Annular Mode and westerly-wind-driven changes in
47 Indian-Atlantic exchange mechanisms. *Geophysical Research Letters*, doi:[10.1002/2015gl064256](https://doi.org/10.1002/2015gl064256).
- 48 Lowe, J.A. and J.M. Gregory, 2006: Understanding projections of sea level rise in a Hadley Centre coupled climate
49 model. *Journal of Geophysical Research*, **111**(C11), C11014, doi:[10.1029/2005jc003421](https://doi.org/10.1029/2005jc003421).
- 50 Löwe, H., F. Riche, and M. Schneebeli, 2013: A general treatment of snow microstructure exemplified by an improved
51 relation for thermal conductivity. *Cryosphere*, **7**(5), 1473–1480, doi:[10.5194/tc-7-1473-2013](https://doi.org/10.5194/tc-7-1473-2013).
- 52 Lowell, T. et al., 2013: Late Holocene expansion of Istorvet ice cap, Liverpool Land, east Greenland. *Quaternary*
53 *Science Reviews*, **63**, 128–140, doi:[10.1016/j.quascirev.2012.11.012](https://doi.org/10.1016/j.quascirev.2012.11.012).
- 54 Lowry, D.P. et al., 2020: Geologic controls on ice sheet sensitivity to deglacial climate forcing in the Ross Embayment,
55 Antarctica. *Quaternary Science Advances*, **1**, 100002, doi:[10.1016/j.qsa.2020.100002](https://doi.org/10.1016/j.qsa.2020.100002).

- 1 Lozier, M.S. et al., 2019: A sea change in our view of overturning in the subpolar North Atlantic. *Science*, **363(6426)**,
2 516–521, doi:[10.1126/science.aau6592](https://doi.org/10.1126/science.aau6592).
- 3 Lozier, S.M. et al., 2017: Overturning in the Subpolar North Atlantic Program: a new international ocean observing
4 system. *Bulletin of the American Meteorological Society*, **98(4)**, 737–752.
- 5 Lübbecke, J.F., J. Durgadoo, and A. Biastoch, 2015: Contribution of increased agulhas leakage to tropical Atlantic
6 warming. *Journal of Climate*, doi:[10.1175/jcli-d-15-0258.1](https://doi.org/10.1175/jcli-d-15-0258.1).
- 7 Luckman, B.H., B.J.R. Sperling, and G.D. Osborn, 2020: The Holocene history of the Columbia Icefield, Canada.
8 *Quaternary Science Reviews*, **242**, 106436, doi:[10.1016/j.quascirev.2020.106436](https://doi.org/10.1016/j.quascirev.2020.106436).
- 9 Luo, Y. and L.M. Rothstein, 2011: Response of the Pacific Ocean Circulation to Climate Change. *Atmosphere-Ocean*,
10 **49(3)**, 235–244, doi:[10.1080/07055900.2011.602325](https://doi.org/10.1080/07055900.2011.602325).
- 11 Lüthi, M.P., 2009: Transient response of idealized glaciers to climate variations. *Journal of Glaciology*, **55(193)**, 918–
12 930, doi:[10.3189/002214309790152519](https://doi.org/10.3189/002214309790152519).
- 13 Lüthi, M.P. and A. Bauder, 2010: Analysis of Alpine glacier length change records with a macroscopic glacier model.
14 *Geographica Helvetica*, **65(2)**, 92–102, doi:[10.5194/gh-65-92-2010](https://doi.org/10.5194/gh-65-92-2010).
- 15 Lüthi, M.P., A. Bauder, and M. Funk, 2010: Volume change reconstruction of Swiss glaciers from length change data.
16 *Journal of Geophysical Research*, **115(F4)**, F04022, doi:[10.1029/2010jf001695](https://doi.org/10.1029/2010jf001695).
- 17 Lüthi, M.P. et al., 2016: A century of geometry and velocity evolution at Ekip Sermia, West Greenland. *Journal of*
18 *Glaciology*, **62(234)**, 640–654, doi:[10.1017/jog.2016.38](https://doi.org/10.1017/jog.2016.38).
- 19 Lyu, K., X. Zhang, and J.A. Church, 2020a: Regional Dynamic Sea Level Simulated in the CMIP5 and CMIP6 Models:
20 Mean Biases, Future Projections, and Their Linkages. *Journal of Climate*, **33(15)**, 6377–6398,
21 doi:[10.1175/jcli-d-19-1029.1](https://doi.org/10.1175/jcli-d-19-1029.1).
- 22 Lyu, K., X. Zhang, J.A. Church, and Q. Wu, 2020b: Processes Responsible for the Southern Hemisphere Ocean Heat
23 Uptake and Redistribution under Anthropogenic Warming. *Journal of Climate*, **33(9)**, 3787–3807,
24 doi:[10.1175/jcli-d-19-0478.1](https://doi.org/10.1175/jcli-d-19-0478.1).
- 25 Lyu, K., X. Zhang, J.A. Church, A.B.A. Slangen, and J. Hu, 2014: Time of emergence for regional sea-level change.
26 *Nature Climate Change*, **4**, 1006–1010, doi:[10.1038/nclimate2397](https://doi.org/10.1038/nclimate2397).
- 27 Ma, X. et al., 2016: Western boundary currents regulated by interaction between ocean eddies and the atmosphere.
28 *Nature*, **535(7613)**, 533–537, doi:[10.1038/nature18640](https://doi.org/10.1038/nature18640).
- 29 Ma, Y. and J.N. Bassis, 2019: The Effect of Submarine Melting on Calving From Marine Terminating Glaciers. *Journal*
30 *of Geophysical Research: Earth Surface*, **124**, 334–346, doi:[10.1029/2018jf004820](https://doi.org/10.1029/2018jf004820).
- 31 MacFerrin, M. et al., 2019: Rapid expansion of Greenland’s low-permeability ice slabs. *Nature*, **573(7774)**, 403–407,
32 doi:[10.1038/s41586-019-1550-3](https://doi.org/10.1038/s41586-019-1550-3).
- 33 Machguth, H. et al., 2016: Greenland meltwater storage in firn limited by near-surface ice formation. *Nature Climate*
34 *Change*, **6**, 390, doi:[10.1038/nclimate2899](https://doi.org/10.1038/nclimate2899).
- 35 Mackie, S., I.J. Smith, J.K. Ridley, D.P. Stevens, and P.J. Langhorne, 2020: Climate response to increasing Antarctic
36 iceberg and ice shelf melt. *Journal of Climate*, **33(20)**, 8917–8938, doi:[10.1175/jcli-d-19-0881.1](https://doi.org/10.1175/jcli-d-19-0881.1).
- 37 Mackintosh, A. et al., 2011: Retreat of the East Antarctic ice sheet during the last glacial termination. *Nature*
38 *Geoscience*, **4(3)**, 195–202, doi:[10.1038/ngeo1061](https://doi.org/10.1038/ngeo1061).
- 39 Magalhães, N., H. Evangelista, T. Condom, A. Rabatel, and P. Ginot, 2019: Amazonian Biomass Burning Enhances
40 Tropical Andean Glaciers Melting. *Scientific Reports*, **9(1)**, 16914, doi:[10.1038/s41598-019-53284-1](https://doi.org/10.1038/s41598-019-53284-1).
- 41 Mak, J., D.P. Marshall, J.R. Maddison, and S.D. Bachman, 2017: Emergent eddy saturation from an energy constrained
42 eddy parameterisation. *Ocean Modelling*, **112**, 125–138, doi:[10.1016/j.ocemod.2017.02.007](https://doi.org/10.1016/j.ocemod.2017.02.007).
- 43 Maksym, T., 2019: Arctic and Antarctic Sea Ice Change: Contrasts, Commonalities, and Causes. *Annual Review of*
44 *Marine Science*, **11(1)**, 187–213, doi:[10.1146/annurev-marine-010816-060610](https://doi.org/10.1146/annurev-marine-010816-060610).
- 45 Maksym, T. and T. Markus, 2008: Antarctic sea ice thickness and snow-to-ice conversion from atmospheric reanalysis
46 and passive microwave snow depth. *Journal of Geophysical Research*, **113(2)**, C02S12,
47 doi:[10.1029/2006jc004085](https://doi.org/10.1029/2006jc004085).
- 48 Malyarenko, A. et al., 2020: A synthesis of thermodynamic ablation at ice–ocean interfaces from theory, observations
49 and models. *Ocean Modelling*, **154**, 101692, doi:[10.1016/j.ocemod.2020.101692](https://doi.org/10.1016/j.ocemod.2020.101692).
- 50 Mankoff, K.D. et al., 2019: Greenland Ice Sheet discharge from 2000 to 2018. *Earth System Science Data*, **11**, 769–
51 786, doi:[10.5194/essd-11-769-2019](https://doi.org/10.5194/essd-11-769-2019).
- 52 Mankoff, K.D. et al., 2020: Greenland Ice Sheet solid ice discharge from 1986 through March 2020. *Earth System*
53 *Science Data*, **12(2)**, 1367–1383, doi:[10.5194/essd-12-1367-2020](https://doi.org/10.5194/essd-12-1367-2020).
- 54 Marcer, M. et al., 2019: Evaluating the destabilization susceptibility of active rock glaciers in the French Alps. *The*
55 *Cryosphere*, **13(1)**, 141–155, doi:[10.5194/tc-13-141-2019](https://doi.org/10.5194/tc-13-141-2019).

- 1 Marcos, M. and A. Amores, 2014: Quantifying anthropogenic and natural contributions to thermosteric sea level rise.
2 *Geophys Res Lett*, **41**, 2502–2507, doi:[10.1002/2014gl059766](https://doi.org/10.1002/2014gl059766).
- 3 Marcos, M. et al., 2019: Coastal Sea Level and Related Fields from Existing Observing Systems. *Surveys in*
4 *Geophysics*, doi:[10.1007/s10712-019-09513-3](https://doi.org/10.1007/s10712-019-09513-3).
- 5 Marcott, S.A. et al., 2019: 10Be age constraints on latest Pleistocene and Holocene cirque glaciation across the western
6 United States. *npj Climate and Atmospheric Science*, **2**(1), 5, doi:[10.1038/s41612-019-0062-z](https://doi.org/10.1038/s41612-019-0062-z).
- 7 Maris, M. et al., 2014: Modelling the evolution of the Antarctic ice sheet since the last interglacial. *The Cryosphere*,
8 **8**(4), 1347–1360.
- 9 Marsh, O.J. et al., 2016: High basal melting forming a channel at the grounding line of Ross Ice Shelf, Antarctica.
10 *Geophysical Research Letters*, **43**(1), 250–255, doi:[10.1002/2015gl066612](https://doi.org/10.1002/2015gl066612).
- 11 Marshall, A.G., H.H. Hendon, T.H. Durrant, and M.A. Hemer, 2015: Madden Julian Oscillation impacts on global
12 ocean surface waves. *Ocean Modelling*, **96**, 136–147, doi:[10.1016/j.ocemod.2015.06.002](https://doi.org/10.1016/j.ocemod.2015.06.002).
- 13 Marshall, A.G., M.A. Hemer, H.H. Hendon, and K.L. McInnes, 2018: Southern annular mode impacts on global ocean
14 surface waves. *Ocean Modelling*, doi:[10.1016/j.ocemod.2018.07.007](https://doi.org/10.1016/j.ocemod.2018.07.007).
- 15 Marshall, J. et al., 2015: The ocean’s role in the transient response of climate to abrupt greenhouse gas forcing. *Climate*
16 *Dynamics*, **44**(7–8), 2287–2299, doi:[10.1007/s00382-014-2308-0](https://doi.org/10.1007/s00382-014-2308-0).
- 17 Marsooli, R., N. Lin, K. Emanuel, and K. Feng, 2019: Climate change exacerbates hurricane flood hazards along US
18 Atlantic and Gulf Coasts in spatially varying patterns. *Nature Communications*, doi:[10.1038/s41467-019-](https://doi.org/10.1038/s41467-019-11755-z)
19 [11755-z](https://doi.org/11755-z).
- 20 Martinec, Z. et al., 2018: A benchmark study of numerical implementations of the sea level equation in GIA modelling.
21 *Geophysical Journal International*, **215**(1), 389–414, doi:[10.1093/gji/ggy280](https://doi.org/10.1093/gji/ggy280).
- 22 Martínez-Asensio, A. et al., 2019: Relative sea-level rise and the influence of vertical land motion at Tropical Pacific
23 Islands. *Global and Planetary Change*, **176**, 132–143, doi:[10.1016/j.gloplacha.2019.03.008](https://doi.org/10.1016/j.gloplacha.2019.03.008).
- 24 Marzeion, B., A.H. Jarosch, and M. Hofer, 2012: Past and future sea-level change from the surface mass balance of
25 glaciers. *The Cryosphere*, **6**(6), 1295–1322, doi:[10.5194/tc-6-1295-2012](https://doi.org/10.5194/tc-6-1295-2012).
- 26 Marzeion, B., P.W. Leclercq, J.G. Cogley, and A.H. Jarosch, 2015: Brief Communication: Global reconstructions of
27 glacier mass change during the 20th century are consistent. *The Cryosphere*, **9**(6), 2399–2404, doi:[10.5194/tc-](https://doi.org/10.5194/tc-9-2399-2015)
28 [9-2399-2015](https://doi.org/9-2399-2015).
- 29 Marzeion, B., G. Kaser, F. Maussion, and N. Champollion, 2018: Limited influence of climate change mitigation on
30 short-term glacier mass loss. *Nature Climate Change*, **8**(4), 305–308, doi:[10.1038/s41558-018-0093-1](https://doi.org/10.1038/s41558-018-0093-1).
- 31 Marzeion, B. et al., 2020: Partitioning the Uncertainty of Ensemble Projections of Global Glacier Mass Change. *Earth’s*
32 *Future*, **8**(7), doi:[10.1029/2019ef001470](https://doi.org/10.1029/2019ef001470).
- 33 Mas e Braga, M., J. Bernales, M. Prange, A. Stroeven, and I. Rogozhina, 2021: Sensitivity of the Antarctic ice sheets to
34 the peak warming of Marine Isotope Stage 11. *The Cryosphere*, **15**, 459–478, doi:[10.5194/tc-15-459-2021](https://doi.org/10.5194/tc-15-459-2021).
- 35 Mason, E. et al., 2010: Procedures for offline grid nesting in regional ocean models. *Ocean Modelling*, **35**(1–2), 1–15,
36 doi:[10.1016/j.ocemod.2010.05.007](https://doi.org/10.1016/j.ocemod.2010.05.007).
- 37 Massom, R.A. et al., 2001: Snow on Antarctic sea ice. *Reviews of Geophysics*, **39**(3), 413–445,
38 doi:[10.1029/2000rg000085](https://doi.org/10.1029/2000rg000085).
- 39 Massom, R.A. et al., 2006: Extreme Anomalous Atmospheric Circulation in the West Antarctic Peninsula Region in
40 Austral Spring and Summer 2001/02, and Its Profound Impact on Sea Ice and Biota. *Journal of Climate*,
41 **19**(15), 3544–3571, doi:[10.1175/jcli3805.1](https://doi.org/10.1175/jcli3805.1).
- 42 Massom, R.A. et al., 2015: External influences on the Mertz Glacier Tongue (East Antarctica) in the decade leading up
43 to its calving in 2010. *Journal of Geophysical Research: Earth Surface*, **120**(3), 490–506,
44 doi:[10.1002/2014jf003223](https://doi.org/10.1002/2014jf003223).
- 45 Massom, R.A. et al., 2018: Antarctic ice shelf disintegration triggered by sea ice loss and ocean swell. *Nature*,
46 **558**(7710), 383–389, doi:[10.1038/s41586-018-0212-1](https://doi.org/10.1038/s41586-018-0212-1).
- 47 Masson-Delmotte, V. et al., 2013: Information from Paleoclimate Archives. In: *Climate Change 2013: The Physical*
48 *Science Basis. Contribution of Working Group I to the Fifth Assessment Report of the IPCC* [Stocker, T.F., D.
49 Qin, G.-K. Plattner, M. Tignor, S.K. Allen, J. Boschung, A. Nauels, Y. Xia, V. Bex, and P.M. Midgley (eds.)].
50 Cambridge University Press, Cambridge, United Kingdom and New York, USA, pp. 383–464,
51 doi:[10.1017/cbo9781107415324.013](https://doi.org/10.1017/cbo9781107415324.013).
- 52 Massonnet, F., V. Guemas, N.S. Fučkar, and F.J. Doblas-Reyes, 2015: The 2014 High Record of Antarctic Sea Ice
53 Extent. *Explaining Extremes of 2014 from a Climate Perspective. Bulletin of the American Meteorological*
54 *Society*, **96**(12), S163–S167, doi:[10.1175/bams-d-15-00093.1](https://doi.org/10.1175/bams-d-15-00093.1).
- 55 Massonnet, F. et al., 2013: A model reconstruction of the Antarctic sea ice thickness and volume changes over 1980-
56 2008 using data assimilation. *Ocean Modelling*, **64**, 67–75, doi:[10.1016/j.ocemod.2013.01.003](https://doi.org/10.1016/j.ocemod.2013.01.003).

- 1 Matero, I.S.O., L.J. Gregoire, R.F. Ivanovic, J.C. Tindall, and A.M. Haywood, 2017: The 8.2 ka cooling event caused
2 by Laurentide ice saddle collapse. *Earth and Planetary Science Letters*, **473**, 205–214,
3 doi:[10.1016/j.epsl.2017.06.011](https://doi.org/10.1016/j.epsl.2017.06.011).
- 4 Mathis, M. and T. Pohlmann, 2014: Projection of physical conditions in the North Sea for the 21st century. *Climate*
5 *Research*, **61**(1), 1–17, doi:[10.3354/cr01232](https://doi.org/10.3354/cr01232).
- 6 Matiu, M. et al., 2021: Observed snow depth trends in the European Alps: 1971 to 2019. *The Cryosphere*, **15**(3), 1343–
7 1382, doi:[10.5194/tc-15-1343-2021](https://doi.org/10.5194/tc-15-1343-2021).
- 8 Mattingly, K.S. et al., 2020: Strong Summer Atmospheric Rivers Trigger Greenland Ice Sheet Melt through Spatially
9 Varying Surface Energy Balance and Cloud Regimes. *Journal of Climate*, **33**(16), 6809–6832,
10 doi:[10.1175/jcli-d-19-0835.1](https://doi.org/10.1175/jcli-d-19-0835.1).
- 11 Maussion, F. et al., 2019a: The Open Global Glacier Model (OGGM) v1.1. *Geoscientific Model Development*, **12**(3),
12 909–931, doi:[10.5194/gmd-12-909-2019](https://doi.org/10.5194/gmd-12-909-2019).
- 13 Maussion, F. et al., 2019b: The Open Global Glacier Model (OGGM) v1.1. *Geoscientific Model Development*, **12**(3),
14 909–931, doi:[10.5194/gmd-12-909-2019](https://doi.org/10.5194/gmd-12-909-2019).
- 15 Mayer, C. et al., 2018: Large ice loss variability at Nioghalvfjærdsfjorden Glacier, Northeast-Greenland. *Nature*
16 *Communications*, **9**(1), 2768, doi:[10.1038/s41467-018-05180-x](https://doi.org/10.1038/s41467-018-05180-x).
- 17 Mayer, M. et al., 2019: An Improved Estimate of the Coupled Arctic Energy Budget. *Journal of Climate*, **32**(22), 7915–
18 7934, doi:[10.1175/jcli-d-19-0233.1](https://doi.org/10.1175/jcli-d-19-0233.1).
- 19 McCarthy, G.D., T.M. Joyce, and S.A. Josey, 2018: Gulf Stream Variability in the Context of Quasi-Decadal and
20 Multidecadal Atlantic Climate Variability. *Geophysical Research Letters*, **45**(20), doi:[10.1029/2018gl079336](https://doi.org/10.1029/2018gl079336).
- 21 McFarlin, J.M. et al., 2018: Pronounced summer warming in northwest Greenland during the Holocene and Last
22 Interglacial. *Proceedings of the National Academy of Sciences*, **115**(25), 6357 LP – 6362,
23 doi:[10.1073/pnas.1720420115](https://doi.org/10.1073/pnas.1720420115).
- 24 McGuire, A.D. et al., 2016: Variability in the sensitivity among model simulations of permafrost and carbon dynamics
25 in the permafrost region between 1960 and 2009. *Global Biogeochemical Cycles*, doi:[10.1002/2016gb005405](https://doi.org/10.1002/2016gb005405).
- 26 McInnes, K.L., R.K. Hoeke, K.J.E. Walsh, J.G. O’Grady, and G.D. Hubbert, 2016: Application of a synthetic cyclone
27 method for assessment of tropical cyclone storm tides in Samoa. *Natural Hazards*, **80**(1), 425–444,
28 doi:[10.1007/s11069-015-1975-4](https://doi.org/10.1007/s11069-015-1975-4).
- 29 McInnes, K.L. et al., 2014: Quantifying storm tide risk in Fiji due to climate variability and change. *Global and*
30 *Planetary Change*, **116**, 115–129, doi:[10.1016/j.gloplacha.2014.02.004](https://doi.org/10.1016/j.gloplacha.2014.02.004).
- 31 McKay, R. et al., 2016: Antarctic marine ice-sheet retreat in the Ross Sea during the early Holocene. *Geology*, **44**(1), 7–
32 10, doi:[10.1130/g37315.1](https://doi.org/10.1130/g37315.1).
- 33 McWilliams, J.C., 2019: A survey of submesoscale currents. *Geoscience Letters*, **6**(1), 1–15, doi:[10.1186/s40562-019-0133-3](https://doi.org/10.1186/s40562-019-0133-3).
- 34
- 35 Meccia, V.L., F. Fabiano, P. Davini, and S. Corti, 2020: Stochastic Parameterizations and the Climate Response to
36 External Forcing: An Experiment With EC-Earth. *Geophysical Research Letters*, **47**(3), e2019GL085951,
37 doi:[10.1029/2019gl085951](https://doi.org/10.1029/2019gl085951).
- 38 Mecking, J.V., S.S. Drijfhout, L.C. Jackson, and M.B. Andrews, 2017: The effect of model bias on Atlantic freshwater
39 transport and implications for AMOC bi-stability. *Tellus, Series A: Dynamic Meteorology and Oceanography*,
40 **69**(1), doi:[10.1080/16000870.2017.1299910](https://doi.org/10.1080/16000870.2017.1299910).
- 41 Medley, B. and E.R. Thomas, 2019: Increased snowfall over the Antarctic Ice Sheet mitigated twentieth-century sea-
42 level rise. *Nature Climate Change*, doi:[10.1038/s41558-018-0356-x](https://doi.org/10.1038/s41558-018-0356-x).
- 43 Meehl, G.A., J.M. Arblaster, C.M. Bitz, C.T.Y. Chung, and H. Teng, 2016: Antarctic sea-ice expansion between 2000
44 and 2014 driven by tropical Pacific decadal climate variability. *Nature Geoscience*, **9**(8), 590–595,
45 doi:[10.1038/ngeo2751](https://doi.org/10.1038/ngeo2751).
- 46 Meehl, G.A. et al., 2019: Sustained ocean changes contributed to sudden Antarctic sea ice retreat in late 2016. *Nature*
47 *Communications*, **10**(1), 14, doi:[10.1038/s41467-018-07865-9](https://doi.org/10.1038/s41467-018-07865-9).
- 48 Méheust, M., R. Stein, K. Fahl, and R. Gersonde, 2018: Sea-ice variability in the subarctic North Pacific and adjacent
49 Bering Sea during the past 25 ka: new insights from IP25 and Uk’37 proxy records. *Arktos*, **4**(1), 8,
50 doi:[10.1007/s41063-018-0043-1](https://doi.org/10.1007/s41063-018-0043-1).
- 51 Meier, H.E.M., 2015: Projected Change – Marine Physics. In: *Second Assessment of Climate Change for the Baltic Sea*
52 *Basin* [The BACC II Author Team (ed.)]. Springer, Cham, Switzerland, pp. 243–252, doi:[10.1007/978-3-319-16006-1_13](https://doi.org/10.1007/978-3-319-16006-1_13).
- 53
- 54 Meier, W.N. and J.S. Stewart, 2019: Assessing uncertainties in sea ice extent climate indicators. *Environmental*
55 *Research Letters*, **14**(3), 035005, doi:[10.1088/1748-9326/aaf52c](https://doi.org/10.1088/1748-9326/aaf52c).

- 1 Meier, W.N., D. Gallaher, and G.G. Campbell, 2013: New estimates of Arctic and Antarctic sea ice extent during
2 September 1964 from recovered Nimbus I satellite imagery. *The Cryosphere*, **7(2)**, 699–705, doi:[10.5194/tc-7-
3 699-2013](https://doi.org/10.5194/tc-7-699-2013).
- 4 Meinshausen, M. et al., 2011: The RCP greenhouse gas concentrations and their extensions from 1765 to 2300.
5 *Climatic change*, **109(1–2)**, 213.
- 6 Melet, A., B. Meyssignac, R. Almar, and G. Le Cozannet, 2018: Under-estimated wave contribution to coastal sea-level
7 rise. *Nature Climate Change*, doi:[10.1038/s41558-018-0088-y](https://doi.org/10.1038/s41558-018-0088-y).
- 8 Melet, A. et al., 2020: Contribution of Wave Setup to Projected Coastal Sea Level Changes. *Journal of Geophysical
9 Research: Oceans*, **125(8)**, doi:[10.1029/2020jc016078](https://doi.org/10.1029/2020jc016078).
- 10 Melzer, B.A. and B. Subrahmanyam, 2017: Decadal changes in salinity in the oceanic subtropical gyres. *Journal of
11 Geophysical Research: Oceans*, **122(1)**, 336–354, doi:[10.1002/2016jc012243](https://doi.org/10.1002/2016jc012243).
- 12 Menary, M.B. and R.A. Wood, 2018: An anatomy of the projected North Atlantic warming hole in CMIP5 models.
13 *Climate Dynamics*, doi:[10.1007/s00382-017-3793-8](https://doi.org/10.1007/s00382-017-3793-8).
- 14 Menary, M.B., L.C. Jackson, and M.S. Lozier, 2020a: Reconciling the Relationship Between the AMOC and Labrador
15 Sea in OSNAP Observations and Climate Models. *Geophysical Research Letters*, **47(18)**,
16 doi:[10.1029/2020g1089793](https://doi.org/10.1029/2020g1089793).
- 17 Menary, M.B., L.C. Jackson, and M.S. Lozier, 2020b: Reconciling the Relationship Between the AMOC and Labrador
18 Sea in OSNAP Observations and Climate Models. *Geophysical Research Letters*, **47(18)**,
19 doi:[10.1029/2020g1089793](https://doi.org/10.1029/2020g1089793).
- 20 Menary, M.B. et al., 2020c: Aerosol-Forced AMOC Changes in CMIP6 Historical Simulations. *Geophysical Research
21 Letters*, **47(14)**, doi:[10.1029/2020g1088166](https://doi.org/10.1029/2020g1088166).
- 22 Mengel, M. and A. Levermann, 2014: Ice plug prevents irreversible discharge from East Antarctica. *Nature Climate
23 Change*, **4**, 451–455, doi:[10.1038/nclimate2226](https://doi.org/10.1038/nclimate2226).
- 24 Mengel, M. et al., 2016: Future sea level rise constrained by observations and long-term commitment. *Proceedings of
25 the National Academy of Sciences*, **113(10)**, 2597–2602, doi:[10.1073/pnas.1500515113](https://doi.org/10.1073/pnas.1500515113).
- 26 Menounos, B. et al., 2019: Heterogeneous Changes in Western North American Glaciers Linked to Decadal Variability
27 in Zonal Wind Strength. *Geophysical Research Letters*, **46(1)**, 200–209, doi:[10.1029/2018g1080942](https://doi.org/10.1029/2018g1080942).
- 28 Mercenier, R., M.P. Lüthi, and A. Vieli, 2018: Calving relation for tidewater glaciers based on detailed stress field
29 analysis. *The Cryosphere*, **12(2)**, 721–739, doi:[10.5194/tc-12-721-2018](https://doi.org/10.5194/tc-12-721-2018).
- 30 Mercenier, R., M.P. Lüthi, and A. Vieli, 2020: How Oceanic Melt Controls Tidewater Glacier Evolution. *Geophysical
31 Research Letters*, **47**, e2019GL086769, doi:[10.1029/2019g1086769](https://doi.org/10.1029/2019g1086769).
- 32 Meredith, M. et al., 2019: Polar Regions. In: *IPCC Special Report on the Ocean and Cryosphere in a Changing Climate*
33 [Pörtner, H.-O., D.C. Roberts, V. Masson-Delmotte, P. Zhai, M. Tignor, E. Poloczanska, K. Mintenbeck, M.
34 Nicolai, A. Okem, J. Petzold, B. Rama, and N. Weyer (eds.)]. In Press, pp. 203–320.
- 35 Merino, N. et al., 2018: Impact of increasing antarctic glacial freshwater release on regional sea-ice cover in the
36 Southern Ocean. *OCEAN MODELLING*, **121**, 76–89, doi:[10.1016/j.ocemod.2017.11.009](https://doi.org/10.1016/j.ocemod.2017.11.009).
- 37 Mernild, S.H., W.H. Lipscomb, D.B. Bahr, V. Radić, and M. Zemp, 2013: Global glacier changes: a revised assessment
38 of committed mass losses and sampling uncertainties. *The Cryosphere*, **7(5)**, 1565–1577, doi:[10.5194/tc-7-
39 1565-2013](https://doi.org/10.5194/tc-7-1565-2013).
- 40 Merrifield, M.A., P.R. Thompson, and M. Lander, 2012: Multidecadal sea level anomalies and trends in the western
41 tropical Pacific. *Geophysical Research Letters*, **39(13)**, n/a–n/a, doi:[10.1029/2012g1052032](https://doi.org/10.1029/2012g1052032).
- 42 Metzner, E.P., M. Salzmann, and R. Gerdes, 2020: Arctic Ocean Surface Energy Flux and the Cold Halocline in Future
43 Climate Projections. *Journal of Geophysical Research: Oceans*, **125(2)**, e2019JC015554,
44 doi:[10.1029/2019jc015554](https://doi.org/10.1029/2019jc015554).
- 45 Meucci, A., I.R. Young, M. Hemer, E. Kirezci, and R. Ranasinghe, 2020: Projected 21st century changes in extreme
46 wind-wave events. *Science Advances*, **6(24)**, 7295–7305, doi:[10.1126/sciadv.aaz7295](https://doi.org/10.1126/sciadv.aaz7295).
- 47 Meyssignac, B. et al., 2017: Evaluating model simulations of twentieth-century sea-level rise. Part II: Regional sea-
48 level changes. *Journal of Climate*, **30(21)**, 8565–8593, doi:[10.1175/jcli-d-17-0112.1](https://doi.org/10.1175/jcli-d-17-0112.1).
- 49 Miles, B.W.J., C.R. Stokes, and S.S.R. Jamieson, 2016: Pan-ice-sheet glacier terminus change in East Antarctica
50 reveals sensitivity of Wilkes Land to sea-ice changes. *Science Advances*, **2(5)**, e1501350,
51 doi:[10.1126/sciadv.1501350](https://doi.org/10.1126/sciadv.1501350).
- 52 Miles, B.W.J., C.R. Stokes, and S.S.R. Jamieson, 2017: Simultaneous disintegration of outlet glaciers in Porpoise Bay
53 (Wilkes Land), East Antarctica, driven by sea ice break-up. *The Cryosphere*, **11(1)**, 427–442, doi:[10.5194/tc-
54 11-427-2017](https://doi.org/10.5194/tc-11-427-2017).
- 55 Miles, B.W.J., C.R. Stokes, A. Vieli, and N.J. Cox, 2013: Rapid, climate-driven changes in outlet glaciers on the Pacific
56 coast of East Antarctica. *Nature*, **500(7464)**, 563–566, doi:[10.1038/nature12382](https://doi.org/10.1038/nature12382).

- 1 Milillo, P. et al., 2017: On the Short-term Grounding Zone Dynamics of Pine Island Glacier, West Antarctica, Observed
2 With COSMO-SkyMed Interferometric Data. *Geophysical Research Letters*, **44**(20), 10,436–10,444,
3 doi:[10.1002/2017g1074320](https://doi.org/10.1002/2017g1074320).
- 4 Milillo, P. et al., 2019: Heterogeneous retreat and ice melt of thwaites glacier, West Antarctica. *Science Advances*, **5**(1),
5 eaau3433, doi:[10.1126/sciadv.aau3433](https://doi.org/10.1126/sciadv.aau3433).
- 6 Millan, R. et al., 2018: Vulnerability of Southeast Greenland Glaciers to Warm Atlantic Water From Operation
7 IceBridge and Ocean Melting Greenland Data. *Geophysical Research Letters*, **45**(6), 2688–2696,
8 doi:[10.1002/2017g1076561](https://doi.org/10.1002/2017g1076561).
- 9 Millan, R. et al., 2020: Constraining an Ocean Model Under Getz Ice Shelf, Antarctica, Using A Gravity-Derived
10 Bathymetry. *Geophysical Research Letters*, **47**(13), e2019GL086522, doi:[10.1029/2019g1086522](https://doi.org/10.1029/2019g1086522).
- 11 Miller, G.H., J.Y. Landvik, S.J. Lehman, and J.R. Southon, 2017: Episodic Neoglacial snowline descent and glacier
12 expansion on Svalbard reconstructed from the 14C ages of ice-entombed plants. *Quaternary Science Reviews*,
13 **155**, 67–78, doi:[10.1016/j.quascirev.2016.10.023](https://doi.org/10.1016/j.quascirev.2016.10.023).
- 14 Miller, G.H., S.J. Lehman, K.A. Refsnider, J.R. Southon, and Y. Zhong, 2013: Unprecedented recent summer warmth
15 in Arctic Canada. *Geophysical Research Letters*, **40**(21), 5745–5751, doi:[10.1002/2013g1057188](https://doi.org/10.1002/2013g1057188).
- 16 Miller, G.H. et al., 2012: Abrupt onset of the Little Ice Age triggered by volcanism and sustained by sea-ice/ocean
17 feedbacks. *Geophysical Research Letters*, **39**(2), doi:[10.1029/2011g1050168](https://doi.org/10.1029/2011g1050168).
- 18 Miller, K.G. et al., 2012: High tide of the warm Pliocene: Implications of global sea level for Antarctic deglaciation.
19 *Geology*, **40**(5), 407–410, doi:[10.1130/g32869.1](https://doi.org/10.1130/g32869.1).
- 20 Miller, K.G. et al., 2020: Cenozoic sea-level and cryospheric evolution from deep-sea geochemical and continental
21 margin records. *Science Advances*, **6**(20), doi:[10.1126/sciadv.aaz1346](https://doi.org/10.1126/sciadv.aaz1346).
- 22 Minderhoud, P.S.J. et al., 2017: Impacts of 25 years of groundwater extraction on subsidence in the Mekong delta,
23 Vietnam. *Environmental Research Letters*, **12**(6), 64006, doi:[10.1088/1748-9326/aa7146](https://doi.org/10.1088/1748-9326/aa7146).
- 24 Mitrovica, J.X., C.C. Hay, R.E. Kopp, C. Harig, and K. Latychev, 2018: Quantifying the sensitivity of sea level change
25 in coastal localities to the geometry of polar ice mass flux. *Journal of Climate*, **31**(9), doi:[10.1175/jcli-d-17-0465.1](https://doi.org/10.1175/jcli-d-17-0465.1).
- 26
- 27 Moffa-Sánchez, P., A. Born, I.R. Hall, D.J.R. Thornalley, and S. Barker, 2014: Solar forcing of North Atlantic surface
28 temperature and salinity over the past millennium. *Nature Geoscience*, **7**(4), 275–278, doi:[10.1038/ngeo2094](https://doi.org/10.1038/ngeo2094).
- 29 Moffa-Sánchez, P. et al., 2019: Variability in the Northern North Atlantic and Arctic Oceans Across the Last Two
30 Millennia: A Review. *Paleoceanography and Paleoclimatology*, **34**(8), 1399–1436,
31 doi:[10.1029/2018pa003508](https://doi.org/10.1029/2018pa003508).
- 32 Moftakhari, H.R., G. Salvadori, A. AghaKouchak, B.F. Sanders, and R.A. Matthew, 2017: Compounding effects of sea
33 level rise and fluvial flooding. *Proceedings of the National Academy of Sciences*, **114**(37), 9785–9790,
34 doi:[10.1073/pnas.1620325114](https://doi.org/10.1073/pnas.1620325114).
- 35 Mohajerani, Y., I. Velicogna, and E. Rignot, 2018: Mass Loss of Totten and Moscow University Glaciers, East
36 Antarctica, Using Regionally Optimized GRACE Mascons. *Geophysical Research Letters*, **45**(14), 7010–7018,
37 doi:[10.1029/2018g1078173](https://doi.org/10.1029/2018g1078173).
- 38 Mollaret, C. et al., 2019: Mountain permafrost degradation documented through a network of permanent electrical
39 resistivity tomography sites. *The Cryosphere*, **13**(10), 2557–2578, doi:[10.5194/tc-13-2557-2019](https://doi.org/10.5194/tc-13-2557-2019).
- 40 Monselesan, D.P., T.J. O’Kane, J.S. Risbey, and J. Church, 2015: Internal climate memory in observations and models.
41 *Geophysical Research Letters*, doi:[10.1002/2014g1062765](https://doi.org/10.1002/2014g1062765).
- 42 Moon, T.A., A.S. Gardner, B. Csatho, I. Parmuzin, and M.A. Fahnestock, 2020: Rapid reconfiguration of the Greenland
43 Ice Sheet coastal margin. *Journal of Geophysical Research: Earth Surface*, **125**(n/a), e2020JF005585,
44 doi:[10.1029/2020jf005585](https://doi.org/10.1029/2020jf005585).
- 45 Moorman, R., A.K. Morrison, and A. McC. Hogg, 2020: Thermal Responses to Antarctic Ice Shelf Melt in an Eddy-
46 Rich Global Ocean–Sea Ice Model. *Journal of Climate*, **33**(15), 6599–6620, doi:[10.1175/jcli-d-19-0846.1](https://doi.org/10.1175/jcli-d-19-0846.1).
- 47 Moreno-Chamarro, E., D. Zanchettin, K. Lohmann, and J.H. Jungclauss, 2017: An abrupt weakening of the subpolar
48 gyre as trigger of Little Ice Age-type episodes. *Climate Dynamics*, **48**(3–4), 727–744, doi:[10.1007/s00382-016-3106-7](https://doi.org/10.1007/s00382-016-3106-7).
- 49
- 50 Mori, N. et al., 2014: Local amplification of storm surge by Super Typhoon Haiyan in Leyte Gulf. *Geophysical*
51 *Research Letters*, **41**(14), 5106–5113, doi:[10.1002/2014g1060689](https://doi.org/10.1002/2014g1060689).
- 52 Mori, N. et al., 2019: Future changes in extreme storm surges based on mega-ensemble projection using 60-km
53 resolution atmospheric global circulation model. *Coastal Engineering Journal*, **61**(3), 295–307,
54 doi:[10.1080/21664250.2019.1586290](https://doi.org/10.1080/21664250.2019.1586290).
- 55 Morim, J., M. Hemer, N. Cartwright, D. Strauss, and F. Andutta, 2018: On the concordance of 21st century wind-wave
56 climate projections. *Global and Planetary Change*, **167**, 160–171, doi:[10.1016/j.gloplacha.2018.05.005](https://doi.org/10.1016/j.gloplacha.2018.05.005).

- 1 Morim, J. et al., 2019: Robustness and uncertainties in multivariate wind-wave climate projections. *Nature Climate*
2 *Change*, **9**, 711–718, doi:[10.1038/s41558-019-0542-5](https://doi.org/10.1038/s41558-019-0542-5).
- 3 Morlighem, M., E. Rignot, and J.K. Willis, 2016a: Improving Bed Topography Mapping of Greenland Glaciers Using
4 NASA’s Oceans Melting Greenland (OMG) Data. *Oceanography*, **29(4)**, 62–71,
5 doi:[10.5670/oceanog.2016.99](https://doi.org/10.5670/oceanog.2016.99).
- 6 Morlighem, M., E. Rignot, J. Mouginot, H. Seroussi, and E. Larour, 2014: Deeply incised submarine glacial valleys
7 beneath the Greenland ice sheet. *Nature Geoscience*, **7(6)**, 418–422, doi:[10.1038/ngeo2167](https://doi.org/10.1038/ngeo2167).
- 8 Morlighem, M., M. Wood, H. Seroussi, Y. Choi, and E. Rignot, 2019: Modeling the response of northwest Greenland to
9 enhanced ocean thermal forcing and subglacial discharge. *The Cryosphere*, **13(2)**, 723–734, doi:[10.5194/tc-13-
10 723-2019](https://doi.org/10.5194/tc-13-723-2019).
- 11 Morlighem, M. et al., 2016b: Modeling of Store Gletscher’s calving dynamics, West Greenland, in response to ocean
12 thermal forcing. *Geophysical Research Letters*, **43(6)**, 2659–2666, doi:[10.1002/2016gl067695](https://doi.org/10.1002/2016gl067695).
- 13 Morlighem, M. et al., 2017: BedMachine v3: Complete Bed Topography and Ocean Bathymetry Mapping of Greenland
14 From Multibeam Echo Sounding Combined With Mass Conservation. *Geophysical Research Letters*, **44(21)**,
15 11,051–11,061, doi:[10.1002/2017gl074954](https://doi.org/10.1002/2017gl074954).
- 16 Morlighem, M. et al., 2020: Deep glacial troughs and stabilizing ridges unveiled beneath the margins of the Antarctic
17 ice sheet. *Nature Geoscience*, **13(2)**, 132–137, doi:[10.1038/s41561-019-0510-8](https://doi.org/10.1038/s41561-019-0510-8).
- 18 Morris, A., G. Moholdt, and L. Gray, 2020: Spread of Svalbard Glacier Mass Loss to Barents Sea Margins Revealed by
19 CryoSat-2. *Journal of Geophysical Research: Earth Surface*, **125(8)**, doi:[10.1029/2019jf005357](https://doi.org/10.1029/2019jf005357).
- 20 Mortimer, C. et al., 2020: Evaluation of long-term Northern Hemisphere snow water equivalent products. *The*
21 *Cryosphere*, **14**, 1579–1594.
- 22 Mosbeux, C., F. Gillet-Chaulet, and O. Gagliardini, 2016: Comparison of adjoint and nudging methods to initialise ice
23 sheet model basal conditions. *Geoscientific Model Development*, **9(7)**, 2549–2562, doi:[10.5194/gmd-9-2549-
24 2016](https://doi.org/10.5194/gmd-9-2549-2016).
- 25 Mottram, R. et al., 2019: An Integrated View of Greenland Ice Sheet Mass Changes Based on Models and Satellite
26 Observations. *Remote Sensing*, **11(12)**, doi:[10.3390/rs11121407](https://doi.org/10.3390/rs11121407).
- 27 Motyka, R.J. et al., 2017: Asynchronous behavior of outlet glaciers feeding Godthåbsfjord (Nuup Kangerlua) and the
28 triggering of Narsap Sermia’s retreat in SW Greenland. *Journal of Glaciology*, **63(238)**, 288–308,
29 doi:[10.1017/jog.2016.138](https://doi.org/10.1017/jog.2016.138).
- 30 Moucha, R. and G.A. Ruetenik, 2017: Interplay between dynamic topography and flexure along the U.S. Atlantic
31 passive margin: Insights from landscape evolution modeling. *Global and Planetary Change*, **149**, 72–78,
32 doi:[10.1016/j.gloplacha.2017.01.004](https://doi.org/10.1016/j.gloplacha.2017.01.004).
- 33 Mouginot, J. et al., 2015: Fast retreat of Zachariaësstrom, northeast Greenland. *Science*, **350(6266)**, 1357–1361,
34 doi:[10.1126/science.aac7111](https://doi.org/10.1126/science.aac7111).
- 35 Mouginot, J. et al., 2019: Forty-six years of Greenland Ice Sheet mass balance from 1972 to 2018. *Proceedings of the*
36 *National Academy of Sciences*, **116(19)**, 9239–9244, doi:[10.1073/pnas.1904242116](https://doi.org/10.1073/pnas.1904242116).
- 37 Mudryk, L. et al., 2020: Historical Northern Hemisphere snow cover trends and projected changes in the CMIP6 multi-
38 model ensemble. *The Cryosphere*, **14(7)**, 2495–2514, doi:[10.5194/tc-14-2495-2020](https://doi.org/10.5194/tc-14-2495-2020).
- 39 Mudryk, L.R., P.J. Kushner, C. Derksen, and C. Thackeray, 2017: Snow cover response to temperature in observational
40 and climate model ensembles. *Geophysical Research Letters*, **44(2)**, 919–926, doi:[10.1002/2016gl071789](https://doi.org/10.1002/2016gl071789).
- 41 Muilwijk, M., L.H. Smedsrud, M. Ilicak, and H. Drange, 2018: Atlantic Water Heat Transport Variability in the 20th
42 Century Arctic Ocean From a Global Ocean Model and Observations. *Journal of Geophysical Research:*
43 *Oceans*, **123(11)**, 8159–8179, doi:[10.1029/2018jc014327](https://doi.org/10.1029/2018jc014327).
- 44 Muis, S., M. Verlaan, H.C. Winsemius, J.C.J.H. Aerts, and P.J. Ward, 2016: A global reanalysis of storm surges and
45 extreme sea levels. *Nature Communications*, **7**, 11969, doi:[10.1038/ncomms11969](https://doi.org/10.1038/ncomms11969).
- 46 Muis, S. et al., 2020: A High-Resolution Global Dataset of Extreme Sea Levels, Tides, and Storm Surges, Including
47 Future Projections. *Frontiers in Marine Science*, **7**, 263, doi:[10.3389/fmars.2020.00263](https://doi.org/10.3389/fmars.2020.00263).
- 48 Muntjewerf, L. et al., 2020a: Greenland Ice Sheet Contribution to 21st Century Sea Level Rise as Simulated by the
49 Coupled CESM2.1-CISM2.1. *Geophysical Research Letters*, **47(9)**, doi:[10.1029/2019gl086836](https://doi.org/10.1029/2019gl086836).
- 50 Muntjewerf, L. et al., 2020b: Accelerated Greenland Ice Sheet Mass Loss Under High Greenhouse Gas Forcing as
51 Simulated by the Coupled CESM2.1-CISM2.1. *Journal of Advances in Modeling Earth Systems*, **12(10)**,
52 doi:[10.1029/2019ms002031](https://doi.org/10.1029/2019ms002031).
- 53 Murari, M.K. et al., 2014: Timing and climatic drivers for glaciation across monsoon-influenced regions of the
54 Himalayan–Tibetan orogen. *Quaternary Science Reviews*, **88**, 159–182, doi:[10.1016/j.quascirev.2014.01.013](https://doi.org/10.1016/j.quascirev.2014.01.013).
- 55 Muresan, I.S. et al., 2016: Modelled glacier dynamics over the last quarter of a century at Jakobshavn Isbræ. *The*
56 *Cryosphere*, **10(2)**, 597–611, doi:[10.5194/tc-10-597-2016](https://doi.org/10.5194/tc-10-597-2016).

- 1 Murray, T. et al., 2015: Extensive retreat of Greenland tidewater glaciers, 2000–2010. *Arctic, Antarctic, and Alpine*
2 *Research*, **47(3)**, 427–447, doi:[10.1657/aaar0014-049](https://doi.org/10.1657/aaar0014-049).
- 3 Nair, A. et al., 2019: Southern Ocean sea ice and frontal changes during the Late Quaternary and their linkages to Asian
4 summer monsoon. *Quaternary Science Reviews*, **213**, 93–104, doi:[10.1016/j.quascirev.2019.04.007](https://doi.org/10.1016/j.quascirev.2019.04.007).
- 5 Najafi, M.R., F.W. Zwiers, and N.P. Gillett, 2015: Attribution of Arctic temperature change to greenhouse-gas and
6 aerosol influences. *Nature Climate Change*, **5(3)**, 246–249, doi:[10.1038/nclimate2524](https://doi.org/10.1038/nclimate2524).
- 7 Narayan, N., A. Paul, S. Mulitza, and M. Schulz, 2010: Trends in coastal upwelling intensity during the late 20th
8 century. *Ocean Science*, **6(3)**, 815–823, doi:[10.5194/os-6-815-2010](https://doi.org/10.5194/os-6-815-2010).
- 9 Nauels, A., M. Meinshausen, M. Mengel, K. Lorbacher, and T.M.L. Wigley, 2017: Synthesizing long-term sea level
10 rise projections – the MAGICC sea level model v2.0. *Geoscientific Model Development*, **10(6)**, 2495–2524,
11 doi:[10.5194/gmd-10-2495-2017](https://doi.org/10.5194/gmd-10-2495-2017).
- 12 Nauels, A. et al., 2019: Attributing long-term sea-level rise to Paris Agreement emission pledges. *Proceedings of the*
13 *National Academy of Sciences*, **116(47)**, 23487–23492, doi:[10.1073/pnas.1907461116](https://doi.org/10.1073/pnas.1907461116).
- 14 Naughten, K.A. et al., 2018: Future Projections of Antarctic Ice Shelf Melting Based on CMIP5 Scenarios. *Journal of*
15 *Climate*, **31(13)**, 5243–5261, doi:[10.1175/jcli-d-17-0854.1](https://doi.org/10.1175/jcli-d-17-0854.1).
- 16 Nesje, A. et al., 2012: The climatic significance of artefacts related to prehistoric reindeer hunting exposed at melting
17 ice patches in southern Norway. *The Holocene*, **22(4)**, 485–496, doi:[10.1177/0959683611425552](https://doi.org/10.1177/0959683611425552).
- 18 Nias, I.J., S.L. Cornford, T.L. Edwards, N. Gourmelen, and A.J. Payne, 2019: Assessing Uncertainty in the Dynamical
19 Ice Response to Ocean Warming in the Amundsen Sea Embayment, West Antarctica. *Geophysical Research*
20 *Letters*, **46(20)**, 11253–11260, doi:[10.1029/2019gl084941](https://doi.org/10.1029/2019gl084941).
- 21 Nicholls, R.J. et al., 2018: Stabilization of global temperature at 1.5°C and 2.0°C: Implications for coastal areas.
22 *Philosophical Transactions of the Royal Society A: Mathematical, Physical and Engineering Sciences*,
23 **376(2119)**, doi:[10.1098/rsta.2016.0448](https://doi.org/10.1098/rsta.2016.0448).
- 24 Nick, F.M. et al., 2013: Future sea-level rise from Greenland’s main outlet glaciers in a warming climate. *Nature*,
25 **497(7448)**, 235–238, doi:[10.1038/nature12068](https://doi.org/10.1038/nature12068).
- 26 Nicolas, J.P. et al., 2017: January 2016 extensive summer melt in West Antarctica favoured by strong El Niño. *Nature*
27 *Communications*, **8(1)**, 15799, doi:[10.1038/ncomms15799](https://doi.org/10.1038/ncomms15799).
- 28 Niederdrenk, A.L. and D. Notz, 2018: Arctic Sea Ice in a 1.5°C Warmer World. *Geophysical Research Letters*, **45(4)**,
29 1963–1971, doi:[10.1002/2017gl076159](https://doi.org/10.1002/2017gl076159).
- 30 Nielsen, L.T., G. Aðalgeirsdóttir, V. Gkinis, R. Nuterman, and C.S. Hvidberg, 2018: The effect of a Holocene climatic
31 optimum on the evolution of the Greenland ice sheet during the last 10 kyr. *Journal of Glaciology*, **64(245)**,
32 477–488, doi:[10.1017/jog.2018.40](https://doi.org/10.1017/jog.2018.40).
- 33 Nitzbon, J. et al., 2020: Fast response of cold ice-rich permafrost in northeast Siberia to a warming climate. *Nature*
34 *Communications*, **11(1)**, 2201, doi:[10.1038/s41467-020-15725-8](https://doi.org/10.1038/s41467-020-15725-8).
- 35 Niwano, M., A. Hashimoto, and T. Aoki, 2019: Cloud-driven modulations of Greenland ice sheet surface melt.
36 *Scientific Reports*, **9**, 10380, doi:[10.1038/s41598-019-46152-5](https://doi.org/10.1038/s41598-019-46152-5).
- 37 Niwano, M. et al., 2018: NHM-SMAP: Spatially and temporally high-resolution nonhydrostatic atmospheric model
38 coupled with detailed snow process model for Greenland Ice Sheet. *Cryosphere*, **12(2)**, 635–655,
39 doi:[10.5194/tc-12-635-2018](https://doi.org/10.5194/tc-12-635-2018).
- 40 Noël, B., L. van Kampenhout, J.T.M. Lenaerts, W.J. van de Berg, and M.R. van den Broeke, 2021: A 21st Century
41 Warming Threshold for Sustained Greenland Ice Sheet Mass Loss. *Geophysical Research Letters*, **n/a(n/a)**,
42 e2020GL090471, doi:[10.1029/2020gl090471](https://doi.org/10.1029/2020gl090471).
- 43 Noël, B. et al., 2018: Six Decades of Glacial Mass Loss in the Canadian Arctic Archipelago. *Journal of Geophysical*
44 *Research: Earth Surface*, **123(6)**, 1430–1449, doi:[10.1029/2017jf004304](https://doi.org/10.1029/2017jf004304).
- 45 Noël, B. et al., 2020: Low elevation of Svalbard glaciers drives high mass loss variability. *Nature Communications*,
46 **11(1)**, 4597, doi:[10.1038/s41467-020-18356-1](https://doi.org/10.1038/s41467-020-18356-1).
- 47 Noetzli, J. et al., 2019: Permafrost thermal state. *State of the Climate in 2018. Bulletin of the American Meteorological*
48 *Society*, **100(9)**, S21–S22, doi:[10.1175/2019bamsstateoftheclimate.1](https://doi.org/10.1175/2019bamsstateoftheclimate.1).
- 49 Notarnicola, C., 2020: Hotspots of snow cover changes in global mountain regions over 2000–2018. *Remote Sensing of*
50 *Environment*, **243**, 111781, doi:[10.1016/j.rse.2020.111781](https://doi.org/10.1016/j.rse.2020.111781).
- 51 Notz, D., 2014: Sea-ice extent and its trend provide limited metrics of model performance. *Cryosphere*, **8(1)**, 229–243,
52 doi:[10.5194/tc-8-229-2014](https://doi.org/10.5194/tc-8-229-2014).
- 53 Notz, D. and J. Marotzke, 2012: Observations reveal external driver for Arctic sea-ice retreat. *Geophysical Research*
54 *Letters*, **39(8)**, doi:[10.1029/2012gl051094](https://doi.org/10.1029/2012gl051094).
- 55 Notz, D. and J. Stroeve, 2016: Observed Arctic sea-ice loss directly follows anthropogenic CO2 emission. *Science*,
56 **354(6313)**, 747–750, doi:[10.1126/science.aag2345](https://doi.org/10.1126/science.aag2345).

- 1 Notz, D. and J. Stroeve, 2018: The Trajectory Towards a Seasonally Ice-Free Arctic Ocean. *Current Climate Change*
2 *Reports*, **4(4)**, 407–416, doi:[10.1007/s40641-018-0113-2](https://doi.org/10.1007/s40641-018-0113-2).
- 3 Notz, D. and SIMIP Community, 2020: Arctic Sea Ice in CMIP6. *Geophysical Research Letters*, **47(10)**,
4 doi:[10.1029/2019gl086749](https://doi.org/10.1029/2019gl086749).
- 5 Notz, D. et al., 2016: The CMIP6 Sea-Ice Model Intercomparison Project (SIMIP): Understanding sea ice through
6 climate-model simulations. *Geoscientific Model Development*, **9(9)**, 3427–3446, doi:[10.5194/gmd-9-3427-](https://doi.org/10.5194/gmd-9-3427-2016)
7 [2016](https://doi.org/10.5194/gmd-9-3427-2016).
- 8 Nowicki, S. et al., 2013: Insights into spatial sensitivities of ice mass response to environmental change from the
9 SeaRISE ice sheet modeling project II: Greenland. *Journal of Geophysical Research: Earth Surface*, **118(2)**,
10 doi:[10.1002/jgrf.20076](https://doi.org/10.1002/jgrf.20076).
- 11 Nowicki, S. et al., 2020a: Experimental protocol for sea level projections from ISMIP6 stand-alone ice sheet models.
12 *Cryosphere*, **14(7)**, 2331–2368, doi:[10.5194/tc-14-2331-2020](https://doi.org/10.5194/tc-14-2331-2020).
- 13 Nowicki, S. et al., 2020b: Experimental protocol for sea level projections from ISMIP6 standalone ice sheet models.
14 *The Cryosphere*, **14**, 2331–2368, doi:[10.5194/tc-14-2331-2020](https://doi.org/10.5194/tc-14-2331-2020).
- 15 Nowicki, S.M. and H. Seroussi, 2018: Projections of Future Sea Level Contributions from the Greenland and Antarctic
16 Ice Sheets: Challenges Beyond Dynamical Ice Sheet Modeling. *Oceanography*,
17 doi:[10.5670/oceanog.2018.216](https://doi.org/10.5670/oceanog.2018.216).
- 18 Nowicki, S.M., A. Payne, E. Larour, and E. Al., 2016: Ice Sheet Model Intercomparison Project (ISMIP6) contribution
19 to CMIP6. *Geoscientific Model Development*, **9(12)**, 4521–4545, doi:[10.5194/gmd-9-4521-2016](https://doi.org/10.5194/gmd-9-4521-2016).
- 20 Nussbaumer, S.U. and H.J. Zumbühl, 2012: The Little Ice Age history of the Glacier des Bossons (Mont Blanc massif,
21 France): a new high-resolution glacier length curve based on historical documents. *Climatic Change*, **111(2)**,
22 301–334, doi:[10.1007/s10584-011-0130-9](https://doi.org/10.1007/s10584-011-0130-9).
- 23 O'Neill, H.B., S.L. Smith, and C. Duchesne, 2019: Long-Term Permafrost Degradation and Thermokarst Subsidence in
24 the Mackenzie Delta Area Indicated by Thaw Tube Measurements. In: *Cold Regions Engineering 2019*. pp.
25 643–651, doi:[10.1061/9780784482599.074](https://doi.org/10.1061/9780784482599.074).
- 26 O'Reilly, C.H., L. Zanna, and T. Woollings, 2019: Assessing External and Internal Sources of Atlantic Multidecadal
27 Variability Using Models, Proxy Data, and Early Instrumental Indices. *Journal of Climate*, **32(22)**, 7727–7745,
28 doi:[10.1175/jcli-d-19-0177.1](https://doi.org/10.1175/jcli-d-19-0177.1).
- 29 Obase, T., A. Abe-Ouchi, K. Kusahara, H. Hasumi, and R. Ohgaito, 2017: Responses of Basal Melting of Antarctic Ice
30 Shelves to the Climatic Forcing of the Last Glacial Maximum and CO2 Doubling. *Journal of Climate*, **30(10)**,
31 3473–3497, doi:[10.1175/jcli-d-15-0908.1](https://doi.org/10.1175/jcli-d-15-0908.1).
- 32 Obu, J., S. Westermann, A. Käab, and A. Bartsch, 2018: Ground Temperature Map, 2000–2016, Northern Hemisphere
33 Permafrost. Alfred Wegener Institute, Helmholtz Centre for Polar and Marine Research, Bremerhaven,
34 Germany, PANGAEA. Retrieved from: <https://doi.org/10.1594/pangaea.888600>.
- 35 Obu, J. et al., 2019: Northern Hemisphere permafrost map based on TTOP modelling for 2000–2016 at 1 km2 scale.
36 *Earth-Science Reviews*, **193**, 299–316, doi:[10.1016/j.earscirev.2019.04.023](https://doi.org/10.1016/j.earscirev.2019.04.023).
- 37 Obu, J. et al., 2020: Pan-Antarctic map of near-surface permafrost temperatures at 1 km2 scale. *The Cryosphere*, **14**,
38 497–519, doi:[10.5194/tc-14-497-2020](https://doi.org/10.5194/tc-14-497-2020).
- 39 Ochwat, N.E., S.J. Marshall, B.J. Moorman, A.S. Criscitiello, and L. Copland, 2021: Meltwater Storage in the firn of
40 Kaskawulsh Glacier, Yukon Territory, Canada. *The Cryosphere*, **in press**, doi:[10.5194/tc-2020-119](https://doi.org/10.5194/tc-2020-119).
- 41 Oerder, V. et al., 2015a: Peru-Chile upwelling dynamics under climate change. *Journal of Geophysical Research:*
42 *Oceans*, **120(2)**, 1152–1172, doi:[10.1002/2014jc010299](https://doi.org/10.1002/2014jc010299).
- 43 Oerder, V. et al., 2015b: Peru-Chile upwelling dynamics under climate change. *Journal of Geophysical Research:*
44 *Oceans*, **120(2)**, 1152–1172, doi:[10.1002/2014jc010299](https://doi.org/10.1002/2014jc010299).
- 45 Oey, L.-Y. and S. Chou, 2016: Evidence of rising and poleward shift of storm surge in western North Pacific in recent
46 decades. *Journal of Geophysical Research: Oceans*, **121(7)**, 5181–5192, doi:[10.1002/2016jc011777](https://doi.org/10.1002/2016jc011777).
- 47 Oka, E. et al., 2017: Long-term change and variation of salinity in the western North Pacific subtropical gyre revealed
48 by 50-year long observations along 137°E. *Journal of Oceanography*, **73(4)**, 479–490, doi:[10.1007/s10872-](https://doi.org/10.1007/s10872-017-0416-2)
49 [017-0416-2](https://doi.org/10.1007/s10872-017-0416-2).
- 50 Oka, E. et al., 2019: Remotely Forced Decadal Physical and Biogeochemical Variability of North Pacific Subtropical
51 Mode Water Over the Last 40 Years. *Geophysical Research Letters*, **46(3)**, 1555–1561,
52 doi:[10.1029/2018gl081330](https://doi.org/10.1029/2018gl081330).
- 53 Olason, E. and D. Notz, 2014: Drivers of variability in Arctic sea-ice drift speed. *Journal of Geophysical Research C:*
54 *Oceans*, **119(9)**, 5755–5775, doi:[10.1002/2014jc009897](https://doi.org/10.1002/2014jc009897).

- 1 Oldenburg, D., K.C. Armour, L.A. Thompson, and C.M. Bitz, 2018a: Distinct Mechanisms of Ocean Heat Transport
2 Into the Arctic Under Internal Variability and Climate Change. *Geophysical Research Letters*, **45(15)**, 7692–
3 7700, doi:[10.1029/2018gl078719](https://doi.org/10.1029/2018gl078719).
- 4 Oldenburg, D., K.C. Armour, L.A. Thompson, and C.M. Bitz, 2018b: Distinct Mechanisms of Ocean Heat Transport
5 Into the Arctic Under Internal Variability and Climate Change. *Geophysical Research Letters*, **45(15)**, 7692–
6 7700, doi:[10.1029/2018gl078719](https://doi.org/10.1029/2018gl078719).
- 7 Olefeldt, D. et al., 2016: Circumpolar distribution and carbon storage of thermokarst landscapes. *Nature*
8 *Communications*, **7**, doi:[10.1038/ncomms13043](https://doi.org/10.1038/ncomms13043).
- 9 Oliver, E.C.J., 2019: Mean warming not variability drives marine heatwave trends. *Climate Dynamics*, **53(3)**, 1653–
10 1659, doi:[10.1007/s00382-019-04707-2](https://doi.org/10.1007/s00382-019-04707-2).
- 11 Oliver, E.C.J. et al., 2019: Projected Marine Heatwaves in the 21st Century and the Potential for Ecological Impact.
12 *Frontiers in Marine Science*, **6**, 734, doi:[10.3389/fmars.2019.00734](https://doi.org/10.3389/fmars.2019.00734).
- 13 Olonscheck, D. and D. Notz, 2017: Consistently estimating internal climate variability from climate model simulations.
14 *Journal of Climate*, **30(23)**, 9555–9573, doi:[10.1175/jcli-d-16-0428.1](https://doi.org/10.1175/jcli-d-16-0428.1).
- 15 Olonscheck, D., T. Mauritsen, and D. Notz, 2019: Arctic sea-ice variability is primarily driven by atmospheric
16 temperature fluctuations. *Nature Geoscience*, **12(6)**, 430–434, doi:[10.1038/s41561-019-0363-1](https://doi.org/10.1038/s41561-019-0363-1).
- 17 Olonscheck, D., M. Rugenstein, and J. Marotzke, 2020: Broad Consistency Between Observed and Simulated Trends in
18 Sea Surface Temperature Patterns. *Geophysical Research Letters*, **47(10)**, e2019GL086773,
19 doi:[10.1029/2019gl086773](https://doi.org/10.1029/2019gl086773).
- 20 Onarheim, I.H., T. Eldevik, L.H. Smedsrud, and J.C. Stroeve, 2018: Seasonal and regional manifestation of Arctic sea
21 ice loss. *Journal of Climate*, **31(12)**, 4917–4932, doi:[10.1175/jcli-d-17-0427.1](https://doi.org/10.1175/jcli-d-17-0427.1).
- 22 Oppenheimer, M. et al., 2019: Sea Level Rise and Implications for Low Lying Islands, Coasts and Communities. In:
23 *IPCC Special Report on the Ocean and Cryosphere in a Changing Climate* [Pörtner, H.-O., D.C. Roberts, V.
24 Masson-Delmotte, P. Zhai, M. Tignor, E. Poloczanska, K. Mintenbeck, M. Nicolai, A. Okem, J. Petzold, B.
25 Rama, and N. Weyer (eds.)]. In Press, pp. 321–445.
- 26 Orton, P., N. Georgas, A. Blumberg, and J. Pullen, 2012: Detailed modeling of recent severe storm tides in estuaries of
27 the New York City region. *Journal of Geophysical Research: Oceans*, **117(C9)**, n/a–n/a,
28 doi:[10.1029/2012jc008220](https://doi.org/10.1029/2012jc008220).
- 29 Orton, P.M. et al., 2018: Flood hazard assessment from storm tides, rain and sea level rise for a tidal river estuary.
30 *Natural Hazards*, 1–29, doi:[10.1007/s11069-018-3251-x](https://doi.org/10.1007/s11069-018-3251-x).
- 31 Østerhus, S. et al., 2019: Arctic Mediterranean exchanges: a consistent volume budget and trends in transports from two
32 decades of observations. *Ocean Science*, **15(2)**, 379–399, doi:[10.5194/os-15-379-2019](https://doi.org/10.5194/os-15-379-2019).
- 33 Overduin, P.P. et al., 2019: Submarine Permafrost Map in the Arctic Modeled Using 1-D Transient Heat Flux
34 (SuPerMAP). *Journal of Geophysical Research: Oceans*, **124(6)**, 3490–3507, doi:[10.1029/2018jc014675](https://doi.org/10.1029/2018jc014675).
- 35 Oyarzún, D. and C.M. Brierley, 2019: The future of coastal upwelling in the Humboldt current from model projections.
36 *Climate Dynamics*, **52(1–2)**, 599–615, doi:[10.1007/s00382-018-4158-7](https://doi.org/10.1007/s00382-018-4158-7).
- 37 Palacios, D. et al., 2020: Climate sensitivity and geomorphological response of cirque glaciers from the late glacial to
38 the Holocene, Sierra Nevada, Spain. *Quaternary Science Reviews*, **248**, 106617,
39 doi:[10.1016/j.quascirev.2020.106617](https://doi.org/10.1016/j.quascirev.2020.106617).
- 40 Palanisamy, H., B. Meyssignac, A. Cazenave, and T. Delcroix, 2015: Is anthropogenic sea level fingerprint already
41 detectable in the Pacific Ocean? *Environmental Research Letters*, **10(8)**, 084024, doi:[10.1088/1748-
42 9326/10/8/084024](https://doi.org/10.1088/1748-9326/10/8/084024).
- 43 Palmer, M.D., G.R. Harris, and J.M. Gregory, 2018: Extending CMIP5 projections of global mean temperature change
44 and sea level rise due to thermal expansion using a physically-based emulator. *Environmental Research*
45 *Letters*, **13(8)**, 84003.
- 46 Palmer, M.D., C.M. Domingues, A.B.A. Slangen, and F. Boeira Dias, 2021: An ensemble approach to quantify global
47 mean sea-level rise over the 20th century from tide gauge reconstructions. *Environmental Research Letters*,
48 **16(4)**, 044043, doi:[10.1088/1748-9326/abdae](https://doi.org/10.1088/1748-9326/abdae).
- 49 Palmer, M.D. et al., 2017: Ocean heat content variability and change in an ensemble of ocean reanalyses. *Climate*
50 *Dynamics*, **49(3)**, 909–930, doi:[10.1007/s00382-015-2801-0](https://doi.org/10.1007/s00382-015-2801-0).
- 51 Palmer, M.D. et al., 2020: Exploring the Drivers of Global and Local Sea-Level Change Over the 21st Century and
52 Beyond. *Earth's Future*, **8(9)**, e2019EF001413, doi:[10.1029/2019ef001413](https://doi.org/10.1029/2019ef001413).
- 53 Paolo, F.S., H.A. Fricker, and L. Padman, 2015: Volume loss from Antarctic ice shelves is accelerating. *Science*,
54 **348(6232)**, 327–331, doi:[10.1126/science.aaa0940](https://doi.org/10.1126/science.aaa0940).
- 55 Paquin, J.P. and L. Sushama, 2015: On the Arctic near-surface permafrost and climate sensitivities to soil and snow
56 model formulations in climate models. *Climate Dynamics*, **44(1–2)**, 203–228, doi:[10.1007/s00382-014-2185-6](https://doi.org/10.1007/s00382-014-2185-6).

- 1 Pardaens, A.K., J.M. Gregory, and J.A. Lowe, 2011: A model study of factors influencing projected changes in regional
2 sea level over the twenty-first century. *Climate Dynamics*, **36(9)**, 2015–2033, doi:[10.1007/s00382-009-0738-x](https://doi.org/10.1007/s00382-009-0738-x).
- 3 Park, H. et al., 2020: Increasing riverine heat influx triggers Arctic sea ice decline and oceanic and atmospheric
4 warming. *Science Advances*, **6(45)**, eabc4699, doi:[10.1126/sciadv.abc4699](https://doi.org/10.1126/sciadv.abc4699).
- 5 Parkes, D. and B. Marzeion, 2018: Twentieth-century contribution to sea-level rise from uncharted glaciers. *Nature*,
6 **563(7732)**, 551–554, doi:[10.1038/s41586-018-0687-9](https://doi.org/10.1038/s41586-018-0687-9).
- 7 Parkinson, C.L., 2019: A 40-y record reveals gradual Antarctic sea ice increases followed by decreases at rates far
8 exceeding the rates seen in the Arctic. *Proceedings of the National Academy of Sciences*, **116(29)**, 14414–
9 14423, doi:[10.1073/pnas.1906556116](https://doi.org/10.1073/pnas.1906556116).
- 10 Parras-Berrocal, I.M. et al., 2020: The climate change signal in the Mediterranean Sea in a regionally coupled
11 atmosphere-ocean model. *Ocean Science*, **16(3)**, 743–765, doi:[10.5194/os-16-743-2020](https://doi.org/10.5194/os-16-743-2020).
- 12 Patterson, M.O. et al., 2014: Orbital forcing of the East Antarctic ice sheet during the Pliocene and Early Pleistocene.
13 *Nature Geoscience*, **7(11)**, 841–847, doi:[10.1038/ngeo2273](https://doi.org/10.1038/ngeo2273).
- 14 Patton, A.I., S.L. Rathburn, and D.M. Capps, 2019: Landslide response to climate change in permafrost regions.
15 *Geomorphology*, **340**, 116–128, doi:[10.1016/j.geomorph.2019.04.029](https://doi.org/10.1016/j.geomorph.2019.04.029).
- 16 Patton, H. et al., 2015: Geophysical constraints on the dynamics and retreat of the Barents Sea ice sheet as a
17 paleobenchmark for models of marine ice sheet deglaciation. *Reviews of Geophysics*, **53(4)**, 1051–1098,
18 doi:[10.1002/2015rg000495](https://doi.org/10.1002/2015rg000495).
- 19 Patton, H. et al., 2017: Deglaciation of the Eurasian ice sheet complex. *Quaternary Science Reviews*, **169**, 148–172,
20 doi:[10.1016/j.quascirev.2017.05.019](https://doi.org/10.1016/j.quascirev.2017.05.019).
- 21 Pattyn, F. and G. Durand, 2013: Why marine ice sheet model predictions may diverge in estimating future sea level rise.
22 *Geophysical Research Letters*, **40(16)**, 4316–4320, doi:[10.1002/grl.50824](https://doi.org/10.1002/grl.50824).
- 23 Pattyn, F. and M. Morlighem, 2020: The uncertain future of the Antarctic Ice Sheet. *Science*, **367(6484)**, 1331–1335,
24 doi:[10.1126/science.aaz5487](https://doi.org/10.1126/science.aaz5487).
- 25 Pattyn, F. et al., 2008: Benchmark experiments for higher-order and full-Stokes ice sheet models (ISMIP-HOM).
26 *Cryosphere*, **2(2)**, 95–108, doi:[10.5194/tc-2-95-2008](https://doi.org/10.5194/tc-2-95-2008).
- 27 Pattyn, F. et al., 2012: Results of the Marine Ice Sheet Model Intercomparison Project, MISIP. *The Cryosphere*, **6(3)**,
28 573–588, doi:[10.5194/tc-6-573-2012](https://doi.org/10.5194/tc-6-573-2012).
- 29 Pavlova, O., S. Gerland, and H. Hop, 2019: Changes in Sea-Ice Extent and Thickness in Kongsfjorden, Svalbard (2003–
30 2016). In: *The Ecosystem of Kongsfjorden, Svalbard* [Hop, H. and C. Wiencke (eds.)]. Advances in Polar
31 Ecology Vol. 2, Springer, Cham, Switzerland, pp. 105–136, doi:[10.1007/978-3-319-46425-1_4](https://doi.org/10.1007/978-3-319-46425-1_4).
- 32 Payne, A.J. et al., 2021: Contrasting contributions to future sea level under CMIP5 and CMIP6 scenarios from the
33 Greenland and Antarctic ice sheets. *Geophysical Research Letters*, **in press**, 1–12.
- 34 Pearson, B., B. Fox-Kemper, S. Bachman, and F. Bryan, 2017: Evaluation of scale-aware subgrid mesoscale eddy
35 models in a global eddy-rich model. *Ocean Modelling*, **115**, 42–58, doi:[10.1016/j.ocemod.2017.05.007](https://doi.org/10.1016/j.ocemod.2017.05.007).
- 36 Pederson, G.T. et al., 2011: The unusual nature of recent snowpack declines in the North American Cordillera. *Science*,
37 **333(6040)**, 332–335, doi:[10.1126/science.1201570](https://doi.org/10.1126/science.1201570).
- 38 Pelle, T., M. Morlighem, and J. Bondzio, 2019: Brief communication: PICOP, a new ocean melt parameterization under
39 ice shelves combining PICO and a plume model. *Cryosphere*, **13**, 1043–1049, doi:[10.5194/tc-13-1043-2019](https://doi.org/10.5194/tc-13-1043-2019).
- 40 Peltier, W.R., D.F. Argus, and R. Drummond, 2015: Space geodesy constrains ice age terminal deglaciation: The global
41 ICE-6G_C (VM5a) model. *Journal of Geophysical Research: Solid Earth*, **120(1)**, 450–487,
42 doi:[10.1002/2014jb011176](https://doi.org/10.1002/2014jb011176).
- 43 Pendleton, S.L. et al., 2019: Rapidly receding Arctic Canada glaciers revealing landscapes continuously ice-covered for
44 more than 40,000 years. *Nature Communications*, **10(1)**, 445, doi:[10.1038/s41467-019-08307-w](https://doi.org/10.1038/s41467-019-08307-w).
- 45 Peng, D., E.M. Hill, A.J. Meltzner, and A.D. Switzer, 2019: Tide Gauge Records Show That the 18.61-Year Nodal
46 Tidal Cycle Can Change High Water Levels by up to 30 cm. *Journal of Geophysical Research: Oceans*,
47 **124(1)**, 736–749, doi:[10.1029/2018jc014695](https://doi.org/10.1029/2018jc014695).
- 48 Peng, G. and W.N. Meier, 2018: Temporal and regional variability of Arctic sea-ice coverage from satellite data.
49 *Annals of Glaciology*, **59(76pt2)**, 191–200, doi:[10.1017/aog.2017.32](https://doi.org/10.1017/aog.2017.32).
- 50 Peng, S. et al., 2013: Change in snow phenology and its potential feedback to temperature in the Northern Hemisphere
51 over the last three decades. *Environmental Research Letters*, **8**, 014008, doi:[10.1088/1748-9326/8/1/014008](https://doi.org/10.1088/1748-9326/8/1/014008).
- 52 Perego, M., S. Price, and G. Stadler, 2014: Optimal initial conditions for coupling ice sheet models to Earth system
53 models. *Journal Of Geophysical Research-Earth Surface*, **119(9)**, 1894–1917, doi:[10.1002/2014jf003181](https://doi.org/10.1002/2014jf003181).
- 54 Perkins-Kirkpatrick, S.E. et al., 2018: The role of natural variability and anthropogenic climate change in the 2017/2018
55 Tasman Sea marine heatwave. *Bulletin of the American Meteorological Society*, 1–4, doi:[10.1175/bams-d-18-0116.1](https://doi.org/10.1175/bams-d-18-0116.1).
- 56

- 1 Noetzli, J., C. Pellet, and B. Staub (eds.), 2019: *Permafrost in Switzerland 2014/2015 to 2017/2018*. Glaciological
2 Report (Permafrost) No. 16-19, Cryospheric Commission of the Swiss Academy of Sciences, 104 pp.,
3 doi:[10.13093/permos-rep-2019-16-19](https://doi.org/10.13093/permos-rep-2019-16-19).
- 4 Petit, T., M.S. Lozier, S.A. Josey, and S.A. Cunningham, 2020: Atlantic Deep Water Formation Occurs Primarily in the
5 Iceland Basin and Irminger Sea by Local Buoyancy Forcing. *Geophysical Research Letters*, **47(22)**,
6 doi:[10.1029/2020gl091028](https://doi.org/10.1029/2020gl091028).
- 7 Petty, A.A., M.M. Holland, D.A. Bailey, and N.T. Kurtz, 2018: Warm Arctic, Increased Winter Sea Ice Growth?
8 *Geophysical Research Letters*, **45(23)**, 12,922–12,930, doi:[10.1029/2018gl079223](https://doi.org/10.1029/2018gl079223).
- 9 Petty, A.A., N.T. Kurtz, R. Kwok, T. Markus, and T.A. Neumann, 2020: Winter Arctic Sea Ice Thickness From
10 ICESat-2 Freeboards. *Journal of Geophysical Research: Oceans*, **125(5)**, e2019JC015764,
11 doi:[10.1029/2019jc015764](https://doi.org/10.1029/2019jc015764).
- 12 Piatt, J.F. et al., 2020: Extreme mortality and reproductive failure of common murrelets resulting from the northeast
13 Pacific marine heatwave of 2014–2016. *PLoS ONE*, **15(1)**, doi:[10.1371/journal.pone.0226087](https://doi.org/10.1371/journal.pone.0226087).
- 14 Pickart, R.S. and M.A. Spall, 2007: Impact of Labrador Sea convection on the North Atlantic meridional overturning
15 circulation. *Journal of Physical Oceanography*, **37(9)**, 2207–2227, doi:[10.1175/jpo3178.1](https://doi.org/10.1175/jpo3178.1).
- 16 Pickering, M.D., N.C. Wells, K.J. Horsburgh, and J.A.M. Green, 2012: The impact of future sea-level rise on the
17 European Shelf tides. *Continental Shelf Research*, **35**, 1–15, doi:[10.1016/j.csr.2011.11.011](https://doi.org/10.1016/j.csr.2011.11.011).
- 18 Pickering, M.D.D. et al., 2017: The impact of future sea-level rise on the global tides. *Continental Shelf Research*, **142**,
19 50–68, doi:[10.1016/j.csr.2017.02.004](https://doi.org/10.1016/j.csr.2017.02.004).
- 20 Pico, T., A. Robel, E. Powell, A.C. Mix, and J.X. Mitrovica, 2019: Leveraging the Rapid Retreat of the Amundsen Gulf
21 Ice Stream 13,000 Years Ago to Reveal Insight Into North American Deglaciation. *Geophysical Research
22 Letters*, **46(21)**, 12101–12107, doi:[10.1029/2019gl084789](https://doi.org/10.1029/2019gl084789).
- 23 Piecuch, C.G., R.M. Ponte, C.M. Little, M.W. Buckley, and I. Fukumori, 2017: Mechanisms underlying recent decadal
24 changes in subpolar North Atlantic Ocean heat content. *Journal of Geophysical Research: Oceans*, **122(9)**,
25 7181–7197, doi:[10.1002/2017jc012845](https://doi.org/10.1002/2017jc012845).
- 26 Piecuch, C.G., P.R. Thompson, R.M. Ponte, M.A. Merrifield, and B.D. Hamlington, 2019: What Caused Recent Shifts
27 in Tropical Pacific Decadal Sea-Level Trends? *Journal of Geophysical Research: Oceans*, **124(11)**, 7575–
28 7590, doi:[10.1029/2019jc015339](https://doi.org/10.1029/2019jc015339).
- 29 Piecuch, C.G. et al., 2018: Origin of spatial variation in US East Coast sea-level trends during 1900–2017. *Nature*,
30 **564(7736)**, 400–404, doi:[10.1038/s41586-018-0787-6](https://doi.org/10.1038/s41586-018-0787-6).
- 31 Pilo, G.S., N.J. Holbrook, A.E. Kiss, and A.M.C. Hogg, 2019: Sensitivity of Marine Heatwave Metrics to Ocean Model
32 Resolution. *Geophysical Research Letters*, **46**, doi:[10.1029/2019gl084928](https://doi.org/10.1029/2019gl084928).
- 33 Plach, A., K.H. Nisancioglu, P.M. Langebroek, A. Born, and S. Le Clec'h, 2019: Eemian Greenland ice sheet simulated
34 with a higher-order model shows strong sensitivity to surface mass balance forcing. *Cryosphere*, **13(8)**, 2133–
35 2148, doi:[10.5194/tc-13-2133-2019](https://doi.org/10.5194/tc-13-2133-2019).
- 36 Plecha, S.M. and P.M.M. Soares, 2020: Global marine heatwave events using the new CMIP6 multi-model ensemble:
37 from shortcomings in present climate to future projections. *Environmental Research Letters*, **15(12)**, 124058,
38 doi:[10.1088/1748-9326/abc847](https://doi.org/10.1088/1748-9326/abc847).
- 39 Pollard, D., R.M. DeConto, and R.B. Alley, 2015: Potential Antarctic Ice Sheet retreat driven by hydrofracturing and
40 ice cliff failure. *Earth and Planetary Science Letters*, **412**, 112–121, doi:[10.1016/j.epsl.2014.12.035](https://doi.org/10.1016/j.epsl.2014.12.035).
- 41 Pollard, D., N. Gomez, R.M. DeConto, and H.K. Han, 2018: Estimating Modern Elevations of Pliocene Shorelines
42 Using a Coupled Ice Sheet-Earth-Sea Level Model. *Journal of Geophysical Research: Earth Surface*, **123(9)**,
43 2279–2291, doi:[10.1029/2018jf004745](https://doi.org/10.1029/2018jf004745).
- 44 Pollard, D., W. Chang, M. Haran, P. Applegate, and R. DeConto, 2016: Large ensemble modeling of the last deglacial
45 retreat of the West Antarctic Ice Sheet: comparison of simple and advanced statistical techniques.
46 *Geoscientific Model Development*, **9(5)**, 1697–1723, doi:[10.5194/gmd-9-1697-2016](https://doi.org/10.5194/gmd-9-1697-2016).
- 47 Pope, J.O., P.R. Holland, A. Orr, G.J. Marshall, and T. Phillips, 2017: The impacts of El Niño on the observed sea ice
48 budget of West Antarctica. *Geophysical Research Letters*, **44(12)**, 6200–6208, doi:[10.1002/2017gl073414](https://doi.org/10.1002/2017gl073414).
- 49 Porada, P., A. Ekici, and C. Beer, 2016: Effects of bryophyte and lichen cover on permafrost soil temperature at large
50 scale. *The Cryosphere*, **10(5)**, 2291–2315, doi:[10.5194/tc-10-2291-2016](https://doi.org/10.5194/tc-10-2291-2016).
- 51 Portela, E., N. Kolodziejczyk, C. Maes, and V. Thierry, 2020: Interior water-mass variability in the Southern-
52 Hemisphere oceans during the last decade. *Journal of Physical Oceanography*, **50(2)**, 361–381,
53 doi:[10.1175/jpo-d-19-0128.1](https://doi.org/10.1175/jpo-d-19-0128.1).
- 54 Prandi, P. et al., 2021: Local sea level trends, accelerations and uncertainties over 1993–2019. *Scientific Data*, **8(1)**, 1–
55 12, doi:[10.1038/s41597-020-00786-7](https://doi.org/10.1038/s41597-020-00786-7).

- 1 Pratap, B., D.P. Dobhal, M. Mehta, and R. Bhambri, 2015: Influence of debris cover and altitude on glacier surface
2 melting: A case study on Dokriani Glacier, central Himalaya, India. *Annals of Glaciology*, **56(70)**, 9–16,
3 doi:[10.3189/2015aog70a971](https://doi.org/10.3189/2015aog70a971).
- 4 Previdi, M. and L.M. Polvani, 2016: Anthropogenic impact on Antarctic surface mass balance, currently masked by
5 natural variability, to emerge by mid-century. *Environmental Research Letters*, **11(9)**, 094001,
6 doi:[10.1088/1748-9326/11/9/094001](https://doi.org/10.1088/1748-9326/11/9/094001).
- 7 Pulliainen, J. et al., 2020: Patterns and trends of Northern Hemisphere snow mass from 1980 to 2018. *Nature*,
8 **581(7808)**, 294–298, doi:[10.1038/s41586-020-2258-0](https://doi.org/10.1038/s41586-020-2258-0).
- 9 Punge, H.J., H. Gallée, M. Kageyama, and G. Krinner, 2012: Modelling snow accumulation on Greenland in Eemian,
10 glacial inception, and modern climates in a GCM. *Climate of the Past*, **8**, 1801–1819, doi:[10.5194/cp-8-1801-2012](https://doi.org/10.5194/cp-8-1801-2012).
- 11
12 Purich, A. and M.H. England, 2019: Tropical Teleconnections to Antarctic Sea Ice During Austral Spring 2016 in
13 Coupled Pacemaker Experiments. *Geophysical Research Letters*, **46(12)**, 6848–6858,
14 doi:[10.1029/2019g1082671](https://doi.org/10.1029/2019g1082671).
- 15 Purich, A., M.H. England, W. Cai, A. Sullivan, and P.J. Durack, 2018: Impacts of broad-scale surface freshening of the
16 Southern Ocean in a coupled climate model. *Journal of Climate*, **31(7)**, 2613–2632, doi:[10.1175/jcli-d-17-0092.1](https://doi.org/10.1175/jcli-d-17-0092.1).
- 17
18 Purich, A. et al., 2016: Tropical pacific SST drivers of recent antarctic sea ice trends. *Journal of Climate*, **29(24)**, 8931–
19 8948, doi:[10.1175/jcli-d-16-0440.1](https://doi.org/10.1175/jcli-d-16-0440.1).
- 20 Purkey, S.G. et al., 2019a: Unabated Bottom Water Warming and Freshening in the South Pacific Ocean. *Journal of*
21 *Geophysical Research: Oceans*, **124(3)**, 1778–1794, doi:[10.1029/2018jc014775](https://doi.org/10.1029/2018jc014775).
- 22 Purkey, S.G. et al., 2019b: Unabated Bottom Water Warming and Freshening in the South Pacific Ocean. *Journal of*
23 *Geophysical Research: Oceans*, **124(3)**, 1778–1794, doi:[10.1029/2018jc014775](https://doi.org/10.1029/2018jc014775).
- 24 Qiao, F., Y. Yuan, J. Deng, D. Dai, and Z. Song, 2016: Wave–turbulence interaction-induced vertical mixing and its
25 effects in ocean and climate models. *Philosophical Transactions of the Royal Society A: Mathematical,*
26 *Physical and Engineering Sciences*, **374(2065)**, 20150201, doi:[10.1098/rsta.2015.0201](https://doi.org/10.1098/rsta.2015.0201).
- 27 Qiao, G., Y. Li, S. Guo, and W. Ye, 2020: Evolving instability of the scar inlet ice shelf based on sequential landsat
28 images spanning 2005–2018. *Remote Sensing*, **12(1)**, 36, doi:[10.3390/rs12010036](https://doi.org/10.3390/rs12010036).
- 29 Qiu, B. and S. Chen, 2012: Multidecadal Sea Level and Gyre Circulation Variability in the Northwestern Tropical
30 Pacific Ocean. *Journal of Physical Oceanography*, **42(1)**, 193–206, doi:[10.1175/jpo-d-11-061.1](https://doi.org/10.1175/jpo-d-11-061.1).
- 31 Qiu, B., S. Chen, B. Qiu, and S. Chen, 2005: Variability of the Kuroshio Extension Jet, Recirculation Gyre, and
32 Mesoscale Eddies on Decadal Time Scales. *Journal of Physical Oceanography*, **35(11)**, 2090–2103,
33 doi:[10.1175/jpo2807.1](https://doi.org/10.1175/jpo2807.1).
- 34 Qu, T., S. Gao, and R.A. Fine, 2020: Variability of the Sub-Antarctic Mode Water Subduction Rate During the Argo
35 Period. *Geophysical Research Letters*, **47(13)**, e2020GL088248, doi:[10.1029/2020g1088248](https://doi.org/10.1029/2020g1088248).
- 36 Qu, X. and A. Hall, 2014: On the persistent spread in snow-albedo feedback. *Climate Dynamics*, **42(1–2)**, 69–81,
37 doi:[10.1007/s00382-013-1774-0](https://doi.org/10.1007/s00382-013-1774-0).
- 38 Quiquet, A., C. Ritz, H.J. Punge, and D. y Méliá, 2013: Greenland ice sheet contribution to sea level rise during the last
39 interglacial period: a modelling study driven and constrained by ice core data. *Climate of the Past*, **9(1)**, 353–
40 366, doi:[10.5194/cp-9-353-2013](https://doi.org/10.5194/cp-9-353-2013).
- 41 Rabatel, A. et al., 2013: Current state of glaciers in the tropical Andes: a multi-century perspective on glacier evolution
42 and climate change. *The Cryosphere*, **7(1)**, 81–102, doi:[10.5194/tc-7-81-2013](https://doi.org/10.5194/tc-7-81-2013).
- 43 Radić, V. et al., 2014: Regional and global projections of twenty-first century glacier mass changes in response to
44 climate scenarios from global climate models. *Climate Dynamics*, **42(1–2)**, 37–58, doi:[10.1007/s00382-013-1719-7](https://doi.org/10.1007/s00382-013-1719-7).
- 45
46 Rae, J.W.B. et al., 2018: CO2 storage and release in the deep Southern Ocean on millennial to centennial timescales.
47 *Nature*, **562(7728)**, 569–573, doi:[10.1038/s41586-018-0614-0](https://doi.org/10.1038/s41586-018-0614-0).
- 48 Rahmstorf, S., M. Perrette, and M. Vermeer, 2012: Testing the robustness of semi-empirical sea level projections.
49 *Climate Dynamics*, **39(3–4)**, 861–875, doi:[10.1007/s00382-011-1226-7](https://doi.org/10.1007/s00382-011-1226-7).
- 50 Rampal, P., J. Weiss, and D. Marsan, 2009: Positive trend in the mean speed and deformation rate of Arctic sea ice,
51 1979–2007. *Journal of Geophysical Research: Oceans*, **114(5)**, doi:[10.1029/2008jc005066](https://doi.org/10.1029/2008jc005066).
- 52 Ran, Y., X. Li, and G. Cheng, 2018: Climate warming over the past half century has led to thermal degradation of
53 permafrost on the Qinghai-Tibet Plateau. *Cryosphere*, **12**, 595–608, doi:[10.5194/tc-12-595-2018](https://doi.org/10.5194/tc-12-595-2018).
- 54 Rashid, M.M. and T. Wahl, 2020: Predictability of Extreme Sea Level Variations Along the U.S. Coastline. *Journal of*
55 *Geophysical Research: Oceans*, **125(9)**, doi:[10.1029/2020jc016295](https://doi.org/10.1029/2020jc016295).

- 1 Rathore, S., N.L. Bindoff, H.E. Phillips, and M. Feng, 2020: Recent hemispheric asymmetry in global ocean warming
2 induced by climate change and internal variability. *Nature Communications*, **11**(1), 2008, doi:[10.1038/s41467-
3 020-15754-3](https://doi.org/10.1038/s41467-020-15754-3).
- 4 Raveland, L., F. Magnin, and P. Deline, 2017: Impacts of the 2003 and 2015 summer heatwaves on permafrost-affected
5 rock-walls in the Mont Blanc massif. *Science of the Total Environment*, **609**, 132–143,
6 doi:[10.1016/j.scitotenv.2017.07.055](https://doi.org/10.1016/j.scitotenv.2017.07.055).
- 7 Ray, R.D., 2009: Secular changes in the solar semidiurnal tide of the western North Atlantic Ocean. *Geophysical
8 Research Letters*, doi:[10.1029/2009gl040217](https://doi.org/10.1029/2009gl040217).
- 9 Raynolds, M.K. et al., 2014: Cumulative geoecological effects of 62 years of infrastructure and climate change in ice-
10 rich permafrost landscapes, Prudhoe Bay Oilfield, Alaska. *Global Change Biology*, **20**(4), 1211–1224,
11 doi:[10.1111/gcb.12500](https://doi.org/10.1111/gcb.12500).
- 12 Reese, R., A. Levermann, T. Albrecht, H. Seroussi, and R. Winkelmann, 2020: The role of history and strength of the
13 oceanic forcing in sea level projections from Antarctica with the Parallel Ice Sheet Model. *Cryosphere*, **14**(9),
14 3097–3110, doi:[10.5194/tc-14-3097-2020](https://doi.org/10.5194/tc-14-3097-2020).
- 15 Reese, R. et al., 2018: The far reach of ice-shelf thinning in Antarctica. *Nature Climate Change*, **8**(1), 53–57,
16 doi:[10.1038/s41558-017-0020-x](https://doi.org/10.1038/s41558-017-0020-x).
- 17 Reguero, B.G., I.J. Losada, and F.J. Méndez, 2019: A recent increase in global wave power as a consequence of oceanic
18 warming. *Nature Communications*, doi:[10.1038/s41467-018-08066-0](https://doi.org/10.1038/s41467-018-08066-0).
- 19 Reichl, B.G. and R. Hallberg, 2018: A simplified energetics based planetary boundary layer (ePBL) approach for ocean
20 climate simulations.. *Ocean Modelling*, **132**, 112–129, doi:[10.1016/j.ocemod.2018.10.004](https://doi.org/10.1016/j.ocemod.2018.10.004).
- 21 Reintges, A., T. Martin, M. Latif, and N.S. Keenlyside, 2017: Uncertainty in twenty-first century projections of the
22 Atlantic Meridional Overturning Circulation in CMIP3 and CMIP5 models. *Climate Dynamics*, **49**(5–6),
23 1495–1511, doi:[10.1007/s00382-016-3180-x](https://doi.org/10.1007/s00382-016-3180-x).
- 24 Renault, L., P. Marchesiello, S. Masson, and J.C. McWilliams, 2019: Remarkable Control of Western Boundary
25 Currents by *<i>Eddy Killing</i>* , a Mechanical Air-Sea Coupling Process. *Geophysical Research Letters*,
26 **46**(5), 2743–2751, doi:[10.1029/2018gl081211](https://doi.org/10.1029/2018gl081211).
- 27 Renault, L. et al., 2016: Modulation of Wind Work by Oceanic Current Interaction with the Atmosphere. *Journal of
28 Physical Oceanography*, **46**(6), 1685–1704, doi:[10.1175/jpo-d-15-0232.1](https://doi.org/10.1175/jpo-d-15-0232.1).
- 29 Renner, A.H.H.H., K.J. Heywood, and S.E. Thorpe, 2009: Validation of three global ocean models in the Weddell Sea.
30 *Ocean Modelling*, **30**(1), 1–15, doi:[10.1016/j.ocemod.2009.05.007](https://doi.org/10.1016/j.ocemod.2009.05.007).
- 31 Réveillet, M., C. Vincent, D. Six, and A. Rabatel, 2017: Which empirical model is best suited to simulate glacier mass
32 balances? *Journal of Glaciology*, **63**(237), 39–54, doi:[10.1017/jog.2016.110](https://doi.org/10.1017/jog.2016.110).
- 33 Réveillet, M. et al., 2018: Relative performance of empirical and physical models in assessing the seasonal and annual
34 glacier surface mass balance of Saint-Sorlin Glacier (French Alps). *Cryosphere*, **12**(4), 1367–1386,
35 doi:[10.5194/tc-12-1367-2018](https://doi.org/10.5194/tc-12-1367-2018).
- 36 Reyes, A. et al., 2014: South Greenland ice-sheet collapse during Marine Isotope Stage 11. *Nature*, **510**(7506), 525–
37 528, doi:[10.1038/nature13456](https://doi.org/10.1038/nature13456).
- 38 Reynhout, S.A. et al., 2019: Holocene glacier fluctuations in Patagonia are modulated by summer insolation intensity
39 and paced by Southern Annular Mode-like variability. *Quaternary Science Reviews*, **220**, 178–187,
40 doi:[10.1016/j.quascirev.2019.05.029](https://doi.org/10.1016/j.quascirev.2019.05.029).
- 41 RGI Consortium, 2017: Randolph Glacier Inventory – A Dataset of Global Glacier Outlines: Version 6.0: Technical
42 Report. Global Land Ice Measurements from Space, CO, USA. Retrieved from: [https://doi.org/10.7265/n5-rgi-
43 60](https://doi.org/10.7265/n5-rgi-60).
- 44 Rhein, M., C. Mertens, and A. Roessler, 2019: Observed Transport Decline at 47°N, Western Atlantic. *Journal of
45 Geophysical Research: Oceans*, **124**(7), 4875–4890, doi:[10.1029/2019jc014993](https://doi.org/10.1029/2019jc014993).
- 46 Rhein, M. et al., 2013: Observations: Ocean. In: *Climate Change 2013 the Physical Science Basis: Working Group I
47 Contribution to the Fifth Assessment Report of the Intergovernmental Panel on Climate Change* [Stocker, T.F.,
48 D. Qin, G.-K. Plattner, M. Tignor, S.K. Allen, J. Boschung, A. Nauels, Y. Xia, V. Bex, and P.M. Midgley
49 (eds.)]. Cambridge University Press, Cambridge, United Kingdom and New York, NY, USA, pp. 255–316,
50 doi:[10.1017/cbo9781107415324.010](https://doi.org/10.1017/cbo9781107415324.010).
- 51 Richter, K. and B. Marzeion, 2014: Earliest local emergence of forced dynamic and steric sea-level trends in climate
52 models. *Environmental Research Letters*, **9**(11), 114009, doi:[10.1088/1748-9326/9/11/114009](https://doi.org/10.1088/1748-9326/9/11/114009).
- 53 Richter, K., B. Marzeion, and R. Riva, 2017: The effect of spatial averaging and glacier melt on detecting a forced
54 signal in regional sea level. *Environmental Research Letters*, doi:[10.1088/1748-9326/aa5967](https://doi.org/10.1088/1748-9326/aa5967).
- 55 Richter, K. et al., 2020: Detecting a forced signal in satellite-era sea-level change. *Environmental Research Letters*,
56 **15**(9), 094079, doi:[10.1088/1748-9326/ab986e](https://doi.org/10.1088/1748-9326/ab986e).

- 1 Ridley, J., J.M. Gregory, P. Huybrechts, and J. Lowe, 2010: Thresholds for irreversible decline of the Greenland ice
2 sheet. *Climate Dynamics*, **35**(6), 1065–1073, doi:[10.1007/s00382-009-0646-0](https://doi.org/10.1007/s00382-009-0646-0).
- 3 Ridley, J.K. and E.W. Blockley, 2018: Brief communication: Solar radiation management not as effective as CO2
4 mitigation for Arctic sea ice loss in hitting the 1.5 and 2°C COP climate targets. *Cryosphere*, **12**(10), 3355–
5 3360, doi:[10.5194/tc-12-3355-2018](https://doi.org/10.5194/tc-12-3355-2018).
- 6 Ridley, J.K., J.A. Lowe, and H.T. Hewitt, 2012: How reversible is sea ice loss? *Cryosphere*, **6**(1), 193–198,
7 doi:[10.5194/tc-6-193-2012](https://doi.org/10.5194/tc-6-193-2012).
- 8 Rietbroek, R., S.-E. Brunnabend, J. Kusche, J. Schröter, and C. Dahle, 2016: Revisiting the contemporary sea-level
9 budget on global and regional scales. *Proceedings of the National Academy of Sciences of the United States of*
10 *America*, **113**(6), 1504–1509, doi:[10.1073/pnas.1519132113](https://doi.org/10.1073/pnas.1519132113).
- 11 Rignot, E., S. Jacobs, J. Mouginot, and B. Scheuchl, 2013: Ice-shelf melting around Antarctica. *Science*, **341**(6143),
12 266–270, doi:[10.1126/science.1235798](https://doi.org/10.1126/science.1235798).
- 13 Rignot, E., J. Mouginot, M. Morlighem, H. Seroussi, and B. Scheuchl, 2014: Widespread, rapid grounding line retreat
14 of Pine Island, Thwaites, Smith, and Kohler glaciers, West Antarctica, from 1992 to 2011. *Geophysical*
15 *Research Letters*, **41**(10), 3502–3509, doi:[10.1002/2014gl060140](https://doi.org/10.1002/2014gl060140).
- 16 Rignot, E. et al., 2019: Four decades of Antarctic Ice Sheet mass balance from 1979–2017. *Proceedings of the National*
17 *Academy of Sciences*, **116**(4), 1–9, doi:[10.1073/pnas.1812883116](https://doi.org/10.1073/pnas.1812883116).
- 18 Rignot, E.I., C. Fenty, X. Kemp, C. Yun, and Cai, 2015: Undercutting of Greenland marine-terminating glaciers in deep
19 glacial fjords. *Geophysical Research Letters*, **42**(14), 5909–5917.
- 20 Ringler, T. et al., 2013: A multi-resolution approach to global ocean modeling. *Ocean Modelling*, **69**, 211–232,
21 doi:[10.1016/j.ocemod.2013.04.010](https://doi.org/10.1016/j.ocemod.2013.04.010).
- 22 Riser, S.C. et al., 2016: Fifteen years of ocean observations with the global Argo array. *Nature Climate Change*, **6**, 145.
- 23 Ritz, C. et al., 2015: Potential sea-level rise from Antarctic ice-sheet instability constrained by observations. *Nature*,
24 **528**(7580), 115–118, doi:[10.1038/nature16147](https://doi.org/10.1038/nature16147).
- 25 Roach, L.A., S.M. Dean, and J.A. Renwick, 2018a: Consistent biases in Antarctic sea ice concentration simulated by
26 climate models. *The Cryosphere*, **12**(1), 365–383, doi:[10.5194/tc-12-365-2018](https://doi.org/10.5194/tc-12-365-2018).
- 27 Roach, L.A., C. Horvat, S.M. Dean, and C.M. Bitz, 2018b: An Emergent Sea Ice Floe Size Distribution in a Global
28 Coupled Ocean-Sea Ice Model. *Journal of Geophysical Research: Oceans*, **123**(6), 4322–4337,
29 doi:[10.1029/2017jc013692](https://doi.org/10.1029/2017jc013692).
- 30 Roach, L.A. et al., 2020: Antarctic Sea Ice Area in CMIP6. *Geophysical Research Letters*, **47**(9),
31 doi:[10.1029/2019gl086729](https://doi.org/10.1029/2019gl086729).
- 32 Robel, A.A., 2017: Thinning sea ice weakens buttressing force of iceberg mélange and promotes calving. *Nature*
33 *Communications*, **8**, 1–7, doi:[10.1038/ncomms14596](https://doi.org/10.1038/ncomms14596).
- 34 Robel, A.A. and A.F. Banwell, 2019: A Speed Limit on Ice Shelf Collapse Through Hydrofracture. *Geophysical*
35 *Research Letters*, **46**(21), 12092–12100, doi:[10.1029/2019gl084397](https://doi.org/10.1029/2019gl084397).
- 36 Robel, A.A., H. Seroussi, and G.H. Roe, 2019: Marine ice sheet instability amplifies and skews uncertainty in
37 projections of future sea-level rise. *Proceedings of the National Academy of Sciences of the United States of*
38 *America*, **116**(30), 14887–14892, doi:[10.1073/pnas.1904822116](https://doi.org/10.1073/pnas.1904822116).
- 39 Roberts, C.D., L. Jackson, and D. McNeall, 2014: Is the 2004–2012 reduction of the Atlantic meridional overturning
40 circulation significant? *Geophysical Research Letters*, **41**(9), 3204–3210, doi:[10.1002/2014gl059473](https://doi.org/10.1002/2014gl059473).
- 41 Roberts, C.D. et al., 2016: On the Drivers and Predictability of Seasonal-to-Interannual Variations in Regional Sea
42 Level. *Journal of Climate*, **29**(21), 7565–7585, doi:[10.1175/jcli-d-15-0886.1](https://doi.org/10.1175/jcli-d-15-0886.1).
- 43 Roberts, M.J. et al., 2018: The Benefits of Global High Resolution for Climate Simulation: Process Understanding and
44 the Enabling of Stakeholder Decisions at the Regional Scale. *Bulletin of the American Meteorological Society*,
45 **99**(11), 2341–2359, doi:[10.1175/bams-d-15-00320.1](https://doi.org/10.1175/bams-d-15-00320.1).
- 46 Roberts, M.J. et al., 2019: Description of the resolution hierarchy of the global coupled HadGEM3-GC3.1 model as
47 used in CMIP6 HighResMIP experiments. *Geoscientific Model Development*, **12**(12), 4999–5028,
48 doi:[10.5194/gmd-12-4999-2019](https://doi.org/10.5194/gmd-12-4999-2019).
- 49 Roberts, M.J. et al., 2020a: Sensitivity of the Atlantic Meridional Overturning Circulation to Model Resolution in
50 CMIP6 HighResMIP Simulations and Implications for Future Changes. *Journal of Advances in Modeling*
51 *Earth Systems*, **12**(8), doi:[10.1029/2019ms002014](https://doi.org/10.1029/2019ms002014).
- 52 Roberts, M.J. et al., 2020b: Sensitivity of the Atlantic Meridional Overturning Circulation to Model Resolution in
53 CMIP6 HighResMIP Simulations and Implications for Future Changes. *Journal of Advances in Modeling*
54 *Earth Systems*, **12**(8), doi:[10.1029/2019ms002014](https://doi.org/10.1029/2019ms002014).

- 1 Roberts, M.J. et al., 2020c: Sensitivity of the Atlantic Meridional Overturning Circulation to Model Resolution in
2 CMIP6 HighResMIP Simulations and Implications for Future Changes. *Journal of Advances in Modeling*
3 *Earth Systems*, **12**(8), doi:[10.1029/2019ms002014](https://doi.org/10.1029/2019ms002014).
- 4 Robinson, A. and H. Goelzer, 2014: The importance of insolation changes for paleo ice sheet modeling. *Cryosphere*,
5 **8**(4), 1419–1428, doi:[10.5194/tc-8-1419-2014](https://doi.org/10.5194/tc-8-1419-2014).
- 6 Robinson, A., R. Calov, and A. Ganopolski, 2011: Greenland ice sheet model parameters constrained using simulations
7 of the Eemian Interglacial. *Climate of the Past*, **7**(2), 381–396.
- 8 Robinson, A., R. Calov, and A. Ganopolski, 2012: Multistability and critical thresholds of the Greenland ice sheet.
9 *Nature Climate Change*, **2**(6), 429–432, doi:[10.1038/nclimate1449](https://doi.org/10.1038/nclimate1449).
- 10 Robinson, A., J. Alvarez-Solas, R. Calov, A. Ganopolski, and M. Montoya, 2017: MIS-11 duration key to
11 disappearance of the Greenland ice sheet. *Nature Communications*, **8**, 16008.
- 12 Robson, J., P. Ortega, and R. Sutton, 2016: A reversal of climatic trends in the North Atlantic since 2005. *Nature*
13 *Geoscience*, **9**(7), 513–517, doi:[10.1038/ngeo2727](https://doi.org/10.1038/ngeo2727).
- 14 Robson, J., R. Sutton, K. Lohmann, D. Smith, and M.D. Palmer, 2012: Causes of the Rapid Warming of the North
15 Atlantic Ocean in the Mid-1990s. *Journal of Climate*, **25**(12), 4116–4134, doi:[10.1175/jcli-d-11-00443.1](https://doi.org/10.1175/jcli-d-11-00443.1).
- 16 Rodehacke, C.B., M. Pfeiffer, T. Semmler, Gurses, and T. Kleiner, 2020: Future sea level contribution from Antarctica
17 inferred from CMIP5 model forcing and its dependence on precipitation ansatz. *Earth System Dynamics*,
18 **11**(4), 1153–1194, doi:[10.5194/esd-11-1153-2020](https://doi.org/10.5194/esd-11-1153-2020).
- 19 Rohling, E.J. et al., 2019: Asynchronous Antarctic and Greenland ice-volume contributions to the last interglacial sea-
20 level highstand. *Nature Communications*, **10**(1), 5040, doi:[10.1038/s41467-019-12874-3](https://doi.org/10.1038/s41467-019-12874-3).
- 21 Romanovsky, V. et al., 2017: Changing Permafrost and its Impacts. In: *Snow, Water, Ice and Permafrost in the Arctic*
22 *(SWIPA) 2017*. Arctic Monitoring and Assessment Programme (AMAP), Oslo, Norway, pp. 65–136.
- 23 Rose, S.K., O.B. Andersen, M. Passaro, C.A. Ludwigsen, and C. Schwatke, 2019: Arctic Ocean Sea Level Record from
24 the Complete Radar Altimetry Era: 1991–2018. *Remote Sensing*, **11**(14), 1672, doi:[10.3390/rs11141672](https://doi.org/10.3390/rs11141672).
- 25 Rösel, A. et al., 2018: Thin Sea Ice, Thick Snow, and Widespread Negative Freeboard Observed During N-ICE2015
26 North of Svalbard. *Journal of Geophysical Research: Oceans*, **123**(2), 1156–1176, doi:[10.1002/2017jc012865](https://doi.org/10.1002/2017jc012865).
- 27 Rosenblum, E. and I. Eisenman, 2017: Sea ice trends in climate models only accurate in runs with biased global
28 warming. *Journal of Climate*, **30**(16), 6265–6278, doi:[10.1175/jcli-d-16-0455.1](https://doi.org/10.1175/jcli-d-16-0455.1).
- 29 Rossby, T., L. Chafik, and L. Houpert, 2020: What can Hydrography Tell Us About the Strength of the Nordic Seas
30 MOC Over the Last 70 to 100 Years? *Geophysical Research Letters*, **47**(12), doi:[10.1029/2020gl087456](https://doi.org/10.1029/2020gl087456).
- 31 Rounce, D.R., R. Hock, and D.E. Shean, 2020: Glacier Mass Change in High Mountain Asia Through 2100 Using the
32 Open-Source Python Glacier Evolution Model (PyGEM). *Frontiers in Earth Science*, **7**, 331,
33 doi:[10.3389/feart.2019.00331](https://doi.org/10.3389/feart.2019.00331).
- 34 Roy, K. and W.R. Peltier, 2017: Space-geodetic and water level gauge constraints on continental uplift and tilting over
35 North America: regional convergence of the ICE-6G_C (VM5a/VM6) models. *Geophysical Journal*
36 *International*, **210**(2), 1115–1142, doi:[10.1093/gji/ggx156](https://doi.org/10.1093/gji/ggx156).
- 37 Royston, S. et al., 2018: Sea-Level Trend Uncertainty With Pacific Climatic Variability and Temporally-Correlated
38 Noise. *Journal of Geophysical Research: Oceans*, **123**(3), 1978–1993, doi:[10.1002/2017jc013655](https://doi.org/10.1002/2017jc013655).
- 39 Ruan, R. et al., 2019: Decelerated Greenland Ice Sheet Melt Driven by Positive Summer North Atlantic Oscillation.
40 *Journal of Geophysical Research: Atmospheres*, **124**(14), 7633–7646, doi:[10.1029/2019jd030689](https://doi.org/10.1029/2019jd030689).
- 41 Rückamp, M., H. Goelzer, and A. Humbert, 2020: Sensitivity of Greenland ice sheet projections to spatial resolution in
42 higher-order simulations: the Alfred Wegener Institute (AWI) contribution to ISMIP6 Greenland using the Ice-
43 sheet and Sea-level System Model (ISSM). *The Cryosphere*, **14**(10), 3309–3327, doi:[10.5194/tc-14-3309-](https://doi.org/10.5194/tc-14-3309-2020)
44 [2020](https://doi.org/10.5194/tc-14-3309-2020).
- 45 Russell, J.L. et al., 2018: Metrics for the Evaluation of the Southern Ocean in Coupled Climate Models and Earth
46 System Models. *Journal of Geophysical Research: Oceans*, **123**(5), 3120–3143, doi:[10.1002/2017jc013461](https://doi.org/10.1002/2017jc013461).
- 47 Ryan, J.C. et al., 2018: Dark zone of the Greenland Ice Sheet controlled by distributed biologically-active impurities.
48 *Nature Communications*, **9**(1), 1065, doi:[10.1038/s41467-018-03353-2](https://doi.org/10.1038/s41467-018-03353-2).
- 49 Ryan, J.C. et al., 2019: Greenland Ice Sheet surface melt amplified by snowline migration and bare ice exposure.
50 *Science Advances*, **5**(3), doi:[10.1126/sciadv.aav3738](https://doi.org/10.1126/sciadv.aav3738).
- 51 Rye, C.D. et al., 2020: Antarctic Glacial Melt as a Driver of Recent Southern Ocean Climate Trends. *Geophysical*
52 *Research Letters*, **47**(11), e2019GL086892, doi:[10.1029/2019gl086892](https://doi.org/10.1029/2019gl086892).
- 53 Rykaczewski, R.R. et al., 2015: Poleward displacement of coastal upwelling-favorable winds in the ocean's eastern
54 boundary currents through the 21st century. *Geophysical Research Letters*, **42**(15), 6424–6431,
55 doi:[10.1002/2015gl064694](https://doi.org/10.1002/2015gl064694).

- 1 Sadai, S., A. Condrón, R. DeConto, and D. Pollard, 2020: Future climate response to Antarctic Ice Sheet melt caused by
2 anthropogenic warming. *Science Advances*, **6(39)**, doi:[10.1126/sciadv.aaz1169](https://doi.org/10.1126/sciadv.aaz1169).
- 3 Saha, S., L. Owen, E. Orr, and M. Caffee, 2018: Timing and nature of Holocene glacier advances at the northwestern
4 end of the Himalayan-Tibetan orogen. *Quaternary Science Reviews*, **187**, 177–202,
5 doi:[10.1016/j.quascirev.2018.03.009](https://doi.org/10.1016/j.quascirev.2018.03.009).
- 6 Sakai, A. and K. Fujita, 2017: Contrasting glacier responses to recent climate change in high-mountain Asia. *Scientific
7 Reports*, **7(1)**, 13717, doi:[10.1038/s41598-017-14256-5](https://doi.org/10.1038/s41598-017-14256-5).
- 8 Sakamoto, T. et al., 2012: MIROC4h: A New High-Resolution Atmosphere-Ocean Coupled General Circulation Model.
9 *Journal of the Meteorological Society of Japan. Ser. II*, **90(3)**, 325–359, doi:[10.2151/jmsj.2012-301](https://doi.org/10.2151/jmsj.2012-301).
- 10 Sallée, J.-B. et al., 2013a: Assessment of Southern Ocean mixed-layer depths in CMIP5 models: Historical bias and
11 forcing response. *Journal of Geophysical Research: Oceans*, **118(4)**, 1845–1862, doi:[10.1002/jgrc.20157](https://doi.org/10.1002/jgrc.20157).
- 12 Sallée, J.-B. et al., 2013b: Assessment of Southern Ocean water mass circulation and characteristics in CMIP5 models:
13 Historical bias and forcing response. *Journal of Geophysical Research: Oceans*, **118(4)**, 1830–1844,
14 doi:[10.1002/jgrc.20135](https://doi.org/10.1002/jgrc.20135).
- 15 Sallée, J.-B. et al., 2021: Summertime increases in upper-ocean stratification and mixed-layer depth. *Nature*, **591(7851)**,
16 592–598, doi:[10.1038/s41586-021-03303-x](https://doi.org/10.1038/s41586-021-03303-x).
- 17 Sánchez-Montes, M.L. et al., 2020: Late Pliocene Cordilleran Ice Sheet development with warm northeast Pacific sea
18 surface temperatures. *Climate of the Past*, **16(1)**, 299–313, doi:[10.5194/cp-16-299-2020](https://doi.org/10.5194/cp-16-299-2020).
- 19 Sasaki, H. et al., 2004: A series of eddy-resolving ocean simulations in the world ocean – OFES (OGCM for the Earth
20 Simulator) project. In: *Oceans '04 MTS/IEEE Techno-Ocean '04*. IEEE, pp. 1535–1541,
21 doi:[10.1109/oceans.2004.1406350](https://doi.org/10.1109/oceans.2004.1406350).
- 22 Sasgen, I. et al., 2020: Return to rapid ice loss in Greenland and record loss in 2019 detected by the GRACE-FO
23 satellites. *Communications Earth & Environment*, **1(1)**, 8, doi:[10.1038/s43247-020-0010-1](https://doi.org/10.1038/s43247-020-0010-1).
- 24 Scambos, T.A. et al., 2017: How much, how fast?: A science review and outlook for research on the instability of
25 Antarctica's Thwaites Glacier in the 21st century. *Global and Planetary Change*, **153**, 16–34,
26 doi:[10.1016/j.gloplacha.2017.04.008](https://doi.org/10.1016/j.gloplacha.2017.04.008).
- 27 Schaeffer, A. and M. Roughan, 2017: Subsurface intensification of marine heatwaves off southeastern Australia: The
28 role of stratification and local winds. *Geophysical Research Letters*, **44(10)**, 5025–5033,
29 doi:[10.1002/2017gl073714](https://doi.org/10.1002/2017gl073714).
- 30 Schaffer, J. et al., 2020: Bathymetry constrains ocean heat supply to Greenland's largest glacier tongue. *Nature
31 Geoscience*, **13(3)**, 227–231, doi:[10.1038/s41561-019-0529-x](https://doi.org/10.1038/s41561-019-0529-x).
- 32 Schemm, S., 2018: Regional Trends in Weather Systems Help Explain Antarctic Sea Ice Trends. *Geophysical Research
33 Letters*, **45(14)**, 7165–7175, doi:[10.1029/2018gl079109](https://doi.org/10.1029/2018gl079109).
- 34 Scherler, D., H. Wulf, and N. Gorelick, 2018: Global Assessment of Supraglacial Debris-Cover Extents. *Geophysical
35 Research Letters*, **45(21)**, 11,798–11,805, doi:[10.1029/2018gl080158](https://doi.org/10.1029/2018gl080158).
- 36 Scheuchl, B., J. Mouginot, E. Rignot, M. Morlighem, and A. Khazendar, 2016: Grounding line retreat of Pope, Smith,
37 and Kohler Glaciers, West Antarctica, measured with Sentinel-1a radar interferometry data. *Geophysical
38 Research Letters*, **43(16)**, 8572–8579, doi:[10.1002/2016gl069287](https://doi.org/10.1002/2016gl069287).
- 39 Schindelegger, M., J.A.M. Green, S.B. Wilmes, and I.D. Haigh, 2018: Can We Model the Effect of Observed Sea Level
40 Rise on Tides? *Journal of Geophysical Research: Oceans*, doi:[10.1029/2018jc013959](https://doi.org/10.1029/2018jc013959).
- 41 Schlegel, N.J., E. Larour, H. Seroussi, M. Morlighem, and J.E. Box, 2015: Ice discharge uncertainties in Northeast
42 Greenland from boundary conditions and climate forcing of an ice flow model. *Journal Of Geophysical
43 Research-Earth Surface*, **120(1)**, 29–54, doi:[10.1002/2014jfr003359](https://doi.org/10.1002/2014jfr003359).
- 44 Schlemm, T. and A. Levermann, 2021: A simple model of mélange buttressing for calving glaciers. *The Cryosphere*,
45 **15**, 531–545, doi:[10.5194/tc-2020-50](https://doi.org/10.5194/tc-2020-50).
- 46 Schloesser, F., T. Friedrich, A. Timmermann, R.M. DeConto, and D. Pollard, 2019: Antarctic iceberg impacts on future
47 Southern Hemisphere climate. *Nature Climate Change*, **9(9)**, 672–677, doi:[10.1038/s41558-019-0546-1](https://doi.org/10.1038/s41558-019-0546-1).
- 48 Schlosser, E., F.A. Haumann, and M.N. Raphael, 2018: Atmospheric influences on the anomalous 2016 Antarctic sea
49 ice decay. *The Cryosphere*, **12(3)**, 1103–1119, doi:[10.5194/tc-12-1103-2018](https://doi.org/10.5194/tc-12-1103-2018).
- 50 Schmale, J. et al., 2017: Modulation of snow reflectance and snowmelt from Central Asian glaciers by anthropogenic
51 black carbon. *Scientific Reports*, **7(1)**, 40501, doi:[10.1038/srep40501](https://doi.org/10.1038/srep40501).
- 52 Schmidt, L.S. et al., 2019: Dynamic simulations of Vatnajökull ice cap from 1980 to 2300. *Journal of Glaciology*,
53 **66(255)**, 97–112, doi:[10.1017/jog.2019.90](https://doi.org/10.1017/jog.2019.90).
- 54 Schöner, W., R. Koch, C. Matulla, C. Marty, and A.M. Tilg, 2019: Spatiotemporal patterns of snow depth within the
55 Swiss-Austrian Alps for the past half century (1961 to 2012) and linkages to climate change. *International
56 Journal of Climatology*, **39(3)**, 1589–1603, doi:[10.1002/joc.5902](https://doi.org/10.1002/joc.5902).

- 1 Schröder, L. et al., 2019: Four decades of Antarctic surface elevation changes from multi-mission satellite altimetry.
2 *The Cryosphere*, **13**, 427–449, doi:[10.5194/tc-13-427-2019](https://doi.org/10.5194/tc-13-427-2019).
- 3 Schroeder, D.M. et al., 2019: Multidecadal observations of the Antarctic ice sheet from restored analog radar records.
4 *ATMOSPHERIC, AND PLANETARY SCIENCES*, **116**, doi:[10.25740/ykq4-9345](https://doi.org/10.25740/ykq4-9345).
- 5 Schroeter, S., W. Hobbs, N.L. Bindoff, R. Massom, and R. Matear, 2018: Drivers of Antarctic sea ice volume change in
6 CMIP5 models. *Journal of Geophysical Research: Oceans*, **123**, 1–25, doi:[10.1029/2018jc014177](https://doi.org/10.1029/2018jc014177).
- 7 Schuler, T. et al., 2020: Reconciling Svalbard Glacier Mass Balance. *Frontiers in Earth Science*, **8**, 156,
8 doi:[10.3389/feart.2020.00156](https://doi.org/10.3389/feart.2020.00156).
- 9 Schweiger, A.J., K.R. Wood, and J. Zhang, 2019: Arctic Sea Ice Volume Variability over 1901–2010: A Model-Based
10 Reconstruction. *Journal of Climate*, **32(15)**, 4731–4752, doi:[10.1175/jcli-d-19-0008.1](https://doi.org/10.1175/jcli-d-19-0008.1).
- 11 Schweinsberg, A.D., J.P. Briner, G.H. Miller, O. Bennike, and E.K. Thomas, 2017: Local glaciation in West Greenland
12 linked to North Atlantic Ocean circulation during the Holocene. *Geology*, **45(3)**, 195–198,
13 doi:[10.1130/g38114.1](https://doi.org/10.1130/g38114.1).
- 14 Schweinsberg, A.D. et al., 2018: Holocene mountain glacier history in the Sukkertoppen Iskappe area, southwest
15 Greenland. *Quaternary Science Reviews*, **197**, 142–161, doi:[10.1016/j.quascirev.2018.06.014](https://doi.org/10.1016/j.quascirev.2018.06.014).
- 16 Screen, J.A. and D. Williamson, 2017: Ice-free Arctic at 1.5°C? *Nature Climate Change*, **7(4)**, 230–231,
17 doi:[10.1038/nclimate3248](https://doi.org/10.1038/nclimate3248).
- 18 Seehaus, T., A.J. Cook, A.B. Silva, and M. Braun, 2018: Changes in glacier dynamics in the northern Antarctic
19 Peninsula since 1985. *Cryosphere*, **12**, 577–594, doi:[10.5194/tc-12-577-2018](https://doi.org/10.5194/tc-12-577-2018).
- 20 Seehaus, T. et al., 2019a: Changes of the tropical glaciers throughout Peru between 2000 and 2016 – mass balance and
21 area fluctuations. *The Cryosphere*, **13(10)**, 2537–2556, doi:[10.5194/tc-13-2537-2019](https://doi.org/10.5194/tc-13-2537-2019).
- 22 Seehaus, T. et al., 2019b: Mass balance and area changes of glaciers in the Cordillera Real and Tres Cruces, Bolivia,
23 between 2000 and 2016. *Journal of Glaciology*, **66(255)**, 124–136, doi:[10.1017/jog.2019.94](https://doi.org/10.1017/jog.2019.94).
- 24 Sellevold, R. and M. Vizcaíno, 2020: Global Warming Threshold and Mechanisms for Accelerated Greenland Ice Sheet
25 Surface Mass Loss. *Journal of Advances in Modeling Earth Systems*, **12(9)**, e2019MS002029,
26 doi:[10.1029/2019ms002029](https://doi.org/10.1029/2019ms002029).
- 27 Sellevold, R. et al., 2019: Surface mass balance downscaling through elevation classes in an Earth system model:
28 application to the Greenland ice sheet. *The Cryosphere*, **13**, 3193–3208, doi:[10.5194/tc-13-3193-2019](https://doi.org/10.5194/tc-13-3193-2019).
- 29 Sen Gupta, A. et al., 2016: Future changes to the Indonesian Throughflow and Pacific circulation: The differing role of
30 wind and deep circulation changes. *Geophysical Research Letters*, **43(4)**, 1669–1678,
31 doi:[10.1002/2016gl067757](https://doi.org/10.1002/2016gl067757).
- 32 Sen Gupta, A. et al., 2020: Drivers and impacts of the most extreme marine heatwaves events. *Scientific Reports*, **10(1)**,
33 19359, doi:[10.1038/s41598-020-75445-3](https://doi.org/10.1038/s41598-020-75445-3).
- 34 Seo, H., R. Murtugudde, M. Jochum, and A.J. Miller, 2008: Modeling of mesoscale coupled ocean–atmosphere
35 interaction and its feedback to ocean in the western Arabian Sea. *Ocean Modelling*, **25(3–4)**, 120–131,
36 doi:[10.1016/j.ocemod.2008.07.003](https://doi.org/10.1016/j.ocemod.2008.07.003).
- 37 Seo, H., K.H. Brink, C.E. Dorman, D. Koracin, and C.A. Edwards, 2012: What determines the spatial pattern in
38 summer upwelling trends on the U.S. West Coast? *Journal of Geophysical Research: Oceans*, **117(C8)**,
39 doi:[10.1029/2012jc008016](https://doi.org/10.1029/2012jc008016).
- 40 Seo, H. et al., 2007: The Scripps Coupled Ocean–Atmosphere Regional (SCOAR) Model, with Applications in the
41 Eastern Pacific Sector. *Journal of Climate*, **20(3)**, 381–402, doi:[10.1175/jcli4016.1](https://doi.org/10.1175/jcli4016.1).
- 42 Sérazin, G. et al., 2016: Quantifying uncertainties on regional sea level change induced by multidecadal intrinsic
43 oceanic variability. *Geophysical Research Letters*, **43(15)**, 8151–8159, doi:[10.1002/2016gl069273](https://doi.org/10.1002/2016gl069273).
- 44 Sérazin, G. et al., 2017: A global probabilistic study of the ocean heat content low-frequency variability: Atmospheric
45 forcing versus oceanic chaos. *Geophysical Research Letters*, **44(11)**, 5580–5589, doi:[10.1002/2017gl073026](https://doi.org/10.1002/2017gl073026).
- 46 Sergienko, O. and D.J. Wingham, 2019: Grounding line stability in a regime of low driving and basal stresses. *Journal*
47 *of Glaciology*, **65(253)**, 833–849, doi:[10.1017/jog.2019.53](https://doi.org/10.1017/jog.2019.53).
- 48 Seroussi, H. et al., 2017: Continued retreat of Thwaites Glacier, West Antarctica, controlled by bed topography and
49 ocean circulation. *Geophysical Research Letters*, **44(12)**, 6191–6199, doi:[10.1002/2017gl072910](https://doi.org/10.1002/2017gl072910).
- 50 Seroussi, H. et al., 2019: initMIP-Antarctica: An ice sheet model initialization experiment of ISMIP6. *The Cryosphere*,
51 **13**, 1441–1471, doi:[10.5194/tc-13-1441-2019](https://doi.org/10.5194/tc-13-1441-2019).
- 52 Seroussi, H. et al., 2020: ISMIP6 Antarctica: A multi-model ensemble of the Antarctic ice sheet evolution over the 21st
53 century. *Cryosphere*, **14(9)**, 3033–3070, doi:[10.5194/tc-14-3033-2020](https://doi.org/10.5194/tc-14-3033-2020).
- 54 Shackleton, S. et al., 2019: Is the Noble Gas-Based Rate of Ocean Warming During the Younger Dryas Overestimated?
55 *Geophysical Research Letters*, **46(11)**, 5928–5936, doi:[10.1029/2019gl082971](https://doi.org/10.1029/2019gl082971).

- 1 Shackleton, S. et al., 2020: Global ocean heat content in the Last Interglacial. *Nature Geoscience*, **13**(1), 77–81,
2 doi:[10.1038/s41561-019-0498-0](https://doi.org/10.1038/s41561-019-0498-0).
- 3 Shakhova, N. et al., 2017: Current rates and mechanisms of subsea permafrost degradation in the East Siberian Arctic
4 Shelf. *Nature Communications*, **8**, 15872, doi:[10.1038/ncomms15872](https://doi.org/10.1038/ncomms15872).
- 5 Shakun, J.D. et al., 2012: Global warming preceded by increasing carbon dioxide concentrations during the last
6 deglaciation. *Nature*, **484**, 49–54, doi:[10.1038/nature10915](https://doi.org/10.1038/nature10915).
- 7 Shakun, J.D. et al., 2015: Regional and global forcing of glacier retreat during the last deglaciation. *Nature*
8 *Communications*, **6**, 8059, doi:[10.1038/ncomms9059](https://doi.org/10.1038/ncomms9059).
- 9 Shannon, S. et al., 2019: Global glacier volume projections under high-end climate change scenarios. *The Cryosphere*,
10 **13**(1), 325–350, doi:[10.5194/tc-13-325-2019](https://doi.org/10.5194/tc-13-325-2019).
- 11 Shean, D.E. et al., 2020: A Systematic, Regional Assessment of High Mountain Asia Glacier Mass Balance. *Frontiers*
12 *in Earth Science*, **7**, 363, doi:[10.3389/feart.2019.00363](https://doi.org/10.3389/feart.2019.00363).
- 13 Shepherd, A. et al., 2019: Trends in Antarctic Ice Sheet Elevation and Mass. *Geophysical Research Letters*, **46**(14),
14 8174–8183, doi:[10.1029/2019gl082182](https://doi.org/10.1029/2019gl082182).
- 15 Shepherd, T.G. et al., 2018: Storylines: an alternative approach to representing uncertainty in physical aspects of
16 climate change. *Climatic Change*, **151**(3), 555–571, doi:[10.1007/s10584-018-2317-9](https://doi.org/10.1007/s10584-018-2317-9).
- 17 Sherman, P., E. Tziperman, C. Deser, and M. McElroy, 2020: Historical and Future Roles of Internal Atmospheric
18 Variability in Modulating Summertime Greenland Ice Sheet Melt. *Geophysical Research Letters*, **47**(6),
19 e2019GL086913, doi:[10.1029/2019gl086913](https://doi.org/10.1029/2019gl086913).
- 20 Shi, J.-R., S.-P. Xie, and L.D. Talley, 2018: Evolving Relative Importance of the Southern Ocean and North Atlantic in
21 Anthropogenic Ocean Heat Uptake. *Journal of Climate*, **31**(18), 7459–7479, doi:[10.1175/jcli-d-18-0170.1](https://doi.org/10.1175/jcli-d-18-0170.1).
- 22 Shi, J.-R., L.D. Talley, S.-P. Xie, W. Liu, and S.T. Gille, 2020: Effects of Buoyancy and Wind Forcing on Southern
23 Ocean Climate Change. *Journal of Climate*, 1–53, doi:[10.1175/jcli-d-19-0877.1](https://doi.org/10.1175/jcli-d-19-0877.1).
- 24 Shimada, R., N. Takeuchi, and T. Aoki, 2016: Inter-annual and geographical variations in the extent of bare ice and
25 dark ice on the Greenland ice sheet derived from MODIS satellite images. *Frontiers in Earth Science*, **4**, 43,
26 doi:[10.3389/feart.2016.00043](https://doi.org/10.3389/feart.2016.00043).
- 27 Shu, Q., Z. Song, and F. Qiao, 2015: Assessment of sea ice simulations in the CMIP5 models. *Cryosphere*, **9**(1), 399–
28 409, doi:[10.5194/tc-9-399-2015](https://doi.org/10.5194/tc-9-399-2015).
- 29 Shu, Q. et al., 2020: Assessment of Sea Ice Extent in CMIP6 With Comparison to Observations and CMIP5.
30 *Geophysical Research Letters*, **47**(9), e2020GL087965, doi:[10.1029/2020gl087965](https://doi.org/10.1029/2020gl087965).
- 31 Shugar, D.H. et al., 2020: Rapid worldwide growth of glacial lakes since 1990. *Nature Climate Change*, **10**(10), 939–
32 945, doi:[10.1038/s41558-020-0855-4](https://doi.org/10.1038/s41558-020-0855-4).
- 33 Sidorenko, D. et al., 2019: Evaluation of FESOM2.0 Coupled to ECHAM6.3: Preindustrial and HighResMIP
34 Simulations. *Journal of Advances in Modeling Earth Systems*, **11**(11), 3794–3815,
35 doi:[10.1029/2019ms001696](https://doi.org/10.1029/2019ms001696).
- 36 Siebert, M., R.B. Alley, E. Rignot, J. Englander, and R. Corell, 2020: Twenty-first century sea-level rise could exceed
37 IPCC projections for strong-warming futures. *One Earth*, **3**(6), 691–703, doi:[10.1016/j.oneear.2020.11.002](https://doi.org/10.1016/j.oneear.2020.11.002).
- 38 Sigl, M. et al., 2018: 19th century glacier retreat in the Alps preceded the emergence of industrial black carbon
39 deposition on high-alpine glaciers. *The Cryosphere*, **12**(10), 3311–3331, doi:[10.5194/tc-12-3311-2018](https://doi.org/10.5194/tc-12-3311-2018).
- 40 Sigmond, M., J.C. Fyfe, and N.C. Swart, 2018: Ice-free Arctic projections under the Paris Agreement. *Nature Climate*
41 *Change*, **8**(5), 404–408, doi:[10.1038/s41558-018-0124-y](https://doi.org/10.1038/s41558-018-0124-y).
- 42 Silvano, A. et al., 2018: Freshening by glacial meltwater enhances melting of ice shelves and reduces formation of
43 Antarctic Bottom Water. *Science Advances*, **4**(4), doi:[10.1126/sciadv.aap9467](https://doi.org/10.1126/sciadv.aap9467).
- 44 Silvano, A. et al., 2020: Recent recovery of Antarctic Bottom Water formation in the Ross Sea driven by climate
45 anomalies. *Nature Geoscience*, **13**(12), 780–786, doi:[10.1038/s41561-020-00655-3](https://doi.org/10.1038/s41561-020-00655-3).
- 46 Silvy, Y., E. Guilyardi, J.-B. Sallée, and P.J. Durack, 2020a: Human-induced changes to the global ocean water masses
47 and their time of emergence. *Nature Climate Change*, **10**(11), 1030–1036, doi:[10.1038/s41558-020-0878-x](https://doi.org/10.1038/s41558-020-0878-x).
- 48 Silvy, Y., E. Guilyardi, J.-B. Sallée, and P.J. Durack, 2020b: Human-induced changes to the global ocean water masses
49 and their time of emergence. *Nature Climate Change*, **10**(11), 1030–1036, doi:[10.1038/s41558-020-0878-x](https://doi.org/10.1038/s41558-020-0878-x).
- 50 Simmonds, I., 2015: Comparing and contrasting the behaviour of Arctic and Antarctic sea ice over the 35 year period
51 1979–2013. *Annals of Glaciology*, **56**(69), 18–28, doi:[10.3189/2015aog69a909](https://doi.org/10.3189/2015aog69a909).
- 52 Simms, A.R., L. Lisiecki, G. Gebbie, P.L. Whitehouse, and J.F. Clark, 2019: Balancing the last glacial maximum
53 (LGM) sea-level budget. *Quaternary Science Reviews*, **205**, 143–153, doi:[10.1016/j.quascirev.2018.12.018](https://doi.org/10.1016/j.quascirev.2018.12.018).
- 54 Simpkins, G.R., Y. Peings, and G. Magnúsdóttir, 2016: Pacific Influences on Tropical Atlantic Teleconnections to the
55 Southern Hemisphere High Latitudes. *Journal of Climate*, **29**(18), 6425–6444, doi:[10.1175/jcli-d-15-0645.1](https://doi.org/10.1175/jcli-d-15-0645.1).

- 1 Simpkins, G.R., L.M. Ciasto, D.W.J. Thompson, and M.H. England, 2012: Seasonal relationships between large-scale
2 climate variability and antarctic sea ice concentration. *Journal of Climate*, **25(16)**, 5451–5469,
3 doi:[10.1175/jcli-d-11-00367.1](https://doi.org/10.1175/jcli-d-11-00367.1).
- 4 Simpson, M.J.R., G.A. Milne, P. Huybrechts, and A.J. Long, 2009: Calibrating a glaciological model of the Greenland
5 ice sheet from the Last Glacial Maximum to present-day using field observations of relative sea level and ice
6 extent. *Quaternary Science Reviews*, **28**, 1631–1657, doi:[10.1016/j.quascirev.2009.03.004](https://doi.org/10.1016/j.quascirev.2009.03.004).
- 7 Singh, H.A., P.J. Rasch, and B.E.J. Rose, 2017: Increased Ocean Heat Convergence Into the High Latitudes With CO₂
8 Doubling Enhances Polar-Amplified Warming. *Geophysical Research Letters*, **44(20)**, 10,583–10,591,
9 doi:[10.1002/2017gl074561](https://doi.org/10.1002/2017gl074561).
- 10 Skinner, L.C., S. Fallon, C. Waelbroeck, E. Michel, and S. Barker, 2010: Ventilation of the Deep Southern Ocean and
11 Deglacial CO₂ Rise. *Science*, **328(5982)**, 1147–1151, doi:[10.1126/science.1183627](https://doi.org/10.1126/science.1183627).
- 12 Slangen, A.B.A., J.A. Church, X. Zhang, and D. Monselesan, 2014a: Detection and attribution of global mean
13 thermosteric sea-level change. *Geophysical Research Letters*, **41(16)**, 5951–5959, doi:[10.1002/2014gl061356](https://doi.org/10.1002/2014gl061356).
- 14 Slangen, A.B.A., J.A. Church, X. Zhang, and D.P. Monselesan, 2015: The sea level response to external forcings in
15 historical simulations of CMIP5 climate models. *Journal of Climate*, **28(21)**, 8521–8539, doi:[10.1175/jcli-d-
16 15-0376.1](https://doi.org/10.1175/jcli-d-15-0376.1).
- 17 Slangen, A.B.A. et al., 2014b: Projecting twenty-first century regional sea-level changes. *Climatic Change*, **124(1–2)**,
18 317–332, doi:[10.1007/s10584-014-1080-9](https://doi.org/10.1007/s10584-014-1080-9).
- 19 Slangen, A.B.A. et al., 2017: Evaluating model simulations of twentieth-century sea level rise. Part I: Global mean sea
20 level change. *Journal of Climate*, **30(21)**, 8539–8563, doi:[10.1175/jcli-d-17-0110.1](https://doi.org/10.1175/jcli-d-17-0110.1).
- 21 Slater, A.G. and D.M. Lawrence, 2013: Diagnosing present and future permafrost from climate models. *Journal of
22 Climate*, **26(15)**, 5608–5623, doi:[10.1175/jcli-d-12-00341.1](https://doi.org/10.1175/jcli-d-12-00341.1).
- 23 Slater, A.G., D.M. Lawrence, and C.D. Koven, 2017: Process-level model evaluation: A snow and heat transfer metric.
24 *The Cryosphere*, **11(2)**, 989–996, doi:[10.5194/tc-11-989-2017](https://doi.org/10.5194/tc-11-989-2017).
- 25 Slater, D.A., P.W. Nienow, D.N. Goldberg, T.R. Cowton, and A.J. Sole, 2017: A model for tidewater glacier
26 undercutting by submarine melting. *Geophysical Research Letters*, **44(5)**, 2360–2368,
27 doi:[10.1002/2016gl072374](https://doi.org/10.1002/2016gl072374).
- 28 Slater, D.A. et al., 2019: Estimating Greenland tidewater glacier retreat driven by submarine melting. *The Cryosphere*,
29 **13(9)**, 2489–2509, doi:[10.5194/tc-13-2489-2019](https://doi.org/10.5194/tc-13-2489-2019).
- 30 Slater, D.A. et al., 2020: Twenty-first century ocean forcing of the Greenland ice sheet for modelling of sea level
31 contribution. *Cryosphere*, **14(3)**, 985–1008, doi:[10.5194/tc-14-985-2020](https://doi.org/10.5194/tc-14-985-2020).
- 32 Slater, T., A.E. Hogg, and R. Mottram, 2020: Ice-sheet losses track high-end sea-level rise projections. *Nature Climate
33 Change*, **10(10)**, 879–881, doi:[10.1038/s41558-020-0893-y](https://doi.org/10.1038/s41558-020-0893-y).
- 34 Slater, T. et al., 2021: Review article: Earth’s ice imbalance. *The Cryosphere*, **15(1)**, 233–246, doi:[10.5194/tc-15-233-
2021](https://doi.org/10.5194/tc-15-233-
35 2021).
- 36 Sloyan, B.M. and T.J. O’Kane, 2015: Drivers of decadal variability in the Tasman Sea. *Journal of Geophysical
37 Research: Oceans*, **120(5)**, 3193–3210, doi:[10.1002/2014jc010550](https://doi.org/10.1002/2014jc010550).
- 38 Sloyan, B.M. et al., 2019: The Global Ocean Ship-Based Hydrographic Investigations Program (GO-SHIP): A Platform
39 for Integrated Multidisciplinary Ocean Science. *Frontiers in Marine Science*, **6**, 445,
40 doi:[10.3389/fmars.2019.00445](https://doi.org/10.3389/fmars.2019.00445).
- 41 Smale, D.A. et al., 2019: Marine heatwaves threaten global biodiversity and the provision of ecosystem services. *Nature
42 Climate Change*, **9(4)**, 306, doi:[10.1038/s41558-019-0412-1](https://doi.org/10.1038/s41558-019-0412-1).
- 43 Small, J. et al., 2014: A new synoptic scale resolving global climate simulation using the Community Earth System
44 Model. *Journal of Advances in Modeling Earth Systems*, **6(4)**, 1065–1094, doi:[10.1002/2014ms000363](https://doi.org/10.1002/2014ms000363).
- 45 Small, R.J., F.O. Bryan, S.P. Bishop, and R.A. Tomas, 2019: Air-sea turbulent heat fluxes in climate models and
46 observational analyses: What drives their variability? *Journal of Climate*, **32(8)**, 2397–2421, doi:[10.1175/jcli-
d-18-0576.1](https://doi.org/10.1175/jcli-
47 d-18-0576.1).
- 48 Small, R.J. et al., 2014: A new synoptic scale resolving global climate simulation using the Community Earth System
49 Model. *Journal of Advances in Modeling Earth Systems*, **6(4)**, 1065–1094, doi:[10.1002/2014ms000363](https://doi.org/10.1002/2014ms000363).
- 50 Small, R.J. et al., 2015: The Benguela Upwelling System: Quantifying the Sensitivity to Resolution and Coastal Wind
51 Representation in a Global Climate Model*. *Journal of Climate*, **28(23)**, 9409–9432, doi:[10.1175/jcli-d-15-
0192.1](https://doi.org/10.1175/jcli-d-15-
52 0192.1).
- 53 Smeed, D.A. et al., 2018: The North Atlantic Ocean Is in a State of Reduced Overturning. *Geophysical Research
54 Letters*, **45(3)**, 1527–1533, doi:[10.1002/2017gl076350](https://doi.org/10.1002/2017gl076350).
- 55 Smith, A. and A. Jahn, 2019: Definition differences and internal variability affect the simulated Arctic sea ice melt
56 season. *Cryosphere*, **13(1)**, 1–20, doi:[10.5194/tc-13-1-2019](https://doi.org/10.5194/tc-13-1-2019).

- 1 Smith, B. et al., 2020: Pervasive ice sheet mass loss reflects competing ocean and atmosphere processes. *Science*,
2 **368(6496)**, 1239–1242, doi:[10.1126/science.aaz5845](https://doi.org/10.1126/science.aaz5845).
- 3 Smith, C.J. et al., 2018: FAIR v1. 3: A simple emissions-based impulse response and carbon cycle model. *Geoscientific*
4 *Model Development*, **11(6)**, 2273–2297.
- 5 Smith, D.E., S. Harrison, C.R. Firth, and J.T. Jordan, 2011: The early Holocene sea level rise. *Quaternary Science*
6 *Reviews*, **30(15)**, 1846–1860, doi:[10.1016/j.quascirev.2011.04.019](https://doi.org/10.1016/j.quascirev.2011.04.019).
- 7 Smith, J.A. et al., 2017: Sub-ice-shelf sediments record history of twentieth-century retreat of Pine Island Glacier.
8 *Nature*, **541(7635)**, 77–80, doi:[10.1038/nature20136](https://doi.org/10.1038/nature20136).
- 9 Smith, K.L., L.M. Polvani, and D.R. Marsh, 2012: Mitigation of 21st century Antarctic sea ice loss by stratospheric
10 ozone recovery. *Geophysical Research Letters*, **39(20)**, 2012GL053325, doi:[10.1029/2012gl053325](https://doi.org/10.1029/2012gl053325).
- 11 Snauffer, A.M., W.W. Hsieh, and A.J. Cannon, 2016: Comparison of gridded snow water equivalent products with in
12 situ measurements in British Columbia, Canada. *Journal of Hydrology*, **541**, 714–726,
13 doi:[10.1016/j.jhydrol.2016.07.027](https://doi.org/10.1016/j.jhydrol.2016.07.027).
- 14 Snow, K. et al., 2015: Sensitivity of abyssal water masses to overflow parameterisations. *Ocean Modelling*, **89**, 84–103,
15 doi:[10.1016/j.ocemod.2015.03.004](https://doi.org/10.1016/j.ocemod.2015.03.004).
- 16 Solgaard, A.M. et al., 2020: Hagen Bræ: A Surging Glacier in North Greenland-35 Years of Observations. *Geophysical*
17 *Research Letters*, **47(6)**, e2019GL085802, doi:[10.1029/2019gl085802](https://doi.org/10.1029/2019gl085802).
- 18 Solomina, O.N. et al., 2015: Holocene glacier fluctuations. *Quaternary Science Reviews*, **111**, 9–34,
19 doi:[10.1016/j.quascirev.2014.11.018](https://doi.org/10.1016/j.quascirev.2014.11.018).
- 20 Solomina, O.N. et al., 2016: Glacier fluctuations during the past 2000 years. *Quaternary Science Reviews*, **149**, 61–90,
21 doi:[10.1016/j.quascirev.2016.04.008](https://doi.org/10.1016/j.quascirev.2016.04.008).
- 22 Somavilla, R., C. González-Pola, and J. Fernández-Díaz, 2017: The warmer the ocean surface, the shallower the mixed
23 layer. How much of this is true? *Journal of Geophysical Research: Oceans*, **122(9)**, 7698–7716,
24 doi:[10.1002/2017jc013125](https://doi.org/10.1002/2017jc013125).
- 25 Sommer, C. et al., 2020: Rapid glacier retreat and downwasting throughout the European Alps in the early 21st century.
26 *Nature Communications*, **11(1)**, 1–10, doi:[10.1038/s41467-020-16818-0](https://doi.org/10.1038/s41467-020-16818-0).
- 27 Somot, S., F. Sevaut, M. Déqué, and M. Crépon, 2008: 21st century climate change scenario for the Mediterranean
28 using a coupled atmosphere–ocean regional climate model. *Global and Planetary Change*, **63(2–3)**, 112–126,
29 doi:[10.1016/j.gloplacha.2007.10.003](https://doi.org/10.1016/j.gloplacha.2007.10.003).
- 30 Song, D., X.H. Wang, X. Zhu, and X. Bao, 2013: Modeling studies of the far-field effects of tidal flat reclamation on
31 tidal dynamics in the East China Seas. *Estuarine, Coastal and Shelf Science*, **133**, 147–160,
32 doi:[10.1016/j.ecss.2013.08.023](https://doi.org/10.1016/j.ecss.2013.08.023).
- 33 Soto-Navarro, J. et al., 2020: Evolution of Mediterranean Sea water properties under climate change scenarios in the
34 Med-CORDEX ensemble. *Climate Dynamics*, **54(3)**, 2135–2165, doi:[10.1007/s00382-019-05105-4](https://doi.org/10.1007/s00382-019-05105-4).
- 35 Sousa, M.C., M. DeCastro, I. Alvarez, M. Gomez-Gesteira, and J.M. Dias, 2017: Why coastal upwelling is expected to
36 increase along the western Iberian Peninsula over the next century? *Science of The Total Environment*, **592**,
37 243–251, doi:[10.1016/j.scitotenv.2017.03.046](https://doi.org/10.1016/j.scitotenv.2017.03.046).
- 38 Spector, P. et al., 2017: Rapid early-Holocene deglaciation in the Ross Sea, Antarctica. *Geophysical Research Letters*,
39 **44(15)**, 7817–7825, doi:[10.1002/2017gl074216](https://doi.org/10.1002/2017gl074216).
- 40 Spence, P. et al., 2014: Rapid subsurface warming and circulation changes of Antarctic coastal waters by poleward
41 shifting winds. *Geophysical Research Letters*, **41(13)**, 4601–4610, doi:[10.1002/2014gl060613](https://doi.org/10.1002/2014gl060613).
- 42 Spence, P. et al., 2017: Localized rapid warming of West Antarctic subsurface waters by remote winds. *Nature Climate*
43 *Change*, **7(8)**, 595–603, doi:[10.1038/nclimate3335](https://doi.org/10.1038/nclimate3335).
- 44 Spolaor, A. et al., 2016: Canadian arctic sea ice reconstructed from bromine in the Greenland NEEM ice core. *Scientific*
45 *Reports*, **6**, 33925, doi:[10.1038/srep33925](https://doi.org/10.1038/srep33925).
- 46 Spreen, G., R. Kwok, and D. Menemenlis, 2011: Trends in Arctic sea ice drift and role of wind forcing: 1992–2009.
47 *Geophysical Research Letters*, **38(19)**, doi:[10.1029/2011gl048970](https://doi.org/10.1029/2011gl048970).
- 48 Spreen, G. et al., 2020: Arctic Sea Ice Volume Export Through Fram Strait From 1992 to 2014. *Journal of Geophysical*
49 *Research: Oceans*, **125(6)**, e2019JC016039, doi:[10.1029/2019jc016039](https://doi.org/10.1029/2019jc016039).
- 50 Stabeno, P.J. and S.W. Bell, 2019: Extreme Conditions in the Bering Sea (2017–2018): Record-Breaking Low Sea-Ice
51 Extent. *Geophysical Research Letters*, **46(15)**, 8952–8959, doi:[10.1029/2019gl083816](https://doi.org/10.1029/2019gl083816).
- 52 Stammer, D. et al., 2019: Ocean Climate Observing Requirements in Support of Climate Research and Climate
53 Information. *Frontiers in Marine Science*, **6**, 444, doi:[10.3389/fmars.2019.00444](https://doi.org/10.3389/fmars.2019.00444).
- 54 Staten, P.W., J. Lu, K.M. Grise, S.M. Davis, and T. Birner, 2018: Re-examining tropical expansion. *Nature Climate*
55 *Change*, **8(9)**, 768–775, doi:[10.1038/s41558-018-0246-2](https://doi.org/10.1038/s41558-018-0246-2).

- 1 Steele, M. and W. Ermold, 2015: Loitering of the retreating sea ice edge in the Arctic Seas. *Journal of Geophysical*
2 *Research: Oceans*, **120(12)**, 7699–7721, doi:[10.1002/2015jc011182](https://doi.org/10.1002/2015jc011182).
- 3 Stein, K., A. Timmermann, E.Y. Kwon, and T. Friedrich, 2020: Timing and magnitude of Southern Ocean sea
4 ice/carbon cycle feedbacks. *Proceedings of the National Academy of Sciences*, **117(9)**, 4498–4504,
5 doi:[10.1073/pnas.1908670117](https://doi.org/10.1073/pnas.1908670117).
- 6 Stein, R. et al., 2017: Holocene variability in sea ice cover, primary production, and Pacific-Water inflow and climate
7 change in the Chukchi and East Siberian Seas (Arctic Ocean). *Journal of Quaternary Science*, **32(3)**, 362–379,
8 doi:[10.1002/jqs.2929](https://doi.org/10.1002/jqs.2929).
- 9 Stellema, A., A. Sen Gupta, and A.S. Taschetto, 2019: Projected slow down of South Indian Ocean circulation.
10 *Scientific Reports*, **9(1)**, 17705, doi:[10.1038/s41598-019-54092-3](https://doi.org/10.1038/s41598-019-54092-3).
- 11 Stendaro, I., M. Rhein, and R. Steinfeldt, 2020: The North Atlantic Current and its Volume and Freshwater Transports
12 in the Subpolar North Atlantic, Time Period 1993–2016. *Journal of Geophysical Research: Oceans*, **125(9)**,
13 e2020JC016065, doi:[10.1029/2020jc016065](https://doi.org/10.1029/2020jc016065).
- 14 Stevens, C. et al., 2020: Ocean mixing and heat transport processes observed under the Ross Ice Shelf control its basal
15 melting. *Proceedings of the National Academy of Sciences of the United States of America*, **117(29)**,
16 doi:[10.1073/pnas.1910760117](https://doi.org/10.1073/pnas.1910760117).
- 17 Stevenson, S., B. Otto-Bliessner, J. Fasullo, and E. Brady, 2016: "El Niño Like" hydroclimate responses to last
18 millennium volcanic eruptions. *Journal of Climate*, **29(8)**, 2907–2921, doi:[10.1175/jcli-d-15-0239.1](https://doi.org/10.1175/jcli-d-15-0239.1).
- 19 Stewart, A.L. and A.F. Thompson, 2013: Connecting Antarctic Cross-Slope Exchange with Southern Ocean
20 Overturning. *Journal of Physical Oceanography*, **43(7)**, 1453–1471, doi:[10.1175/jpo-d-12-0205.1](https://doi.org/10.1175/jpo-d-12-0205.1).
- 21 Stewart, A.L. and A.F. Thompson, 2015: Eddy-mediated transport of warm Circumpolar Deep Water across the
22 Antarctic Shelf Break. *Geophysical Research Letters*, **42(2)**, 432–440, doi:[10.1002/2014gl062281](https://doi.org/10.1002/2014gl062281).
- 23 Stewart, A.L., A. Klocker, and D. Menemenlis, 2018: Circum-Antarctic Shoreward Heat Transport Derived From an
24 Eddy- and Tide-Resolving Simulation. *Geophysical Research Letters*, **45(2)**, 834–845,
25 doi:[10.1002/2017gl075677](https://doi.org/10.1002/2017gl075677).
- 26 Stewart, C.L., P. Christoffersen, K.W. Nicholls, M.J.M. Williams, and J.A. Dowdeswell, 2019: Basal melting of Ross
27 Ice Shelf from solar heat absorption in an ice-front polynya. *Nature Geoscience*, **12**, 435–440,
28 doi:[10.1038/s41561-019-0356-0](https://doi.org/10.1038/s41561-019-0356-0).
- 29 Stewart, K.D., A.M.C. Hogg, M.H. England, and D.W. Waugh, 2020: Response of the Southern Ocean Overturning
30 Circulation to Extreme Southern Annular Mode Conditions. *Geophysical Research Letters*, **47(22)**,
31 e2020GL091103, doi:[10.1029/2020gl091103](https://doi.org/10.1029/2020gl091103).
- 32 Stibal, M. et al., 2017: Algae Drive Enhanced Darkening of Bare Ice on the Greenland Ice Sheet. *Geophysical Research*
33 *Letters*, **44(22)**, 11,463–11,471, doi:[10.1002/2017gl075958](https://doi.org/10.1002/2017gl075958).
- 34 Stone, E.J., D.J. Lunt, J.D. Annan, and J.C. Hargreaves, 2013: Quantification of the Greenland ice sheet contribution to
35 Last Interglacial sea level rise. *Climate of the Past*, **9(2)**, 621–639, doi:[10.5194/cp-9-621-2013](https://doi.org/10.5194/cp-9-621-2013).
- 36 Stopa, J.E., F. Arduin, and F. Girard-Arduin, 2016: Wave climate in the Arctic 1992–2014: seasonality and trends.
37 *The Cryosphere*, **10(4)**, 1605–1629, doi:[10.5194/tc-10-1605-2016](https://doi.org/10.5194/tc-10-1605-2016).
- 38 Stopa, J.E., F. Arduin, E. Stutzmann, and T. Lecocq, 2019: Sea State Trends and Variability: Consistency Between
39 Models, Altimeters, Buoys, and Seismic Data (1979–2016). *Journal of Geophysical Research: Oceans*, **124(6)**,
40 3923–3940, doi:[10.1029/2018jc014607](https://doi.org/10.1029/2018jc014607).
- 41 Storlazzi, C.D. et al., 2018: Most atolls will be uninhabitable by the mid-21st century because of sea-level rise
42 exacerbating wave-driven flooding. *Science Advances*, **4(4)**, doi:[10.1126/sciadv.aap9741](https://doi.org/10.1126/sciadv.aap9741).
- 43 Stouffer, R.J. et al., 2006: Investigating the Causes of the Response of the Thermohaline Circulation to Past and Future
44 Climate Changes. *J. Climate*, **19**, 1365–1387, doi:[10.1175/jcli3689.1](https://doi.org/10.1175/jcli3689.1).
- 45 Straneo, F. and C. Cenedese, 2015: The Dynamics of Greenland's Glacial Fjords and Their Role in Climate. *Annual*
46 *Review of Marine Science*, **7(1)**, 89–112, doi:[10.1146/annurev-marine-010213-135133](https://doi.org/10.1146/annurev-marine-010213-135133).
- 47 Streletskiy, D.A. et al., 2017: Thaw Subsidence in Undisturbed Tundra Landscapes, Barrow, Alaska, 1962–2015.
48 *Permafrost and Periglacial Processes*, **28(3)**, 566–572, doi:[10.1002/ppp.1918](https://doi.org/10.1002/ppp.1918).
- 49 Stroeve, J. and D. Notz, 2018: Changing state of Arctic sea ice across all seasons. *Environmental Research Letters*,
50 **13(10)**, 103001, doi:[10.1088/1748-9326/aade56](https://doi.org/10.1088/1748-9326/aade56).
- 51 Stroeve, J., A. Barrett, M. Serreze, and A. Schweiger, 2014: Using records from submarine, aircraft and satellites to
52 evaluate climate model simulations of Arctic sea ice thickness. *The Cryosphere*, **8(5)**, 1839–1854,
53 doi:[10.5194/tc-8-1839-2014](https://doi.org/10.5194/tc-8-1839-2014).
- 54 Stroeve, J.C. et al., 2012: Trends in Arctic sea ice extent from CMIP5, CMIP3 and observations. *Geophysical Research*
55 *Letters*, **39(16)**, doi:[10.1029/2012gl052676](https://doi.org/10.1029/2012gl052676).

- 1 Stuhne, G.R. and W.R. Peltier, 2015: Reconciling the ICE-6G_C reconstruction of glacial chronology with ice sheet
2 dynamics: The cases of Greenland and Antarctica. *Journal of Geophysical Research*, **120(9)**, 1841–1865.
- 3 Sugimoto, S., K. Hanawa, T. Watanabe, T. Suga, and S.-P.P. Xie, 2017: Enhanced warming of the subtropical mode
4 water in the North Pacific and North Atlantic. *Nature Climate Change*, **7**, 656, doi:[10.1038/nclimate3371](https://doi.org/10.1038/nclimate3371).
- 5 Sun, Q., M.M. Whitney, F.O. Bryan, and Y.- Tseng, 2017: A box model for representing estuarine physical processes in
6 Earth system models. *Ocean Modelling*, **112**, 139–153, doi:[10.1016/j.ocemod.2017.03.004](https://doi.org/10.1016/j.ocemod.2017.03.004).
- 7 Sun, S. et al., 2019: Topographic Shelf Waves Control Seasonal Melting Near Antarctic Ice Shelf Grounding Lines.
8 *Geophysical Research Letters*, **46(16)**, 9824–9832, doi:[10.1029/2019gl083881](https://doi.org/10.1029/2019gl083881).
- 9 Sun, S. et al., 2020: Antarctic ice sheet response to sudden and sustained ice-shelf collapse (ABUMIP). *Journal of*
10 *Glaciology*, 4–11, doi:[10.1017/jog.2020.67](https://doi.org/10.1017/jog.2020.67).
- 11 Suo, L., Y. Gao, D. Guo, and I. Bethke, 2017: Sea-ice free Arctic contributes to the projected warming minimum in the
12 North Atlantic. *Environmental Research Letters*, **12(7)**, 74004, doi:[10.1088/1748-9326/aa6a5e](https://doi.org/10.1088/1748-9326/aa6a5e).
- 13 Supply, A. et al., 2018: Precipitation Estimates from SMOS Sea-Surface Salinity. *Quarterly Journal of the Royal*
14 *Meteorological Society*, **144(S1)**, 103–119, doi:[10.1002/qj.3110](https://doi.org/10.1002/qj.3110).
- 15 Sutherland, D.A. et al., 2019: Direct observations of submarine melt and subsurface geometry at a tidewater glacier.
16 *Science*, **365(6451)**, 369–374, doi:[10.1126/science.aax3528](https://doi.org/10.1126/science.aax3528).
- 17 Sutter, J., P. Gierz, K. Grosfeld, M. Thoma, and G. Lohmann, 2016: Ocean temperature thresholds for Last Interglacial
18 West Antarctic Ice Sheet collapse. *Geophysical Research Letters*, **43(6)**, 2675–2682,
19 doi:[10.1002/2016gl067818](https://doi.org/10.1002/2016gl067818).
- 20 Sutter, J. et al., 2020: Limited Retreat of the Wilkes Basin Ice Sheet During the Last Interglacial. *Geophysical Research*
21 *Letters*, **47(13)**, 1–8, doi:[10.1029/2020gl088131](https://doi.org/10.1029/2020gl088131).
- 22 Svensson, C. and D.A. Jones, 2004: Dependence between sea surge, river flow and precipitation in south and west
23 Britain. *Hydrology and Earth System Sciences*, **8(5)**, 973–992, doi:[10.5194/hess-8-973-2004](https://doi.org/10.5194/hess-8-973-2004).
- 24 Swapna, P., J. Jyoti, R. Krishnan, N. Sandeep, and S.M. Griffies, 2017: Multidecadal Weakening of Indian Summer
25 Monsoon Circulation Induces an Increasing Northern Indian Ocean Sea Level. *Geophysical Research Letters*,
26 **44(20)**, 10,560–10,572, doi:[10.1002/2017gl074706](https://doi.org/10.1002/2017gl074706).
- 27 Swart, N.C., S.T. Gille, J.C. Fyfe, and N.P. Gillett, 2018: Recent Southern Ocean warming and freshening driven by
28 greenhouse gas emissions and ozone depletion. *Nature Geoscience*, **11(11)**, 836–841, doi:[10.1038/s41561-018-0226-1](https://doi.org/10.1038/s41561-018-0226-1).
- 29 Sweet, W. and J. Park, 2014: From the extreme to the mean: Acceleration and tipping points of coastal inundation from
30 sea level rise. *Earth's Future*, **2(12)**, 579–600, doi:[10.1002/2014ef000272](https://doi.org/10.1002/2014ef000272).
- 31 Swingedouw, D., P. Braconnot, P. Delecluse, E. Guilyardi, and O. Marti, 2006: The impact of global freshwater forcing
32 on the thermohaline circulation: adjustment of North Atlantic convection sites in a CGCM. *Climate Dynamics*,
33 **28(2–3)**, 291–305, doi:[10.1007/s00382-006-0171-3](https://doi.org/10.1007/s00382-006-0171-3).
- 34 Sydeman, W.J. et al., 2014: Climate change and wind intensification in coastal upwelling ecosystems. *Science*,
35 **345(6192)**, 77–80, doi:[10.1126/science.1251635](https://doi.org/10.1126/science.1251635).
- 36 Sylla, A., J. Mignot, X. Capet, and A.T. Gaye, 2019: Weakening of the Senegalo-Mauritania Upwelling System under
37 climate change. *Climate dynamics*, **53**, 4447–4473.
- 38 Tabone, I., J. Blasco, A. Robinson, J. Alvarez-Solas, and M. Montoya, 2018: The sensitivity of the Greenland Ice Sheet
39 to glacial-interglacial oceanic forcing. *Climate of the Past*, **14(4)**, 455–472, doi:[10.5194/cp-14-455-2018](https://doi.org/10.5194/cp-14-455-2018).
- 40 Tadesse, M., T. Wahl, and A. Cid, 2020: Data-Driven Modeling of Global Storm Surges. *Frontiers in Marine Science*,
41 **7**, 260, doi:[10.3389/fmars.2020.00260](https://doi.org/10.3389/fmars.2020.00260).
- 42 Takahashi, C. and M. Watanabe, 2016: Pacific trade winds accelerated by aerosol forcing over the past two decades.
43 *Nature Climate Change*, **6(8)**, 768–772, doi:[10.1038/nclimate2996](https://doi.org/10.1038/nclimate2996).
- 44 Takayabu, I. et al., 2015: Climate change effects on the worst-case storm surge: A case study of Typhoon Haiyan.
45 *Environmental Research Letters*, doi:[10.1088/1748-9326/10/6/064011](https://doi.org/10.1088/1748-9326/10/6/064011).
- 46 Talke, S.A. and D.A. Jay, 2013: Nineteenth century North American and Pacific tidal data: Lost or just forgotten?
47 *Journal of Coastal Research*, **29(6a)**, 118–127, doi:[10.2112/jcoastres-d-12-00181.1](https://doi.org/10.2112/jcoastres-d-12-00181.1).
- 48 Talke, S.A., A.C. Kemp, and J. Woodruff, 2018: Relative Sea Level, Tides, and Extreme Water Levels in Boston
49 Harbor From 1825 to 2018. *Journal of Geophysical Research: Oceans*, **123(6)**, 3895–3914,
50 doi:[10.1029/2017jc013645](https://doi.org/10.1029/2017jc013645).
- 51 Talley, L., 2013: Closure of the Global Overturning Circulation Through the Indian, Pacific, and Southern Oceans:
52 Schematics and Transports. *Oceanography*, **26(1)**, 80–97, doi:[10.5670/oceanog.2013.07](https://doi.org/10.5670/oceanog.2013.07).
- 53 Tandon, N.F., P.J. Kushner, D. Docquier, J.J. Wettstein, and C. Li, 2018: Reassessing Sea Ice Drift and Its Relationship
54 to Long-Term Arctic Sea Ice Loss in Coupled Climate Models. *Journal of Geophysical Research: Oceans*,
55 **123(6)**, 4338–4359, doi:[10.1029/2017jc013697](https://doi.org/10.1029/2017jc013697).
- 56

- 1 Tapia Baldis, C. and D. Trombotto Liaudat, 2019: Rockslides and rock avalanches in the Central Andes of Argentina
2 and their possible association with permafrost degradation. *Permafrost and Periglacial Processes*, **30(4)**, 330–
3 347, doi:[10.1002/ppp.2024](https://doi.org/10.1002/ppp.2024).
- 4 Tarasov, L., A.S. Dyke, R.M. Neal, and W.R. Peltier, 2012: A data-calibrated distribution of deglacial chronologies for
5 the North American ice complex from glaciological modeling. *Earth and Planetary Science Letters*, **315**, 30–
6 40, doi:[10.1016/j.epsl.2011.09.010](https://doi.org/10.1016/j.epsl.2011.09.010).
- 7 Taylor, K.E., R.J. Stouffer, and G.A. Meehl, 2012: An Overview of CMIP5 and the Experiment Design. *Bulletin of the*
8 *American Meteorological Society*, **93(4)**, 485–498, doi:[10.1175/bams-d-11-00094.1](https://doi.org/10.1175/bams-d-11-00094.1).
- 9 Tedesco, M. and X. Fettweis, 2020: Unprecedented atmospheric conditions (1948–2019) drive the 2019 exceptional
10 melting season over the Greenland ice sheet. *The Cryosphere*, **14**, 1209–1223, doi:[10.5194/tc-14-1209-2020](https://doi.org/10.5194/tc-14-1209-2020).
- 11 Terada, M., S. Minobe, and C. Deutsch, 2020: Mechanisms of future changes in equatorial upwelling: CMIP5
12 intermodel analysis. *Journal of Climate*, **33(2)**, 497–510, doi:[10.1175/jcli-d-19-0128.1](https://doi.org/10.1175/jcli-d-19-0128.1).
- 13 Tesi, T. et al., 2020: Resolving sea ice dynamics in the north-western Ross Sea during the last 2.6 ka: From seasonal to
14 millennial timescales. *Quaternary Science Reviews*, **237**, 106299, doi:[10.1016/j.quascirev.2020.106299](https://doi.org/10.1016/j.quascirev.2020.106299).
- 15 Thackeray, C.W. and C.G. Fletcher, 2016: Snow albedo feedback: Current knowledge, importance, outstanding issues
16 and future directions. *Progress in Physical Geography*, **40(3)**, 392–408, doi:[10.1177/0309133315620999](https://doi.org/10.1177/0309133315620999).
- 17 Thackeray, C.W., C.G. Fletcher, and C. Derksen, 2015: Quantifying the skill of CMIP5 models in simulating seasonal
18 albedo and snow cover evolution. *Journal of Geophysical Research*, **120(12)**, 5831–5849,
19 doi:[10.1002/2015jd023325](https://doi.org/10.1002/2015jd023325).
- 20 Thackeray, C.W., X. Qu, and A. Hall, 2018: Why Do Models Produce Spread in Snow Albedo Feedback? *Geophysical*
21 *Research Letters*, **45(12)**, 6223–6231, doi:[10.1029/2018gl078493](https://doi.org/10.1029/2018gl078493).
- 22 The IMBIE team, 2021: Antarctic and Greenland Ice Sheet mass balance 1992–2020 for IPCC AR6.
23 doi:[10.5285/77B64C55-7166-4A06-9DEF-2E400398E452](https://doi.org/10.5285/77B64C55-7166-4A06-9DEF-2E400398E452).
- 24 The IMBIE Team, 2020: Mass balance of the Greenland Ice Sheet from 1992 to 2018. *Nature*, **579**, 233–239,
25 doi:[10.1038/s41586-019-1855-2](https://doi.org/10.1038/s41586-019-1855-2).
- 26 The IMBIE Team et al., 2018: Mass balance of the Antarctic Ice Sheet from 1992 to 2017. *Nature*, **558(7709)**, 219–
27 222, doi:[10.1038/s41586-018-0179-y](https://doi.org/10.1038/s41586-018-0179-y).
- 28 Thøgersen, K., A. Gilbert, T.V. Schuler, and A. Malthe-Sørenssen, 2019: Rate-and-state friction explains glacier surge
29 propagation. *Nature Communications*, **10(1)**, 2823, doi:[10.1038/s41467-019-10506-4](https://doi.org/10.1038/s41467-019-10506-4).
- 30 Thomas, E.R. et al., 2019: Antarctic Sea Ice Proxies from Marine and Ice Core Archives Suitable for Reconstructing
31 Sea Ice over the Past 2000 Years. *Geosciences*, **9(12)**, 506, doi:[10.3390/geosciences9120506](https://doi.org/10.3390/geosciences9120506).
- 32 Thomas, Z.A. et al., 2020: Tipping elements and amplified polar warming during the Last Interglacial. *Quaternary*
33 *Science Reviews*, **233**, 106222, doi:[10.1016/j.quascirev.2020.106222](https://doi.org/10.1016/j.quascirev.2020.106222).
- 34 Thompson, A.F., A.L. Stewart, P. Spence, and K.J. Heywood, 2018: The Antarctic Slope Current in a Changing
35 Climate. *Reviews of Geophysics*, **56(4)**, 741–770, doi:[10.1029/2018rg000624](https://doi.org/10.1029/2018rg000624).
- 36 Thomson, J. and W.E. Rogers, 2014: Swell and sea in the emerging Arctic Ocean. *Geophysical Research Letters*, **41(9)**,
37 3136–3140, doi:[10.1002/2014gl059983](https://doi.org/10.1002/2014gl059983).
- 38 Tierney, J.E. et al., 2020: Glacial cooling and climate sensitivity revisited. *Nature*, **584(7822)**, 569–573,
39 doi:[10.1038/s41586-020-2617-x](https://doi.org/10.1038/s41586-020-2617-x).
- 40 Timko, P.G. et al., 2013: Skill testing a three-dimensional global tide model to historical current meter records. *Journal*
41 *of Geophysical Research: Oceans*, **118(12)**, 6914–6933, doi:[10.1002/2013jc009071](https://doi.org/10.1002/2013jc009071).
- 42 Timmermann, R. and H.H. Hellmer, 2013: Southern Ocean warming and increased ice shelf basal melting in the
43 twenty-first and twenty-second centuries based on coupled ice-ocean finite-element modelling. *Ocean*
44 *Dynamics*, **63(9)**, 1011–1026, doi:[10.1007/s10236-013-0642-0](https://doi.org/10.1007/s10236-013-0642-0).
- 45 Timmermann, R. and S. Goeller, 2017: Response to Filchner-Ronne Ice Shelf cavity warming in a coupled ocean-ice
46 sheet model – Part 1: The ocean perspective. *Ocean Science*, **13(5)**, 765–776, doi:[10.5194/os-13-765-2017](https://doi.org/10.5194/os-13-765-2017).
- 47 Timmermans, B., D. Stone, M. Wehner, and H. Krishnan, 2017: Impact of tropical cyclones on modeled extreme wind-
48 wave climate. *Geophysical Research Letters*, doi:[10.1002/2016gl071681](https://doi.org/10.1002/2016gl071681).
- 49 Timmermans, B.W., C.P. Gommenginger, G. Dodet, and J.-R. Bidlot, 2020: Global Wave Height Trends and
50 Variability from New Multimission Satellite Altimeter Products, Reanalyses, and Wave Buoys. *Geophysical*
51 *Research Letters*, **47(9)**, doi:[10.1029/2019gl086880](https://doi.org/10.1029/2019gl086880).
- 52 Tinker, J., J. Lowe, J. Holt, A. Pardaens, and A. Wiltshire, 2015: Validation of an ensemble modelling system for
53 climate projections for the northwest European shelf seas. *Progress in Oceanography*, **138**, 211–237,
54 doi:[10.1016/j.pocean.2015.07.002](https://doi.org/10.1016/j.pocean.2015.07.002).
- 55 Tinker, J., J. Lowe, A. Pardaens, J. Holt, and R. Barciela, 2016: Uncertainty in climate projections for the 21st century
56 northwest European shelf seas. *Progress in Oceanography*, **148**, 56–73, doi:[10.1016/j.pocean.2016.09.003](https://doi.org/10.1016/j.pocean.2016.09.003).

- 1 Todd, A. et al., 2020: Ocean-Only FAFMIP: Understanding Regional Patterns of Ocean Heat Content and Dynamic Sea
2 Level Change. *Journal of Advances in Modeling Earth Systems*, **12**, e2019MS002027,
3 doi:[10.1029/2019ms002027](https://doi.org/10.1029/2019ms002027).
- 4 Todd, J. et al., 2018: A Full-Stokes 3-D Calving Model Applied to a Large Greenlandic Glacier. *Journal of Geophysical*
5 *Research: Earth Surface*, **123**(3), 410–432, doi:[10.1002/2017jf004349](https://doi.org/10.1002/2017jf004349).
- 6 Tomita, H., T. Hihara, S. Kako, M. Kubota, and K. Kutsuwada, 2019: An introduction to J-OFURO3, a third-generation
7 Japanese ocean flux data set using remote-sensing observations. *Journal of Oceanography*, **75**(2), 171–194,
8 doi:[10.1007/s10872-018-0493-x](https://doi.org/10.1007/s10872-018-0493-x).
- 9 Törnqvist, T.E. and M.P. Hijma, 2012: Links between early Holocene ice-sheet decay, sea-level rise and abrupt climate
10 change. *Nature Geoscience*, **5**(9), 601–606, doi:[10.1038/ngeo1536](https://doi.org/10.1038/ngeo1536).
- 11 Torsvik, T. et al., 2019: Impact of tidewater glacier retreat on the fjord system: Modeling present and future circulation
12 in Kongsfjorden, Svalbard. *Estuarine, Coastal and Shelf Science*, **220**, 152–165,
13 doi:[10.1016/j.ecss.2019.02.005](https://doi.org/10.1016/j.ecss.2019.02.005).
- 14 Trenberth, K.E. and J.T. Fasullo, 2018: Applications of an updated atmospheric energetics formulation. *Journal of*
15 *Climate*, **31**(16), 6263–6279, doi:[10.1175/jcli-d-17-0838.1](https://doi.org/10.1175/jcli-d-17-0838.1).
- 16 Trenberth, K.E., Y. Zhang, J.T. Fasullo, and L. Cheng, 2019: Observation-Based Estimates of Global and Basin Ocean
17 Meridional Heat Transport Time Series. *Journal of Climate*, **32**(14), 4567–4583, doi:[10.1175/jcli-d-18-0872.1](https://doi.org/10.1175/jcli-d-18-0872.1).
- 18 Trofaier, A.M., S. Westermann, and A. Bartsch, 2017: Progress in space-borne studies of permafrost for climate
19 science: Towards a multi-ECV approach. *Remote Sensing of Environment*, **203**, 55–70,
20 doi:[10.1016/j.rse.2017.05.021](https://doi.org/10.1016/j.rse.2017.05.021).
- 21 Trotta, F., N. Pinardi, E. Fenu, A. Grandi, and V. Lyubartsev, 2017: Multi-nest high-resolution model of submesoscale
22 circulation features in the Gulf of Taranto. *Ocean Dynamics*, **67**(12), 1609–1625, doi:[10.1007/s10236-017-1110-z](https://doi.org/10.1007/s10236-017-1110-z).
- 23 Trusel, L.D. et al., 2015: Divergent trajectories of Antarctic surface melt under two twenty-first-century climate
24 scenarios. *Nature Geoscience*, **8**, 927–932, doi:[10.1038/ngeo2563](https://doi.org/10.1038/ngeo2563).
- 25 Trüssel, B.L., R.J. Motyka, M. Truffer, and C.F. Larsen, 2013: Rapid thinning of lake-calving Yakutat Glacier and the
26 collapse of the Yakutat Icefield, southeast Alaska, USA. *Journal of Glaciology*, **59**(213), 149–161, doi:
27 [10.3189/2013j0g12j081](https://doi.org/10.3189/2013j0g12j081).
- 28 Tsubouchi, T. et al., 2021: Increased ocean heat transport into the Nordic Seas and Arctic Ocean over the period 1993–
29 2016. *Nature Climate Change*, **11**(1), 21–26, doi:[10.1038/s41558-020-00941-3](https://doi.org/10.1038/s41558-020-00941-3).
- 30 Tsujino, H. et al., 2020: Evaluation of global ocean–sea-ice model simulations based on the experimental protocols of
31 the Ocean Model Intercomparison Project phase 2 (OMIP-2). *Geoscientific Model Development*, **13**(8), 3643–
32 3708, doi:[10.5194/gmd-13-3643-2020](https://doi.org/10.5194/gmd-13-3643-2020).
- 33 Turetsky, M.R. et al., 2020: Carbon release through abrupt permafrost thaw. *Nature Geoscience*, **13**(2), 138–143,
34 doi:[10.1038/s41561-019-0526-0](https://doi.org/10.1038/s41561-019-0526-0).
- 35 Turki, I., N. Massei, and B. Laignel, 2019: Linking sea level dynamic and exceptional events to large-scale atmospheric
36 circulation variability: A case of the Seine Bay, France. *Oceanologia*, **61**(3), 321–330,
37 doi:[10.1016/j.oceano.2019.01.003](https://doi.org/10.1016/j.oceano.2019.01.003).
- 38 Turner, J., T. Bracegirdle, T. Phillips, G. Marshall, and S. Hosking, 2013: An Initial Assessment of Antarctic Sea Ice
39 Extent in the CMIP5 Models. *Journal of Climate*, **26**, 1473–1484.
- 40 Turner, J. et al., 2017: Atmosphere–ocean–ice interactions in the Amundsen Sea Embayment, West Antarctica. *Reviews*
41 *of Geophysics*, **55**, 235–276, doi:[10.1002/2016rg000532](https://doi.org/10.1002/2016rg000532).
- 42 Turner, J. et al., 2020: Recent Decrease of Summer Sea Ice in the Weddell Sea, Antarctica. *Geophysical Research*
43 *Letters*, **47**(11), e2020GL087127, doi:[10.1029/2020gl087127](https://doi.org/10.1029/2020gl087127).
- 44 Turney, C.S.M. et al., 2020: Early Last Interglacial ocean warming drove substantial ice mass loss from Antarctica.
45 *Proceedings of the National Academy of Sciences*, **117**(8), 3996–4006, doi:[10.1073/pnas.1902469117](https://doi.org/10.1073/pnas.1902469117).
- 46 Uemura, R. et al., 2018: Asynchrony between Antarctic temperature and CO2 associated with obliquity over the past
47 720,000 years. *Nature communications*, **9**(1), 1–11, doi:[10.1038/s41467-018-03328-3](https://doi.org/10.1038/s41467-018-03328-3).
- 48 Ullman, D.J. et al., 2016: Final Laurentide ice-sheet deglaciation and Holocene climate–sea level change. *Quaternary*
49 *Science Reviews*, **152**, 49–59, doi:[10.1016/j.quascirev.2016.09.014](https://doi.org/10.1016/j.quascirev.2016.09.014).
- 50 Uotila, P. et al., 2019: An assessment of ten ocean reanalyses in the polar regions. *Climate Dynamics*, **52**(3), 1613–
51 1650, doi:[10.1007/s00382-018-4242-z](https://doi.org/10.1007/s00382-018-4242-z).
- 52 Valdes, P., 2011: Built for stability. *Nature Geoscience*, **4**(7), 414–416, doi:[10.1038/ngeo1200](https://doi.org/10.1038/ngeo1200).
- 53 Valdivieso, M. et al., 2017: An assessment of air–sea heat fluxes from ocean and coupled reanalyses. *Climate*
54 *Dynamics*, **49**(3), 983–1008, doi:[10.1007/s00382-015-2843-3](https://doi.org/10.1007/s00382-015-2843-3).
- 55

- 1 Välisuo, I., T. Vihma, R. Pirazzini, and M. Schäfer, 2018: Interannual Variability of Atmospheric Conditions and
2 Surface Melt in Greenland in 2000–2014. *Journal of Geophysical Research: Atmospheres*, **123(18)**, 10,410–
3 443,463, doi:[10.1029/2018jd028445](https://doi.org/10.1029/2018jd028445).
- 4 Van Breedam, J., H. Goelzer, and P. Huybrechts, 2020: Semi-equilibrated global sea-level change projections for the
5 next 10 000 years. *Earth System Dynamics*, **11(4)**, 953–976, doi:[10.5194/esd-11-953-2020](https://doi.org/10.5194/esd-11-953-2020).
- 6 Van de Wal, R.S.W. and M. Wild, 2001: Modelling the response of glaciers to climate change by applying volume-area
7 scaling in combination with a high resolution GCM. *Climate Dynamics*, **18(3)**, 359–366,
8 doi:[10.1007/s003820100184](https://doi.org/10.1007/s003820100184).
- 9 van den Hurk, B., E. van Meijgaard, P. de Valk, K.-J. van Heeringen, and J. Gooijer, 2015: Analysis of a compounding
10 surge and precipitation event in the Netherlands. *Environmental Research Letters*, **10(3)**, 35001.
- 11 van der Linden, E.C., D. Le Bars, R. Bintanja, and W. Hazeleger, 2019: Oceanic heat transport into the Arctic under
12 high and low CO2 forcing. *Climate Dynamics*, **53(7–8)**, 4763–4780, doi:[10.1007/s00382-019-04824-y](https://doi.org/10.1007/s00382-019-04824-y).
- 13 van Kampenhout, L. et al., 2017: Improving the Representation of Polar Snow and Firn in the Community Earth System
14 Model. *Journal of Advances in Modeling Earth Systems*, **9(7)**, 2583–2600, doi:[10.1002/2017ms000988](https://doi.org/10.1002/2017ms000988).
- 15 van Kampenhout, L. et al., 2020: Present-Day Greenland Ice Sheet Climate and Surface Mass Balance in CESM2.
16 *Journal of Geophysical Research: Earth Surface*, **125(2)**, doi:[10.1029/2019jf005318](https://doi.org/10.1029/2019jf005318).
- 17 Van Pelt, W. et al., 2019: A long-term dataset of climatic mass balance, snow conditions, and runoff in Svalbard (1957-
18 2018). *Cryosphere*, **13(9)**, 2259–2280, doi:[10.5194/tc-13-2259-2019](https://doi.org/10.5194/tc-13-2259-2019).
- 19 van Tricht, K. et al., 2016: Clouds enhance Greenland ice sheet meltwater runoff. *Nature Communications*, **7**, 10266,
20 doi:[10.1038/ncomms10266](https://doi.org/10.1038/ncomms10266).
- 21 Vandecrux, B. et al., 2019: Firn data compilation reveals widespread decrease of firn air content in western Greenland.
22 *The Cryosphere*, **13(3)**, 845–859, doi:[10.5194/tc-13-845-2019](https://doi.org/10.5194/tc-13-845-2019).
- 23 Varela, R., I. Álvarez, F. Santos, M. Gómez-Gesteira, and others, 2015: Has upwelling strengthened along worldwide
24 coasts over 1982–2010? *Scientific reports*, **5**, 10016, doi:[10.1038/srep10016](https://doi.org/10.1038/srep10016).
- 25 Varela, R., F.P. Lima, R. Seabra, C. Meneghesso, and M. Gómez-Gesteira, 2018: Coastal warming and wind-driven
26 upwelling: A global analysis. *Science of The Total Environment*, **639**, 1501–1511,
27 doi:[10.1016/j.scitotenv.2018.05.273](https://doi.org/10.1016/j.scitotenv.2018.05.273).
- 28 Vargo, L.J. et al., 2020: Anthropogenic warming forces extreme annual glacier mass loss. *Nature Climate Change*,
29 **10(9)**, 856–861, doi:[10.1038/s41558-020-0849-2](https://doi.org/10.1038/s41558-020-0849-2).
- 30 Vaughan, D.G. et al., 2013: Observations: Cryosphere. In: *Climate Change 2013: The Physical Science Basis. Contribution of Working Group I to the Fifth Assessment Report of the Intergovernmental Panel on Climate Change* [Stocker, T.F., G.-K. D. Qin, M. Plattner, S.K. Tignor, J. Allen, A. Boschung, Y. Nauels, V.B. Xia, and P.M. Midgley (eds.)], Cambridge University Press, Cambridge, United Kingdom and New York, NY, USA, pp. 317–382, doi:[10.1017/cbo9781107415324.012](https://doi.org/10.1017/cbo9781107415324.012).
- 35 Vecchi, G.A. and B.J. Soden, 2007: Global warming and the weakening of the tropical circulation. *Journal of Climate*,
36 doi:[10.1175/jcli4258.1](https://doi.org/10.1175/jcli4258.1).
- 37 Vecchi, G.A. et al., 2006: Weakening of tropical Pacific atmospheric circulation due to anthropogenic forcing. *Nature*,
38 **441(7089)**, 73–76, doi:[10.1038/nature04744](https://doi.org/10.1038/nature04744).
- 39 Velicogna, I. et al., 2020: Continuity of Ice Sheet Mass Loss in Greenland and Antarctica From the GRACE and
40 GRACE Follow-On Missions. *Geophysical Research Letters*, **47(8)**, e2020GL087291,
41 doi:[10.1029/2020gl087291](https://doi.org/10.1029/2020gl087291).
- 42 Venturelli, R.A. et al., 2020: Mid-Holocene Grounding Line Retreat and Readvance at Whillans Ice Stream, West
43 Antarctica. *Geophysical Research Letters*, **47(15)**, doi:[10.1029/2020gl088476](https://doi.org/10.1029/2020gl088476).
- 44 Verfaillie, D. et al., 2018: Multi-component ensembles of future meteorological and natural snow conditions for 1500 m
45 altitude in the Chartreuse mountain range, Northern French Alps. *Cryosphere*, **12(4)**, 1249–1271,
46 doi:[10.5194/tc-12-1249-2018](https://doi.org/10.5194/tc-12-1249-2018).
- 47 Vermassen, F. et al., 2020: A Major Collapse of Kangerlussuaq Glacier’s Ice Tongue Between 1932 and 1933 in East
48 Greenland. *Geophysical Research Letters*, **47(4)**, e2019GL085954, doi:[10.1029/2019gl085954](https://doi.org/10.1029/2019gl085954).
- 49 Vichi, M. et al., 2019: Effects of an Explosive Polar Cyclone Crossing the Antarctic Marginal Ice Zone. *Geophysical Research Letters*, **46(11)**, 5948–5958, doi:[10.1029/2019gl082457](https://doi.org/10.1029/2019gl082457).
- 51 Vieira, G. et al., 2010: Thermal state of permafrost and active-layer monitoring in the antarctic: Advances during the
52 international polar year 2007–2009. *Permafrost and Periglacial Processes*, **21(2)**, 182–197,
53 doi:[10.1002/ppp.685](https://doi.org/10.1002/ppp.685).
- 54 Vihma, T., P. Tisler, and P. Uotila, 2012: Atmospheric forcing on the drift of Arctic sea ice in 1989–2009. *Geophysical Research Letters*, **39(2)**, doi:[10.1029/2011gl050118](https://doi.org/10.1029/2011gl050118).

- 1 Vijay, S. et al., 2019: Resolving Seasonal Ice Velocity of 45 Greenlandic Glaciers With Very High Temporal Details.
2 *Geophysical Research Letters*, **46(3)**, 1485–1495, doi:[10.1029/2018gl081503](https://doi.org/10.1029/2018gl081503).
- 3 Vinogradova, N. et al., 2019: Satellite Salinity Observing System: Recent Discoveries and the Way Forward. *Frontiers*
4 *in Marine Science*, **6**, 243, doi:[10.3389/fmars.2019.00243](https://doi.org/10.3389/fmars.2019.00243).
- 5 Vitousek, S. et al., 2017: Doubling of coastal flooding frequency within decades due to sea-level rise. *Scientific*
6 *Reports*, **7(1)**, 1–9, doi:[10.1038/s41598-017-01362-7](https://doi.org/10.1038/s41598-017-01362-7).
- 7 Vizcaino, M. et al., 2015: Coupled simulations of Greenland Ice Sheet and climate change up to A.D. 2300.
8 *Geophysical Research Letters*, **42(10)**, 3927–3935, doi:[10.1002/2014gl061142](https://doi.org/10.1002/2014gl061142).
- 9 Voldoire, A. et al., 2019: Evaluation of CMIP6 DECK Experiments With CNRM-CM6-1. *Journal of Advances in*
10 *Modeling Earth Systems*, **11**, 2177–2213, doi:[10.1029/2019ms001683](https://doi.org/10.1029/2019ms001683).
- 11 Vousdoukas, M.I., L. Mentaschi, E. Voukouvalas, M. Verlaan, and L. Feyen, 2017: Extreme sea levels on the rise along
12 Europe’s coasts. *Earth’s Future*, **5(3)**, 304–323.
- 13 Vousdoukas, M.I. et al., 2018: Global probabilistic projections of extreme sea levels show intensification of coastal
14 flood hazard. *Nature Communications*, **9(1)**, 2360, doi:[10.1038/s41467-018-04692-w](https://doi.org/10.1038/s41467-018-04692-w).
- 15 Wada, Y., 2016: Modeling groundwater depletion at regional and global scales: Present state and future prospects.
16 *Surveys in Geophysics*, **37(2)**, 419–451.
- 17 Wada, Y. et al., 2012: Past and future contribution of global groundwater depletion to sea-level rise. *Geophysical*
18 *Research Letters*, **39(9)**, n/a–n/a, doi:[10.1029/2012gl051230](https://doi.org/10.1029/2012gl051230).
- 19 Wada, Y. et al., 2016: Fate of water pumped from underground and contributions to sea-level rise. *Nature Climate*
20 *Change*, doi:[10.1038/nclimate3001](https://doi.org/10.1038/nclimate3001).
- 21 Wagner, T.J.W. and I. Eisenman, 2015: How Climate Model Complexity Influences Sea Ice Stability. *Journal of*
22 *Climate*, **28(10)**, 3998–4014, doi:[10.1175/jcli-d-14-00654.1](https://doi.org/10.1175/jcli-d-14-00654.1).
- 23 Wagner, T.J.W. et al., 2019: Large spatial variations in the flux balance along the front of a Greenland tidewater glacier.
24 *Cryosphere*, **13(3)**, 911–925, doi:[10.5194/tc-13-911-2019](https://doi.org/10.5194/tc-13-911-2019).
- 25 Wahl, T. and D.P. Chambers, 2015: Evidence for multidecadal variability in US extreme sea level records. *Journal of*
26 *Geophysical Research: Oceans*, **120(3)**, 1527–1544.
- 27 Wahl, T. et al., 2017: Understanding extreme sea levels for broad-scale coastal impact and adaptation analysis. *Nature*
28 *Communications*, **8**, doi:[10.1038/ncomms16075](https://doi.org/10.1038/ncomms16075).
- 29 Wählin, A.K. et al., 2020: Ice front blocking of ocean heat transport to an Antarctic ice shelf. *Nature*, **578**, 568–571,
30 doi:[10.1038/s41586-020-2014-5](https://doi.org/10.1038/s41586-020-2014-5).
- 31 Walsh, J.E., F. Fetterer, J. Scott Stewart, and W.L. Chapman, 2017: A database for depicting Arctic sea ice variations
32 back to 1850. *Geographical Review*, **107(1)**, 89–107, doi:[10.1111/j.1931-0846.2016.12195.x](https://doi.org/10.1111/j.1931-0846.2016.12195.x).
- 33 Walsh, J.E. et al., 2018: Downscaling of climate model output for Alaskan stakeholders. *Environmental Modelling &*
34 *Software*, **110**, 38–51, doi:[10.1016/j.envsoft.2018.03.021](https://doi.org/10.1016/j.envsoft.2018.03.021).
- 35 Wandres, M., C. Pattiaratchi, and M.A. Hemer, 2017: Projected changes of the southwest Australian wave climate
36 under two atmospheric greenhouse gas concentration pathways. *Ocean Modelling*, **117**, 70–87,
37 doi:[10.1016/j.ocemod.2017.08.002](https://doi.org/10.1016/j.ocemod.2017.08.002).
- 38 Wang, C., L. Zhang, S.-K.K. Lee, L. Wu, and C.R. Mechoso, 2014: A global perspective on CMIP5 climate model
39 biases. *Nature Climate Change*, **4(3)**, 201–205, doi:[10.1038/nclimate2118](https://doi.org/10.1038/nclimate2118).
- 40 Wang, D., T.C. Gouhier, B.A. Menge, and A.R. Ganguly, 2015: Intensification and spatial homogenization of coastal
41 upwelling under climate change. *Nature*, **518(7539)**, 390–394, doi:[10.1038/nature14235](https://doi.org/10.1038/nature14235).
- 42 Wang, G. et al., 2019: Compounding tropical and stratospheric forcing of the record low Antarctic sea-ice in 2016.
43 *Nature Communications*, **10(1)**, 13, doi:[10.1038/s41467-018-07689-7](https://doi.org/10.1038/s41467-018-07689-7).
- 44 Wang, H., S.A. Legg, and R.W. Hallberg, 2015: Representations of the Nordic Seas overflows and their large scale
45 climate impact in coupled models. *Ocean Modelling*, **86**, 76–92, doi:[10.1016/j.ocemod.2014.12.005](https://doi.org/10.1016/j.ocemod.2014.12.005).
- 46 Wang, J., J.A. Church, X. Zhang, and X. Chen, 2021: Reconciling global mean and regional sea level change in
47 projections and observations. *Nature Communications*, **12**, 990, doi:[10.1038/s41467-021-21265-6](https://doi.org/10.1038/s41467-021-21265-6).
- 48 Wang, L., C. Derksen, R. Brown, and T. Markus, 2013: Recent changes in pan-Arctic melt onset from satellite passive
49 microwave measurements. *Geophysical Research Letters*, **40(3)**, 522–528, doi:[10.1002/grl.50098](https://doi.org/10.1002/grl.50098).
- 50 Wang, L. et al., 2016: Investigating the spread in surface albedo for snow-covered forests in CMIP5 models. *Journal of*
51 *Geophysical Research*, **121(3)**, 1104–1119, doi:[10.1002/2015jd023824](https://doi.org/10.1002/2015jd023824).
- 52 Wang, L. et al., 2020: Recent Shift in the Warming of the Southern Oceans Modulated by Decadal Climate Variability.
53 *Geophysical Research Letters*, **n/a(n/a)**, e2020GL090889, doi:[10.1029/2020gl090889](https://doi.org/10.1029/2020gl090889).
- 54 Wang, L. et al., 2021: Recent Shift in the Warming of the Southern Oceans Modulated by Decadal Climate Variability.
55 *Geophysical Research Letters*, **48(3)**, e2020GL090889, doi:[10.1029/2020gl090889](https://doi.org/10.1029/2020gl090889).

- 1 Wang, Q. et al., 2014: The Finite Element Sea Ice-Ocean Model (FESOM) v.1.4: formulation of an ocean general
2 circulation model. *Geoscientific Model Development*, **7**(2), 663–693, doi:[10.5194/gmd-7-663-2014](https://doi.org/10.5194/gmd-7-663-2014).
- 3 Wang, Q. et al., 2019: Ocean Heat Transport Into the Barents Sea: Distinct Controls on the Upward Trend and
4 Interannual Variability. *Geophysical Research Letters*, **46**(22), 13180–13190, doi:[10.1029/2019gl083837](https://doi.org/10.1029/2019gl083837).
- 5 Wang, W., C.S. Zender, D. van As, and N.B. Miller, 2019: Spatial Distribution of Melt Season Cloud Radiative Effects
6 Over Greenland: Evaluating Satellite Observations, Reanalyses, and Model Simulations Against In Situ
7 Measurements. *Journal of Geophysical Research: Atmospheres*, **124**, 57–71, doi:[10.1029/2018jd028919](https://doi.org/10.1029/2018jd028919).
- 8 Wang, W. et al., 2016: Evaluation of air-soil temperature relationships simulated by land surface models during winter
9 across the permafrost region. *The Cryosphere*, **10**(4), 1721–1737, doi:[10.5194/tc-10-1721-2016](https://doi.org/10.5194/tc-10-1721-2016).
- 10 Wang, Y. et al., 2018: Elucidating the Role of Anthropogenic Aerosols in Arctic Sea Ice Variations. *Journal of Climate*,
11 **31**(1), 99–114, doi:[10.1175/jcli-d-17-0287.1](https://doi.org/10.1175/jcli-d-17-0287.1).
- 12 Wang, Y.-L. and C.-R. Wu, 2018: Discordant multi-decadal trend in the intensity of the Kuroshio along its path during
13 1993–2013. *Scientific Reports*, **8**(1), 14633, doi:[10.1038/s41598-018-32843-y](https://doi.org/10.1038/s41598-018-32843-y).
- 14 Wang, Y.-L., C.-R. Wu, and S.-Y. Chao, 2016: Warming and weakening trends of the Kuroshio during 1993–2013.
15 *Geophysical Research Letters*, **43**(17), 9200–9207, doi:[10.1002/2016gl069432](https://doi.org/10.1002/2016gl069432).
- 16 Ward, P.J. et al., 2018: Dependence between high sea-level and high river discharge increases flood hazard in global
17 deltas and estuaries. *Environmental Research Letters*, **13**(8), 084012, doi:[10.1088/1748-9326/aad400](https://doi.org/10.1088/1748-9326/aad400).
- 18 Warrick, R. et al., 1990: Sea Level Rise. In: *Climate Change: The IPCC Scientific Assessment* [Houghton, J.T., G.J.
19 Jenkins, and J.J. Ephraums (eds.)]. Cambridge University Press, Cambridge, United Kingdom and New York,
20 NY, USA, pp. 259–281.
- 21 Washam, P., A. Münchow, and K.W. Nicholls, 2018: A Decade of Ocean changes impacting the ice shelf of Petermann
22 Gletscher, Greenland. *Journal of Physical Oceanography*, **48**(10), 2477–2493, doi:[10.1175/jpo-d-17-0181.1](https://doi.org/10.1175/jpo-d-17-0181.1).
- 23 Watanabe, M., J.L. Dufresne, Y. Kosaka, T. Mauritsen, and H. Tatebe, 2021: Enhanced warming constrained by past
24 trends in equatorial Pacific sea surface temperature gradient. *Nature Climate Change*, **11**, 33–37,
25 doi:[10.1038/s41558-020-00933-3](https://doi.org/10.1038/s41558-020-00933-3).
- 26 Waugh, D.W., A. McC. Hogg, P. Spence, M.H. England, and T.W.N. Haine, 2019: Response of Southern Ocean
27 Ventilation to Changes in Midlatitude Westerly Winds. *Journal of Climate*, **32**(17), 5345–5361,
28 doi:[10.1175/jcli-d-19-0039.1](https://doi.org/10.1175/jcli-d-19-0039.1).
- 29 WCRP Global Sea Level Budget Group, 2018a: Global sea-level budget 1993–present. *Earth System Science Data*,
30 **10**(3), 1551–1590, doi:[10.5194/essd-10-1551-2018](https://doi.org/10.5194/essd-10-1551-2018).
- 31 WCRP Global Sea Level Budget Group, 2018b: Global sea-level budget 1993–present. *Earth System Science Data*,
32 **10**(3), 1551–1590, doi:[10.5194/essd-10-1551-2018](https://doi.org/10.5194/essd-10-1551-2018).
- 33 Wearing, M.G. and J. Kingslake, 2019: Holocene Formation of Henry Ice Rise, West Antarctica, Inferred From Ice-
34 Penetrating Radar. *Journal of Geophysical Research: Earth Surface*, **124**(8), 2224–2240,
35 doi:[10.1029/2018jf004988](https://doi.org/10.1029/2018jf004988).
- 36 Webber, B.G.M., K.J. Heywood, D.P. Stevens, and K.M. Assmann, 2019: The Impact of Overturning and Horizontal
37 Circulation in Pine Island Trough on Ice Shelf Melt in the Eastern Amundsen Sea. *Journal of Physical
38 Oceanography*, **49**(1), 63–83, doi:[10.1175/jpo-d-17-0213.1](https://doi.org/10.1175/jpo-d-17-0213.1).
- 39 Weber, M.E. et al., 2014: Millennial-scale variability in Antarctic ice-sheet discharge during the last deglaciation.
40 *Nature*, **510**(7503), 134–138, doi:[10.1038/nature13397](https://doi.org/10.1038/nature13397).
- 41 Webster, M. et al., 2018: Snow in the changing sea-ice systems. *Nature Climate Change*, **8**(11), 946–953,
42 doi:[10.1038/s41558-018-0286-7](https://doi.org/10.1038/s41558-018-0286-7).
- 43 Wei, T., Q. Yan, W. Qi, M. Ding, and C. Wang, 2020: Projections of Arctic sea ice conditions and shipping routes in
44 the twenty-first century using CMIP6 forcing scenarios. *Environmental Research Letters*, **15**(10), 104079,
45 doi:[10.1088/1748-9326/abb2c8](https://doi.org/10.1088/1748-9326/abb2c8).
- 46 Weijer, W., W. Cheng, O.A. Garuba, A. Hu, and B.T. Nadiga, 2020: CMIP6 Models Predict Significant 21st Century
47 Decline of the Atlantic Meridional Overturning Circulation. *Geophysical Research Letters*, **47**(12),
48 doi:[10.1029/2019gl086075](https://doi.org/10.1029/2019gl086075).
- 49 Weijer, W. et al., 2019: Stability of the Atlantic Meridional Overturning Circulation: A Review and Synthesis. *Journal
50 of Geophysical Research: Oceans*, 2019JC015083, doi:[10.1029/2019jc015083](https://doi.org/10.1029/2019jc015083).
- 51 Welty, E. et al., 2020: Worldwide version-controlled database of glacier thickness observations. *Earth System Science
52 Data*, **12**, 3039–3055, doi:[10.5194/essd-2020-87](https://doi.org/10.5194/essd-2020-87).
- 53 Wernecke, A., T.L. Edwards, I.J. Nias, P.B. Holden, and N.R. Edwards, 2020: Spatial probabilistic calibration of a
54 high-resolution Amundsen Sea Embayment ice sheet model with satellite altimeter data. *Cryosphere*, **14**(5),
55 1459–1474, doi:[10.5194/tc-14-1459-2020](https://doi.org/10.5194/tc-14-1459-2020).

- 1 Wernli, H. and L. Papritz, 2018: Role of polar anticyclones and mid-latitude cyclones for Arctic summertime sea-ice
2 melting. *Nature Geoscience*, **11**(2), 108–113, doi:[10.1038/s41561-017-0041-0](https://doi.org/10.1038/s41561-017-0041-0).
- 3 Whitehouse, P.L., 2018: Glacial isostatic adjustment modelling: Historical perspectives, recent advances, and future
4 directions. *Earth Surface Dynamics*, **6**(2), 401–429, doi:[10.5194/esurf-6-401-2018](https://doi.org/10.5194/esurf-6-401-2018).
- 5 Whitehouse, P.L., M.J. Bentley, and A.M. Le Brocq, 2012: A deglacial model for Antarctica: geological constraints and
6 glaciological modelling as a basis for a new model of Antarctic glacial isostatic adjustment. *Quaternary
7 Science Reviews*, **32**, 1–24, doi:[10.1016/j.quascirev.2011.11.016](https://doi.org/10.1016/j.quascirev.2011.11.016).
- 8 Wille, J.D. et al., 2019: West Antarctic surface melt triggered by atmospheric rivers. *Nature Geoscience*, **12**(11), 911–
9 916, doi:[10.1038/s41561-019-0460-1](https://doi.org/10.1038/s41561-019-0460-1).
- 10 Williams, G. et al., 2015: Thick and deformed Antarctic sea ice mapped with autonomous underwater vehicles. *Nature
11 Geoscience*, **8**(1), 61–67, doi:[10.1038/ngeo2299](https://doi.org/10.1038/ngeo2299).
- 12 Williams, K.D. et al., 2018: The Met Office Global Coupled Model 3.0 and 3.1 (GC3.0 and GC3.1) Configurations.
13 *Journal of Advances in Modeling Earth Systems*, **10**(2), 357–380, doi:[10.1002/2017ms001115](https://doi.org/10.1002/2017ms001115).
- 14 Williams, R.G., V. Roussenov, D. Smith, and M.S. Lozier, 2014: Decadal Evolution of Ocean Thermal Anomalies in
15 the North Atlantic: The Effects of Ekman, Overturning, and Horizontal Transport. *Journal of Climate*, **27**(2),
16 698–719, doi:[10.1175/jcli-d-12-00234.1](https://doi.org/10.1175/jcli-d-12-00234.1).
- 17 Williams, R.G., V. Roussenov, M.S. Lozier, and D. Smith, 2015: Mechanisms of Heat Content and Thermocline
18 Change in the Subtropical and Subpolar North Atlantic. *Journal of Climate*, **28**(24), 9803–9815,
19 doi:[10.1175/jcli-d-15-0097.1](https://doi.org/10.1175/jcli-d-15-0097.1).
- 20 Williamson, C.J. et al., 2019: Glacier Algae: A Dark Past and a Darker Future. *Frontiers in Microbiology*, **10**, 524,
21 doi:[10.3389/fmicb.2019.00524](https://doi.org/10.3389/fmicb.2019.00524).
- 22 Wills, R.C.J., K.C. Armour, D.S. Battisti, and D.L. Hartmann, 2019: Ocean–Atmosphere Dynamical Coupling
23 Fundamental to the Atlantic Multidecadal Oscillation. *Journal of Climate*, **32**(1), 251–272, doi:[10.1175/jcli-d-
24 18-0269.1](https://doi.org/10.1175/jcli-d-18-0269.1).
- 25 Wilson, D.J. et al., 2018: Ice loss from the East Antarctic Ice Sheet during late Pleistocene interglacials. *Nature*,
26 **561**(7723), 383–386, doi:[10.1038/s41586-018-0501-8](https://doi.org/10.1038/s41586-018-0501-8).
- 27 Wilson, D.J. et al., 2020: Sea-ice control on deglacial lower cell circulation changes recorded by Drake Passage deep-
28 sea corals. *Earth and Planetary Science Letters*, **544**, doi:[10.1016/j.epsl.2020.116405](https://doi.org/10.1016/j.epsl.2020.116405).
- 29 Wilson, N., F. Straneo, and P. Heimbach, 2017: Satellite-derived submarine melt rates and mass balance (2011–2015)
30 for Greenland’s largest remaining ice tongues. *Cryosphere*, **11**(6), 2773–2782, doi:[10.5194/tc-11-2773-2017](https://doi.org/10.5194/tc-11-2773-2017).
- 31 Winton, M., S.M. Griffies, B.L. Samuels, J.L. Sarmiento, and T.L.F. Licher, 2013: Connecting changing ocean
32 circulation with changing climate. *Journal of Climate*, **26**(7), 2268–2278, doi:[10.1175/jcli-d-12-00296.1](https://doi.org/10.1175/jcli-d-12-00296.1).
- 33 Wittenberg, A.T., 2009: Are historical records sufficient to constrain ENSO simulations? *Geophysical Research
34 Letters*, **36**(12), L12702, doi:[10.1029/2009gl0138710](https://doi.org/10.1029/2009gl0138710).
- 35 Wittmann, M. et al., 2017: Impact of dust deposition on the albedo of Vatnajökull ice cap, Iceland. *The Cryosphere*, **11**,
36 741–754, doi:[10.5194/tc-11-741-2017](https://doi.org/10.5194/tc-11-741-2017).
- 37 Wolovick, M.J. and J.C. Moore, 2018: Stopping the flood: could we use targeted geoengineering to mitigate sea level
38 rise? *The Cryosphere*, **12**(9), 2955–2967, doi:[10.5194/tc-12-2955-2018](https://doi.org/10.5194/tc-12-2955-2018).
- 39 Wong, T.E., A.M.R. Bakker, and K. Keller, 2017: Impacts of Antarctic fast dynamics on sea-level projections and
40 coastal flood defense. *Climatic Change*, **144**(2), 347–364, doi:[10.1007/s10584-017-2039-4](https://doi.org/10.1007/s10584-017-2039-4).
- 41 Wood, M. et al., 2018: Ocean-Induced Melt Triggers Glacier Retreat in Northwest Greenland. *Geophysical Research
42 Letters*, **45**(16), 8334–8342, doi:[10.1029/2018gl078024](https://doi.org/10.1029/2018gl078024).
- 43 Wood, M. et al., 2021: Ocean forcing drives glacier retreat in Greenland. *Science Advances*, **7**(1),
44 doi:[10.1126/sciadv.aba7282](https://doi.org/10.1126/sciadv.aba7282).
- 45 Woodworth, P.L. et al., 2016: Towards a global higher-frequency sea level dataset. *Geoscience Data Journal*, **3**(2), 50–
46 59.
- 47 Wöppelmann, G. and M. Marcos, 2016: Vertical land motion as a key to understanding sea level change and variability.
48 *Reviews of Geophysics*, **54**(1), 64–92, doi:[10.1002/2015rg000502](https://doi.org/10.1002/2015rg000502).
- 49 Worby, A.P. et al., 2008: Thickness distribution of Antarctic sea ice. *Journal of Geophysical Research*, **113**(C5),
50 C05S92, doi:[10.1029/2007jc004254](https://doi.org/10.1029/2007jc004254).
- 51 Wouters, B., A.S. Gardner, and G. Moholdt, 2019: Global Glacier Mass Loss During the GRACE Satellite Mission
52 (2002–2016). *Frontiers in Earth Science*, **7**, 96, doi:[10.3389/feart.2019.00096](https://doi.org/10.3389/feart.2019.00096).
- 53 Wu, B., X. Lin, and L. Yu, 2020: North Pacific subtropical mode water is controlled by the Atlantic Multidecadal
54 Variability. *Nature Climate Change*, **10**(3), 238–243, doi:[10.1038/s41558-020-0692-5](https://doi.org/10.1038/s41558-020-0692-5).
- 55 Wu, L. et al., 2012: Enhanced warming over the global subtropical western boundary currents. *Nature Climate Change*,
56 **2**(3), 161–166, doi:[10.1038/nclimate1353](https://doi.org/10.1038/nclimate1353).

- 1 Wu, W. et al., 2018: Mapping Dependence Between Extreme Rainfall and Storm Surge. *Journal of Geophysical*
2 *Research: Oceans*, **123(4)**, 2461–2474, doi:[10.1002/2017jc013472](https://doi.org/10.1002/2017jc013472).
- 3 Xiao, W., O. Esper, and R. Gersonde, 2016: Last Glacial - Holocene climate variability in the Atlantic sector of the
4 Southern Ocean. *Quaternary Science Reviews*, **135**, 115–137, doi:[10.1016/j.quascirev.2016.01.023](https://doi.org/10.1016/j.quascirev.2016.01.023).
- 5 Xiao, X. et al., 2017: Deglacial and Holocene sea-ice variability north of Iceland and response to ocean circulation
6 changes. *Earth and Planetary Science Letters*, **472**, 14–24, doi:[10.1016/j.epsl.2017.05.006](https://doi.org/10.1016/j.epsl.2017.05.006).
- 7 Xie, S., T.H. Dixon, D.M. Holland, D. Voytenko, and I. Vaňková, 2019: Rapid iceberg calving following removal of
8 tightly packed pro-glacial mélange. *Nature Communications*, **10(1)**, 3250, doi:[10.1038/s41467-019-10908-4](https://doi.org/10.1038/s41467-019-10908-4).
- 9 Xu, W., L. Ma, M. Ma, H. Zhang, and W. Yuan, 2017: Spatial-temporal variability of snow cover and depth in the
10 Qinghai-Tibetan plateau. *Journal of Climate*, **30**, 1521–1533, doi:[10.1175/jcli-d-15-0732.1](https://doi.org/10.1175/jcli-d-15-0732.1).
- 11 Yamaguchi, R. and T. Suga, 2019: Trend and Variability in Global Upper-Ocean Stratification Since the 1960s. *Journal*
12 *of Geophysical Research: Oceans*, **n/a(n/a)**, doi:[10.1029/2019jc015439](https://doi.org/10.1029/2019jc015439).
- 13 Yamamoto, A. et al., 2015: Global deep ocean oxygenation by enhanced ventilation in the Southern Ocean under long-
14 term global warming. *Global Biogeochemical Cycles*, **29(10)**, 1801–1815, doi:[10.1002/2015gb005181](https://doi.org/10.1002/2015gb005181).
- 15 Yan, Q., Z. Zhang, and H. Wang, 2016: Investigating uncertainty in the simulation of the Antarctic ice sheet during the
16 mid-Piacenzian. *Journal of Geophysical Research: Atmospheres*, **121(4)**, 1559–1574,
17 doi:[10.1002/2015jd023900](https://doi.org/10.1002/2015jd023900).
- 18 Yan, Q., Z. Zhang, H. Wang, and R. Zhang, 2014: Simulation of Greenland ice sheet during the mid-Pliocene warm
19 period. *Chinese science bulletin*, **59(2)**, 201–211.
- 20 Yan, X., R. Zhang, and T.R. Knutson, 2018: Underestimated AMOC Variability and Implications for AMV and
21 Predictability in CMIP Models. *Geophysical Research Letters*, **45(9)**, 4319–4328, doi:[10.1029/2018gl077378](https://doi.org/10.1029/2018gl077378).
- 22 Yang, H. et al., 2016a: Intensification and poleward shift of subtropical western boundary currents in a warming
23 climate. *Journal of Geophysical Research: Oceans*, **121(7)**, 4928–4945, doi:[10.1002/2015jc011513](https://doi.org/10.1002/2015jc011513).
- 24 Yang, H. et al., 2016b: Intensification and poleward shift of subtropical western boundary currents in a warming
25 climate. *Journal of Geophysical Research: Oceans*, **121(7)**, 4928–4945, doi:[10.1002/2015jc011513](https://doi.org/10.1002/2015jc011513).
- 26 Yang, H. et al., 2020: Poleward Shift of the Major Ocean Gyres Detected in a Warming Climate. *Geophysical Research*
27 *Letters*, **47(5)**, doi:[10.1029/2019gl085868](https://doi.org/10.1029/2019gl085868).
- 28 Yang, J.-A., S. Kim, N. Mori, and H. Mase, 2018: Assessment of long-term impact of storm surges around the Korean
29 Peninsula based on a large ensemble of climate projections. *Coastal Engineering*, **142**, 1–8,
30 doi:[10.1016/j.coastaleng.2018.09.008](https://doi.org/10.1016/j.coastaleng.2018.09.008).
- 31 Yao, Y., J. Wang, J. Yin, and X. Zou, 2020: Marine Heatwaves in China's Marginal Seas and Adjacent Offshore
32 Waters: Past, Present, and Future. *Journal of Geophysical Research: Oceans*, **125(3)**, e2019JC015801,
33 doi:[10.1029/2019jc015801](https://doi.org/10.1029/2019jc015801).
- 34 Yashayaev, I., 2007: Hydrographic changes in the Labrador Sea, 1960–2005. *Progress in Oceanography*, **73(3–4)**, 242–
35 276, doi:[10.1016/j.poccean.2007.04.015](https://doi.org/10.1016/j.poccean.2007.04.015).
- 36 Yashayaev, I. and J.W. Loder, 2016: Recurrent replenishment of Labrador Sea Water and associated decadal-scale
37 variability. *Journal of Geophysical Research: Oceans*, **121(11)**, 8095–8114, doi:[10.1002/2016jc012046](https://doi.org/10.1002/2016jc012046).
- 38 Yau, A.M., M.L. Bender, A. Robinson, and E.J. Brook, 2016: Reconstructing the last interglacial at Summit,
39 Greenland: Insights from GISP2. *Proceedings of the National Academy of Sciences*, **113(35)**, 9710–9715,
40 doi:[10.1073/pnas.1524766113](https://doi.org/10.1073/pnas.1524766113).
- 41 Yeager, S., 2015: Topographic Coupling of the Atlantic Overturning and Gyre Circulations. *Journal of Physical*
42 *Oceanography*, **45(5)**, 1258–1284, doi:[10.1175/jpo-d-14-0100.1](https://doi.org/10.1175/jpo-d-14-0100.1).
- 43 Yin, J., 2012: Century to multi-century sea level rise projections from CMIP5 models. *Geophysical Research Letters*,
44 **39(17)**, n/a–n/a, doi:[10.1029/2012gl052947](https://doi.org/10.1029/2012gl052947).
- 45 Yin, J. and R.J. Stouffer, 2007: Comparison of the Stability of the Atlantic Thermohaline Circulation in Two Coupled
46 Atmosphere–Ocean General Circulation Models. *Journal of Climate*, **20(17)**, 4293–4315,
47 doi:[10.1175/jcli4256.1](https://doi.org/10.1175/jcli4256.1).
- 48 Yokohata, T. et al., 2020: Model improvement and future projection of permafrost processes in a global land surface
49 model. *Progress in Earth and Planetary Science*, **7(1)**, 69, doi:[10.1186/s40645-020-00380-w](https://doi.org/10.1186/s40645-020-00380-w).
- 50 Young, I.R. and A. Ribal, 2019: Multiplatform evaluation of global trends in wind speed and wave height. *Science*,
51 **364(6440)**, 548–552, doi:[10.1126/science.aav9527](https://doi.org/10.1126/science.aav9527).
- 52 Young, N.E. and J.P. Briner, 2015: Holocene evolution of the western Greenland Ice Sheet: Assessing geophysical ice-
53 sheet models with geological reconstructions of ice-margin change. *Quaternary Science Reviews*, **114**, 1–17,
54 doi:[10.1016/j.quascirev.2015.01.018](https://doi.org/10.1016/j.quascirev.2015.01.018).

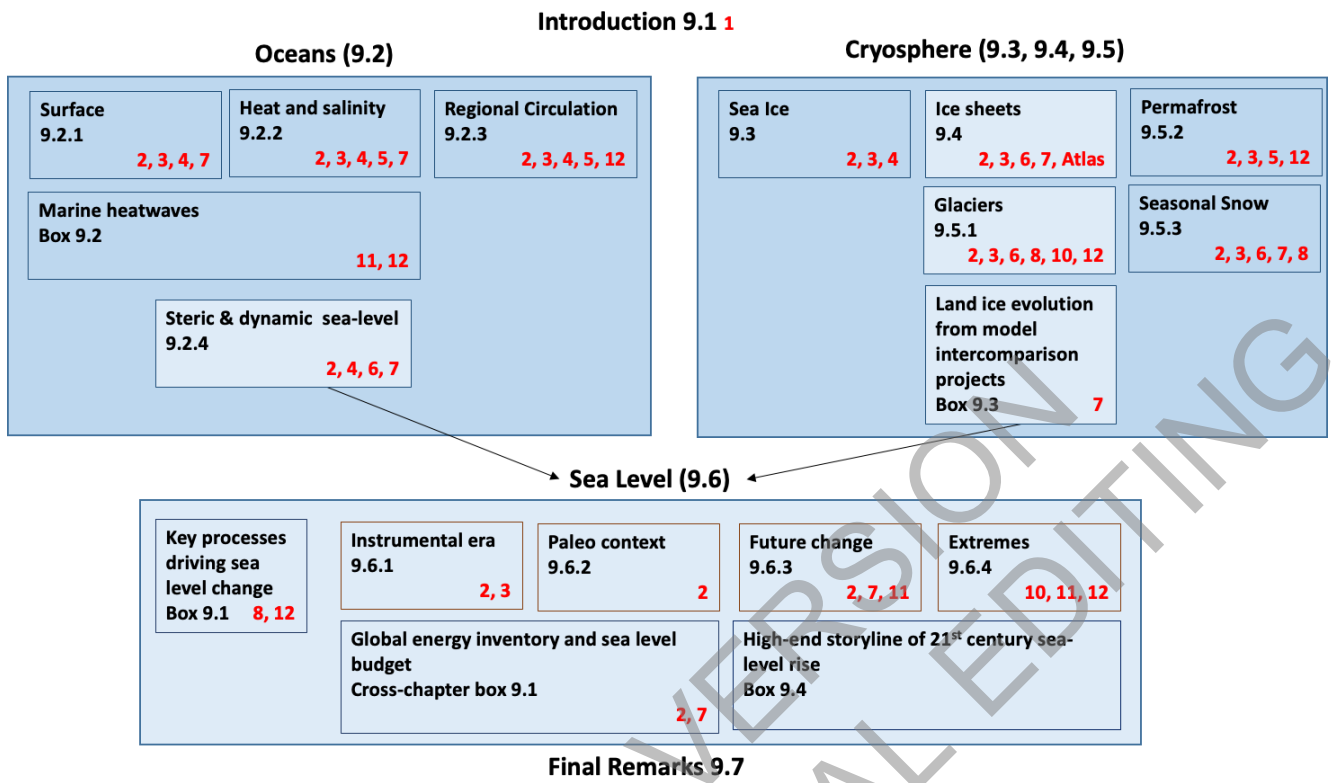
- 1 Yu, H., E. Rignot, H. Seroussi, M. Morlighem, and Y. Choi, 2019: Impact of Iceberg Calving on the Retreat of
2 Thwaites Glacier, West Antarctica Over the Next Century With Different Calving Laws and Ocean Thermal
3 Forcing. *Geophysical Research Letters*, **46(24)**, 14539–14547, doi:[10.1029/2019gl084066](https://doi.org/10.1029/2019gl084066).
- 4 Yu, L., 2019: Global Air-Sea Fluxes of Heat, Fresh Water, and Momentum: Energy Budget Closure and Unanswered
5 Questions. *Ann. Rev. Marine Sci.*, **11**, 227–248, doi:[10.1146/annurev-marine-010816](https://doi.org/10.1146/annurev-marine-010816).
- 6 Yu, L. et al., 2017: The global ocean water cycle in atmospheric reanalysis, satellite, and ocean salinity. *J. Climate*,
7 **30(10)**, 3829–3852, doi:[10.1175/jcli-d-16-0479.1](https://doi.org/10.1175/jcli-d-16-0479.1).
- 8 Yu, Y.Q., H.L. Liu, and P.F. Lin, 2012: A quasi-global 1/10° eddy-resolving ocean general circulation model and its
9 preliminary results. *Chinese Science Bulletin*, **57(30)**, 3908–3916, doi:[10.1007/s11434-012-5234-8](https://doi.org/10.1007/s11434-012-5234-8).
- 10 Yuan, N. et al., 2017: Increase of the Antarctic Sea Ice Extent is highly significant only in the Ross Sea. *Scientific*
11 *Reports*, **7**, 41096, doi:[10.1038/srep41096](https://doi.org/10.1038/srep41096).
- 12 Yukimoto, S. et al., 2019: The meteorological research institute Earth system model version 2.0, MRI-ESM2.0:
13 Description and basic evaluation of the physical component. *Journal of the Meteorological Society of Japan*,
14 **97(5)**, 931–965, doi:[10.2151/jmsj.2019-051](https://doi.org/10.2151/jmsj.2019-051).
- 15 Zängl, G., D. Reinert, P. Ripodas, and M. Baldauf, 2015: The ICON (ICOsahedral Non-hydrostatic) modelling
16 framework of DWD and MPI-M: Description of the non-hydrostatic dynamical core. *Quarterly Journal of the*
17 *Royal Meteorological Society*, **141(687)**, 563–579, doi:[10.1002/qj.2378](https://doi.org/10.1002/qj.2378).
- 18 Zanna, L., S. Khatiwala, J.M. Gregory, J. Ison, and P. Heimbach, 2019a: Global reconstruction of historical ocean heat
19 storage and transport. *Proceedings of the National Academy of Sciences*, **116(4)**, 201808838,
20 doi:[10.1073/pnas.1808838115](https://doi.org/10.1073/pnas.1808838115).
- 21 Zanna, L., S. Khatiwala, J.M. Gregory, J. Ison, and P. Heimbach, 2019b: Global reconstruction of historical ocean heat
22 storage and transport. *Proceedings of the National Academy of Sciences*, **116(4)**, 1126–1131,
23 doi:[10.1073/pnas.1808838115](https://doi.org/10.1073/pnas.1808838115).
- 24 Zanowski, H. and R. Hallberg, 2017: Weddell Polynya Transport Mechanisms in the Abyssal Ocean. *Journal of*
25 *Physical Oceanography*, **47(12)**, 2907–2925, doi:[10.1175/jpo-d-17-0091.1](https://doi.org/10.1175/jpo-d-17-0091.1).
- 26 Zanowski, H., R. Hallberg, and J.L. Sarmiento, 2015: Abyssal Ocean Warming and Salinification after Weddell
27 Polynyas in the GFDL CM2G Coupled Climate Model. *Journal of Physical Oceanography*, **45(11)**, 2755–
28 2772, doi:[10.1175/jpo-d-15-0109.1](https://doi.org/10.1175/jpo-d-15-0109.1).
- 29 Zarfl, C., A.E. Lumsdon, J. Berlekamp, L. Tydecks, and K. Tockner, 2015: A global boom in hydropower dam
30 construction. *Aquatic Sciences*, **77(1)**, 161–170.
- 31 Zekollari, H. and P. Huybrechts, 2015: On the climate-geometry imbalance, response time and volume-area scaling of
32 an alpine glacier: insights from a 3-D flow model applied to Vadret da Morteratsch, Switzerland. *Annals of*
33 *Glaciology*, **56(70)**, 51–62, doi:[10.3189/2015aog70a921](https://doi.org/10.3189/2015aog70a921).
- 34 Zekollari, H., M. Huss, and D. Farinotti, 2019: Modelling the future evolution of glaciers in the European Alps under
35 the EURO-CORDEX RCM ensemble. *The Cryosphere*, **13(4)**, 1125–1146, doi:[10.5194/tc-13-1125-2019](https://doi.org/10.5194/tc-13-1125-2019).
- 36 Zekollari, H., M. Huss, and D. Farinotti, 2020: On the Imbalance and Response Time of Glaciers in the European Alps.
37 *Geophysical Research Letters*, **47(2)**, e2019GL085578, doi:[10.1029/2019gl085578](https://doi.org/10.1029/2019gl085578).
- 38 Zemp, M. et al., 2015: Historically unprecedented global glacier decline in the early 21st century. *Journal of*
39 *Glaciology*, **61(228)**, 745–762, doi:[10.3189/2015jog15j017](https://doi.org/10.3189/2015jog15j017).
- 40 Zemp, M. et al., 2019: Global glacier mass changes and their contributions to sea-level rise from 1961 to 2016. *Nature*,
41 **568(7752)**, 382–386, doi:[10.1038/s41586-019-1071-0](https://doi.org/10.1038/s41586-019-1071-0).
- 42 Zemp, M. et al., 2020: Brief communication: Ad hoc estimation of glacier contributions to sea-level rise from the latest
43 glaciological observations. *The Cryosphere*, **14(3)**, 1043–1050, doi:[10.5194/tc-14-1043-2020](https://doi.org/10.5194/tc-14-1043-2020).
- 44 Zhai, F., D. Hu, Q. Wang, and F. Wang, 2014: Long-term trend of Pacific South Equatorial Current bifurcation over
45 1950–2010. *Geophysical Research Letters*, **41(9)**, 3172–3180, doi:[10.1002/2014gl059934](https://doi.org/10.1002/2014gl059934).
- 46 Zhang, B. et al., 2019: Geodetic and model data reveal different spatio-temporal patterns of transient mass changes over
47 Greenland from 2007 to 2017. *Earth and Planetary Science Letters*, **515**, 154–163,
48 doi:[10.1016/j.epsl.2019.03.028](https://doi.org/10.1016/j.epsl.2019.03.028).
- 49 Zhang, J., 2014: Modeling the impact of wind intensification on Antarctic sea ice volume. *Journal of Climate*, **27(1)**,
50 202–214, doi:[10.1175/jcli-d-12-00139.1](https://doi.org/10.1175/jcli-d-12-00139.1).
- 51 Zhang, L., T.L. Delworth, W. Cooke, and X. Yang, 2019a: Natural variability of Southern Ocean convection as a driver
52 of observed climate trends. *Nature Climate Change*, **9(1)**, 59–65, doi:[10.1038/s41558-018-0350-3](https://doi.org/10.1038/s41558-018-0350-3).
- 53 Zhang, L., T.L. Delworth, W. Cooke, and X. Yang, 2019b: Natural variability of Southern Ocean convection as a driver
54 of observed climate trends. *Nature Climate Change*, **9(1)**, 59–65, doi:[10.1038/s41558-018-0350-3](https://doi.org/10.1038/s41558-018-0350-3).

- 1 Zhang, R., 2015: Mechanisms for low-frequency variability of summer Arctic sea ice extent. *Proceedings of the*
2 *National Academy of Sciences of the United States of America*, **112**(15), 4570–4575,
3 doi:[10.1073/pnas.1422296112](https://doi.org/10.1073/pnas.1422296112).
- 4 Zhang, R. et al., 2019: A Review of the Role of the Atlantic Meridional Overturning Circulation in Atlantic
5 Multidecadal Variability and Associated Climate Impacts. *Reviews of Geophysics*, **57**(2), 316–375,
6 doi:[10.1029/2019rg000644](https://doi.org/10.1029/2019rg000644).
- 7 Zhang, T., J.A. Heginbottom, R.G. Barry, and J. Brown, 2000: Further statistics on the distribution of permafrost and
8 ground ice in the Northern Hemisphere. *Polar Geography*, **24**(2), 126–131, doi:[10.1080/10889370009377692](https://doi.org/10.1080/10889370009377692).
- 9 Zhang, T., R.G. Barry, K. Knowles, J.A. Heginbottom, and J. Brown, 1999: Statistics and characteristics of permafrost
10 and ground-ice distribution in the Northern Hemisphere. *Polar Geography*, **23**(2), 132–154,
11 doi:[10.1080/10889379909377670](https://doi.org/10.1080/10889379909377670).
- 12 Zhang, Y. and A.M. Baptista, 2008: SELFE: A semi-implicit Eulerian–Lagrangian finite-element model for cross-scale
13 ocean circulation. *Ocean Modelling*, **21**(3–4), 71–96, doi:[10.1016/j.ocemod.2007.11.005](https://doi.org/10.1016/j.ocemod.2007.11.005).
- 14 Zhang, Y., H. Renssen, H. Seppä, and P.J. Valdes, 2017: Holocene temperature evolution in the Northern Hemisphere
15 high latitudes – Model-data comparisons. *Quaternary Science Reviews*, **173**, 101–113,
16 doi:[10.1016/j.quascirev.2017.07.018](https://doi.org/10.1016/j.quascirev.2017.07.018).
- 17 Zhang, Y., Z. Zhang, D. Chen, B. Qiu, and W. Wang, 2020: Strengthening of the Kuroshio current by intensifying
18 tropical cyclones. *Science*, **368**(6494), 988–993, doi:[10.1126/science.aax5758](https://doi.org/10.1126/science.aax5758).
- 19 Zhang, Y. et al., 2016: Studies of the Canadian Arctic Archipelago water transport and its relationship to basin-local
20 forcings: Results from AO-FVCOM. *Journal of Geophysical Research: Oceans*, **121**(6), 4392–4415,
21 doi:[10.1002/2016jc011634](https://doi.org/10.1002/2016jc011634).
- 22 Zhang, Y.J., F. Ye, E. Stanev, and S. Grashorn, 2016: Seamless cross-scale modeling with SCHISM. *Ocean Modelling*,
23 **102**, 64–81, doi:[10.1016/j.ocemod.2016.05.002](https://doi.org/10.1016/j.ocemod.2016.05.002).
- 24 Zhang, Z. et al., 2016: Observed 3D Structure, Generation, and Dissipation of Oceanic Mesoscale Eddies in the South
25 China Sea. *Scientific Reports*, **6**, doi:[10.1038/srep24349](https://doi.org/10.1038/srep24349).
- 26 Zhao, S., S. Zhang, W. Cheng, and C. Zhou, 2019: Model Simulation and Prediction of Decadal Mountain Permafrost
27 Distribution Based on Remote Sensing Data in the Qilian Mountains from the 1990s to the 2040s. *Remote*
28 *Sensing*, **11**(2), 183, doi:[10.3390/rs11020183](https://doi.org/10.3390/rs11020183).
- 29 Zheng, W. et al., 2018: Accelerating glacier mass loss on Franz Josef Land, Russian Arctic. *Remote Sensing of*
30 *Environment*, **211**, 357–375, doi:[10.1016/j.rse.2018.04.004](https://doi.org/10.1016/j.rse.2018.04.004).
- 31 Zhong, H., P.-J. van Overloop, and P.H.A.J.M. van Gelder, 2013: A joint probability approach using a 1-D
32 hydrodynamic model for estimating high water level frequencies in the Lower Rhine Delta. *Natural Hazards*
33 *and Earth System Sciences*, **13**(7), 1841–1852, doi:[10.5194/nhess-13-1841-2013](https://doi.org/10.5194/nhess-13-1841-2013).
- 34 Zhong, X. et al., 2018: Spatiotemporal variability of snow depth across the Eurasian continent from 1966 to 2012.
35 *Cryosphere*, **12**, 227–245, doi:[10.5194/tc-12-227-2018](https://doi.org/10.5194/tc-12-227-2018).
- 36 Zhu, D. et al., 2019: Controls of soil organic matter on permafrost thermal and carbon dynamics. *Nature*
37 *Communications*, **10**, 3172.
- 38 Zhu, Y., R.-H. Zhang, D. Li, and D. Chen, 2020: The thermocline biases in the tropical North Pacific and their
39 attributions. *Journal of Climate*, **34**(5), 1–17, doi:[10.1175/jcli-d-20-0675.1](https://doi.org/10.1175/jcli-d-20-0675.1).
- 40 Zickfeld, K., V.K. Arora, and N.P. Gillett, 2012: Is the climate response to CO₂ emissions path
41 dependent? *Geophysical Research Letters*, **39**(5), n/a–n/a, doi:[10.1029/2011gl050205](https://doi.org/10.1029/2011gl050205).
- 42 Zickfeld, K., S. Solomon, and D.M. Gilford, 2017: Centuries of thermal sea-level rise due to anthropogenic emissions
43 of short-lived greenhouse gases. *Proceedings of the National Academy of Sciences*, **114**(4), 657–662,
44 doi:[10.1073/pnas.1612066114](https://doi.org/10.1073/pnas.1612066114).
- 45 Zika, J.D., J.M. Gregory, E.L. McDonagh, A. Marzocchi, and L. Clement, 2021: Recent water mass changes reveal
46 mechanisms of ocean warming. *Journal of Climate*, 1–52, doi:[10.1175/jcli-d-20-0355.1](https://doi.org/10.1175/jcli-d-20-0355.1).
- 47 Zika, J.D. et al., 2018: Improved estimates of water cycle change from ocean salinity: the key role of ocean warming.
48 *Environmental Research Letters*, **13**(7), 74036, doi:[10.1088/1748-9326/aace42](https://doi.org/10.1088/1748-9326/aace42).
- 49 Zunz, V., H. Goosse, and F. Massonnet, 2013: How does internal variability influence the ability of CMIP5 models to
50 reproduce the recent trend in Southern Ocean sea ice extent? *The Cryosphere*, **7**(2), 451–468, doi:[10.5194/tc-7-](https://doi.org/10.5194/tc-7-451-2013)
51 [451-2013](https://doi.org/10.5194/tc-7-451-2013).
- 52

1 **Figures**

2

3



4

5

6 **Figure 9.1:** Visual guide to chapter 9 with relevant chapter numbers indicated in red.

7

8

9

10

11

12

13

14

15

16

17

18

19

20

21

22

23

24

25

26

27

28

29

30

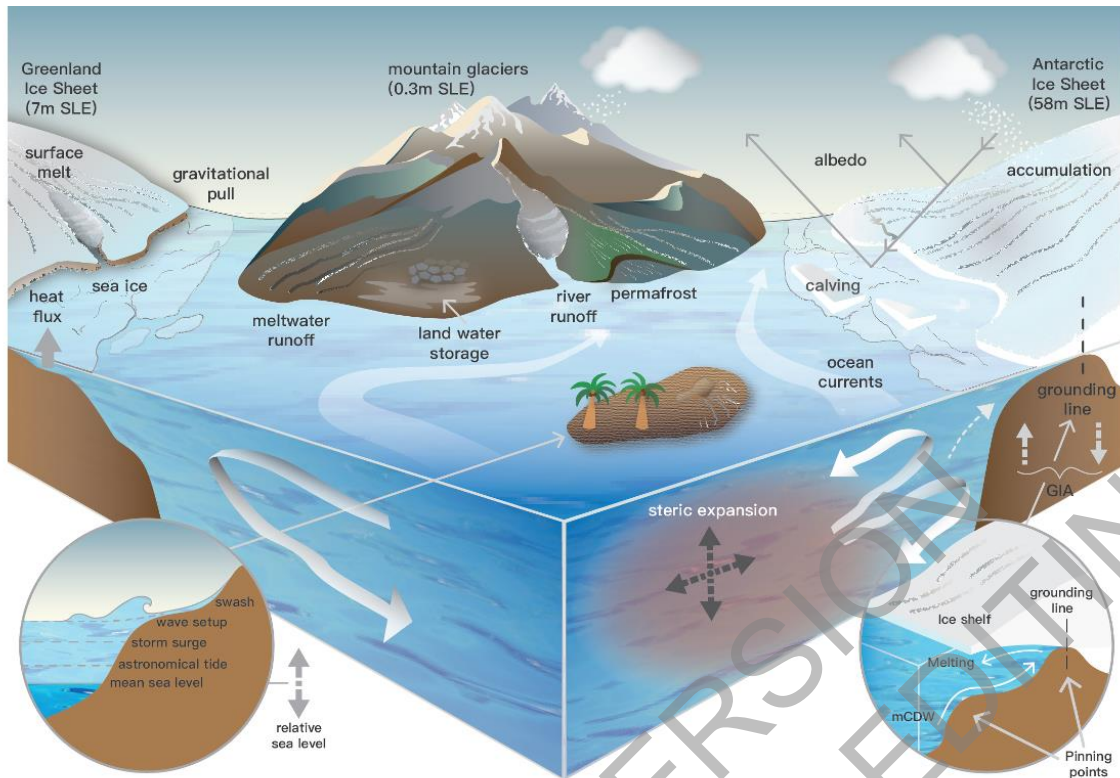
31

32

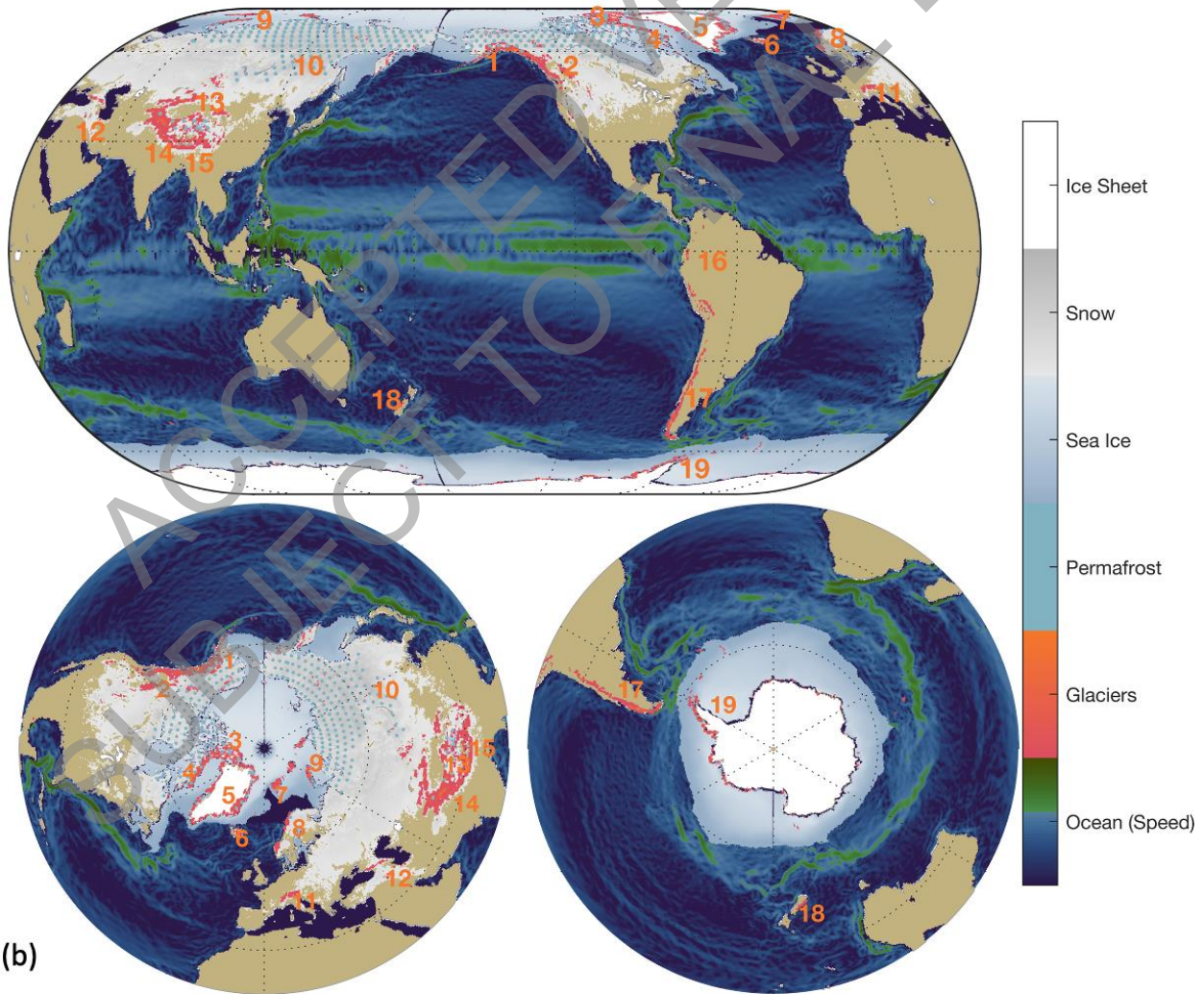
33

1
2
3

ACCEPTED VERSION
SUBJECT TO FINAL EDITING



(a)



(b)

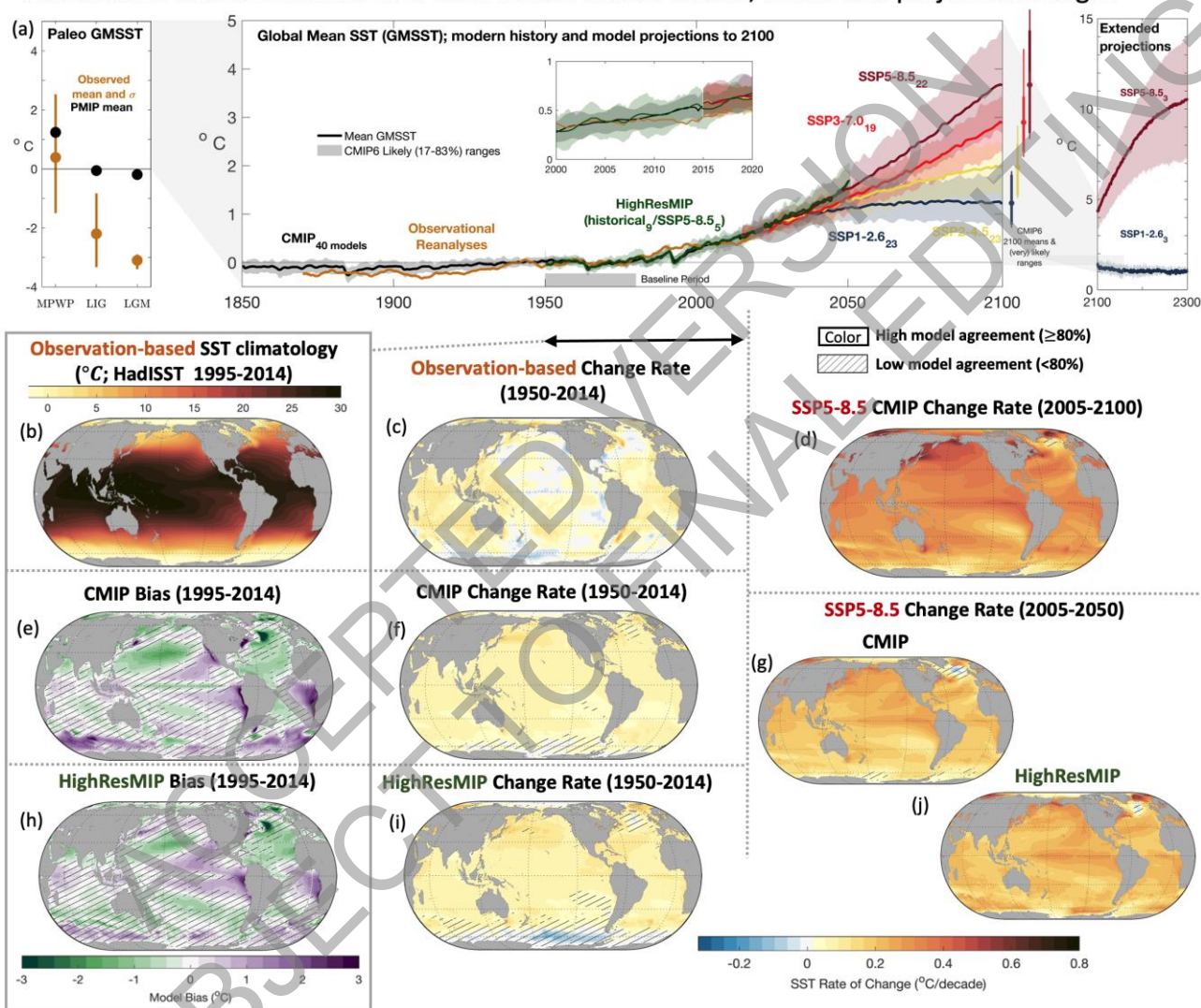
1
2

1 **Figure 9.2: Components of ocean, cryosphere and sea level assessed in this chapter.** (a) Schematic of processes
2 (mCDW=modified Circumpolar Deep Water, GIA=Glacial Isostatic Adjustment). White arrows indicate
3 ocean circulation. Pinning points indicate where the grounding line is most stable and ice sheet retreat
4 will slow. (b) Geographic distribution of ocean and cryosphere components (numbers indicate (RGI
5 Consortium, 2017) glacierized regions, see Figures 9.20 and 9.21 for labels). Sea ice shaded to indicate
6 the annual mean concentration. Green ocean colours indicate larger surface current speed. Further details
7 on data sources and processing are available in the chapter data table (Table 9.SM.9).
8

ACCEPTED VERSION
SUBJECT TO FINAL EDITING

Sea Surface Temperature (SST) Anomalies and Maps

Observation-based estimates and CMIP6 multi-model means, biases and projected changes



1
2

1 **Figure 9.3: Sea Surface Temperature (SST) and its changes with time.** (a) Time series of global mean SST anomaly relative to 1950-1980 climatology. Shown are
2 observational reanalyses (HadISST) and multi-model means from the CMIP historical, CMIP projections, and HighResMIP experiment. (b) Map of observed SST
3 (1995-2014 climatology HadISST), (e) bias of CMIP and (h) bias of HighResMIP (bottom left) over 1995-2014. Also shown are 1950-2014 c) historical SST changes
4 from observations, (f) CMIP and (i) HighResMIP, and (d) 2005-2100 SST change rate, (g) 2005-2050 change rate for SSP5-8.5 for the CMIP ensemble, and (j) 2005-
5 2050 change rate for SSP5-8.5 for the HighResMIP ensemble. No overlay indicates regions with high model agreement, where $\geq 80\%$ of models agree on sign of
6 change; diagonal lines indicate regions with low model agreement, where $< 80\%$ of models agree on sign of change (see Cross-Chapter Box Atlas.1 for more
7 information). Further details on data sources and processing are available in the chapter data table (Table 9.SM.9).
8

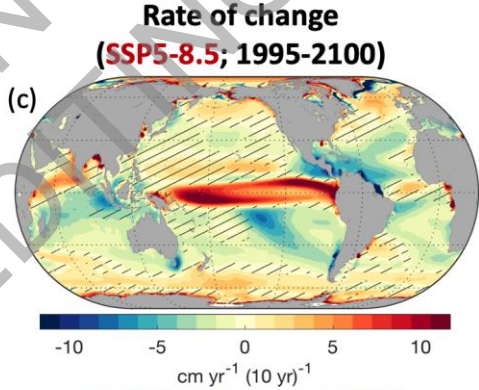
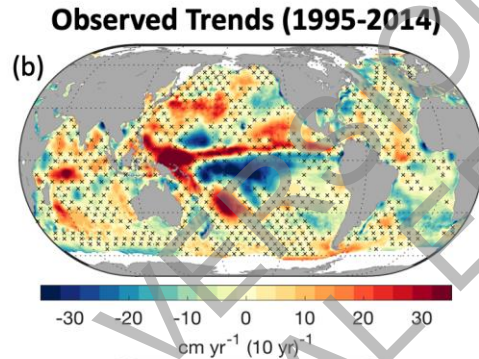
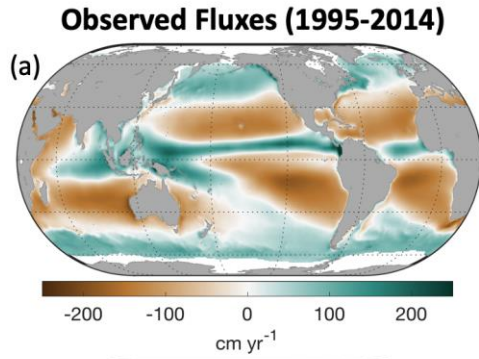
1

Surface fluxes of freshwater, heat, and momentum (wind stress)

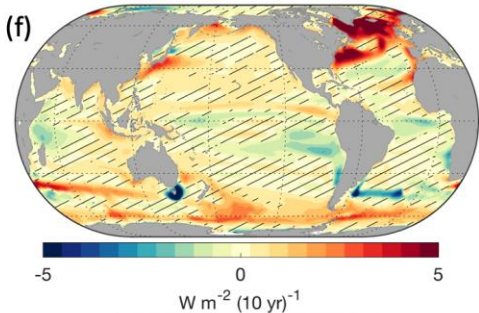
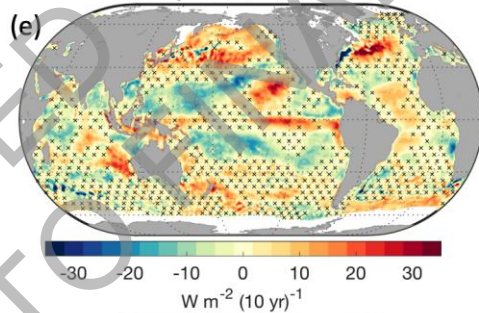
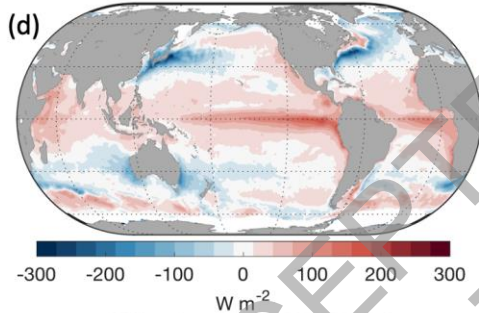
Observed fluxes and trends, and projected rates of change in SSP5-8.5

Color Significant/High model agreement ($\geq 80\%$)
Diagonal lines Low model agreement ($< 80\%$)
XXXX Non-significant (observations)

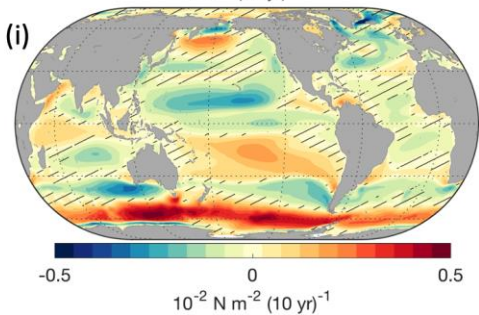
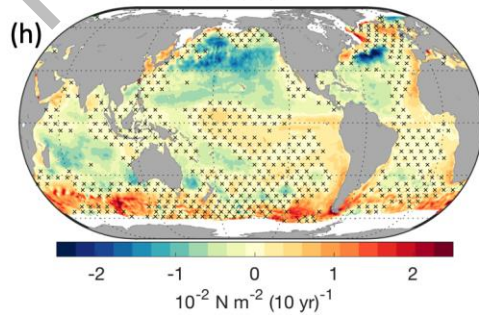
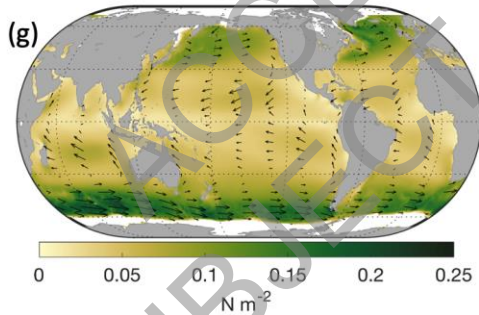
Freshwater Flux
 17 CMIP models



Net Heat Flux
 22 CMIP models



Wind Stress
 11 CMIP models



2
3

1 **Figure 9.4: Global maps of observed mean fluxes (a, d, g), the observed trends in these fluxes (b, e, h) and the projected rate of change in these fluxes from SSP5-8.5 (c, f,**
2 **i).** Shown are the freshwater flux (a, b, c), net heat flux (d, e, f), and momentum flux or wind stress magnitude (g, h, i), with positive numbers indicating ocean
3 freshening, warming, and accelerating respectively. The means and observed trends are calculated between 1995-2014 (freshwater and wind stress) or 2001-2014
4 (heat) and the SSP5-8.5 projected rates are between 1995-2100 using 20-year averages at each end of the time period. Observations show objective interpolation from
5 CERES EBAF v4 (Kato et al., 2018), OAFflux-HR (Yu, 2019), and GPCP (Adler et al., 2003) of fluxes and flux trends. (b, e, h) Observed trends with no overlay
6 indicates regions where the trends are significant at $p = 0.34$ level. Crosses indicate regions where trends are not significant. For (c, f, i) projections, no overlay
7 indicates regions with high model agreement, where $\geq 80\%$ of models agree on the sign of change; diagonal lines indicate regions with low model agreement, where
8 $< 80\%$ of models agree on the sign of change (see Cross-Chapter Box Atlas.1 for more information). Further details on data sources and processing are available in the
9 chapter data table (Table 9.SM.9).

Ocean Mixed Layer Depth (MLD) in Winter and Summer

Observed MLD, model MLD biases, and projected changes in MLD

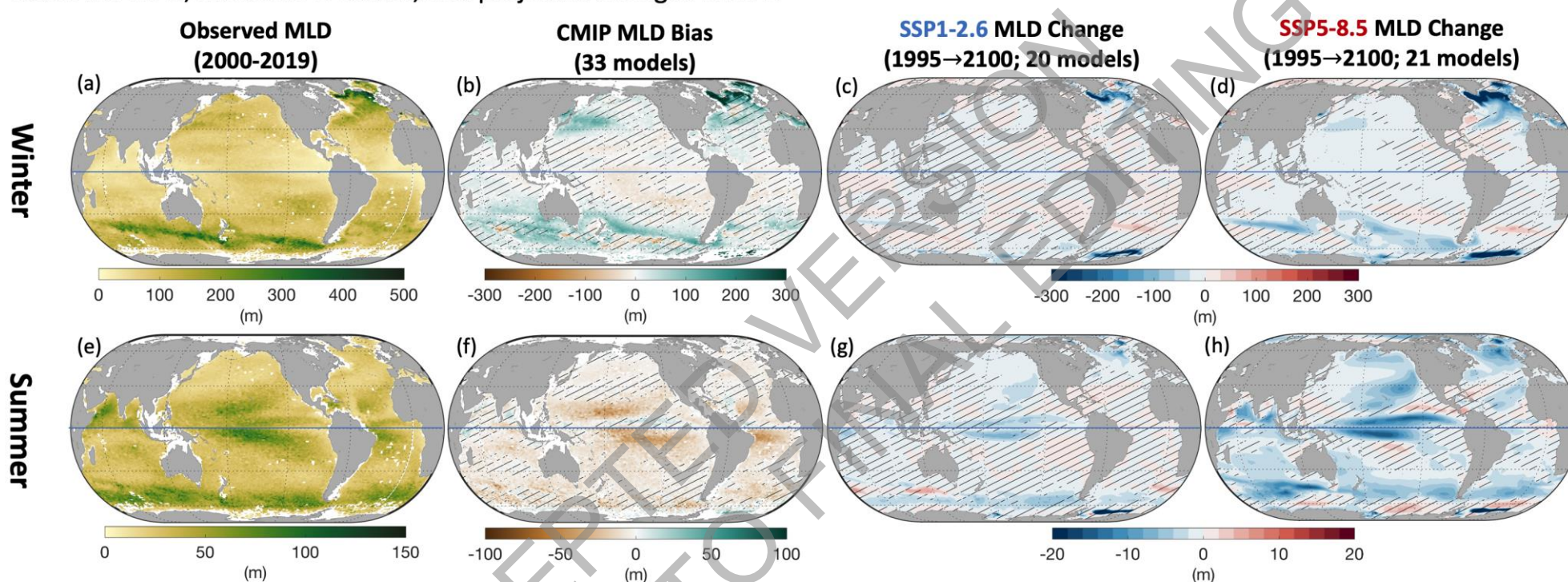
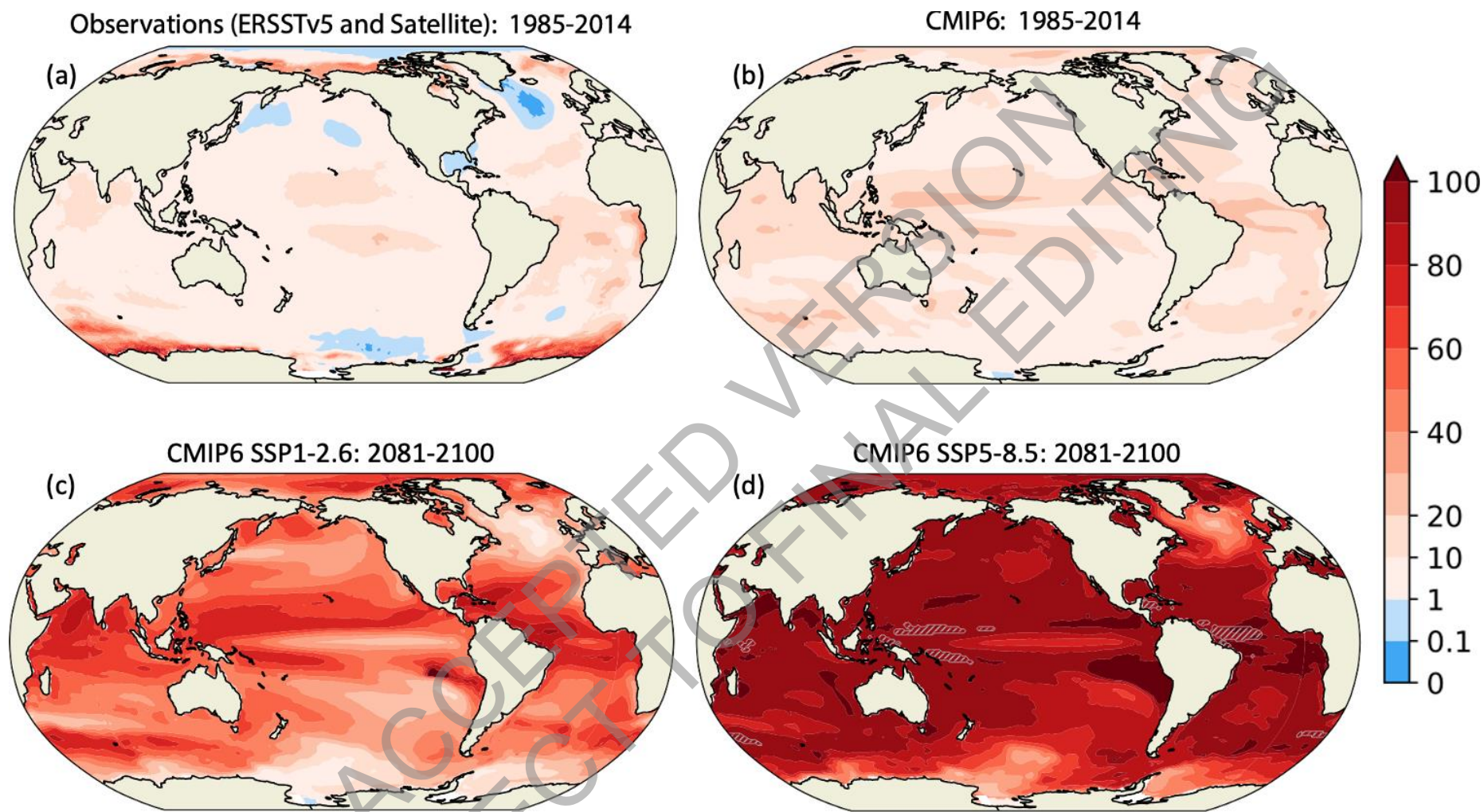


Figure 9.5: Mixed layer depth in (a-d) winter and (e-h) summer. (a, e) Observed climatological mean mixed layer depth (based on density threshold) from the Argo Mixed Layer Depth (Holte et al., 2017) from observations 2000–2019. (b, f) Bias between the observation-based estimate (2000–2019) and the 1995–2014 CMIP6 climatological mean mixed layer depth. (c, d, g, h) Projected MLD change from 1995–2014 to 2081–2100 under (c, g) SSP1-2.6 and (d, h) SSP5-8.5 scenarios. The (a, b, c, d) Winter row shows DJF in the Northern Hemisphere and JJA in the Southern Hemisphere, and the (e, f, g, h) Summer row shows JJA in the Northern Hemisphere and DJF in the Southern Hemisphere. The mixed layer depth is the depth where the potential density is 0.03 kg m^{-3} denser than at 10m. No overlay indicates regions with high model agreement, where $\geq 80\%$ of models agree on the sign of change; diagonal lines indicate regions with low model agreement, where $< 80\%$ of models agree on the sign of change (see Cross-Chapter Box Atlas.1 for more information). Further details on data sources and processing are available in the chapter data table (Table 9.SM.9).

1

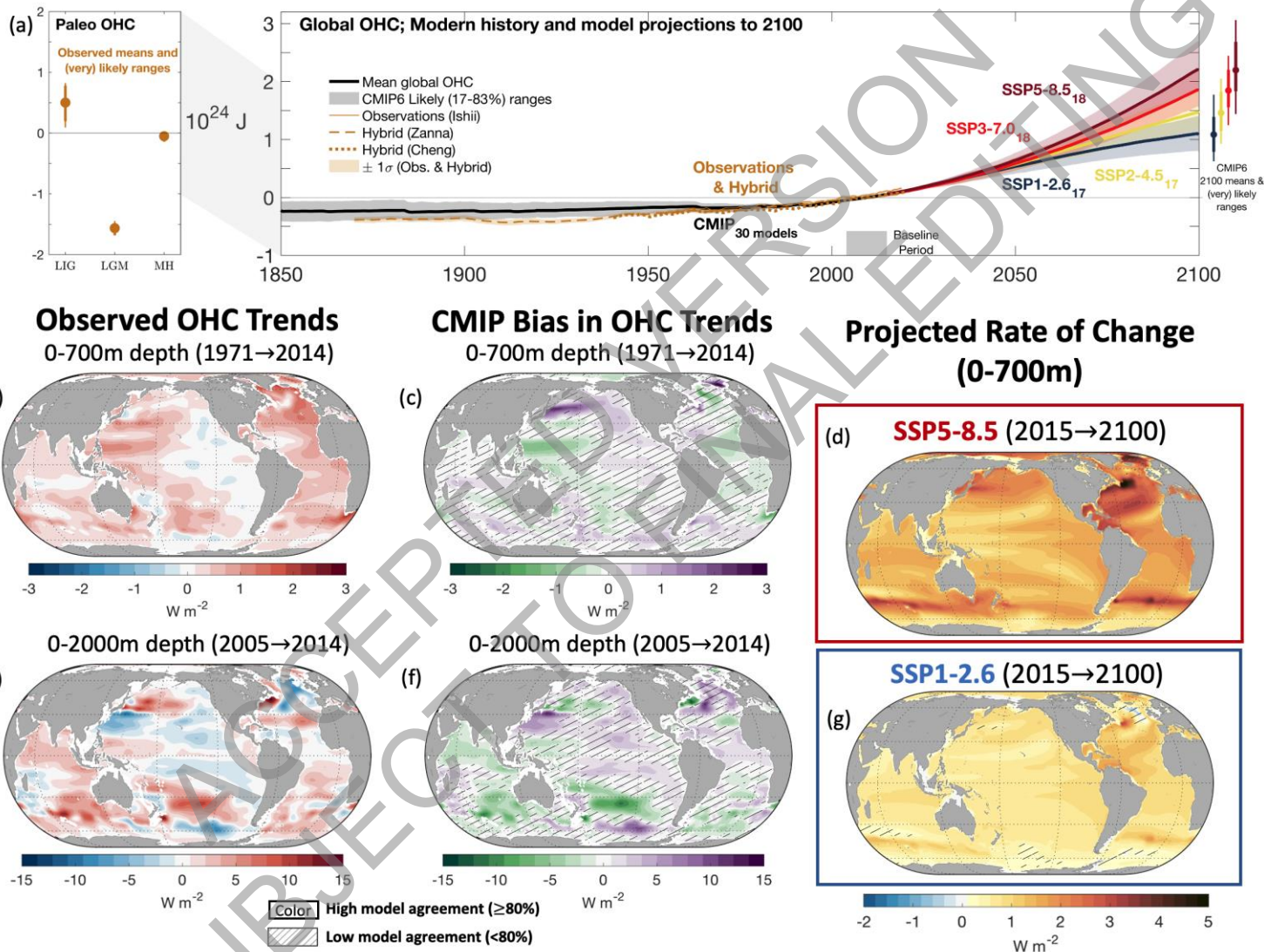
2
3
4
5
6
7

Box 9.2, Figure 1: Observed and simulated regional probability ratio of marine heatwaves (MHWs) for the 1985-2014 period and for the end of the 21st century under two different greenhouse gas emissions scenarios. The probability ratio is the proportion by which the number of MHW days per year has increased relative to preindustrial times. A MHW is defined as a deviation beyond the daily 99th percentile (11-day window) in the deseasonalized sea surface temperature. (a) The MHW probability ratio from satellite observations (NOAA OISST V2.1; Huang et al. 2020) during 1985-2014. The mean warming pattern (difference in ERSST5

1 (Huang et al. 2017) sea surface temperature between the 1985-2014 and 1854-1900 periods) has been added to the satellite observations to calculate the
2 probability ratio. (b-d) CMIP6 simulated multi-model mean probability ratio of the (b) 1985-2014 period, and 2081-2100 period in the (c) SSP1 2.6 and (d) SSP5
3 8.5 scenarios. The areas with grey diagonal lines in (d) indicate permanent MHWs (> 360 heatwave days per year). These 14 CMIP6 models are included in the
4 analysis: ACCESS-CM2, CESM2, CESM2-WACCM, CMCCCM2-SR5, CNRM-CM6-1, CNRM-ESM2-1, CanESM5, EC-Earth3, IPSL-CM6A-LR, MIROC6,
5 MRI-ESM2-0, NESM3, NorESM2-LM, NorESM2-MM. Further details on data sources and processing are available in the chapter data table (Table 9.SM.9).
6
7
8
9
10
11
12
13
14
15
16
17
18

Ocean Heat Content (OHC) Anomalies and Maps

Observation-based estimates and CMIP6 multi-model means, biases and projected changes

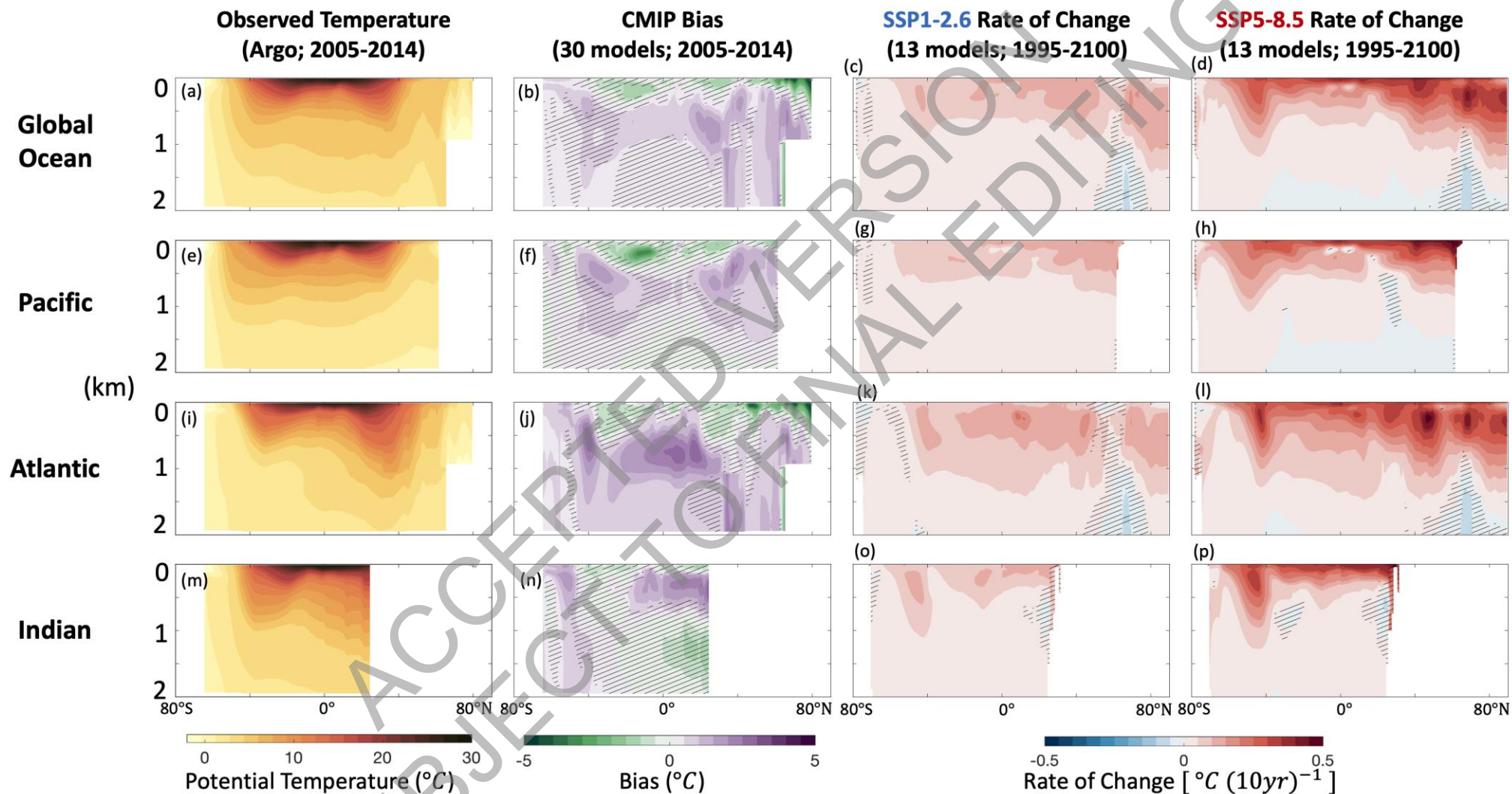


1 **Figure 9.6: Ocean heat content (OHC) and its changes with time.** (a) Time series of global ocean heat content anomaly relative to a 2005-2014 climatology in the upper 2000m
2 of the ocean. Shown are observations (Ishii et al., 2017; Baggenstos et al., 2019; Shackleton et al., 2020), model-observation hybrids (Cheng et al., 2019; Zanna et al.,
3 2019), and multi-model means from the CMIP6 historical (29 models) and SSP scenarios (label subscripts indicate number of models per SSP). (b-g) Maps of Ocean
4 Heat Content across different time periods, in different layers, and from different data sets/experiments. Maps show the CMIP6 ensemble bias and observed (Ishii et
5 al., 2017) trends of OHC for (b, c) 0-700m for the period 1971-2014, and (e, f) 0-2000m for the period 2005-2017. CMIP6 ensemble mean maps show projected rate of
6 change 2015-2100 for (d) SSP5-8.5 and (g) SSP1-2.6 scenarios. Also shown are the projected change in 0-700m OHC for (d) SSP1-2.6 and (g) SSP5-8.5 in the CMIP6
7 ensembles, for the period 2091-2100 versus 2005-2014. No overlay indicates regions with high model agreement, where $\geq 80\%$ of models agree on the sign of change;
8 diagonal lines indicate regions with low model agreement, where $< 80\%$ of models agree on the sign of change (see Cross-Chapter Box Atlas.1 for more information).
9 Further details on data sources and processing are available in the chapter data table (Table 9.SM.9).

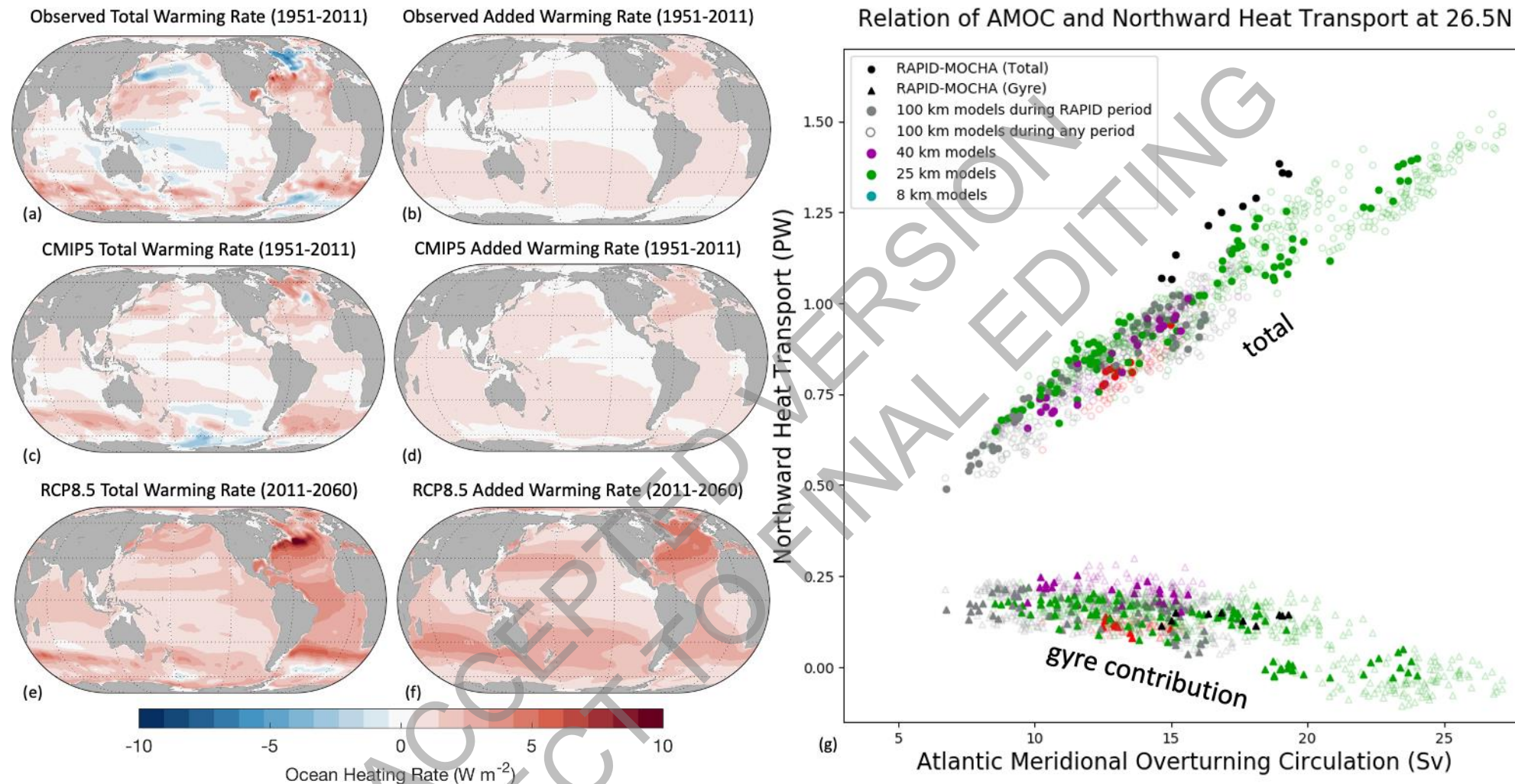
Zonal-mean potential temperature as a function of depth and latitude

Observed mean, CMIP6 biases, and projected rates of change, for each ocean basin

Color High model agreement ($\geq 80\%$)
 Hatched Low model agreement ($< 80\%$)



1 **Figure 9.7: Meridional-depth profiles of zonal-mean potential temperature in the ocean and its rate of change in the upper 2000m of the Global, Pacific, Atlantic, and**
2 **Indian Oceans.** Shown are (a, e, i, m) observed temperature (Argo climatology 2005-2014), (b, f, j, n) bias of the CMIP6 ensemble over this period, and future
3 changes under (c, g, k, o) SSP1-2.6 and (d, h, l, p) SSP5-8.5. No overlay indicates regions with high model agreement, where $\geq 80\%$ of models agree on the sign of
4 change; diagonal lines indicate regions with low model agreement, where $< 80\%$ of models agree on the sign of change (see Cross-Chapter Box Atlas.1 for more
5 information). Further details on data sources and processing are available in the chapter data table (Table 9.SM.9).
6
7
8
9
10
11
12
13
14
15
16
17
18
19
20
21
22
23
24
25
26
27
28
29
30

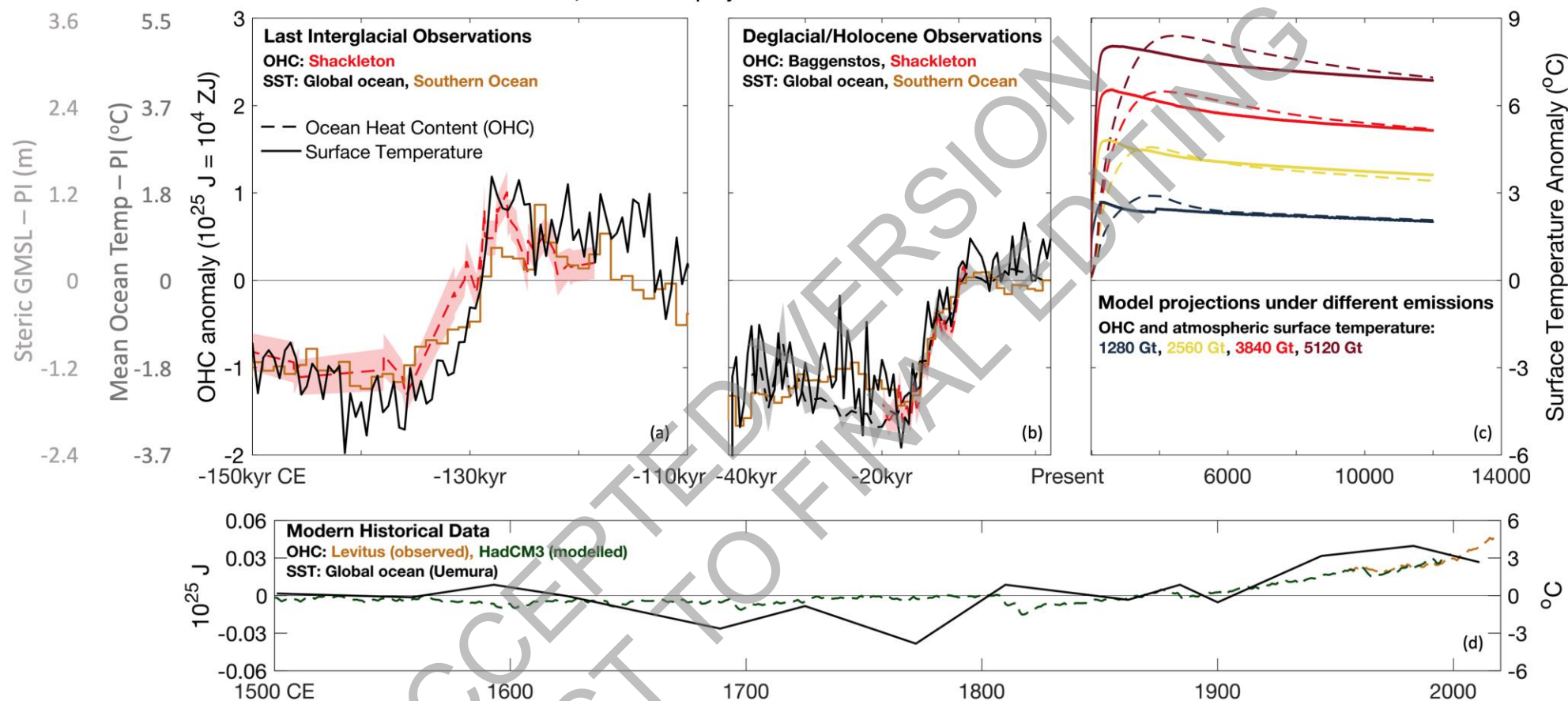


1

2 **Figure 9.8: Decomposition of ocean simulated ocean heat content and northward heat transport.** (a, c, e) Total ocean heat content (0-2000 m) warming rate as observed and
 3 simulated by CMIP5 models over the historical period (1951-2011) and under the RCP8.5 future (2011-2060) versus the associated decomposed (b, d, f) added heat
 4 contribution (neglecting changes in ocean circulation) to the total (Bronselaer and Zanna, 2020). (g) Relationship between northward heat transport and Atlantic
 5 Meridional Overturning Circulation in HighResMIP models (1950-2050) and observations during the RAPID period (2004-2018). Further details on data sources and
 6 processing are available in the chapter data table (Table 9.SM.9).

Long-term trends of ocean heat content and surface temperature

Observed and modelled historical data, and model projections under different emissions scenarios



1

2 **Figure 9.9: Long-term trends of ocean heat content and surface temperature.** (a, b) Ice-core rare gas estimates of past mean ocean heat content OHC (ZJ), scaled to global
 3 mean ocean temperature (°C), and to steric GMSL (m) per CCB-2 (red dashed line), compared to surface temperatures (black solid line, gold solid line; °C rightmost
 4 axis). Southern Ocean SST from multiple proxies in 11 sediment cores and from ice core deuterium excess (Uemura et al., 2018). a) Penultimate glacial interval to last
 5 interglacial, 150,000-100,000 yr B2K (Shackleton et al., 2020). b) Last glacial interval to modern interglacial, 40,000-0 yr B2K (Baggenstos et al., 2019; Shackleton et
 6 al., 2019). Changes in OHC (dashed lines) track changes in Southern Ocean SST (solid lines). c) Long-term projected (2000 to 12000 CE) changes of OHC (dashed

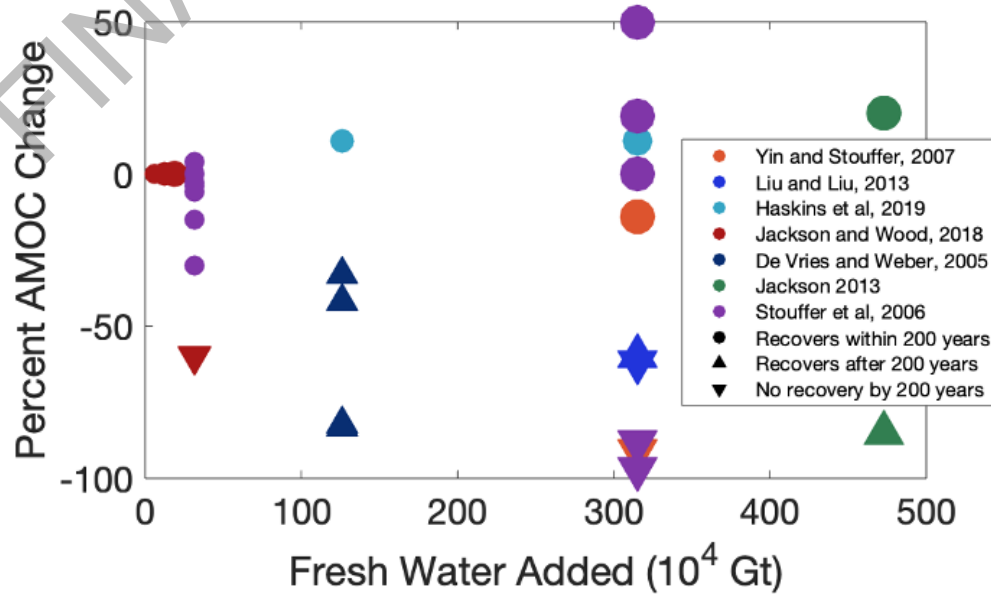
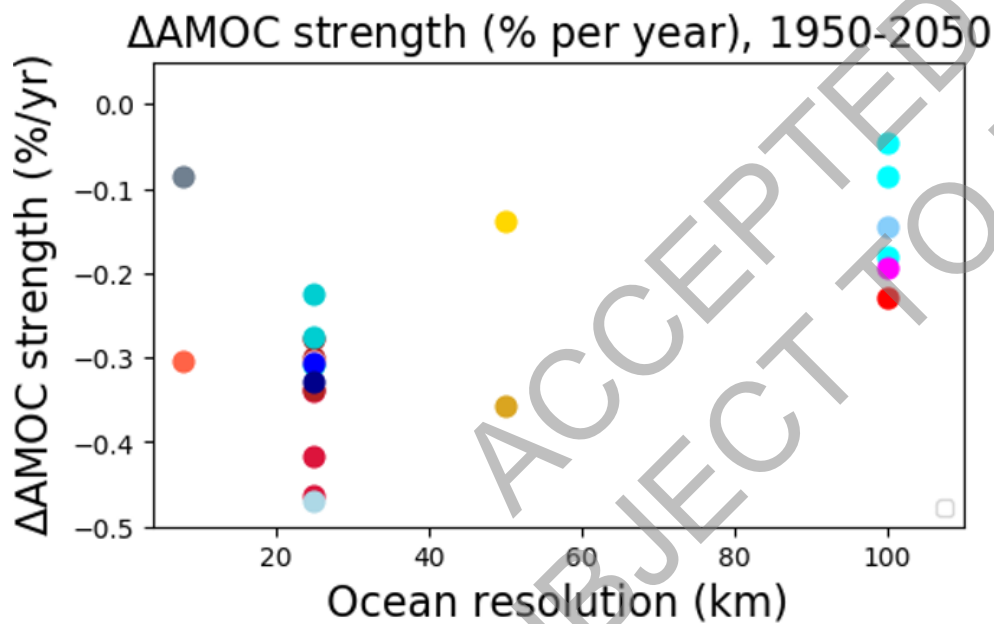
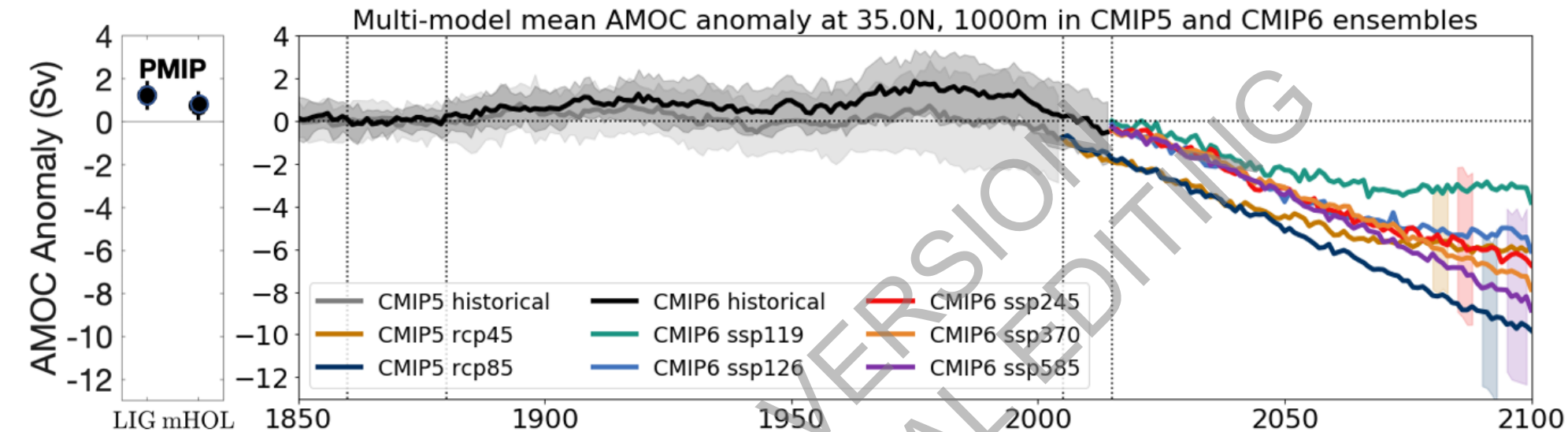
Do Not Cite, Quote or Distribute

9-218

Total pages: 257

1 lines) in response to four greenhouse gas emissions scenarios (Clark et al., 2016) scale similarly to large-scale paleo changes but lag projected global mean SST (solid
2 lines). d) model simulated 1500-1999 OHC (Gregory et al., 2006) and 1955-2019 observations (Levitus et al., 2012) updated by NOAA NODC. All data expressed as
3 anomalies relative to preindustrial time. Further details on data sources and processing are available in the chapter data table (Table 9.SM.9).
4

5
6
7
8
9
10
11
12
13
14
15
16
17



1

1 **Figure 9.10: AMOC strength in simulations and sensitivity to resolution and forcing.** (Top left) AMOC magnitude in PMIP experiments. (Top right) Time series of AMOC
2 from CMIP5 and CMIP6 based on (Menary et al., 2020). (Bottom left) Percent change in AMOC strength per year at different resolutions over the 1950-2050 period
3 with colours for model families (Roberts et al., 2020). (Bottom right) A compilation (Jackson and Wood, 2018) of percentage changes in the simulated AMOC after
4 applying an additional freshwater flux in the subpolar North Atlantic at the surface for a limited time (de Vries and Weber, 2005; Stouffer et al., 2006; Yin and
5 Stouffer, 2007; Jackson, 2013; Liu and Liu, 2013; Jackson and Wood, 2018; Haskins et al., 2019). Symbols indicate whether the AMOC recovers within 200 years
6 (circles), is starting to recover (upwards arrow) or does not recover within 200 years (downwards arrow). Symbol size indicates rate of freshwater input. Further details
7 on data sources and processing are available in the chapter data table (Table 9.SM.9).
8
9
10
11
12
13
14
15
16
17
18
19
20
21
22
23

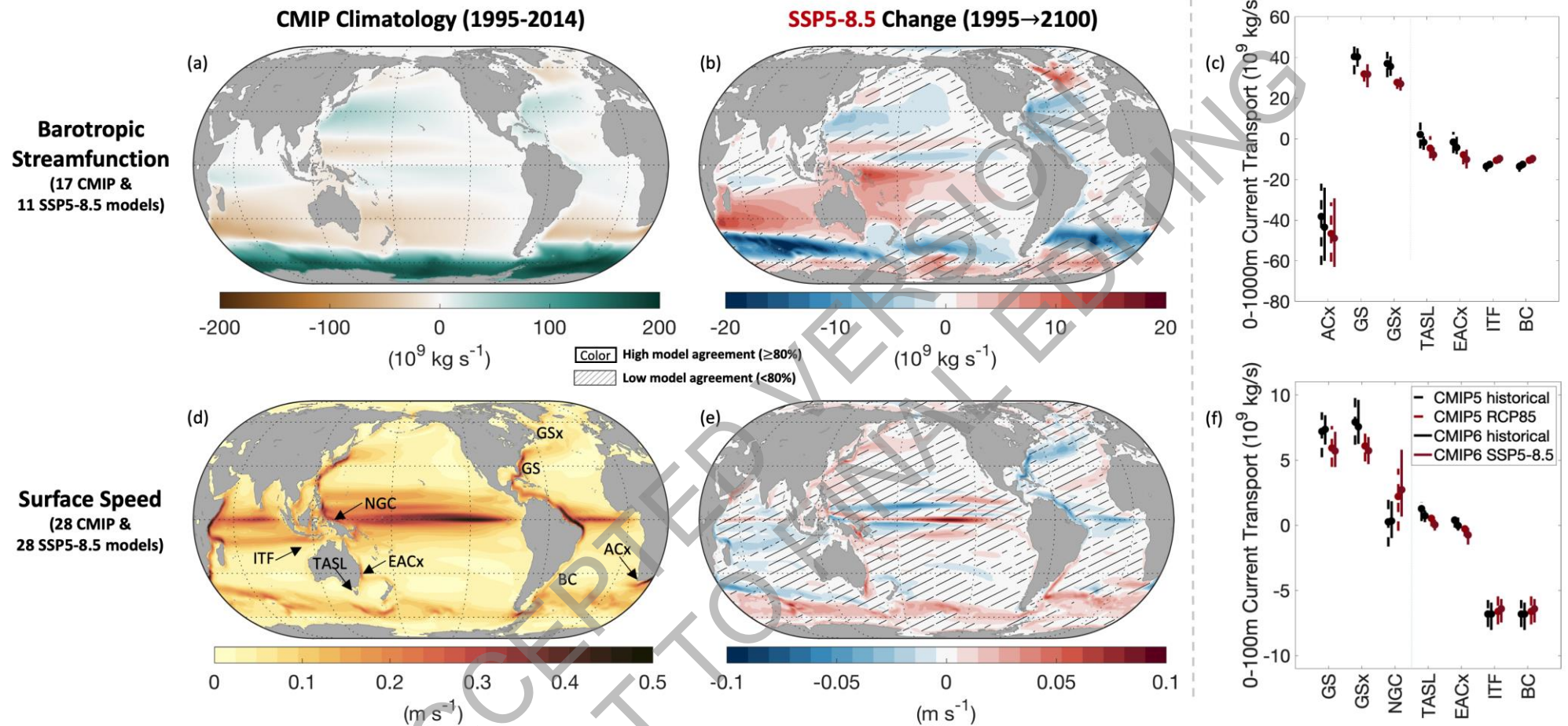
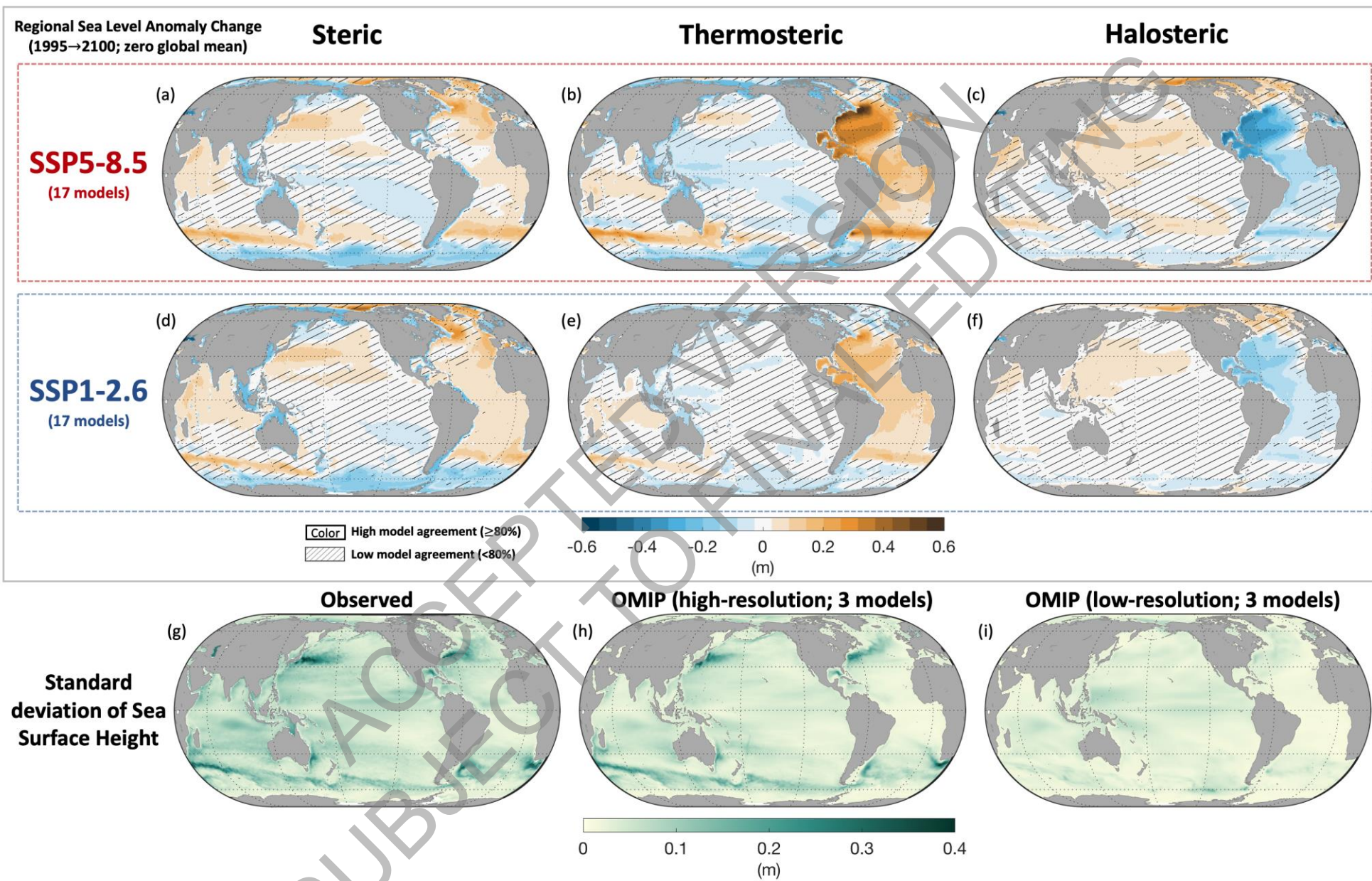
1
2
3
4
5
6
7
8
9

Figure 9.11: Simulated barotropic streamfunction, surface speed and major current transport in CMIP5 and CMIP6. (a) Mean barotropic streamfunction (S_v) 1995-2014 and projected barotropic streamfunction change (S_v , 2018-2100 vs. 1995-2014) under (b) SSP5-8.5. (d) Mean surface (0-100 m) speed (m/s) and projected surface speed change (m/s , 2081-2100) versus 1995-2014 under (e) SSP5-8.5. (c, f) Median and likely range of 1995-2014 and 2081-2100 transport of 3 currents with the largest transport change and 4 with the largest fractional change (Sen Gupta et al., 2016). (c) Deep currents: Agulhas Extension (ACx), Gulf Stream (GS), Gulf Stream Extension (GSx), Tasman Leakage (TASL), East Australia Current Extension (EACx), Indonesian Throughflow (ITF), and Brazil Current (BC). (f) Shallow currents: as for deep but with New Guinea Current (NGC), and without ACx. No overlay indicates regions with high model agreement, where $\geq 80\%$ of models agree on the sign of change; diagonal lines indicate regions with low model agreement, where $< 80\%$ of models agree on the sign of change (see Cross-Chapter Box Atlas.1 for more information). Further details on data sources and processing are available in the chapter data table (Table 9.SM.9).



1 **Figure 9.12: (a-f) CMIP6 multi-model mean projected change contributions to relative sea level change in (a,d) steric sea level anomaly, (b, e) thermosteric sea level**
2 **anomaly, and (c, f) halosteric sea level anomaly between 1995-2014 and 2081-2100 using a method that does not require a reference level (Landerer et al.,**
3 **2007). Global mean change has been removed from these figures, consistent with the methods in Sections 9.6.3 and 9.A.4.3 and the definitions of (Gregory et al.,**
4 **2019). See Figure 9.27 for GMSL. (g-i) Standard deviation of ocean dynamic sea-level change from (g) Aviso observations (10 day highpass filter), (h) 5-day mean of**
5 **high-resolution OMIP-2 models forced with observed fluxes, and (i) 5-day mean of low-resolution OMIP-2 models which are comparable in resolution to the models**
6 **in (a-f). No overlay indicates regions with high model agreement, where $\geq 80\%$ of models agree on the sign of change; diagonal lines indicate regions with low model**
7 **agreement, where $< 80\%$ of models agree on the sign of change (see Cross-Chapter Box Atlas.1 for more information). Further details on data sources and processing**
8 **are available in the chapter data table (Table 9.SM.9).**
9

Arctic sea-ice historical records and CMIP6 projections

Anomaly time series, maps of seasonal sea-ice concentration and changes, and projected sea-ice metrics in SSP2-4.5

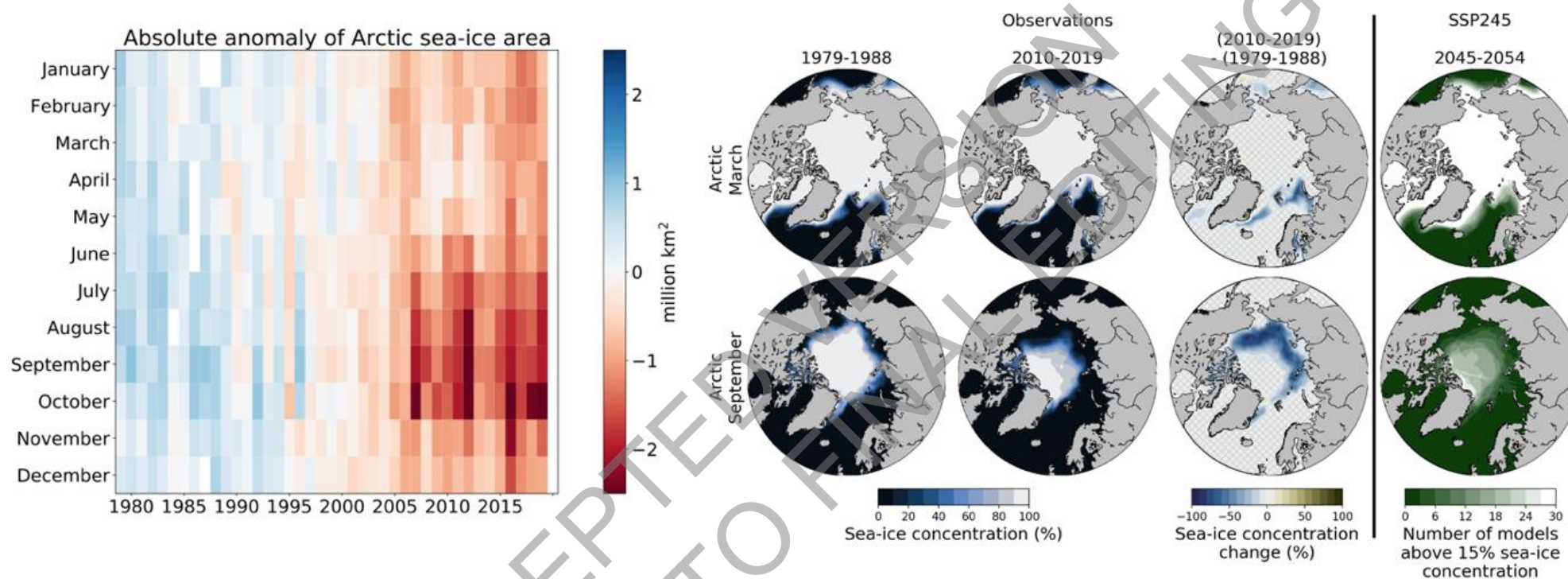
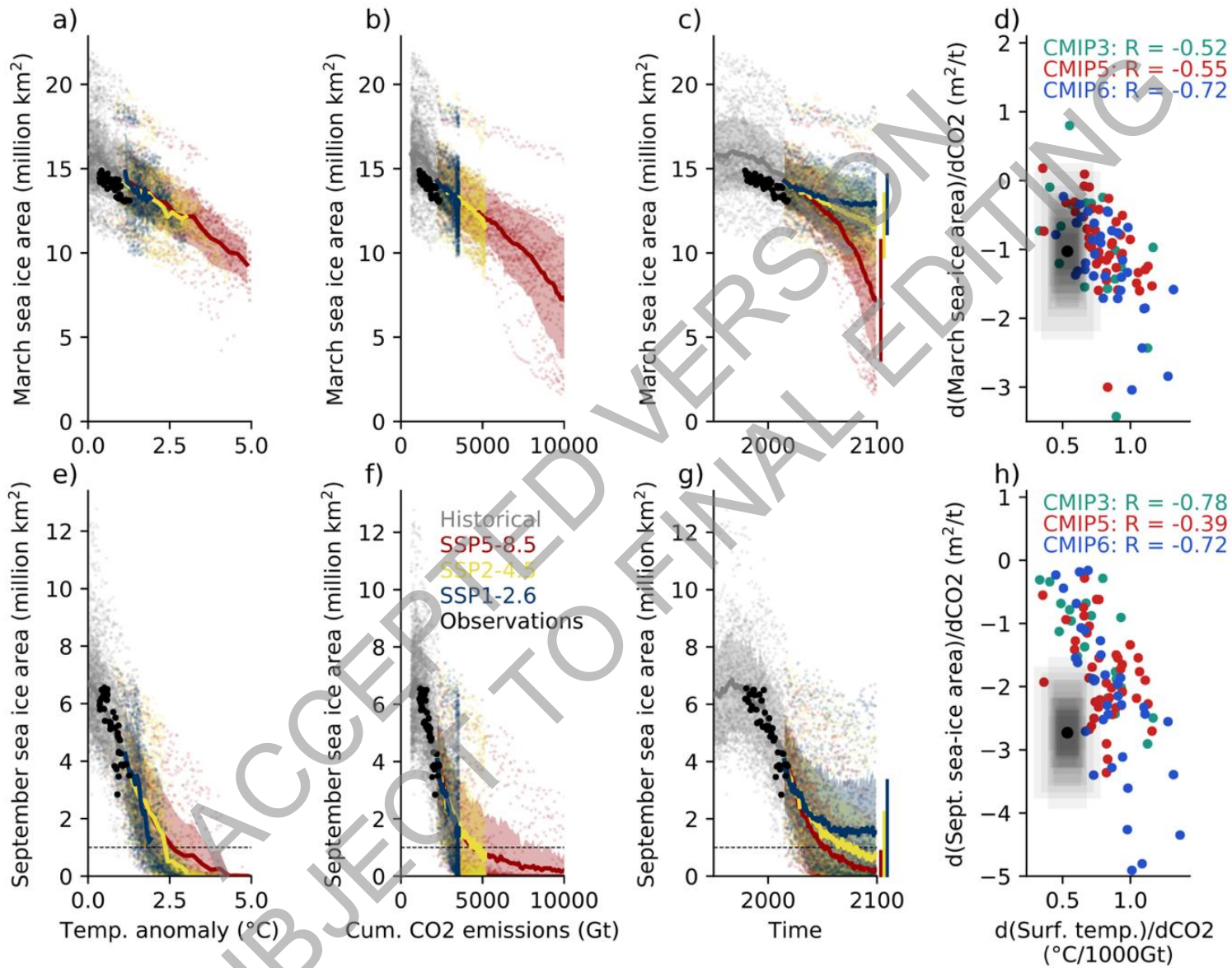


Figure 9.13: Arctic sea-ice historical records and CMIP6 projections. Left: Absolute anomaly of monthly-mean Arctic sea-ice area during the period 1979 to 2019 relative to the average monthly-mean Arctic sea-ice area during the period 1979 to 2008. Right: Sea-ice concentration in the Arctic for March and September, which usually are the months of maximum and minimum sea-ice area, respectively. First column: Satellite-retrieved mean sea-ice concentration during the decade 1979-1988. Second column: Satellite-retrieved mean sea-ice concentration during the decade 2010-2019. Third column: Absolute change in sea-ice concentration between these two decades, with grid lines indicating non-significant differences. Fourth column: number of available CMIP6 models that simulate a mean sea-ice concentration above 15 % for the decade 2045-2054. The average observational record of sea-ice area is derived from the UHH sea-ice area product (Doerr et al., 2021), based on the average sea-ice concentration of OSISAF/CCI (OSI-450 for 1979-2015, OSI-430b for 2016-2019)(Lavergne et al., 2019), NASA Team (version 1, 1979-2019)(Cavalieri et al., 1996) and Bootstrap (version 3, 1979-2019)(Comiso, 2017) that is also used for the figure panels showing observed sea-ice concentration. Further details on data sources and processing are available in the chapter data table (Table 9.SM.9).



1 **Figure 9.14: Monthly mean March (a-d) and September (e-h) sea-ice area as a function of global surface air temperature (GSAT) anomaly (a,e); cumulative**
2 **anthropogenic CO₂ emissions (b,f); year (c,g) in CMIP6 model simulations (shading, ensemble mean as bold line) and in observations (black dots).** Panels d
3 and h show the sensitivity of sea-ice loss to anthropogenic CO₂ emissions as a function of the modelled sensitivity of GSAT to anthropogenic CO₂ emissions. In panels
4 d and h, the black dot denotes the observed sensitivity, while the shading around it denotes internal variability as inferred from CMIP6 simulations (after Notz and
5 SIMIP Community, 2020). Further details on data sources and processing are available in the chapter data table (Table 9.SM.9).
6
7
8
9
10
11
12
13
14
15
16
17
18
19
20
21
22
23

Antarctic sea-ice historical records and CMIP6 projections

Anomaly time series, maps of seasonal sea-ice concentration and changes, and projected sea-ice metrics in SSP2-4.5

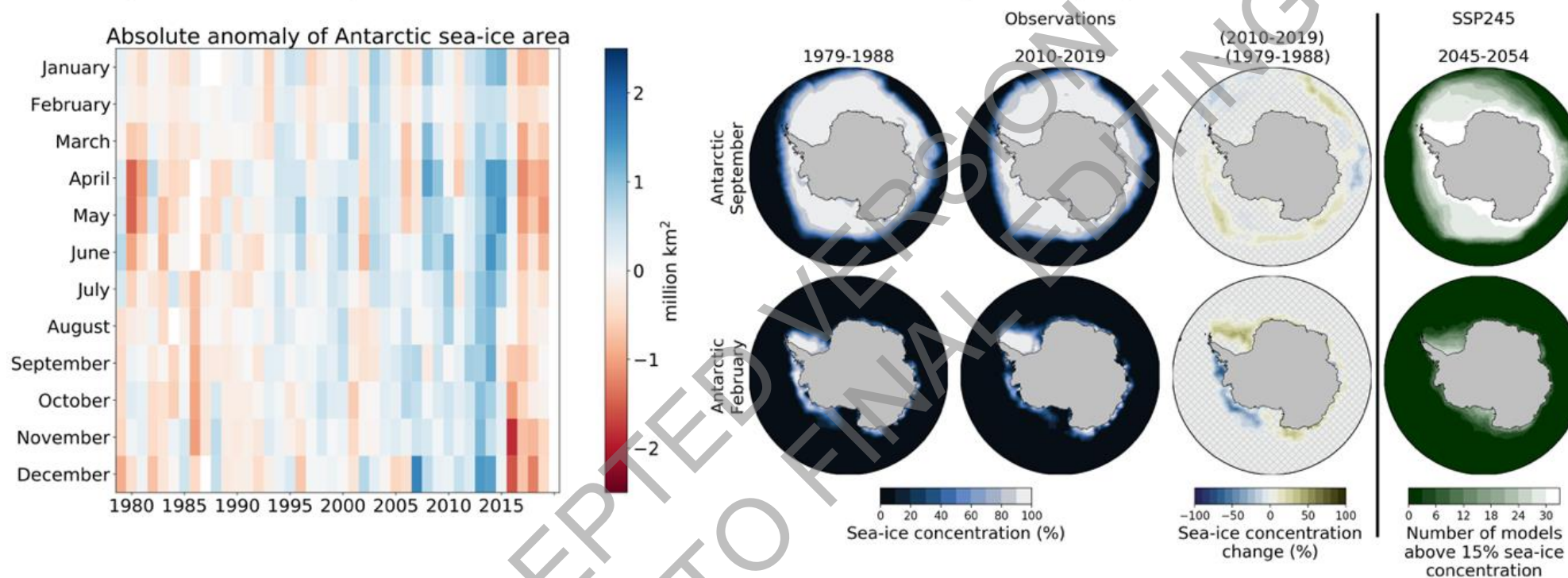
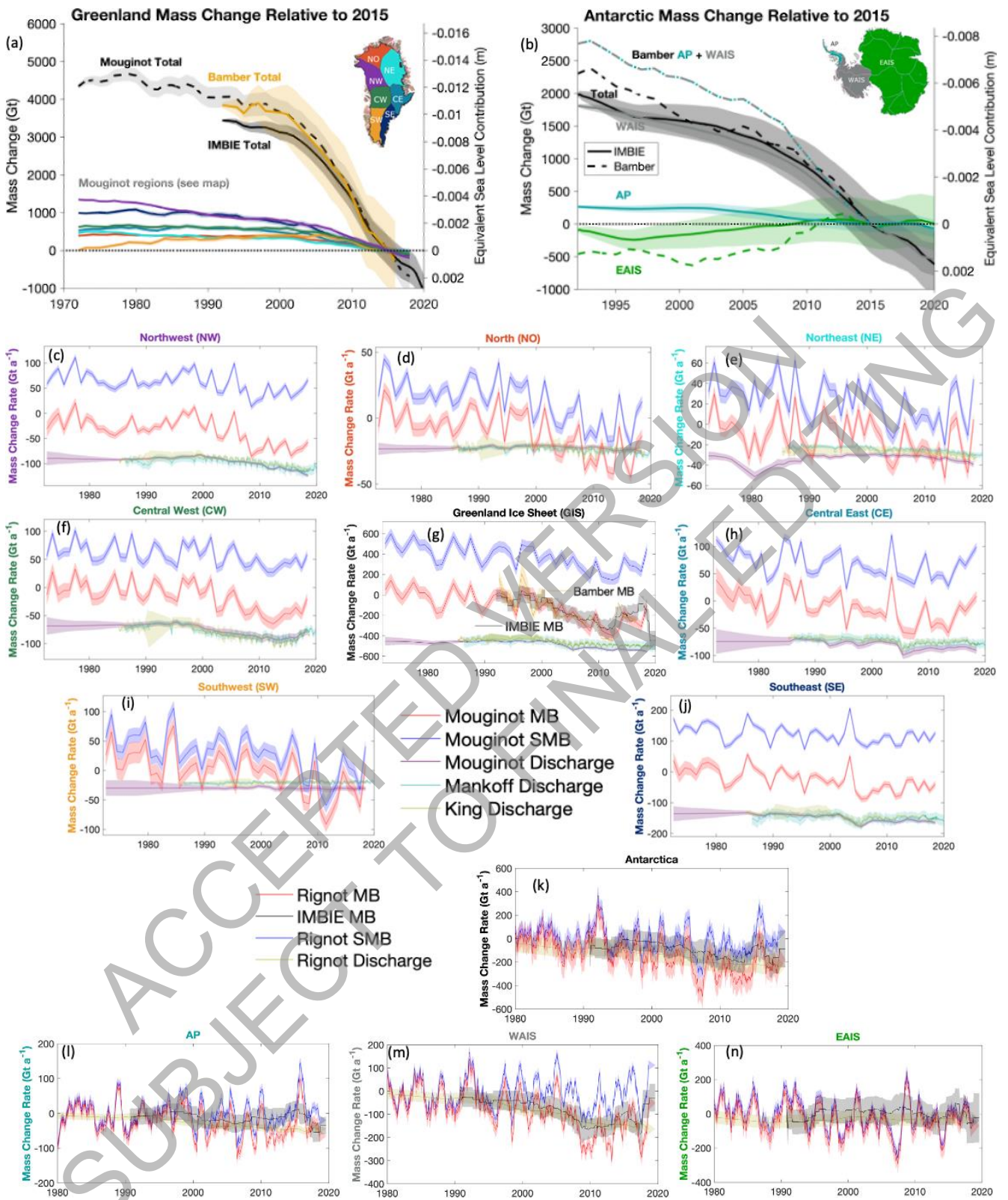


Figure 9.15: Antarctic sea-ice historical records and CMIP6 projections. Left: Absolute anomaly of observed monthly-mean Antarctic sea-ice area during the period 1979 to 2019 relative to the average monthly-mean Antarctic sea-ice area during the period 1979 to 2008. Right: Sea-ice coverage in the Antarctic as given by the average of the three most widely used satellite-based estimates for September and February, which usually are the months of maximum and minimum sea-ice coverage, respectively. First column: Mean sea-ice coverage during the decade 1979-1988. Second column: Mean sea-ice coverage during the decade 2010-2019. Third column: Absolute change in sea-ice concentration between these two decades, with grid lines indicating non-significant differences. Fourth column: number of available CMIP6 models that simulate a mean sea-ice concentration above 15 % for the decade 2045-2054. The average observational record of sea-ice area is derived from the UHH sea-ice area product (Doerr et al., 2021), based on the average sea-ice concentration of OSISAF/CCI (OSI-450 for 1979-2015, OSI-430b for 2016-2019)(Lavergne et al., 2019), NASA Team (version 1, 1979-2019)(Cavalieri et al., 1996) and Bootstrap (version 3, 1979-2019)(Comiso, 2017) that is also used for the figure panels showing observed sea-ice concentration. Further details on data sources and processing are available in the chapter data table (Table 9.SM.9).

1



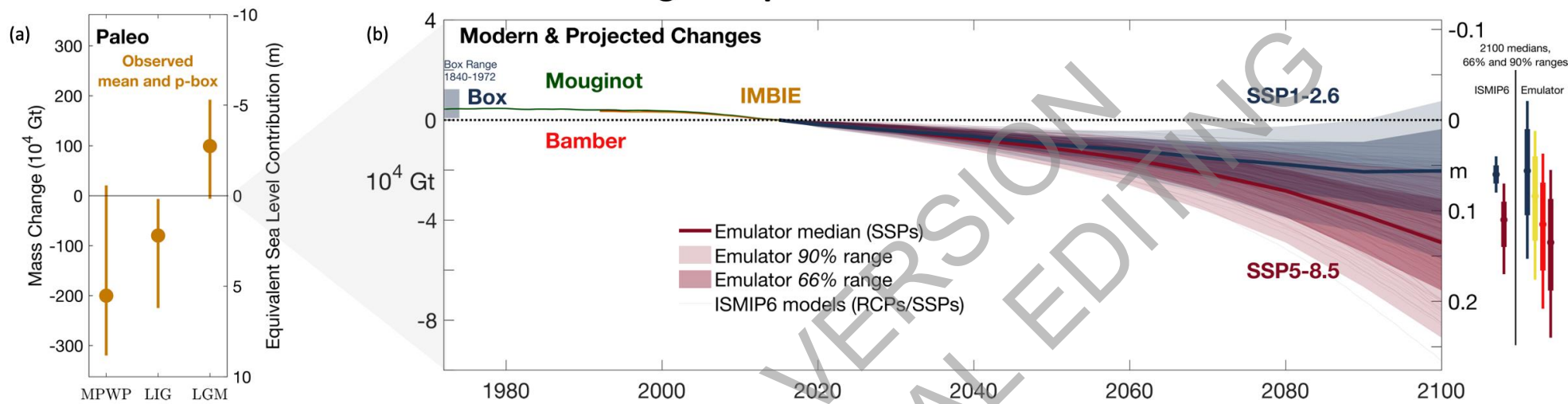
2
3
4
5
6
7
8
9

Figure 9.16: Mass changes and mass change rates for Greenland and Antarctic ice sheet regions. (Upper Left) Time series of mass changes in Greenland for each of the major drainage basins shown in the inset figure (Bamber et al., 2018b; Mouginitot et al., 2019) for the periods 1972 – 2016, 1992–2018, and 1992–2020. (Upper Right) Time series of mass changes for three portions of Antarctica (Bamber et al., 2018b) for the period 1992 – 2016 and 1992–2020. (Lower rows) Estimates of mass change rates of surface mass

1 balance, discharge and mass balance in seven Greenland regions (Bamber et al., 2018b; Mankoff et al.,
2 2019; Mougnot et al., 2019; King et al., 2020). (Bottom rows) Estimates of mass change rates of surface
3 mass balance, discharge and mass balance for three regions of Antarctica (Bamber et al., 2018b; The
4 IMBIE Team et al., 2018; Rignot et al., 2019). Further details on data sources and processing are
5 available in the chapter data table (Table 9.SM.9).
6
7

ACCEPTED VERSION
SUBJECT TO FINAL EDITING

Greenland Ice Sheet Cumulative Mass Change & Equivalent Sea Level Contribution



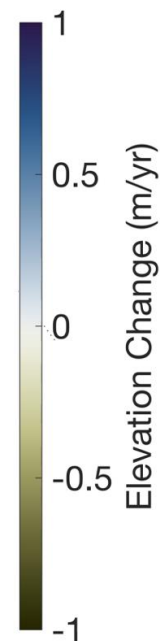
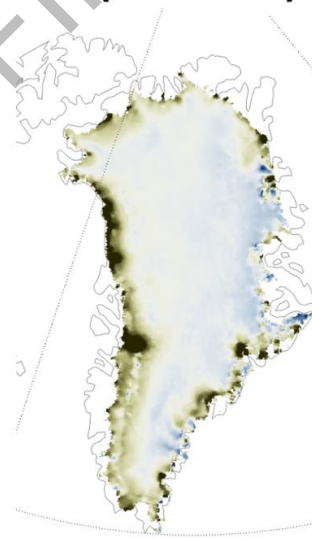
(c) Mid-Pliocene Warm Period

(d) Last Interglacial

(e) Last Glacial Maximum

(f) Observations (2010-2017)

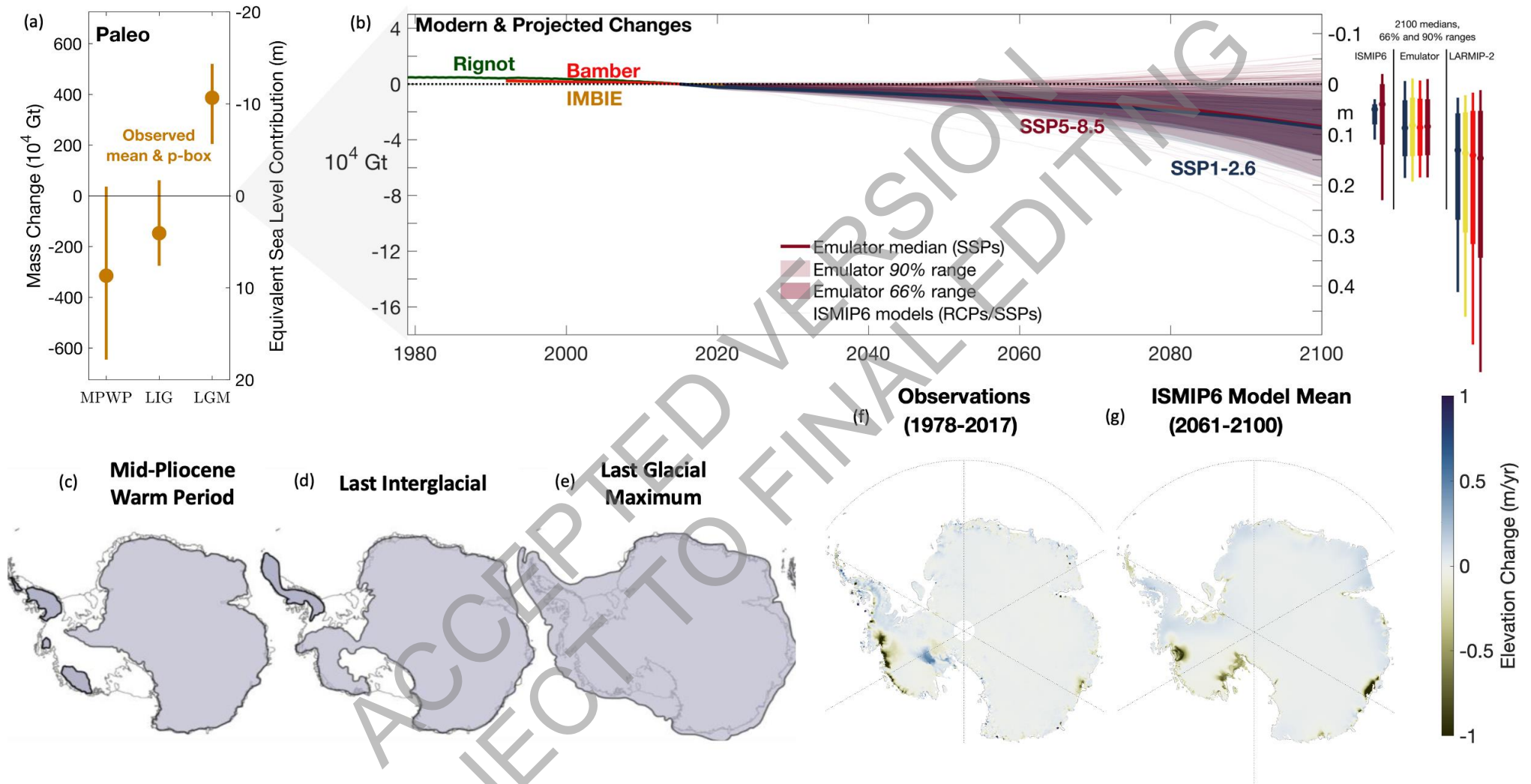
(g) ISMIP6 Model Mean (2093-2100)



1
2
3
4
5
6
7
8
9
10
11
12
13
14
15
16
17
18
19
20
21
22

Figure 9.17: Greenland Ice Sheet cumulative mass change and equivalent sea level contribution. (a) A p-box (Section 9.6.3.2) based estimate of the range of values of paleo Greenland ice sheet mass and sea level equivalents relative to present day and the median over all central estimates (Simpson et al., 2009; Argus and Peltier, 2010; Colville et al., 2011; Dolan et al., 2011; Fyke et al., 2011; Robinson et al., 2011; Born and Nisancioglu, 2012; Miller et al., 2012; Dahl-Jensen et al., 2013; Helsen et al., 2013; Nick et al., 2013; Quiquet et al., 2013; Stone et al., 2013; Colleoni et al., 2014; Lecavalier et al., 2014; Robinson and Goelzer, 2014; Calov et al., 2015; Dutton et al., 2015; Koenig et al., 2015; Peltier et al., 2015; Stuhne and Peltier, 2015; Vizcaino et al., 2015; Goelzer et al., 2016; Khan et al., 2016; Yau et al., 2016; de Boer et al., 2017; Calov et al., 2018; Simms et al., 2019); and (b) cumulative mass loss (and sea level equivalent) from 1972 (Mouginot et al., 2019) and 1992 (Bamber et al., 2018b; The IMBIE Team, 2019), the estimated mass loss from 1840 (Box and Colgan, 2013; Kjeldsen et al., 2015) indicated with a shaded box and projections from ISMIP6 by 2100 under RCP8.5/SSP5-85 and RCP2.6/SSP1-26 scenarios (thin lines from (Goelzer et al., 2020; Edwards et al., 2021; Payne et al., 2021) and likely range of the ISMIP6 emulation (shades and bold line (Edwards et al., 2021)) are shown in time. Schematic interpretations of individual reconstructions (Lecavalier et al., 2014; Goelzer et al., 2016; Berends et al., 2019) of the spatial extent of the Greenland ice sheet are shown for the (c) mid-Pliocene Warm Period, (d) the Last Interglacial and (e) the Last Glacial Maximum: grey shading shows extent of grounded ice. Maps of mean elevation changes (f) 2010-2017 derived from CryoSat 2 radar altimetry (Bamber et al., 2018b) and (g) ISMIP6 model mean (2093-2100) projected changes for the MIROC5 climate model under the RCP8.5 scenario (Goelzer et al., 2020). Further details on data sources and processing are available in the chapter data table (Table 9.SM.9).

Antarctic Ice Sheet Cumulative Mass Change & Equivalent Sea Level Contribution



1

2 **Figure 9.18:** (a) A p-box (Section 9.6.3.2) based estimate of the range of values of paleo Antarctic ice sheet mass and sea level equivalents relative to present day and the median
 3 over all central estimates (Bamber et al., 2009; Argus and Peltier, 2010; Dolan et al., 2011; Mackintosh et al., 2011; Golledge et al., 2012; Miller et al., 2012;
 4 Whitehouse et al., 2012; Golledge et al., 2013; Ivins et al., 2013; Argus et al., 2014; Briggs et al., 2014; Golledge et al., 2014; Maris et al., 2014; De Boer et al., 2015;

Do Not Cite, Quote or Distribute

9-233

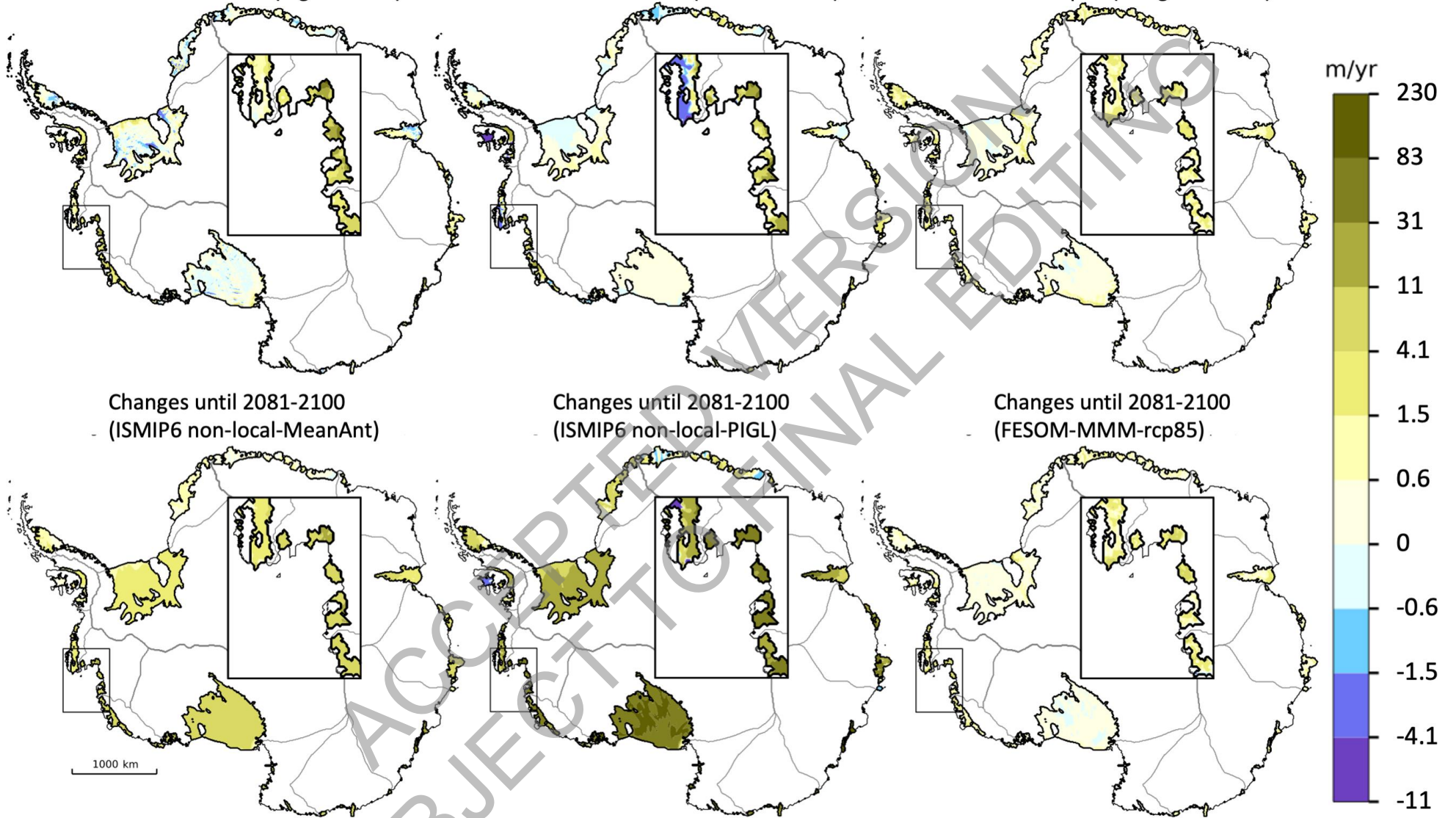
Total pages: 257

1 Dutton et al., 2015; Golledge et al., 2015; Pollard et al., 2015; DeConto and Pollard, 2016; Gasson et al., 2016; Goelzer et al., 2016; Yan et al., 2016; de Boer et al.,
2 2017; Golledge et al., 2017; Kopp et al., 2017; Simms et al., 2019) ; and cumulative mass loss (and sea level equivalent) since 2015, with satellite observations shown
3 from 1993 (Bamber et al., 2018a; The IMBIE Team et al., 2018; WCRP Global Sea Level Budget Group, 2018) and observations from 1979 (Rignot et al., 2019),
4 ISMIP6 projected changes by 2100 under RCP8.5/SSP5-8.5 and RCP2.6/SSP1-2.6 scenarios (thin lines from (Seroussi et al., 2020; Edwards et al., 2021; Payne et al.,
5 2021) and 17th to 83rd, 5th to 95th percentile ranges of the ISMIP6 emulation (shaded line, (Edwards et al., 2021)). Right, 17th to 83rd, 5th to 95th percentile ranges for
6 ISMIP6, emulator, and LARMIP-2 including SMB at 2100. Schematic interpretations of individual reconstructions (Anderson et al., 2002; Bentley et al., 2014; De
7 Boer et al., 2015; Goelzer et al., 2016) of the spatial extent of the Antarctic ice sheet are shown for the (b) mid-Pliocene Warm Period, (c) the Last Interglacial and (d)
8 the Last Glacial Maximum (Fretwell et al., 2013); grey shading shows extent of grounded ice. Maps of mean elevation changes (e) 1978-2017 derived from multi-
9 mission satellite altimetry (Schröder et al., 2019) and (f) ISMIP6 (2061-2100) projected changes for an ensemble using the NorESM1-M climate model under the
10 RCP8.5 scenario (Seroussi et al., 2020). Further details on data sources and processing are available in the chapter data table (Table 9.SM.9).
11
12
13
14
15
16
17
18
19
20

Observational Estimate (Rignot et al.)

ISMIP6 Non-Local PIGL (Jourdain et al.)

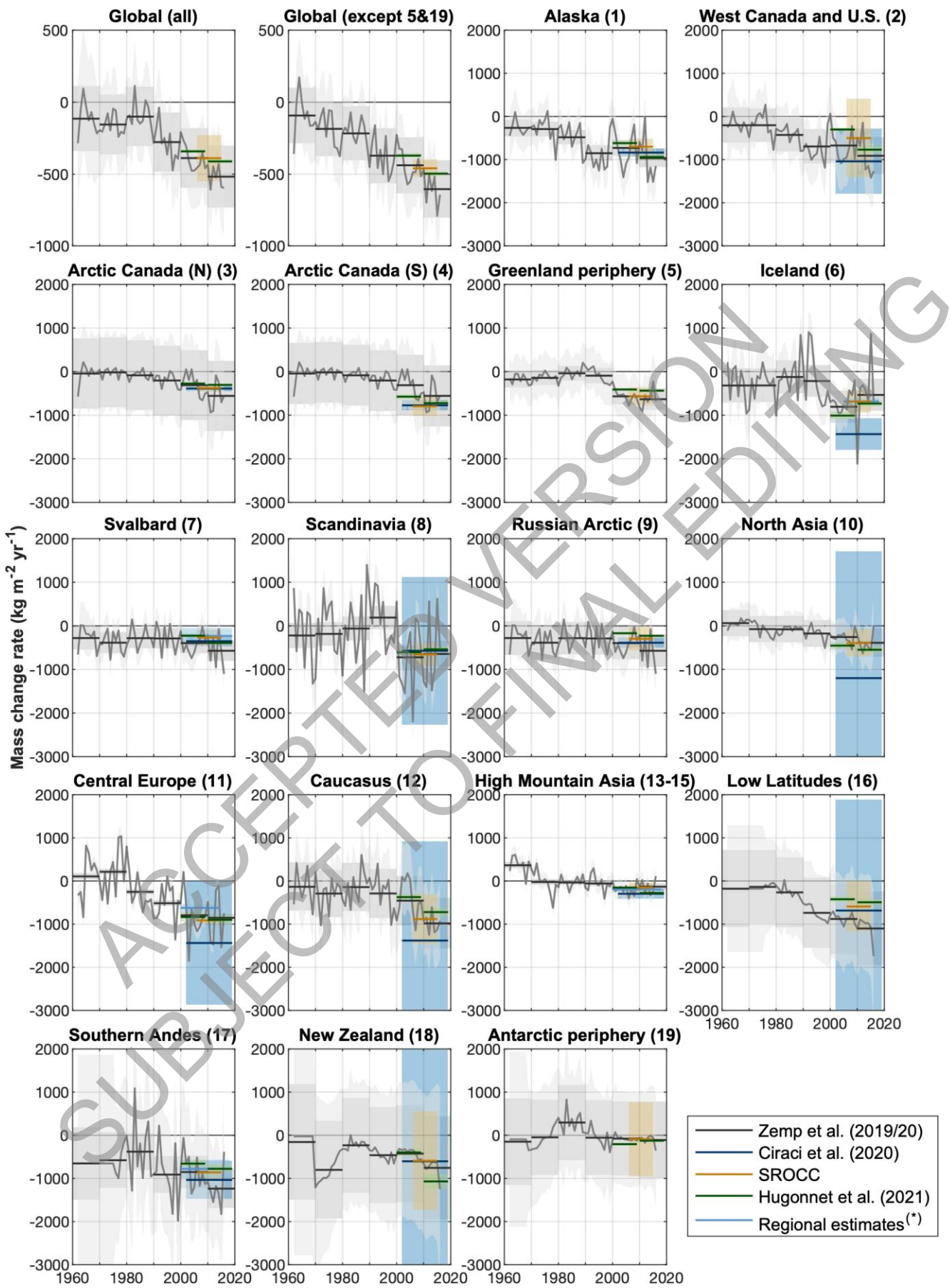
FESOM-MMM-rcp85 (Naughten et al.)



1
2

1 **Figure 9.19: Ice shelf basal melt rates for present-day (upper panels) and changes from present-day to the end of the 21st century under the RCP8.5 scenario (lower**
2 **panels).** Present-day melt rates were estimated through: the input-output method constrained by satellite observations and atmosphere/snow simulations (Rignot et al.,
3 2013) and representative of 2003-2008 (upper left); the non-local-PIGL parameterization constrained by observation-based ocean properties (Jourdain et al., 2020) and
4 representative of 1995-2014 (upper centre); the Finite Element Sea-ice/ice-shelf Ocean Model (FESOM) simulation over 2006-2015, forced by atmospheric conditions
5 from a CMIP5 multi-model mean (MMM) under the RCP8.5 scenario ((Naughten et al., 2018) upper right). Future anomalies are calculated as 2081-2100 minus
6 present-day using the ISMIP6 non-local-MeanAnt and non-local-PIGL parameterizations (Jourdain et al., 2020) lower left and centre respectively) based on projections
7 from the NorESM1-M CMIP5 model, and the FESOM-MMM projection (lower right). Note the symmetric-log colour bar (linear around zero, logarithmic for stronger
8 negative and positive values). Inset highlights the Amundsen Sea Region. Further details on data sources and processing are available in the chapter data table (Table
9 9.SM.9).

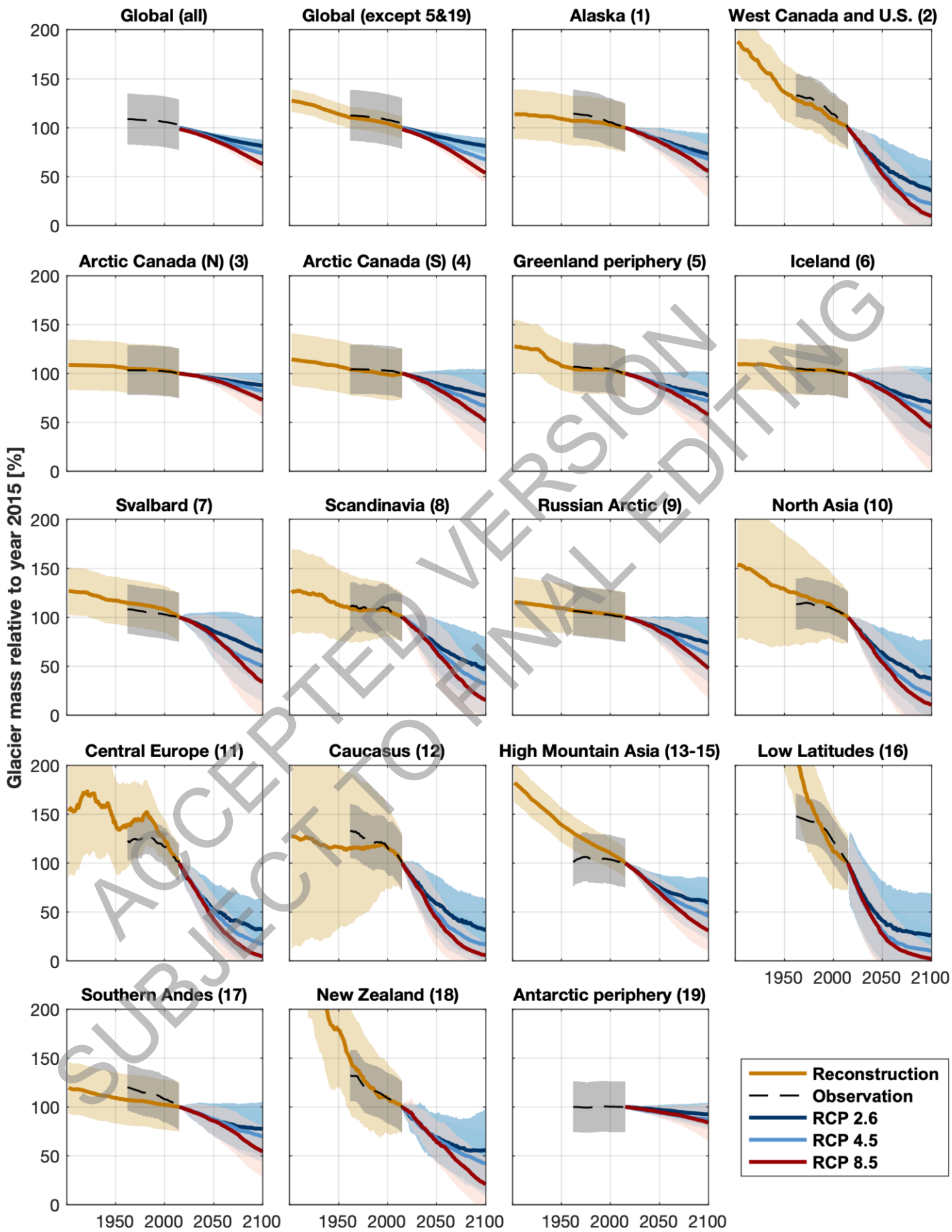
1



2
3

1 **Figure 9.20: Global and regional glacier mass change rate between 1960 and 2019.** The time series of annual and
2 decadal mean mass change are based on glaciological and geodetic balances (Zemp et al. (2019) and
3 Zemp et al. (2020)). Superimposed are the 2002-2019 average rates by (Ciraci et al., 2020) based on the
4 Gravity Recovery and Climate Experiment (GRACE), 2006-2015 estimated rates as assessed in SROCC
5 and the new decadal averages (2000-2009 and 2010-2019) by Hugonnet et al. (9998). (*) New regional
6 estimates for the Andes (Dussaillant et al., 2019), High Mountain Asia (Shean et al., 2020), Iceland
7 (Aðalgeirsdóttir et al., 2020), Central Europe (Sommer et al., 2020) and Svalbard (Schuler et al., 2020)
8 are also shown. The uncertainty reported in each study is shown. See Figure 9.2 for the location of each
9 region. Further details on data sources and processing are available in the chapter data table (Table
10 9.SM.9).

ACCEPTED VERSION
SUBJECT TO FINAL EDITING



1 **Figure 9.21: Global and regional glacier mass evolution between 1901 and 2100 relative to glacier mass in 2015.**
2 Reconstructed glacier mass change through the 20th century (Marzeion et al., 2015) and observed during
3 1961-2016 (Zemp et al., 2019). Projected (2015-2100) glacier mass evolution is based on the median of
4 three Representative Concentration Pathways (RCPs) emission scenarios (Marzeion et al., 2020).
5 Uncertainties are in all cases the 90% confidence interval. For a better comparison between regions, the
6 maximum relative mass change was set to 200%, although for three regions, the volume changes between
7 1901 and 2015 exceeded that value. For the Low Latitude, New Zealand, and High Mountain Asia
8 glaciers, the changes were larger than 1000%, 350%, and 250%, respectively. See Figure 9.2 for the
9 location of each region. Further details on data sources and processing are available in the chapter data
10 table (Table 9.SM.9).
11

ACCEPTED VERSION
SUBJECT TO FINAL EDITING

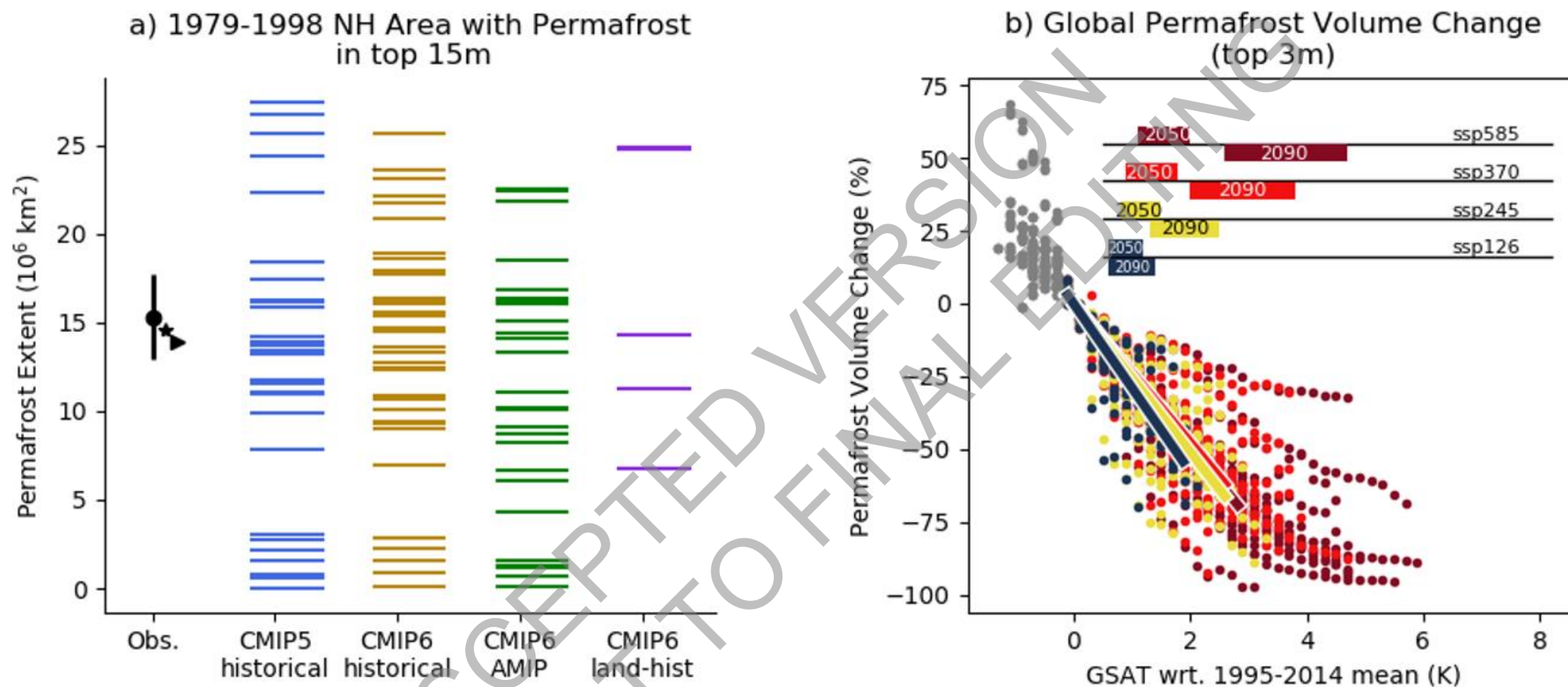
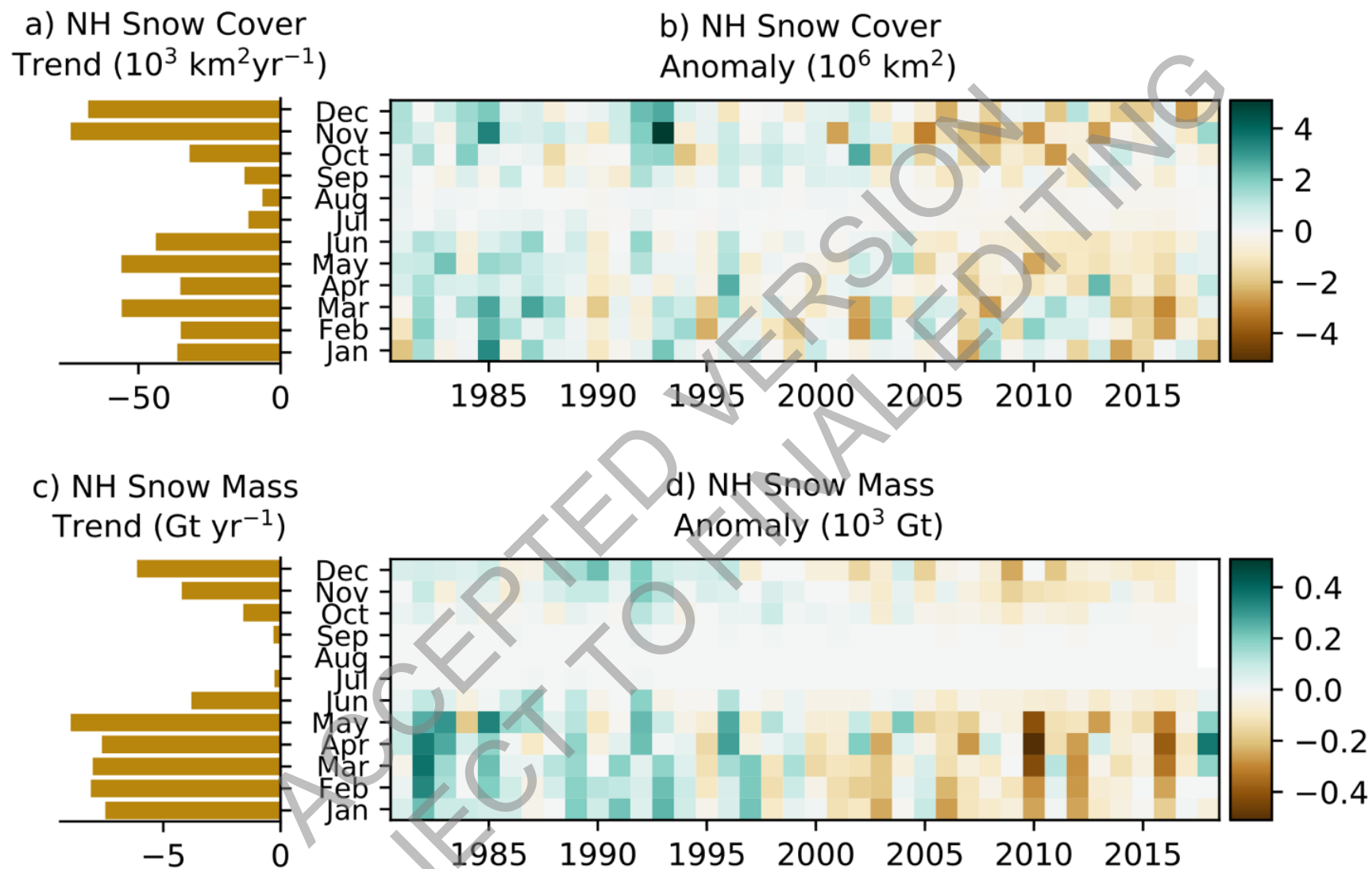
1
23
4
5
6
7
8
9
10
11

Figure 9.22: Simulated versus observed permafrost extent and permafrost volume change by warming level. a) Diagnosed Northern Hemisphere permafrost extent (area with perennially frozen ground at 15 m depth, or at the deepest model soil level if this is above 15 m) for 1979-1998, for available CMIP5 and CMIP6 models, from the first ensemble member of the historical coupled run, and for CMIP6 AMIP (atmosphere+land surface, prescribed ocean) and land-hist (land only, prescribed atmospheric forcing) runs. Estimates of current permafrost extents based on physical evidence and reanalyses are indicated as black symbols (triangle: Obu et al. (2018); star: Zhang et al. (1999); circle: central value and associated range from Gruber (2012)). b) Simulated global permafrost volume change between the surface and 3 m depth as a function of the simulated GSAT change, from the first ensemble members of a selection of scenarios, for available CMIP6 models. Further details on data sources and processing are available in the chapter data table (Table 9.SM.9).



1
2 **Figure 9.23: Observed monthly Northern Hemisphere (a) snow cover trends and (b) anomalies, and (c) snow mass trends and (d) anomalies.** From the observation-based
3 ensemble discussed in the text (Mudryk et al., 2020). Trends and anomalies are calculated over the 1981-2018 period. Further details on data sources and processing
4 are available in the chapter data table (Table 9.SM.9).

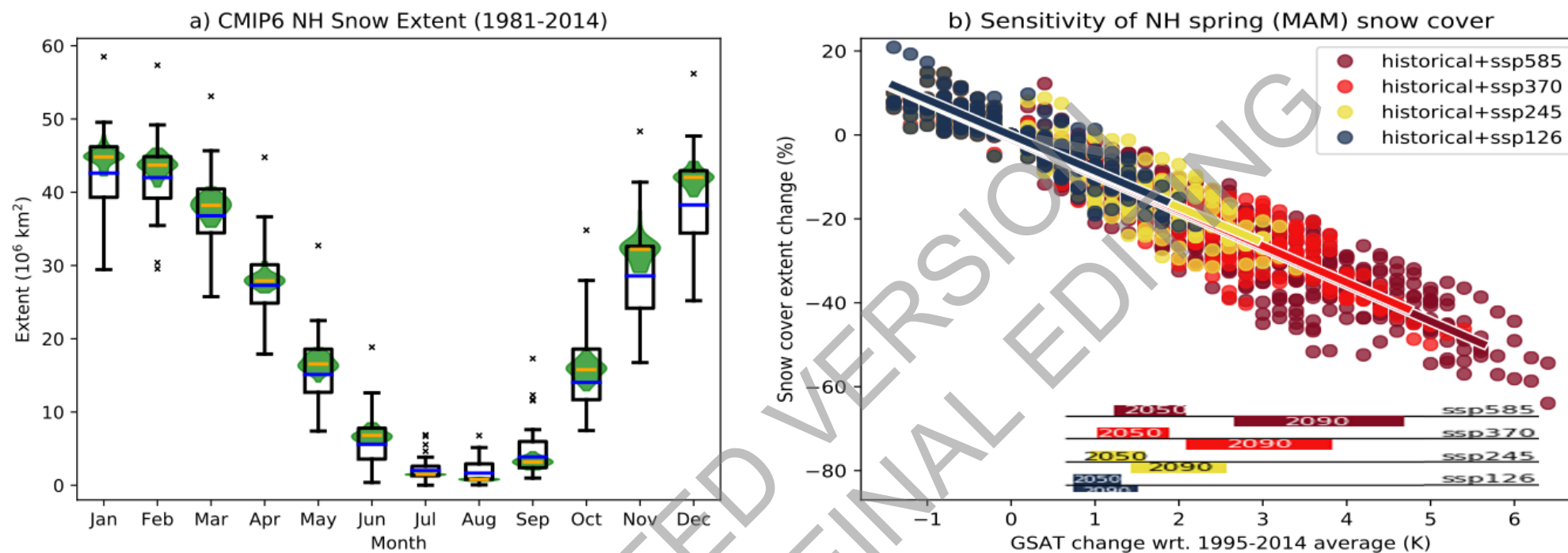
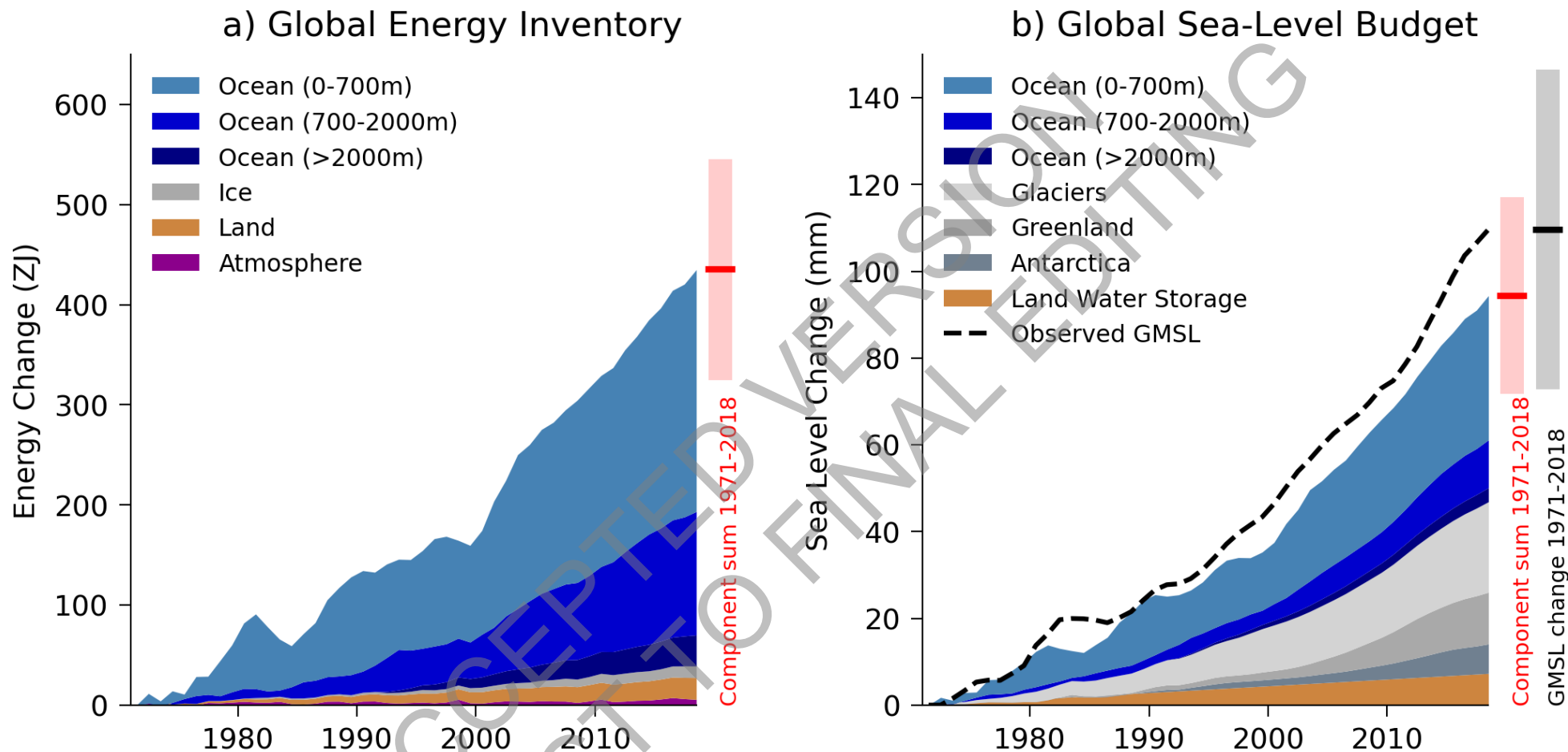


Figure 9.24: Simulated CMIP6 and observed snow cover extent (SCE). a) Simulated CMIP6 and observed (Mudryk et al., 2020) SCE (in millions of km²) for 1981-2014. Boxes and whiskers with outliers represent monthly mean values for the individual CMIP6 models averaged over 1981-2014, with the red bar indicating the median of the CMIP6 multi-model ensemble for that period. The observed interannual distribution over the period is represented in green, with the yellow bar indicating the median. b) Spring (March to May) Northern Hemisphere snow cover extent against GSAT (relative to the 1995-2014 average) for the CMIP6 Tier 1 scenarios (SSP1-2.6, SSP2-4.5, SSP3-7.0 and SSP5-8.5), with linear regressions. Each data point is the mean for one CMIP6 simulation (first ensemble member for each available model) in the corresponding temperature bin. Further details on data sources and processing are available in the chapter data table (Table 9.SM.9).



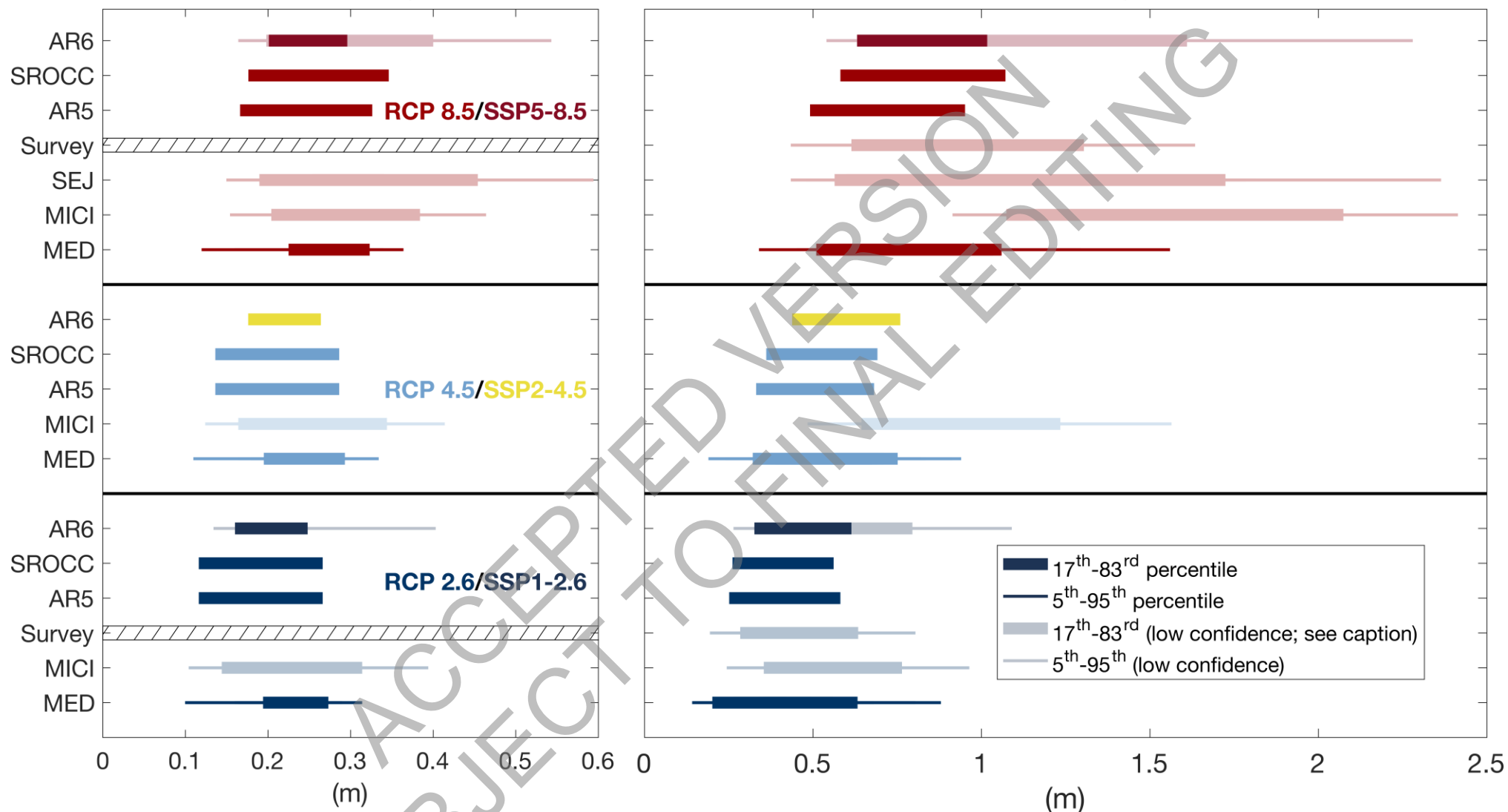
1
2
3
4
5
6
7

Cross-Chapter 9.1, Figure 1: Global Energy Inventory and Sea Level Budget. a) Observed changes in the global energy inventory for 1971-2018 (shaded time series) with component contributions as indicated in the figure legend. Earth System Heating for the whole period and associated uncertainty is indicated to the right of the plot (red bar = central estimate; shading = *very likely* range); b) Observed changes in components of global mean sea-level for 1971-2018 (shaded time series) as indicated in the figure legend. Observed global mean sea-level change from tide gauge reconstructions (1971-1993) and satellite altimeter measurements (1993-2018) is shown for comparison (dashed line) as a 3-year running mean to reduce sampling

1 noise. Closure of the global sea-level budget for the whole period is indicated to the right of the plot (red bar = component sum central estimate;
2 red shading = *very likely* range; black bar = total sea level central estimate; grey shading = *very likely* range). Full details of the datasets and
3 methods used are available in Annex I. Further details on energy and sea-level components are reported in Table 7.1 and Table 9.5.
4
5
6
7
8
9
10
11
12
13
14
15
16
17
18

2050 GMSL Projections

2100 GMSL Projections



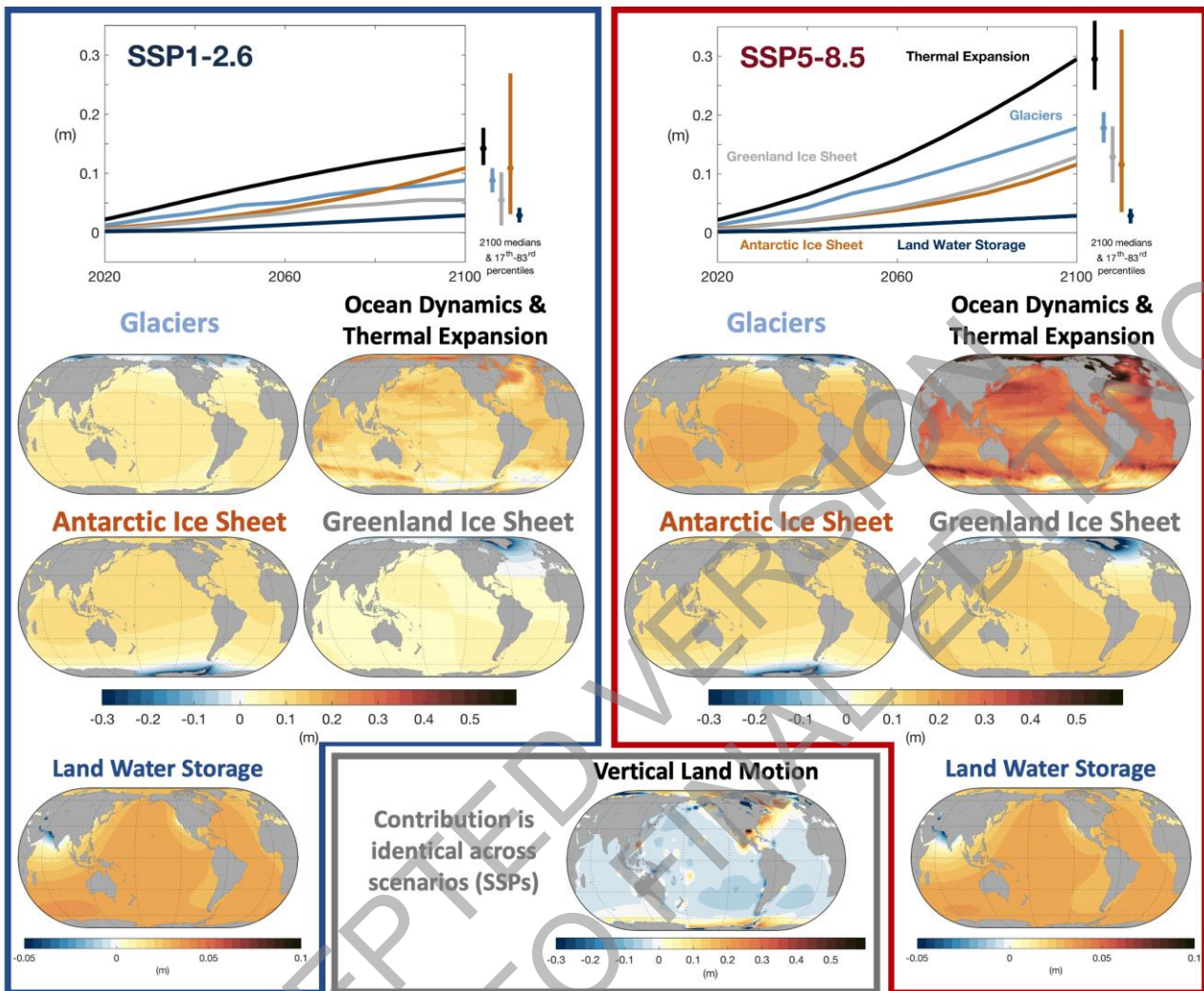
1
2
3

Figure 9.25: Literature global mean sea level (GMSL) projections (m) for 2050 (left) and 2100 (right) since 1995-2014, for RCP 8.5/SSP5-8.5 (top set), RCP 4.5/SSP2-4.5 (middle set), and RCP 2.6/SSP1-2.6 (bottom set). Projections are standardised to account for minor differences in time periods. Thick bars span from the 17th-83rd

1 percentile projections, and thin bars span the 5th-95th percentile projections. The different assessments of ice sheet contributions are indicated by ‘MED’ (ice sheet
2 projections including only processes in whose quantification there is *medium confidence*), ‘MICI’ (ice sheet projections which incorporate Marine Ice Cliff Instability),
3 and ‘SEJ’ (structured expert judgement (SEJ) to assess the central range of the ice-sheet projection distributions). ‘Survey’ indicates the results of a 2020 survey of sea-
4 level experts on GMSL rise from all sources (Horton et al., 2020). Projection categories incorporating processes in which there is *low confidence* (‘MICI’ and ‘SEJ’)
5 are lightly shaded. Dispersion among the different projections represents *deep uncertainty*, which arises as a result of *low agreement* regarding appropriate conceptual
6 models describing ice sheet behaviour and *low agreement* regarding probability distributions used to represent key uncertainties. Individual studies are shown in Tables
7 9.SM.5, 9.SM.6. Further details on data sources and processing are available in the chapter data table (Table 9.SM.9).

1
2

Projected Sea Level Change Contributions under SSP1-2.6 and SSP5-8.5



3
4
5
6
7
8
9

Figure 9.26: Median global mean and regional relative sea-level projections (m) by contribution for the SSP1-2.6 and SSP5-8.5 scenarios. (upper time series) Global mean contributions to sea-level change as a function of time, relative to 1995-2014. (lower maps) Regional projections of the sea-level contributions in 2100 relative to 1995-2014 for SSP5-8.5 and SSP1-2.6. Vertical land motion is common to both SSPs. Further details on data sources and processing are available in the chapter data table (Table 9.SM.9).

1

Projected global mean sea level rise under different SSP scenarios

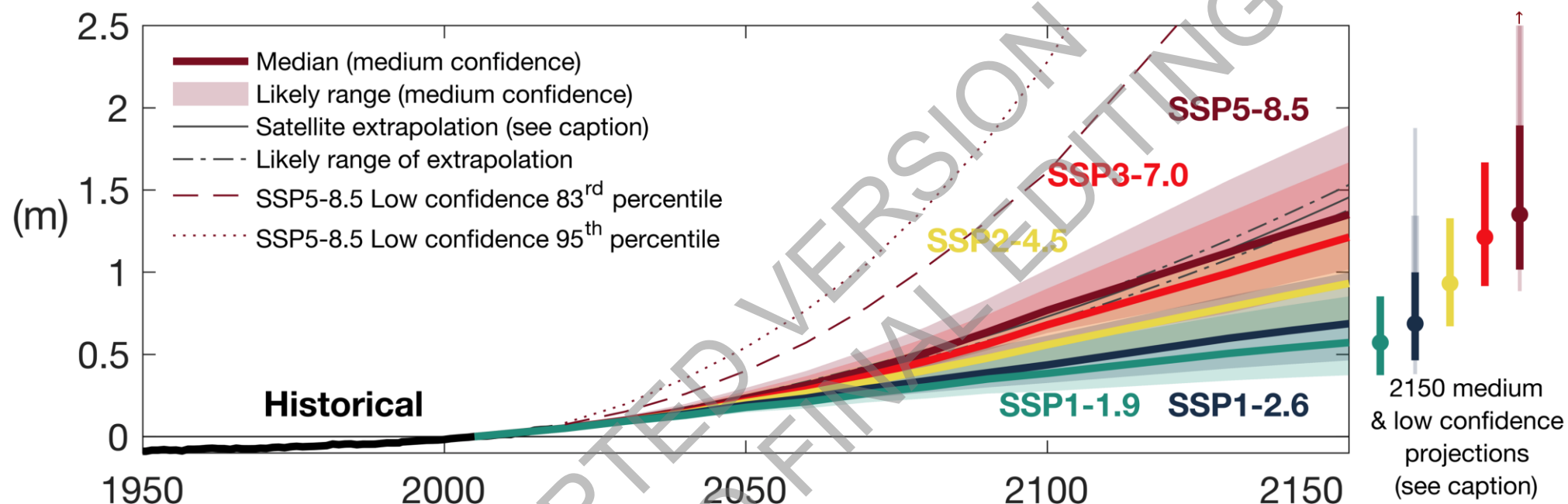
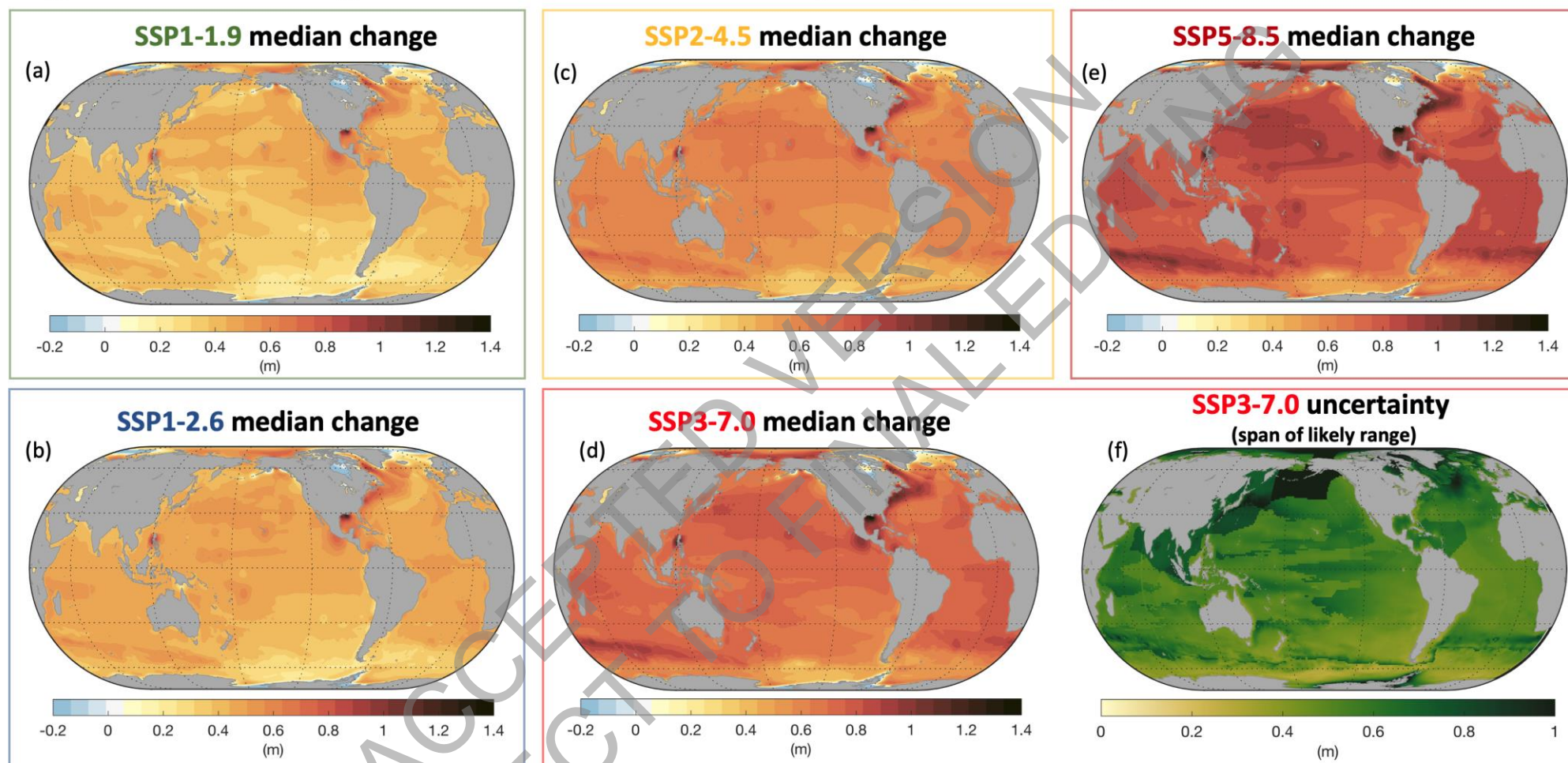


Figure 9.27: Projected global mean sea level rise under different SSP scenarios. Likely global mean sea-level change for SSP scenarios resulting from processes in whose projection there is *medium confidence*. Projections and likely ranges at 2150 are shown on right. Lightly shaded ranges and thinner lightly shaded ranges on the right show the 17th-83rd and 5th-95th percentile ranges for projections including *low confidence* processes for SSP1-2.6 and SSP5-8.5 only, derived from a p-box including Structured Expert Judgement and Marine Ice Cliff Instability projections. Black lines show historical GMSL change, and thick solid and dash-dotted black lines show the mean and likely range extrapolating the 1993-2018 satellite altimeter trend and acceleration. Further details on data sources and processing are available in the chapter data table (Table 9.SM.9).

2
3
4
5
6
7
8
9
10
11
12
13
14
15

Regional sea level change at 2100 for different scenarios (with respect to 1995-2014)



1

2

3

4

5

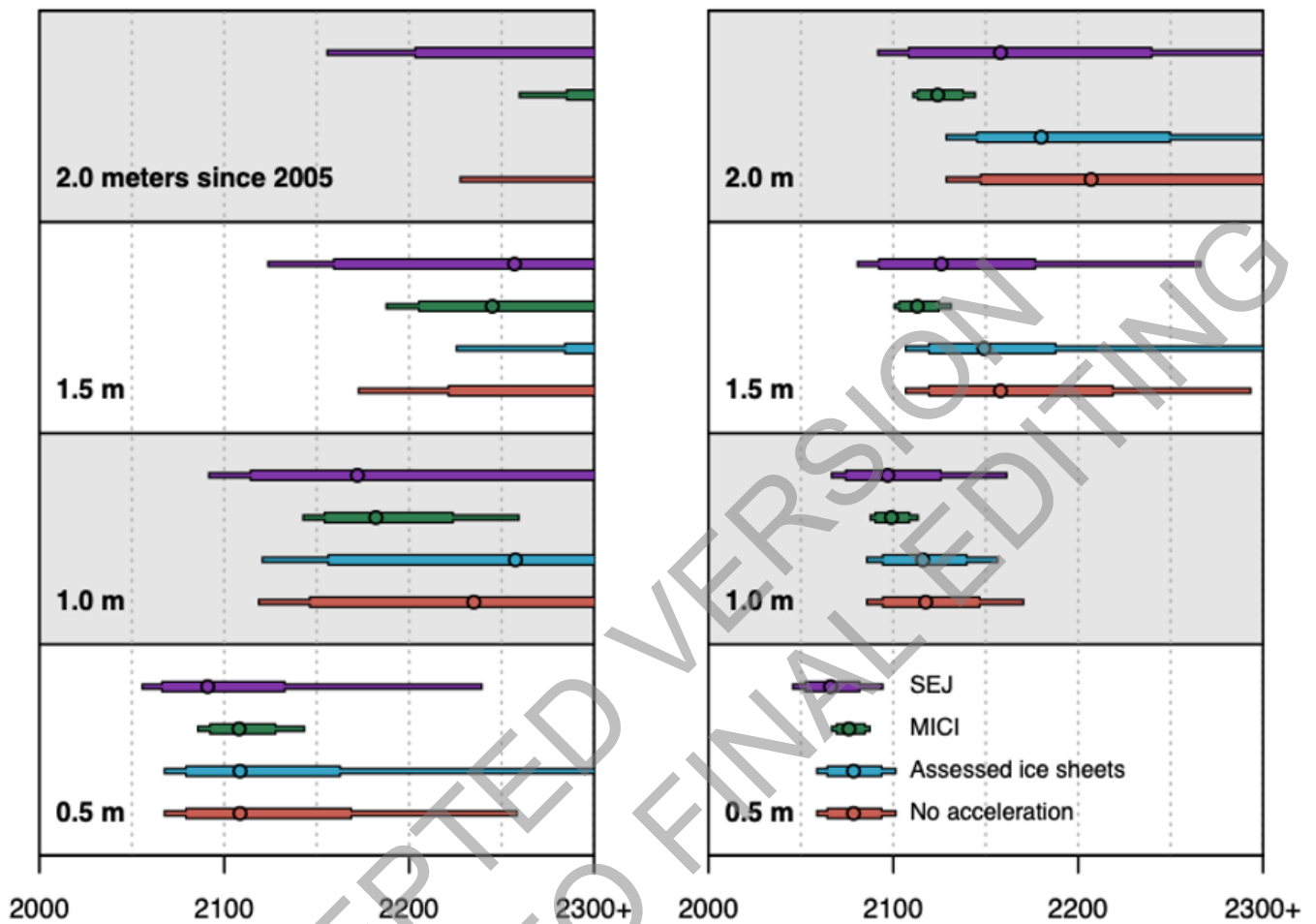
Figure 9.28: Regional sea level change at 2100 for different scenarios (with respect to 1995-2014). Median regional relative sea-level change from 1995 to 2014 up to 2100 for (a) SSP1-1.9, (b) SSP1-2.6, (c) SSP2-4.5, (d) SSP3-7.0, (e) SSP5-8.5, and (f) width of the likely range for SSP3-7.0. The high uncertainty in projections around Alaska and the Aleutian Islands arises from the tectonic contribution to vertical land motion, which varies greatly over short distances in this region. Further details on data sources and processing are available in the chapter data table (Table 9.SM.9).

1

Projected timing of sea-level rise milestones Under different forcing scenarios and methodologies

SSP1-2.6

SSP5-8.5



2
3
4
5
6
7
8
9
10
11
12
13
14
15
16
17
18
19
20
21
22
23

Figure 9.29: Timing of when GMSL thresholds of 0.5, 1.0, 1.5 and 2.0 m are exceeded, based upon four different ice-sheet projection methods informing post-2100 projections. Methods are labelled based on their treatment of ice sheets. “No acceleration” assumes constant rates of mass change after 2100. “Assessed ice sheet” models post-2100 ice sheet losses using a parametric fit (Supplementary Material 9.SM.4) extending to 2300 based on a multimodel assessment of contributions under RCP2.6 and RCP8.5 at 2300. Structured Expert Judgement (SEJ) employs ice-sheet projections from Bamber et al. (2019) Marine Ice Cliff Instability (MICI) combines the parametric fit (Supplementary Material 9.SM3.4) for Greenland with Antarctic projections based on DeConto et al. (2021). Circles/thick bars/thin bars represent the 50th, 17th-83rd, and 5th-95th percentiles of the exceedance timing for the indicated projection method. Further details on data sources and processing are available in the chapter data table (Table 9.SM.9).

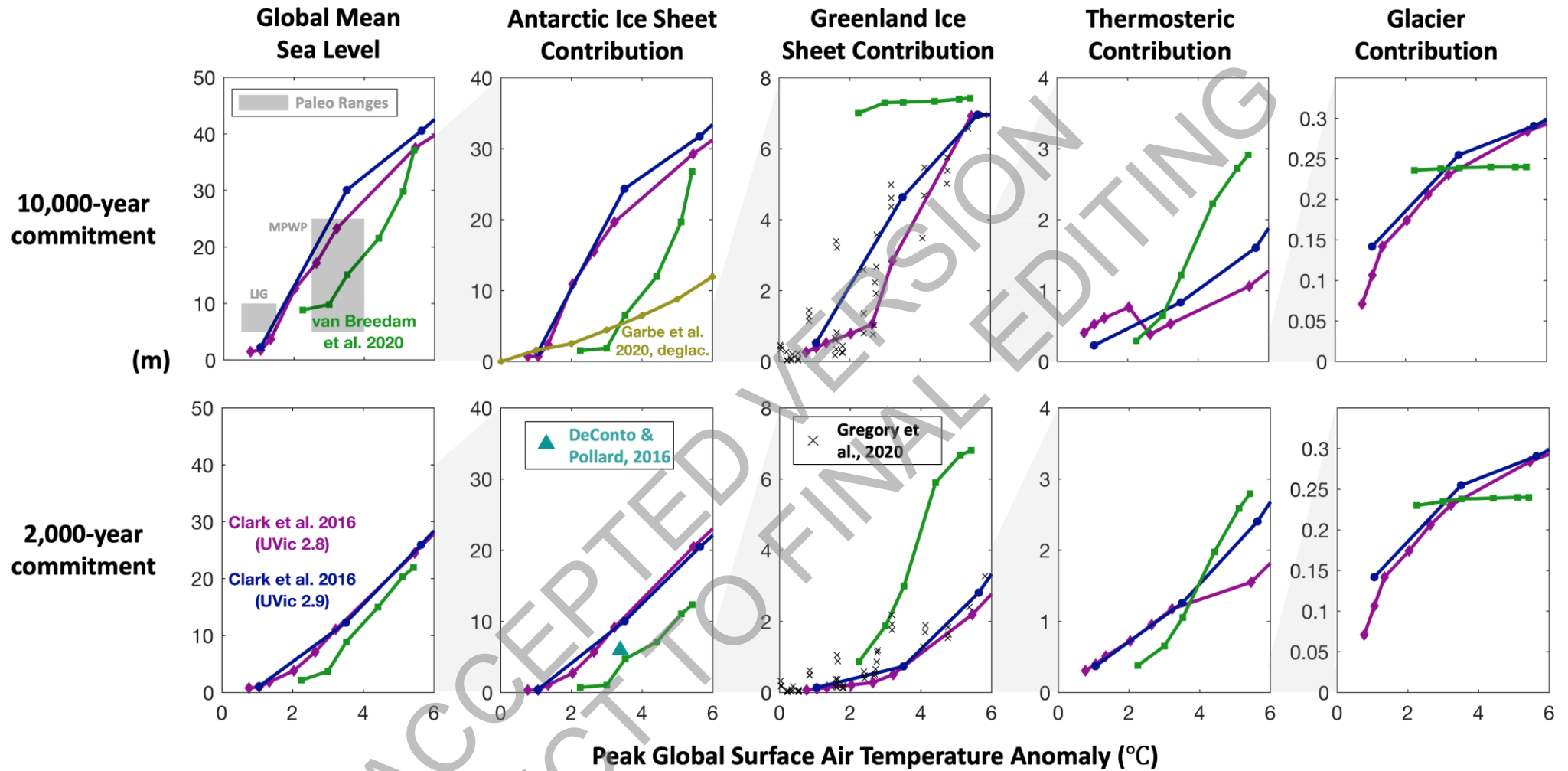
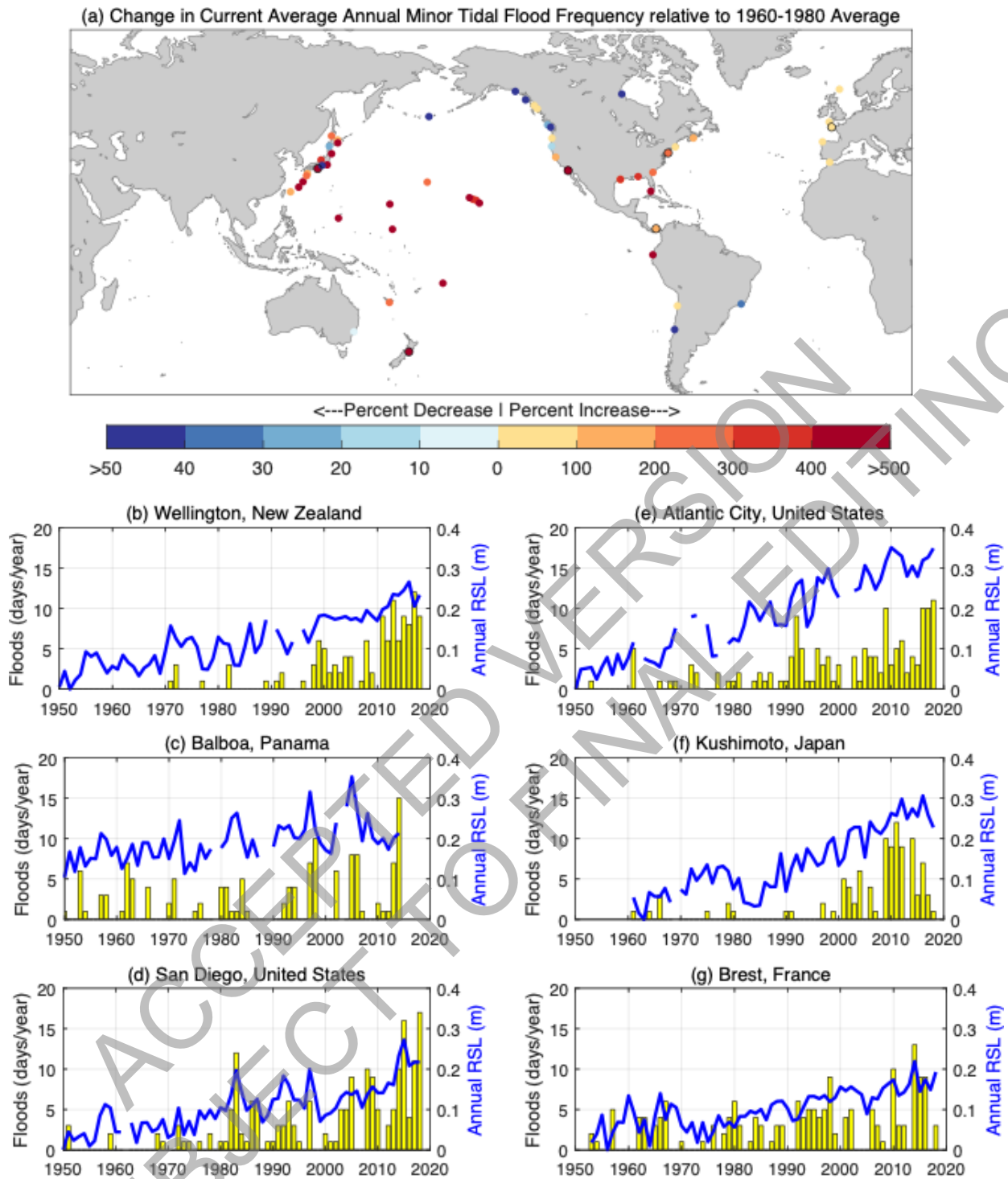


Figure 9.30: Global mean sea-level commitment as a function of peak global surface air temperature. From models (Clark et al., 2016; DeConto and Pollard, 2016; Garbe et al., 2020; Van Breedam et al., 2020) and paleo data on 2000-year (lower row) and 10,000 year (upper row) timescales. Columns indicate different contributors to GMSL rise (from left to right: total GMSL change, Antarctic Ice Sheet, Greenland Ice Sheet, global mean thermosteric sea-level rise, and glaciers). Further details on data sources and processing are available in the chapter data table (Table 9.SM.9).

1
2
3
4
5
6

1



2
3
4
5
6
7
8
9
10
11

Figure 9.31: Historical occurrences of minor extreme still water levels. Defined as the 99th percentile of daily observed water levels over 1995-2014. (a) Percent change in occurrences over 1995-2014 relative to those over 1960-1980. (b-g) Annual mean sea level (blue) and annual occurrences of extreme still water levels over the 1995-2014 99th percentile daily maximum (yellow) at six selected tide gauge locations. Further details on data sources and processing are available in the chapter data table (Table 9.SM.9).

Median Amplification Factor of Extreme Still Water Level by:

2050

2100

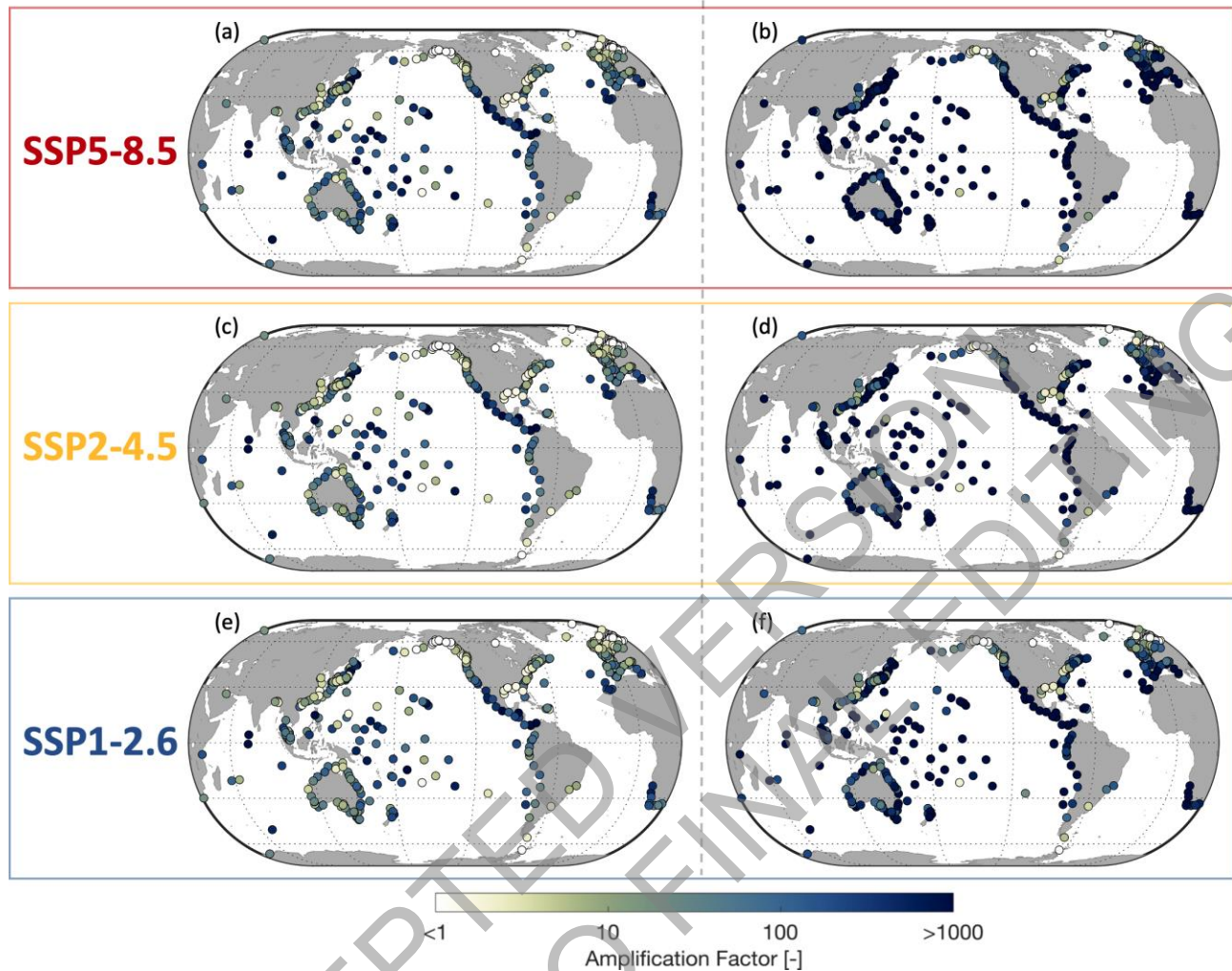


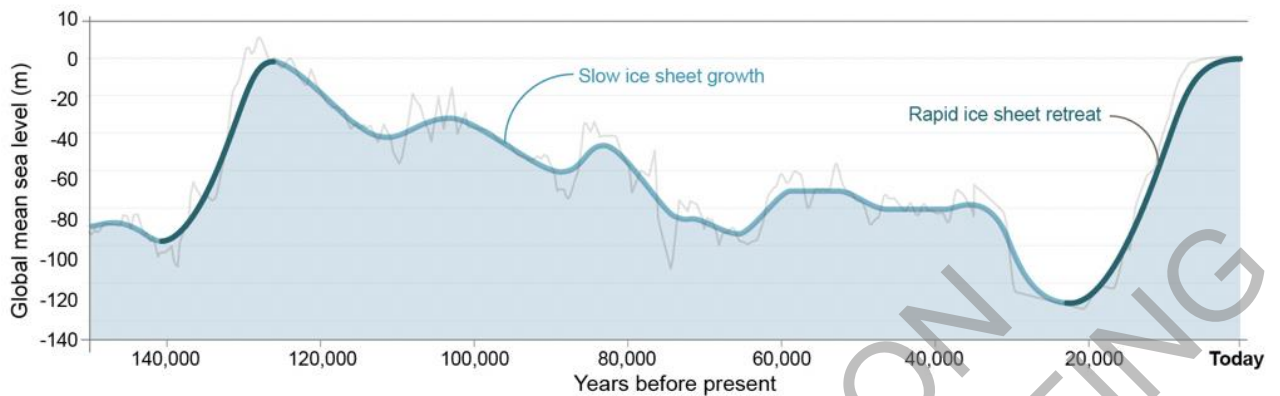
Figure 9.32: Projected median frequency amplification factors for the 1% average annual probability extreme still water level in 2050 (a, c, e) and 2100 (b, d, f). Based on a peak-over-threshold (99.7%) method applied to the historical extreme still water levels of GESLA2 following SROCC and additionally fitting a Gumbel distribution between MHHW and the threshold following (Buchanan et al., 2016), using the regional sea-level projections of this chapter (Section 9.6.3.3) for (a, b) SSP5-8.5, (c, d) SSP2-4.5 and (e, f) SSP1-2.6. Further details on data sources and processing are available in the chapter data table (Table 9.SM.9).

1
2
3
4
5
6
7
8
9
10
11
12
13
14
15
16
17
18
19
20
21
22
23
24

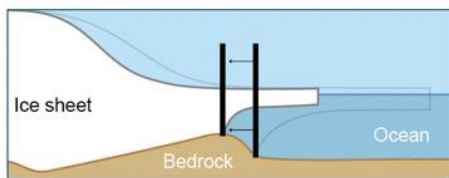
1

FAQ 9.1: Can melting of the ice sheets be reversed?

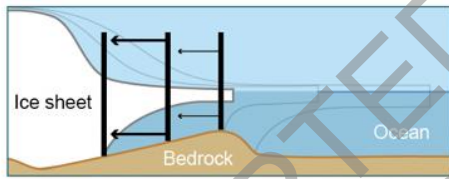
Once ice sheets are **destabilised**, it takes them tens of thousands of years to re-grow. These changes strongly affect **sea level**.



Melting driven by ocean temperature



When bedrock dips seaward or is flat, the retreat stops when warming stops. When ice sheet retreats, **less ice** is released into ocean

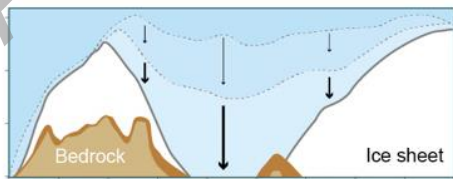


When bedrock dips landward the retreat is quick and self-sustained. When ice sheet retreats, **more ice** is released into ocean – ice sheet retreats further

Melting driven by air temperature



The ice sheet is very thick therefore its surface is very high and the air at high altitude is very cold



As the ice sheet melts, its **surface goes down** until it reaches a threshold, where the surrounding air is warmer and melts the ice even more quickly

FAQ 9.1, Figure 1: Ice sheets growth and decay (Top) Changes in ice-sheet volume modulate sea level variations.

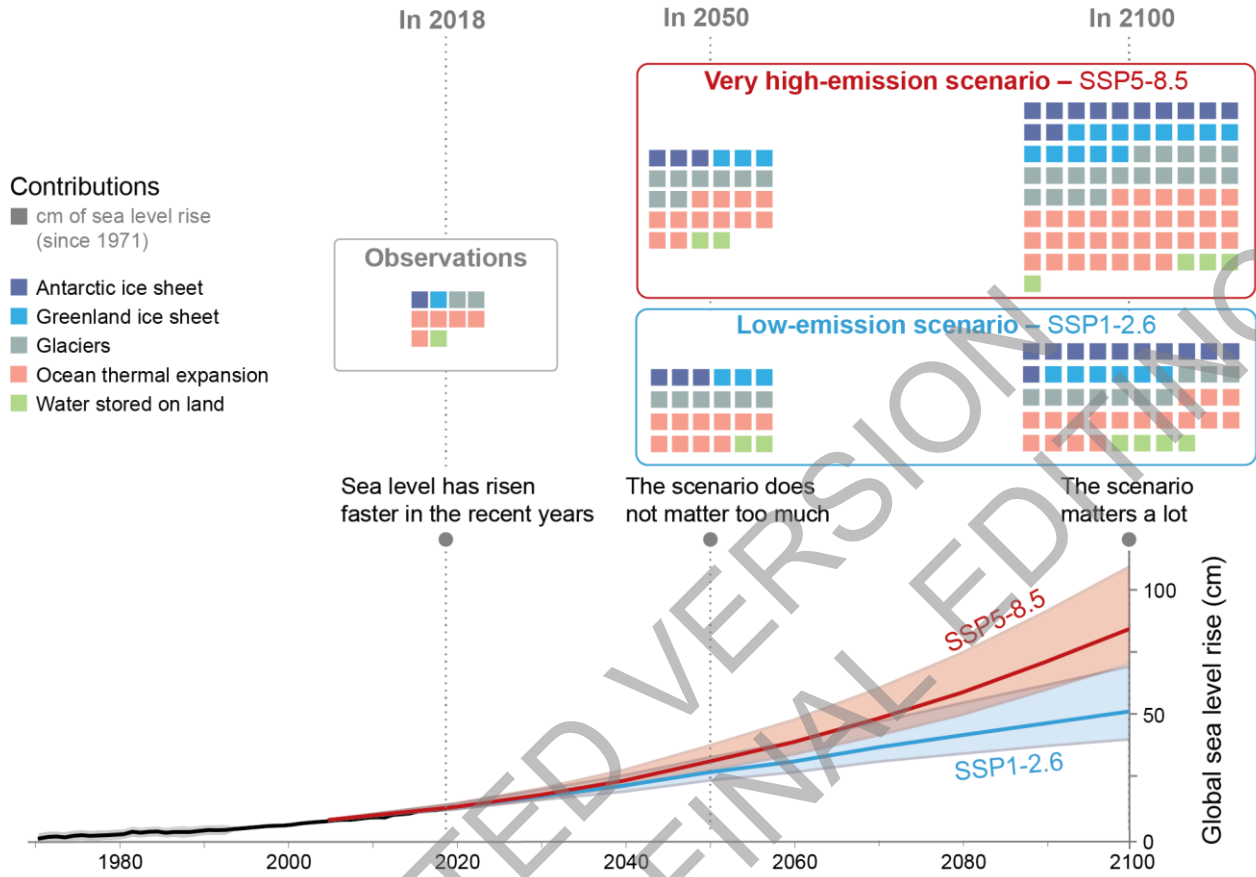
The grey line depicts data from a range of physical environmental sea-level recorders such as coral reefs (see Table 9.SM.5) while the blue line is a smoothed version of it. (Bottom, left) Example of destabilisation mechanism in Antarctica. (Bottom, right) Example of destabilisation mechanism in Greenland.

2
3
4
5
6
7
8
9
10
11
12
13
14
15
16
17
18
19
20
21
22

1
2

FAQ 9.2: How much will sea level rise in the next few decades?

Emissions scenarios influence little sea level rise of the coming decades but has a huge effect on sea level at the end of the century.



FAQ 9.2, Figure 1: Observed and projected global mean sea level rise and the contributions from its major constituents.

3
4
5
6
7
8
9
10
11
12
13
14
15
16
17
18
19
20
21
22
23
24
25
26
27

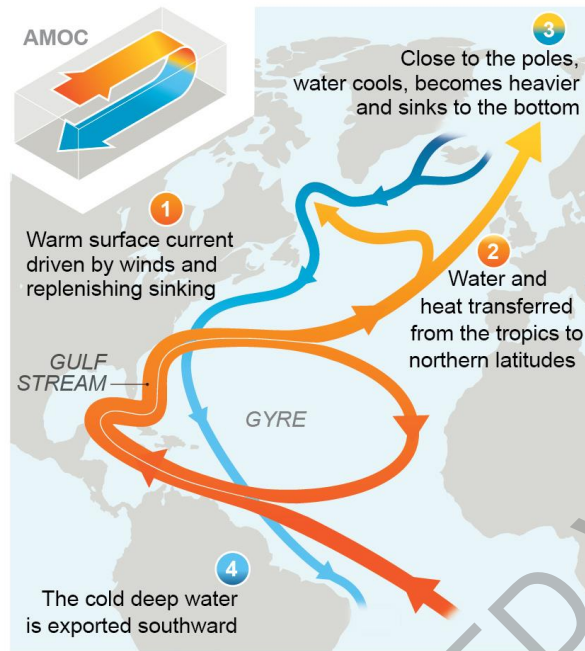
1

FAQ 9.3: Will the Gulf Stream shut down?

The Gulf Stream, a warm current, is expected to weaken but not cease. This slowdown will affect regional weather and sea level.

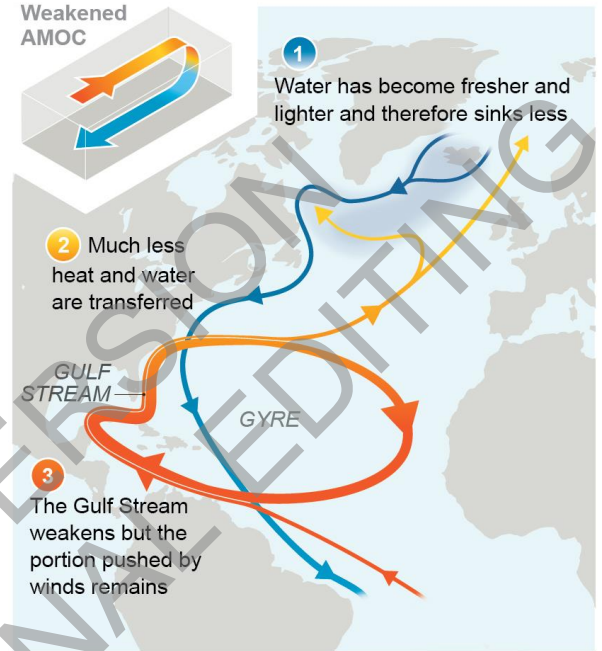
Today

The Gulf Stream is part of both the horizontal, subtropical gyre and the vertical, Atlantic Meridional Overturning Circulation (AMOC)



In a warmer world

Climate change weakens the AMOC, which slows the Gulf Stream down



2

3 **FAQ 9.3, Figure 1: Horizontal (gyre) and vertical (Atlantic Meridional Overturning Circulation - AMOC)**
 4 **circulations in the Atlantic today (left) and in a warmer world (right).** The Gulf Stream is a
 5 warm current composed of both circulations.

6

ACCEPTED FOR PUBLICATION
 SUBJECT TO FINAL EDITING